2011

PETROLOGIC, GEOCHEMICAL, AND GEOCHRONOLOGIC CONSTRAINTS ON THE TECTONIC EVOLUTION OF THE SOUTHERN APPALACHIAN OROGEN, BLUE RIDGE PROVINCE OF WESTERN NORTH CAROLINA

Eric Douglas Anderson
University of Kentucky, geology_eric@yahoo.com

ABSTRACT OF DISSERTATION

Eric Douglas Anderson

The Graduate School

University of Kentucky

2011

PETROLOGIC, GEOCHEMICAL, AND GEOCHRONOLOGIC CONSTRAINTS ON THE TECTONIC EVOLUTION OF THE SOUTHERN APPALACHIAN OROGEN, BLUE RIDGE PROVINCE OF WESTERN NORTH CAROLINA

ABSTRACT OF DISSERTATION

---

a dissertation submitted in partial fulfillment of the
requirements for the degree of Doctor of Philosophy in the
College of Arts and Sciences
at the University of Kentucky

By
Eric Douglas Anderson

Lexington, Kentucky

Director: Dr. David P. Moecher, Associate Professor
of Earth and Environmental Sciences,
Lexington, Kentucky

2011

ABSTRACT OF DISSERTATION

PETROLOGIC, GEOCHEMICAL, AND GEOCHRONOLOGIC CONSTRAINTS ON THE TECTONIC EVOLUTION OF THE SOUTHERN APPALACHIAN OROGEN, BLUE RIDGE PROVINCE OF WESTERN NORTH CAROLINA

The Blue Ridge Province of western North Carolina contains a wide variety of metamorphosed igneous and sedimentary rocks that record the tectonic effects of Precambrian and Paleozoic orogenic cycles. Tectonic interpretations of the events that led to the present configuration are varied and often conflicting. This investigation examines metamorphosed mafic rocks that are widely interpreted to have formed during the closure of ocean basins. Metabasites, and specifically eclogites, have a tendency to mark tectonic sutures and frequently preserve pressure (P), temperature (T), and age data (t) that can be gleaned from mineral equilibria and U-Pb isotopic compositions. As such, the examination of the metabasites is considered the key to understanding the orogenic history of the southern Blue Ridge where these metabasites occur. Chapter 2 is an investigation of the retrograde reactions related to the decompression of sodic pyroxenes that react to form diopside-plagioclase-hornblende-quartz symplectites as stability fields are overstepped during isothermal decompression. In Chapter 3 metabasites from the central and eastern Blue Ridge are re-examined and P-T pathways of these lithologies are determined. The argument is made that the Taconic orogeny of the Blue Ridge is the result of a continent-continent collision event that culminated in a mega-mélange that coincides with the Cullowhee terrane and the eastern Blue Ridge mélange of western North Carolina. Chapter 4 contains the results of a geochronological investigation of the Precambrian basement complex of the eastern Great Smoky Mountains. Chapter 5 is a whole rock geochemical study of the same basement complex. In Chapter 6, a potential lithologic correlation between the southern Blue Ridge basement and the Arequipa-Antofalla block of Peru is discussed. The geologic history of western South America from the Mesoproterozoic through Cambrian is summarized, a potential isotope-based lithologic correlation is proposed, and the early tectonic history of the central Blue Ridge is discussed. Chapter 7 contains brief summaries of Chapters 1-6.
KEYWORDS: Blue Ridge, Grenville, Taconic, orogeny, tectonics

_____
Student's Signature

_____
Date

PETROLOGIC, GEOCHEMICAL, AND GEOCHRONOLOGIC CONSTRAINTS ON THE TECTONIC EVOLUTION OF THE SOUTHERN APPALACHIAN OROGEN, BLUE RIDGE PROVINCE OF WESTERN NORTH CAROLINA

By

Eric Douglas Anderson

_____
Director of Dissertation

_____
Director of Graduate Studies

_____

RULES FOR THE USE OF DISSERTATIONS

Unpublished dissertations submitted for the Doctor's degree and deposited in the University of Kentucky Library are as a rule open for inspection, but are to be used only with due regard to the rights of the authors. Bibliographical references may be noted, but quotations or summaries of parts may be published only with the permission of the author, and with the usual scholarly acknowledgments.

Extensive copying or publication of the dissertation in whole or in part also requires the consent of the Dean of the Graduate School of the University of Kentucky.

A library that borrows this dissertation for use by its patrons is expected to secure the signature of each user.

Name Date

_____

_____

_____

_____

_____

_____

_____

_____

_____

_____

_____

_____

DISSERTATION

Eric Douglas Anderson

The Graduate School

University of Kentucky

2011

ACKNOWLEDGMENTS

Gratitude is expressed towards my dissertation adviser, Dr. David Moecher for his guidance, patience, dedication to geology, insightful suggestions, and time management skills. Dr. Moecher allows students to conduct research without forcing the results to fit into a pre-determined model, and this freedom of mind is greatly appreciated. The author is indebted to Carl Merschat and the North Carolina Geological Survey for two guided tours of the Blue Ridge basement complex. The Kentucky Geological Survey graciously provided the use of their X-ray facilities. Henry Francis and Jason Backus of the KGS dedicated hours of their time to guide XRF analysis and directed the sample-preparation process. Skilled assistance with zircon and monazite age determination was provided by Axel Schmitt and Marty Grove of the UCLA Keck Lab and is greatly appreciated. Scott Southworth and Michael Kunk of the U.S. Geological Survey freely shared ideas, information, and provided a critical Ar-Ar age for the Dellwood metabasite. Carl Henderson, the microbeam guru at the University of Michigan helped to image zircons prior to analysis at UCLA. Thanks go to Steve Dunn for sharing eclogite thin sections from Gurskøy, Norway, and to Spencer Cotkin for sharing a collection of eclogite thin sections from Flatraket, Norway. The insightful reviews of Eric Essene and an anonymous referee helped resolve inconsistencies and errors in Chapter 2, published in 2007 in the journal *Contributions to Mineralogy and Petrology*. Mark Steltenpohl and an anonymous reviewer greatly improved Chapter 3, published in the journal *Tectonics* in 2009. Dr. William A. Thomas made numerous insightful comments to correct serious errors and misconceptions in a previous version of Chapter 6. Dr. Thomas also reminded me that hunches and science are two different things. Eric Tohver reviewed Chapter 6 and made suggestions that significantly improved the chapter; his efforts are greatly appreciated. I would like to thank the members of my Dissertation Committee: Dr. Christopher S. Romanek, Dr. Edward Woolery, and Dr. Steven W. Yates of the Chemistry Department for their reviews and suggestions. I would like to thank Drs. Berman, Ludwig, Janousek, Farrow, and Erban for developing their ultra-sophisticated thermobarometric, geochronologic, and geochemical freeware.

In addition to the technical and instrumental assistance above, I would like to thank my wife, Jenell for her patience, support, advice, and understanding. I would like to thank my parents Larz and Glenice for their encouragement related to the study of science and support through college. Grants from the Geological Society of America (graduate research grant), the Graduate School of the University of Kentucky, and the Brown-McFarlan Fund of the Department of Earth and Environmental Sciences at the University of Kentucky were instrumental for covering research costs and travel to conferences. Without this assistance, the project would not have been possible. National Science foundation grants #NSF EAR 0635688, EAR 0001322, and EAR 0824714 made microbeam and SIMS analyses possible. Finally, I would like to thank the engineers of CAMECA for providing superb analytical tools.

TABLE OF CONTENTS

LIST OF TABLES

LIST OF FIGURES

CHAPTER 1: INTRODUCTION

Overview

The present configuration of the southern Appalachian orogen is the result of a nearly 1.5 Ga-long tectonic history. There are at least eight orogenies that potentially modified the Appalachian basement complex exposed in western North Carolina (Figures 1.1, 1.2). Mesoproterozoic to Neoproterozoic orogenies include: 1) the Elzeverian orogeny (*circa* 1245-1220); 2) the Shawinigan orogeny (*circa* 1200-1140); and 3) the Grenville orogeny (*circa* 1090-980 Ma) (ages from Hynes and Rivers, 2010). The Grenville orogen in North America is widely interpreted to have resulted from the collision of Laurentia and Amazonia (e.g. Loewy et al., 2003; Tohver et al., 2004; Hynes and Rivers, 2010; Fisher et al. 2010), so it may be appropriate to consider the effects of the Elzeverian-, Shawinigan- and Grenville-age tectonic events in the southern Blue Ridge in terms of the South American Sunsás orogeny. Later orogenies that potentially modified the southern Blue Ridge basement include five orogenies that occurred during the Paleozoic Era: Taconic, Cherokee, Acadian, Neoacadian, and Alleghanian (Hibbard et al., 2010; Hatcher, 2002). Although the Appalachians are a major tectonic feature on Earth, and studies of Appalachian tectonics may have served as a springboard for innovative geologic thinking (Tollo et al., 2010), vast tracts of basement complex rocks exist in the southern Appalachians that have only been examined on a reconnaissance level in terms of geochronology and geochemistry. The present investigation is centered on one such area: the basement rocks of the eastern Great Smoky Mountains, western North Carolina. Some studies have been conducted in and around the Great Smoky Mountain National Park (Hatcher et al., 2005, Southworth et al., 2005 and references therein), but few geochronological investigations have been conducted in the central Blue Ridge related to the Precambrian basement. Geologic mapping of the field area has been completed at the 1:100,000 scale (Southworth et al., 2005; Merschat et al., 2008), and several quadrangles have been mapped at the 1:24,000 scale, providing a framework for the investigation.

Geological Setting

The geologic history of the Blue Ridge Province of western North Carolina consists of several compressive and extensional deformation episodes potentially caused by continent-continent and island arc collisions related to the closure of one or more ocean basins (Rankin et al., 1989; Hibbard et al., 2007). Interpretations of seismic profiles (e.g. Cook et al., 1979, 1981; Cook and Vasudevan, 2006) conclude that the southern Blue Ridge is part of a large composite thrust sheet that contains the western Blue Ridge, central Blue Ridge, eastern Blue Ridge, Inner Piedmont, Cat Square, and Carolinia terranes. The Blue Ridge thrust sheet has a thickness ranging from six to fifteen kilometers and was transported en-mass a distance of several-hundreds of kilometers during the Alleghanian orogeny (Carboniferous-Permian).

The western Blue Ridge (Figure 1.1) is composed of Middle Proterozoic age orthogneiss and paragneiss units that are overlain by the Ocoee Supergroup, a thick (> 9-

kilometers) siliciclastic sequence of immature sediments that were deposited in fault-bounded rift basins during the Neoproterozoic (King et al., 1958; Rankin, 1975). One model for Neoproterozoic rifting holds that the breakup of the Rodinian supercontinent occurred at *circa* 570 Ma, leading to the opening of the Iapetus Ocean, followed by Neoproterozoic to early Paleozoic opening of the "Taconic Seaway", a small ocean basin separating Laurentia from a ribbon of rifted continental fragments and island arcs along the length of the Laurentian margin (Cawood et al., 2001). The proposed ribbon of continental fragments may have occurred due to "ridge jump" of a spreading center that moved inboard from the Laurentian margin.

Tectonostratigraphic subdivisions (Figure 1.2) are loosely based on Hatcher et al., 2005. "Eastern Blue Ridge" refers to lithologies exposed between the Chattahoochee-Holland Mountain fault and the Brevard fault zone. These same lithologies comprise the Jefferson terrane (Horton et al., 1989, 1986), the Toe terrane (Raymond et al., 1989), and the western portion of the Tugaloo terrane of Hatcher (2002). The eastern Blue Ridge contains the Lick Ridge and Boone eclogites investigated here, and consists of amphibolite, pelitic schist, quartzofeldspathic gneiss, various migmatites, and ultramafic rocks of the Ashe Metamorphic Suite (Rankin, 1970; McSween et al., 1989) that were metamorphosed during the Taconic (Miller et al., 2006)

The central Blue Ridge includes the Hayesville-Soque River thrust sheet (Hatcher et al., 2005) located between the Hayesville and Chattahoochee-Holland Mountain faults (Figure 1.1). The central Blue Ridge is composed of high-grade metamorphic rocks that include migmatitic orthogneiss, paragneiss, HP (high pressure)-metabasites exposed near Dellwood, and Taconic hypersthene-granulites that occur at Winding Stair Gap (Eckert, 1989, Moecher et al., 2004). The central Blue Ridge appears to have experienced a higher grade of metamorphism and contains more abundant migmatites, amphibolites, and ultramafic rocks relative to the western Blue Ridge (Hatcher et al., 2005). Results of geologic mapping conducted by the Hatcher group at UT Knoxville suggest that the central Blue Ridge is composed of two separate terranes; the Cowrock terrane, located mostly in Georgia, and the Cartoogechaye terrane, positioned stratigraphically above the Cowrock terrane (Hatcher et al., 2004, 2005). Orthogneisses of the central Blue Ridge Cartoogechaye terrane are the primary focus of Chapters 4 and 5.

The Mars Hill terrane, like the central Blue Ridge is adjacent to the eastern Blue Ridge and appears to be anomalously old relative to the Mesoproterozoic rocks that occur along strike. Evidence for the ancient nature of the Mars Hill terrane includes a whole-rock Rb-Sr isochron age of 1815 $\pm$ 31 Ma (Monrad and Gully, 1983). The Mars Hill terrane is also noted for its lithologic diversity, and appears to record an episode of Mesoproterozoic granulite facies metamorphism (Merschat, 1977). The southwestern extent of the Mars Hill terrane is unclear; "Mars Hill terrane-like" lithologies have been documented as far south as Sylva and Fines Creek, beyond the "established" boundaries of the terrane, and consequently overlap with the central Blue Ridge lithologies examined here (Berquist et al., 2003). Some workers argue that the Mars Hill terrane is part of the western Blue Ridge because the basement is stitched by Neoproterozoic A-type dikes, and covered by Neoproterozoic strata, characteristics shared by the western Blue Ridge (e.g. Hatcher et al. 2005).

An early Paleozoic regional-metamorphic episode (Hadley and Goldsmith, 1963; Moecher et al., 2005) produced a Barrovian isograd pattern that increases from chlorite-

grade (greenschist facies) in the northwest to sillimanite- and hypersthene-grade (granulite facies) towards the southeast, culminating in the Wayah metamorphic core complex (Eckert et al., 1989). Subsequent overprinting in the Blue Ridge and Inner Piedmont may be related to Neo-Acadian metamorphism (~365-350 Ma, Hatcher et al., 2005), and thrusting of the Blue Ridge thrust sheet onto the Valley and Ridge Province along the Great Smoky and Guest Creek faults at *circa* 280 Ma (Southworth et al, 2005). Dextral transpressional episodes occurred during the Silurian and Devonian that may have caused significant terrane dispersion in the Appalachian Blue Ridge (Dennis, 2007; Stewart et al., 1997). Taconic, Cherokee, Acadian, Neoacadian, and Alleghanian metamorphic and plutonic events have been documented in different terranes of the Blue Ridge. Some terranes were affected by several Paleozoic orogenies. At present, the age distribution of metamorphism, plutonism, and clastic wedge deposition is not fully understood in the southern Appalachian Blue Ridge.

Goals of the Investigation

The purpose of the current study is to use petrology, geothermobarometry, geochronology, and geochemical data of the Blue Ridge to test the validity of existing tectonic models. Emphasis is placed on understanding the Taconic orogeny (~450-480 Ma) and various related tectonic models. Present models for the Taconic orogeny are varied and conflicting. Some models suggest that the Taconic orogeny was the result of a collision between Laurentia and the Piedmont terrane that began in the lower Ordovician as the Piedmont arc advanced over an east-dipping subduction zone (Hatcher, 1989; Stewart et al., 1997). Other models for the Taconic orogeny include the development of a block-in-matrix mélange in the central Blue Ridge that formed due to the lithological mixing of the western Blue Ridge (Sherwood terrane) and the Piedmont (Toe terrane) to form the Cullowhee terrane (Raymond et al., 1989). Another hypothesis of Raymond et al. (1989) suggests that the block-in-matrix Cullowhee terrane may have resulted from the development of a Franciscan Formation-type blueschist complex that was later overprinted by amphibolite-facies metamorphism. Yet another model of the Taconic orogeny is implied from studies of South American geology, where the Famatinian orogeny (540-330 Ma; Aceñolaza and Toselli, 1976) resulted from continent-continent collision between South America and Laurentia (Dalla Salda et al., 1992). In this model, the presence of peri-Gondwanan elements in the southern Blue Ridge (i.e. Carolinia) and peri-Laurentian elements in southern South America (i.e. Occidentalia) may be explained by terrane transfer between continents occurring in the Taconic-Famatinian orogeny.

Focus is also placed on understanding the origin of the central Blue Ridge basement complex. A fundamental question is: what composes the basement complex of the central Blue Ridge? Although Hadley and Goldsmith (1963) interpreted the basement complex of the eastern Great Smoky Mountains as a mix of granitic, metasedimentary, and metavolcanic gneisses components, the ages and tectonic relations between the lithologies is uncertain. Hatcher (1978) and Montes and Hatcher (1999) imply that the central Blue Ridge basement may be composed of metasedimentary-metavolcanic rock equivalents of the Ashe or Tallulah Falls Formation. Merschat et al. (2010) imply that the central Blue Ridge basement complex is largely metasedimentary in origin.

Contributions to Geological Science

In the present work, a suite of metamorphic rocks from the Dellwood region of the central Blue Ridge is analyzed for whole rock chemical compositions. A high pressure (HP) metabasite was discovered that became the focus of Chapters 2 and 3. Eclogites and HP granulites of gneiss terranes are rarely pristine; they commonly contain retrograde mineral assemblages and fabrics that form during tectonic exhumation processes as metamorphic facies boundaries were crossed during decompression. In eclogites from gneiss terranes, omphacite that formed at peak eclogite-facies P-T conditions breaks down at amphibolite-facies conditions to form "symplectites" composed of plagioclase, diopside, quartz, and hornblende. To estimate minimum pressure conditions, workers commonly "reintegrate" symplectite compositions using an electron microprobe analyzer and use reintegrated-omphacite compositions to estimate precursor omphacite compositions that are then used for pressure calculations. However, the technique is somewhat questionable because it is unclear whether the symplectite-forming reactions(s) occur under closed-system conditions or not. In a contribution to metamorphic petrology, the reactions related to the formation of symplectites after omphacite are examined and the validity of reintegration of symplectites is tested. The study (Chapter 2) is a microprobe-based examination of naturally-occurring-HP metabasites from the southern Blue Ridge and the Calledonides of Norway. Most of Chapter 2 was previously published in *Contributions to Mineralogy and Petrology*, (2007) volume 154, issue 3, pages 253-277, and appears here with minor editing.

Taconic (~460 Ma) eclogites of the southern Appalachian basement are central to tectonic models of the Blue Ridge as they mark the location of sutures between collisional terranes. In the geologic record there are several types of eclogite. Low-T eclogite (Carswell, 1990) forms via the subduction of oceanic crust beneath a continental margin. Medium-T eclogite (Carswell, 1990) forms during continental subduction events, with examples occurring in a dozen-or-so gneiss terranes that include the Caledonides of Norway (e.g. Labrousse et al., 2004), and the Kaghan Valley of the western Himalaya (Parrish et al., 2006). In Chapter 3, the P-T paths of Taconic medium-T eclogites of the eastern Blue Ridge are re-examined, and a P-T path is estimated for the newly recognized Taconic garnet granulites and HP-amphibolites of the central Blue Ridge basement complex. This contribution also includes the calculation of a prograde path for the Boone eclogite (Abbott and Greenwood, 2001). A tectonic model is proposed in which HP metabasites formed due to continental collision and subduction of continental crust at the Laurentian margin of the southern Blue Ridge. Most of the material from Chapter 3 appears in *Tectonics* (2009), volume 28, TC5012, 27 pages, doi:10.1029/2008TC002319. Some changes were made to the 2009 material as presented here in Chapter 3.

Chapter 4 is a geochronologic study of central and western Blue Ridge orthogneisses, that includes new U-Pb zircon (SIMS) ages. In addition, Th-Pb monazite ages are determined from western Blue Ridge cover sequences and from a central Blue Ridge migmatite. Zircon ages from the present study are consistent with three episodes of Mesoproterozoic plutonism. Additional plutonic events are indicated by detrital zircons older than 1292, and by plutonic zircons that are younger than 1020 Ma. Three metamorphic events are delineated that include a Taconic igneous/metamorphic

migmatization event. Results of Th-Pb monazite geochronology define four age modes that correspond to the Taconic, Cherokee (Silurian), Acadian, and Alleghanian orogenies. The most frequent age mode preserved in monazite is correlated to the Cherokee orogeny.

In Chapter 5, the granitoid classification system of Frost et al. (2001) and Frost and Frost (2008) is applied to a suite of orthogneisses from the central and western Blue Ridge to discern the tectonic setting of igneous emplacement. The results indicate that two arc-related Mesoproterozoic episodes produced most of the basement orthogneisses that were sampled. The third and youngest Mesoproterozoic episode produced ferroan granites that were presumably produced by the melting of overly-thickened continental crust during the Grenville orogeny.

While evaluating and classifying the granitoids of the study area, a potential isotope-based lithologic correlation between Blue Ridge basement and the Arequipa-Antofalla block of South America was determined. The correlation is based on U-Pb ages of igneous and metamorphic zircon, whole rock Pb-Pb isotopic compositions, Nd-Sm ages, and whole rock Rb-Sr ages. Constraints of the isotopic correlation are used to produce a paleogeographic reconstruction of the Laurentian-Amazonian portion of Rodinia prior to Neoproterozoic rifting. The occurrence of correlated gneiss terranes in the southern Blue Ridge of Laurentia and the western margin of South America would support tectonic models in which Mesoproterozoic basement was transferred from South America to Laurentia at ~1150 Ma (e.g. Tohver et al., 2004; Fisher et al., 2010).

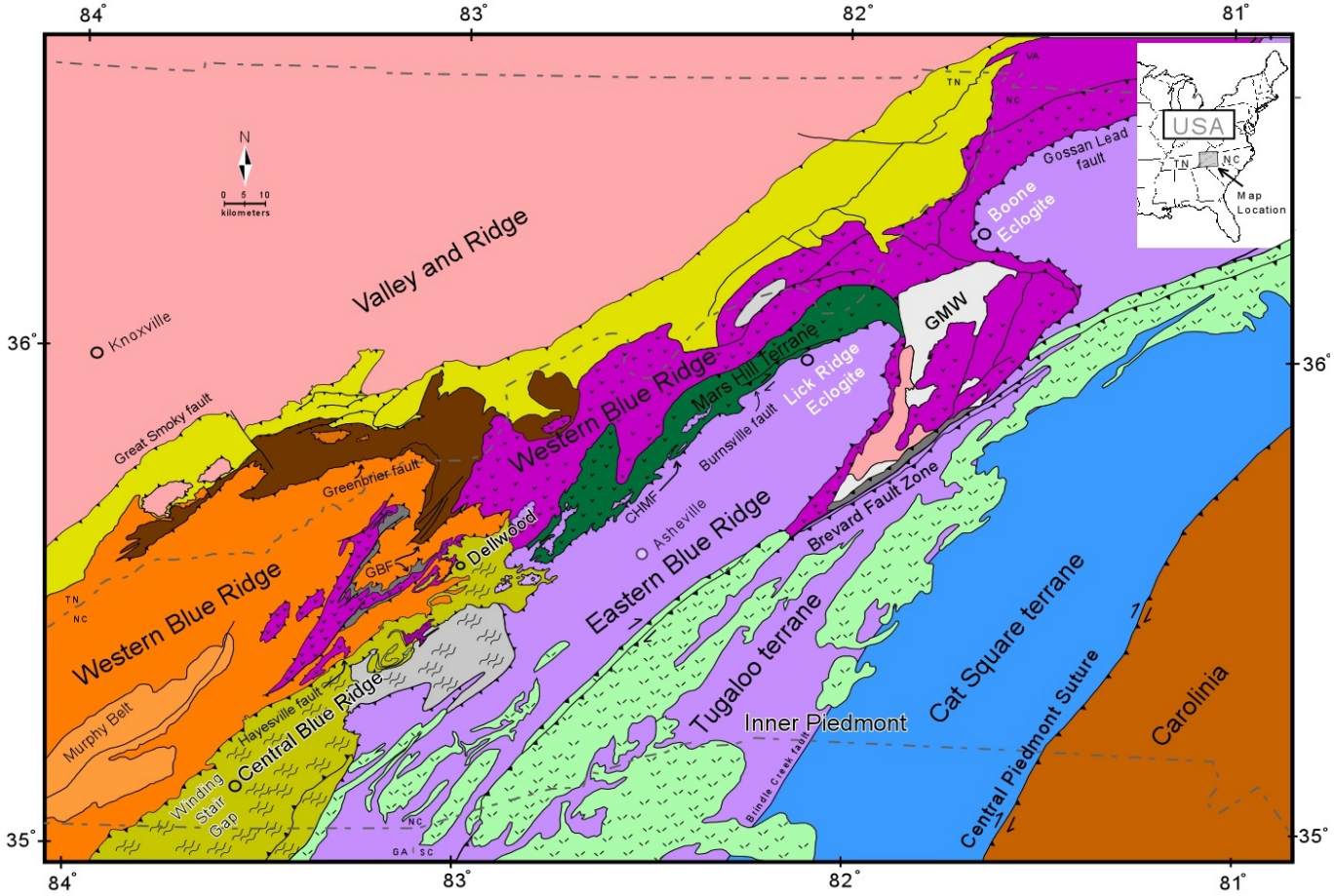

Figure 1.1. Geologic map of western North Carolina. (explanation follows)

Figure 1.1. Geologic map of western North Carolina with geologic provinces, selected faults, and locations of investigated HP rocks. GBF=Greenbrier fault; CHMF=Chattahoochee-Holland Mountain fault. Map compiled from Rankin et al. (1990), Woodward et al. (1991), Adams et al. (1995), Hatcher et al. (2004), and Hatcher et al. (2005).

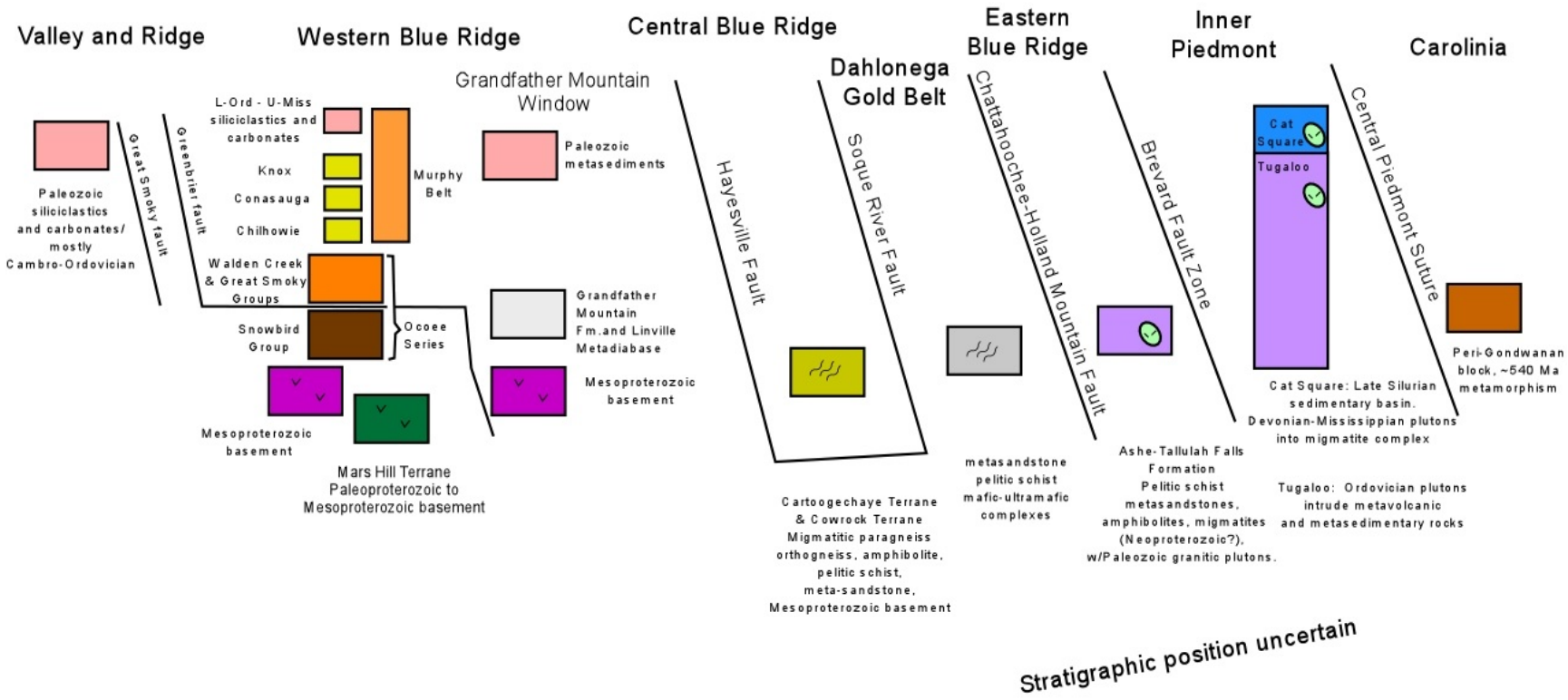

Figure 1.2. Legend to geologic map.

CHAPTER 2: OMPHACITE BREAKDOWN REACTIONS AND RELATION TO ECLOGITE EXHUMATION RATES

Introduction

Clinopyroxene + plagioclase symplectites after omphacite are a common feature in metabasites of high pressure (HP) and ultra-high-pressure (UHP) metamorphic belts (e.g., Eskola, 1921; Griffin and Råheim, 1973; O'Brien et al., 1990; Droop et al., 1990; Zhao et al., 2001). In the absence of coesite or preserved omphacite, clinopyroxene + plagioclase symplectites after omphacite (hereafter referred to as "Cpx-Pl symplectites") are commonly used to infer prior eclogite, HP granulite, or HP amphibolite facies conditions, interpretations that may be crucial for understanding the tectonic history of a collisional orogen. Cpx-Pl symplectites can form in response to post-peak decompression as eclogite facies rocks pass through granulite and/or upper amphibolite facies conditions. This inference was initially made by Eskola (1921) based on petrographic features of metabasites from the Western Gneiss Region of Norway. Eskola inferred that alkali-free diopside + albite symplectites formed from the isochemical breakdown of omphacite due to decompression beyond the omphacite stability field. Later studies (Vogel 1966) have supported Eskola's idea of an isochemical reaction. Vogel proposed "unmixing" (exsolution) of the precursor omphacite by the reaction:

$$\square_{1/2}Ca_{1/2}AlSi_2O_6 \text{ (Ca-Eskola component)} + NaAlSi_2O_6 \text{ (Jadeite)} = 1.5\ Na_{2/3}Ca_{1/3}[Al_{4/3}Si_{8/3}O_8]\ (Ab_{67}An_{33}) \qquad [1]$$

Boland and van Roermund (1983) also suggested exsolution ("discontinuous" and "continuous" precipitation) as a mechanism for the formation of Cpx-Pl symplectites after omphacite. The idea that Cpx-Pl symplectites represent decompressed omphacite and that rocks containing such features are relict eclogites has gained wide acceptance (e.g., Peacock and Goodge, 1995; O'Brien, 1989b; Jamtveit, 1987; Möller, 1998; Zhao et al., 2001). Some workers accept the assumption that the symplectite-forming reaction is isochemical (e.g., Abbott and Greenwood, 2001; Markl and Bucher, 1997; Shervais et al., 2003) and reintegrate symplectite assemblages to estimate an original omphacite composition. The jadeite component of the reintegrated omphacite composition is used to calculate a minimum pressure using the equilibrium:

$$Jd + Qtz = Ab \quad \text{(Holland, 1980, 1983)} \qquad [2]$$

Uncertainties exist related to the inferred exsolution mechanism and the isochemical nature of omphacite-breakdown reactions. Mysen and Griffin (1973) noted that the exsolution of plagioclase from stoichiometric pyroxene components (jadeite, $NaAlSi_2O_6$; Ca-Tschermak, $CaAl_2SiO_6$) requires the addition of SiO_2. They proposed several sub-silicic "third phases" that would make the reaction isochemical, but noted that these "third phases" were never observed in symplectic assemblages they examined.

Mysen and Griffen (1973) also considered several reactions involving Ca-Eskola component that produce plagioclase without consuming SiO_2. Oxidation of ferrous omphacite to form ferric augite + plagioclase during uplift and cooling was proposed as a likely mechanism for the formation of Cpx-Pl symplectites (Mysen and Griffin, 1973). In a study of kyanite-eclogites from the Adula Nappe, Central Alps, Heinrich (1982) suggested that fluid transport (on a scale of meters) facilitated cation transport on a millimeter scale. Fluids were proposed to be an integral part of net-transfer reactions that resulted in amphibolite-facies overprinting of eclogite-facies rocks, implying open-system behavior at the grain scale. Studies of retrograde reactions from Bohemian Massif eclogites (Messiga and Bettini, 1990), and the Southern Sulu UHP eclogites (Yang, 2004) utilizing mass-balance analysis concluded that various retrograde assemblage reactions are *not* isochemical. Messiga and Bettini (1990) determined that sodium in plagioclase coronas on garnet was not derived from adjacent garnet or orthopyroxene; Yang (2004) determined that various symplectites occurring at omphacite grain boundaries were not isochemical with adjacent omphacite.

The purpose of the present study is to (1) investigate the mechanism(s) responsible for the formation of Cpx-Pl symplectites after omphacite in metabasites via high resolution BSE imaging, elemental X-ray mapping and focused beam compositional traverses of symplectic phases; (2) test the validity of Cpx-Pl symplectite reintegration by comparing symplectite compositions to un-reacted omphacitic compositions determined via electron microprobe broadbeam analysis, and (3) quantify the location and kinetics of symplectite-forming reactions in P-T space. Rocks that have completely equilibrated at eclogite facies conditions provide no record of a P-T pathway. Disequilibrium assemblages in metabasites, such as Cpx-Pl symplectites and coronas around garnet, do preserve P-T pathway information if interpreted correctly (e.g., Rubie, 1990). A variety of Cpx + Pl $\pm$ Hbl $\pm$ Qtz symplectites after omphacite from metabasites of the Blue Ridge Province of the southern Appalachian orogen (USA), and the Western Gneiss Region (WGR) of Norway are examined in detail. Minerals abbreviations are after Kretz (1983); abbreviations used for pyroxene solid solution endmembers include Ac = acmite/aegirine; CaTs = Ca-Tschermak's component; Es = esseneite, and CaEs = Ca-Eskola component.

Geological Setting of Samples

Southern Blue Ridge (USA)

Occurrences of HP rocks are rare within the Appalachian orogen of eastern Laurentia (Berkshire massif: Maggs et al., 1986; Laird and Albee, 1981: Newfoundland: Church, 1969). Several occurrences of eclogite from the southern Appalachian Blue Ridge province appear to be concentrated along terrane margins that separate a series of parauthochtonous to allochthonous terranes that were accreted to the western margin of Laurentia during the Paleozoic (Hatcher et al., 2005). The HP metabasites investigated from the southern Blue Ridge occur near the boundary of the eastern Blue Ridge terrane and Grenville-aged, western Blue Ridge basement (Figures 1.1, 1.2). The Lick Ridge

eclogite (or Bakersville eclogite: Willard and Adams, 1994) occurs as a series of ~1 kilometer-scale, tectonically-emplaced blocks that are exposed near the base of the eastern Blue Ridge. Eclogite and ultramafic pods are enclosed by pelitic schist, mica gneiss, metagraywacke, and amphibolite, approximately 400 meters above a ~0.2-kilometer-wide, right-lateral shear zone (Silurian-Devonian aged Burnsville fault) that separates the underlying western Blue Ridge basement from the eastern Blue Ridge (Adams et al., 1995). The Dellwood metabasite occurs as a ~0.5-km-long pod enclosed by migmatitic muscovite-biotite gneiss, various biotite-hornblende gneisses, muscovite-biotite-garnet schists, and orthogneiss of the central Blue Ridge basement complex. The Boone eclogites occur ~7 km northwest of Boone, North Carolina, are enclosed by hornblende schist and pelitic schist, and may represent HP relics that have survived widespread amphibolite-facies overprinting (Abbott and Raymond, 1997; Abbott and Greenwood, 2001). The Lick Ridge and Boone eclogites occur in a similar structural position, occurring near the base of the eastern Blue Ridge as inclusions in a Taconic (Middle Ordovician) subduction complex (Miller et al., 2006) that was variably overprinted by Acadian (middle Paleozoic) and Alleghanian (late Paleozoic) deformation.

Western Gneiss Region, Norwegian Caledonides

The Western Gneiss Region is a composite terrane consisting of Baltic, Mesoproterozoic continental basement, overlain by several Caledonian nappes, exposed as the largest of a series of basement windows in Norway and Sweden. Granodioritic, granitic, and gabbroic migmatites, were reworked during the Scandian phase of the Caledonian orogeny (Krabbendam et al., 2000; Cuthbert et al., 2000). In the central and northwestern WGR, mafic and felsic eclogites occur as meter- to kilometer-scale lenses in high-grade gneiss (Griffin et al., 1985). Coesite-bearing and relict coesite UHP (ultra-high-pressure) eclogites, are preserved in the northwestern WGR (Smith, 1984, 1988; Wain, 1997). Eclogites from Flatraket and Gurskøy of the "Nordfjord area" are examined in the present study. Although lacking coesite, the samples were collected adjacent to coesite-bearing eclogite localities (Cuthbert et al., 2000) and are assumed to have experienced UHP conditions. In recent tectonic interpretations of the Nordfjord area, HP and UHP eclogites formed in response to the NW-directed subduction of Baltic continental crust beneath Laurentian continental crust during the Caledonian orogeny (Andersen et al. 1991). Recent studies (Labrousse et al., 2004; Terry et al., 2000) suggest that UHP and HP lithologies from various areas of the WGR were exhumed from depths of nearly 100 km at plate tectonic rates (2 – 25 mm/yr.)

Mineral Assemblages

Blue Ridge Thrust Complex: SW of Grandfather Mountain Window

Eclogites from Lick Ridge are composed mainly of omphacite, garnet, quartz and rutile (Figure 2.1) with retrograde hornblende, plagioclase, and traces of titanite, apatite,

and zircon (Willard and Adams, 1994; Page et al., 2003). Garnet is typically rimmed by coronas of plagioclase and hornblende. Garnet cores are commonly inclusion-rich, with quartz, rutile, titanite, epidote, clinopyroxene and hornblende occurring as the included phases (Page et al., 2003). Matrix pyroxene exhibits various exsolution textures including oriented quartz rods, compound inclusions composed of hornblende + quartz, and lamellar clinopyroxene-hornblende intergrowths (Page et al., 2005). Clinopyroxene grains that have reacted to form lamellar intergrowths of plagioclase + clinopyroxene + hornblende + quartz are investigated in the present study. Some matrix clinopyroxene contains zones of unreacted omphacite that are relatively pristine, lacking inclusions or exsolution features. The petrography of the Lick Ridge eclogite has been described in detail previously (Willard and Adams, 1994; Page et al., 2003, 2005).

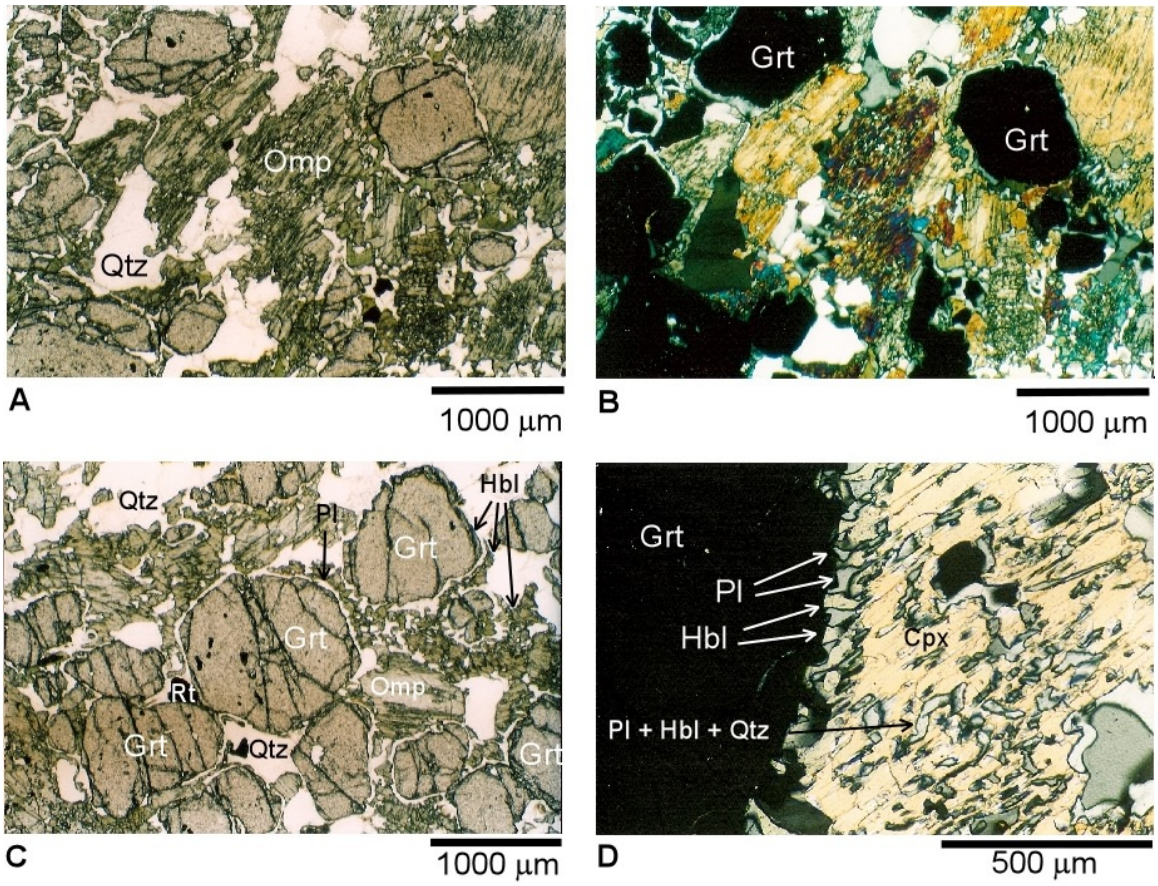

Figure 2.1. Photomicrographs of the Lick Ridge eclogite. A) Omphacite, garnet, quartz and rutile under PPL (Plane polarized light). B) Symplectic Cpx and reaction rims around garnet under XN (crossed Nicols). C) Eclogite with plagioclase + hornblende rims on garnet, and symplectic pyroxene. PPL. D) Retrograde reactions at garnet rim, XN. Mineral abbreviations after Kretz (1983).

Blue Ridge Thrust Complex: Eastern Great Smoky Mountains

Metabasite samples from the central Blue Ridge basement complex north of Dellwood, NC have a matrix assemblage consisting of clinopyroxene, garnet, hornblende, plagioclase, titanite, and ilmenite (Figure 2.2). Samples collected from the center of the km-scale Dellwood metabasite body contain abundant clinopyroxene + garnet; other samples collected from the outer margin of the mafic lens contain only traces of clinopyroxene with a greater abundance of hornblende. Most clinopyroxene grains show some degree of breakdown to form Cpx-Pl symplectites, with rods or lamellae of plagioclase, hornblende, and quartz enclosed by clinopyroxene; some matrix pyroxenes have apparently not reacted. Garnet is subhedral to euhedral, ~0.5 to 3 mm in diameter with inclusions of clinopyroxene, Cl-amphibole, epidote, plagioclase, titanite, ilmenite, rutile, quartz, apatite, and dolomite. Plagioclase occurs as subhedral grains within the matrix, as rims surrounding garnet, and lamellar and rod-shaped inclusions in symplecte assemblages. Rutile is less abundant than titanite or ilmenite, occurs within the matrix or as inclusions in garnet, and is commonly rimmed by titanite. The metabasites from Dellwood are classified as (Opx-free) garnet granulites and HP-amphibolites. Plagioclase is an abundant matrix phase in all samples and is interpreted as part of the peak metamorphic assemblage. Although quartz occurs as inclusions within garnet and clinopyroxene, it is lacking as a matrix phase, consistent with SiO_2 contents of 43-45 wt. % determined by XRF (X-ray fluorescence) analysis (data in chapter 5; samples DEL03-3, 3B, 3C, 3D, DEL05-3B2).

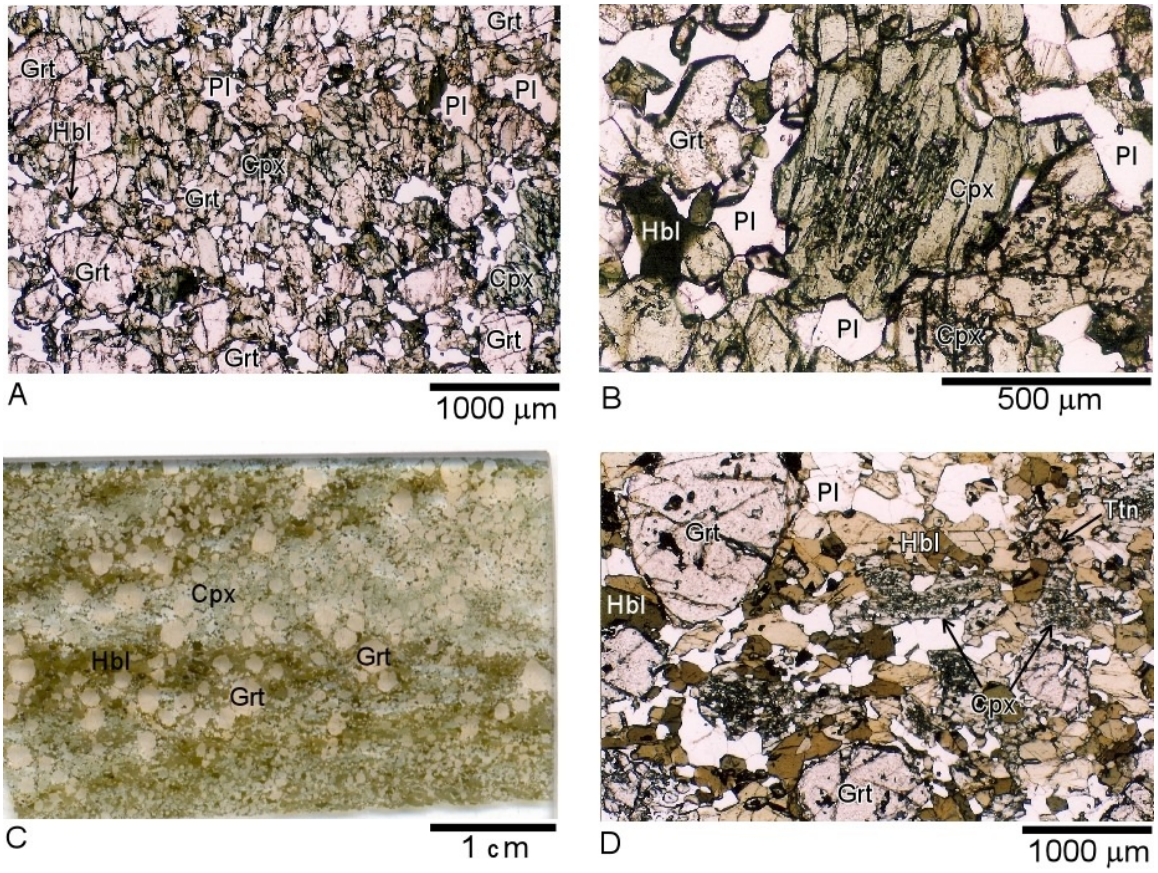

Figure 2.2. Photomicrographs of metabasites sampled north of Dellwood, NC, central Blue Ridge basement complex. A) Photomicrograph of matrix phases (clinopyroxene, garnet, plagioclase with minor hornblende) in garnet granulite (sample DEL05-3B2), PPL. B) Matrix pyroxene with symplectitic phases in core, sample DEL05-3B2, PPL. C) Scan of thin section DEL03-3B showing Cpx- and Hbl-rich banding in HP amphibolite. D) Cpx-Pl symplectites, garnet, plagioclase, hornblende, and titanite in HP-amphibolite DEL03-3B, PPL.

Blue Ridge Thrust Complex NE of Grandfather Mtn. Window

Boone eclogites (Abbott and Raymond, 1997) are banded on the cm-scale. Some bands are rich in clinopyroxene, plagioclase, and garnet; other layers contain more abundant hornblende, quartz, or epidote. In the present study, bands composed of clinopyroxene, plagioclase, garnet, hornblende, epidote, quartz, and ilmenite ("retrograde eclogites") are investigated. In thin section, precursor clinopyroxene has completely reacted to form fine-grained diopside-plagioclase symplectites (Figure 2.3). Cpx-Pl symplectite contains vermicular plagioclase rods, typically 5 – 10 μm in diameter, included in diopside. Some Cpx -Pl symplectites have a plumose structure, with curved

plagioclase lamellae. Optical continuity in remnant clinopyroxene suggests that precursor omphacite grains were 5 – 10 mm in diameter (Abbott and Raymond, 1997). Garnets are small (~250 – 750 μm), subhedral to euhedral, and typically enclosed by Cpx-Pl symplectite. Ilmenite displays coronas of titanite and plagioclase. Garnet is rimmed by hornblende, plagioclase, and rare magnetite. Titanite, quartz, rutile, ilmenite, apatite, zircon, and pyrite occur as inclusions in Boone eclogite garnet.

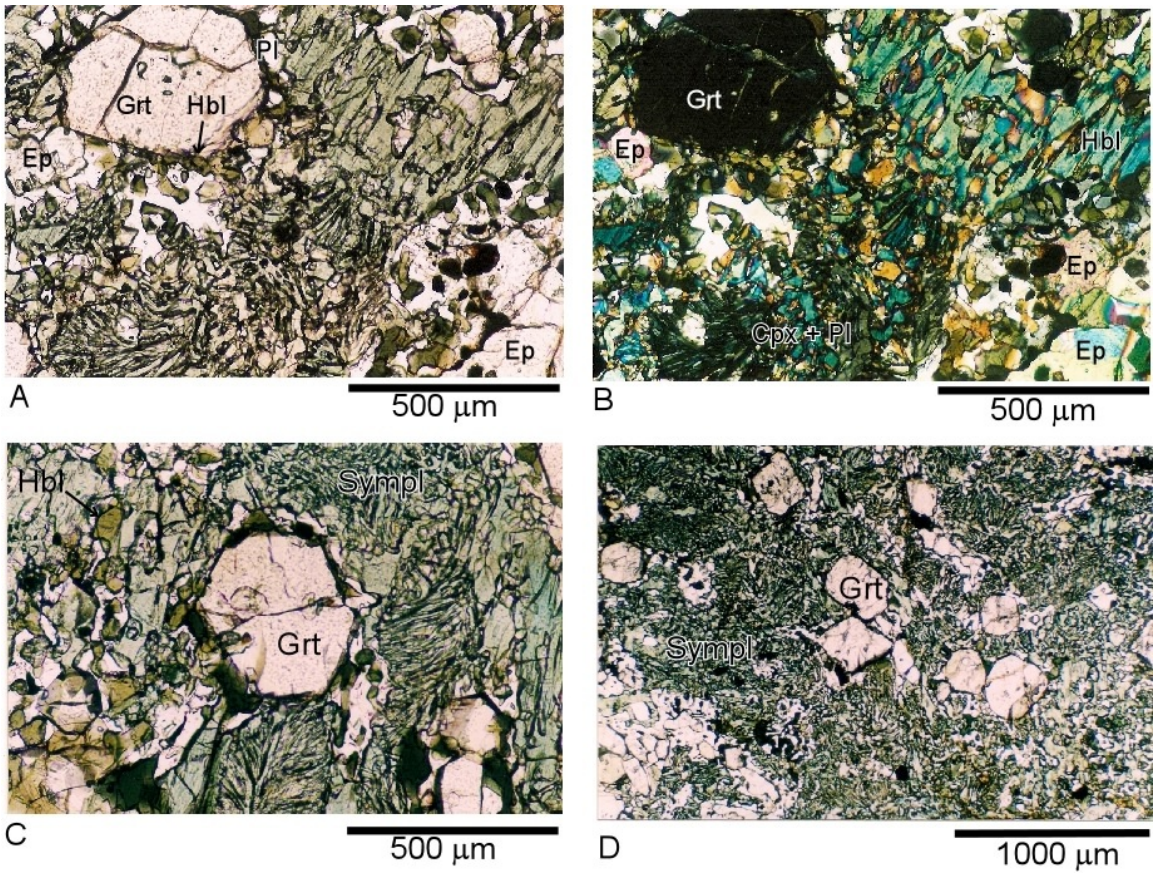

Figure 2.3. Photomicrographs of Boone eclogite. A) Clinopyroxene, garnet, plagioclase, and epidote with omphacite completely replaced by diopside-plagioclase-hornblende symplectites, PPL. B) Same image under XN. C) Small garnets with Hbl + Pl rims, plumose Cpx + Plag symplectite after omphacite, PPL. D) Cpx + Pl symplectite after omphacite, PPL.

Western Gneiss Region, Norway

Eclogites from Flatraket, Norway contain omphacite, garnet and rutile, and have been examined in detail in previous studies (e.g., Cotkin et al., 1988; Krabbendam et al., 2000; Wain et al., 2001). Clinopyroxene + plagioclase + hornblende symplectites occur

between optically distinct matrix clinopyroxene grains and at garnet-clinopyroxene grain boundaries. Under plane light, symplectites appear dark brown, are very-fine grained, and symplectite colonies have a maximum width of approximately 500 μm (Figure 2.4).

Retrograde eclogites from Gurskøy are composed largely of garnet and omphacite (Figure 2.4) and were collected as boudins in felsic gneiss (Dunn and Medaris, 1989). Plagioclase-diopside symplectites appear to be concentrated at omphacite grain boundaries; some symplectites completely replace single grains of optically-continuous omphacite. Garnet is subhedral, with a fairly uniform size of approximately 1 mm, and rimmed by plagioclase and hornblende.

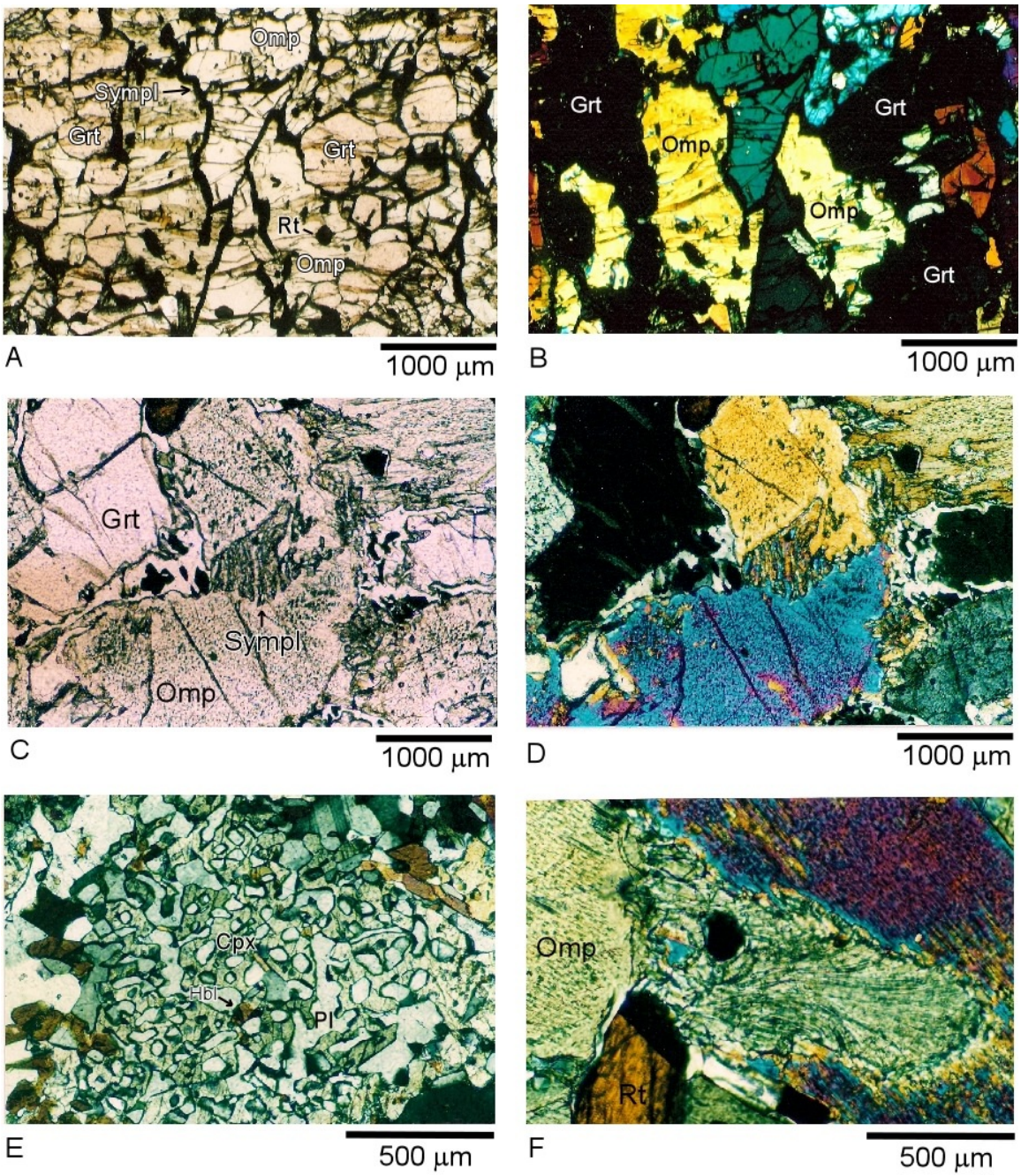

Figure 2.4. Symplectites in eclogite, WGR Norway. A) Cpx-Pl-Hbl symplectites at grain boundaries, Flatraket sample, PPL; B) Same view under XN; C) Cpx-Pl symplectite at grain boundary between two omphacite grains, Gurskøy, Norway, PPL. D) Same image under XN. E) Cpx-Pl-Hbl symplectite after omphacite, showing cross-section of plagioclase rods, Gurskøy, Norway, PPL; F) Plumose Cpx-Pl symplectite colony, Gurskøy, Norway, XN.

Mineral Chemistry

Mineral compositions were determined using the ARL-SEMQ microprobe at the University of Kentucky. Most minerals were analyzed in point mode, using WDS at 15 kV and 15 nA, except for plagioclase, which was analyzed using a rastered beam (10 x 10 μm) at 15 kV and 10 nA to minimize loss of Na and K. Typical count times were 10-20 seconds on peak, and 5-10 seconds for background counts. Natural USNM standards were used, ZAF corrections were made using Probewin v. 5.32. Compositional traverses of garnet and across various phases in symplectites were performed using a mean atomic number background correction.

Garnet formulae were recalculated on the basis of 12 oxygens; all Fe was assumed to be Fe^{2+}. Pyroxene formulae were calculated on the basis of 6 oxygens, with Fe^{2+} and Fe^{3+} estimated by stoichiometry (Droop, 1987). Pyroxene endmember components were calculated using an endmember-removal sequence spread sheet (Vogel 1966, Smyth 1980). Ten end-members were calculated in the order: aegirine $NaFe^{3+}Si_2O_6$ (Ac), jadeite $NaAlSi_2O_6$ (Jd), $KFe^{3+}AlSiO_6$ (I), Ca-Ti Tschermak's component ($CaTiAl_2O_6$), esseneite $CaFe^{3+}AlSiO_6$ (Es), Ca-Tschermak's component $CaAlAlSiO_6$ (CaTs), johannsenite $CaMnSi_2O_6$ (Jo), wollastonite $Ca_2Si_2O_6$ (Wo), enstatite $Mg_2Si_2O_6$ (En) and ferrosilite $Fe_2Si_2O_6$ (Fs). Minimum content of Ca-Eskola component (CaEs) ($_{1/2}Ca_{1/2}AlSi_2O_6$) was calculated using the method of Page et al. (2005); i.e. twice the cation deficiency in a 6-cation normalization with all Fe as Fe^{2+}. The Ca-Eskola estimation (null in all pyroxenes analyzed, with the exception of broadbeam reintegrations) was made independently of the endmember removal spreadsheet that utilizes a Fe^{3+}estimate. Pyroxenes are classified using International Mineralogical Association criteria (Morimoto et al., 1988). The pyroxene endmember calculation scheme described above was used to classify pyroxenes and to estimate X_{jd} of Cpx for thermobarometric calculations. Hornblende formulae were calculated assuming 13 cations excluding Ca, Na, and K; Fe^{3+} was estimated by stoichiometry (Eqn. 6 of Droop, 1987).

Lick Ridge, Appalachian Blue Ridge

Matrix pyroxenes are zoned, with omphacitic cores and diopsidic rims. Cores have an average composition of $Jd_{21}CaTs_{09}Ac_{05}CaEs_0Di_{49}Hd_{16}$, with average estimated $Fe^{3+}/Fe^{2+} = 0.43$, $Fe^{2+}/(Fe^{2+} + Mg) = 0.24$ and Na = 0.23 – 0.30 pfu. Core compositions plot as a cluster within the omphacite field, with $X_{jd} = 0.2 – 0.3$ on the Quad-Jd-Ac plot (Figure 2.5). Pyroxene compositions from Cpx-Pl symplectites are diopsidic and have compositions similar to matrix omphacite rims, with an average composition of $Jd_{02}CaTs_{08}Ac_{08}Di_{63}Hd_{19}$, $Fe^{2+}/(Fe^{2+} + Mg) = 0.24$ and Na = 0.07 – 0.13 pfu. Garnet compositional traverses show flat, homogenous core compositions of approximately $Alm_{44}Grs_{25}Prp_{30}Sps_{01}$, followed by a small spike in Mg and concomitant dip in Ca. The outer ~100 μm rims have increasing Fe, decreasing Mg, and slightly lower Ca content. Mn concentrations are low throughout. Plagioclase compositions from plagioclase +

hornblende coronas surrounding garnet have compositions that are similar to plagioclase from Cpx-Pl symplectites, ranging from Ab_{71}-Ab_{76}, with an average value of ~ $Ab_{72}An_{28}$. Representative analyses of phases are presented in Appendix A.

Dellwood, Appalachian Blue Ridge

Several compositions of pyroxene occur in Dellwood garnet granulite and HP-amphibolite, including diopside, aegirine-augite, and omphacite (Figures 2.5, 2.6, 2.7). The most sodic pyroxene is non-symplectitic omphacite, occurs as a matrix phase, and has a composition of ~ $Jd_{19}CaTs_{06}Ac_{05}CaEs_{0}Di_{42}Hd_{28}$. Matrix pyroxene in garnet granulite has X_{jd} of 0 – 0.19, X_{ac} = 0 – 0.17, with average X_{jd} = 0.08, average X_{ac} = 0.09, average Na = 0.18 pfu, average Al = 0.29 pfu and average $Fe^{2+}/(Fe^{2+} + Mg)$ = 0.37. Pyroxene inclusions occurring in garnet of garnet granulite are classified as diopside, aegirine and omphacite with X_{jd} = 0 – 0.19, X_{ac} = 0 – 0.19, with average X_{jd} = 0.08, average X_{ac} = 0.05, average Na = 0.13 pfu, average Al = 0.21 pfu, and average $Fe^{2+}/(Fe^{2+} + Mg)$ = 0.34. Pyroxene inclusions in garnet contain up to 10% esseneite component. Matrix pyroxene rims have compositions that are similar to symplectic pyroxene and diopsidic. Average X_{jd} = 0.06, average X_{ac} = 0.08, average Na = 0.15 pfu, average Al = 0.24 pfu, and average $Fe^{2+}/(Fe^{2+} + Mg)$ = 0.36 in pyroxene rims and symplectic pyroxene of garnet granulite.

Garnets have relatively flat compositional zoning profiles within cores, with typical core compositions ranging from $Alm_{55}Grs_{32}Prp_{12}Sps_{01}$ to $Alm_{55}Grs_{28}Prp_{15}Sps_{02}$. From core to rim, Mg content gradually increases and Mn decreases, consistent with preservation of a component of prograde growth zoning (Medaris et al., 1995, 2006; Štípská and Powell, 2005). Some garnet profiles show a spike in Ca and drop in Mg, approximately 150 μm from the rim. The outer ~20 μm rims of garnet are characterized by increased Ca and Fe concentrations, and decreased Mg content consistent with slight retrograde re-equilibration. The largest garnets (2 – 3 mm) are euhedral, occur within hornblende-rich samples, and have core compositions that are enriched in Mn and depleted in Mg (~$Alm_{54}Grs_{30}Prp_{05}Sps_{12}$) relative to garnet rims (~$Alm_{58}Grs_{27}Prp_{13}Sps_{02}$), consistent with the preservation of prograde growth zoning. Garnets with low Mn content were preferred for thermobarometry.

Plagioclase compositions vary with textural position. The most sodic feldspars occur as matrix grains (Ab_{78} – Ab_{83}) and as intergrowths in Cpx-Pl symplectites (Ab_{75} – Ab_{80}). Plagioclase in coronas surrounding garnet has slightly lower Na content (Ab_{69} – Ab_{73}). Plagioclase with much lower Na content occurs as inclusions in granulite garnet (Ab_{50} – Ab_{60}). Matrix plagioclase has reverse compositional zoning with rim compositions typically 2-5 mole% higher in anorthite component relative to plagioclase cores. Amphibole from matrix and symplectite assemblages is classified as edenite, pargasite, and ferropargasite (Leake et al., 1997). Amphibole inclusions in garnet (granulite samples) are classified as pargasite and magnesiosadanagaite and contain up to 1.88 wt% Cl.

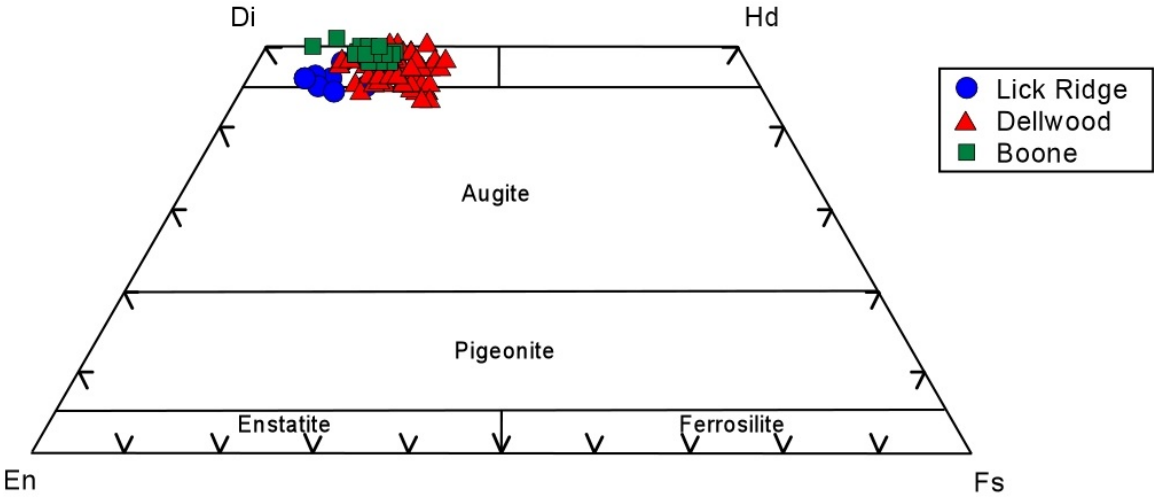

Figure 2.5. Ca-Mg-Fe Clinopyroxenes of the central and eastern Blue Ridge, western North Carolina. Endmember plots from Morimoto et al., 1988; Di = diopside, Hd = hedenbergite, En = enstatite, Fs = ferrosilite, Wo = wollastonite.

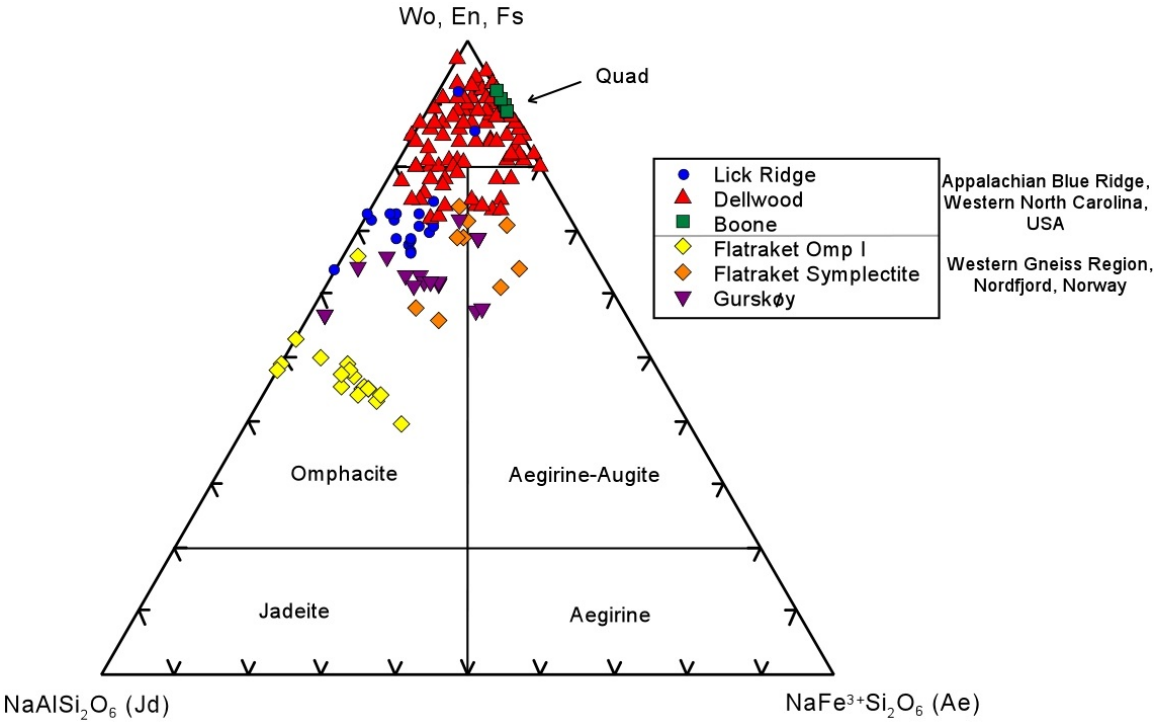

Figure 2.6. Clinopyroxene compositions from Blue Ridge and WGR metabasites. Dellwood clinopyroxenes are compositionally diverse, and include diopside, augite, aegirine-augite, and omphacite. Endmember plots from Morimoto et al., 1988; Wo = wollastonite, En = enstatite, Fs = ferrosilite.

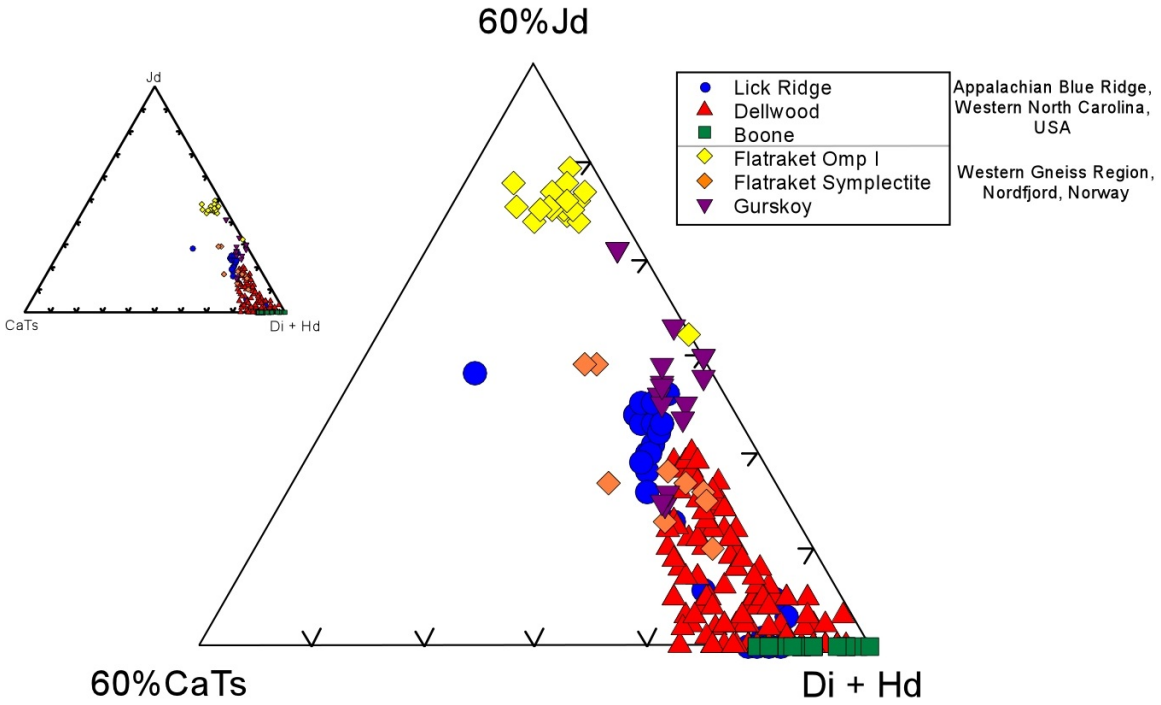

Figure 2.7. Clinopyroxene compositions shown in Jd-CaTs-Di + Hd space.

Boone, Appalachian Blue Ridge

Pyroxene from Boone retrograde eclogite occurs as Cpx-Pl symplectite and plot within the diopside field on the pyroxene quad (Figure 2.5), with an average composition of $Jd_0CaTs_{05}Ac_{09}Ess_{09}CaEs_0Di_{49}Hd_{29}$. Pyroxenes are low in Na, containing < 0.1 Na pfu. Garnet compositional profiles appear flat throughout garnet cores, having a composition of ~$Alm_{58}Grs_{27}Prp_{14}Sps_{03}$. Some garnet compositional profiles show a spike in Ca concentrations approximately 100 µm from the rim. Garnet contains slightly higher Mn concentrations in cores (~Sps_{03}) relative to rims (Sps_{01}). Plagioclase compositions range from ~Ab_{64} to Ab_{60}. Some mineral compositions from the Boone eclogite, including a reintegrated omphacite composition and thermobarometric estimates have been published previously (Abbott and Greenwood, 2001).

Flatraket, Western Gneiss Region

Matrix clinopyroxenes from Flatraket eclogite are omphacitic and unzoned, with an average composition of ~$Jd_{39}CaTs_{05}Ac_{13}CaEs_0Di_{27}Hd_{13}$. Symplectitic pyroxene contains less Na (0.25 – 0.4 pfu) relative to matrix pyroxene (0.4 - 0.6 pfu), has variable compositions (~$Jd_{8\text{-}25}CaTs_{6\text{-}12}Ac_{10\text{-}25}Di_{31\text{-}43}Hd_{16\text{-}24}$), and plots within the omphacite and aegirine-augite fields (Figures 2.6, 2.7). The larger garnets in the Flatraket eclogite

sample have homogeneous core compositions ~ $Alm_{55}Grs_{25}Prp_{19}Sps_{01}$, surrounded by a ~100 μm rim with variable compositions of ~ $Alm_{61}Grs_{16}Prp_{22}Sps_{01}$. Garnet rims contain less Fe, Ca, and are enriched in Mg relative to core compositions. Plagioclase in Cpx-Pl-Hbl symplectites contains no orthoclase component and has a composition of ~$Ab_{90}An_{10}$.

Gurskøy, Western Gneiss Region

Matrix omphacite of the Gurskøy eclogite sample has an average composition of ~$Jd_{21}CaTs_{08}Ac_{20}Di_{31}Hd_{20}$ (Figures 2.6, 2.7). Compositional traverses across garnets indicate relatively homogenous interior compositions ~ $Alm_{56}Grs_{23}Prp_{20}Sps_{01}$, with decreasing X_{Fe}, almandine, and grossular component in the outer 40 μm. Pyrope component increases abruptly at the rim ~ $Alm_{45}Grs_{22}Prp_{31}Sps_{02}$. Gurskøy compositional traverses across garnet indicate prograde zoning at the rim (decreasing Fe/Mg). Plagioclase compositions are related to textural position, with lower Ab content at garnet rims, and higher Ab content in symplectites. Plagioclase from retrograde eclogite ranges from ~Ab_{56} – Ab_{60} at garnet rims, and has a composition of ~Ab_{84} within symplectite.

Symplectite Pyroxene: Compositional Variations and Textures

Lick Ridge, Appalachian Blue Ridge

X-ray elemental intensity maps of matrix pyroxenes from Lick Ridge reveal omphacitic cores and diopsidic rims (Figure 2.8A). Diopsidic rims surrounding the outer ~200 μm of omphacite appear bright in Ca-intensity maps. Cpx-Pl symplectites occur at omphacite rims and within omphacite cores (Figure 2.8A). Higher resolution images of internal Cpx-Pl symplectites (Figure 2.8B,C) show that hornblende and minor quartz are part of the symplectite mineral assemblage. Compositional trends in symplectic pyroxene can be seen in Figure 2.8B,C. Pyroxenes adjacent to plagioclase are Ca-rich, and depleted in Al and Na relative to omphacite that has not reacted. Some lamellae of plagioclase and hornblende appear to follow the trace of {110} in omphacite (Figure 2.8D). Crystallographic control of symplectic plagioclase and hornblende can be seen more clearly in Figure 2.8E. This Al-intensity map oriented perpendicular to (001) reveals plagioclase and hornblende growth following {110}, producing a grid pattern of plagioclase and hornblende.

Some omphacite grains from Lick Ridge contain needles of hornblende + quartz, without associated plagioclase (Figure 2.8F). These features, referred to as "hornblende with quartz 'caps'" by Page et al. (2005) appear to have overgrown fine orthopyroxene lamellae in omphacite. The fine orthopyroxene exsolution lamellae (< 1 μm) appear bright in BSE images (Figure 2.8F). [Orthopyroxene lamellae occur in samples analyzed by Page et al. (2003, 2005) were interpreted as evidence for an excursion through the granulite-facies]. Microimaging reveals three distinct microtextures in omphacites from Lick Ridge: 1) exsolution of orthopyroxene; 2) the development of hornblende with

quartz caps; and 3) the formation of Cpx-Pl symplectites (plagioclase + hornblende + minor quartz controlled by {110}). Orthopyroxene exsolution appears to have preceded the growth of Hbl-Qtz needles and Cpx-Pl-Hbl-Qtz symplectites as one fabric appears to have formed at the expense of the other.

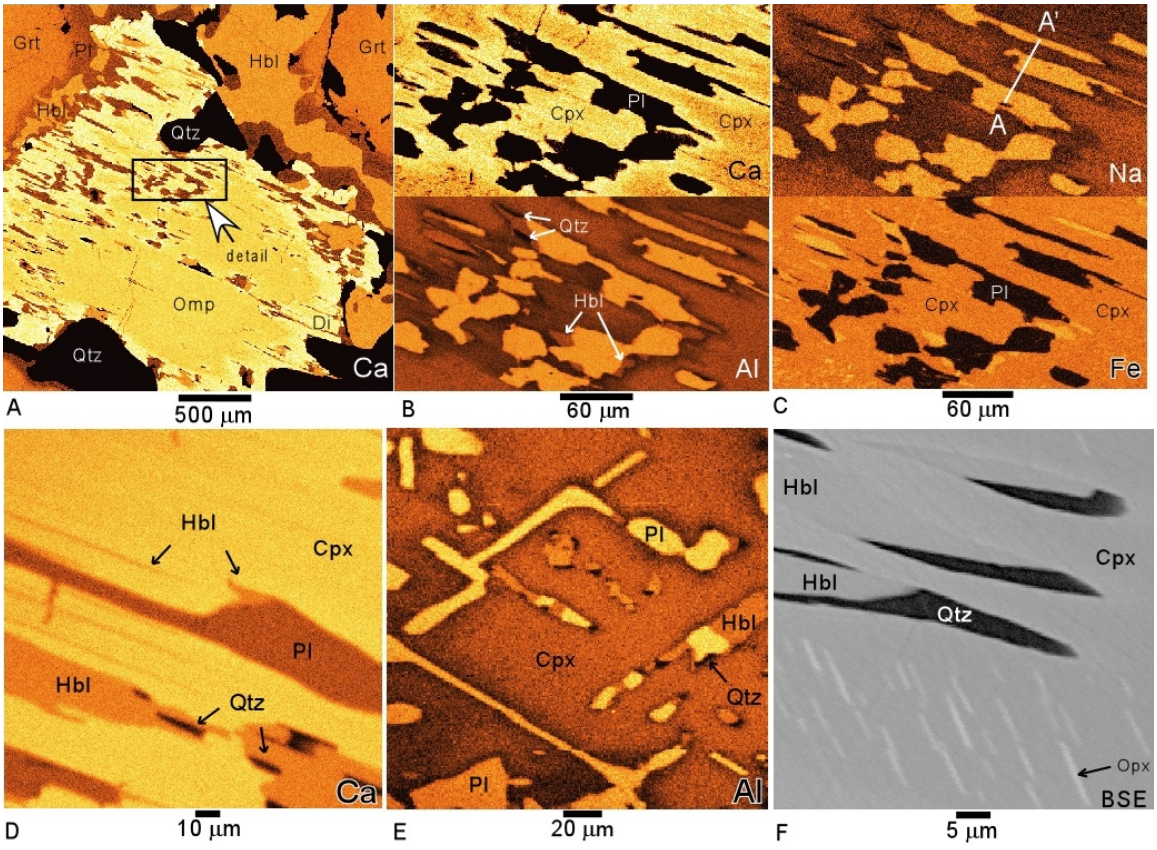

Figure 2.8. X-Ray elemental intensity maps of Lick Ridge eclogite. A) Ca-map of omphacite. Core of omphacite is Na-rich relative to rim and symplectic pyroxene. Ca-rich zones can be seen as bright areas of omphacite rim. B) and C) Ca-, Al-, Na-, and Fe-maps of detail from Figure 2.8A (box). Ca-enrichment and Na-depletion in pyroxene can be seen at grain boundaries adjacent to plagioclase. Location of compositional traverse (Figure 2.9A) is shown in the Na-map. Hornblende is clearly seen in Al and Fe maps, but is nearly invisible in BSE, Ca-, and Na-maps. D) Ca-map showing fine lamellae of hornblende and plagioclase oriented parallel to clinopyroxene cleavage. E) Al-map of omphacite. View perpendicular to c-axis shows plagioclase, hornblende, and quartz growth controlled by {110}. F) BSE image of hornblende with quartz caps in clinopyroxene. Bright orthopyroxene lamellae in omphacite are absent adjacent to compound inclusions of hornblende + quartz.

Compositional trends in internal symplectite phases are shown semiquantitatively in Figure 2.9A, a compositional traverse across diopside and plagioclase lamellae in

symplectite, with traverse location given in Figure 2.8C and Figure 2.9B. The symplectic pyroxene is compositionally zoned with cores that are Mg-rich, Al-poor relative to compositions at grain boundaries adjacent to plagioclase. Mg compositional profiles in symplectic diopside form concave-up curves, while Al compositions are concave-down. Thin, sub-μm wide lamellae, identified as quartz produce Si spikes in the compositional profile plot (Figure 2.9A) between plagioclase and diopside. A thin quartz lamella can be seen in Figure 2.9B that occurs between diopside and plagioclase. Hornblende is present in this BSE image as well, but difficult to resolve due to similarities in the mean atomic numbers of clinopyroxene and hornblende in this sample.

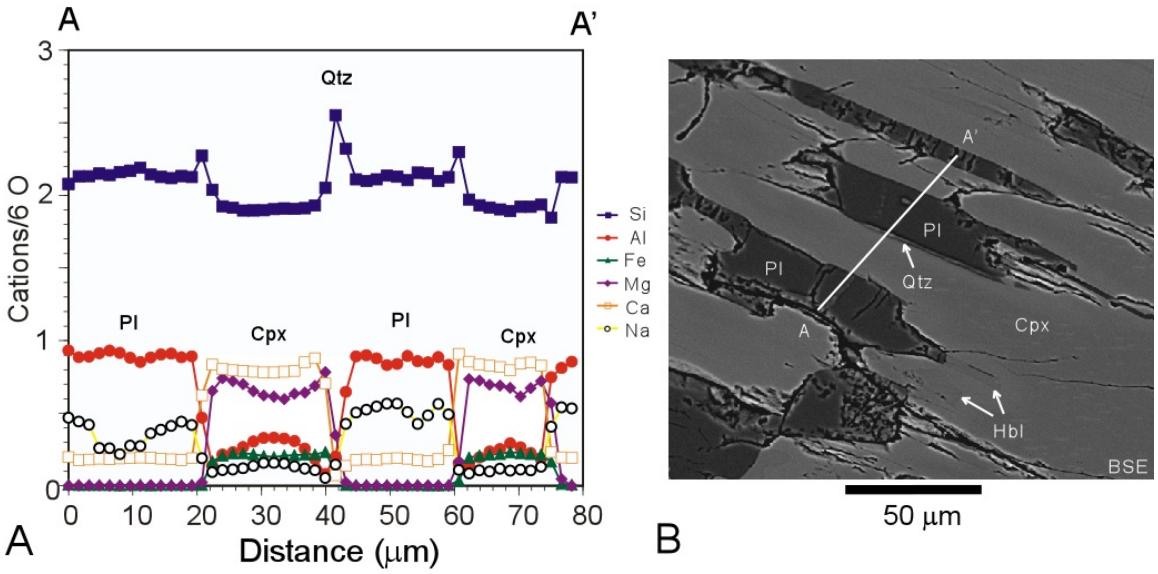

Figure 2.9. Compositional traverse across symplectic plagioclase (Pl) and clinopyroxene (Cpx), Lick Ridge eclogite. Y axis: cations calculated on the basis of 6 oxygens from microprobe WDS data. Quartz occurs as thin (~ 1 μm) lamellae between plagioclase and clinopyroxene, can be seen in BSE image 2.9B, and is responsible for silicon spikes seen in the compositional traverse plot 2.9A.

Dellwood, Appalachian Blue Ridge

Cpx-Pl symplectites from the Dellwood metabasites are shown in X-ray elemental intensity maps presented in Figure 2.10. The coarsest matrix pyroxenes are anhedral, and commonly rimmed by plagioclase. Matrix pyroxenes that have not reacted to form symplectite have Na-rich cores with diopsidic rims that are Ca-rich and Na-poor relative to omphacitic cores. Matrix pyroxenes that have reacted commonly contain a symplectite assemblage of clinopyroxene + plagioclase + hornblende + quartz within pyroxene cores. Quartz occurs as a minor phase in the symplectites (1 – 2 % by volume) and can be seen in higher resolution X-ray maps (Figure 2.10C,E).

A representative compositional traverse across a plagioclase rod within symplectic pyroxene is plotted in Figure 2.10D. The traverse location and symplectite assemblage can be seen in the Al-intensity map (Figure 2.10E). Pyroxene compositions gradually change from point B to the plagioclase crystal. Over this ~ 50 μm interval, Al and Na concentrations gradually drop, as Mg and Ca concentrations gradually rise. Fe concentrations change little over this interval.

Isolated hornblende with quartz caps (no associated plagioclase or quartz) occur as inclusions within matrix pyroxene of HP amphibolite from Dellwood, and are texturally similar to occurrences in the Lick Ridge eclogite (Figure 2.8F).

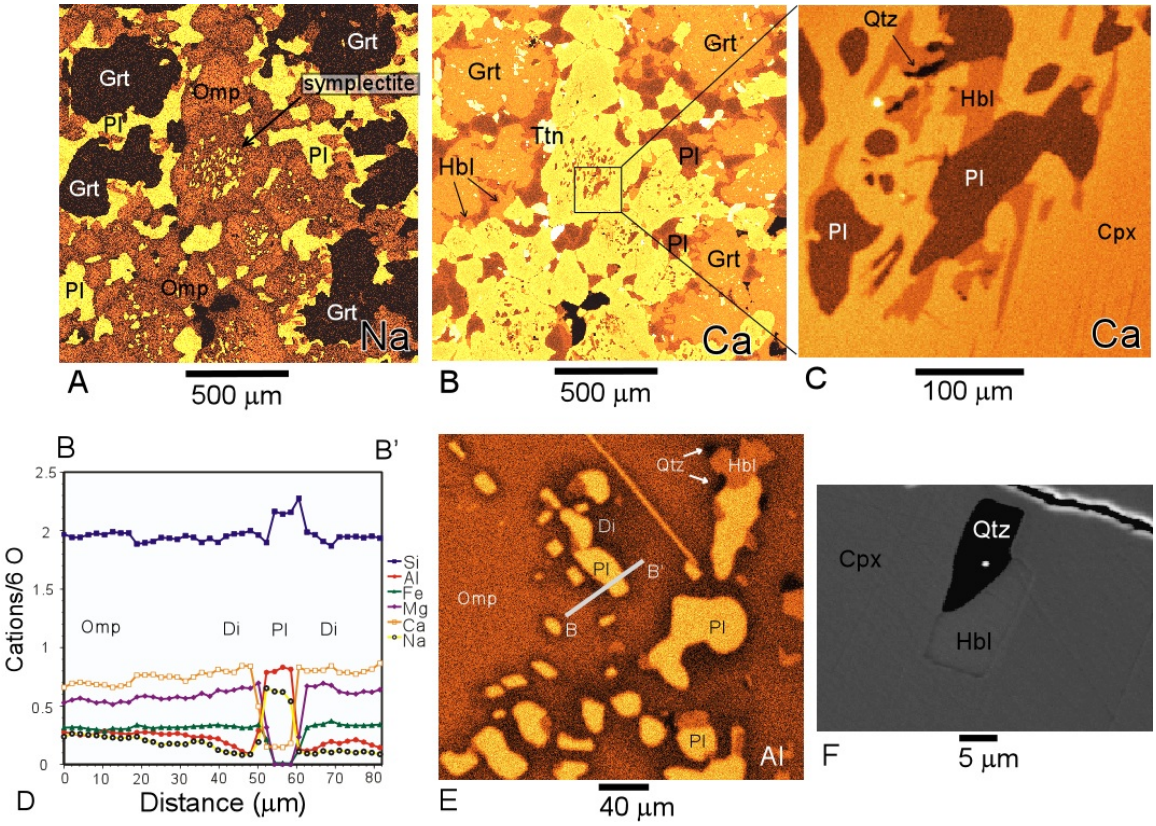

Figure 2.10. X-ray elemental intensity maps, compositional traverse, and BSE image of Dellwood garnet granulite. A) and B) Na- and Ca-maps of representative matrix assemblages from sample DEL05-3B2. Na-zoning can be seen in omphacite, which is Na-depleted adjacent to Cpx-Pl symplectite. Garnets are anhedral, and typically surrounded by plagioclase and hornblende rims. Reverse zoning in plagioclase, and abundant titanite inclusions in garnet are evident in the Ca map. C) Ca map detail showing rods of plagioclase, hornblende, and traces of quartz in Cpx-Pl symplectite. D) Compositional traverse across plagioclase in symplectite. X axis: distance in micrometers; Y axis: cations calculated on the basis of six oxygen from microprobe data. E) Al X-ray intensity map of symplectic omphacite with location of compositional

traverse. Diopside (Di) appears as dark halos surrounding plagioclase. Quartz appears black. F) Hornblende-with-quartz-cap inclusion in Cpx, Dellwood HP amphibolite, sample DEL03-3B.

Boone, Appalachian Blue Ridge

Symplectites after omphacite from Boone, NC retrograde eclogites contain diopside and plagioclase (Figure 2.11). No quartz needles or hornblende intergrowths were observed in the Boone eclogites. Compositional profiles across hornblende and plagioclase coronas are extremely flat (Figure 2.11C). Limited compositional variation is seen in plagioclase or hornblende that rims a small (100 μm) garnet. The traverse of symplectic diopside (Figure 2.11D) also plots as a relatively flat profile. Diopside lamellae are zoned with respect to Al, with Al-rich cores, and Al-poor compositions at grain boundaries. Al-zoning in symplectic pyroxene can be seen in the Al X-ray map, and is most evident in the largest diopside lamellae. The Al profile is concave-down in shape. Mg- and Si-profiles have a slight concave-up shape.

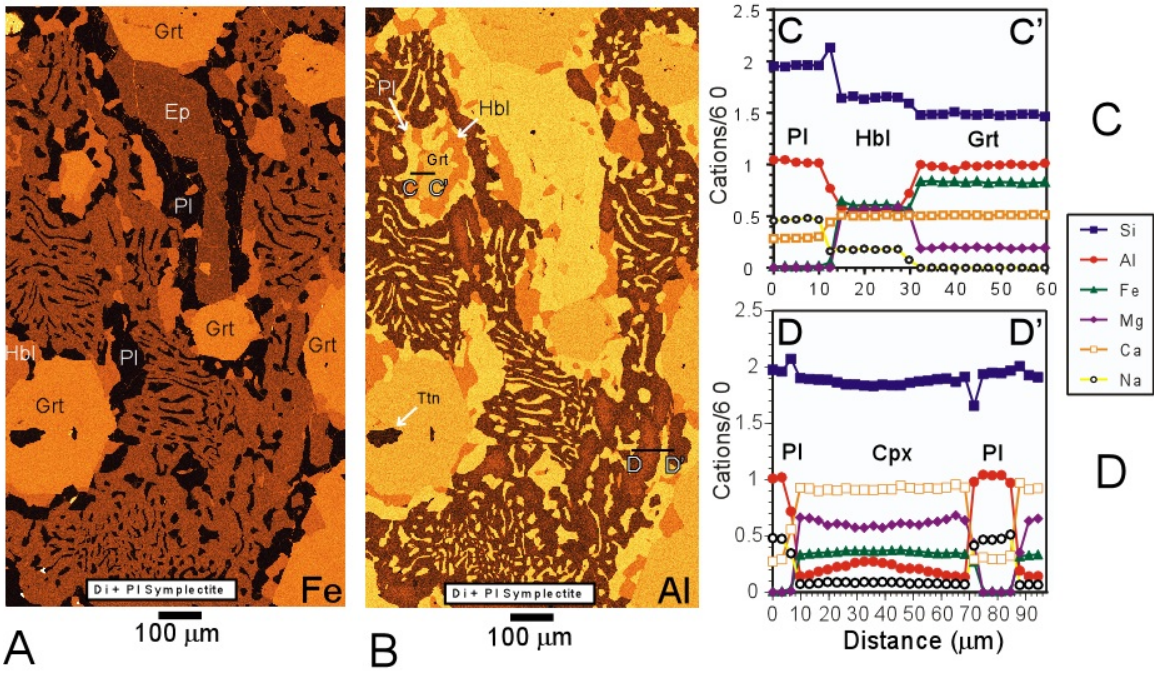

Figure 2.11. X-ray elemental intensity maps and compositional traverses from Boone retrograde eclogite. A) Fe-intensity map; B) Al-intensity map. Plagioclase (Pl) appears black in the Fe-map, and occurs as vermicular intergrowths with diopside (Di). C) Compositional traverse across plagioclase-hornblende-garnet at garnet rim. D) Compositional profile across plagioclase and clinopyroxene. Traverse locations are

shown in the Al-intensity map. X axis: distance in micrometers, Y axis: cations calculated on the basis of 6 oxygens from microprobe WDS data.

Nordfjord Area, Western Gneiss Region, Norway

Symplectites after omphacite from the Flatraket retrograde eclogite are well developed at omphacite-omphacite grain boundaries (Figure 2.12A). The widest bands of symplectite occur at omphacite-omphacite grain boundaries; thinner symplectite colonies occur at garnet-omphacite grain boundaries, typically outside of a hornblende rim surrounding garnet. Patchy Ca-zoning patterns in garnet are apparent in the Ca-intensity map (Figure 2.12A). Garnet cores are enriched in Ca relative to thick (>100 μm) rims. Matrix omphacite grains have homogeneous chemical compositions. A representative compositional traverse across matrix omphacite is presented in Figure 2.12B. Compositional profiles of matrix omphacite are essentially flat. No compositional traverses were constructed from traverses across phases in symplectite due to the fine-grained nature of the symplectites that are too small for resolution with the microprobe.

Symplectite "colonies" of the Flatraket sample are morphologically similar to those described by other workers (Eskola, 1921; Boland and van Roermund, 1983; Waters, 2002). Specifically, the size of clinopyroxene, hornblende and plagioclase lamellae vary within symplectites: fine lamellae occur at the boundary between symplectite colonies and matrix omphacite, coarser lamellae occur in the centers of symplectite colonies (Figure 2.12C). From morphological and quantitative examination of eclogites from the Statlandet and Nordfjord areas of the WGR, Waters (2002) suggests that symplectite colonies form at omphacite-omphacite grain boundaries and propagate into matrix omphacite along a reaction front. A typical reaction front is shown in Figure 2.12C, at the boundary of finest-grained symplectite and unreacted omphacite. Jadeite component in clinopyroxene varies systematically in Stadlandet and Nordfjord samples; ~ 47% in matrix omphacite, ~ 30% in coarser lamellae, ~ 10% in fine clinopyroxene lamellae at the reaction front margin (Waters, 2002). This interpretation is consistent with earlier petrographic studies of Cpx-Pl symplectites from the WGR that suggest a migrating reaction front (Eskola, 1921).

A compositional traverse across omphacite, hornblende and garnet from Flatraket sample F28-C is plotted in Figure 2.12.D, with traverse location shown as an inset BSE image. The compositional profile indicates extensive solid solution of Al in hornblende. Hornblende is Al-rich at the grain boundary with garnet, and is Al-poor at the grain boundary with omphacite, producing a ramp-shaped profile. Concentrations in Si have opposite trends; hornblende is Si-rich at the omphacite grain boundary, and ramp down towards relatively Si-poor compositions at the garnet grain boundary. Na and Fe profiles resemble steps, with Na and Fe abundances in hornblende having concentrations that are intermediate to omphacite and garnet compositions.

Cpx-Pl symplectites from Gurskøy eclogite are broadly similar to Flatraket symplectite in terms of morphology (Figure 2.12.C,E). These symplectites are

concentrated at omphacite grain boundaries and contain curved lamellae of plagioclase and diopside. However, the symplectic mineral assemblages from Flatraket and Gurskøy samples are different; Gurskøy Cpx-Pl symplectites lack hornblende and quartz. Matrix omphacite from Flatraket is compositionally homogenous, while matrix omphacite from Gurskøy contains abundant inclusions of hornblende with quartz caps (Figure 2.12.F). These hornblende-quartz inclusions, rimmed by thin (~3 μm) zones of diopside, are remarkably similar to the hornblende with quartz caps that occur in retrograde eclogite from Lick Ridge (e.g., Figure 2.8F, Page et al., (2005) Figure 2).

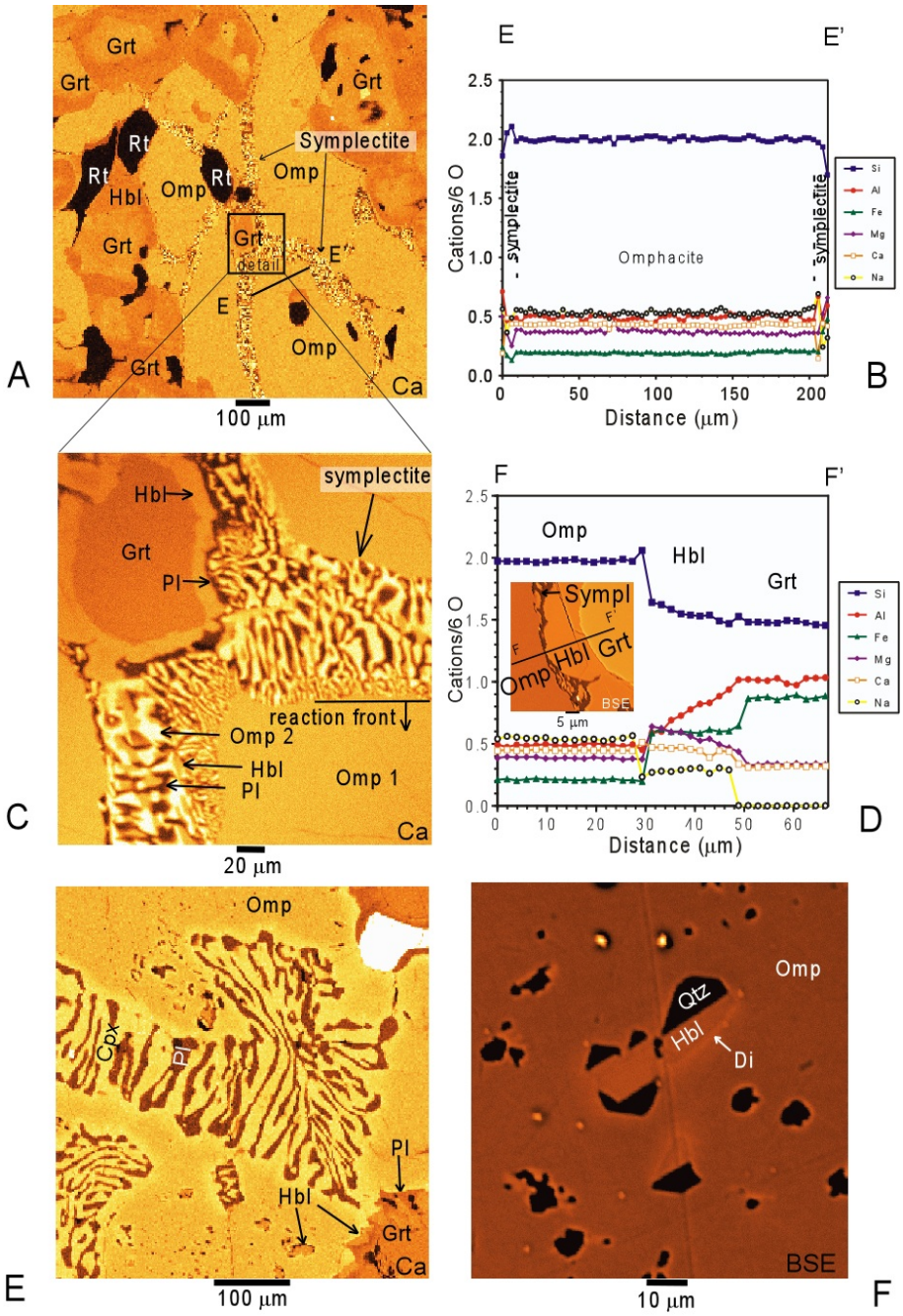

Figure 2.12. X-ray elemental intensity maps and compositional traverse from WGR eclogites, Nordfjord region.

(legend follows)

Figure Legend 2.12. A) Flatraket eclogite. Ca-intensity map of omphacite, garnet, rutile assemblage with grain-boundary symplectites and location of compositional traverse. B) Compositional traverse across matrix omphacite. C) Flatraket eclogite. Ca-intensity map of Cpx-Pl-Hbl symplectite "colonies" from Flatraket eclogite, detail from Figure 2.12.A (box) Symplectites form at omphacite-omphacite grain boundaries, and at garnet-omphacite boundaries. Reaction fronts are defined by fine-grained symplectites, and propagate into omphacite. D) Compositional traverse across omphacite, hornblende, and garnet with extensive solid solution in hornblende. Al-concentrations in hornblende are high adjacent to garnet, and low adjacent to symplectite and omphacite. E) Gurskøy eclogite. Ca-map of symplectite "colony" composed of diopside + plagioclase at grain boundary between two distinct omphacite crystals. F) Gurskøy eclogite. BSE image of hornblende with quartz "caps", with diopside rim, included in matrix omphacite.

Mass Balance

Methods and Results

Broadbeam microprobe analysis was used to "reintegrate" symplectite compositions to estimate precursor pyroxene compositions. The symplectite-forming reactions are examined in terms of open- versus closed-system behavior by comparing the bulk composition of symplectites to unreacted matrix pyroxene. Symplectites were analyzed using averaged microprobe WDS analyses collected as area scans in grids. Each point was collected using a rastered beam with dimensions of 10 μm x 10 μm. Although larger rastered areas allow for fewer analytical spots, grids of small areas were analyzed to minimize systematic errors. Symplectites, adjacent unreacted pyroxene, and standards were analyzed using the same analytical conditions and a mean atomic number background correction. Microprobe analyses were normalized to 100% for plotting purposes with all iron as FeO. For each comparison, symplectite and unreacted pyroxene were as close as possible (10's – 100's of μm away); most symplectite and unreacted pyroxene occur within the same grain. No comparison was attempted for the Boone eclogite due to the lack of unreacted pyroxene.

Compositions of Cpx-Pl symplectite (spot locations in Figure 2.13) are broadly similar to unreacted pyroxene compositions (Appendix B), with the exception of the Gurskøy samples, in which symplectite contains up to ~ 4.7 wt. % more Al_2O_3 and ~ 3.8% wt.% less FeO relative to unreacted omphacite. [SiO_2] and [Al_2O_3] plot near the 1:1 correlation line (Figure 2.15), or are higher in reintegrated symplectite. [FeO], [MgO], [CaO], and [Na_2O] plot on the 1:1 reference line, or are higher in unreacted pyroxene.

When reintegrated symplectites from the Blue Ridge and WGR are recalculated as pyroxenes in a six-anion normalization with all Fe as Fe^{2+}, there are cation deficiencies (i.e. Σ cations < 4) and $Al^{VI} > Al^{IV} + Na$, suggesting non-stoichiometric pyroxene compositions (Smyth, 1980) that may be reconciled by the presence of CaEs component in precursor pyroxene. (Vogel, 1966; Mysen and Griffin, 1973; Smyth, 1980; Katayama et al., 2000; Smith, 2006; Day and Mulcahy, 2007). Estimates of X_{CaEs} and other

endmembers are presented in Appendix B and were made using the method of Katayama et al. (2000). According to these calculations, precursor pyroxenes from Gurskøy, Flatraket, Lick Ridge, and Dellwood HP-amphibolite contained significant CaEs (~23, 12.3, 15, and 5.6 mol % respectively) relative to the adjacent unreacted pyroxene (~0 mol % CaEs). Similar X_{CaEs} estimates are obtained using the method of Page et al. (2003): ~20, 9, 11, and 4 mol% respectively). The estimate of X_{CaEs} = 0.20-0.23 from the Gurskøy reintegration leads to unrealistically high temperature estimates of ~1400 ^{o}C at 30 kbar, using the P-T phase relations of Gasparik (1986) as redrawn by Page et al. (2005, Figure 3). Scatter for the Gurskøy comparison in Figure 2.13, specifically the discrepancy between [Al] and [Fe] in symplectite versus adjacent omphacite, and the high Si (2.03-2.07 pfu) in the reintegrated Gurskøy pyroxene suggest that this reintegration does not represent a real pyroxene composition and that the estimate of X_{CaEs} = 0.20-0.23 is not valid. The X_{CaEs} estimates from Flatraket, Lick Ridge and Dellwood reintegrations give more realistic P-T conditions when plotted in the P-T phase diagram of Page et al. (2005) (Figure 3) but provide unreliable P-T estimates due to the unknown effects of Fe solid solution in natural garnet and pyroxene on the experimentally derived phase relations (Gasparik ,1986; Page et al., 2005).

Results of broadbeam reintegrations of Hbl-Qtz inclusions and the enclosing Cpx are presented in Appendix C, with endmember calculations after Katayama et al. (2000) and analysis locations in Figure 2.12. All broadbeam reintegrations of Hbl with quartz "caps" result in non-stoichiometric pyroxene formulae. In these four reintegrations, Σ cations < 4 in 6-anion normalizations with all Fe^{2+}, $Al^{VI} > Al^{IV}$ + Na in 3 of the 4 mineral recalculations, and Si < 2.0 pfu in all recalculations. The estimated CaEs ranges from 8-12 % in the Lick Ridge eclogite to 2 % in the Dellwood garnet granulite. Broadbeam estimates of CaEs from the reintegration of Hbl-Qtz inclusions in Lick Ridge omphacite are much higher than previous estimates of Page et al. (2005), who estimated a maximum of 4% CaEs. The disparity may be due to 1) differences in methods and 2) the modes of hornblende and quartz are higher in the broadbeam reintegration (Figure 2.13A) relative to the ~12% Hbl, ~6% Qtz modes used in calculations of Page et al. (2005). Nevertheless, the resemblance of the reintegrated formulas to true pyroxenes strongly suggests that Hbl + Qtz inclusions exsolved from non-stoichiometric pyroxene. The precursor pyroxenes are interpreted to be supersilicic (Smith, 2006). As stability was overstepped, SiO_2 and hornblende were exsolved, and preserved as inclusions in stoichiometric clinopyroxene.

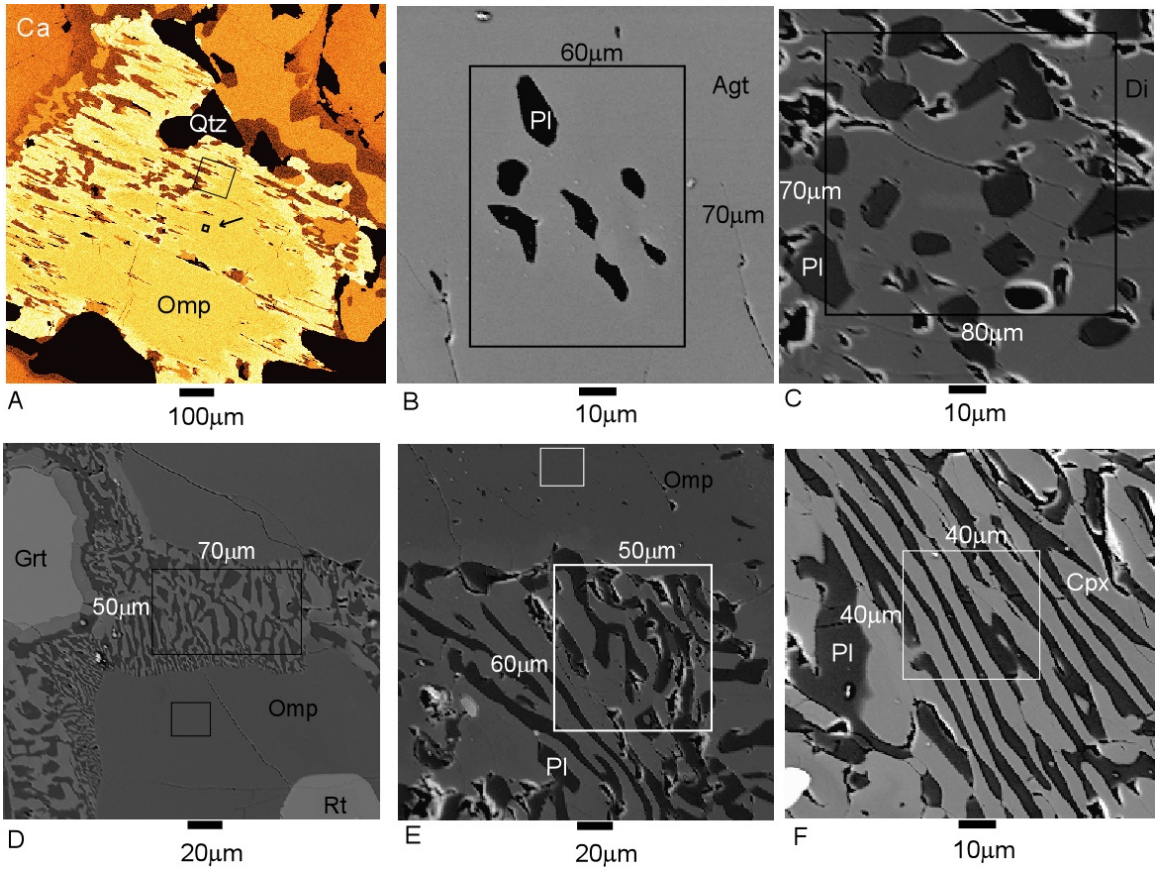

Figure 2.13. X-ray map and BSE images of microprobe broadbeam analysis locations. A) Ca-X-ray map of symplectic Lick Ridge omphacite with large square showing approximate location where 100 points were collected, each having the dimensions ~10 x 10 μm. Smaller square with arrow represents approximate location of 9 points collected in "adjacent unreacted pyroxene". B) Dellwood garnet granulite sample DEL05-3B2, with location of 60 x 70 μm grid covering symplectite in aegirine-augite (Agt). C) Dellwood HP-amphibolite, sample DEL03-3B, with location of 70 x 80 μm grid. D) BSE image of symplectite at omphacite grain boundaries, Flatraket, WGR Norway sample F28-C. Large rectangle represents location of symplectite analyses; small square is approximate location of adjacent unreacted pyroxene. E) BSE image of Gurskøy eclogite with location of broadbeam analysis in lobate Cpx-Pl symplectite, and location of adjacent unreacted pyroxene. The small, dark inclusions in matrix omphacite are primarily Qtz + Hbl.

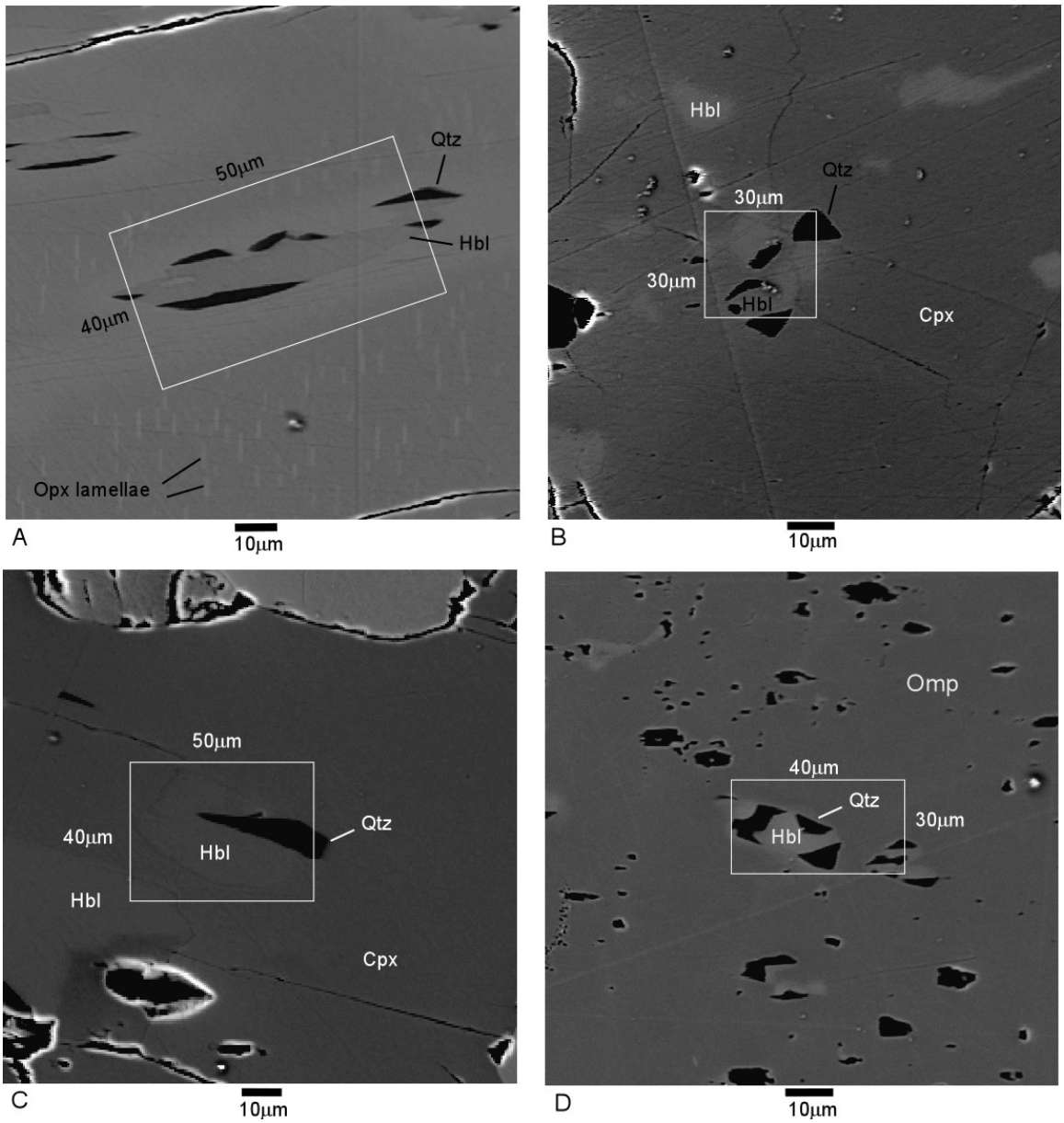

Figure 2.14. BSE Images with locations of broadbeam analyses of hornblende + quartz inclusions and surrounding clinopyroxene. A) Lick Ridge eclogite, eastern Blue Ridge; B) Dellwood HP-amphibolite (central Blue Ridge); C) Dellwood garnet granulite (central Blue Ridge), light gray in reintegrated area is Hbl, black phase is quartz; D) Gurskøy eclogite (WGR) with abundant quartz inclusions (black) in omphacite.

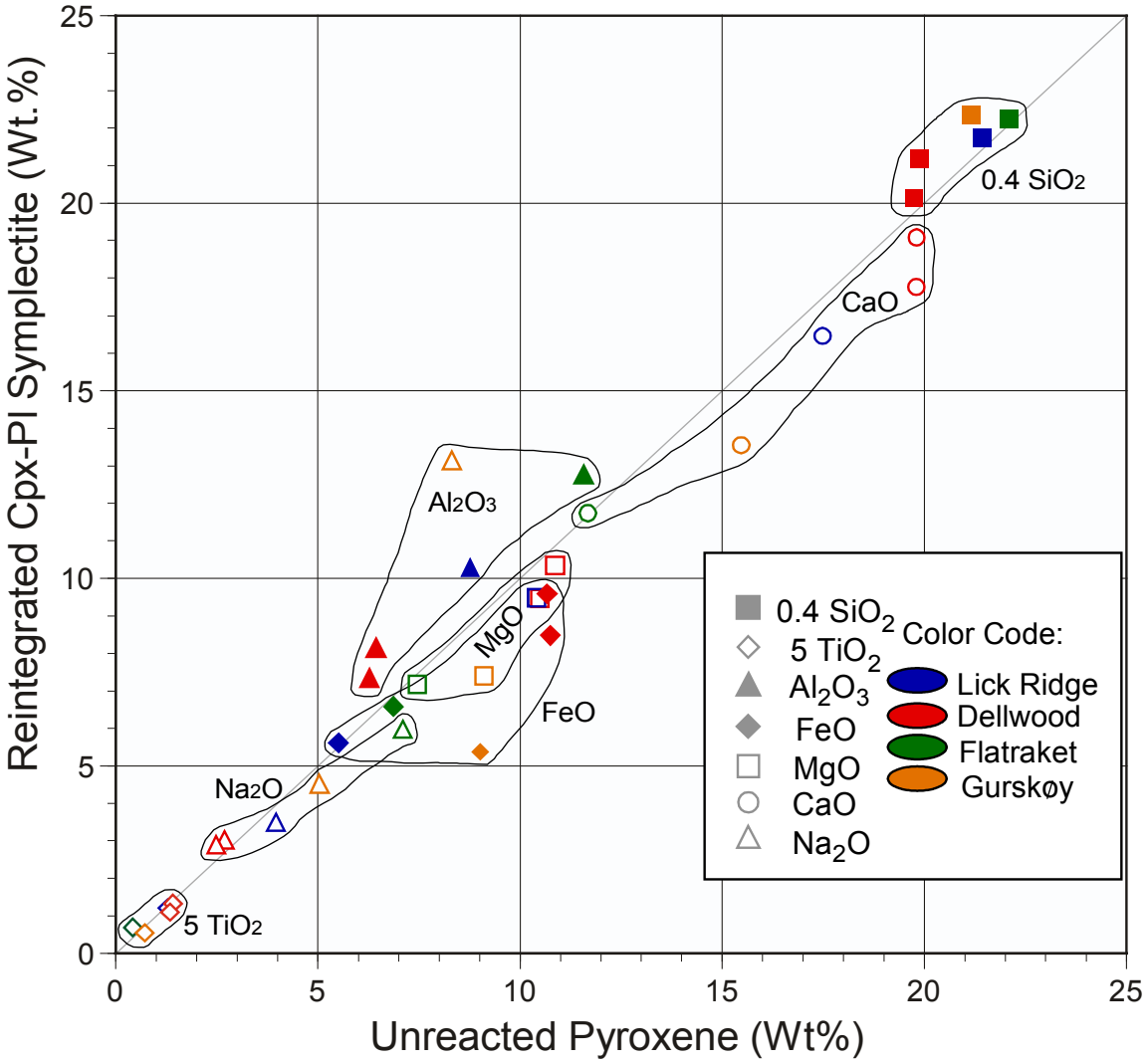

Figure 2.15. Comparative plot of reintegrated Cpx-Pl symplectite compositions versus unreacted pyroxene compositions. Data from broadbeam microprobe analyses (Appendix B). Major elements are plotted as oxide wt.%, total Fe calculated as FeO. Analysis locations shown in Figures 2.13, 2.14.

Thermobarometry and Decompression Rates

Methods

Thermobarometric estimates were made to understand the P-T pathways of Appalachian Blue Ridge and WGR metabasites, and to estimate the P-T conditions at which Cpx-Pl symplectites form. Minimum pressures of eclogite facies conditions were estimated by convention, using jadeite stability (Reaction 2). Temperatures of omphacite-garnet assemblages were estimated using the garnet-clinopyroxene Fe-Mg exchange thermometer (Berman et al., 1995):

$$3Di + Alm = 3\ Hed + Prp \quad [3]$$

Additional P-T estimates were made from WDS analyses of three retrograde metamorphic assemblages: (1) garnet rim-plagioclase-hornblende-quartz-H_2O; (2) clinopyroxene-plagioclase-hornblende symplectites; and (3) garnet-plagioclase-clinopyroxene-quartz. Methods used for all calculations are summarized in Appendix D. Garnet analyses with the highest Mg/Fe ratio and matrix pyroxene cores with highest jadeite component were used for garnet-clinopyroxene thermometry. The high Mg/Fe garnet compositions occur near garnet rims, just inside retrograde rims in Lick Ridge, Dellwood, and Flatraket metabasites. A range of P-T conditions was estimated by inputting a range of pyroxene and garnet compositions into TWQ (Berman, 1988,1990; Berman et al., 1995; Berman et al., 1996). A ferric iron calculation (Droop, 1987) was made for all clinopyroxene and hornblende used in P-T estimates. The method of estimating P-T conditions of Cpx+Hbl+Pl symplectites is outlined by Waters (2002).

Estimating P-T conditions from reactions in Dellwood garnet granulite was problematic due to the lack of quartz as a matrix phase and within retrograde garnet rim assemblages. Cpx-Grt-Pl-Qtz barometry was applied to matrix assemblages and inclusion suites in garnet using a reduced activity for SiO_2 ($\alpha_{SiO2} = 0.5$). Garnet rim equilibria were estimated from the locus of the intersections of nine reactions that do not involve quartz, listed in Appendix D (rxns 16-24). Reduced silica activities decreased the pressure estimates of Dellwood granulites by ~2 kbar, however these results are viewed as tentative, due to the silica activity estimation. $P_{fluid} = P_{total}$ for all calculations.

Lick Ridge, Appalachian Blue Ridge

Results of thermobarometric estimates from the Lick Ridge eclogite (this study) are compiled along with estimates of others in Figure 2.16A**.** The P-T path of the Lick Ridge eclogite, surrounding schist and amphibolite is different from the P-T path of Page et al. (2003), largely due to differences in estimates from garnet rim-hornblende-plagioclase assemblages. Page et al. (2003) estimated P-T conditions of ~ 9-11 kbar at 500-550 ^oC; conditions of ~12.5 to15 kbar at 740 – 800 ^oC are estimated here. The path of Page et al. (2003) forms a closed loop; the path in Figure 2.15A resembles an open

hairpin. Using our higher-temperature estimates, the conditions at which garnet-rim reactions occur (field 7) overlaps with P-T estimates from Cpx-Pl-Hbl symplectite equilibria (reactions [4,5]), suggesting that the two processes (breakdown of garnet rims, and formation of Cpx-Pl symplectites) may have occurred simultaneously. Retrograde eclogite conditions (fields 5,6,7) and specifically the P-T estimates from Cpx-Pl symplectites (field 6) overlap with P-T estimates from the lithologies that enclose eclogite. This allows for the possibility that the Lick Ridge eclogite formed in situ; adjacent garnet amphibolite and mica schists of the AMS may have experienced eclogite-facies conditions, but record only amphibolite facies conditions.

Metamorphic zircon ID-TIMS ages (459 +1.5/-0.6) and metamorphic titanite ID-TIMS ages (393.5 $\pm$ 3.8 Ma) of mineral separates from the Lick Ridge eclogite (Miller (B.V) et al., 2000, 2006) allow the exhumation rate, decompression rate, and cooling rates of the Lick Ridge eclogite to be estimated. Miller et al. (2000) suggest that metamorphic zircon textures are consistent with zircon growth during near-peak eclogite facies metamorphism, and interpret the titanite ages (~393 Ma) and 420 $\pm$ 15 Ma zircon rim ages as recording an Acadian amphibolite-facies metamorphic event. However, the distribution of isotopic effects due to Acadian (400-338 Ma) metamorphism are scattered in the Blue Ridge thrust sheets, leading to several alternate interpretations of geochronologic data (Moecher et al., 2005). The early Paleozoic cooling history of the Spruce Pine thrust sheet and the Lick Ridge eclogite that it contains is uncertain, and estimated here using a model of slow uplift and cooling through titanite closure temperatures (estimated as 600 ^{o}C) from peak temperatures experienced during Taconic metamorphism. Determination of metamorphic ages from titanite and zircon from the Dellwood region may clarify the meaning of the Acadian titanite ages at Lick Ridge. Using pressure estimates from the decompression pathway of Figure 2.16A, and U-Pb ages cited above, the estimated exhumation rate for the Lick Ridge eclogite is 0.7 mm/year (~66 km to 20 km depth in 65 m.y.). The corresponding decompression estimate is 0.22 kbar/m.y. (from 20 to 6 kbar in 65 m.y.). The cooling rate is approximately 3 ^{o}C/ m.y (~800 to 600^{o}C in 65 m.y.).

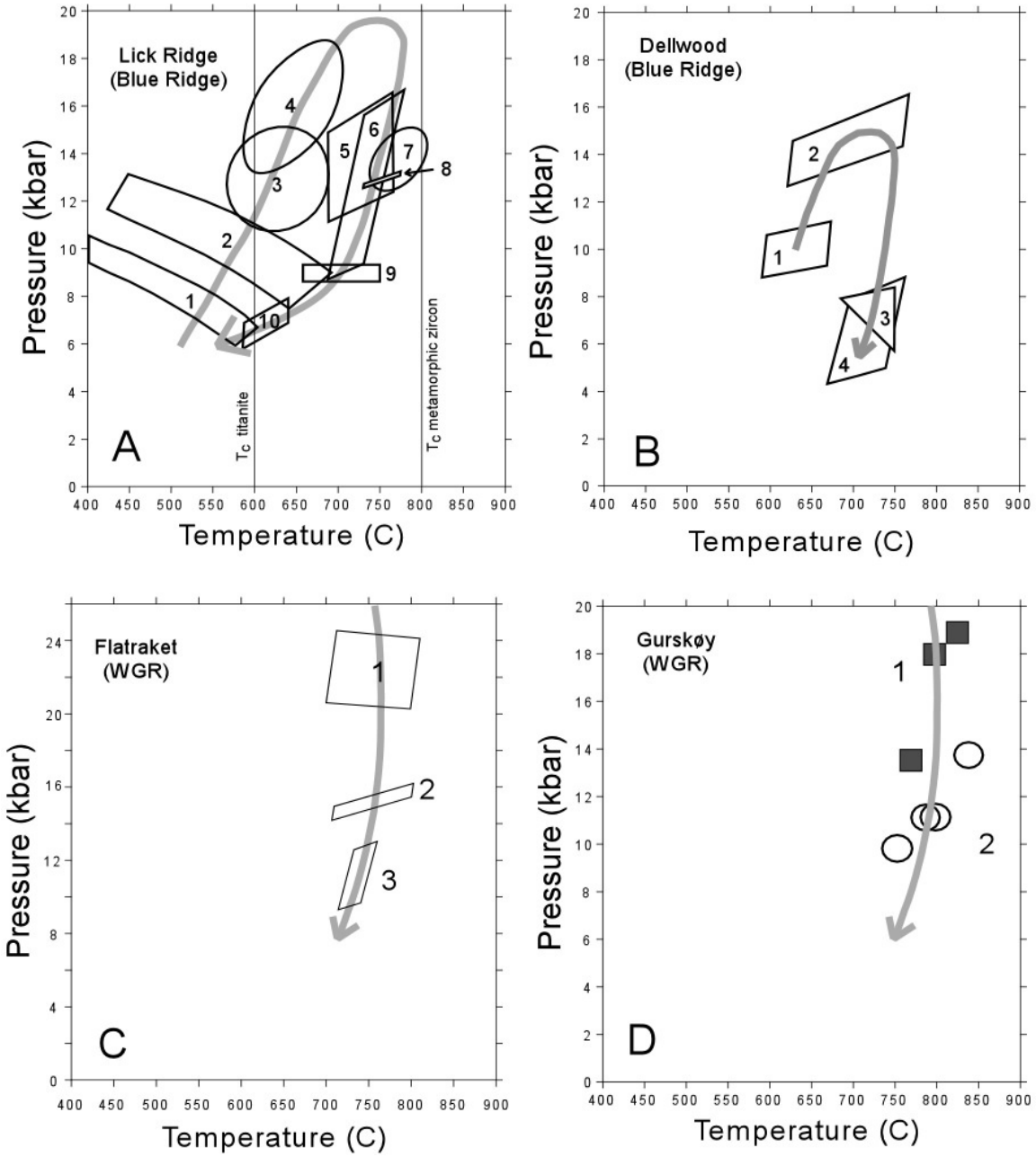

Figure 2.16. P-T estimates and paths of ABR and WGR metabasites.

(legend follows)

Figure Legend 2.16: A) Lick Ridge eclogite and surrounding schists (ABR). Fields (1) through (4): P-T estimates from inclusions in eclogite garnet (Page et al., 2003); (5) Estimates from retrograde assemblages using Grt-Cpx-Opx-Pl-Qtz equilibria (Page et al., 2003); (6) Estimated conditions from Cpx-Pl-Hbl symplectites (reactions [4, 5] Table 2.6; this study); (7) Estimates from Hbl-Grt (rim)-Pl-Qtz (reactions [6-12], this study); (8) Jd-Qtz-Ab and Grt-Cpx equilibria (pressure minimum, reactions [2, 3]; this study); (9) P-T estimates from adjacent garnet amphibolites (Waters et al., 2000); (10) P-T estimates from adjacent mica schists (Adams et al., 1995). Vertical lines show approximate closure temperatures for metamorphic zircon (~800 ^{o}C) and titanite (~600 ^{o}C). Gray arrow shows a possible P-T path for the Lick Ridge eclogite. B) Dellwood garnet granulite (ABR, sample DEL05-3B2). (1) Cpx-Grt-Pl-Qtz (GADS-GAHS, with reduced silica activity) estimates from inclusions and adjacent Grt core compositions (reactions [13-15]); (2) Grt-Pl-Cpx-Qtz estimates from matrix compositions (reactions [13-15], reduced silica activity); (3) P-T estimates from garnet rim reactions (Hbl-Grt-Pl, reactions [16-24]). (4) P-T estimates based on Cpx-Pl-Hbl symplectite equilibria (reactions [4,5]). Proposed P-T path shown as gray arrow. C) Flatraket, Norway. Field (1), eclogite facies shear zone estimates, garnet-clinopyroxene-phengite barometer, sample aw-99, Wain et al., (2001), Fe^{3+} calculation of Droop (1987); field (2) Jd-Qtz-Ab and Grt-Cpx equilibria (pressure minimum, reactions [2, 3]) sample F28-C, this study ; field (3) Cpx-Pl-Hbl symplectite equilibria, this study, sample F28-C (reactions [4,5]). Note change in scale on y-axis. D**)** P-T estimates for eclogite, Gurskøy, Norway. Field (1) P-T estimates of Dunn and Medaris (1989) from Jd-Qtz-Ab and Grt-Cpx equilibria (pressure minimum) and retrograde Grt-Pl-Cpx-Qtz reactions; field (2) Retrograde conditions estimated from garnet-rim assemblages (Hbl-Grt-Pl-Qtz) in eclogite and garnet granulite (this study, reactions [6-12]).

Dellwood Metabasite

Analyses of diopside + plagioclase inclusions and the enclosing garnets were used to estimate prograde metamorphic conditions of 9-11 kbar at 600-660 °C by applying equilibria [13-15] (Appendix D). Microprobe traverses across garnet adjacent to inclusions show limited compositional zoning across inclusion-garnet grain boundaries, indicating the inclusions are appropriate for thermobarometry. Garnet compositions were determined adjacent to inclusions to insure that the appropriate diopside + plagioclase + garnet trios were used for P-T estimates. Estimates of 13 to 16.5 kbar at 625 to 760 °C result from Grt-Pl-Cpx-Qtz equilibria. Retrograde conditions from garnet rim-hornblende–plagioclase equilibria (quartz-free reactions [16-24]) range from 6-8.5 kbar at 690 – 750 °C. P-T estimates from retrograde Cpx-Pl-Hbl symplectite assemblages (reactions [4-5]) range from 5 – 8.5 kbar at 675 – 750 °C. Results plotted in Figure 2.16B produce a clockwise P-T path, that begin at amphibolite facies conditions in field (1), followed by higher P-T conditions at upper-amphibolite to eclogite-facies conditions (field 2). The path ends with nearly isothermal decompression recorded by retrograde reactions in fields (3), and (4).

Boone Retrograde Eclogite

Previous estimates of peak metamorphic conditions from the Boone eclogites are 13.5-18.9 kbar at 640-840 °C, calculated from reintegrated omphacite compositions (X_{Jd} = 0.27 – 0.42), and garnet cores (Abbott and Greenwood, 2001). Broadbeam reintegrations of Cpx- Pl symplectites from the present study (X_{Jd} = 0.17 – 0.20) are lower than reintegrated omphacite compositions of Abbott and Greenwood (2001). No new estimates from Jd-Qtz-Ab and Grt-Cpx equilibria are presented here due to (1) the small garnet size that could potentially lead to false "apparent" temperatures due to diffusion of Fe and Mg (Spear, 1995; Figures 17-24) and (2) uncertainties in Fe^{3+}/ Fe^{2+} concentrations in reintegrated omphacite.

P-T estimates from Grt (rim)-Hbl-Pl-Qtz equilibria (reactions [6-12]) suggest conditions of 11-13 kbar at 760-825 °C. The resulting temperature estimate falls within the range estimated from garnet-omphacite equilibria (640-840°C; Abbott and Greenwood, 2001). U-Pb geochronologic ages of metamorphic minerals from the Boone eclogite have not been determined.

Western Gneiss Region Eclogites

Eclogite facies P-T conditions of ~ 22 kbar, 753 °C (Wain et al., 2001) were estimated from the Flatraket Complex using the garnet-clinopyroxene-phengite barometer (Waters and Martin, 1993), and temperature estimates from the garnet-clinopyroxene Fe-Mg exchange thermometer (Powell, 1985). The highest P-T conditions plotted in Figure 1.16C (from Wain et al., 2001) were estimated from fine-grained granular eclogite, sample aw99, using the Fe^{3+} estimation of Droop (1987). P-T estimates of ~14-16 kbar at

710 – 800 ºC (this study) were calculated using reactions [2] and [3], using high Mg-garnet compositions (just inside retrograde rim) and homogenous omphacite core compositions from sample F28-C. Retrograde conditions of ~ 720 – 760 ºC at 9.5 – 13 kbar were estimated from Cpx-Pl-Hbl symplectite assemblages (sample F28-C, this study), using reactions [4] and [5], and the same method of Fe^{3+} estimation. No estimates were made for Grt rim-Hbl-Pl assemblages due to variable compositions in the outer rims of garnet.

Other workers have calculated P-T conditions using Cpx-Pl-Hbl equilibria and compositions of symplectite phases from the Nordfjord area of the WGR. Waters (2002) estimated temperatures of 600-700 ºC at 7 – 14 kbar for Nordfjord and Stadlandet eclogites. Labrousse et al. (2004) estimated temperatures ranging from 550 – 650 ºC at 4.5 – 13 kbar from symplectites of six WGR eclogite samples. Although P-T estimates produced here (from symplectite equilibria) are very similar to those of Waters (2002), our temperature estimates are slightly higher (720-760 ºC). Differences in temperature estimates may be due to differences in software (TWQ 1.02 versus THERMOCALC) (Holland and Powell, 1998), or may be real (due to differences in local P-T conditions and the corresponding mineral compositions).

An isothermal decompression path was plotted for Gurskøy using previously determined P-T estimates (Dunn and Medaris, 1989) based on Grt-Pl-Cpx-Qtz and Jd-Ab-Qtz equilibria, and Grt rim-Hbl-Pl-Qtz equilibria (reactions [6-12]) from eclogite and garnet granulite mineral compositions (this study). The calculated P-T path (Figure 2.16D) is nearly isothermal, and plots with a temperature range of ~750 – 800 ºC. No estimates were made from Cpx-Pl symplectites assemblages from Gurskøy eclogites due to the lack of hornblende in these symplectites.

In an evaluation of structural, thermobarometric, and geochronologic data sets of the WGC, Labrousse et al. (2004) calculated exhumation rates for the Nordfjord area of the WGR. For the interval between 18 and 7 kbar, an exhumation rate of 2.3 mm/year (from 60 to 28 km in 14 m.y.) was estimated for the Nordfjord region (Labrousse et al., 2004). Decompression and cooling rates can readily be calculated from their data: 0.6 kbar/m.y. (from 18 to 7 kbar in 14 m.y.). The estimated cooling rate for the Nordfjord area is ~13 ºC/m.y. (from 780 to 600 ºC in 14 m.y.) for this interval (Labrousse et al., 2004).

Other HP Terranes

Pressure-temperature paths, cooling rates, and decompression rates determined from several UHP and HP terranes are graphically compared in Figures 2.17, 2.18, and 2.19. Eclogites from all of these terranes contain retrograde symplectite after omphacite. Most of these eclogites experienced temperatures ranging from 600-750 ºC during decompression from 20 to 10 kbar. The Zermatt-Saas ophiolite shows lower temperatures over this pressure range due to differences in tectonic setting: lower temperatures are characteristic of Alpine-Himalayan blueschist belts (Ernst, 1988). The anomalous deflection towards higher temperatures in the decompression path of the

D'Entrecasteaux eclogites, Papua New Guinea (light blue curve, Figure 2.17) resulted from an episode of granodiorite plutonism (Hill and Baldwin, 1993). Decompression and cooling rates estimated for the Lick Ridge eclogite are lower than rapidly exhumed UHP terranes such as the WGR, Pakistan Himalayas, Alps, and Papua, New Guinea. T-t and P-t curves of the Nordfjord area (WGR, Norway) are similar to other rapidly-decompressed and rapidly-cooled UHP terranes plotted in Figures 2.18, 2.19.

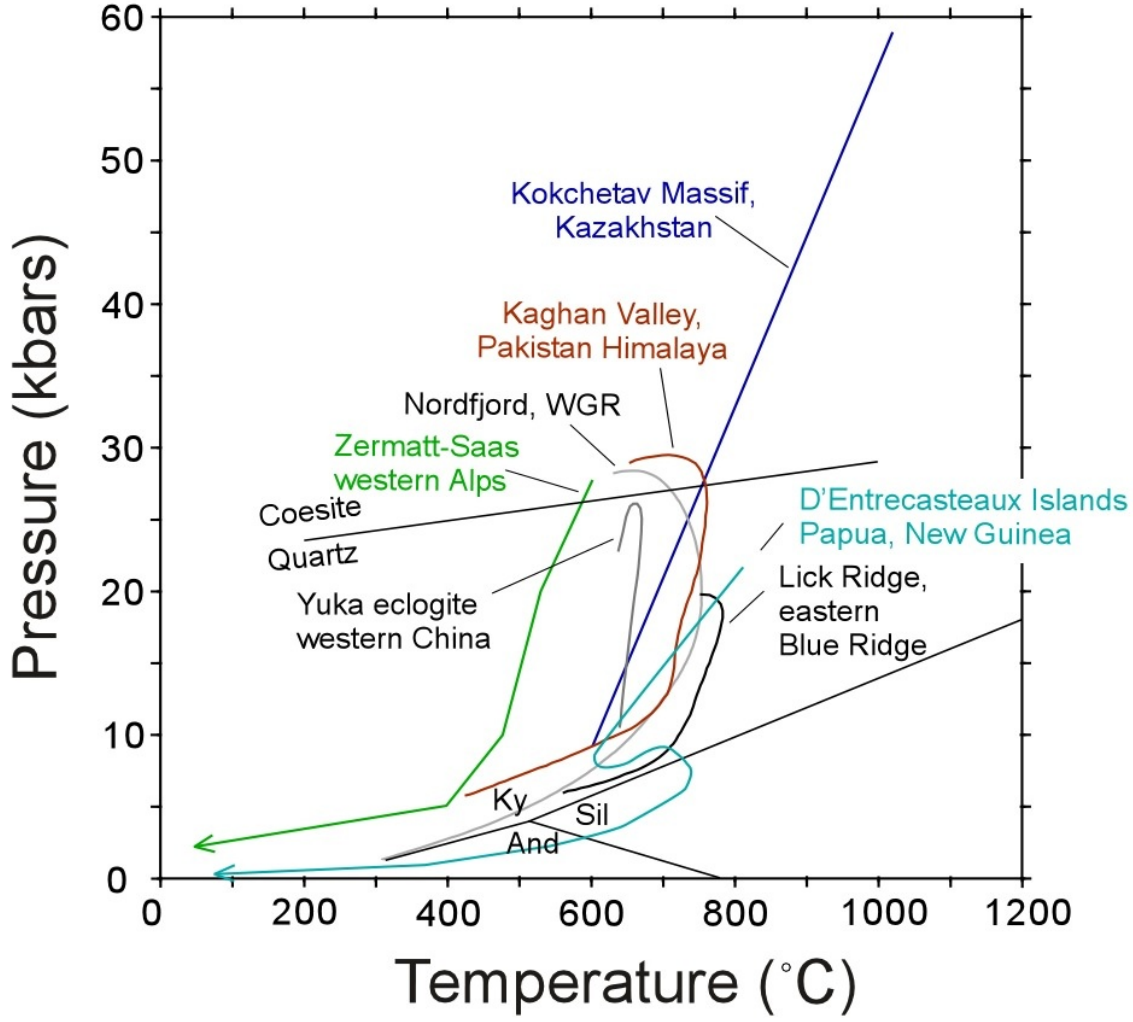

Figure 2.17. Comparison of retrograde P-T paths of HP and UHP eclogites. Kokchetav massif, Kazakhstan (Hacker et al., 2003; Okamoto et al., 2000); Kaghan Valley, Pakistan Himalaya (Gough, 2002; Parrish et al., 2006); Nordfjord region, WGR, Norway (Labrousse et al., 2004); Zermatt-Saas ophiolite at Lago di Cignana, Western Alps (Amato et al., 1999); Yuka eclogite, north Qaidam Mountains, China (Zhang et al., 2005); D'Entrecasteaux Islands, Papua, New Guinea (Hill and Baldwin, 1993); Lick Ridge, Eastern Blue Ridge (this study, and references in Figure 2.16).

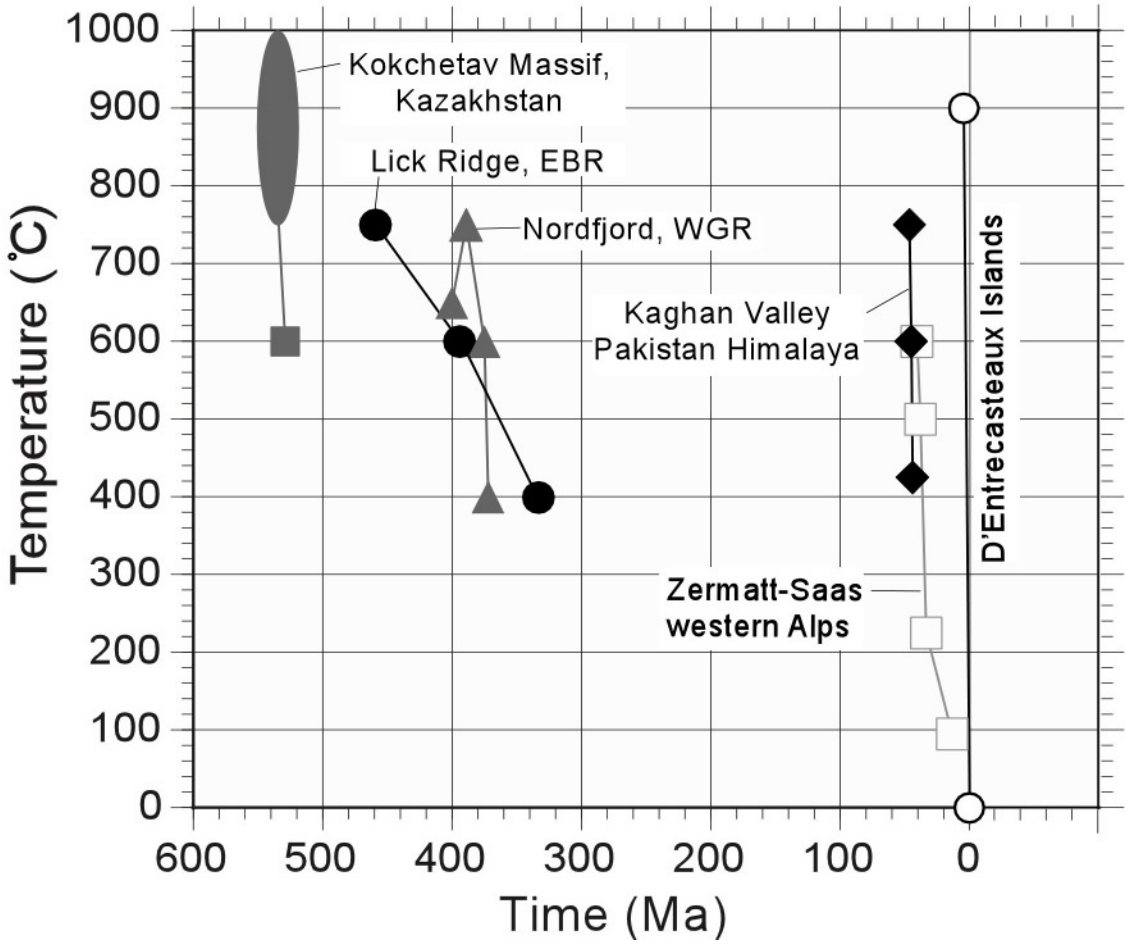

Figure 2.18. T-t (Temperature-Time) comparison of HP and UHP terranes. Figures 2.18 and 2.19 were derived by integrating P-T paths of Figure 2.17 and geochronologic data from the following sources: Kokchetav massif: Hacker et al. (2003); Shatsky et al. (1999); Lick Ridge, eastern Blue Ridge: Miller et al. (2006); Nordfjord, WGR, Norway: Labrousse et al. (2004); Schärer & Labrousse (2003); Labrousse (2001); Kaghan Valley, Pakistan Himalaya: Parrish et al. (2006); Treloar et al. (2003); D'Entrecasteaux Islands, Papua, New Guinea: Baldwin et al. (2004); Zermatt-Saas ophiolite at Lago di Cignana, Western Alps: Amato et al. (1999); Hurford et al. (1989, 1991).

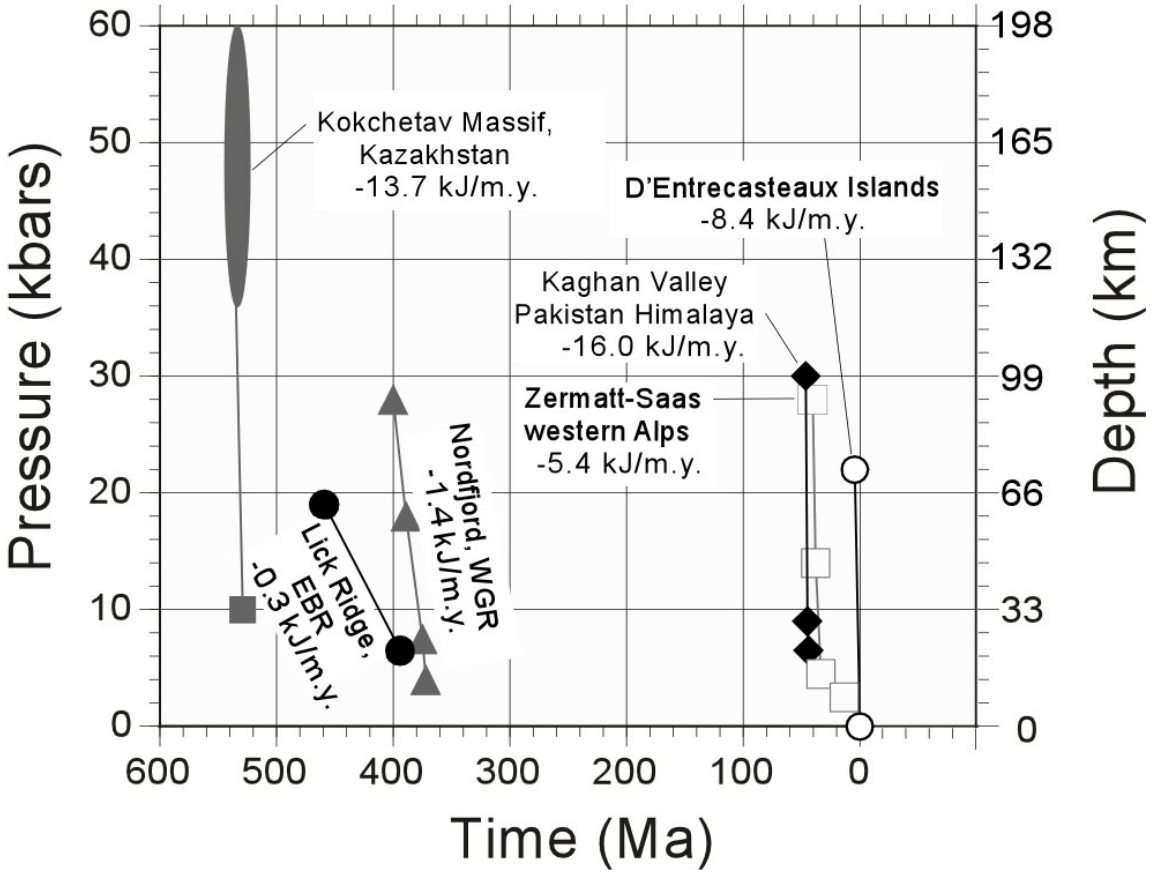

Figure 2.19. P-t (pressure-time) comparison of HP and UHP terranes. Free energy produced by overstepping omphacite stability is estimated as (kJ/m.y.) and discussed in the text.

Discussion

The examination of metabasites in the present study indicates that the net omphacite-breakdown reaction is essentially Omp = Di-Hd (ss) + Pl $\pm$ Hbl $\pm$ Qtz, and not a simple combination of Jd + Qtz = Ab and CaTs + Qtz = An. In Dellwood samples the reaction appears to be low-Na Ac or high-Na Di = Di-Hd (ss) + Pl + Hbl + Qtz. The temperature range for formation of the Cpx-Pl symplectites examined is ~650 to 775 ^{o}C. Boone symplectites are an exception, formed at higher temperatures (~ 760 – 825 ^{o}C), and contain low [Na] in the symplectitic diopside. Cpx-Pl symplectites form over a pressure interval of ~ 3 – 16 kbar that appears to be correlated with X_{Jd} in omphacite, with high-X_{Jd} Cpx breaking down at higher pressures, low- X_{Jd} Cpx reacting at lower pressures during decompression.

There appear to be two primary reaction mechanisms in retrograde omphacite. Low-Na omphacite (or aegirine-augite) with low decompression and cooling rates (~0.22 kb/ and ~3 °C/m.y.; e.g., "low pressure" eclogites and high pressure amphibolites/granulites) breaks down via an exsolution-like process yielding crystallographically-controlled plagioclase + hornblende + quartz lamellae within clinopyroxene or at grain boundaries. Chemical zoning is well developed in pyroxene adjacent to plagioclase and hornblende lamellae and at grain boundaries (Figures 2.9, 2.10, 2.11). This reaction mechanism differs from true exsolution in that the host and exsolving phase are not isostructural (or nearly so) end members. Omphacite I from HP WGR eclogite breaks down to form complex, fine-grained, grain-boundary or internal symplectic intergrowths of omphacite II (less sodic) + plagioclase + hornblende. Matrix omphacite is unzoned (Figures 2.12 B, D). Lack of diffusion-controlled chemical zoning in matrix omphacite adjacent to symplectite, and symplectite-forming reactions in HP/UHP WGR settings are associated with rapid uplift rates (2-3 mm a^{-1}), steep decompression paths (~0.6 kb/ and 13 °C/m.y.), and disequilibrium on a micron scale.

The widespread occurrence of symplectic textures in rapidly decompressed HP and UHP rocks is the fingerprint of rapid eduction or uplift and significant over-stepping of a strongly pressure dependent reaction along a nearly isothermal decompression path. Although decompression is rapid, the degree of cooling through the isothermal interval is obviously low, thus maintaining favorable reaction kinetics at nearly peak-T conditions. The reaction may be considered wholesale breakdown of the omphacite lattice, with product phases nucleating at the site of breakdown. In contrast, nucleation of 'exsolution' lamellae and diffusion-controlled coarsening is diagnostic of low degrees of overstepping of the omphacite-breakdown reaction along P-T paths with a greater component of cooling, and longer periods of time at high T, with a longer characteristic length scale for diffusion. None of the samples examined exhibits a preferred orientation of reaction products; the reaction proceeds essentially statically, without the catalytic effect of strain-induced recrystallization.

The degree of overstepping of omphacite breakdown is approximated in Figure 2.19. Overstepping of jadeite stability is expressed as ΔG_{Rxn2}/m.y., and was estimated as ΔG_{Rxn2}/m.y. = ΔP_{Rxn2}/m.y. x ΔV_{Rxn2}. ΔP_{Rxn2}/m.y. was obtained from the P-t path in Figure 2.19. ΔV_{Rxn2} (~ 1.639 J/bar/mol taken from output of TWQ 2.02 [Berman 1988]) is taken as an estimate of the volume change of the more complex reaction experienced for the isothermally decompressed omphacite at 700 °C. Negative ΔG_{Rxn2} results from decompression, and indicates that the symplectite-forming reactions are spontaneous. Values of ΔG_{Rxn2}/m.y. range from -0.3 to -16.0 kJ/m.y., and differ by nearly two orders of magnitude, due to decompression rates that differ by over an order of magnitude.

In most of the broadbeam comparisons the Cpx-Pl symplectites appear to be largely isochemical with adjacent unreacted clinopyroxene. Reintegrations from Lick Ridge, Dellwood, and Flatraket appear isochemical; the Gurskøy reintegration does not. However the trends in Figure 2.15 indicate that there is not a perfect 1:1 correlation between symplectite and adjacent pyroxene compositions, and that [Si] and [Al] are higher in some symplectite; [Fe], [Mg], and [Ca] are higher in some unreacted pyroxene.

The explanation for these trends is uncertain, but may be (1) entirely due to errors inherent in microprobe broadbeam data reduction, e.g. using a pyroxene standard to reintegrate symplectic plagioclase. This explanation is plausible for most of the data (and would completely invalidate the calculation of CaEs from symplectite) but unlikely for the Gurskøy symplectite having ~4.7 wt.% more Al_2O_3 and ~3.8 wt.% less FeO relative to unreacted pyroxene; (2) due to diffusion of Fe, Mg, and Ca out of symplectite with Al and Si remaining fixed. (3) due to diffusion of Al and Si into symplectite during decompression, with Fe, Mg, and Ca remaining fixed. An alternative explanation is that the trends of Figure 2.9 are largely real, that sympectites and adjacent omphacite are *nearly* isochemical, and that zones richer in CaEs component (such as the distinct symplectitic cores in the Dellwood metabasites, (Figures 2.10A, 2.13B) reacted to form symplectite during decompression while rims with lower X_{CaEs} did not. This explanation is plausible for the ABR examples, however, it is difficult to conceive how reintegrated phases in grain-boundary type symplectites (e.g. Flatraket, Figure 2.12A, C) produce a more representative approximation of early (HP) omphacite compositions than the cores of larger unreacted omphacite. Perhaps the matrix omphacite from Flatraket was supersilicic at HP/UHP conditions and silica exsolution occurred during decompression. Excess silica may have migrated from CaEs-bearing matrix omphacite to grain boundaries where it was incorporated into symplectite phases.

Variations in compositional profiles across clinopyroxene and plagioclase lamellae in Cpx-Pl symplectites (Figures 2.9A, 2.10D, 2.11D) are interpreted as evidence for thermally activated lattice diffusion. Compositional profiles suggest that some of the plagioclase in symplectic pyroxene forms from reactions involving chemical components derived in-situ, i.e. by the diffusion of Na and Al from omphacite towards plagioclase nucleation sites. Lattice diffusion appears to be the mechanism of cation transfer over a range of ~40 μm in ABR symplectites. However in the Gurskøy symplectite reintegration, high Al-content in symplectite relative to adjacent omphacite cannot be accounted for by the redistribution of Na and Al within clinopyroxene grains. In eclogite composed essentially of omphacite and garnet, a likely external source of Al is garnet. A compositional profile from a hornblende rim on garnet from Flatraket (Figure 2.12D) indicates high-Al hornblende near garnet, and low-Al hornblende adjacent to symplectite. This profile suggests that the transfer of Al away from garnet breakdown reactions may occur via lattice diffusion of Al through hornblende. The continued transfer of Al from garnet to nucleation sites in Cpx-Pl symplectites may occur via grain boundary diffusion as well as diffusion along {110} in pyroxene.

The paradox that quartz occurs within some Cpx-Pl symplectites after omphacite (quartz should be consumed by the reactions Jd + Qtz = Ab and CaTs + Qtz = An) can be explained by the presence of Ca-Eskola component in precursor clinopyroxene. Significant amounts of CaEs are indicated when reintegrated Cpx-Pl symplectite compositions are recalculated as pyroxenes. If the Gurskøy reintegration is disregarded (the resulting recalculated pyroxene formula is questionable), the reintegrated symplectites from Flatraket, Lick Ridge and Dellwood have X_{CaEs} that ranges from 4-15 mole % when endmember calculation methods of Katayama et al., (2000) and Page et al.,

(2005) are applied. If CaEs was a component of these pyroxenes at high pressure (>15 kbar), it is plausible that all of the following reactions occurred during the breakdown of clinopyroxene to form Cpx-Pl symplectite:

$$CaEs + Jd = 1.5\ Pl\ (Ab_{67}An_{33})\ (Vogel, 1966)\ [1]$$
$$Jd + Qtz = Ab\ [2]$$
$$CaTs + Qtz = An\ [25]$$
$$2\ CaEs = CaTs + 3\ Qtz\ (Smyth, 1980)\ [26]$$
$$CaEs = An + 2\ Qtz\ (Gasparik, 1986)\ [27]$$

Quartz normative Cpx-Pl symplectite assemblages and the presence of quartz needles may result from quartz-producing reactions [26, 27] "swamping" the quartz-consuming reactions [2,25]. Quartz-free symplectites may occur when the quartz-consuming reactions swamp the quartz-producing reactions. The Gurskøy symplectites contain distinct quartz-free, hornblende-free intergrowths of diopside + plagioclase that form in matrix omphacite included by abundant quartz + hornblende needles (Figure 2.12E). A possible explanation for these modally distinct symplectic assemblages, as well as similar occurrences in the Lick Ridge omphacites, is that the breakdown of CaEs occurred early during decompression, and led to the formation of Hbl+Qtz inclusions. Jd breakdown reactions occurred later during decompression, and the formation of diopside + plagioclase symplectites formed at the expense of Hbl+Qtz inclusions.

CHAPTER 3: FORMATION OF HIGH-PRESSURE METABASITES IN THE SOUTHERN APPALACHIAN BLUE RIDGE VIA TACONIC CONTINENTAL SUBDUCTION

Introduction

Continental subduction to depths in excess of 100 km and rapid exhumation is now widely recognized as the fundamental process for production and preservation of the largest tracts of high pressure (HP) to ultra-high pressure (UHP) rocks exposed on Earth (Liou et al., 2004; Ernst, 2006). The type locality of UHP metamorphism is the Western Gneiss Region of the Norwegian Caledonides, which formed by subduction of the Baltic continental margin followed by rapid, extension-driven exhumation at 1-10 cm a^{-1} (Johnston et al., 2007). HP and UHP eclogites in East Greenland reveal that rocks now comprising part of the northern Laurentian continental margin were similarly subducted and exhumed in the middle Paleozoic (Gilotti and McClelland, 2007). Thus both continental margins were subducted during Caledonian collision.

In contrast, eclogites occur at only two known localities in the entire Appalachian orogen: at Lick Ridge, near the boundary between the eastern and western Blue Ridge in western North Carolina (Willard and Adams, 1994) (Figure 3.1), and in the central Carolina Terrane (Shervais et al., 2003). Other occurrences of metabasites identified as retrograde eclogite or HP granulite/amphibolite occur within the eastern Blue Ridge of the southern Appalachian Blue Ridge proximal to the western Blue Ridge terraneboundary in western North Carolina and Georgia (Figure 3.1). These include retrograde eclogite exposed north of the Grandfather Mountain window (Abbott and Raymond, 1997; Abbott and Greenwood, 2001; Anderson and Moecher, 2007), garnet granulites of the Lake Chatuge mafic-ultramafic complex (Dallmeyer, 1974), and clinopyroxene-garnet granulites and amphibolites in the eastern Great Smoky Mountains. (Anderson and Moecher, 2007) (Figure 3.1). Only one definitive occurrence of blueschist occurs in the Appalachians (New Brunswick: van Staal et al., 1990), but it is younger (Late Ordovician-Early Silurian) than the southern Appalachian eclogites.

The Lick Ridge eclogite is a key element in models of Paleozoic collisional tectonics for the southern Appalachian orogen. It implies that a much larger tract of the Blue Ridge crust was subducted to depths greater than the thickness of typical continental crust, even though most of those rocks do not mineralogically record that subduction. Thermobarometric calculations for the most common Lick Ridge assemblages indicate that omphacite and garnet formed at 13-17 kbar and 650-730 ºC (Willard and Adams,1994). P-T estimates based on compositions of inclusions in garnet, retrograde phases, and metamorphic assemblages in the surrounding schists and amphibolites provide a well-constrained, clockwise P-T path with a component of isothermal decompression (Page et al., 2003; Anderson and Moecher, 2007). Zircon ID-TIMS U-Pb ages for the Lick Ridge eclogite (459.0 + 1.6/-0.6 Ma; B.V. Miller et al., 2000, 2006) indicate that eclogite-facies metamorphism was a Taconian event (Appendix E). At other locations along the boundary zone between the eastern and western Blue Ridge, Taconian

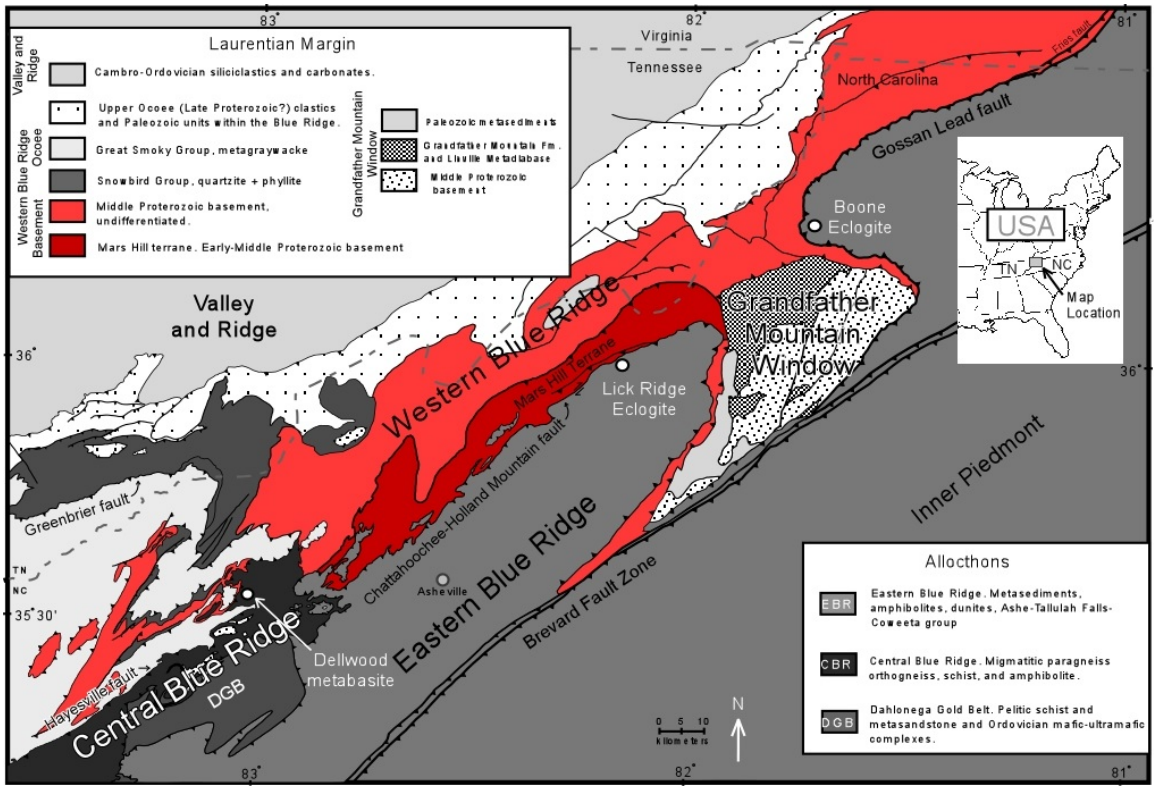

Figure 3.1. Simplified geologic map of the study area. Tectonic elements of parts of the southern Appalachian Blue Ridge and locations of high-pressure lithologies examined in this study are shown. Map compiled from Rankin et al. (1990); Woodward et al. (1991); Adams et al. (1995); Hatcher et al. (2004); and Hatcher et al. (2005).

mineral assemblages record upper amphibolite to granulite-facies. Migmatitic gneisses exposed at Winding Stair Gap yield a zircon U-Pb ID-TIMS age (458 $\pm$ 1 Ma; Moecher et al., 2004) and thermobarometry (P = 8.0 $\pm$ 0.6 kbar; T = 850 $\pm$ 20 ^{o}C) consistent with granulite-facies metamorphism occurring contemporaneously with eclogite-facies metamorphism along strike to the northeast.

Several tectonic models account for the presence of eclogites in the eastern Blue Ridge (e.g. Stewart et al., 1997; Abbott and Greenwood, 2001; Miller et al., 2006). A fundamental assumption in these models is that they require subduction of oceanic crust, or a subducted seamount, that was later obducted cratonward onto the Laurentian margin. Referred to here as the "obducted ophiolite" models, they imply that the eastern Blue Ridge eclogites should be low-temperature types (LT; < 550 ^{o}C; Banno, 1970; Carswell,

1990), typical of B-type (Benioff) subduction zones. However, thermobarometric estimates indicate that eclogites of the EBR are medium-temperature type eclogites (MT; 550-900 ºC), (Adams and Trupe, 1997; Abbott and Greenwood, 2001; Page et al., 2003). According to the obducted ophiolite model, eclogite-facies metabasites formed prior to westward obduction onto the Laurentian margin, however the U-Pb ages of zircon from the Lick Ridge eclogite (459.0 + 1.6/-0.6 Ma) are statistically indistinguishable from the U-Pb age of zircons from Winding Stair Gap migmatitic granulite (458 ± 1 Ma), and not older as proposed by the model.

Subduction of the Laurentian continental margin (Gilotti and McClelland, 2007) is a viable alternative model for formation of southern Appalachian HP rocks during the Taconian orogeny. Furthermore, Ordovician HP rocks are reported from the Seve Nappe Complex, the Upper Allocthon of the Caledonide orogen in western Norway (Corfu et al., 2002). This generation of HP rocks resulted from a subduction event earlier than and distinct from the more widespread Siluro-Devonian HP and UHP events of the Western Gneiss Region, and suggests that the continental collision process was protracted and complex. The older Caledonian HP rocks and their tectonic setting might provide insight into the evolution of the polymetamorphic occurrences in the southernmost Appalachian-Caledonian chain (Steltenpohl et al., 2003). Herein we test models for generating HP rocks that bear on the manner of early Paleozoic collision of southern Laurentia. New thermobarometric estimates have been made for metabasites from Boone and Dellwood, NC. P-T paths of southern Appalachian Blue Ridge metabasites are compared to numerous P-T paths from various types of subduction zones (circum-Pacific and Alpine-Himalayan blueschist-eclogite belts; central Variscan suture; and Western Gneiss Region, Norway). The P-T paths are interpreted in the context of seismic-reflection profiles (Cook et al., 1979; 1981) and lithospheric subduction dynamics (Coakley and Gurnis, 1995) to develop an internally consistent model for Taconian orogenesis in the southern Appalachian orogen.

Methods

Mineral Analysis

Mineral compositions were determined using the ARL-SEMQ electron probe microanalyzer at the University of Kentucky. Most minerals were analyzed in point mode, using WDS at 15 kV and 15 nA; plagioclase, muscovite and biotite are analyzed using a rastered beam (~5 x 5 μm) at 15 kV and 10 nA to minimize loss of Na and K. Typical count times are10-20 seconds on peak, and 5-10 seconds for background counts. Natural USNM silicates and oxides were used as standards, ZAF corrections are made using Probewin v. 5.32.

Garnet formulae are recalculated on the basis of 12 oxygen; all Fe is assumed to be Fe^{2+}. Pyroxene formulae are calculated on the basis of 6 oxygen, with Fe^{2+} and Fe^{3+} estimated by stoichiometry (Droop, 1987). Pyroxene end-member components are calculated using an end-member removal scheme (Vogel, 1966; Smyth, 1980). Ten end-

members were calculated in the order: aegirine $NaFe^{3+}Si_2O_6$ (Ac), jadeite $NaAlSi_2O_6$ (Jd), $KFe^{3+}AlSiO_6$ (I), Ca-Ti Tschermak's component ($CaTiAl_2O_6$), esseneite $CaFe^{3+}AlSiO_6$ (Es), Ca-Tschermak's component $CaAlAlSiO_6$ (CaTs), johannsenite $CaMnSi_2O_6$ (Jo), wollastonite $Ca_2Si_2O_6$ (Wo), enstatite $Mg_2Si_2O_6$ (En) and ferrosilite $Fe_2Si_2O_6$ (Fs). The pyroxene end member calculation scheme described above is used to classify pyroxenes and to estimate X_{Jd} of Cpx for thermobarometric calculations. Hornblende formulae are calculated assuming 13 cations excluding Ca, Na, and K; Fe^{3+} is estimated by stoichiometry (Equation 6 of Droop, 1987). Pyroxene and amphibole classification is based on IMA criteria (Morimoto et al., 1988; Leake et al., 1997).

Thermobarometry

In general, P-T paths are based on prograde estimates from inclusion-in-garnet compositions, matrix garnet and clinopyroxene compositions, and retrograde conditions from retrograde mineral compositions. The assumption that inclusions in garnet preserve prograde conditions is based on the interpretation of the garnet profiles, i.e., increasing Mg/Fe from core to rim indicates prograde garnet growth; the sharp drop in Mg/Fe at garnet rims indicates retrograde conditions. Prograde P-T conditions from the Dellwood metabasite were estimated using compositions of plagioclase and clinopyroxene inclusions in garnet. Prograde conditions from the Boone metabasites are estimated using Hbl-Qtz-Grt equilibria applied to hornblende inclusions in garnet. Prograde P-T conditions of the Lick Ridge eclogite were estimated by Page et al. (2003) using mineral compositions of clinopyroxene, hornblende, epidote, titanite, rutile, and biotite inclusions in garnet. Compositional traverses across inclusions in garnet are made to avoid both strongly-zoned inclusions and potential late reequilibration effects. Simple inclusions are preferred over compound inclusions, and inclusion compositions are matched with adjacent garnet compositions for each P-T estimate. Minimum pressures of eclogite facies conditions are estimated by convention, using jadeite stability (Holland, 1980, 1983):

$$Jd + Qtz = Ab \quad [1]$$

Temperatures of Cpx+Grt-bearing assemblages are estimated using the garnet clinopyroxene Fe-Mg exchange thermometer (Berman et al., 1995):

$$3Di + Alm = 3Hed + Prp \quad [2]$$

The garnet granulites and HP-amphibolites from Dellwood do not contain evidence of a precursor eclogite-facies mineral assemblage. Plagioclase occurs as a matrix phase and reaction [1] cannot be used to estimate minimum pressure. The equilibrium Grt + Qtz =Cpx + Pl is relevant for calculating P and T in these samples. Quartz is present as inclusions in garnet but it is not present in the matrix. The absence

of quartz implies silica activity (a_{SiO_2}) < 1 during equilibration of the matrix assemblage. In the absence of direct constraints on a_{SiO_2}, P-T conditions for the Grt + Pl + Cpx assemblage were calculated assuming a range of reduced silica activity (a_{SiO_2} = 0.2 to 0.8) in the garnet-plagioclase clinopyroxene-quartz equilibria (equations 13-14, Table 3.2). The results cited here use a_{SiO_2} = 0.5. A variation in a_{SiO_2} of + 0.3 results in a pressure shift of + 2 kbar. In view of the presence of quartz as inclusions in garnet, we consider a_{SiO_2} =0.5 to be a minimum value during equilibration of the matrix assemblage, and thus the calculated peak P-T conditions for the Dellwood metabasite to be minimum values. Due to the lack of preservation of peak omphacite, and presence of symplectic intergrowths of clinopyroxene and plagioclase, peak P-T estimates for the Boone retrograde eclogite are based on reintegrated omphacite compositions following Abbott and Greenwood (2001) (X_{Jd} = 0.42). Estimates of retrograde P-T conditions are made from several assemblages, including garnet rim-plagioclase-hornblende-quartz and clinopyroxene-plagioclase-hornblende symplectites after omphacite (Waters, 2002). Specific equilibria for each assemblage and sample are listed in Appendix F. P-T estimates are calculated using TWEEQU (Berman, 1988, 1990; Berman et al., 1995, 1996). A ferric iron calculation (Droop, 1987) is used for all equilibria that involve clinopyroxene or hornblende. X-ray maps are collected prior to quantitative analysis to better understand the relationship of textural position to mineral chemistry.

Geochronology

Zircons from leucosome and melanosome of migmatitic paragneiss occurring ~19 km NNE of the metabasites in the study area were separated by standard procedures (heavy liquids, Franz isodynamic separator), mounted in epoxy, polished, and imaged under BSE and CL with the Cameca SX-100 microprobe at the University of Michigan. U-Pb zircon ages were determined using the Cameca 1270 ion microprobe (SIMS) at the Keck Lab, UCLA using standard spot size analysis, the AS3 standard (Paces and Miller, 1993), oxygen "flooding" (P ~ 3 x 10^{-5} Torr) to increase Pb yield, and 7-10 analytical cycles or "blocks". Data are reduced using ZIPS v3.0.4 (written by C.D. Coath) using measured $^{204}Pb/^{206}Pb$ to correct for common lead, and plotted with Isoplot v.3.50 (Ludwig, 2003).

Petrography and Mineral Chemistry

Dellwood Basement Lithologies

The "Dellwood metabasite" occurs as a ~0.5 km-wide mass mapped as an amphibolite member of the "Carolina gneiss" basement complex, a formation composed of migmatitic muscovite-biotite gneiss, migmatitic hornblende-biotite gneisses,

muscovite biotite-garnet schists, porphyroclastic orthogneiss, and amphibolite (Hadley and Goldsmith, 1963) (Figure 3.1). Inferred structural cross sections (Montes, 1997) show the Dellwood metabasite occurring approximately 1 kilometer above the Hayesville fault and the faulted contact between Laurentian basement orthogneiss (footwall) and the central Blue Ridge Cartoogechaye terrane in the hanging wall. The core of the amphibolite body is unfoliated, with a weak compositional layering but no crystallographically- or shape-preferred orientation of constituent phases. The outer margin of the metabasite consists of fine-grained, foliated amphibolite composed of abundant hornblende with plagioclase, garnet, and clinopyroxene. Garnet growth in all amphibolites samples predates equilibration of the matrix assemblage. Evidence for various retrograde reactions includes resorbed garnets, the growth of plagioclase and amphibole at garnet rims, and the breakdown of omphacite to form diopside + plagioclase + hornblende + quartz symplectites. Mineral assemblages of the metabasite constitute greenish Cpx-rich amphibolite and Grt-Cpx granulite. Migmatitic orthogneiss and paragneiss enclosing the Dellwood metabasite contains isoclinally folded leucosomes that are refolded to open folds with a weak axial plane foliation that formed at biotite grade conditions (Massey and Moecher, 2005). No folds are observed in the amphibolite mass, and it appears to be a mega-boudin or tectonic block entrained in a matrix of orthogneiss, migmatitic biotite gneiss, and various two-mica schists.

Dellwood Sample DEL05-3B2

Sample DEL05-3B2 is medium- to fine-grained, macroscopically homogenous, with an estimated mode of clinopyroxene 41%, garnet 40%, plagioclase 10%, hornblende 5%, titanite 2%, ilmenite 1%, with apatite < 1% (Figure 3.2A). The sample has the lowest modal hornblende relative to other metabasite samples collected from the Dellwood location. The latter are classified as HP-amphibolites and consist of ~ hornblende 35%, garnet 25%, clinopyroxene 22%, plagioclase 15%, titanite 2%, ilmenite 1%, with traces of rutile, apatite, and zircon (Figure 3.2B). Quartz is absent as a matrix phase in all of the Dellwood metabasite samples, suggesting that the igneous protoliths were silica undersaturated. SiO_2 content of four Dellwood metabasite samples range from 43-46 wt. %, with further discussion to follow in Chapter 4. DEL05-3B2 is classified as garnet granulite due to the occurrence of the assemblage clinopyroxene + garnet + plagioclase (O'Brien and Rötzler, 2003). Omphacitic and aegirine-augite clinopyroxene show some degree of breakdown to form symplectitic rods of plagioclase, hornblende, and minor quartz enclosed by diopsidic pyroxene (Figure 3.3A). Microbeam reintegrations indicate that these Cpx-Pl-Hbl-Qtz symplectites after omphacite and aegirine-augite are isochemical with adjacent unreacted clinopyroxene (Chapter 2). Garnet is subhedral to euhedral, typically 0.5 – 1.5 mm in diameter, and contains inclusions of clinopyroxene, Cl-rich hornblende, epidote, plagioclase, titanite, quartz, and apatite (Figure 3.3B). Plagioclase occurs as subhedral grains within the matrix, as rims surrounding garnet, and as rod-shaped inclusions in symplectites after clinopyroxene. Clinoyroxene is classified as low-Na omphacite, low-Na aegirine-augite, and high-Na

diopside with compositions related to textural position (Figure 3.4). Cpx inclusions in garnet have an average composition of $Ac_{08}Jd_{05}Ess_{02}CaTs_{06}I_{01}Di_{51}Hd_{27}$ with average Al = 0.21 pfu and average Na = 0.13 pfu. Matrix pyroxene cores have the highest Na and Al concentrations, with an average composition of $Ac_{09}Jd_{09}CaTs_{09}I_{01}Di_{45}Hd_{27}$, average Al = 0.29 pfu, average Na = 0.18 pfu. Compositions of symplectic clinopyroxene are similar to matrix pyroxene rims, with an average composition of $Ac_{08}Jd_{06}Ess_{01}CaTs_{08}I_{01}Di_{49}Hd_{27}$, average Al = 0.24 pfu and average Na = 0.15 pfu. Representative mineral compositions are given in Appendix G.

Garnet cores are almandine-rich; average = $Alm_{54}Grs_{33}Pyp_{10\text{-}12}Sps_{02}$ (Figures 3.5A,B). Mg/Fe gradually increases from core to rim, and Ca decreases slightly, indicative of prograde garnet growth zoning (Medaris et al., 1995; Štípská and Powell, 2005; Medaris et al., 2006). Mg/Fe decreases in the outer ~20 micrometers in garnet traverses, consistent with slight retrograde re-equilibration. Garnet with highest Mg/Fe occurs just inside the retrograde rim and has a composition of ~ $Alm_{55}Grs_{32}Pyp_{13\text{-}14}Sps_{01}$. Garnet compositions from Dellwood, Lick Ridge and Boone are compared in Figure 3.6. Although the Dellwood granulite is not a retrograde eclogite, compositions are plotted for comparison purposes. Fields defining group A (inclusions in kimberlite, basalt, or ultramafic rocks), group B (bands or lenses in migmatitic gneiss terranes), and group C (bands or lenses from glaucophane schist / ophiolitic rocks) are from Coleman et al. (1965) and Mottana (1986). Garnet composition (Figure 3.6) is not particularly useful for understanding the origins of the HP garnets that were analyzed: the divisions of Coleman et al. (1965) imply that garnet compositions from Boone and Dellwood formed in glaucophane schist (Type C) complexes; Lick Ridge garnets plot on the group B (migmatitic gneiss)-group C boundary. When the more recent classification fields of Motanna (1986) are applied, most HP Blue Ridge garnet compositions plot within the intersection of group B and group C garnets, and tectonic affiliations are not clearly implied.

Plagioclase composition varies with textural position. The most sodic feldspar occurs as matrix grains (Ab_{78} – Ab_{83}) and intergrowths in symplectite after clinopyroxene (Ab_{75} – Ab_{80}). Plagioclase in coronas surrounding garnet has slightly lower Na content (Ab_{69} – Ab_{73}). Plagioclase with low-Na content occurs as inclusions within garnet (Ab_{50} – Ab_{60}). Matrix plagioclase shows reverse compositional zoning with rim compositions typically 2-5% higher in X_{An} relative to plagioclase cores.

Amphibole compositions vary with textural position (Figure 3.7). Inclusions in garnet are primarily ferropargasite and chlorian ferropargasite, with some chlorian sadanagaite and pargasite present. Low Si (~5.3 Si on the basis of 23 O) amphibole inclusions in garnet were found only in Dellwood garnet granulite, and were not present as inclusions in Lick Ridge eclogite or Boone retrograde eclogite. Cl was detected (up to 1.9 elemental wt. % Cl) only in amphibole inclusions of Dellwood granulite garnets. Cl was not detectable in Boone or Lick Ridge amphibole inclusions in preliminary EDS scans. Matrix hornblende in Dellwood metabasites is compositionally similar to amphibole in garnet rim assemblages, as well as symplectic hornblende after clinopyroxene, with compositions that are pargasitic to ferropargasitic. Some symplectic

hornblende has slightly lower Na_A, ranging from 0.4-0.5 pfu, and is classified as tschermakite and magnesiohornblende.

Garnet-Muscovite-Biotite Schist, MV02-7, Dellwood Region

P-T estimates were made for a garnet-muscovite-biotite schist in contact with the Dellwood metabasite (~600 meters ENE) to address the tectonic relationship between metabasite and enclosing basement lithologies: were mafic blocks metamorphosed prior to becoming intermixed with blocks of felsic orthogneiss and schist, or did heterogeneous basement complex lithologies reach HP conditions as a single entity? Schist sample MV02-7 underwent retrograde folding and ductile deformation that produced porphyroclastic garnet and mica fish (Clemons and Moecher, 2009). To avoid the potential effects of deformation-induced resetting of mineral equilibria (Moecher and Wintsch, 1994) P-T estimates were made from relatively undeformed inclusions in garnet. Photomicrographs, X-ray maps, and representative analyses are presented in Figures 3.2C, 3.3C, and Appendix G.

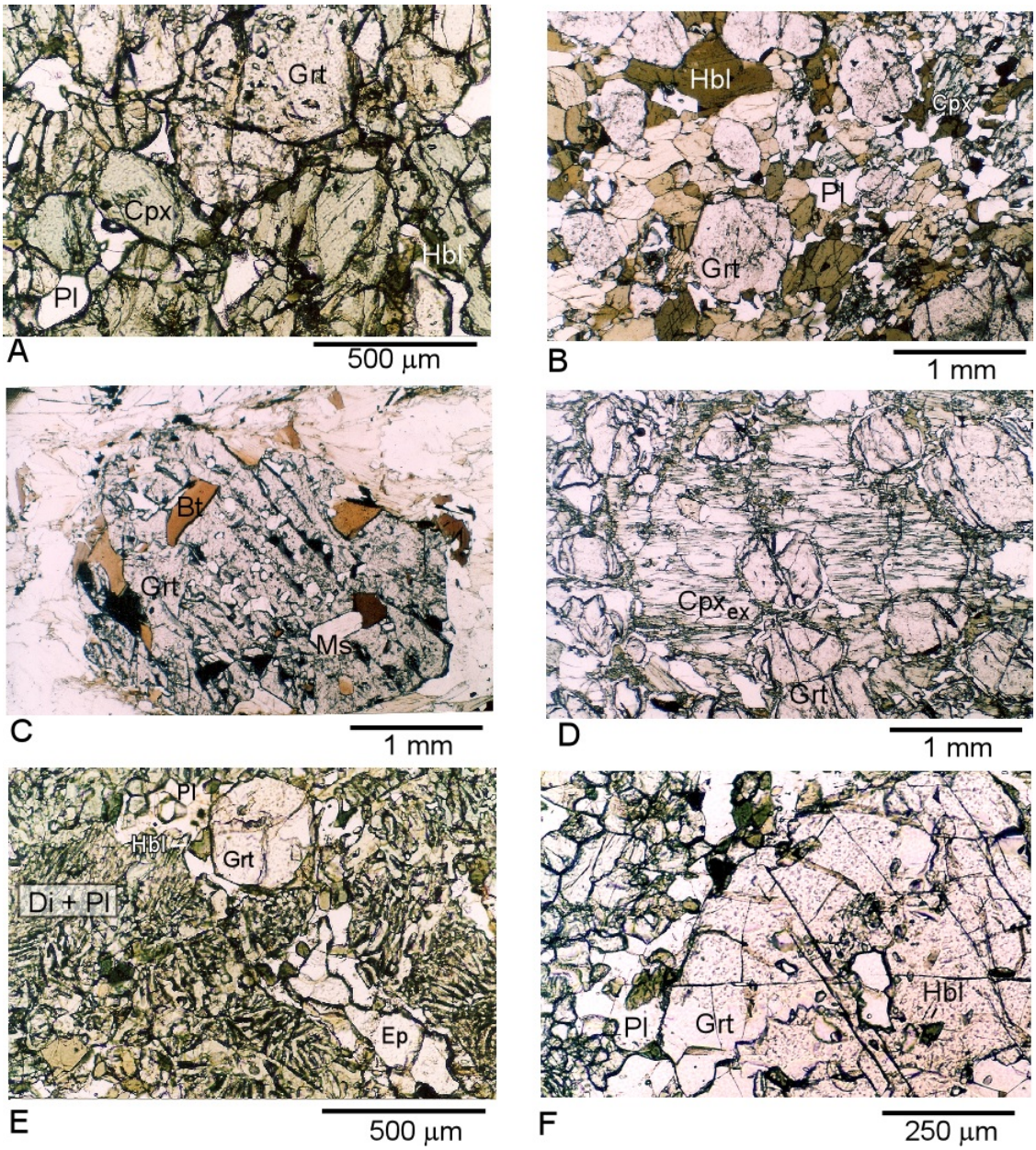

Figure 3.2. Photomicrographs of metabasites and schist from the central and eastern Blue Ridge, Western North Carolina. A) Dellwood garnet granulite, DEL05-3B2, PPL; B) Dellwood HP-amphibolite, DEL03-3B, PPL. C) Schist adjacent to Dellwood metabasite, MV02-7, with inclusions in garnet, PPL. D) Lick Ridge eclogite, sample NC98-1, PPL. E) Boone eclogite, sample Z05-2B, with diopside + plagioclase symplectites after omphacite, PPL. F) Boone eclogite, Z05-1B garnet with inclusions of hornblende + quartz, PPL. Mineral abbreviations after Kretz (1983).

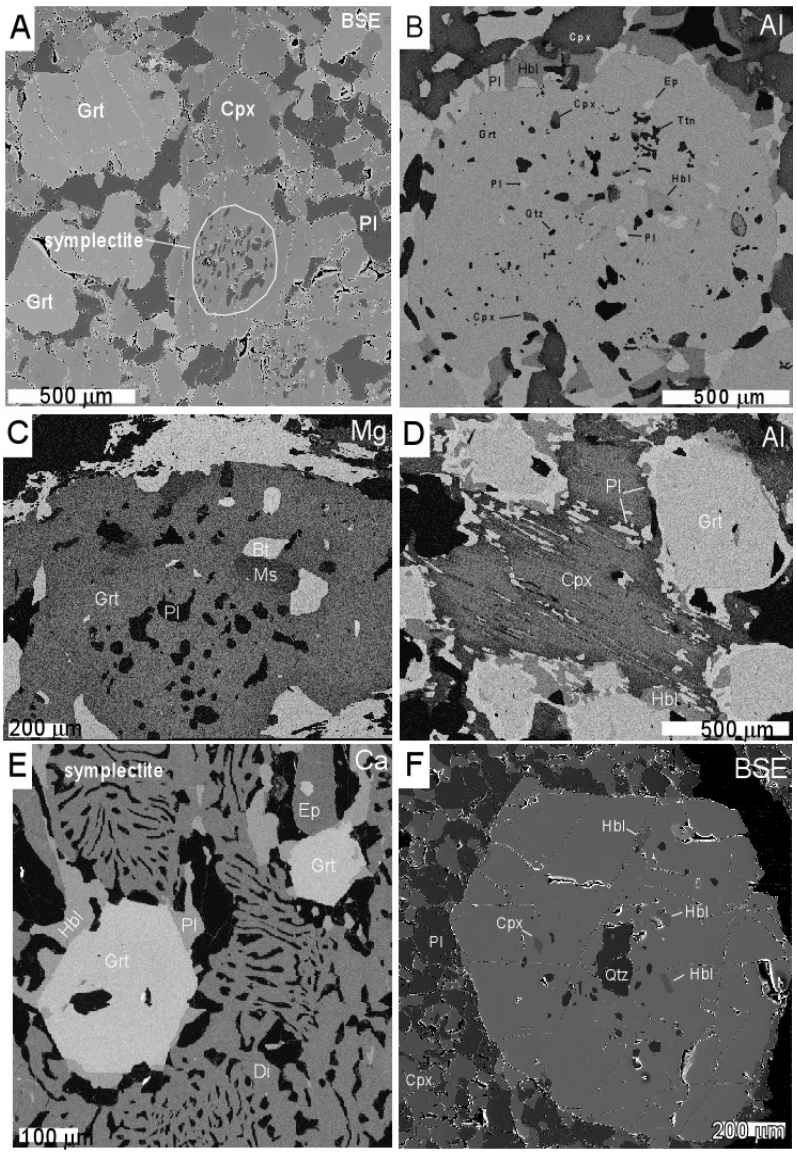

Figure 3.3. BSE and elemental intensity X-ray maps of metabasites and schist from western North Carolina. A) BSE image of Dellwood garnet granulite, DEL05-3B2, with resorbed garnet rims and internal Cpx-Pl-Hbl-Qtz symplectite after low-Na omphacite. B) Al-intensity map of inclusions in garnet used for thermobarometry, Dellwood sample DEL05-3B2. C) Mg-intensity map of inclusions in garnet, muscovite schist sample MV02-7, Dellwood area. D) Al-intensity map of Lick Ridge eclogite, sample NC98-1. E) BSE image of diopside-plagioclase symplectite after omphacite, Boone eclogite sample Z05-2B. F) Garnet with inclusions, Boone retrograde eclogite sample Z05-1B.

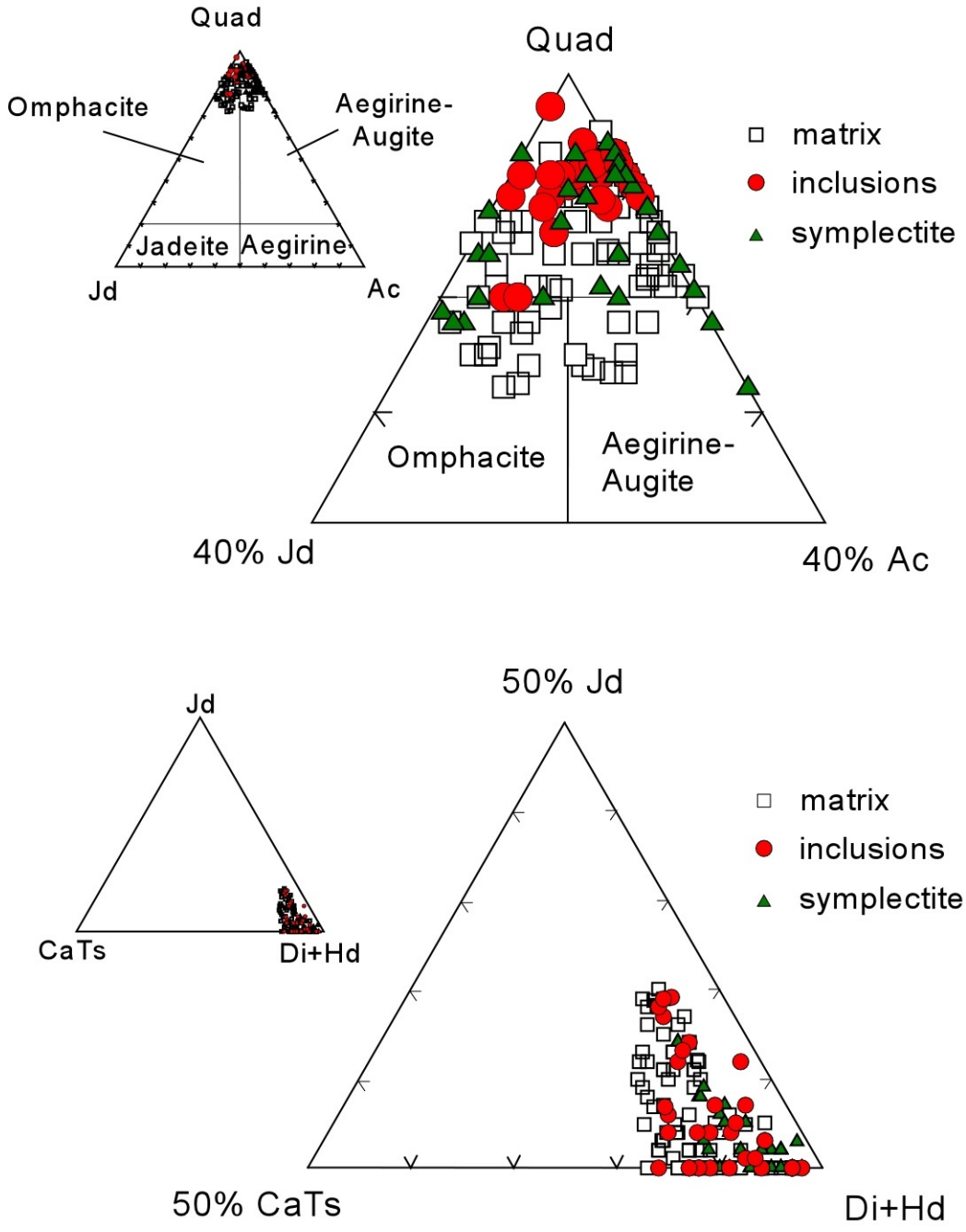

Figure 3.4. Pyroxene compositions, Dellwood granulite and HP-amphibolite. Top: Quad-Jd-Ac plot. Bottom: Jd-CaTs-Di + Hd plot. Endmember plots from Morimoto et al. (1988); Quad = Ca-Mg-Fe pyroxenes; Jd = jadeite; Ac = aegirine or acmite; CaTs = Ca-Tschermak's component; Di = diopside; Hd = hedenbergite.

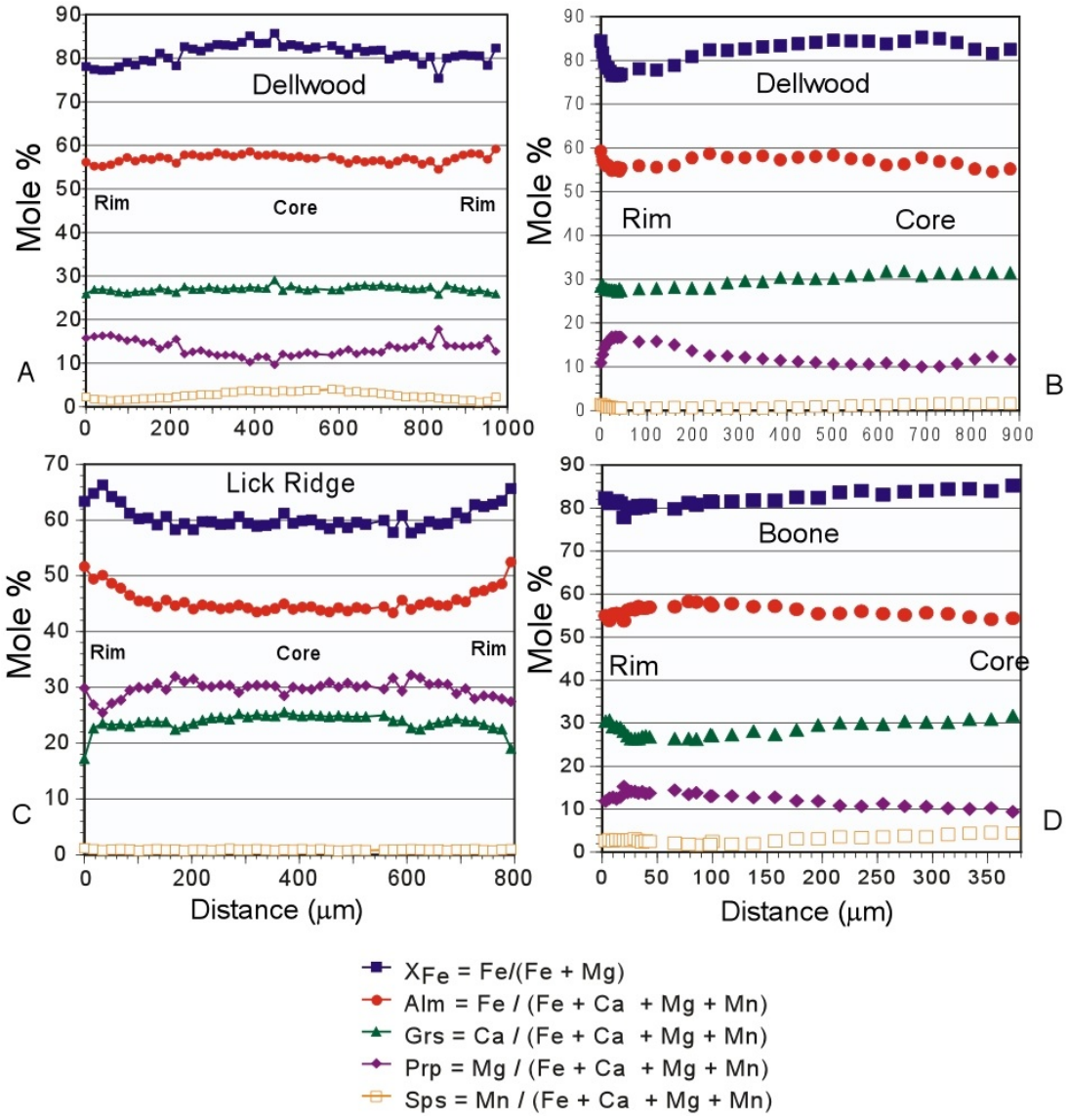

Figure 3.5. Garnet compositional traverses. A) Dellwood garnet granulite, DEL05-3B2; B) Dellwood HP-amphibolite, DEL03-3B; C) Lick Ridge retrograde eclogite, NC98-1; D) Boone retrograde eclogite, Z05-1B.

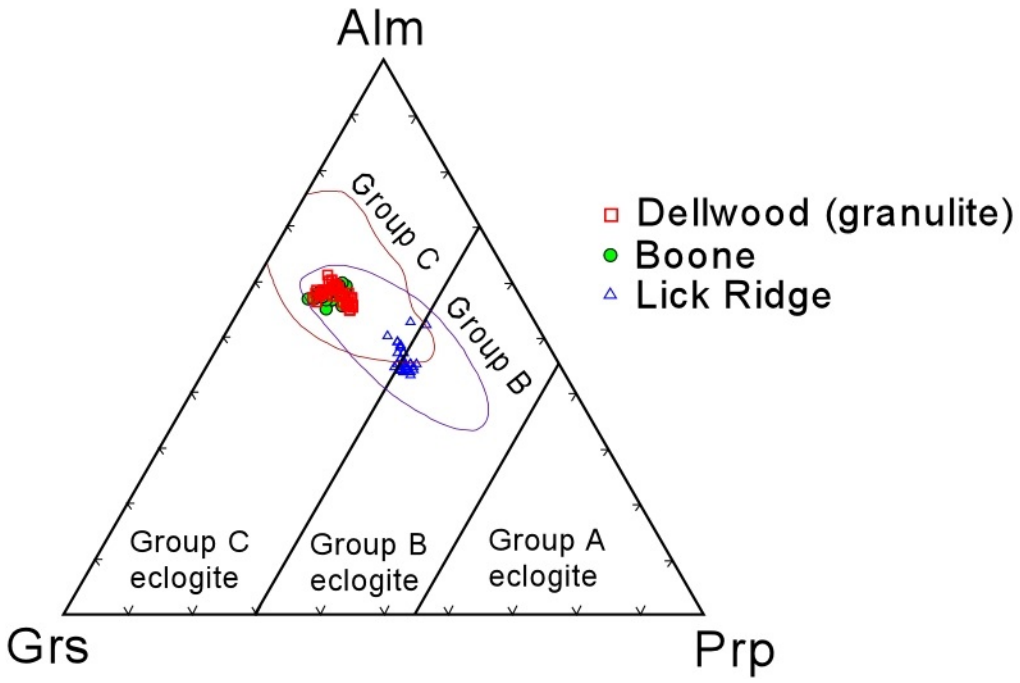

Figure 3.6. Garnet compositions of Dellwood granulite, Boone and Lick Ridge retrograde eclogite. Group A (kimberlite inclusions), B (migmatitic gneiss), C (glaucophane schist) eclogite fields after Coleman et al. (1965), Group B, C ellipses after Mottana (1986).

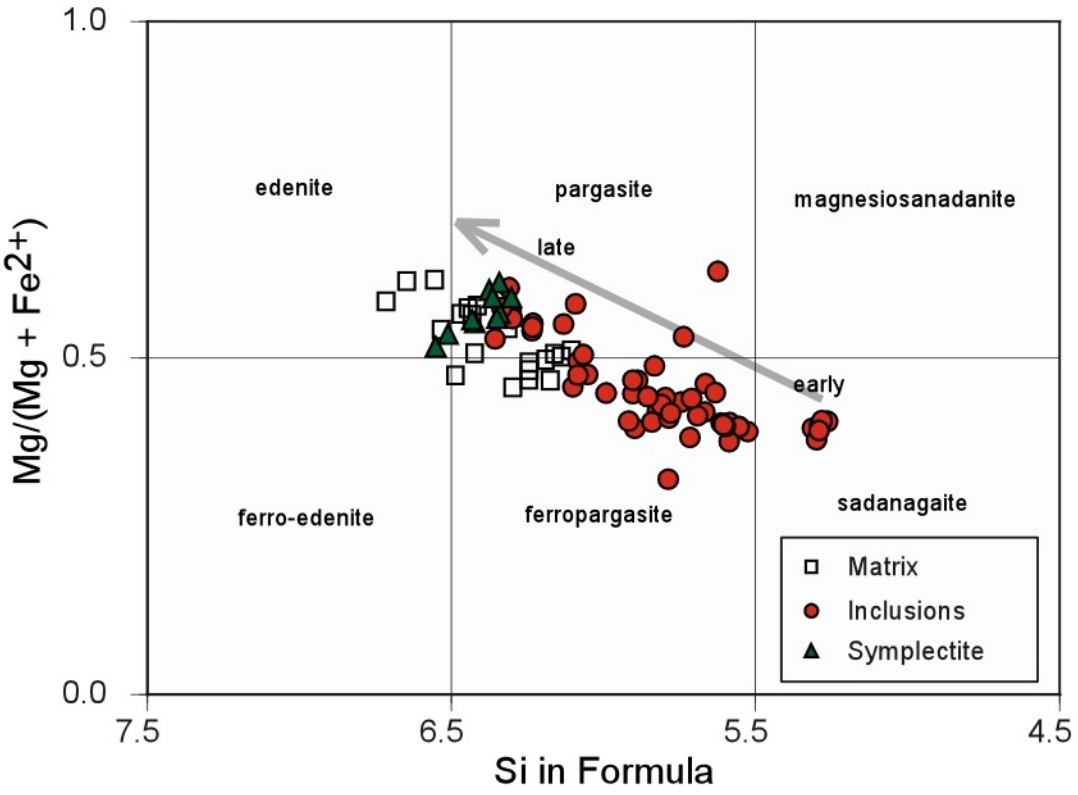

Figure 3.7. Calcic amphibole compositions of Dellwood granulite and HP-amphibolites. IMA classification, Leake et al. (1997).

Lick Ridge Eclogite

Eclogites from Lick Ridge are massive to weakly layered, medium- to coarse-grained with a peak eclogite facies assemblage of omphacite, garnet, quartz and rutile (Figure 3.2D) and variable amounts of retrograde plagioclase and hornblende. Mineral modes (sample NC98-1) are approximately clinopyroxene 40%, garnet 40%, quartz 10%, hornblende 5%, and plagioclase 5%, with traces of rutile, titanite, apatite, and zircon. Garnets are typically 1 - 2 mm in diameter, contain a variety of mineral inclusions, and are rimmed by coronas of plagioclase and hornblende. Garnet contains inclusions of

quartz, rutile, titanite, epidote, clinopyroxene, hornblende, and biotite (Willard and Adams, 1994; Page et al., 2003). Matrix omphacitic clinopyroxene ranges from 1 - 8 mm, with grains exhibiting undulatory extinction and subgrain boundaries. Some omphacite completely reacted to form clinopyroxene-plagioclase symplectite whereas other pyroxene cores appear to be unreacted, having an average composition of $\sim Jd_{21}CaTs_{09}Ac_{05}Di_{49}Hd_{16}$ and estimated $Fe^{3+} / Fe^{2+} = 0.43$. Clinopyroxene in Cpx-Pl-Hbl-Qtz symplectite is diopsidic and has compositions similar to matrix omphacite rims, with an average composition of $Jd_{03}CaTs_{08}Ac_{07}Di_{63}Hd_{19}$. Garnet cores are relatively homogenous ($\sim Alm_{44}Grs_{25}Pyp_{30}Sps_{01}$), followed by a small spike in Mg and concomitant dip in Ca (Figure 3.5C). The outer 100 μm show patterns of increasing Fe, decreasing Mg, and slightly lower Ca. Mn concentrations are low throughout. Plagioclase compositions from plagioclase + hornblende coronas surrounding garnet range from Ab_{71} to Ab_{76}, with an average value of ~ Ab_{72}. Representative analyses of phases are given in Appendix G. Additional mineral compositions and petrography have been published previously (Willard and Adams, 1994; Page et al., 2003, 2005; Anderson and Moecher, 2007).

Boone Retrograde Eclogite

Retrograde eclogites from the eastern Blue Ridge that occur north of the Grandfather Mtn. Window (Figure 3.1) are banded on the cm-scale, defined by layers rich in clinopyroxene, plagioclase, and garnet alternating with layers with greater abundance of hornblende, quartz, or epidote. In samples of retrograde eclogite, coarse (5 – 10 mm) precursor clinopyroxene has completely reacted to form fine-grained diopside-plagioclase symplectites after omphacite (Figures 3.2F, 3.3E) (Abbott and Greenwood, 2001; Anderson and Moecher, 2007). Diopside-plagioclase symplectite after omphacite is pale green under plane-polarized light and contains vermicular, irregular lamellae that are 5 – 10 μm thick. Modal abundances in retrograde eclogite examined are approximately: 45% Cpx –Pl symplectite; 35% garnet; 10% epidote; 4% quartz; 5% hornblende; 1% ilmenite, with traces of titanite. Ilmenite typically has coronas of titanite and plagioclase. Garnet is subhedral to euhedral, rimmed by hornblende, plagioclase, and trace magnetite (Figure 3.3E). Garnet contains inclusions of hornblende, titanite, quartz, rutile, ilmenite, apatite, zircon, pyrite, and rare clinopyroxene. Clinopyroxene from Boone metabasites is diopsidic and low in Na, containing < 0.1 Na pfu, with an average composition of $\sim Jd_{0}CaTs_{05}Ae_{09}Di_{54}Hd_{32}$. The representative garnet compositional profile from Boone (Figure 3.5D) shows Fe and Mg increasing from core to rim, and X_{Fe}, Ca, and Mn decreasing from core to rim. The highest Mg/Fe ratio occurs ~20 μm from the garnet rim, having a compositions of ~ $Alm_{55}Grs_{28}Pyp_{15}Sps_{03}$. The outermost garnet rim compositions show a decrease in Mg, and Fe, and an increase in Ca and X_{Fe}, consistent with retrograde cooling. All of the plagioclase from Boone retrograde eclogite appears to be retrograde with a narrow range of compositions. Symplectic plagioclase after omphacite and plagioclase from garnet rim assemblages range between $\sim Ab_{65}An_{35}$ and $Ab_{60}An_{40}$. Hornblende occurs at garnet rims and as inclusions in garnet (Figures 3.2F,

3.3E, F) and shows limited compositional variation. All of the amphiboles from Boone are calcic amphiboles, most of the amphibole in retrograde garnet rim assemblages is pargasitic, and the majority of amphibole inclusions in garnet are magnesiohastingsite ($^{IV}Al < Fe^{3+}$) (Leake et al., 1997).

Results and Interpretation

Thermobarometry

P-T estimates from HP-metabasites of the eastern Blue Ridge (Lick Ridge and Boone eclogites) and the central Blue Ridge (Dellwood and Winding Stair Gap) are shown in Figure 3.8. The P-T path of the Lick Ridge eclogite (Figure 3.8A) forms a well-constrained, clockwise, hairpin-shaped loop. P-T estimates from inclusions in garnet (Figure 3.8A, fields 1-4) are at or below the inferred peak P-T conditions, and consistent with entrapment during prograde garnet growth (Page et al., 2003). Peak P-T conditions are not fully constrained, however a minimum pressure of ~ 17 kbar at 700 - 750 °C is suggested by the presence of high-Jd omphacite ($X_{Jd} = 0.60$) and garnet-clinopyroxene Fe-Mg exchange thermometry (reactions [1,2]) (Page et al., 2003). The absence of coesite inclusions in garnet (Page et al., 2005) implies that the quartz-coesite isopleth can be used as an upper limit for pressure. Attainment of eclogite-facies conditions, inferred here at ~19 kbar and 750 °C, and P-T estimates from retrograde reactions [3-12] suggest nearly isothermal decompression at granulite- to upper amphibolite-facies conditions. A retrograde path into the granulite facies is required by thermobarometry and the presence of orthopyroxene in symplectite assemblages after omphacite (Page et al., 2003). The nearly isothermal decompression path calculated here (Figure 3.8A) differs from the P-T path estimated by Page et al. (2003), largely due to differences in P-T estimates fromgarnet rim-hornblende-plagioclase-quartz equilibria (Figure 3.8A, field 7). In the present study, garnet-rim equilibria utilizing the outermost garnet rim compositions (reactions 6-12) yield ~13-15 kbar and 725 – 800 °C. The similarity of P-T conditions estimated from
garnet-rim assemblages and symplectites (reactions 3-4), suggests that garnet breakdown may have occurred simultaneously with omphacite-breakdown reactions, consistent with textural observations (Figure 3.2D). The P-T conditions recorded by adjacent, un-sheared Ashe Metamorphic Suite garnet amphibolites (Figure 3.8A, field 9; 8.6 – 9.3 kbar and 660-750 °C; Waters et al. 2000) overlaps with P-T conditions determined from retrograde Lick Ridge symplectite (Figure 3.8A, field 7; ~9 kbar and 700 °C, equations 3-4). P-T estimates from Dellwood garnet granulite also define a clockwise loop (Figure 3.8B). Upper-amphibolite-facies conditions are indicated from Cpx-Pl-Grt-Qtz equilibria applied to inclusions in garnet (Figure 2.8B, field 1). HP conditions of 14-16 kbar at 625 –750 °C are indicated from Cpx-Pl-Grt-Qtz equilibria estimates utilizing garnet with maximum Mg/Fe, matrix clinopyroxene compositions, and reduced silica activity

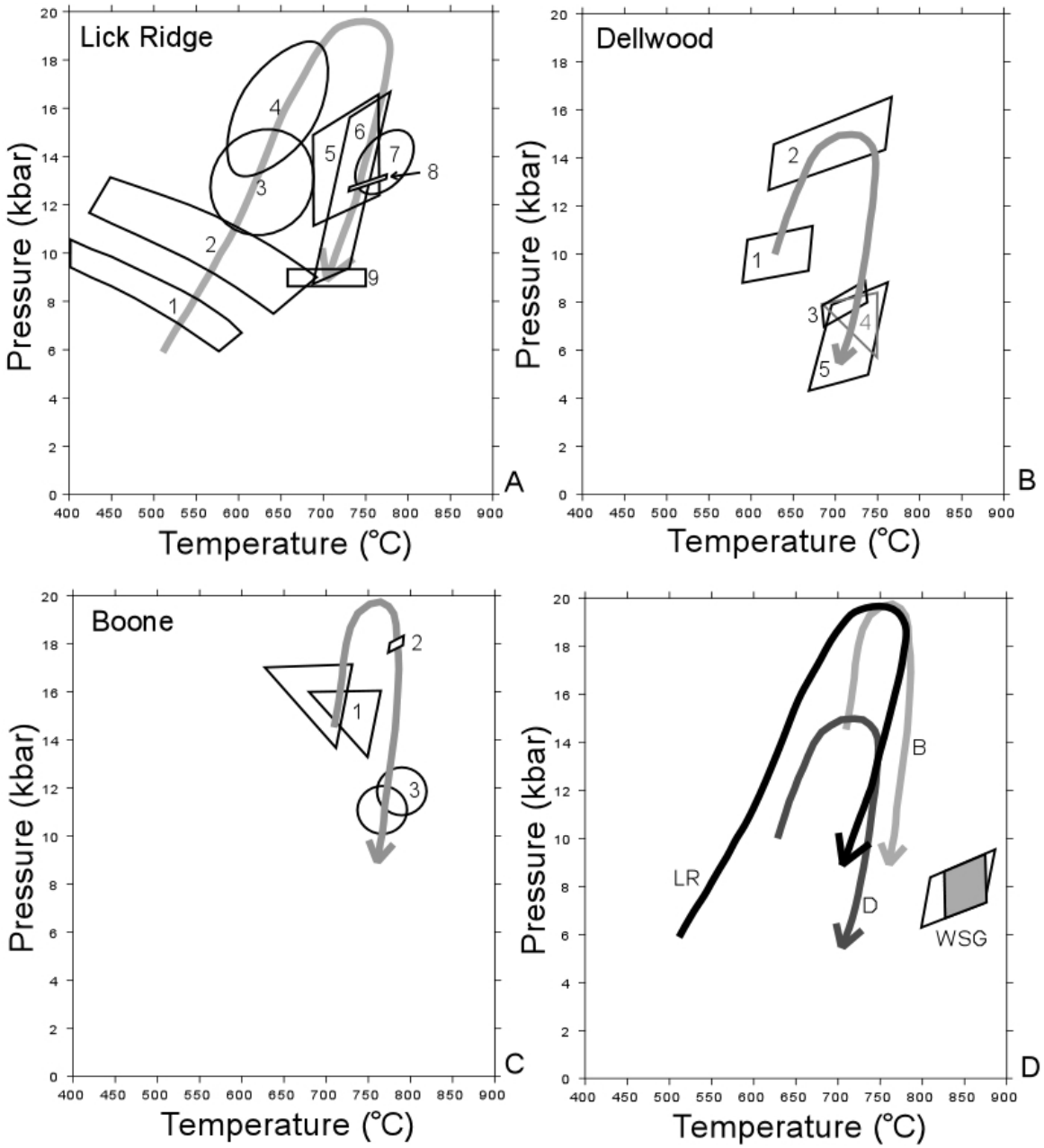

Figure 3.8. P-T estimates from western North Carolina metabasites. (Legend follows).

Figure Legend 3.8. P-T Estimates from Western North Carolina Metabasites. A) Lick Ridge eclogite, fields (1) through (4): P-T estimates from inclusions in eclogite garnet (Page et al., 2003); (5) Estimates from high-Mg garnet, clinopyroxene, orthopyroxene, plagioclase, and quartz (Page et al., 2003); (6) Estimated conditions from symplectite assemblages (reactions [3,4] Table 3.2; this study); (7) estimate from Grt-Pl-Hbl-Qtz-H_2O, garnet rim assemblages (reactions [6-12], this study); (8) Omphacite-garnet equilibria, minimum pressure estimate (reactions [1,2]; this study); (9) P-T estimates from adjacent garnet amphibolites (Waters et al. 2000; Miller et al. 2006). B) Dellwood garnet granulite, DEL05-3B2. (1) Grt-Pl-Cpx-Qtz estimates based on inclusions in garnet, rxns [13-15], reduced silica activity; (2): Grt-Pl-Cpx-Qtz estimates, high-Mg garnet, matrix clinopyroxene, rxns [13-15], reduced silica activity; (3) P-T estimate from adjacent schist, MV02-7,Grt-Ms-Bt-Pl-Qtz-H_2O rxns [25-27]; (4) estimate from Grt-Pl-Hbl-H_2O, garnet rim assemblages, rxns [16-24]; (5) estimate from symplectites after clinopyroxene, reactions [3,4]). C) Boone retrograde eclogite: 1) Hbl-Qtz-Grt-H_2O equilibria based on inclusions in garnet, rxns [28-37]; 2) Minimum pressure from Grt-Omp-Qtz equilibria, using reintegrated omphacite composition of Abbott and Greenwood (2001), rxns [1,2]; 3) Retrograde garnet rim reactions, Grt-Pl-Hbl-Qtz-H_2O rxns [6-12]. D) Compilation of P-T pathways, with additional estimate of conditions from Winding Stair Gap migmatitic gneiss, from Moecher et al. (2004).

(equations 16-24, Figure 3.8B field (2)). The path continues with nearly isothermal decompression at granulite to upper-amphibolite facies, indicated by estimates based on retrograde metamorphic reactions (reactions 3-4 and 16-24). Estimates from the adjacent schist (~ 7-9 kbar and 675 – 740 °C, sample MV02-7) coincide with the retrograde path estimated for the Dellwood metabasite.

P-T estimates from hornblende-rich samples from the Dellwood metabasite body (e.g. HP-amphibolite sample DEL03-3B, Figure 3.2B) overlap with estimates from Cpx-rich HP granulite (DEL03-3B2, Figure 3.2A). Estimates of 14-16 kbar at 660-740 °C were obtained using Cpx-Pl-Grt-Qtz equilibria, reduced silica activities (0.50), and mineral compositions from sample DEL03-3B.

New P-T estimates from Boone metabasites (Figure 3.8C) define a clockwise loop with inferred peak conditions at eclogite facies and nearly-isothermal decompression through garnet granulite or upper-amphibolite facies. Hornblende-garnet-quartz equilibria (reactions 28-37, Figure 3.8C, field (1)) based on inclusion compositions in garnet indicate conditions of 14 – 17 kbar at 625 – 750 °C, consistent with prograde garnet growth at upper-amphibolite to eclogite facies conditions. TWQ estimates (reactions 1, 2; using reintegrated omphacite compositions and clinopyroxene inclusions in garnet, Figure 3.8C, field (2)) suggest a minimum pressure of ~18 kbar at 775 °C, similar to previously reported estimates of ~16 kbar at 720 °C (Abbott and Greenwood, 2001). Isothermal decompression is indicated by estimates of 10-13 kbar at 725 – 825 °C (Figure 3.8C, field (3)) based on garnet rim-plagioclase-hornblende equilibria (equations 6-12). The high temperatures (~800 °C) indicated from garnet rim equilibria may be directly related to the formation of coarse-grained diopside-plagioclase symplectites after omphacite: the breakdown of omphacite and development of coarse Pl + Di symplectites (Figures 3.2F, 3.3E) may have been enhanced by isothermal decompression at elevated temperature (Anderson and Moecher, 2007). P-T estimates are compiled in Figure 3.8D to produce nested P-T paths interpreted as a record of HP Taconic metamorphism in the central and easterm Blue Ridge that has survived widespread Acadian and Alleghanian overprinting. P-T estimates from Winding Stair Gap are included, and indicate granulite facies conditions at ~7-9 kbar and 800 – 875 °C.

Timing of HP Metamorphism

Regional metamorphism in the Dellwood basement complex and surrounding are of the central Blue Ridge is manifested by the migmatization of a range of precursor sedimentary and igneous lithologies. Zircons from leucosome and melanosome of migmatitic biotite-plagioclase gneiss (Figures 3.9, 3.10) sampled ~6 km north of the Dellwood metabasite body were analyzed by ion microprobe to constrain the timing of regional metamorphism. An age of 456 + 17.5/-13.5 Ma (94% C.I.) was determined using the "zircon age extractor" plot function of Isoplot V.3.5 (Ludwig, 2003, Sambridge and Compston, 1994). Figure 3.10.A is a weighted average of the concordia ages determined from 14 analyses of zircons separated from migmatite (DEL03-1) and the leucosome (DEL03-1L). Paleozoic-aged spots, with "correlation of concordia ellipse"

values below 0.4 were culled and ommitted from this calculation as well as three points determined to have ages younger than 400 Ma. A concordia age of 444 ± 16 Ma (2σ) (Figure 3.10.B) results from the weighted average of eight points from seven zircon grains separated from the late leucosome (DEL03-1L). A wide range of ages from Paleoproterozoic (~1800 Ma) through Alleghanian (~320 Ma) were determined from ion probe analysis of zircons from this sample (Appendix H). The Taconic ages determined from the smaller-sized zircon population suggest that near-peak thermal conditions and melting were achieved at *circa* 456 Ma. Larger (1 mm long) zircons separated from the same migmatite have considerably older (1.0 – 1.3 Ma) ion-probe core ages. The wide range of ages determined from older, potentially detrital cores implies that the migmatite's protolith is of sedimentary origin.

In support of a Taconic age for regional metamorphism, an ^{40}Ar-^{39}Ar hornblende plateau age of 449 ± 2 Ma was obtained from hornblende separated from the Dellwood metabasite body studied here (Kunk et al., 2006; similar ages were obtained Dallmeyer, 1975), consistent with cooling through the closure temperature of Ar in hornblende at *circa* 7 m.y. after attainment of metamorphic peak temperature. The zircon geochronology of the central Blue Ridge, and the data determined from migmatites DEL03-1, DEL03-1L is discussed further in Chapter 4.

Discussion

Comparison of Subduction P-T Paths

P-T pathways of circum-Pacific and Alpine-Himalayan paleosubduction zones exposing transitional blueschist-eclogite facies rocks are plotted with P-T paths from the Blue Ridge metabasites (this study) in Figure 3.11A. Most of the paths resulting from the subduction of oceanic crust and arc trench sediments never exceed temperatures of 550 °C, thus conforming to the definition of low-T eclogite (Carswell, 1990). All of the calculated P-T paths from the central and eastern Blue Ridge occur at temperatures that are distinctly higher (~200 °C hotter) than paths determined for circum-pacific and Alpine-Himalayan belts. Prograde P-T estimates determined for the Lick Ridge eclogite (Page et al., 2003) overlap somewhat with the retrograde circum-pacific P-T paths, indicating that a Franciscan-type tectonic setting for the eastern Blue Ridge during the Taconic cannot be completely ruled out on the basis of P-T estimates. However, these higher temperatures indicate that the eastern Blue Ridge HP assemblages are more appropriately considered medium temperature eclogites (and granulites) (550-900 °C; Carswell, 1990), typical of tectonically thickened continental crust. The metamorphic conditions experienced during subduction and eduction of low-T versus medium-T eclogites are different. Low-T blueschist-eclogite belts can be overprinted by low-P amphibolite/greenschist assemblages during adiabatic decompression or with continued heating during decompression ("western alpine type endmember" of Ernst, 1988), or nearly coincident retracing of the prograde path during retrogression ("Franciscan type"; Ernst, 1988) resulting in blueschist facies overprinting of low-T eclogite (Ernst, 1988;

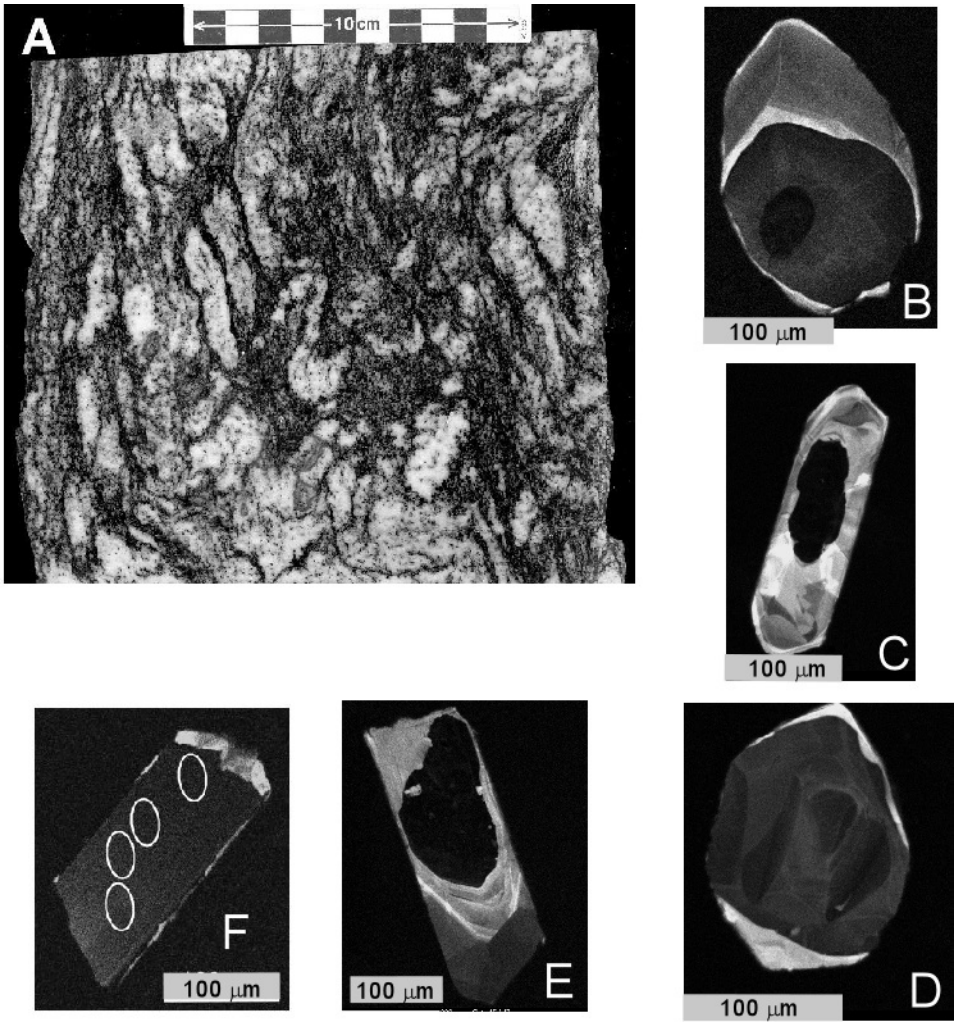

Figure 3.9. Images of central Blue Ridge migmatite, Sample DEL03-1. A) Scan of slab, central Blue Ridge migmatite, DEL03-1 with folded cm-scale leucosomes. B-F CL images of representative analyzed zircon grains.

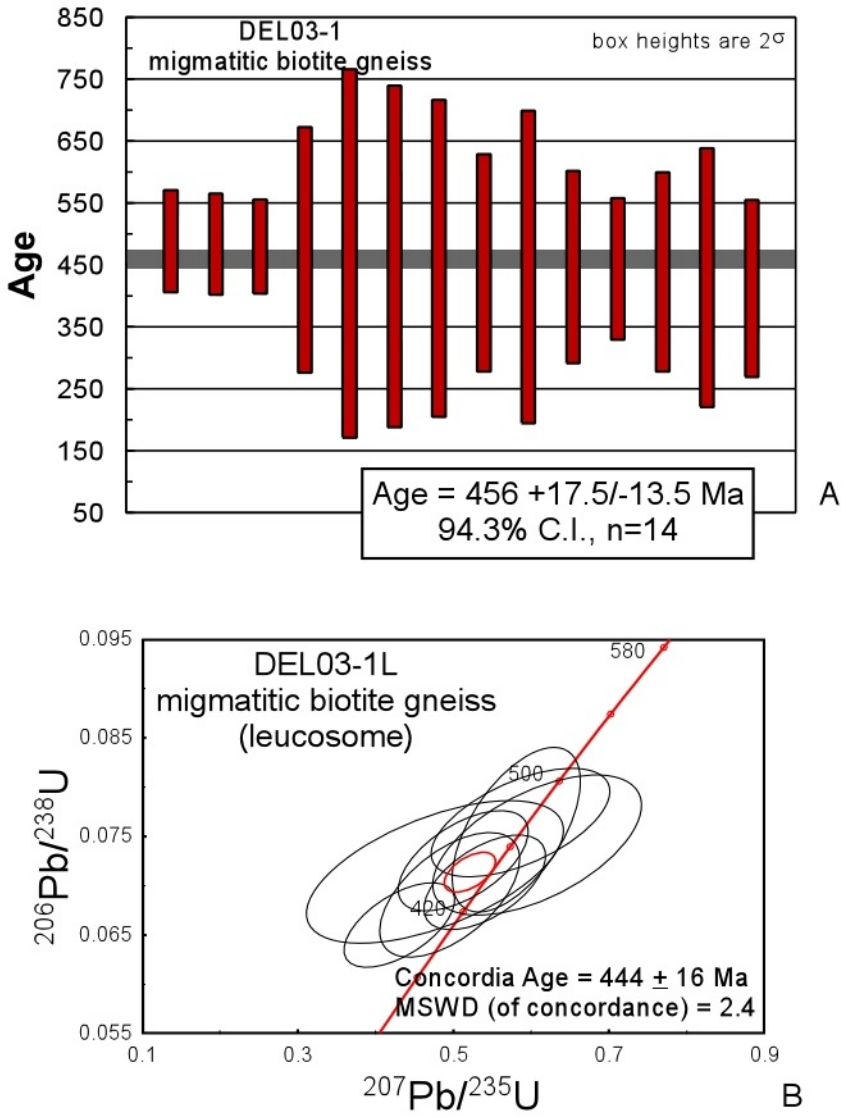

Figure 3.10. U-Pb zircon ages from central Blue Ridge migmatite sample DEL03-1. A) U-Pb age of 456.5 ± 17/-13.5 Ma (94% C.I.) was calculated from a weighted average of 14 ion-microprobe spots from migmatite and leucosome. B) Concordia age determined from the weighted average of zircons separated from late leucosome, 444 ± 16 Ma (2σ).

Tsujimori et al., 2006). In contrast, the P-T paths of Blue Ridge metabasites indicate prograde P-T conditions at amphibolite facies, peak conditions in the lower eclogite or garnet-granulite facies, and retrograde conditions at granulite or amphibolite facies.

In Figure 3.11B, P-T paths from the Blue Ridge metabasites are compared to P-T paths determined from eclogites of the Pakistan Himalaya, WGR (Norway) and the Variscan orogeny of Europe. Eocene UHP (coesite-bearing) eclogites from the Kaghan Valley region of the Pakistan Himalaya are interpreted to have formed from the subduction of Indian plate continental crust below the Kohistan arc to the north (Parrish et al., 2006). WGR eclogite facies metamorphism resulted from the subduction of Baltica beneath Laurentia during the Scandian tectophase of the Caledonian orogeny (e.g. Andersen et al., 1991; Cuthbert et al., 2000). Maximum P-conditions generally decrease from micro-diamond + coesite-bearing gneiss and UHP eclogite in the north (Moldefjord region, Dobrzhinetskaya et al., 1995; Wain, 1997) towards lower P-T conditions preserved near Sunnfjord further to the south (Krogh, 1980; Cuthbert et al., 2000; Engvik et al., 2000; Labrousse et al., 2004). P-T paths from the late Paleozoic Variscan (Hercynian) orogeny of Europe include data from the Bohemian Massif, Schwartzwald, Massif Central and Iberian Massif. Although the geologic history of the HP, low- to medium-T units of the Variscan belt is controversial, these P-T pathways appear to have resulted from the collision of Laurasia and Gondwana. An early (Devonian) phase involved the subduction of oceanic crust. A second (early Carboniferous) stage characterizes the Variscan orogeny and produced P-T paths that are nearly identical to the Blue Ridge metabasite paths (Figure 3.11B). Thinned continental crust was subducted into the mantle *circa* 340 Ma, followed by a slab break-off event (Davies and von Blankenburg, 1995) and rapid, buoyancy-driven exhumation at 340-330 Ma (van Breeman et al., 1982; Carswell and Jamtveit, 1990; Dallmeyer et al., 1992; Costa et al., 1993; Kröner et al., 1998; O'Brien, 2000). The prograde path calculated from retrograde eclogites of the Odenwald (Will and Schmädicke, 2001) is nearly identical to the prograde path of the Lick Ridge eclogite (Page et al., 2003). The P-T loop of the retrograde eclogites from Oberpfalz Forrest (O'Brien, 1989a, b) is nearly identical to the path calculated here for the Dellwood garnet granulite (Figure 2.11B). P-T estimates from Winding Stair Gap granulite (Moecher et al., 2004) are similar to estimates from Variscan granulites (e.g. Cabo Ortegal, Kuijper et al., 1985).

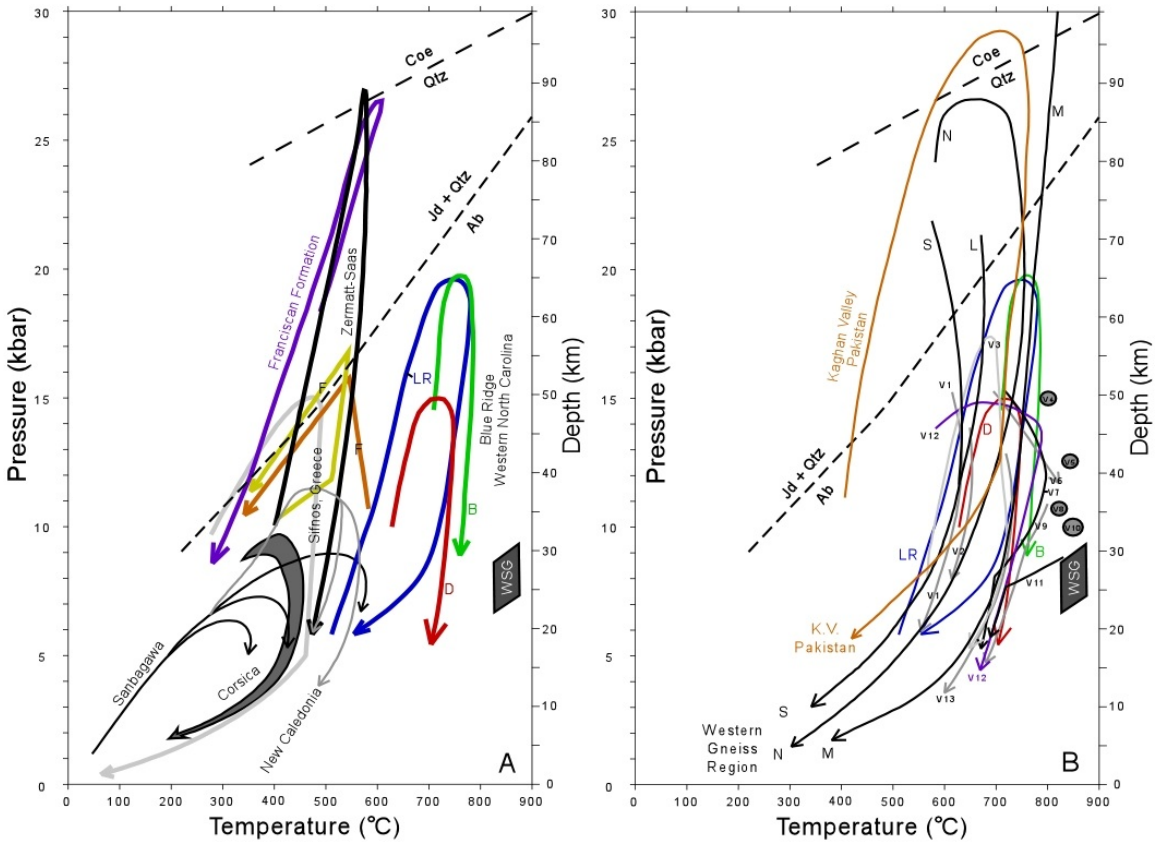

Figure 3.11. Comparison of circum-Pacific/Alpine-Himalayan and continental subduction P-T Paths. (Legend follows).

Figure Legend 3.11. A) P-T Paths from Subducted Oceanic Crust and Arc-Trench Sediments (Blueschist Belts and Associated Low-T Eclogites) Compared with P-T paths of HP Complexes of Western North Carolina. Data from: Sanbagawa: Kunugiza et al. (1986); Corsica: Gibbons et al. (1986); Stifnos: Schliestedt (1990); Zermatt-Saas: Bucher et al. (2005); Franciscan Fm: Tsujimori et al. (2006); Krogh et al. (1994);Wakabayashi, (1999). Blue Ridge estimates from Figure 3.8D and references therein; LR = Lick Ridge eclogite; B = Boone retrograde eclogite; D = Dellwood metabasites; WSG = Winding Stair Gap migmatite. B) P-T paths from continental subduction belts compared with P-T paths of HP-complexes of western North Carolina. Data from: Kaghan Valley: Parrish et al. (2006); Western Gneiss Region: Labrousse et al. (2004), [M = Moldefjord, N = Nordfjord, L = Lavik, S = Sunnfjord]; Variscan Orogen: O'Brien et al. (1990); V1 Munchberg: Franz et al. (1986); V2 Münchberg: Blümel (1986); V3 Odenwald: Will and Schmädicke (2001); V4 Limousin eclogite: Bernard-Griffiths and Jahn (1981); V5 Bragança/Morais: Munhá and Marques (1987), V6 Rouergue: Briand et al. (1988); V7 Oberpfalz: O'Brien (1989a); V8 Bragança/Morais: Munhá and Marques (1987); V9 Oberpfalz: Blümel (1983); V10 Cabo Ortegal: Kuijper et al. (1985); V11 Lyonnais: Dufour (1985); V12 Oberpfalz: O'Brien (1989b); V13 Schwartzwald: Klein and Wimmenauer (1984). Blue Ridge estimates from Figure 3.8D and references therein.

Implications for the Blue Ridge Tectonics

The similarity between P-T paths of the Blue Ridge metabasites and continental subduction complexes (Figure 3.11B) supports a model with HP-metabasites of western North Carolina having formed in a continental subduction complex. Peak pressure conditions from Blue Ridge metabasites allow for the estimate of burial/subduction of crustal material to depths of at least 65 km. The nearly-isothermal trend of decompression paths (Figure 3.8D), new zircon U-Pb and hornblende ^{40}Ar-^{39}Ar age estimates from the Dellwood metabasites of the central Blue Ridge basement complex, and preservation of prograde growth zoning in garnet are consistent with rapid eduction of the central and eastern Blue Ridge to depths of 25-30 km.

There are other consistencies with the hypothesis that parts of the central and eastern Blue Ridge are exhumed continental crustal subduction complexes. These are 1) the presence of peridotites and 2) widely reported mega mélange/disrupted terrane/block-in-matrix fabrics from the eastern and central Blue Ridge. Garnet peridotites ("orogenic peridotites", "peridotite massifs", "alpine-type peridotites") are a common feature of the

dozen-or-so continental subduction complexes that have been investigated (Brueckner and Medaris, 2000). Although there are no garnet peridotites in the central or eastern Blue Ridge, chromite dunites and websterites are fairly common. The central and eastern Blue Ridge could be considered a lower-P analog to the WGR of Norway. Prograde garnet growth in the Dellwood metabasite is consistent with intrusion at shallow to intermediate depths (20-50 km) followed by prograde metamorphism that occurred as the metabasite descended (Brueckner and Medaris, 2000). However, more data, including age constraints and trace element trends are required to confidently categorize the Dellwood metabasite and numerous km-scale alpine ultramafic masses (dunites, websterites, harzburgites, pyroxenites, and serpentinized equivalents) of the western Blue Ridge basement (Merschat and Cattanach, 2008) and eastern Blue Ridge mélange that lack evidence for magmatic emplacement (e.g. Webster-Addie, Buck Creek, Day Book, Woody, Dark Ridge meta-ultramafic bodies) (Raymond, 1995; Swanson et al., 2005; Ryan et al., 2005; Warner and Hepler, 2005; Peterson and Ryan, 2009).

Structurally, the central and eastern Blue Ridge differ from the adjacent western Blue Ridge in western North Carolina in that they contain elements typical of subduction complexes. Horton et al. (1989) included the Jefferson terrane in his list of "disrupted terranes" referring to blocks of heterogeneous lithologies with heterogeneous ages set in a matrix of schist that are common in mélange complexes. In western North Carolina, the Jefferson terrane includes the Ashe Metamorphic Suite and the central Blue Ridge metabasites described here. Raymond et al. (1989) subdivided the southern Blue Ridge into four tectonostratigraphic terranes based upon mélange distribution. The "Cullowhee terrane" occurs at the western edge of the eastern Blue Ridge, and contains lithologically mixed fragments of western basement (Sherwood terrane) and eastern Blue Ridge rocks (Toe terrane). High-grade metamorphosed mélanges with block-in-matrix structure are potentially *the* dominant structural style of the eastern Blue Ridge and the Cullowhee terrane. Block-in-matrix structures consist of blocks of amphibolite, biotite-gneiss, granitic orthogneiss, and calc-silicate clasts ranging from cm- to km-scale, and matrices include mica schist, biotite migmatite, and biotite schist (Raymond et al., 1989). Lacazette and Rast (1989) also describe a "mega-mélange" at Chunky Gal Mountain that may extend from northern Georgian into parts of Virginia. It was originally proposed by Anderson and Moecher (2009) that this mega-mélange formed in the western North Carolina Blue Ridge due to the westward subduction of Mesoproterozoic basement rocks and Neoproterozoic cover sequences (Ashe-Tallulah Falls-Coweeta Group) that were thrust beneath the Laurentian margin during the Lower through Middle Ordovician to produce a continental crustal subduction mélange. This mélange includes the central Blue Ridge terranes as well as the Mars Hill terrane (usually ascribed as a western Blue Ridge terrane), and is referred to here as the eastern Blue Ridge mélange after Lacazette and Rast (1989), although it is virtually identical to the Cullowhee terrane of Raymond et al. (1989).

P-T estimates for the two-mica schist analyzed from the Dellwood basement complex (MV02-7) resulted in a disparity in pressure estimates relative to the Dellwood metabasite P-T estimates (7-9 kbar for the two-mica schist, versus 14-16 kbar for the

metabasite). A similar situation has been noted in the WGR of Norway, and led to a longstanding argument related to the disparity in P-T estimates between mafic eclogites, pelitic schist, and felsic orthogneiss (e.g. Cuthbert et al., 1983; Krabbendam et al., 2000; Cuthbert et al, 2000). Three alternative solutions to the WGR problem appear pertinent here: 1) the Dellwood metabasites were tectonically emplaced into country rock (including orthogneiss and pelitic schist) that never experienced HP conditions; 2) the country rock, taken as the entire Dellwood basement complex, was subjected to and equilibrated to HP conditions, but felsic rocks, including the two mica schist (MV02-7), reequilibrated to a low pressure assemblage whilst the map-scale mafic pods retained their HP record through metastability; or 3) Devonian strike-slip faulting has translated domains within the central and western Blue Ridge, juxtaposing low-P blocks against high-P blocks.

Polarity of Subduction

Determining the polarity of Taconic continental subduction in western North Carolina is nontrivial due to widespread late Paleozoic retrograde metamorphism and deformation, the latter involving large-scale strike-slip (likely several hundred kilometers) and thrust (~260 km) translation. Anderson and Moecher (2009) proposed westward subduction of crustal material below the Laurentian margin, echoing the conclusions of previous studies that include Bird and Dewey (1970), Brown (1970), DeWindt (1975), Rast and Kohles (1986), Hanan and Sinha (1989), Drummond et al. (1994), Lissenberg et al., (2005), Tull et al., (2007), Barineau et al. (2008), and Holm-Denoma and Das. (2008).

Seismic studies have produced data that potentially support a model of westward subduction of continental crust below the Middle Ordovician Laurentian margin. Seismic reflection images produced by the Consortium for Continental Reflection Profiling (COCORP) (Figure 3.12) show a set of west-dipping reflectors below the Charlotte belt and Carolina Slate belt of Carolinia labeled "J" in Figure 3.13, 3.14. The reflectors dip ~18^{o} to the northwest and are visible between 6.0 and 9.0 s (~18-27 km). Sub-horizontal reflectors below reflector "J" at 11 – 12 s occur near Moho depths, and may indicate the top of the present-day mantle (Cook et al., 1979; Cook and Vasudevan, 2006). Reflector J indicates that a significant westward-dipping structure is preserved below the Blue Ridge thrust sheet. These reflectors are tentatively correlated here as the lower extension of the eastern Blue Ridge mélange. If this correlation is correct, the rock units immediately below "J" may contain lithologies that can be correlated to surface exposures in the central and eastern Blue Ridge including high-grade migmatites, granulites, and eclogites. The top of reflector "J" can be restored to the central Blue Ridge-eastern Blue Ridge boundary by displacing the Blue Ridge thrust sheet approximately 240 km towards the southeast, assuming the upper sheet is 10 km thick, and the reflector maintains a constant slope of 18^{o}. However, this restoration estimate does not consider Silurian-Devonian strike-slip transpression that potentially has a profound effect on a reconstructed cross section (e.g. Dennis, 2007). Subsequent

COCORP seismic reflection profiling conducted further south, near the southern boundary of the Carolina Slate belt, did not show evidence for a reflector similar to reflector "J" (Cook et al., 1981). Hibbard et al. (2010) interpret this same "reflector J" as the Silurian-aged (pre ~430 Ma) suture between Carolinia and Laurentia, having formed via continental subduction during the "Cherokee" orogeny. Other possibile interpretations are that the west-dipping reflector represents the top of an oceanic crust reflector related to an Ordovician peri-Laurentian island arc (e.g. Mac Niocaill et al., 1996, Horton et al., 2010; McClellan et al., 2007) or an Ordovician continental arc built on the peri-Laurentian margin (Holm-Denoma and Das, 2010).

In a study of Ordovician volcanic-arc rocks of the central Appalachian Piedmont of Maryland and Virginia, Horton et al. (2010) conclude that Ordovician volcanic and plutonic arc rocks occur throughout the Appalachian orogen from Newfoundland to Alabama. Magmatic activity spans a 30-35 Ma interval from 483 Ma (Occaquan Granite; Aleinikoff et al., 2002) to 453 $\pm$ 4 Ma (Chopawamsic Formation) and 448 $\pm$ 4 Ma (Quatico Formation; Horton et al., 2010). No polarity model is proposed for the Maryland-Virginia region.

In the Talladega Belt of Alabama and Georgia (Figure 3.15) Holm-Denoma and Das (2010) interpreted a mid-Ordovician back-arc basin to have formed above attenuated crust of the Laurentian margin above a west-dipping subduction zone. The study is based on U-Pb zircon ages, geochemical and isotope data and geologic mapping. There are significant differences in the tectonic setting between the Taladega Belt and the central and eastern Blue Ridge of western North Carolina. Specifically, there is no indication of a Taconic HP metamorphic event in the Talladega Belt (Tull, 1978; Guthrie et al., 1995) and metamorphism is constrained to the interval between 360 and 320 Ma (McClellan et al., 2007). An alternative interpretation of the Ordovician volcanic and plutonic rocks of the Talladega belt was made by McClellan et al. (2007) who propose that the Hillabee Greenstone represents the southernmost extension of an Early to Middle Ordovician arc complex that formed outboard of Laurentia.

A detailed petrologic investigation of the Elkahatchee quartz diorite, the largest exposed pluton of the eastern Blue Ridge, led to the interpretation that the parental magmas of the Elkahatchee quartz diorite formed by continental margin magmatism associated with the westward subduction of oceanic crust beneath Laurentia (Drummond et al., 1994). U-Pb zircon ages of 496 $\pm$ 14 and Rb-Sr whole-rock ages of 490 $\pm$ 28 Ma (Russell et al., 1987) were interpreted as crystallization ages of the Elkahatchee quartz diorite. More recent SHRIMP-RG based U-Pb zircon studies of the Elkahatchee pluton determined ages as young as 370 Ma, Proterozoic xenocrystic zircons, and older Paleozoic xenocrystic zircons (Tull et al., 2009). The study of Tull et al. (2009) concluded that the Elkahatchee pluton is likely a complex, diachronous map unit, and pre-Taconic subduction in the Alabama-Georgia Appalachian orogen was considered questionable.

An investigation of the Baltimore Mafic Complex (BMC), the largest mafic complex in the Appalachians, led to the interpretation of ensialic magmatism. Hanan and Sinha (1989) suggested that BMC peridotites and gabbros formed in an ensialic back arc

basin to the west of the James Run volcanic suite, both of which resulted from magmas produced by a westward dipping subduction complex. Sinha et al. (1997) interpreted the tectonic setting of the BMC as a sub-arc plutonic complex that formed at 489 ± 7 Ma.

Geophysical modeling studies also support the concept of westward subduction. Specifically, Coakley and Gurnis (1995) proposed that westward subduction occurred below the Laurentian margin based on lithospheric modeling of far-field tilting of the Michigan Basin to accommodate the deposition of the Black River and Trenton stratigraphic intervals. The best-fit model invokes westward subduction of a slab of negatively buoyant crust, descending at moderate dip (20-30°) for 10-15 Ma. Subduction initiated along the eastern margin of Laurentia at ~470 – 460 Ma and lasted for 10 – 15 Ma (Coakley and Gurnis, 1995).

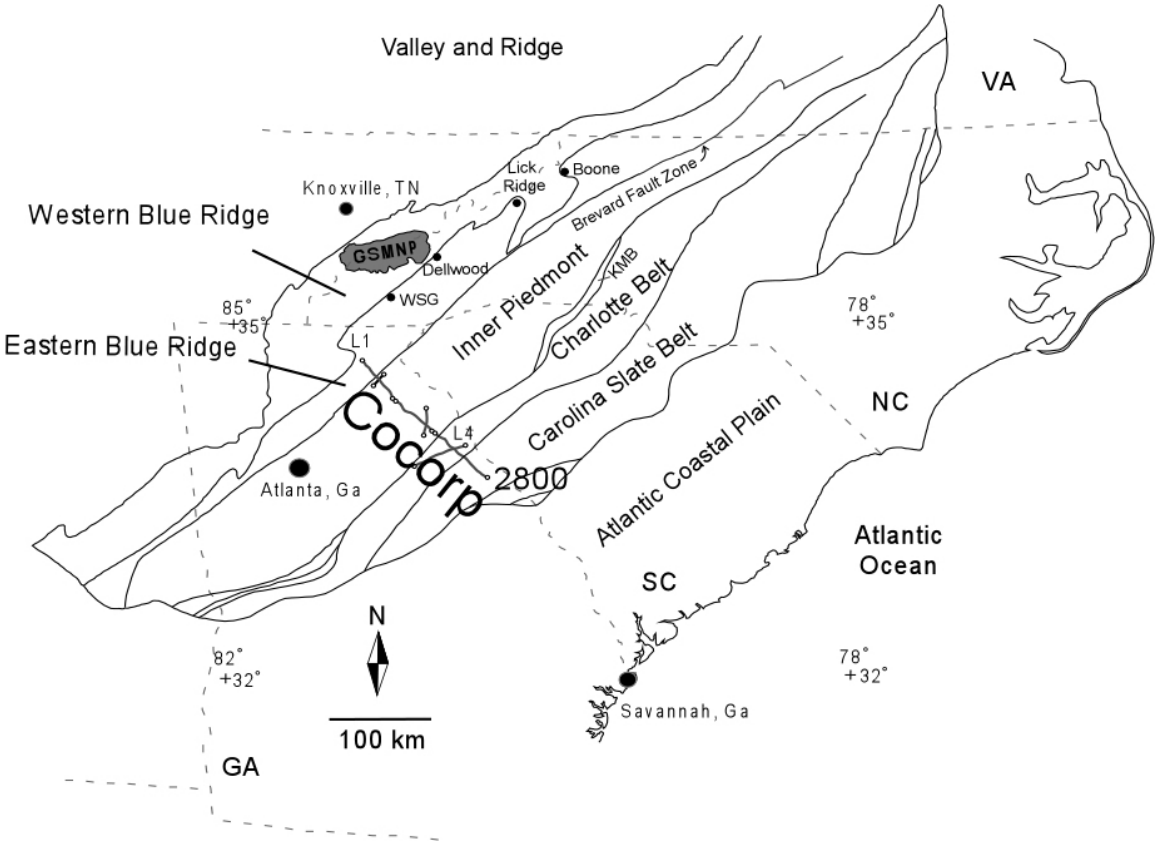

Figure 3.12. Location of COCORP seismic profile line 1. Blue Ridge thrust sheet, northeastern Georgia, modified from Cook et al., (1979).

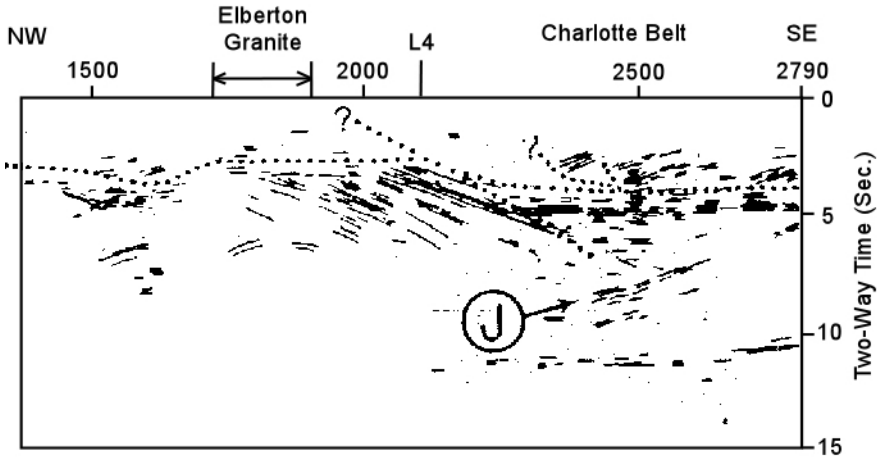

Figure 3.13. Line drawing of major events on COCORP line 1. From Cook et al. (1979).

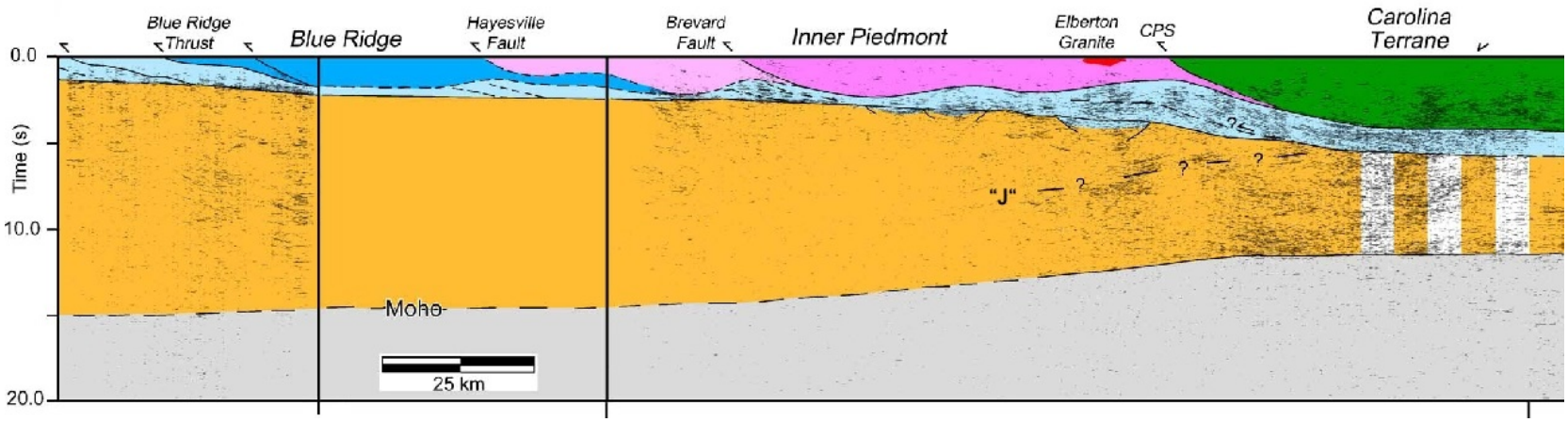

Figure 3.14. Interpreted seismic data from reprocessed seismic lines. TN-1, GA-1, GA-5, and GA-8, Cook and Vasudevan (2006). West dipping reflector is labeled "J".

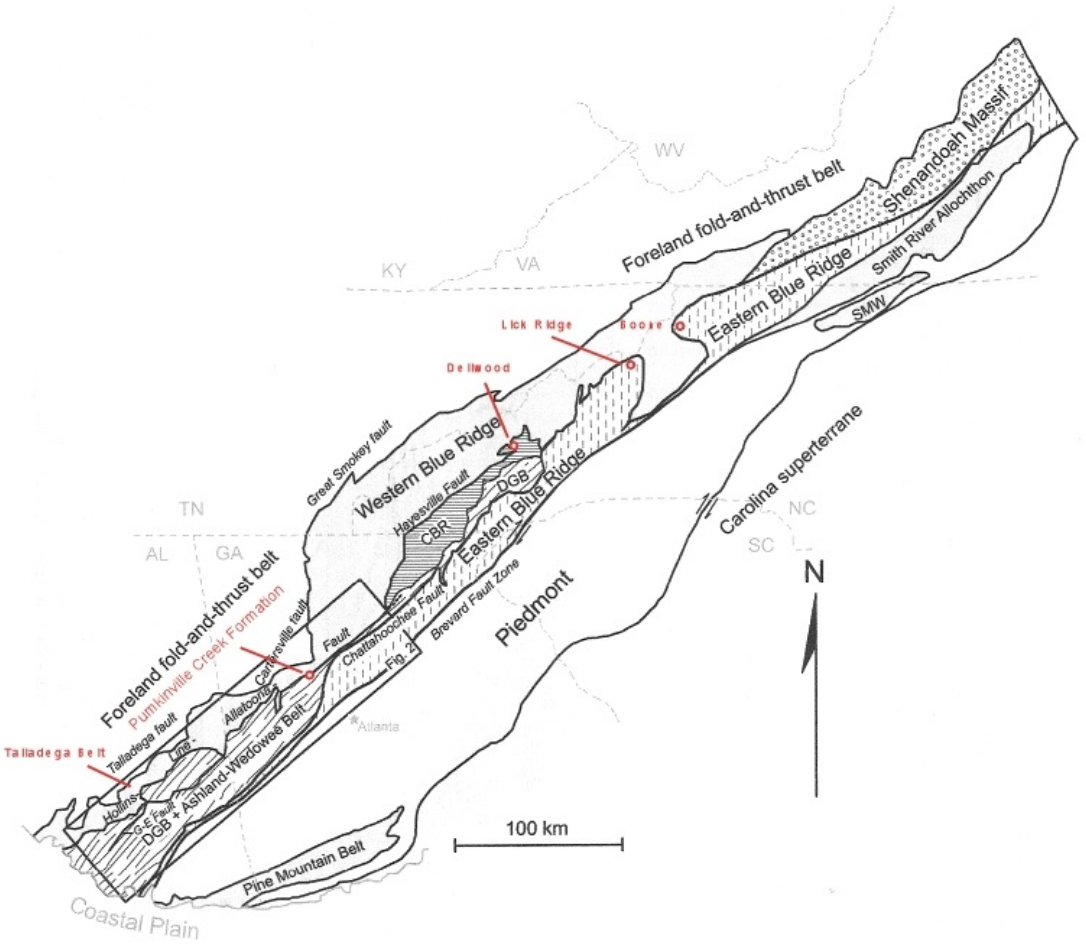

Figure 3.15. Location map with Talledega Belt and Pumpkinville Creek Formations. Also shown are the Dellwood, Lick Ridge and Boone locations in North Carolina. Modified from Holm-Denoma and Das, 2010. Abbreviations: DGB-Dahlonega Gold Belt, CBR-central Blue Ridge, G-E fault-Goldwater-Enitachopco fault, SMW Sauratown Mountain window.

Devonian Transpression and Tectonic Models

Paleomagnetic data from the northern Appalachian terranes identified several arcs within the Iapetus Ocean during the Early to Middle Ordovician. These include a peri-Laurentian arc at ~10-20°S, an intra-oceanic arc named the Exploits arc at ~30°S, and a peri-Avalonian arc at 50-60°S (Mac Niocaill et al., 1996). Reproductive communication of Celtic fauna between the peri-Avalonian arc, Exploits arc, and the Precordillera suggest that these terranes were well separated from the Laurentian margin prior to collisional events along the Laurentian and South American margin (Mac Niocaill et al., 1996). The paleomagnetic and paleontological interpretations require an open Ordovician ocean adjacent to the Appalachian margin and preclude a continent-continent collision between Laurentia and Gondwana during the Taconic-Famatinian orogeny (e.g. Dalla Salda, 1992a,b, Dalziel et al., 1996, Mac Niocaill et al., 1996). A paleogeographic reconstruction (after Mac Niocaill et al., 1996) for the Arenig (Lower Ordovician; ~478-471 Ma) is shown in Figure 3.16. Although no paleomagentic data were used to constrain the position of potential Southern Appalachian Ordovician-aged magmatic arcs, some characteristics of the pre-Taconic tectonic setting of southern Laurentia can be inferred from the Ordovician magmatic arc complexes that extend from Newfoundland to Alabama (Horton et al., 2010). Specifically, the tectonic setting of the Taconic orogeny of the central and eastern Blue Ridge of North Carolina may have involved multiple arcs (Mac Niocaill et al., 1996), bimodal volcanism on the Laurentian margin (e.g. Holm-Denoma and Das, 2010), and the accretion of terranes of Gondwanan affinity (e.g. Carolinia, a.k.a. the Carolina Super terrane, Carolina Zone, the Carolina terrane, Hibbard, 2000; Hibbard et al., 2002). Extensive along-strike variation is inferred from Alleghanian metamorphic ages in the Talledaga Belt (McClellan et al., 2007) versus Taconic metamorphism in the central and eastern Blue Ridge (Moecher et al., 2004, Miller et al., 2006, 2010).

In a comparative study of the terranes of the Southern Blue Ridge, Dennis (2007) proposed a Late Silurian paleogeographic reconstruction of the Appalachian orogen that can be used to estimate the extent of Devonian strike-slip tectonic reconfiguration events (Figure 3.17). Dennis (2007) interprets the adjacent terranes of the Blue Ridge of North and South Carolina as having contrasting metamorphic ages. Despite extensive Ordovician plutonism in the Inner Piedmont terrane, there is no evidence of an Ordovician metamorphic event. Peak metamorphism occurred in the eastern and central Blue Ridge at ~460 Ma, in the Inner Piedmont at ~360 Ma, and in Carolinia at ~540 Ma (Dennis, 2007). In the Late-Silurian reconstruction of Dennis (2007), the Piedmont terrane consists of an Ordovician plutonic arc (Tugaloo terrane) and a Silurian basin (Cat Square terrane) that are restored to a position near the New York promontory. Dennis (2007) suggests that the Inner Piedmont, and possibly parts of the eastern Blue Ridge were translated at least 400 kilometers south along the Brevard fault zone. The kinematic change from compressional to dextral strike-slip motion is proposed to have occurred after 430 Ma. Translation may also have occurred along the Burnsville Fault, interpreted as a reactivated portion of the Taconic suture that occurs between the Lick Ridge eclogite

and the Mars Hill terrane of the western Blue Ridge (Adams et al., 1995). In the Late-Silurian reconstruction of Dennis (2007), no attempt is made to extrapolate the southern extent of Carolinia.

Several alternate tectonic interpretations relative to docking of Carolinia (Carolina superterrane) based on the age and provenance of the Cat Square terrane, geochronologic studies, and foreland basin stratigraphy have been proposed (e.g. Bream, 2002; Hatcher 2002). In Merschat et al. (2010), Carolinia initially collided near the New York Promontory. Intrusion of the Corncord-Salisbury plutonic suite into Carolinia (e.g. McSween and Harvey, 1997), upper amphibolite metamorphism of the Cat Square terrane (Merschat and Kalbas, 2002), and 360-340 Ma Ar/Ar cooling ages from the western edge of Carolinia (Dallmeyer et al., 1986) support the interpretation that Carolinia overthrust the Cat Square terrane, part of the Tugaloo terrane, and the Laurentian margin during the Neoacadian Orogeny. Consequently, details related to the docking of Carolinia are presently a subject of debate.

The tectonic history of the Inner Piedmont is important for modeling the Taconic orogeny of western North Carolina. Perhaps the most widely-accepted model calls for the eastward subduction of oceanic crust beneath the Piedmont arc (Figure 3.18) due to the interpretation that Ordovician arc-granites in the Piedmont were derived by the closure of a small ocean basin between the Laurentian margin and the Piedmont arc (e.g., Hatcher, 1987, Stewart et al., 1997; Abbott and Greenwood, 2001; Miller et al., 2006). Dennis (2007) suggests that the Piedmont arc was not outboard of western North Carolina during the Taconic orogeny, and consequently the model of eastward subduction of MORB beneath the Piedmont arc may need to be reconsidered.

The P-T paths of the central and eastern Blue Ridge indicate that crustal material was subducted to depths of 50-65 kilometers and metamorphosed at HP conditions (upper amphibolite, eclogite, and granulite facies) . It would appear unlikely that medium-T eclogites and the continental-collision-type subduction complex inferred here would form spontaneously, and a driving mechanism such as the collision with an outboard terrane with the Laurentian margin is sought out here. Although a collision between Laurentia and Gondwana has been proposed previously (Dalla Salda, 1992a,b; Dalziel et al., 1997), paleomagnetic and paleontologic studies (e.g. Mac Niocaill et al., 1996) as well as stratigraphic considerations (Thomas et al., 2002) suggest that such a collision never occurred. Given the Silurian reconstruction of Dennis (2007) as well as tectonic models developed from the Talladega-Dahlonega belts of Alabama-Georgia (McClellan et al., 2007; Holm-Denoma and Das, 2010), a model is proposed here in which a southern extension of Carolinia collided with the peri-Laurentian margin at ~460 Ma (Figure 3.19, 3.20). In Figure 3.17.B, Carolinia extends as far south as the present day Virginia-North Carolina border. The southern limit of Carolinia during the Ordovician is unknown due to the presence of the Brunswick (Charleston) terrane and the Wiggens-Suwannee suture along the southern Appalachian margin (Hatcher, 2010). It is proposed here that Carolinia extended south of present-day Virginia, and collided with the Laurentian margin in the vicinity of the Tennessee embayment during the Taconic orogeny. The change in the age of metamorphism from the Dahlonega gold belt (Middle Mississippian)

to the Cowrock terrane (Middle Ordovician) is potentially related to the southern geographic limit of Carolinia. Only one episode of prograde metamorphism has been recognized in the Dahlonega Gold belt (McConnell and Abrams, 1984). The Dahlonega gold belt and other eastern Blue Ridge units in northern Georgia yield hornblende $^{40}Ar/^{39}Ar$ plateau ages ranging from ~330-332 Ma (Dallmeyer, 1988) indicating cooling through ~500°C occurred in the Middle Mississipian. In contrast, the Cowrock and Cartoogechaye blocks contain mafic-ultramafic complexes that experienced HP granulite facies metamorphism in the Taconic (Lake Chatuge and Buck Creek; Meen, 1988; Emilio, 1998), with granulite-facies conditions of the Cartoogechaye terrane (Winding stair gap locality) U-Pb zircon (TIMS) ages yielding 458 ± 1 Ma (Moecher et al., 2004).

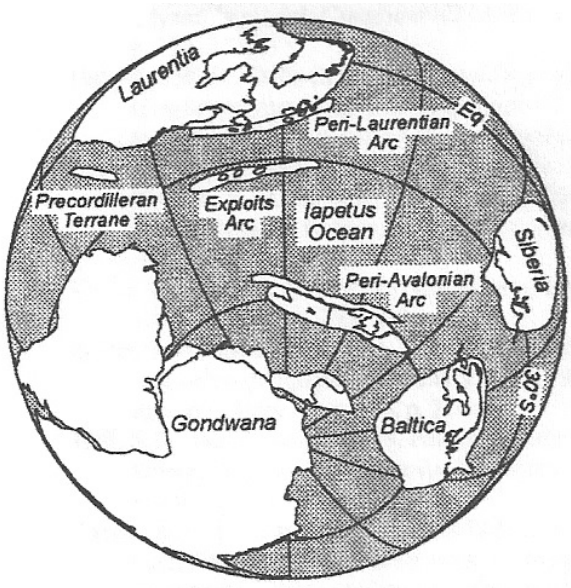

Figure 3.16. Arenig paleogeographic reconstruction of the Iapetus Ocean. (Mac Niocaill et al., 1996).

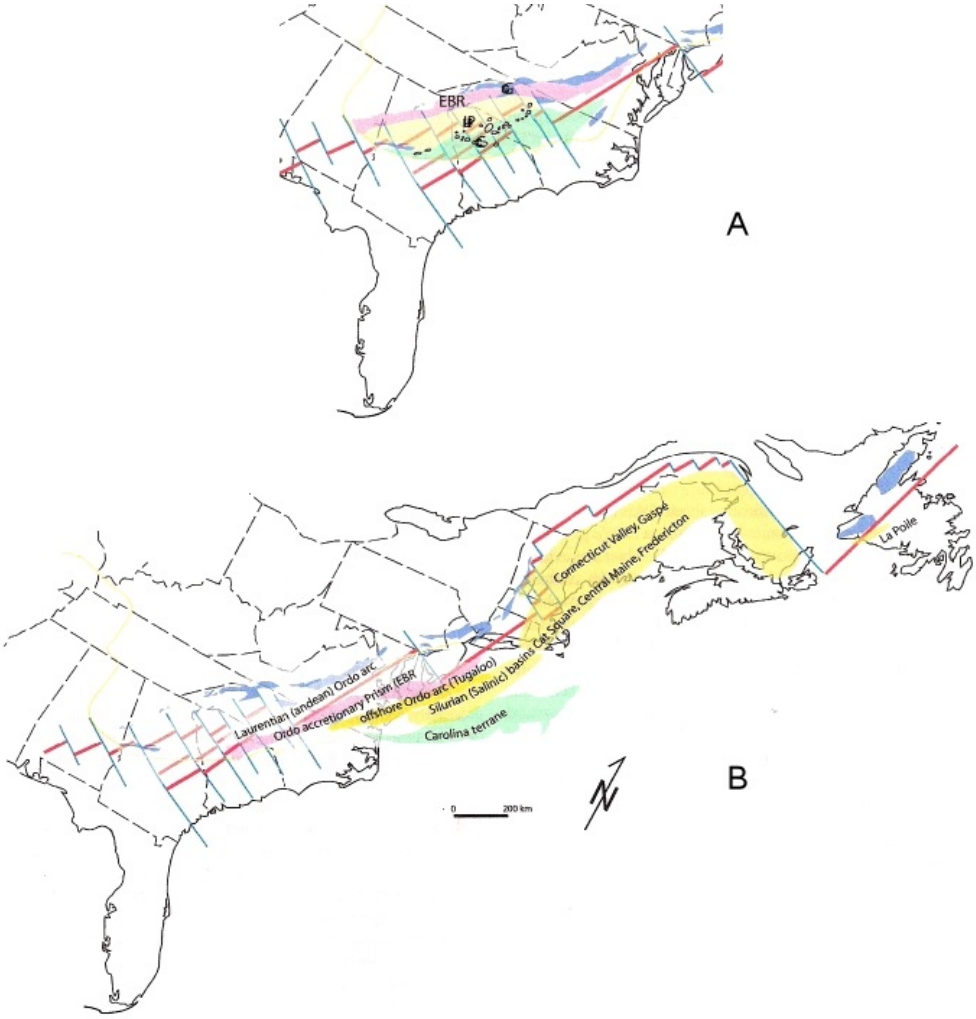

Figure 3.17. Late-Silurian reconstruction. A) Present-day distribution of terranes. G-Grenville basement, EBR-eastern Blue Ridge, IP-Inner Piedmont, C-Carolinia/Carolina terrane. B) Late Silurian reconstruction with Silurian basins restored to the New York Promontory region. From Dennis (2007).

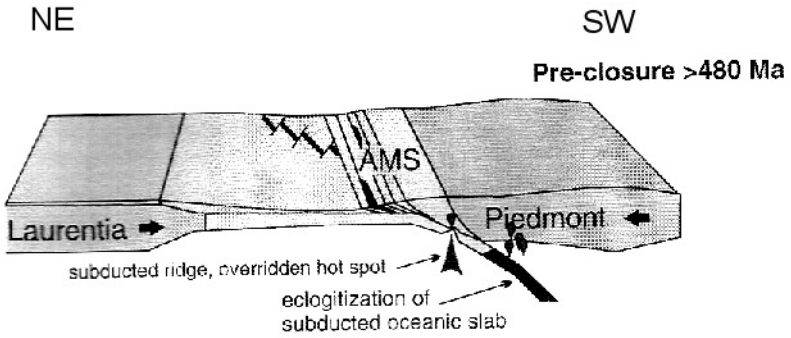

Figure 3.18. Tectonic model with eastward subduction below the Piedmont arc. (from Miller et al., 2006).

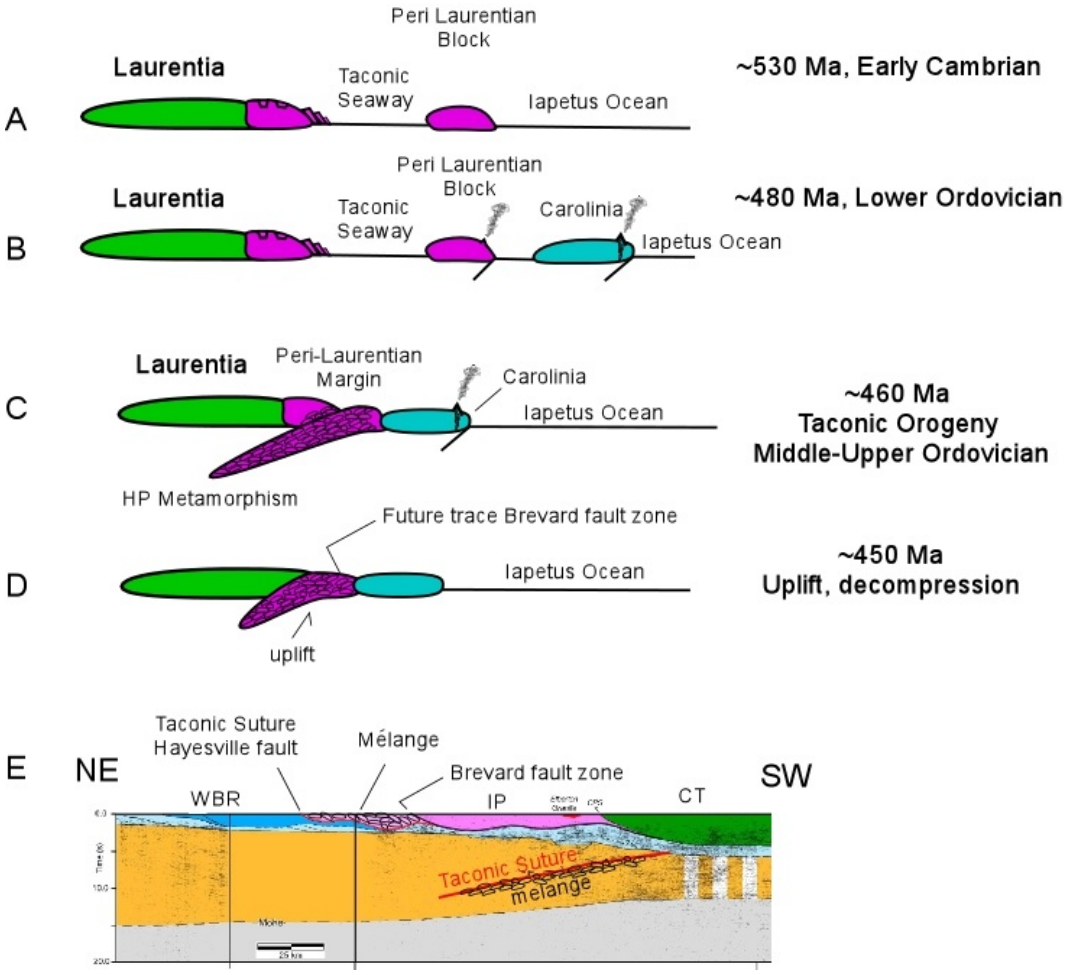

Figure 3.19. Tectonic schematic of the Taconic orogeny of western North Carolina. A) Rift to drift stratigraphic interval with carbonates deposited at the margin of the Taconic Seaway (Hibbard et al, 2007, McCausland et al., 2007). B) Ordovician magmatic arcs form along the Laurentian margin over an interval of 30-35 Ma, from ~483 to ~448 Ma (Horton et al., 2010). C) Southern Carolinia collides with the peri-Laurentian block, resulting in subduction of Mesoproterozoic continental crust, Cambro-Ordovician sea floor, and Precambrian-Ordovician siliciclastic cover sequences. D) Uplift, decompression, and waning volcanism at ~450 Ma. E) Interpretations shown on reprocessed COCORP seismic image (present-day), with surface and proposed subsurface locations of the Taconic suture and continental-collision melanges. WBR-western Blue Ridge, IP-Inner Piedmont, CT-Carolinia terrane. Seismic image from Cook and Vasudevan, 2006.

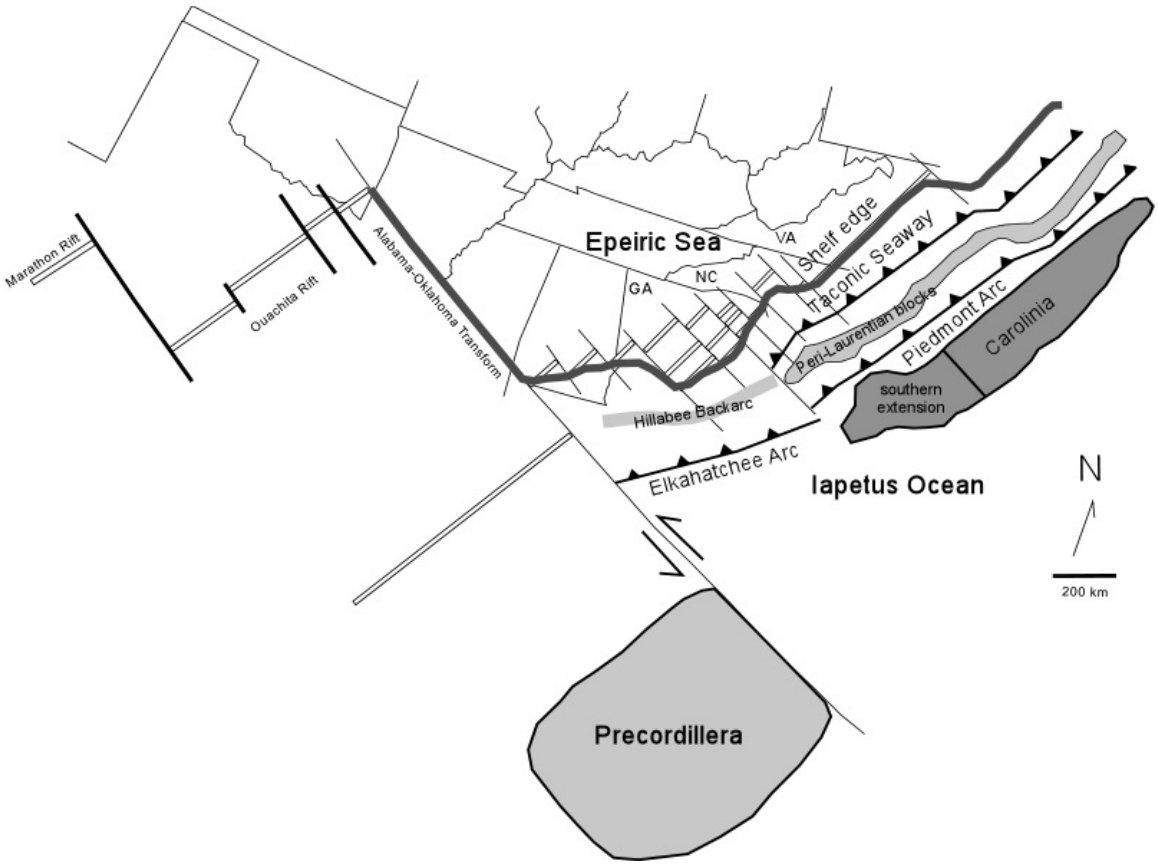

Figure 3.20. Paleogeographic reconstruction of the southern and central Blue Ridge at ~480 Ma. Elkahatchee arc is positioned across modern Florida (Tull et al., 2007). Piedmont arc outboard of peri-Laurentian blocks. Carolinia is shown extending to the south, prior to Taconic collision with the central Blue Ridge. Exploits arc and peri-Avalonian arcs (Mac Niocaill, 1996) not shown. Modified from Thomas and Astini (1996), Dennis (2007), and Tull et al., (2007).

Comparison with the Norwegian Caledonides

Several comparisons can be made between the eastern Blue Ridge mélange and the HP lithologies produced by the subduction of Baltica beneath Laurentia during the Scandian tectophase of the Caledonian orogeny. Although eclogites are much more common in the WGR relative to the eastern Blue Ridge mélange, in both locations most eclogite outcrops are rimmed by amphibolite. In the WGR, km-scale eclogite bodies, lenticular pods, and meter-decimeter scale tabular eclogite bodies are preserved without retrogression to amphibolite facies (Cuthbert et al., 2000). In the southern Blue Ridge, amphibolite-facies retrogression appears to have been more complete – eclogites and HP Grt-Cpx rocks appear to be preserved only as km-scale mafic occurrences (Lick Ridge,

Boone, Dellwood, Lake Chatuge). Evidence for Taconic HP metamorphism is therefore relatively scarce in the Blue Ridge, having been overprinted by retrograde metamorphism on a larger scale. Felsic eclogites occur within the WGR, but are lacking, were completely overprinted, or await discovery in the eastern Blue Ridge mélange. Felsic Bt-Hbl-Ep-Ttn-Plag-Kfs gneiss (the same assemblage as felsic gneiss of the WGR) is abundant in the eastern Blue Ridge mélange, and may represent orthogneiss that experienced HP conditions during Taconic subduction but experienced widespread, late overprinting. Integrated geochronologic-thermobarometric studies of the WGR demonstrate that rapid exhumation and cooling followed peak Scandian HP/UHP metamorphism (Terry et al., 2000; Labrousse et al., 2004; Walsh et al., 2007). Late Devonian rapid exhumation resulted from crustal extension that continued into the Mesozoic (Osmundsen et al., 2003). Western Norway (and the opposing continental margin in East Greenland; Gilotti and McLelland, 2007) did not experience subsequent phases of continental collision that would have tectonically modified Caledonian crust in the manner that occurred in the southern Appalachians. The isothermal decompression segment of P-T paths for eastern Blue Ridge mélange metabasites (Figure 3.8D) and the sole hornblende ^{40}Ar-^{39}Ar cooling age of 449 Ma (Kunk et al., 2006) suggest that rapid exhumation of the eastern Blue Ridge mélange occurred immediately after attainment of peak pressures. Limited geochronology (Dallmeyer, 1975; Connelly and Dallmeyer, 1993; Moecher et al., 2005; Kunk et al., 2006) hints at potential Silurian and Devonian events in the Blue Ridge province, but Late Devonian to Early Carboniferous ("Neo-Acadian") and Carboniferous (Alleghanian) orogenesis overprinted Taconian structures, fabrics and assemblages to the extent that it is impossible in many rocks to recognize any relict features.

CHAPTER 4: ZIRCON AND MONAZITE U-PB AND TH-PB GEOCHRONLOGY OF BASEMENT ROCKS, DELLWOOD AREA WESTERN NORTH CAROLINA

Introduction

Lithologies from the eastern Great Smoky Mountain basement complex are sampled and analyzed in an effort to understand their origin and to resolve conflicting tectonic interpretations. Montes (1997) proposed that the migmatitic, biotite- and hornblende-biotite gneisses of the Dellwood basement complex are equivalents of the Tallulah Falls Formation, a Neoproterozoic amphibolite-bearing metaclastic cover sequence. Merschat and Cattanach (2008) classify similar Cartoogechaye basement complex rocks in the adjacent Clyde quadrangle as Mesoproterozoic to Neoproterozoic, but note that the stratigraphic relations are uncertain. Other workers, including Southworth et al. (2005a,b), mapped the basement complex rocks of the Dellwood quadrangle as a combination of Mesoproterozoic lithologies. The existence and location of the purported Hayesville fault also comes into question when considering the various basement units and the additional data presented here may offer further constraints. Montes (1997) and Montes and Hatcher (1999) locate the Hayesville fault near the western margin of the basement complex exposed in the Dellwood quadrangle. The presence of hornblende-bearing lithologies in the hanging wall, and the relative lack of hornblende-bearing lithologies in the footwall was used to locate the fault. Southworth et al. (2005a,b) mapped the location of the Hayesville fault ~5 kilometers further south at the contact between Mesoproterozoic migmatitic biotite gneiss (hanging wall) and Neoproterozoic metagraywackes of the Copperhill Formation (Ocoee Supergroup) in the footwall.

Another tectonic question is the location of the southwestern limit of the Mars Hill terrane. Ownby et al. (2004) suggest that the Mars Hill terrane (Figure 1.1) contains unusually old (as old as 1.8 Ga) basement lithologies with surface exposures near Sylva, Frankin, and Dellwood. Ownby et al. (2004) infer that the Mars Hill terrane potentially extends into Georgia, and may include the basement gneiss complex of the Dellwood area. In an effort to constrain the age of events in the central Blue Ridge basement complex and to resolve interpretive incongruities, samples were collected from outcrops in the Dellwood, Clyde, Whittier, Cove Creek Gap, Bunches Bald, Sylva North, Smokemont, Hazelwood, Fines Creek, Sylva North, and Lemon Gap quadrangles. Zircon and monazite U-Pb and Th-Pb ages were determined using SIMS (secondary ion mass spectrometry). New data presented here are discussed in the context of existing data sets from other locations to develop a regionally consistent tectonic model for the evolution of the southern Appalachian Blue Ridge.

Geologic Setting

Early geologic maps of the eastern Great Smoky Mountains include works of Kerr (1875), and Keith (1904). A detailed 1:24,000 scale geologic map of the Dellwood

quadrangle was produced by Hadley and Goldsmith (1963) as part of an investigation of the geology of the eastern Great Smoky Mountains. Hadley and Goldsmith recognized augen gneiss, granitoid gneiss and an older basement complex lithology named the "Carolina Gneiss" (Keith, 1904) that contains quartzose, muscovitic, and biotite gneisses, minor mica schist, layered hornblende-biotite gneiss, and amphibolite.

The North Carolina Geological Survey (NCGS) completed geologic mapping in sixteen of the 1:24,000 geologic quadrangles that make up the western half of the Asheville 1:100,000 scale geologic map (Cattanach and Merschat, 2005) and adjoin the eastern margin of the present study area. During the course of the investigation, NCGS geologists abandoned older map units, including the Carolina Gneiss and Roan Gneiss and proposed new formation names. The central Blue Ridge Cartoogechaye terrane rocks investigated here are classified and mapped on the N.C. Geological Survey western half of the Asheville 1:100,000 scale map (Merschat and Cattanach, 2008) as 1) biotite gneiss; 2) mylonitic biotite gneiss; 3) felsic gneiss; 4) muscovite-biotite gneiss; 5) metagraywacke; and 6) amphibolite. In 2005, a 1:100,000 scale map of the Great Smoky Mountains National Parks region was compiled by the U.S. Geological Survey (Southworth et al., 2005a,b). Although the N.C. Geological Survey and U.S. Geological Survey maps abut at a longitude of 83^{o}E, the map units are somewhat different.

In the present study, the analyzed rocks have been classified as one of six lithologies. 1) "Biotite gneiss" is primarily composed of plagioclase, quartz and biotite, lacks the felsic porphyroclasts of the biotite augen gneiss, is commonly migmatitic, and often crosscut by late leucocratic dikes. 2) "Hornblende-biotite gneiss" contains both hornblende and biotite as a mafic phase and may be migmatitic. 3) "Muscovite-biotite gneiss" and schist occurs in the Dellwood and Clyde quadrangles and contains a greater abundance of muscovite relative to migmatitic biotite gneiss. 4) "Biotite augen gneiss" contains large (commonly > 1 cm) feldspar porphyroclasts suggesting a plutonic origin for the protolith of these metaplutonic rocks. Biotite augen gneiss includes a sample of Max Patch Granite from the Lemon Gap quadrangle, and a tectonized orthogneiss from the Ravensford body. Some mylonites appear to have formed from the deformation of biotite augen gneiss, (e.g. SC04-6, MV02-8) and are referred to as "mylonitic biotite augen gneiss" due to the mylonitic fabrics observed in thin section. 5) "Amphibolites" contain hornblende + plagioclase $\pm$ garnet, are distinctly more mafic, darker colored, and hornblende-rich relative to hornblende-biotite gneiss. Amphibolites are much less migmatitic relative to hornblende-biotite gneiss, although leucocratic layers and veins are common. The clinopyroxene-bearing "Dellwood metabasite" samples are plotted as amphibolites. The final lithologic category is 6) "metasedimentary cover rocks" that includes schists of the Great Smoky Group and Murphy Belt. Several map units used by the NC and US Geological Surveys contain layers or clasts of distinct rock types. In these situations, mineralogically distinct layers, pods or clasts of orthogneiss were sampled in an attempt to characterize the geochemistry of basement complex endmembers. In such a situation, the lithologic classification of a gneiss sample may not appear to resemble the map unit that was used to describe the formation as a whole.

Previous Isotopic Studies

Recent whole rock Pb and Sm-Nd isotopic investigations of the Appalachian orogen have concluded that the entire central and southern Appalachian basement complex (rocks older than 900 Ma) is exotic to Laurentia, and was accreted to Laurentia during the Grenville orogeny to form a suture that may coincide with the NY-AL lineament (Loewy et al., 2003; Fisher et al., 2010). Other Pb and Sm-Nd investigations (Tohver et al., 2004) have suggested that 1) the Mars Hill terrane of the southern Blue Ridge is in turn exotic with respect to the southern Appalachian "Grenville" basement complex; and 2) the Mars Hill terrane is of Amazonian provenance, with transfer of the Mars Hill terrane from Amazonia to Laurentia having occurred during the Grenville orogeny, but post ~1.15 Ga.

SIMS U-Pb studies of zircon have been widely applied to recognize the timing and distribution of Proterozoic magmatism in basement rocks of the Appalachians. Carrigan et al. (2003) determined that most of the larger (> ~100 μm) magmatic zircons from the western, central (including the Mars Hill terrane) and eastern Blue Ridge have rim material that formed *circa* 1000 Ma. Zircon core ages from the western Blue Ridge (NW of Hayesville and Fries faults) suggest the occurrence of magmatic events at 1020-1080 Ma, and 1130-1180 Ma. Zircons from eastern Blue Ridge basement formed during a magmatic episode that occurred at 1140-1170 Ma. Most of the SIMS analyses of magmatic zircons from Mars Hill terrane are considerably older with ages ranging between 1200-1300 and 1600-1800 Ma (Officer, 2003; Ownby et al., 2004; Berquist et al., 2005; Fisher et al., 2010).

Mesoproterozoic rocks of the Great Smoky Mountain National Park region (western Blue Ridge) were chronologically divided into four groups by U.S.Geological Survey scientists (Southworth et al, 2005a). The oldest rocks, "Group 1", consist of migmatitic biotite gneiss, hornblende-biotite gneiss, paragneiss, amphibolite, and ultramafic and mafic lithologies. Group 1 rocks appear to be widespread in the central Blue Ridge basement of the Dellwood and Clyde quadrangles, and the U.S. Geological Survey's "migmatitic biotite gneiss" has been correlated with lithologies mapped to the east as "Earlies Gap Biotite Gneiss" by the NCGS (Southworth, 2005a; Merschat and Wiener, 1988). Group 1 rocks were undated by Southworth et al. (2005a), however a leucocratic dike that cross cuts migmatitic biotite gneiss was sampled from the south end of Ela dome, and yielded a SHRIMP age of 1194 Ma. This magmatic event (intrusion of the dike) suggests a minimum age of 1194 Ma for migmatitic biotite gneiss and the Group 1 rocks. The 1194-1192 Ma dike is associated with leucocratic granite and porphyritic quartz monzonite, designated Group 2, and proposed to be the oldest dated rock in the western Blue Ridge. Group 1 lithologies were intruded by Group 3 rocks in a magmatic pulse that occurred between 1178-1116 Ma. Group 3 rocks may represent recycled material based on the presence of inherited zircon cores showing Group 2 ages of 1190 and 1180 Ma. Orthogneisses belonging to Group 3 include the Spring Creek Granitoid Gneiss, occurring east of the Pigeon River (1178 Ma, Southworth et al., 2005a; P. Berquist, 2004, oral comm.), foliated biotite granitic gneiss from the Bryson City dome

(1117 Ma), and monzogranitic gneiss occurring from east of the Pigeon River to the Cataloochee area (1148 Ma, P.Berquist, 2004, oral comm.) A major deformation event occurred between the plutonic emplacement of Group 3 and Group 4 rocks, between 1117 and 1081 Ma. Group 4 orthogneiss crystallized between 1081 and 1029 Ma and is comprised of porphyritic granite occurring at the center of Ela dome (1056 Ma), granodiorite occurring on the west side of Cove Mountain (1040 Ma, correlated with the Max Patch Granite occurring to the NW), and biotite augen gneiss occurring as L-S tectonites in the Qualla-Dellwood and Cherokee-Raven Fork belts (1029 Ma) (Southworth et al., 2005a).

Previous Th-Pb Monazite Studies

Kohn (2001) dated monazites of staurolite-, kyanite- and sillimanite-grade Great Smoky Group schists using chemical dating via EMPA (electron microprobe analyzer), and initially determined that regional metamorphism of the Great Smoky Mountains was an Acadian event, with a major age distribution peak at ~370 Ma, a minor hump at ~320 Ma, no ages older than 425 Ma, and none younger than 280 Ma. Kohn recommended that on the basis of his findings, the widespread interpretation of Taconic-aged regional metamorphism and Taconian tectonics in the Great Smoky Mountains should be revised. Kohn and Malloy (2004) re-analyzed monazites in Great Smoky Group schists using EMPA and SIMS methods, and interpreted age distribution plots to represent a single age of ~400 Ma, again linking Barrovian metamorphism in the western Blue Ridge to the Acadian orogeny. In yet another re-evaluation of monazite ages from the Great Smoky Group schists, Corrie and Kohn (2007) used the ID-TIMS method in conjunction with micro-drilling to determine unequivocally Taconic U-Pb monazite ages of 450 $\pm$ 5 Ma.

Eckert (2002) analyzed five samples of monazite from the central and western Blue Ridge using EMPA and determined ages of 487 $\pm$ 7 Ma from Great Smoky Group samples, 459 $\pm$ 7 Ma for the central Blue Ridge, and 449 $\pm$ 9 Ma for granulite facies metamorphism at Winding Stair Gap, findings that contradict Acadian metamorphism declared by Kohn (2001) and Kohn and Malloy (2004) and supporting the hypothesis that widespread amphibolite- to granulite-facies metamorphism in the central and western Blue Ridge was indeed Taconian. Eckert's monazite ages range from 349-575 Ma; younger dates may have resulted from Acadian (~380 Ma) lead loss.

Moecher et al. (2002) also determined Taconian ages for monazites from Grt-St-Ky-Ms-Bt gneiss of the central Blue Ridge, near the Hayesville fault (location MM-22 in this study) and two samples of Great Smoky Group schist: Grt-St-Ky-Ms-Bt-Qtz-Pl-Rt (location GT02-2 in this study), and Grt-Bt-Ms-Pl-Qtz metapsammites collected near Soco Gap. The majority of ages fell in the range 440-480 Ma (Taconian), some ages (5 of ~350 analyses) range from 360-410 Ma (Acadian), four rims appear Alleghanian ($\leq$ 330 Ma, and 18 points ranged from 520-540 Ma. This data set was interpreted as documenting the dominant phase of monazite growth resulting from Taconic metamorphism, with tentative weak overprinting occurring during the Acadian and

Alleghanian tectophases; the significance of the 520-540 ages is poorly understood (Moecher et al., 2002, 2003).

Hietpas et al. (2010) and Moecher et al. (2011)analyzed detrital monazite grains that were isolated from stream sediments of the French Broad River and its tributaries. Ion probe ages were determined from monazite cores separated from modern stream sediments that were transported from the eastern, central, and western Blue Ridge and the western Inner Piedmont. Resulting Th-Pb monazite age distribution plots largely record a single Taconic age of ~460 Ma, although zircon and monazite records some middle to late Paleozoic ages.

Methods

Secondary Ion Mass Spectrometry (SIMS)

Metamorphic rocks from the central and western Blue Ridge were slabbed with a rock saw and crushed by hand in a ceramic mortar and pestle. Heavy liquids and a Franz isodynamic separator were used to isolate zircons that were pipetted in liquid alcohol using a micro-pipetter under binocular microscope, dried, and mounted onto double-sticky tape. Epoxy was poured into one-inch round forms, allowed to cure, polished lightly, and imaged with the Cameca SX-100 microprobe at the University of Michigan using BSE and Cl detectors. U-Pb zircon ages were determined using the Cameca 1270 ion microprobe (SIMS) at the Keck Laboratory, UCLA using standard spot size analysis, the AS3 standard (1099 $\pm$ 3 Ma: Paces and Miller, 1993) as an age and U standard, oxygen "flooding" (P $\simeq$ 3 x 10^{-5} Torr) to increase Pb yield, and 5-10 analytical cycles or "blocks" for each spot. Data were reduced using ZIPS v3.0.4 (written by C.D. Coath) using measured $^{204}Pb/^{206}Pb$ to correct for common lead, and plotted with Isoplot v.3.50 (Ludwig, 2003). Unless otherwise noted, uncertainty is reported here at the 2σ confidence interval, while concordia diagrams are plotted at the 1σ confidence level.

Detailed protocols for $^{208}Pb/^{232}Th$ dating of monazite using the Cameca 1270 ion microprobe are presented in Harrison et al. (1995), Grove and Harrison (1999), and Hietpas et al. (2010). Monazites were analyzed using a $^{16}O^-$ primary beam current of ~4 nA, a spot size of 20 x 30 micrometers, and 7 analytical cycles or "blocks", using the UCLA monazite standard "544", having a determined age of 45 $\pm$ 1.4 Ma (Harrison et al., 1999). High-energy ions (-20 to –30 eV energy offsets) were used to analyze ^{208}Pb and Th species to mitigate potential matrix effects related to variable Th concentrations in monazite. A common lead correction, based on measured ^{204}Pb was applied to the data, after adjusting for intensity lost for high-energy $^{208}Pb^+$, and a $^{144}NdThO^{2+}$ isobaric interference resolved by calculations based on measured $^{143}NdThO^{2+}$. Although it is possible to use SIMS data to resolve U-Pb ages from monazite, the low U and Pb concentrations in the 544 standard are less than ideal for the application of the U-Pb method.

Sample Locations

Rock sample from the eastern Great Smoky Mountains were collected at outcrops that occur in the Dellwood, Bunches Bald, Clyde, Fines Creek, Cove Creek, Sylva North, and Whittier quadrangles. Metasedimentary rocks of the Ocoee Supergroup were collected within the Great Smoky Mountain National Park with the permission of the National Park Service. Samples include a wide variety of orthogneiss, paragneiss, migmatites, and amphibolites of the central Blue Ridge basement complex. Additional suites of rocks were collected at previously described locations including the Lick Ridge eclogite and Boone eclogite of the eastern Blue Ridge. Topographic maps showing sample locations, and a table with GPS coordinates are presented in Appendix I.

Petrology

Introduction

A considerable body of work has been published by other workers related to the petrography, lithologic contacts, and structural elements of the rocks exposed in the western, central, and eastern Blue Ridge of western North Carolina. Pertinent studies include projects undertaken by the U.S. Geological Survey (Hadley and Goldsmith, 1963; Southworth et al., 2005a,b), and investigations done by the NCGS (Merschat and Wiener, 1988; Cattanach and Merschat, 2005). An excellent geologic overview of the southern Appalachian orogen is given in Hatcher and Butler (1979). Other studies, containing more structural emphasis were published by Massey (2003), Moecher and Massey (2005), Raymond et al. (1989), Lacazette and Rast (1989), Stewart et al. (1997), Montes (1997), and Loughry (2010). The purpose here is to provide petrographic descriptions of the rocks that were sampled, to outline the rock classification strategy used here, and to summarize the structures observed in outcrop and thin section.

Biotite Gneiss

Biotite gneiss is light to dark gray, medium- to coarse-grained and is composed primarily of plagioclase, quartz, and biotite, with some K-feldspar (Figure 4.1). Mineral modes vary considerably, and some samples contain significant amounts of garnet and muscovite. Feldspar is generally more abundant than quartz, and biotite modes are variable (~10-60%) with higher abundances in melanosomes of migmatitic biotite gneiss. Accessory minerals include titanite, apatite, ilmenite, and zircon. Biotite gneiss is foliated, with the foliation defined by subparallel biotite crystals, muscovite crystals, quartz ribbons, and flattened feldspar grains. This gneissic layering (Figure 4.2) has been designated "S_2" by Eckert (1984), followed by Massey (2003) and Massey and Moecher (2005). S0 (bedding) and S_1, (an early schistosity parallel to bedding) have been recognized in psammitic and pelitic rocks of the metasedimentary cover sequences

(Massey, 2003; Massey and Moecher 2005), but not distinguished in basement orthogneisses and paragneisses of this study. S_3 is a non-penetrative fabric that deforms S_2 and is commonly seen in outcrop and evident at map scale as open- to tight-folds that may have an axial planar crenulation cleavage. Photographs of representative biotite gneiss lithology, with structural interpretations are shown in Figures 4.2 and 4.3. In thin section, the S_3 fabric is associated with brittle deformation of feldspar porphyroclasts, folded cleavages, and recrystallized quartz and titanite. Biotite gneiss is a common rock type in the central Blue Ridge, occurring as large (km-scale) mapable units and as discrete layers in straight gneiss or folded layered gneiss. Biotite gneiss is locally migmatitic, with well-developed leucosome-melanosome segregations, and widespread melt injections (apophyses) that indicate the occurrence of partial melting. Migmatitic biotite gneiss crops out in the southeastern Dellwood quadrangle, with notable locations and contact relations given by Hadley and Goldsmith (1963). Migmatitic biotite gneiss also is found to the west at Ela dome and at the southern margin of Bryson City dome (Southworth et al., 2005a). Some, if not most of the migmatitic biotite gneiss map units contain lenses and clasts of other rock types, specifically quartzofeldspathic gneiss, muscovite-biotite schist and gneiss, amphibolite, hornblende-biotite gneiss, and rare calc-silicate pods. Examples of lithologic mixing in migmatitic biotite gneiss can be seen at outcrop MV02-6 (Dellwood), where amphibolite, mica schist, and metagranite clasts occur in a matrix of migmatitic biotite gneiss. Other examples are found in the Cherokee-Raven Fork belt and Qualla-Dellwood belt west of Soco Gap and described by Southworth et al. (2005a). Lithologic mixing, specifically block-in-matrix structures having matrices composed of biotite migmatite and biotite schist (Raymond et al., 1989), occur throughout the "Cartoogechaye terrane" of Hatcher (2005) and "Cullowhee terrane" of Raymond et al. (1989), and are well exposed within a ~5 km-wide belt that extends from south of Sylva to Clyde, NC, between the Hayesville fault and the Chattahoochee-Holland Mountain fault (the Hayesville thrust sheet). The migmatitic biotite gneiss map unit of Southworth et al. (2005a) was correlated with the Earlies Gap Biotite Gneiss map unit (Carter and Wiener, 1999) that occurs further east in the western half of the Asheville 1:100,000 scale quadrangle. However Merschat and Cattenach (2008) distinguish Cartoogechaye terrane biotite gneiss that occurs in the Clyde, Canton, and Fines Creek quads (inferred Neoproterozoic) from the Earlies Gap Biotite Gneiss (Mesoproterozoic basement lithology) as different map units.

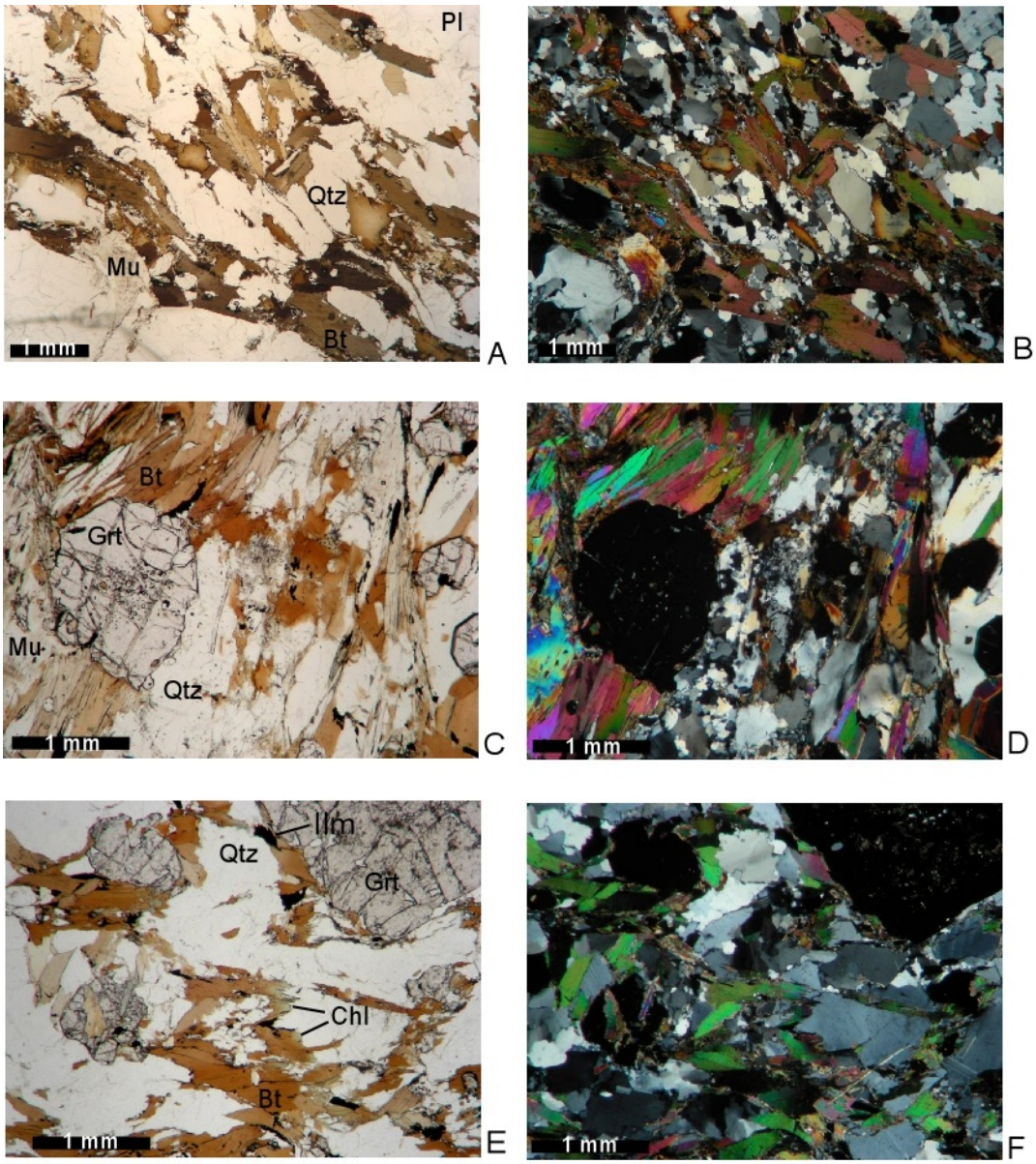

Figure 4.1. Photomicrographs of biotite gneiss. A) Sample DEL03-1, migmatitic biotite gneiss under plane-polarized light (PPL); B) crossed Nicols (XN); C) sample MM-22, migmatitic biotite gneiss, PPL; D) XN; E) sample JUN04-1B, biotite gneiss, PPL; F) XN. Figure 4.1 (continued): Mineral abbreviations: Qtz = quartz, Bt = biotite, Grt = garnet, Mu = muscovite, Pl = plagioclase.

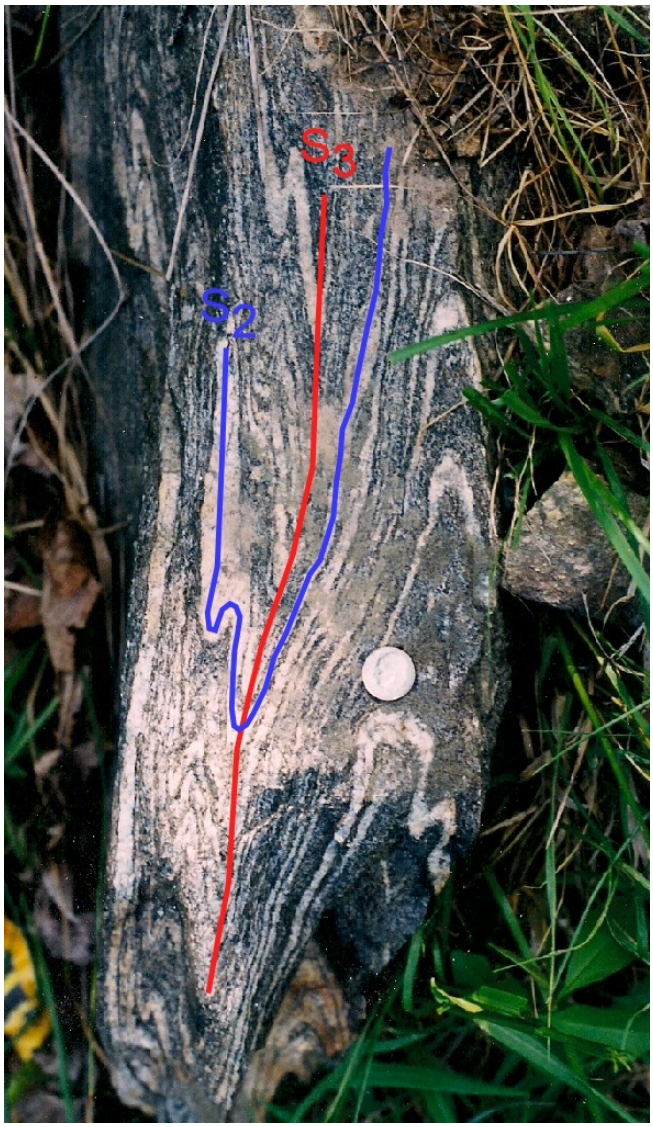

Figure 4.2. Biotite gneiss, sample DEL03-1, Dellwood quadrangle. S_2 is defined by felsic (white) and biotite (black) gneissic bands; S_3 is shown here as the axial plane defined by folded S_2 surfaces. Dime for scale.

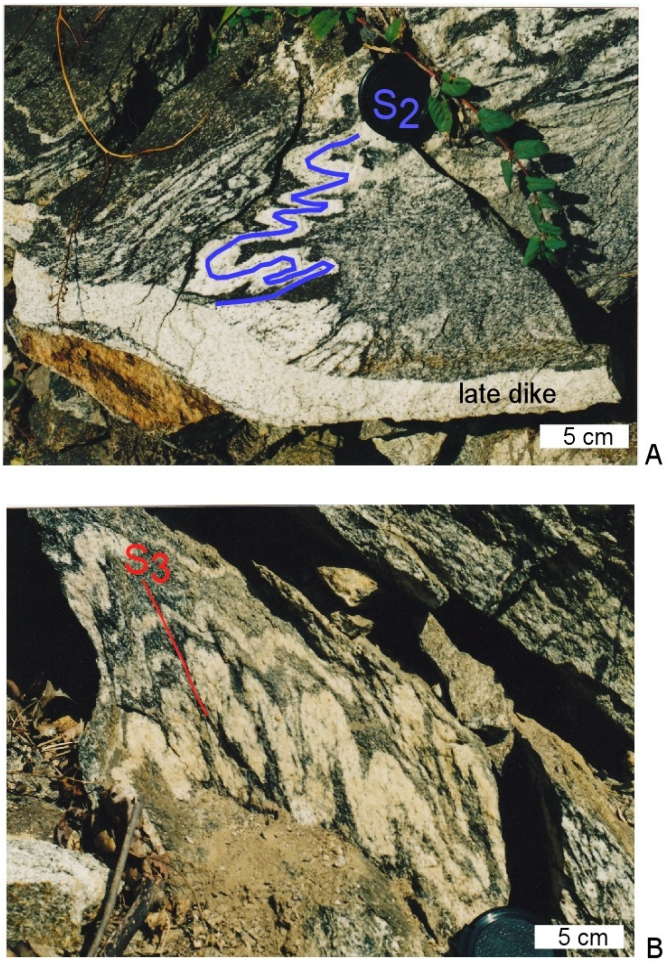

Figure 4.3. Migmatitic biotite gneiss sample HM03-3, Clyde quadrangle. A) Leucosome defines S_2 that was folded to produce F_3 folds, and crosscut by a late leucocratic dike. B) Isoclinal folds in migmatitic biotite gneiss, sample HM03-3, with late axial planar slip cleavage (S_3).

Hornblende-Biotite Gneiss

Hornblende-biotite gneiss varies from pale green to dark green in hornblende-rich occurrences. Some hornblende-biotite gneiss contains less hornblende and is medium-

gray in color. Major mineral components include alkali feldspar, quartz, hornblende, biotite and plagioclase with accessory titanite, epidote, apatite, garnet, ilmenite, spinel, and zircon (Figure 4.4). Large, map-scale bodies of migmatitic to layered hornblende-biotite and biotite-hornblende gneiss occur in the Dellwood quadrangle, and were mapped by Hadley and Goldsmith (1963) as a component of the now abandoned "Carolina Gneiss Formation". In the most recent regional-scale geologic maps, hornblende-biotite gneiss is mapped as a distinct Mesoproterozoic formation in the Dellwood, NC area (Southworth et al., 2005a), and is a component of Cartoogechayee terrane biotite gneiss in the Clyde, Sandymush, and Canton quadrangles that occur within the western portion of the Asheville 1:100,000 scale map (Merschat and Cattanach, 2008, Merschat and Wiener, 1988). Loughry (2010) distinguished three types of hornblende-bearing gneiss in the Dellwood quadrangle: 1) metaplutonic orthogneiss; 2) foliated and deformed orthogneiss equivalents; and 3) migmatitic hornblende-biotite gneiss. Massive orthogneiss occurs in the cores of the larger hornblende-biotite gneiss units, whereas strongly foliated and deformed hornblende-biotite gneiss occurs at the margins of large hornblende-biotite bodies near the contacts with the enclosing biotite gneiss (Loughry, 2010). Specific hornblende-biotite gneiss outcrops, including the southeast ridge of Purchase Knob, and Goat Rock Ridge, are described by Hadley and Goldsmith (1963). Photomicrographs are given in Figure 4.4; outcrop photographs are shown in Figure 4.5.

Biotite Augen Gneiss

Biotite augen gneiss varies in color from light to medium gray to reddish-brown and contains coarse augen composed of white to pink microcline and oligoclase in a matrix of foliated quartz, plagioclase, K-feldspar, and biotite. The augen allowed Hadley and Goldsmith (1963) to classify augen gneiss as a meta-plutonic rock, whereas other biotite gneisses exposed in the eastern Great Smoky Mountains, lacking coarse augen, were interpreted as a suite of metavolcanic rocks. Samples analyzed here include augen gneiss from the Ravensford body exposed along the Cherokee-Raven Fork belt (sample CH02-2B) and augen gneiss from the Qualla-Dellwood belt (location OS03-1, Figure 4.6). The Ravensford body, described in detail by Hadley and Goldsmith (1963) is strongly lineated, with the lineation defined by rods of oligoclase. Color varies between light and dark gray, depending on modal variations of plagioclase and biotite. In thin section, sample CH02-2B is strongly deformed, showing a well developed S-C fabric, expressed by highly fractured plagioclase crystals, with recrystallized quartz and titanite throughout. Major minerals include plagioclase, quartz, biotite, and alkali feldspar with minor muscovite, titanite, epidote, apatite, magnetite-ilmenite, zircon (Figure 4.7). Large (mapable) bodies of biotite augen gneiss are also exposed in the western half of the Dellwood quadrangle. Biotite augen gneiss occurs throughout the Dellwood basement complex, occurring as layers and pods, with occurrences classified as part of the Mesoproterozoic-aged Migmatitic Biotite Gneiss unit of Southworth et al. (2005a,b). There are considerable variations in mineral modes (e.g. feldspar, biotite, quartz, muscovite content) among the biotite augen gneiss rocks, suggesting that the rocks

making up this group may in fact be petrogenetically unrelated. Several samples of mylonite (Figures 4.8, 4.9) appear to have been derived from the ductile deformation of biotite augen gneiss.

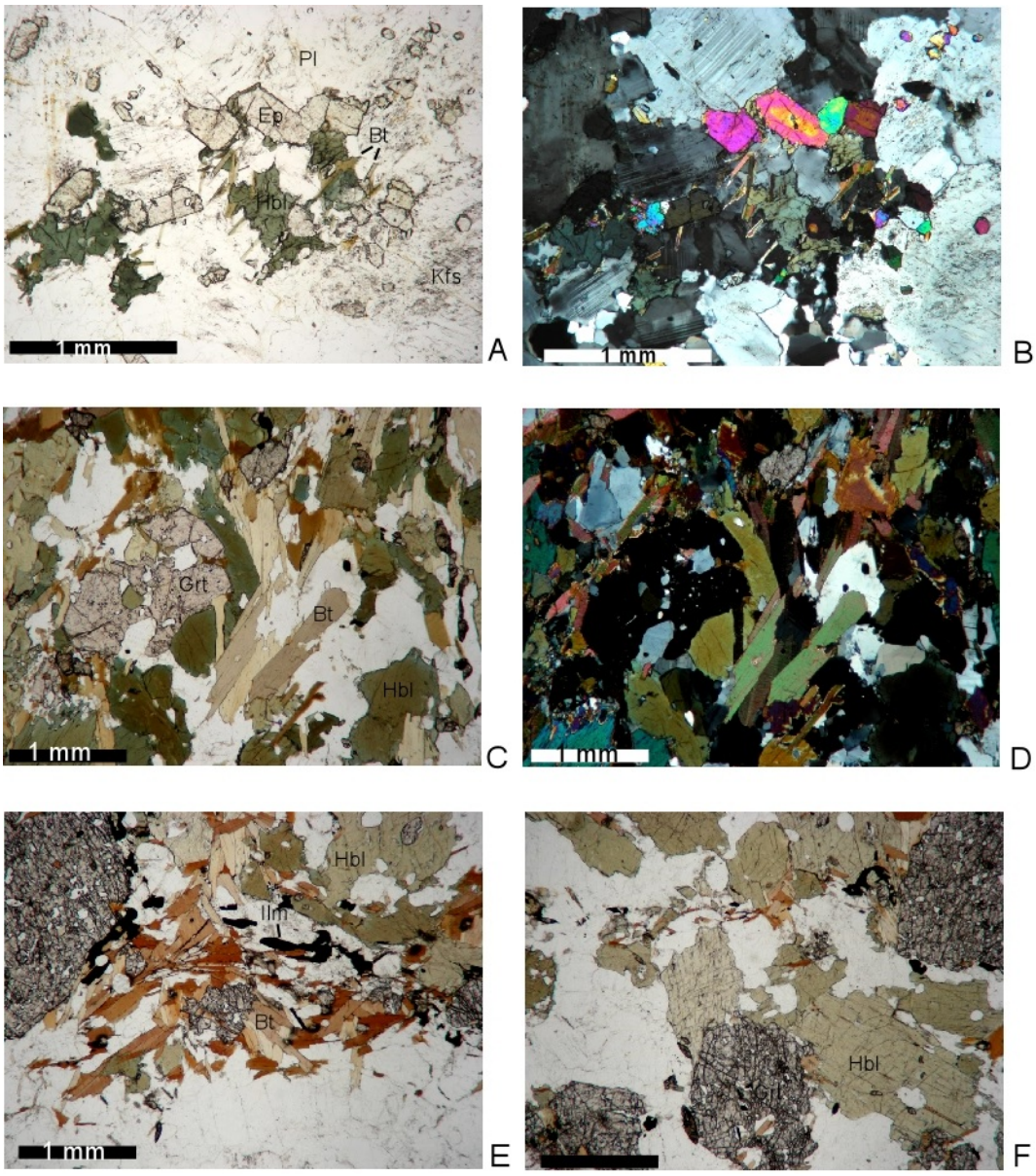

Figure 4.4. Photomicrographs of hornblende-biotite gneiss. (Figure caption follows).

Figure Caption 4.4.
A) HM03-5B, layer within Sandymush felsic gneiss, eastern Clyde quadrangle PPL (plane-polarized light); B) XN (crossed Nicols); C) MLL04-1C, mafic layer within migmatitic biotite gneiss unit, Hayesville thrust sheet, Mount Lynn Lowry overlook, Blue Ridge Parkway; D) XN; E) CG03-2, lens of hornblende-biotite gneiss from Coleman Gap, Clyde quadrangle, PPL; F) CG03-2, PPL

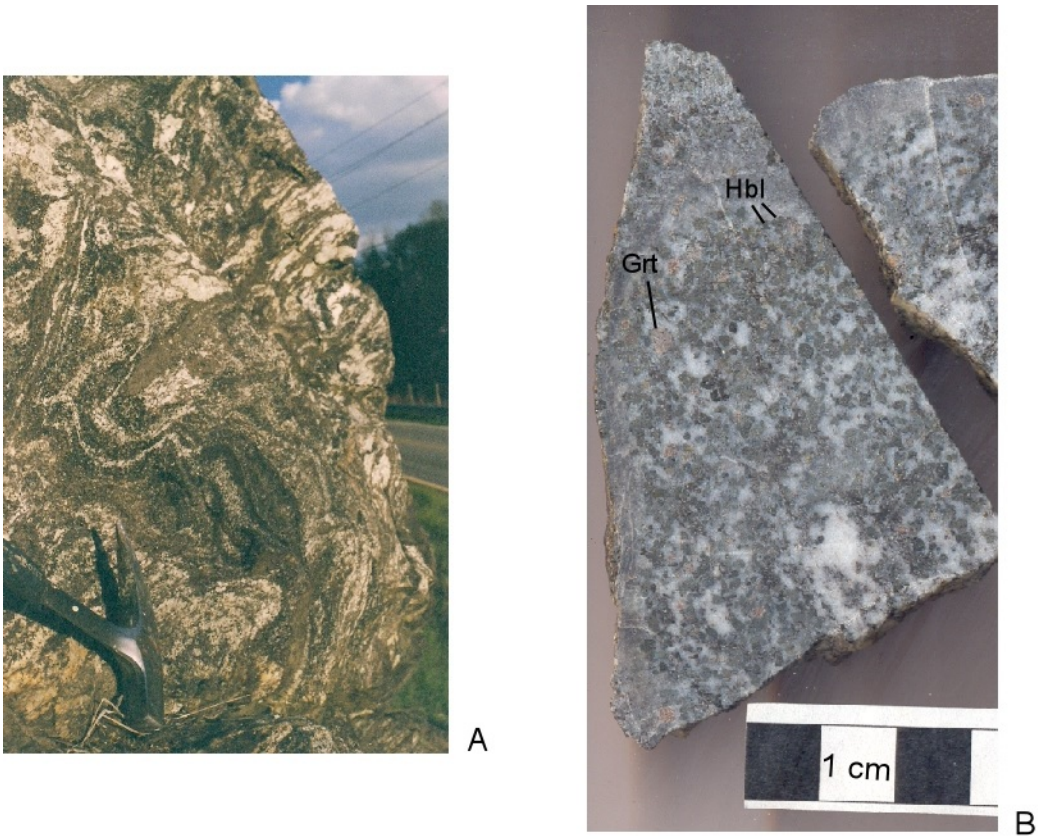

Figure 4.5. Images from Coleman Gap roadcut, central Blue Ridge. A) Polydeformed biotite gneiss with layers of hornblende biotite gneiss, location CG03, Clyde quadrangle, hammer for scale; B) scanned slab of hornblende-biotite gneiss, sample CG03-3, showing garnet (maroon), hornblende (dark green), and plagioclase (white).

A

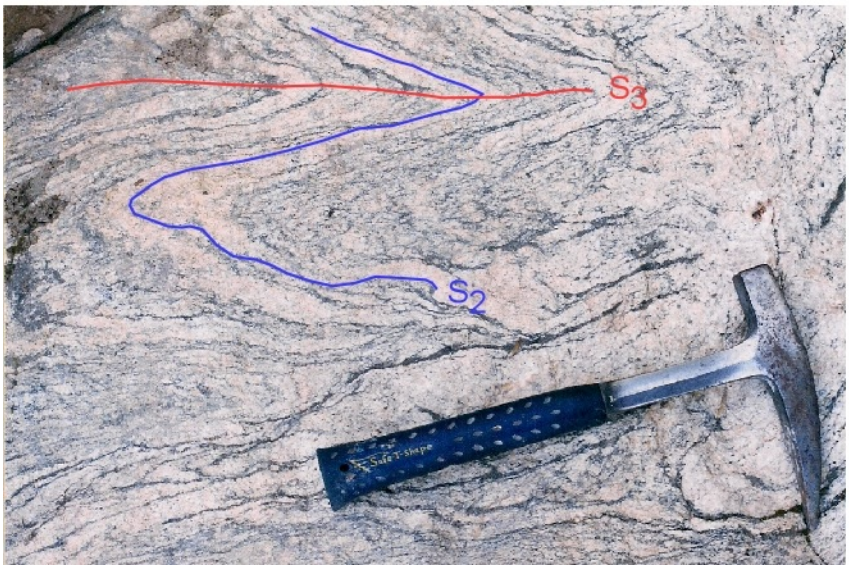

B

Figure 4.6. Outcrop photographs of biotite augen gneiss. Location OS03-1, Qualla-Dellwood belt, Old Soco Road, Sylva North quadrangle. A) Antiform in orthogneiss, hammer for scale; B) Tight folds in orthogneiss. S_2 is defined by folded layers of orthogneiss. S_3 includes the axial planar slip cleavage related to folded S_2 layers, hammer for scale.

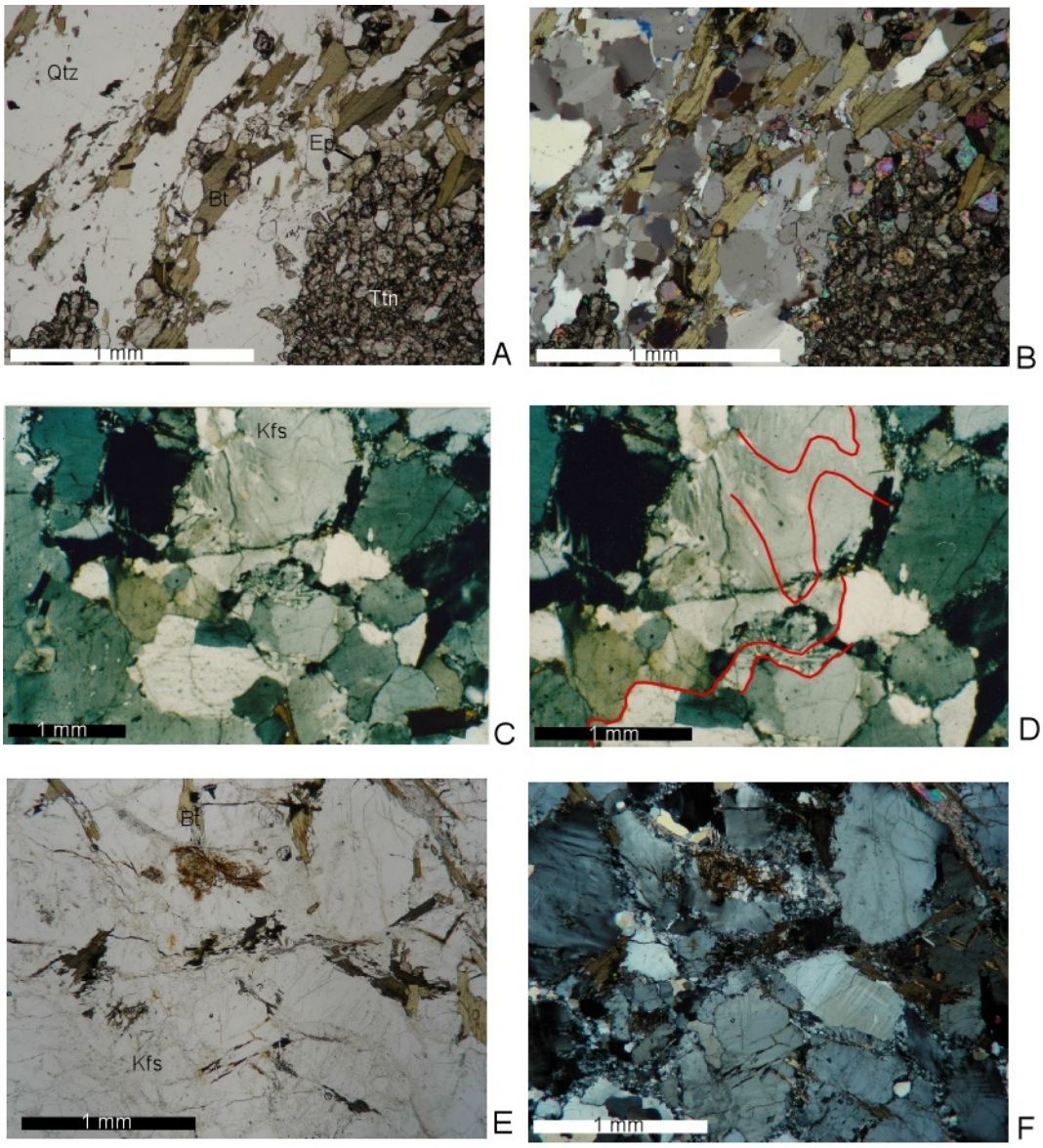

Figure 4.7. Photomicrographs of biotite augen gneiss. A) CH02-2B, augen gneiss from the Ravensford body, Cherokee, NC. Deformation fabrics include subgrains and bulge nucleation textures in quartz, and the recrystallization of titanite to form subgrains. PPL; B) CH02-2B, XN; C) MV02-4A, showing microfolds in K-feldspar rich augen gneiss. Dellwood basement complex, XN; C) CH02-2B, same photomicrograph with folded mineral cleavage and microfolds highlighted in red, XN; D) OS03-1, biotite augen gneiss from the Qualla-Dellwood belt, Old Soco Road, PPL; E) OS03-1. Under crossed Nicols the grid-shaped pattern of microlithons can be seen. Strain is expressed by grain-size reduction at feldspar and quartz grain boundaries, with grain size reduction occasionally penetrating into feldspar grain interiors.

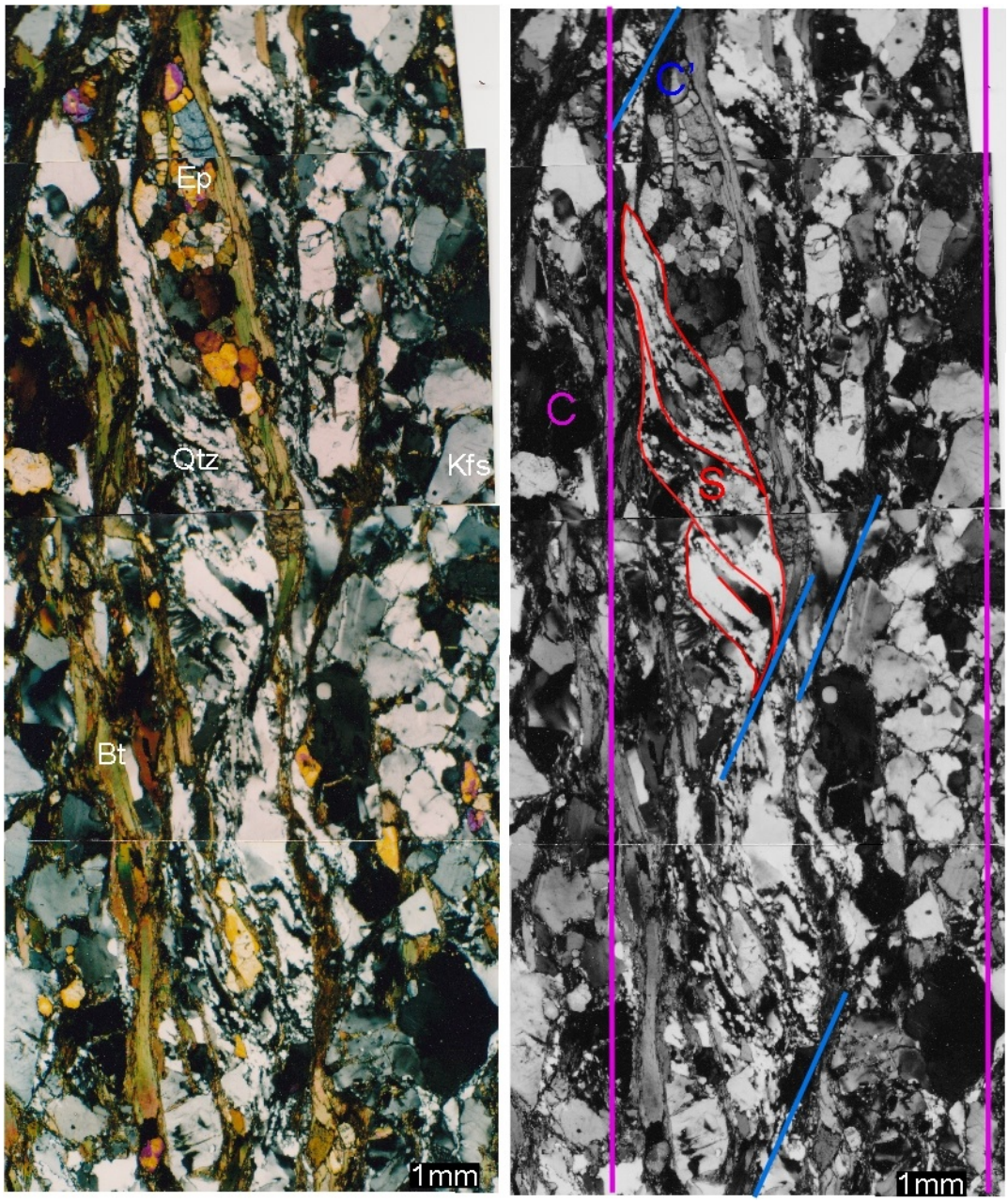

Figure 4.8. Photomicrographs of mylonitic orthogneiss. A) MV02-8A, sampled at Ned's Branch, south of Purchase Knob, Dellwood quadrangle, showing mylonitic fabric in S-C tectonite (Lister and Snoke, 1984) (XN). B) Microfabric interpretation: S=sigmoidal schistosity defined by boudinaged and recrystallized quartz ribbons; C= shear bands (cisailement) expressed as aligned biotite grains; C'=shear bands oblique to S (XN).

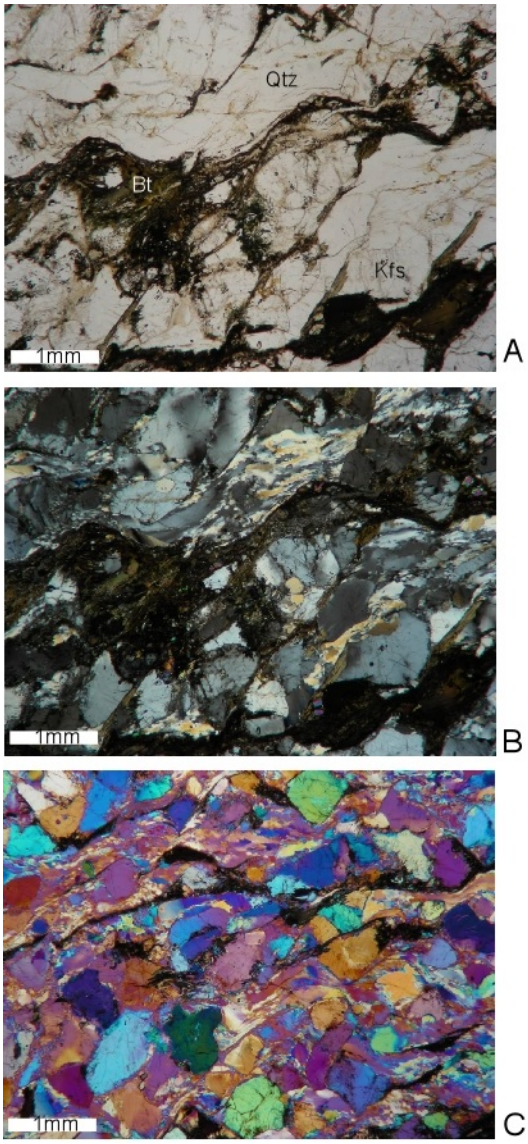

Figure 4.9. Photomicrographs of mylonitic orthogneiss. Sample SC04-6, sampled east of Purchase Knob, Dellwood quadrangle. A) SC04-6 PPL; B) Same image under XN; C) Similar image with λ plate inserted.

Amphibolite

Amphibolite occurs as dark green to black pods, distinct layers, and as kilometer-scale bodies enclosed by orthogneiss, biotite gneiss, and schist thoughout the central Blue Ridge basement complex. Amphibolite slabs also are enclosed by layered meta-plutonic rocks of the western Blue Ridge, with an example given by Hadley and Goldsmith (1963) from a location north of Big Cove. Dozens of discrete, elongated amphibolite masses were mapped in the western half of the Asheville 1:100,000 scale quadrangle (Merschat and Cattanach, 2008) occurring as inclusions throughout the Mesoproterozoic basement complex. Mapable amphibolite pods were found in the Max Patch Granite, Spring Creek Granitoid Gneiss, Sandymush Felsic Gneiss, and Earlies Gap formations. A large (~600 x 400 m) amphibolite body consists of clinopyroxene-garnet granulite, clinopyroxene-hornblende-garnet granulite, and garnet amphibolite occurs north of Dellwood, NC and was described in detail in Chapters 1 and 2, with additional photomicrographs shown in Figure 4.10. The other amphibolites examined here lack clinopyroxene, and are composed of plagioclase, hornblende, and garnet, with minor quartz, biotite after hornblende, and accessory titanite, epidote, ilmenite, and apatite. Amphibolites sampled south of Purchase Knob (Samples H03-3,-4) are strongly lineated, with a lineation defined by plagioclase rods and aligned hornblende crystals.

Other Lithologies

Distinct bodies of muscovite-rich schist and gneiss are found in the central Blue Ridge Basement complex. Kilometer-scale bodies containing muscovite-biotite schists were mapped in the Clyde quadrangle by Merschat and Cattenach (2008). An excellent exposure of this unit, that contains blocks of various lithologies in a matrix of muscovite-biotite gneiss and schist, can be found along I-40 at Coleman Gap in the Clyde quadrangle. Whole rock analyses of the present study include analyses determined from smaller outcrops of muscovite-biotite schist (eg. H03-1, MV02-7) that occur in the basement complex near Dellwood, NC. No zircons were dated from these samples of muscovite-biotite gneiss, but in retrospect, it would have been a good age to resolve. Thermobarometric estimates from MV07-7 were presented in Chapter 1.

Monazite was separated and dated from several units of the metasedimentary cover sequences, structurally located above the central and western Blue Ridge basement complex. Th-Pb monazite ages were determined from Great Smoky Group schists 1) located south of Leatherwood Top in the Dellwood quadrangle (MV02-1A), and 2) located south east of the Big Witch Gap tunnel off of the Blue Ridge parkway in the Bunches Bald quadrangle. Photomicrographs of deformed Great Smoky Group schists are shown in Figure 4.11. Monazite was dated from a garnet schist of the Mineral Bluff Formation, from the Murphy belt, sampled in the Marble quadrangle on the west side of US Route 141, near the junction of Kinners Road. Monazite U-Pb ages were determined from a sample of migmatitic biotite gneiss collected just south of the Hayesville fault, sample MM22-B.

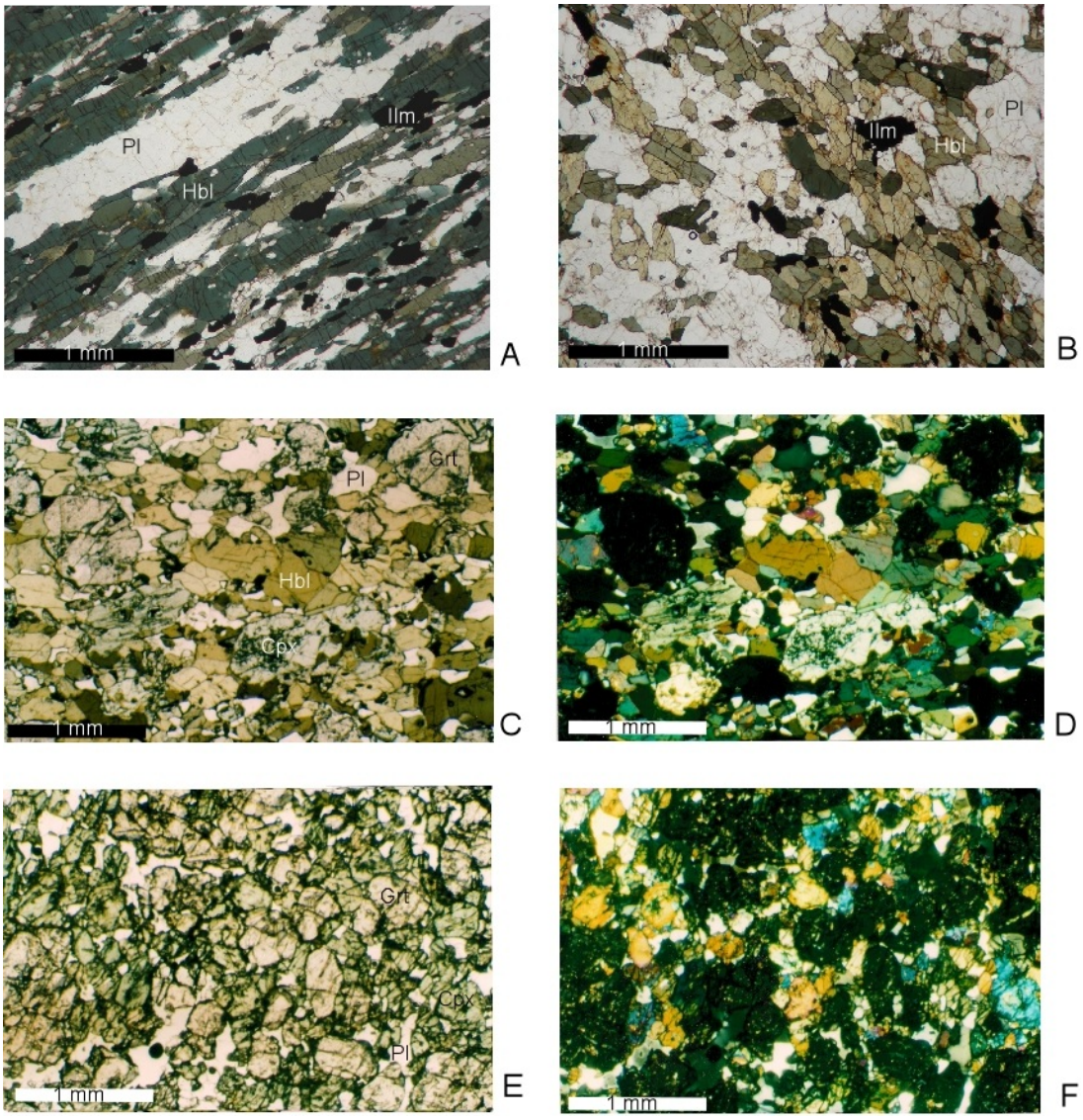

Figure 4.10. Photomicrographs of amphibolite from the Dellwood quadrangle. A) H03-4C, lineated amphibolite collected above Hemphill creek, southeast of the Cataloochee divide, PPL; B) H03-4F, amphibolite largely composed of plagioclase, hornblende, and ilmenite, PPL; C) DEL03-3B, un-foliated HP-amphibolite assemblage exposed near NC Route 276, Dellwoood quadrangle, PPL; D) same image of garnet + hornblende + clinopyroxene + plagioclase assemblage, XN; E) DEL05-3B2, HP garnet granulite assemblage, consisting of garnet + clinopyroxene + plagioclase; F) DEL05-3B2, XN.

Zircon and Monazite Characterization

Zircon grains extracted from 14 meta-igneous rocks were imaged and examined for morphology and internal structure using BSE and CL imaging. Most of the zircons appear light-pink, frosty-white, or pink under transmitted light. Many of the larger grains appear darker, due to metamictization and the presence of inclusions and fractures. Several of the zircon populations contain a mixture of large metamict grains having obvious xenocrystic cores and smaller clear grains. Length to width ratio is variable, ranging from 1:1 to 1:6. Zircons from sample FC04-1B are noticeably darker (amber-colored) with spherical grains and rounded terminations common. Representative zircons were dated using the U-Pb method via SIMS. A summary of the resulting ages is given in Table 4.1 with ion probe data given in Appendix J.

Zircon Geochronology: Results and Interpretation

Biotite Gneiss

DEL03-1 Migmatitic Biotite Gneiss

Zircons were separated from migmatitic biotite gneiss (DEL03-1) as well as a leucosome from the same location (DEL03-1L). Slabs of the samples are shown in Figure 4.12, CL images of polished zircon grains and ion probe pit locations are shown in Figure 4.13, and forty six ion probe analyses determined on polished grains from both samples are plotted in Figure 4.14.A, revealing a wide range of determined ages. The oldest zircon ages were determined from xenocrystic cores rimmed by one or more zones of later zircon growth, with zircon core ages determined to show a broad spectrum of Paleoproterozoic and Mesoproterozoic ages (1911, 1630 with 1205 rim, 1429, 1349, 1290, and 1198 Ma). An example of these age relations can be seen in Figure 4.13.L, where a ~ 1628 Ma xenocrystic core is overgrown by ~1205 Ma material, which is capped by thin rims that appear bright under CL. By examining all of the data determined from these samples, it appears that zircon rims record two stages of metamorphic zircon growth, the first of which occurred at ~997 $\pm$ 18 Ma (weighted average, Figure 4.14.B) and produced entirely new zircon crystals as well as thick metamorphic rims that envelop older xenocrystic cores. The second metamorphic event occurred around 897 $\pm$ 31 Ma (weighted average, Figure 4.14.C), producing thick, low-U caps on the terminations of older crystals. The CL image shown in Figure 4.13.I shows an undated xenocrystic core mantled by ~997 Ma metamorphic zircon, that is in turn capped by ~897 Ma rims. Some of the thinner rims on zircon that appear bright under CL are difficult to date with the ion probe (in polished grain mounts), and potentially grew during the proposed 897 Ma metamorphic event. Also present in these migmatitic

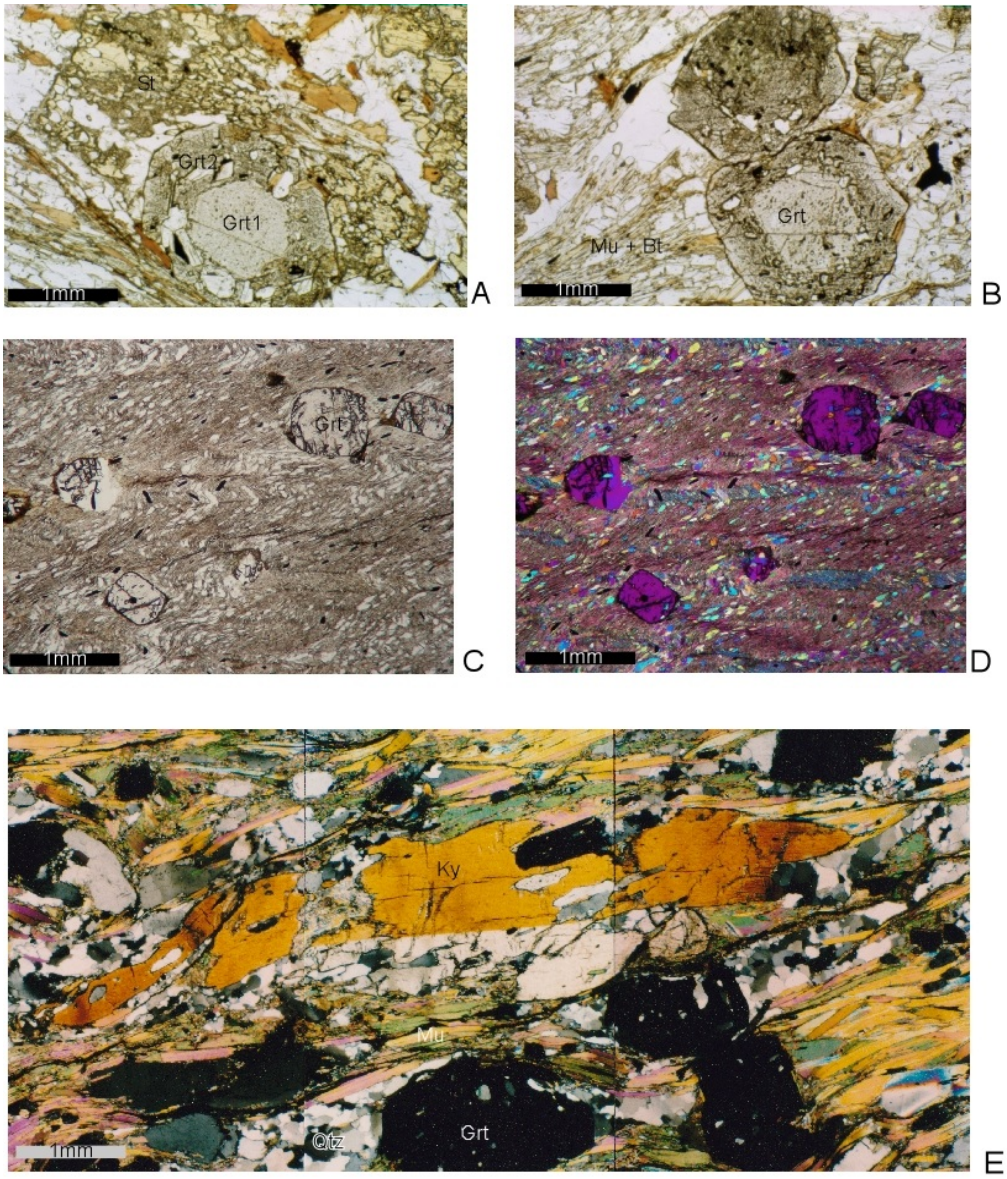

Figure 4.11. Photomicrographs of Great Smoky Group and Snowbird Group cover lithologies. A) GT02-2, Great Smoky Group schist, collected near Big Witch Gap, Bunches Bald quad, with two distinct zones of garnet growth, overgrown by staurolite porphyroblast, PPL; B) GT02-2, foliation (S_2) is deflected around garnet porphyroblast, PPL; C) CCG03-6, garnet schist from the Wading Branch Formation, Cove Creek Gap quadrangle, with crenulation cleavage, PPL; D) CCG03-6, λ-plate inserted; E) MV02-1B, Great Smoky Group/Copper Hill Formation schist, with boudinaged, sheared kyanite porphyroblast, flattened garnet theta-clasts, and mica fish.

Table 4.1. Summary of U-Pb Zircon Ages from the Central Blue Ridge, Western North Carolina.

Sample	Location	Lithology	n (analyses)	Concordia age (Ma)	± (2σ) (Ma)	Metamorphic Rims (Ma)	± (2σ) (Ma)	detrital (Ma)	± (2σ) (Ma)
DEL03-1	D	migmatitic biotite gneiss	1 crystal[1]	460	11	997	18	742	71
						897	31	1044	+52/-55
DEL03-1L	D	leucosome	14[2]	456	+17.6/-13.5			1202	63
								1285	61
								1349	37
								1426	57
								1628	41
								1911	39

[1] ion tunneling into a single unpolished zircon

[2] weighted average calculation from 14 analyses of zircons pooled from DEL03-1, DEL03-1L

Sample locations: D=Dellwood;

Table 4.1 (Continued). Summary of U-Pb Zircon Ages from the Central Blue Ridge, Western North Carolina.

Sample	Location	Lithology	n (analyses)	Concordia age (Ma)	± (2σ) (Ma)	inheritance (Ma)	± (2σ) (Ma)
MM22	H	migmatitic bt gneiss	7	478	22	997	60
CG03-2	C	hbl-bt gneiss	9	965	50	1042	84
CH02-2B	W	bt augen gneiss	5	1010	52		
MV02-2	D	bt augen gneiss	4	997	51	1109	42
HM03-5B	C	hbl-bt gneiss	4	1007	60	1147	43
FC04-1B	FC	bt gneiss	4	1047	79	1145	41
						1336	51
OS03-1B	SN	bt augen gneiss	4	1122	47	1188	84
SC04-6	D	bt augen gneiss	6	1129	36	1209	78
MV02-3	D	bt augen gneiss	1	1169	46		
DEL04-5	D	hbl-bt gneiss	5	1142	70	1282	73
						1244	26
NB04-1A	D	bt augen gneiss	1	1153	40		
PK03-3	D	bt augen gneiss	3	1172	46		

Sample locations: D=Dellwood;H= Hazelwood; C=Clyde; W=Whittier; FC=Fines Creek; SN=Sylva North quad

samples is a generation of Paleozoic zircons, some of which display oscillatory growth zoning under CL; others appear homogeneous and dark under CL. U-Pb data from fourteen analyzed spots from zircons of DEL03-1 and DEL03-1L yield an age of 456 $\pm$ 17.6/-13.5 Ma, with a weighted average histogram given in the previous chapter. Some of these Taconic-aged crystals show evidence of containing older xenocrystic cores under CL (Figure 4.13.E). Another Taconic age estimate of 460 $\pm$ 11 Ma (2σ) was determined from a single unpolished zircon grain (DEL03-1 mount 2, grain D, Figure 4.15, Appendix K). Using the ion probe to "tunnel" into unpolished grains is advantageous in that it minimizes the effects of potential inherited xenocrystic cores that may yield discordant and geologically meaningless ages.

The interpretation of the isotopic data is complicated. Each of the three metamorphic events determined from these migmatites (460, 897, and 997 Ma) may have potentially involved the lithologic mixing of older rocks to produce the wide spectrum of inherited zircon core ages. Alternatively, this migmatitic biotite gneiss formed from a sedimentary protolith similar to the Ocoee (WBR) or Ashe (EBR) cover sequences that typically contain a wide spectrum of detrital zircon (Bream et al., 2004; Moecher et al., 2010; Chakraborty et al., 2011). Perhaps the migmatitic biotite gneiss is more akin to other central Blue Ridge paragneisses such as the Wolf Pen migmatite, Chunky Gal Mountain, and Otto Formation (Merschat et al., 2010). In any event, if sample DEL03-1 is a high-grade metasedimentary rock, the Proterozoic xenocrystic cores with 997 and 897 Ma metamorphic rims may have been detrital grains in the protolith at the time of deposition. It is suggested that these three metamorphic events occurred in the central Blue Ridge, however, if this sample is truly a high-grade metasedimentary rock, the zircons could have been derived from distant sources (thousands of kilometers away), reflecting orogenic events that occurred in a different terrane.

Of the 26 grains that were analyzed, significant post-Grenvillian ages include one zircon with an age of 742 $\pm$ 71 Ma, and another dated 554 $\pm$ 83 Ma. Five grains have ages ranging from 436 to 304 Ma allowing for the possibility that high temperature events and new zircon growth occurred after the Taconic orogeny (Early Silurian through Late Pennsylvanian). However, most of these younger ages have a high degree of uncertainty (relatively large error ellipses, or discordant age determinations). Isoplot V.3.5 is unable to "unmix" the ages of the Paleozoic zircons into distinct age modes using the Sambridge and Compston (1994) method. Given the migmatitic fabrics observed in these samples (apophyses and late leucocratic dikes), the high temperatures determined from adjacent outcrops using thermobarometry (~700-750^{o}C, location DEL03-3, Chapter 3), and overwhelming evidence for a population of Taconic zircons, this migmatitic biotite gneiss is interpreted to be a Taconic migmatite derived by the partial melting of a Neoproterozoic sedimentary protolith.

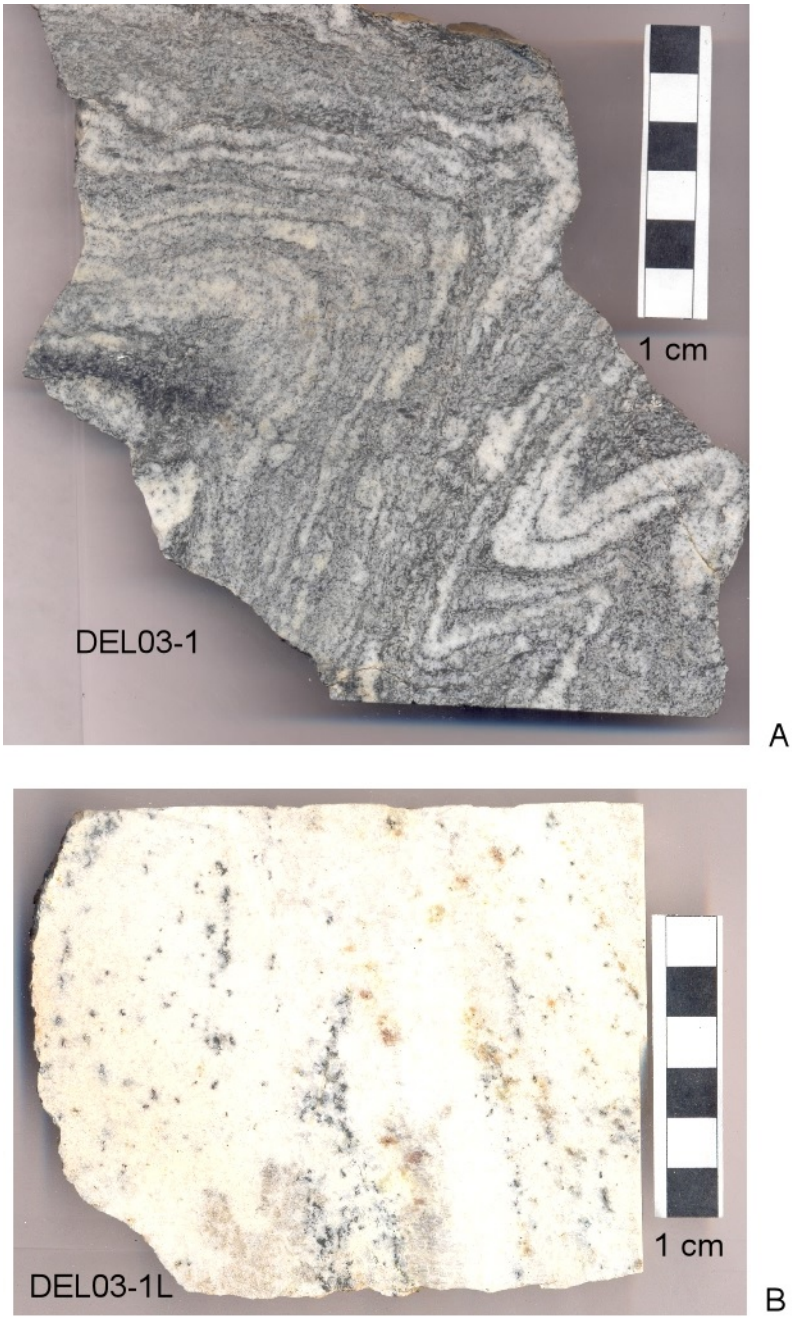

Figure 4.12. Slabs of migmatitic biotite gneiss, DEL03-1 and DEL03-1L. A) Central Blue Ridge migmatitic biotite gneiss, sample DEL03-1. B) Sample DEL03-1L, a massive leucosome from the same outcrop, Dellwood quadrangle.

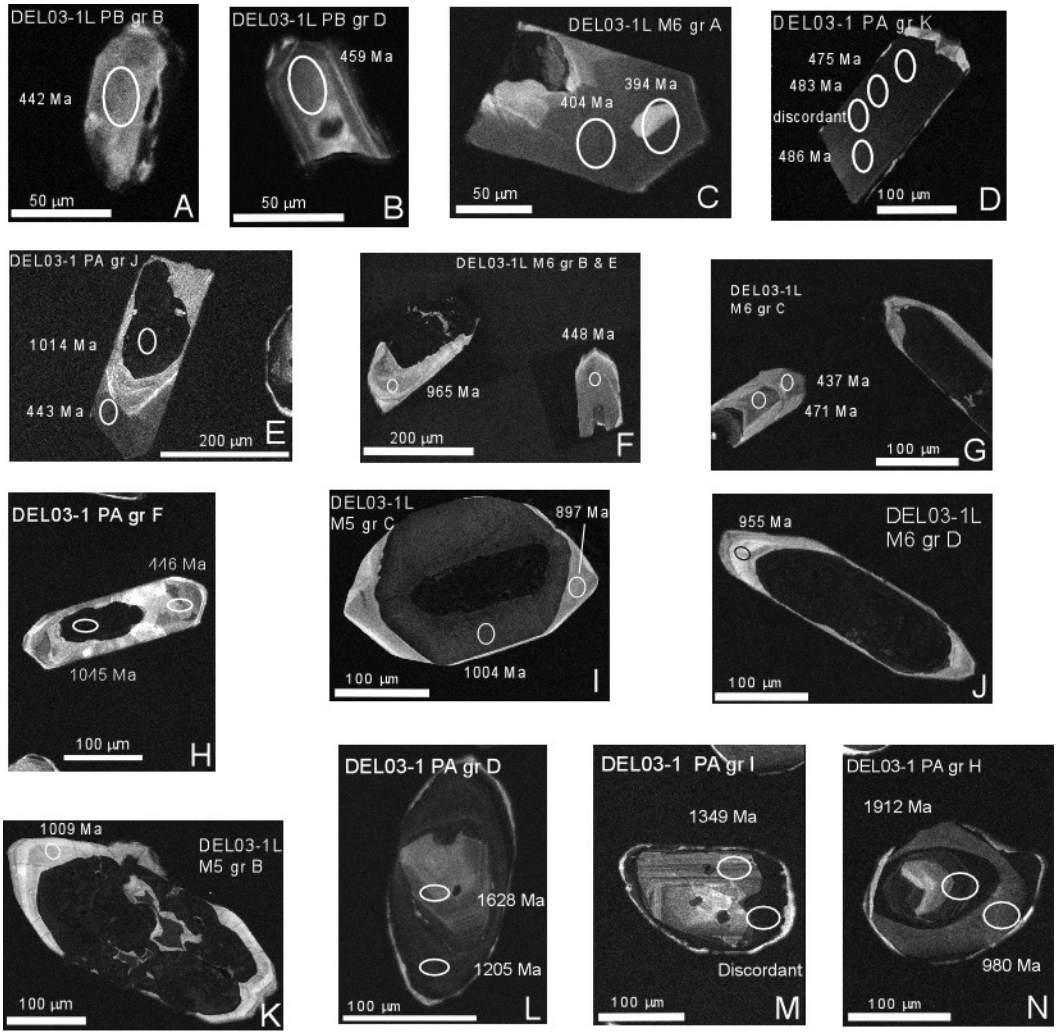

Figure 4.13. CL images of polished zircons from migmatitic biotite gneiss, DEL03-1, and leucocratic dike DEL03-1L. Approximate analysis spot locations shown in white along with concordia ages.

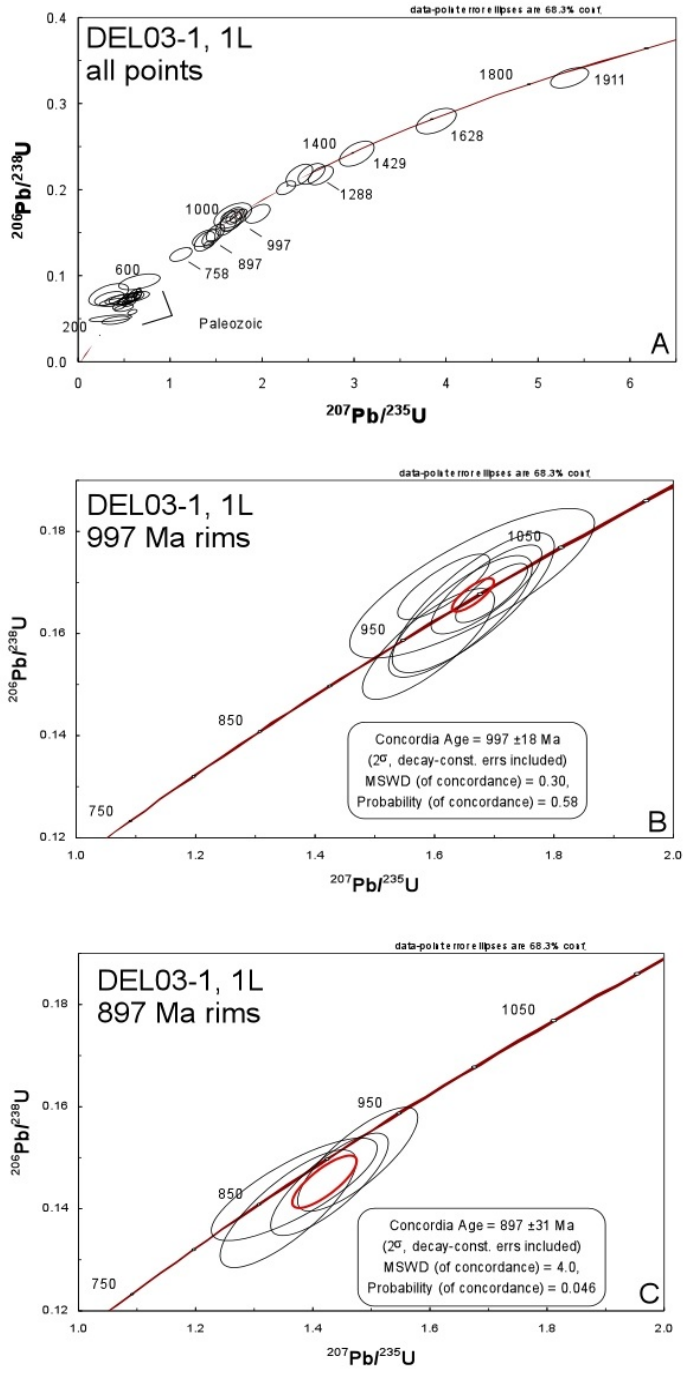

Figure 4.14. Concordia plots from migmatitic biotite gneiss. (Legend follows)

Figure Legend 4.14 A) Summary diagram showing 46 ion probe analyses from samples DEL03-1 and DEL03-1L with ages ranges in Ma. B) Metamorphic rim age of 997 Ma determined from weighted average of spots pooled from DEL03-1 and DEL03-1L. C) Metamorphic rim age of 897 from weighted average of analyses pooled from DEL03-1 and DEL03-1L.

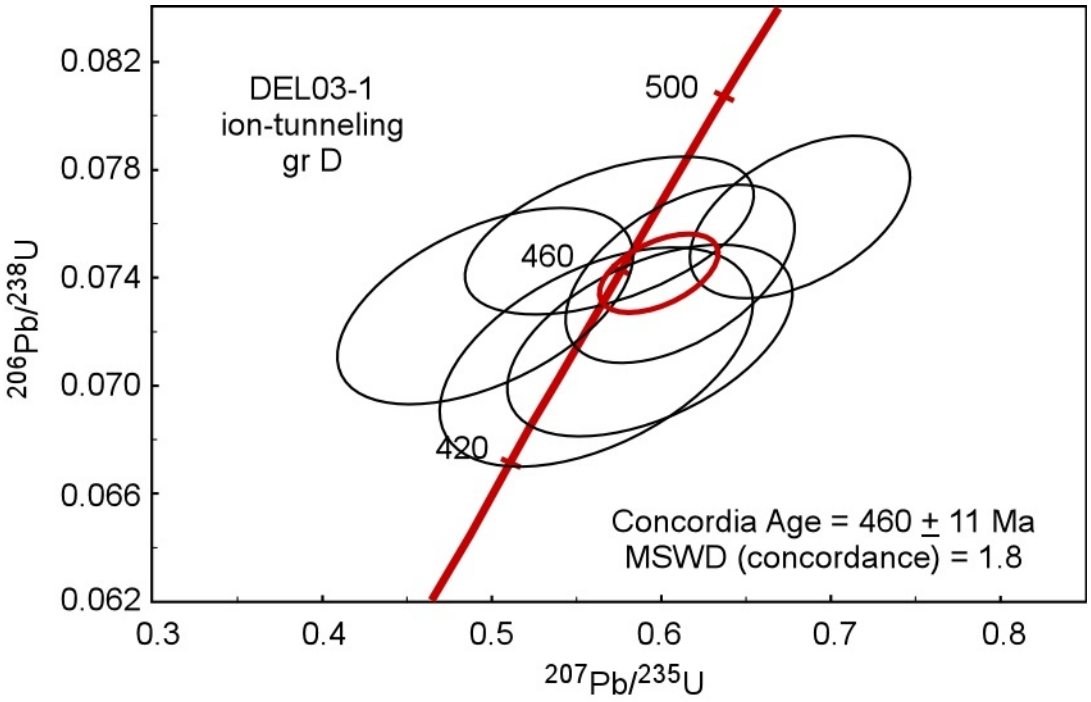

Figure 4.15. Concordia plot of "ion-tunneling" data, DEL03-1. A Taconic age of 460 ± 11 Ma (2σ) was determined via "ion tunneling" into an unpolished grain from migmatitic biotite gneiss, with each ellipse representing a block of 5 analytical cycles. Data in Appendix K.

MM-22B, Migmatitic Biotite Gneiss

Migmatitic biotite gneiss sample MM-22B was collected along the Blue Ridge Parkway near the Mount Lynn Lowry overlook, a site that has been studied previously (Massey, 2003; Moecher et al., 2005). Small (≤100 micrometer) zircons and monazites were separated from migmatitic biotite gneiss, mounted, and analyzed with the Cameca ion microprobe at UCLA. Monazite chemical ages have been determined from this outcrop, however the investigation was done on sample MM-22A, a garnet-kyanite paragneiss, not MM-22B, the migmatitic biotite gneiss examined here. Whole rock geochemical analyses were determined from three additional samples from the same outcrop (MLL-04-1A, B, and C). Of the seven zircon grains analyzed, three points were averaged to yield an age of 478 ± 22 Ma (Figure 4.16.A). Three other points show reverse discordance on the concordia diagram with ages ranging from 562 to 573. The age of the seventh grain is 977 ± 60 Ma and CL imaging suggests that this analysis was performed on a xenocrystic core of a detrital grain that shows oscillatory zoning (Figure 4.16.B). There appears to be older, xenocrystic material in the cores of the three zircons that yielded ages of 562-573, as well as reverse discordance on the concordia plot; for these reasons, these three points (562-573 Ma) are not considered geologically

meaningful, or at least their significance is not fully understood. Reverse discordance has been attributed to U-loss (Faure, 1986), but in this case (using an ion probe), the reverse discordance may be an artifact of enhanced ion yields from labile Pb (Wiedenbeck, 1995)

Monazite Th-Pb age estimates from twelve ion probe spots on seven grains of MM-22B appear to be a mixture of two age components (Figure 4.17.A). Approximately 85% of the grains have an age of 434.4 ± 9.5 Ma; 15% of the grains have an age of 457 ± 31 Ma (Figure 4.17.B). BSE images of grains are shown in Figure 4.17.C. Ages were calculated using the Sambridge-Compston "unmix ages" algorithm of Isoplot ver. 3.50 (Sambridge and Compston, 1994; Ludwig, 2003). The Ordovician 457 ± 31 Ma Th-Pb monazite age is essentially the same as the U-Pb zircon TIMS age determined by Moecher et al. (2004) from the central Blue Ridge Winding Stair Gap migmatite (458 ± 1 Ma) that occurs in the same structural setting ascribed to the Cartoogechaye terrane. Monazite Th-Pb data is given in Appendix L.

MV02-2, Biotite Gneiss

U-Pb zircon ages were determined from four spots on four zircons separated from a sample of garnet-biotite gneiss that was sampled north of Jonathan Creek, north of U.S. Route 276, west of the golf course. An image of the slab, showing the typical light and dark bands that define the gneissosity, is shown in Figure 4.18.A. Also shown in Figure 4.18 are CL images of the analyzed zircon grains with approximate pit locations and calculated concordia ages. Zircons separated from this sample include several spherical-shaped grains (e.g. grain F in Figure 4.18.C) that appear to be of metamorphic origin (Corfu et al., 2003). Although more data would be useful, the U-Pb ages from this sample were divided into two modes, occurring at 997 Ma and 1109 Ma (Figure 4.19).

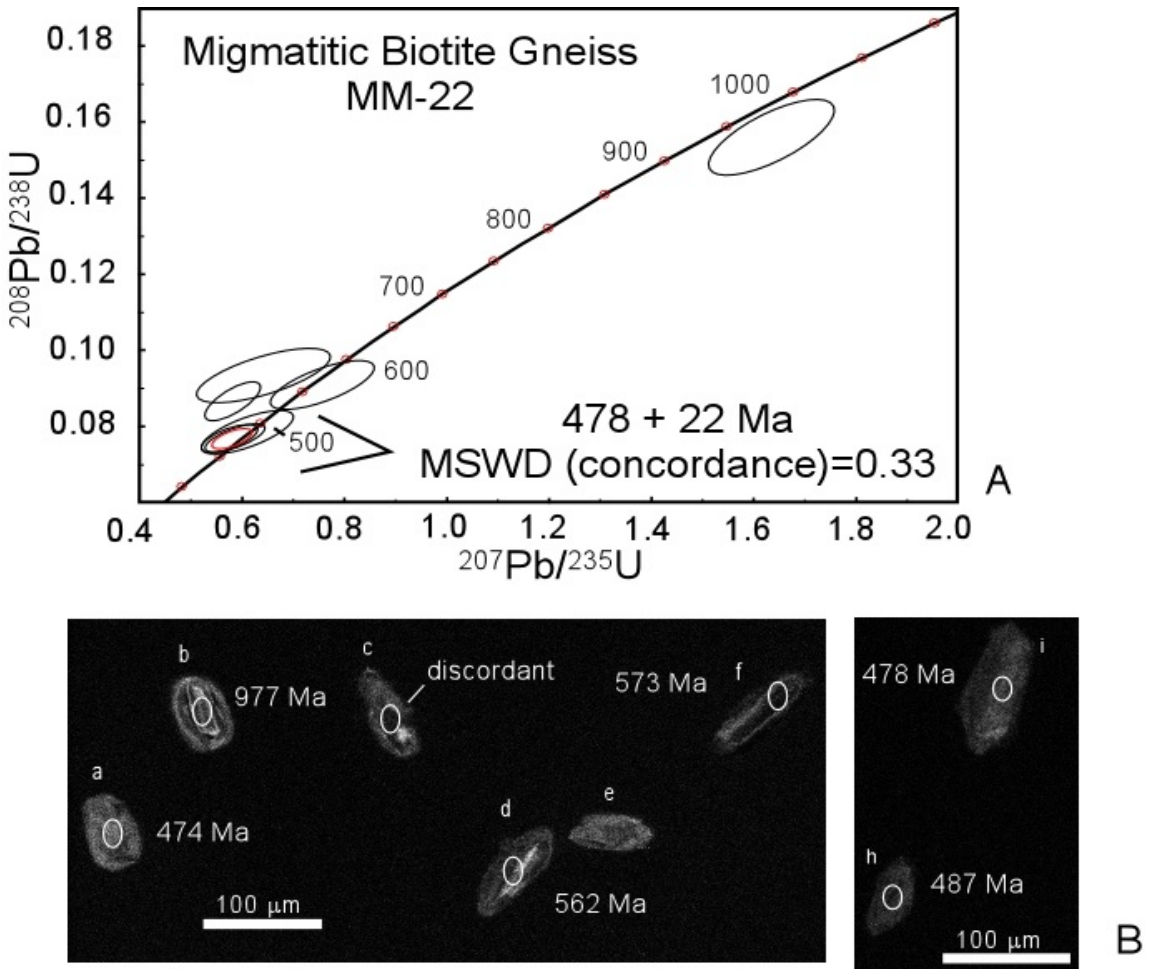

Figure 4.16. Concordia diagram and CL images from migmatitic gneiss sample MM-22. A) Plot of all points, with weighted average determined from three spots. B) CL images of polished zircons with approximate spot locations and determined ages.

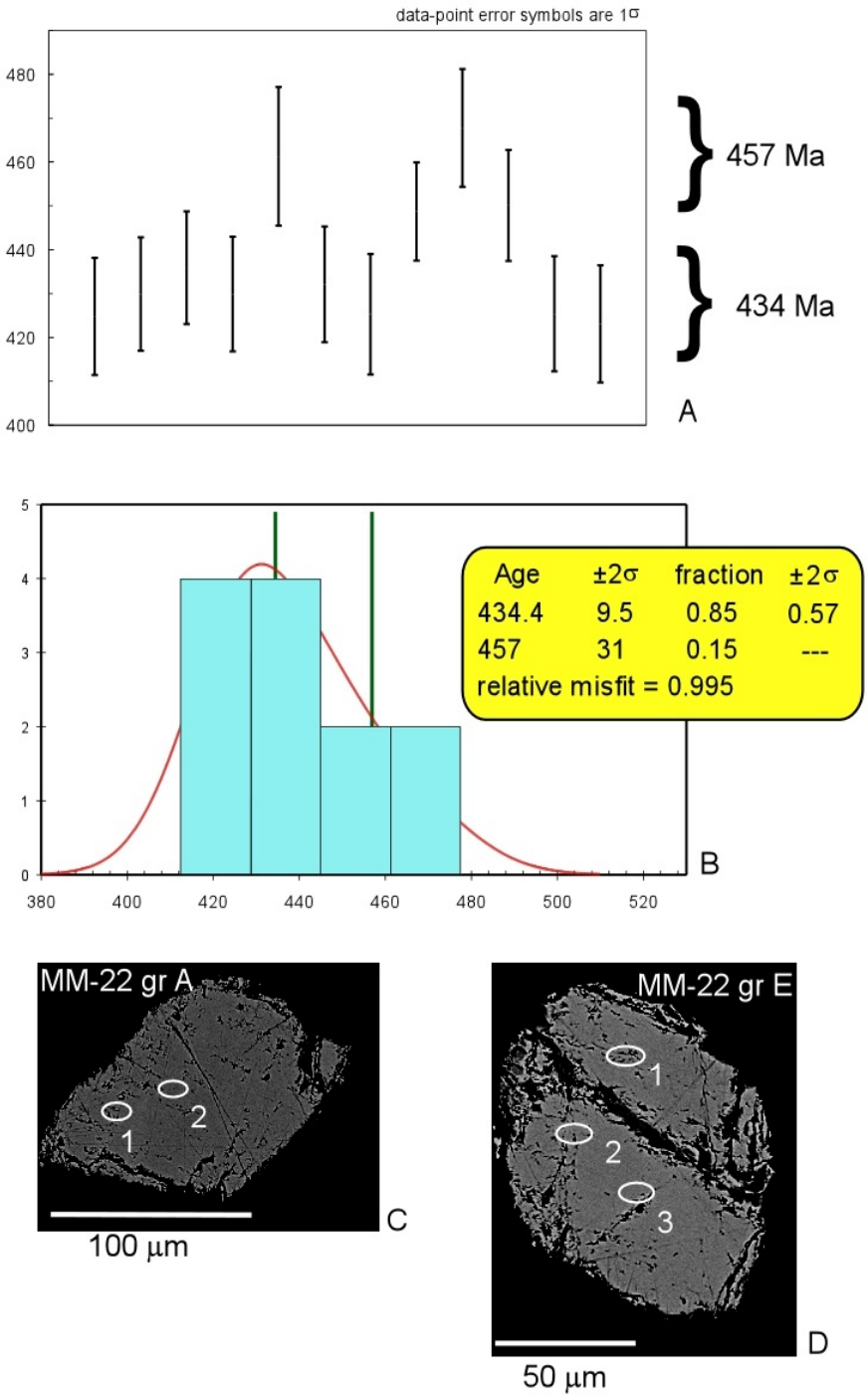

Figure 4.17. Monazite Th-Pb age summary, migmatitic biotite gneiss MM-22. A) Histogram showing the age distribution of monazite ages. B) Age fraction calculation from Isoplot. C) BSE images of monazite grains with approximate pit locations.

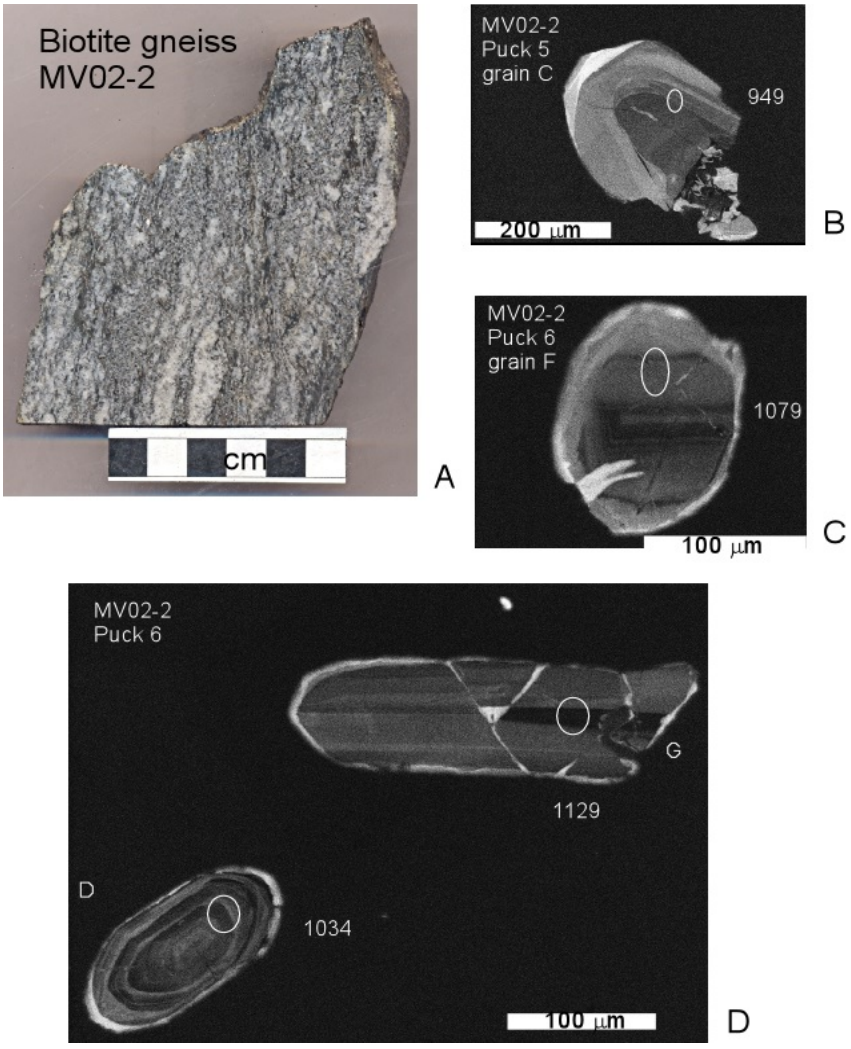

Figure 4.18. Slab and CL images of zircon from biotite gneiss, MV02-2. A) Scanned image of slab. B-D) CL images of zircon grains with pit locations and concordia ages in Ma.

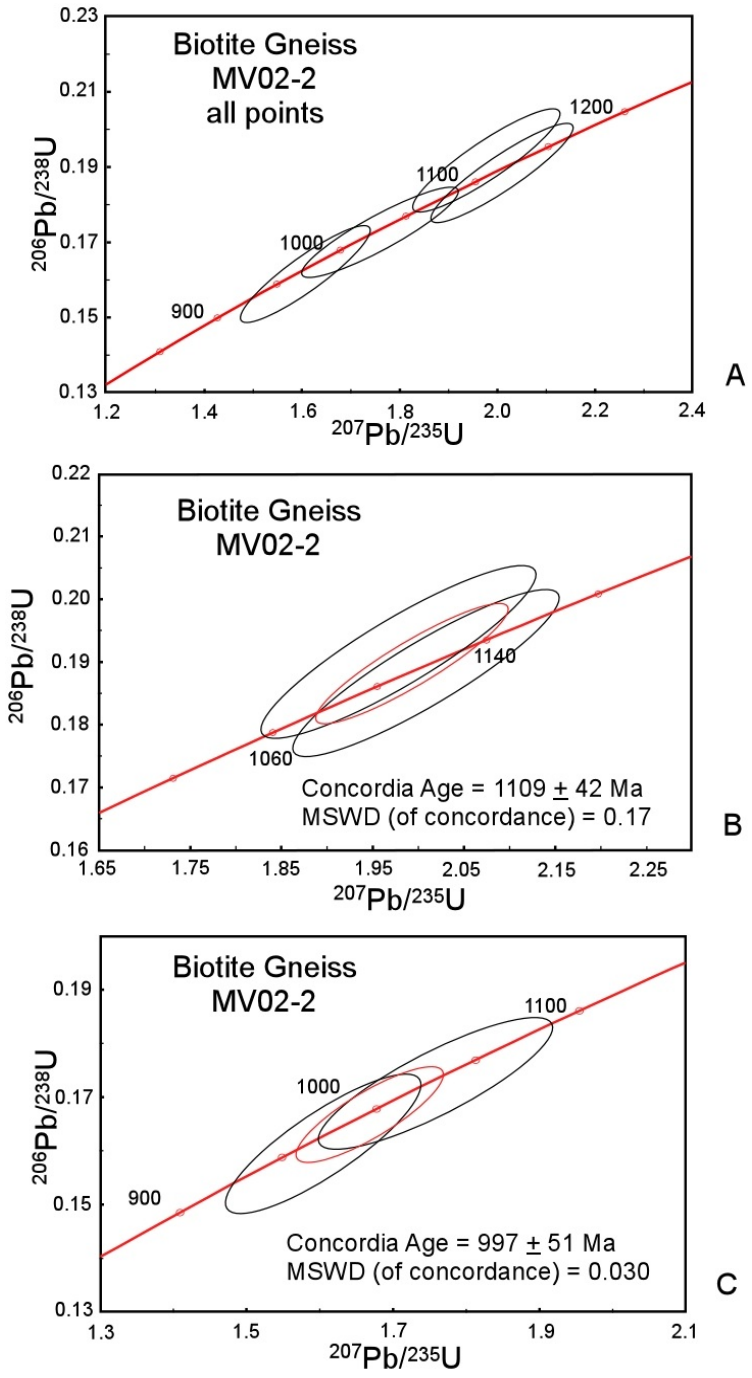

Figure 4.19. Concordia diagrams determined from biotite gneiss, MV02-2. A) Concordia plot of all data from MV02-2. B) 1109 Ma age determined from the weighted mean of two spots. C) 997 Ma concordia age determined from the weighted mean of two spots.

Hornblende-Biotite Gneiss,

DEL04-5, Hornblende-Biotite Gneiss

DEL04-5 was collected on the east side of U.S. Highway 276 in the Dellwood quadrangle. The outcrop appears to be part of a relatively large (~1.5 km x 0.3 km) block of hornblende-bearing orthogneiss that is enclosed by biotite- and muscovite-biotite gneiss of the central Blue Ridge basement complex. The gneiss contains scarce modal hornblende relative to the other samples of hornblende-biotite gneiss, and is unique in that it contains large (>2 cm) augen or porphyroclasts composed of alkali feldspar. Flattened pink feldspar grains can be seen in an image of a thin section chip (Figure 3.27.A). Zircons show U-rich cores with oscillatory zoning, with U-poor rims forming thick mantles (Figure 4.20). A concordia plot of the SIMS data (Figure 4.21) shows age ellipses that appear to be distributed into different age modes. The oldest age, 1282 $\pm$ 73 Ma, is close to the 1287-1292 age mode previously determined from a study of hornblende-biotite gneiss of the Dellwood quadrangle by Loughry (2010). A weighted mean of three points yields a second age of 1244 $\pm$ 26 Ma, interpreted here as the crystallization age. This age falls outside of the modes determined by Loughry for the Dellwood basement complex. The 1244 Ma age overlaps with the age estimate of 1200-1260 for Earlies Gap granulites that occur to the east (Merschat and Cattanach, 2008; Fullagar et al., 1979; Officer et al., 2003; Ownby et al., 2004). One zircon core has a younger age of 1142 $\pm$ 70 Ma and displays oscillatory zoning (magmatic). The younger zircon may have crystallized during a Mesoproterozoic remelting event that reworked older 1244 granitoids.

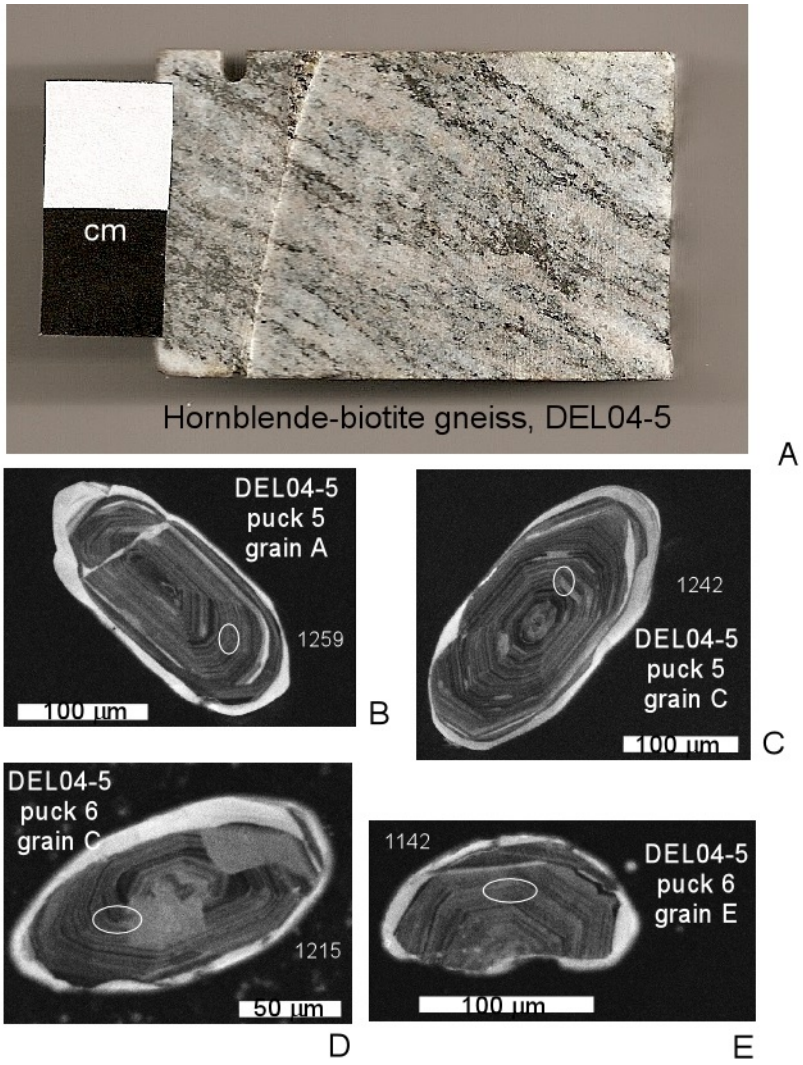

Figure 4.20. Slab and CL images of zircon, hornblende-biotite gneiss, DEL04-5. A) Slab from sample DEL04-5 with flattened alkali feldspar; biotite and hornblende comprise the dark, mafic phase. B-E) CL images of zircon from DEL04-5 with pit location and concordia age in Ma.

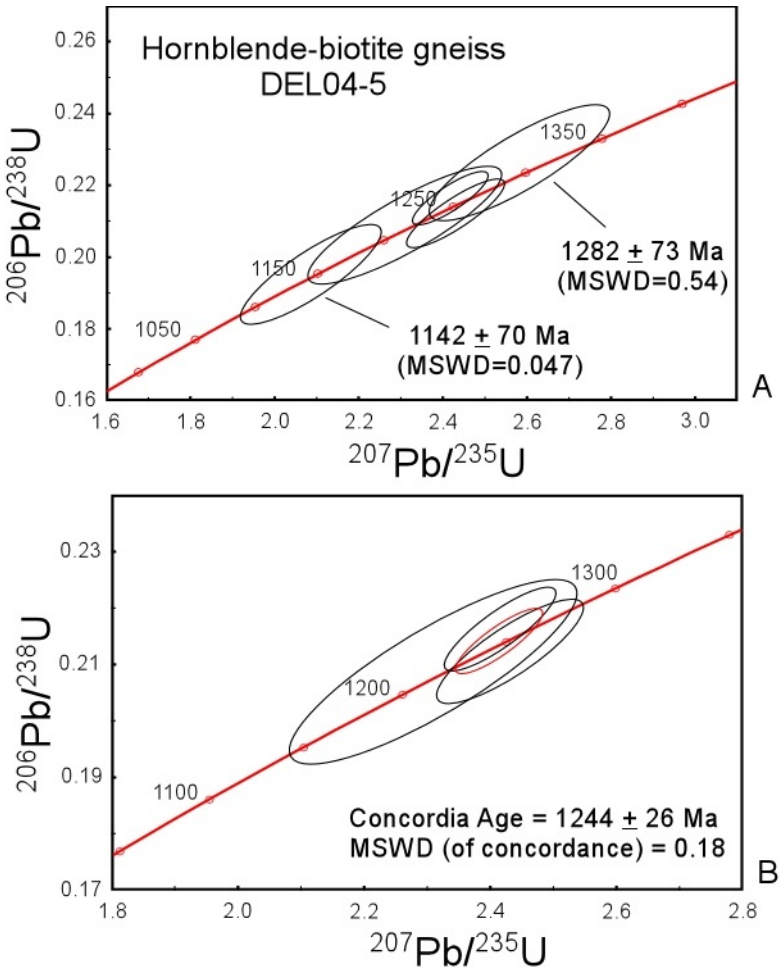

Figure 4.21. Concordia plots from hornblende-biotite gneiss zircons, DEL04-5. A) Plot of all data from polished grains. Ellipses interpreted to represent three age modes, with 1142 and 1282 Ma ages marked. B) Weighted mean age of 1244 ± 26 Ma determined from the average of three spots from zircon cores.

CG03-2, Hornblende-Biotite Gneiss

U-Pb ages were determined from nine spots on nine grains that were isolated from a layer of hornblende-biotite gneiss that occurs at the Coleman Gap outcrop, sampled along Coleman Gap Road, above I-40 in the Clyde quadrangle. Unfortunately, the nine points are not sufficient to thoroughly resolve the distribution of ages from this lithologically and texturally complex sample. Concordia plots are shown in Figure 4.22, with slabs and zircon CL images given in Figure 4.23. The first diagram contains error ellipses from all nine ion probe spots, with ages ranging from 1042 to 420 Ma (Figure 4.22.A). Three age modes were determined in a more comprehensive study of hornblende-biotite gneiss from the central Blue Ridge. These ages are 1030-1055, 1153-

1170, and 1287-1292 Ma (Loughry, 2010). A cumulative probability plot from two grains in the present investigation yields an age of 1042 ± 84 Ma (Figure 3.22.B), an age that falls within the youngest age mode from Loughry (2010). An age of 965 ± 50 Ma was determined from a weighted mean of two points. The ~965 Ma zircons from hornblende-biotite gneiss display oscillatory zoning under CL (Figure 3.30), indicative of an igneous origin, unlike the ~997 Ma rims of the migmatitic biotite gneiss that lack oscillatory zoning, and appear to be of metamorphic origin. In the present study, more Neoproterozoic to Paleozoic ages were determined relative to the widely Mesoproterozoic ages determined by Loughry (2010). These Neoproterozoic to Paleozoic grains tend to be smaller (50-100 micrometer) relative to the larger (~100-200 micrometer) Mesoproterozoic grains of Loughry (2010). Several grains analyzed here appear to contain xenocrystic cores, and yielded discordant ages.

HM03-5B, Hornblende-Biotite Gneiss

Sample HM03-5B was collected in the easternmost Clyde quadrangle, where it occurs as a felsic, hornblende-biotite orthogneiss, mapped as part of the Sandymush Felsic Gneiss unit of Merschat and Cattanach (2008). The high abundance of quartz and alkali feldspar can be seen in a scanned image of the slab (Figure 4.24). Also shown in Figure 4.24 are CL and BSE images of the zircons with spot locations and concordia ages. The zircons are characterized by large cores that show oscillatory zoning and are dark (U-rich) under CL. These older cores appear to have undergone fracturing and corrosion prior to the growth of thick mantles of newer material that is bright under CL and may show fine oscillatory zoning. Four spots were analyzed from four crystals, with all points plotted in Figure 4.25.A. Two ages were determined from the older cores that yield a weighted mean age of 1147 ± 43 Ma (2σ). Two ages determined from the younger, thick rim material yield a weighted mean age of 1007 ± 60 Ma (2σ). The younger rim material appears to have the same age as the 997 ± 18 Ma rims determined from migmatitic biotite gneiss in the Dellwood quadrangle (DEL03-1, 1L).

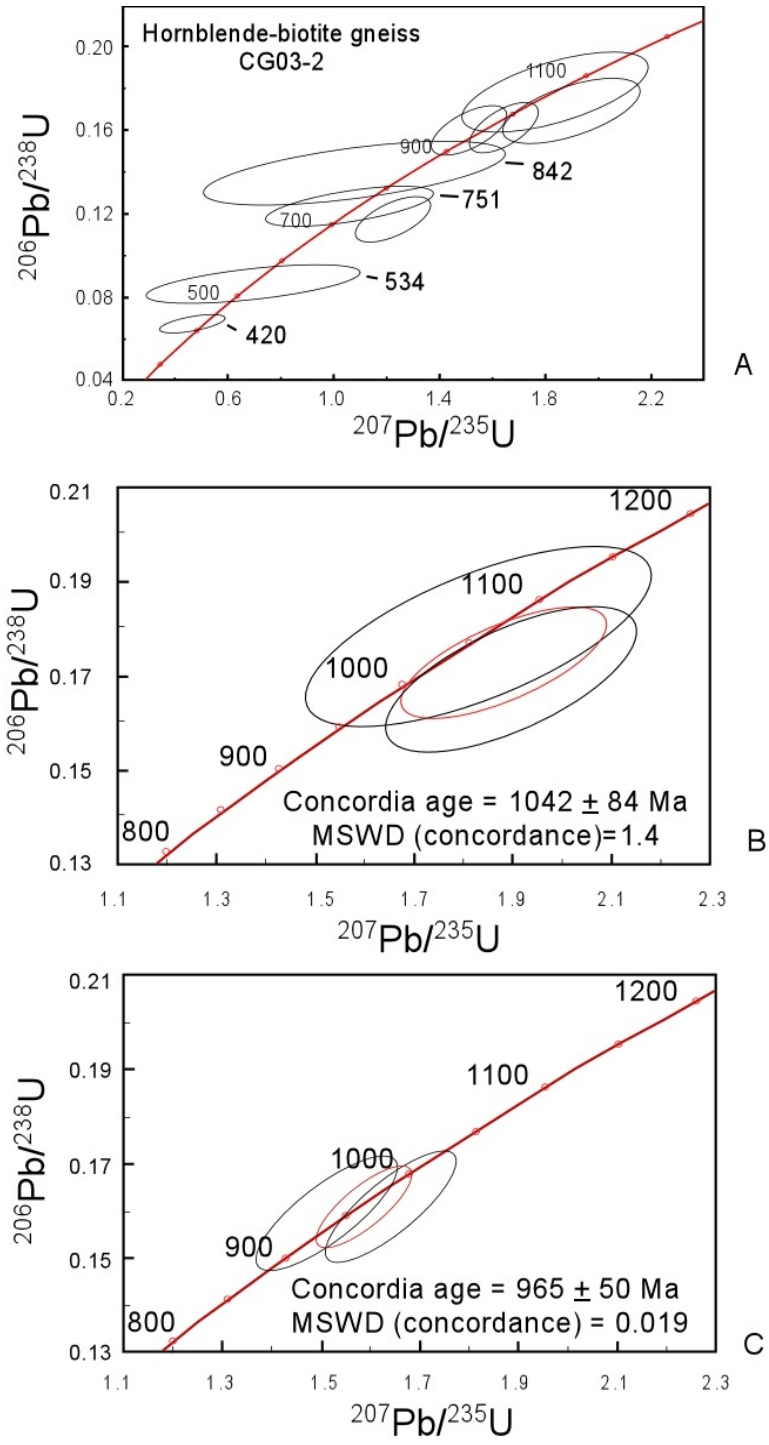

Figure 4.22. Concordia plots of zircon ages determined from hornblende-biotite gneiss, CG03-2. A) Plot of all 9 points. B) 1042 ± 84 Ma determined from a weighted mean of two points. C) 965 ± 50 Ma determined from a weighted mean of two points.

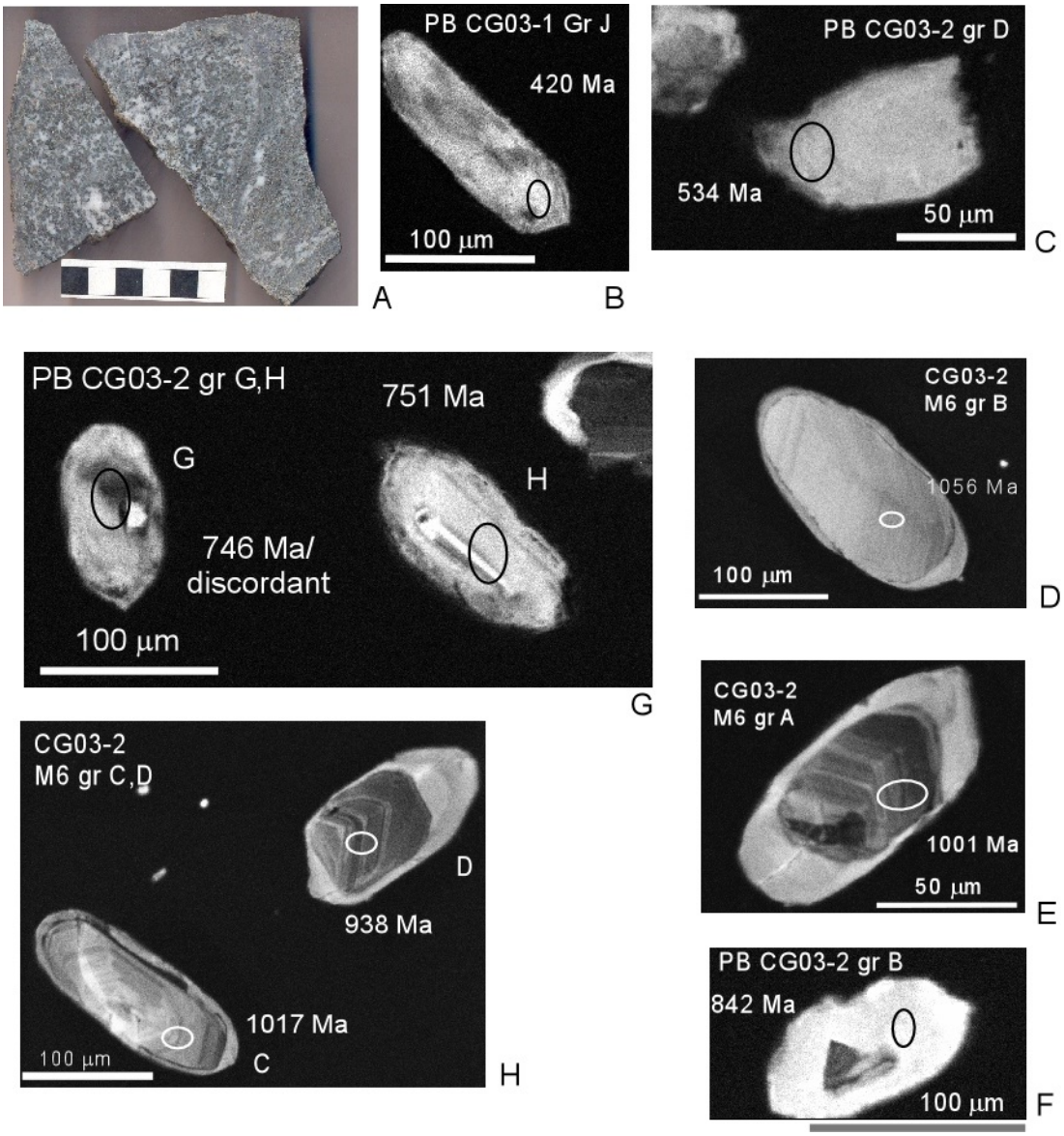

Figure 4.23. Slab and CL images of zircons from hornblende-biotite gneiss, sample CG03-2. A) Slab of hornblende-biotite gneiss, CG03-2, with cm-scale. B-H) CL images of zircon grains with approximate pit locations and concordia ages. Traces of xenocrystic cores can be seen in image G in grains G and H.

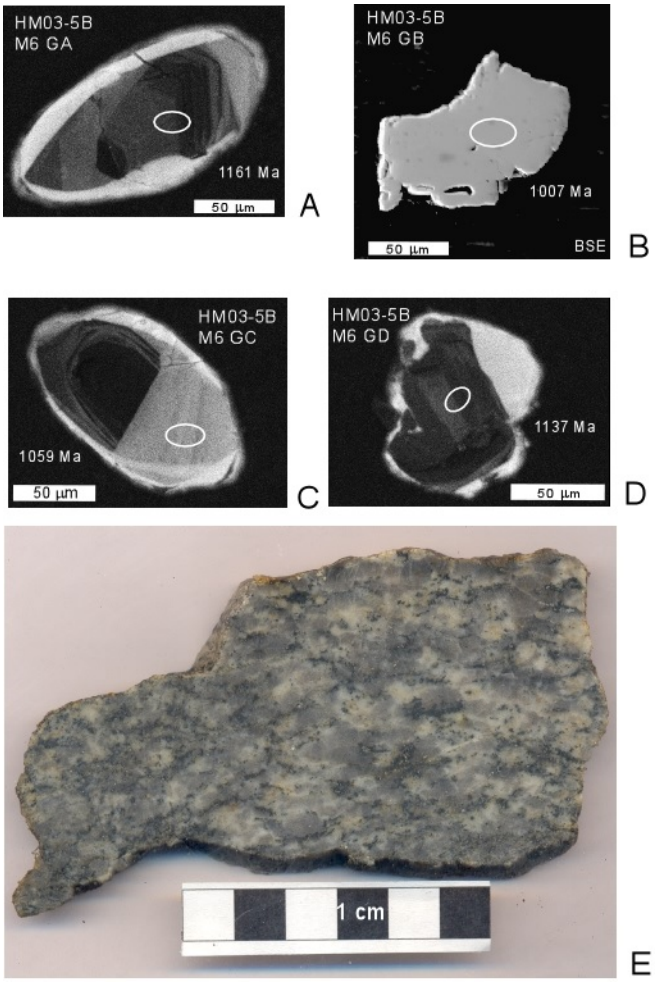

Figure 4.24. CL and BSE images from hornblende-biotite gneiss, HM03-5B. A- D) grains A,B,C, and D from grain mount #6. Grain B is interpreted to be a fragment of younger rim material that spalled off of a larger zircon crystal. E) Scan of slab from HM03-5B. Quartz appears gray, alkali feldspar is white, hornblende and biotite are black to dark green.

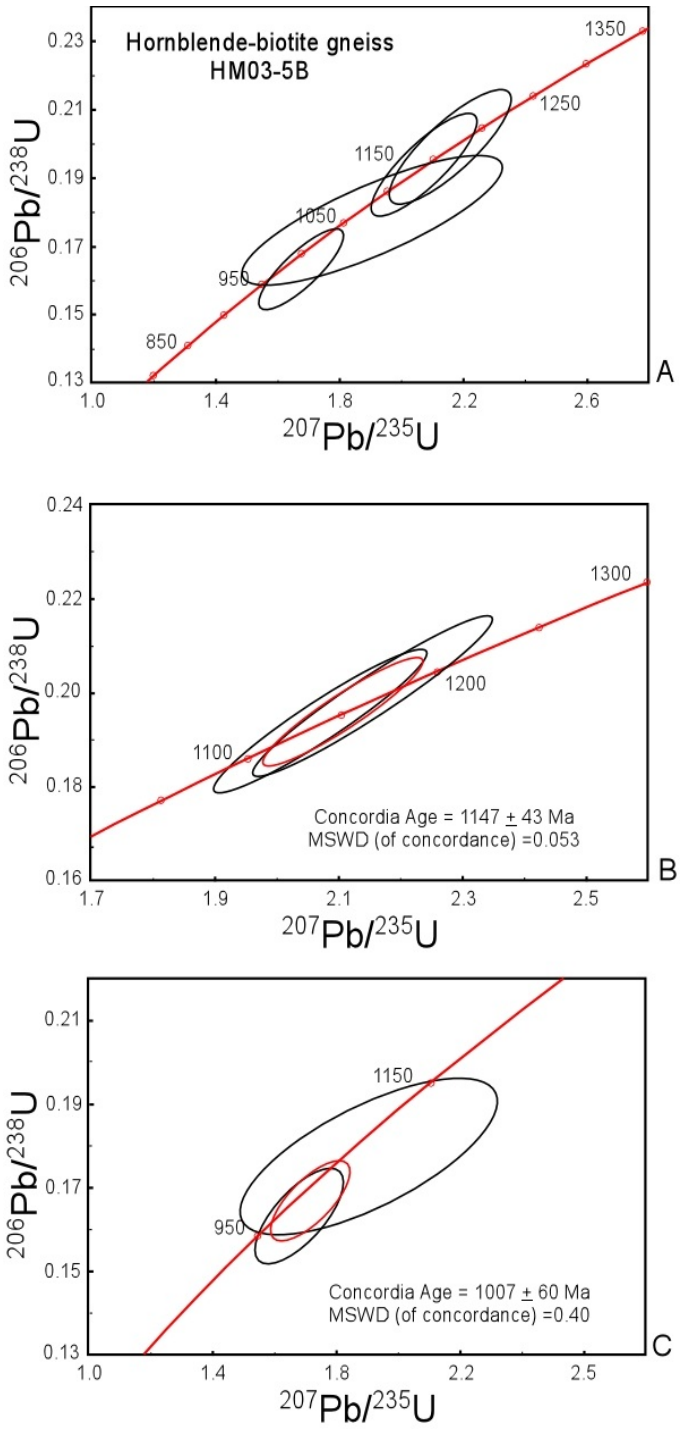

Figure 4.25. Concordia plots from hornblende-biotite orthogneiss, HM03-5B, central Blue Ridge. A) Concordia plot of all points from HM03-5B. B) Weighted mean calculated from older zircon cores. C) Weighted mean calculated from thick zircon rims.

Biotite Augen Gneiss

CH02-2B, Biotite Augen Gneiss

Sample CH02-2B was sampled at Cherokee Gap, on U.S. Route 19 southeast of Cherokee, in the Whittier Quadrangle. The sample is an L-S tectonite, containing coarse augen composed of feldspar porphyroclasts, and belongs to the "Ravensford body" of Hadley and Goldsmith (1963), traditionally designated as western Blue Ridge orthogneiss. Five points on five polished grains were analyzed, with spot locations and ages shown in Figure 4.26. Of these five spots, one age was low relative to the others (604 Ma). Three points were averaged to give a weighted mean age estimate of 992 $\pm$ 41 Ma. Southworth and Aleinikoff have also estimated the age of biotite augen gneiss from the same Ravensford body, sampled at the head of Big Cove on the north side of the bridge over Raven Fork in the Smokemont quadrangle. Zircons from this previous study yielded a SHRIMP U-Pb age of 1029 Ma (Southworth and Aleinikoff, in press). The concordia age determined here (992 Ma) is lower than the 1029 Ma age. However, upon closer inspection, the zircon grains from "puck B" closely resemble the unpolished grain from "puck 2"; it would appear that during the preparation of puck B, the grains were under-polished. Puck A, was polished enough to reveal oscillatory zoning within the core, and grain B from "puck A" yields an age of 1010 Ma, that is in closer agreement to the 1029 Ma age determined by Southworth and Aleinikoff. Given the low degree of polishing, it would appear that the 992 Ma age represents the age of metamorphic rim material that encases the older, ~1029 Ma core material. The 992 Ma age is in agreement with the 997 Ma metamorphic rim age determined from DEL03-1 and DEL03-1L of the central Blue Ridge.

Several unpolished zircon grains from CH02-2B were also examined using the "ion-tunneling" or "depth-profiling" approach, with notable results shown in Figure 4.27.C. Twelve blocks or analytical cycles were determined incrementally, as the ion probe tunneled through an unpolished rim through a total depth of approximately 0.3 micrometers. The outermost rim appears to be Taconic aged, however single analytical blocks yield ages having a high degree of uncertainty; the rims could be Acadian or Neo-Acadian aged. As tunneling progressed towards the core, the data indicate a tendency towards Mesoproterozoic-aged zircon material. It appears as though Taconic deformation in the western Blue Ridge resulted in the development of very thin (< 0.3 micron) zircon rims growing outside of ~997 Ma metamorphic rims, that in turn encased the older ~1029 Ma zircons.

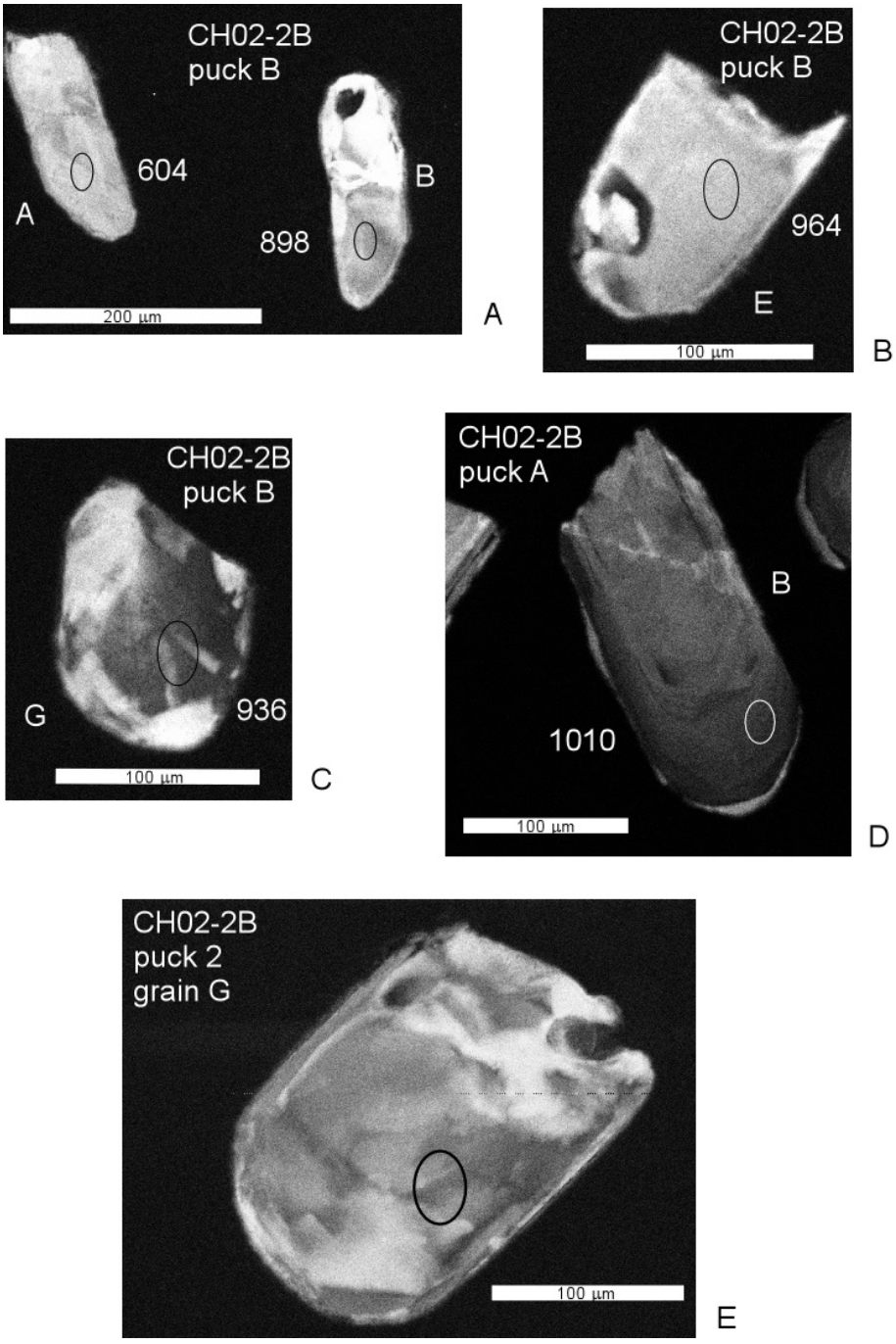

Figure 4.26. CL Images of zircons from biotite augen gneiss, sample CH02-2B. A),B),C), CL images from lightly-polished puck B, with approximate pit location and concordia age in Ma. D) CL image of well-polished puck A, grain B, oscillatory zoning visible. E) CL image of unpolished grain G from puck 2, with location of ion-tunneling pit.

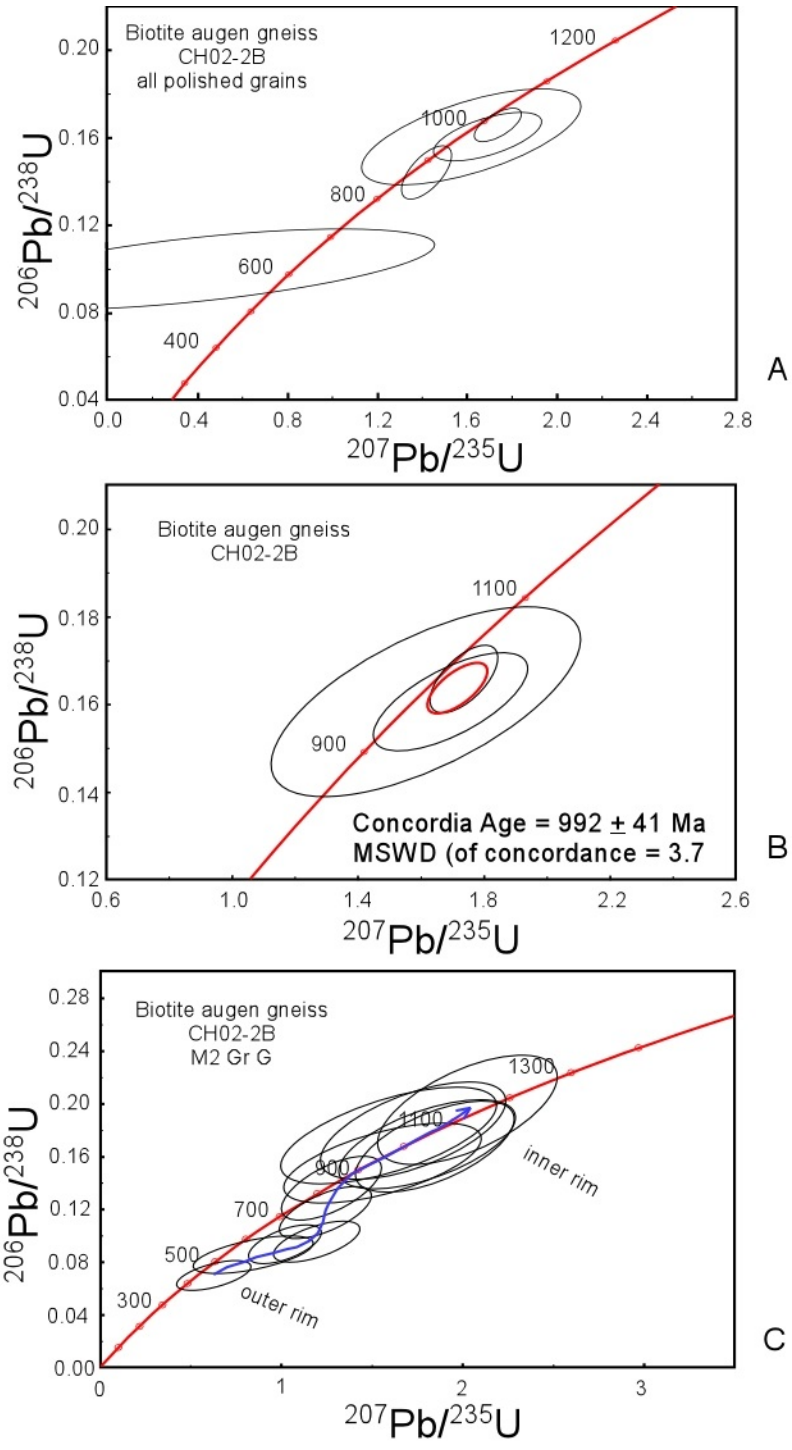

Figure 4.27. Concordia diagrams from biotite augen gneiss, sample CH02-2B. (Legend follows).

Figure Legend 4.27

A) Summary plot with 5 points from pucks A and B. B) Weighted mean of 992 Ma calculated from three points. C) Concordia plot from ion-tunneling through an unpolished rim. Total pit depth is approximately 0.3 micrometers Outer rim shows a Paleozoic age (Taconic?), with progressively older ages resulting from continued tunneling. Inner rim age is Mesoproterozoic; each ellipse represents a single analytical block or cycle from the CAMECA 1270 ion microscope, with data in Appendix K.

OS03-1A, Biotite Augen Gneiss

Samples of orthogneiss were collected on Old Soco Road along Hornbuckle Creek in the Sylva North quadrangle. These outcrops have been referred to as the Qualla-Dellwood belt, and are traditionally designated as western Blue Ridge basement (Southworth et al., 2005a). Although large K-feldspar augen are not present in the scanned slab, there are bands or lenses of granitic material, interspersed with layers of biotite-rich bands (Figure 4.28), suggesting that this sample is an orthogneiss, derived by the deformation of a precursor granite. CL images of zircon from OS03-1A reveal U-rich cores having irregular zoning patterns, surrounded by relatively thick, U-poor rims that appear bright under CL and show oscillatory zoning. Four points determined from the older core material are plotted in Figure 4.29. Three points were averaged to yield a weighted mean age of 1122 $\pm$ 47 Ma. The fourth point is significantly older (1188 $\pm$ 84 Ma), and is interpreted to represent an older, xenocrystic core, that represents a second age mode. These results suggest that the Qualla-Dellwood (1122 Ma) and Cherokee-Raven Fork belts (1029 Ma, Southworth and Alleinikoff, in press) are composed of distinct orthogneisses. The primary mode of zircon ages from OS03-1A (1122 Ma) is more similar to the adjacent Granitic Gneiss unit sampled at Cataloochee Estates (1168 Ma, Southworth and Aleinikoff, in press). The disparity between the ages determined from the Cherokee-Raven fork belt (1029) and the Qualla-Dellwood belt could support Southworth et al.'s inference that a major Alleghanian fault (or possibly a Devonian dextral fault?) exists between the two belts. The proposed Alleghanian fault was based on differences in metamorphic conditions determined in the two belts and their cover sequences.

Alternatively, the thick, low-U rims that display oscillatory zoning in OS03-1A remain undated, and they could signify the recycling of older material from the Qualla Dellwood belt at *circa* 1029 Ma. Both of these adjacent western blue Ridge basement "belts" may be composed of a mixture of different-aged Mesoproterozoic orthogneisses, with prevalent age modes resulting from ~1029 and 1120-1180 Ma plutonic events.

PK03-3, Biotite Augen Gneiss

PK03-1 was sampled west of Purchase Knob, in a gated community that lies in the Dellwood quadrangle. Small (~3mm) augen can be seen in Figure 4.30, along with CL images of the zircons analyzed. Zircon grains show oscillatory zoning in the cores, and have relatively thick, low-U rims. The boundary between the core and rim appears irregular and corroded. Three points from three grains determined from zircon cores yield a weighted mean age of 1172 $\pm$ 46 Ma (Figure 4.31).

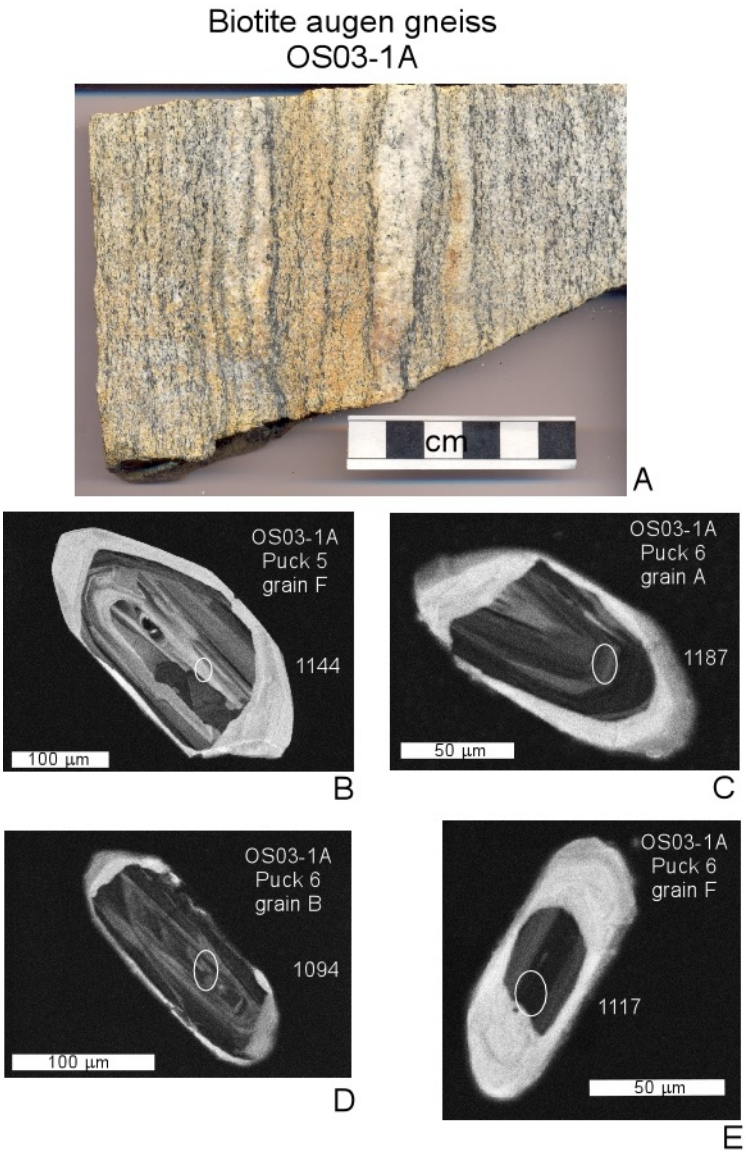

Figure 4.28. Slab and CL images of zircon, biotite augen gneiss, OS03-1A. A) Slab from OS03-1A with bands of granitic material. Orange streaks due to weathering. B-E) CL images of zircon, with pit locations and ages in Ma.

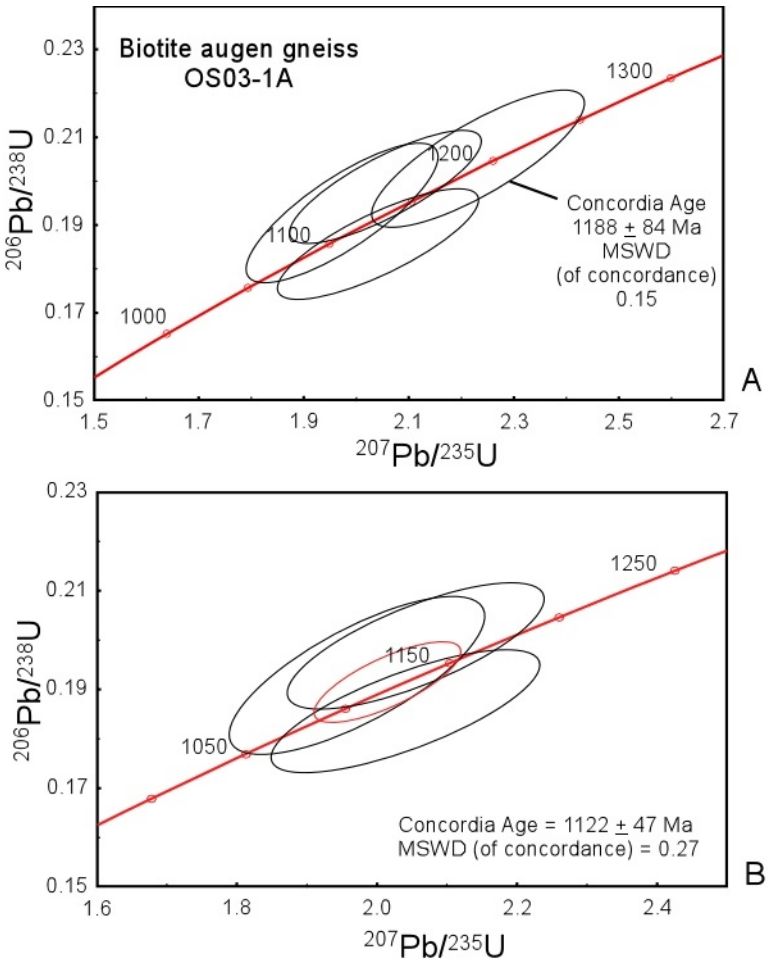

Figure 4.29. Concordia Plots from biotite augen gneiss, OS03-1A. A) Plot of all points from polished grains, with a single 1188 ± 84 Ma age. B) Weighted mean age of 1122 ± 47 Ma determined from the average of three cores.

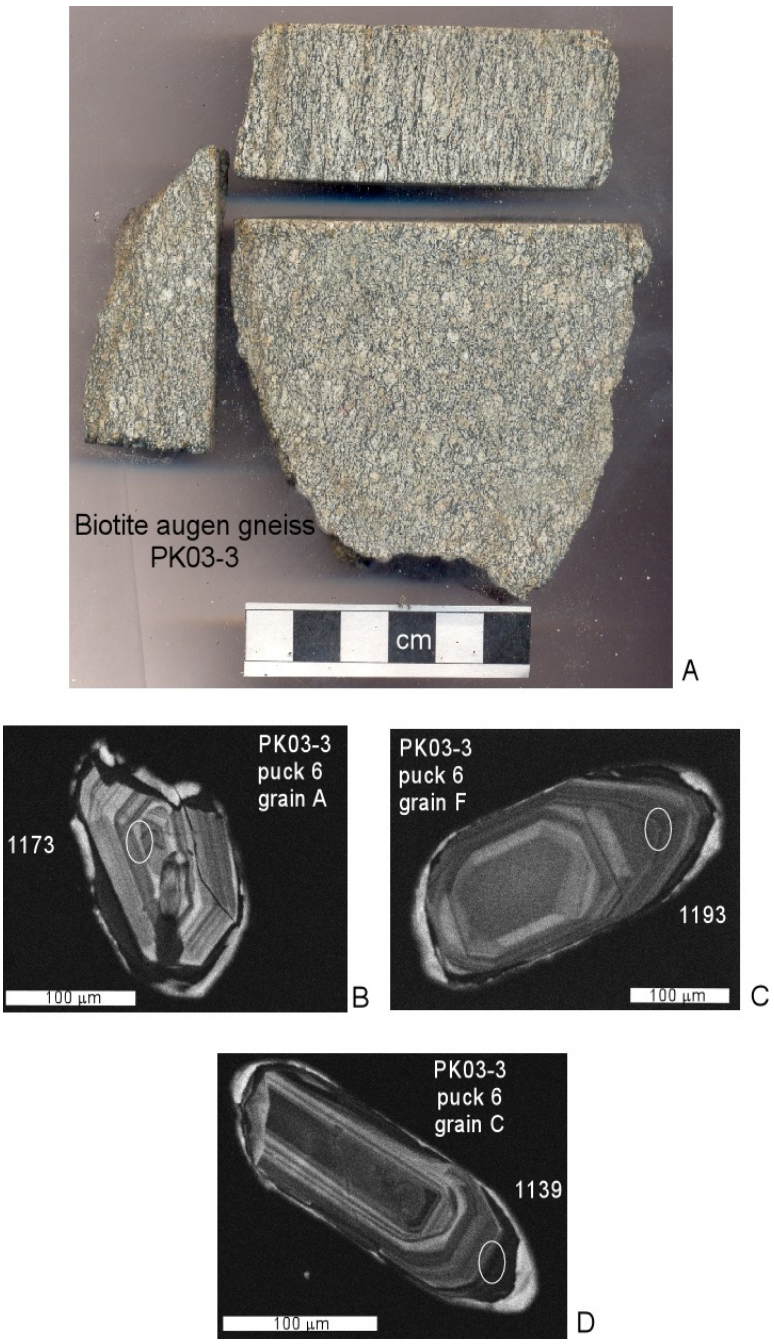

Figure 4.30. Slab and CL images of zircon, biotite augen gneiss, PK03-3. A) Slabs of sample orthogneiss PK03-3. Gneissosity can be seen in the top slab, small feldspar augen are visible in the largest slab. B-D) CL images of zircons with analysis pits and determined concordia ages in Ma.

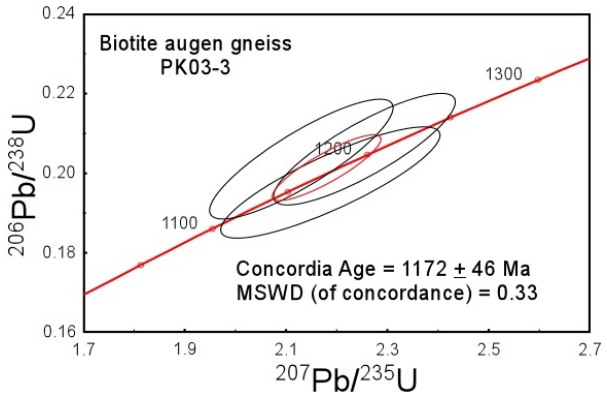

Figure 4.31. Concordia plot from biotite augen gneiss PK03-3 zircons.

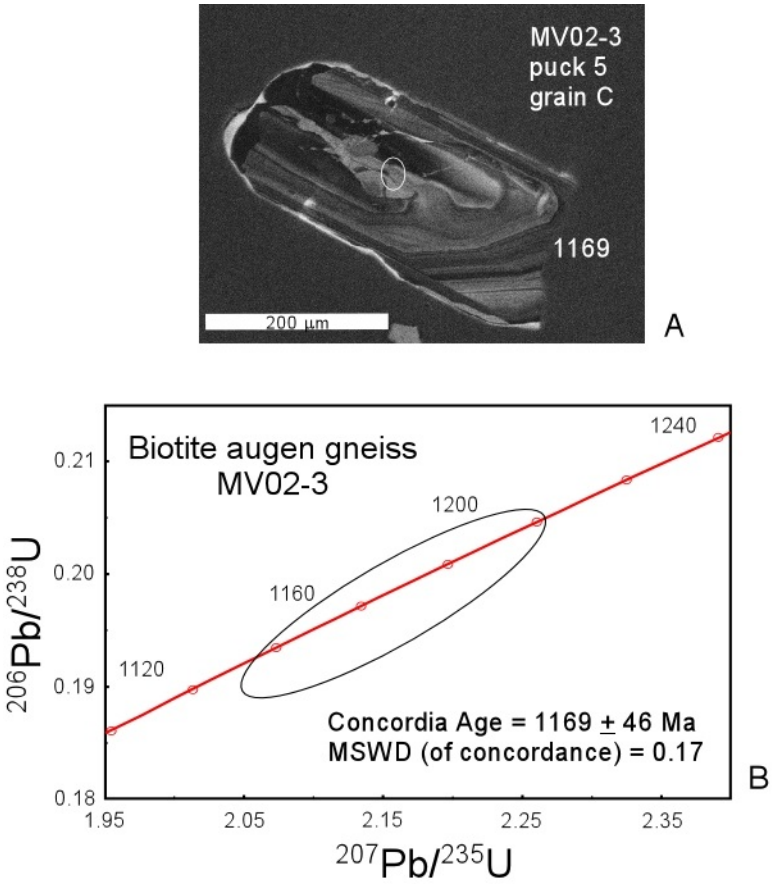

Figure 4.32. CL image and concordia plot, biotite augen gneiss, MV02-3. A) CL image of zircon from MV02-3. B) Concordia plot from a single grain.

MV02-3, Biotite Augen Gneiss

A variety of orthogneisses and were sampled north of Jonathan Creek on the road leading into Mitchell Cove. One point from one grain was analyzed to yield a U-Pb age of 1169 $\pm$ 46 Ma, with CL image and concordia diagram given in Figure 4.32.

SC04-6, Biotite Augen Gneiss

A suite of deformed orthogneiss was collected west of Purchase Knob, in the Dellwood quadrangle, along a gravel road that leads to the science center. Several of these samples are mylonitic. Six zircons were analyzed from sample SC04-6, with a slab of the sample and CL images of the zircon grains shown in Figure 4.33. Zircon cores are gray to black (U-rich) with convoluted zoning; rims show variable thickness, with some thick rim material (~30 micrometers) composed of zircon material that is bright under CL (U-poor). Five points from five grains exhibiting consistent oscillatory zoning characteristics (i.e. magmatic crystallization) yield a weighted mean age of 1129 $\pm$ 36 Ma. A sixth point has a concordia age of 1209 Ma, was omitted from the age calculation because it appears to be inherited (Figure 4.34).

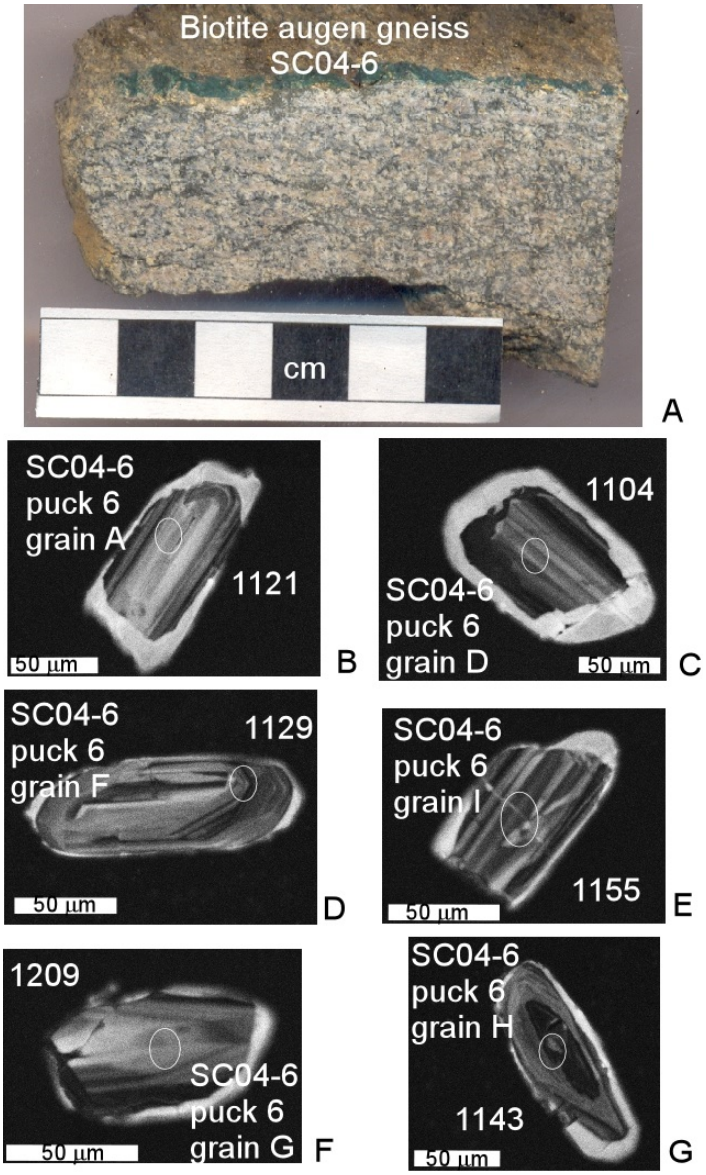

Figure 4.33. Slab and CL images of zircon, biotite augen gneiss, SC04-6. A) Slab of the sample, from the Dellwood quadrangle. B-G) CL images of zircon with analysis pits and concordia ages in Ma.

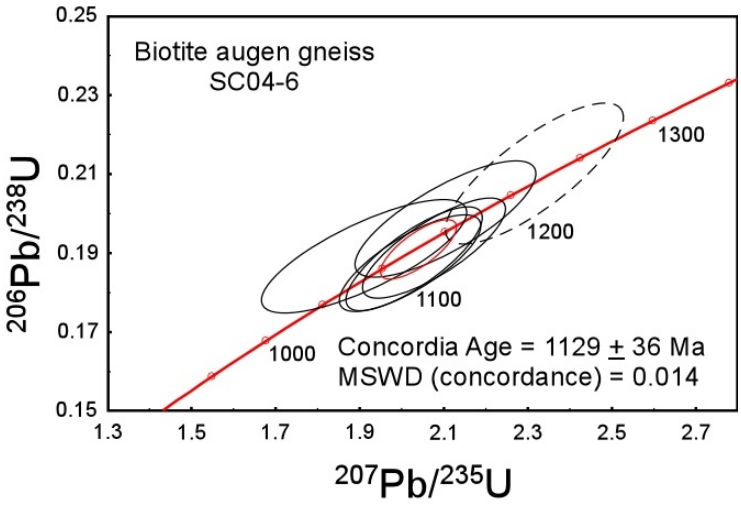

Figure 4.34. Concordia diagram, biotite augen gneiss, SC04-6. Of the six analyses plotted, five were used to calculate a weighted mean age of 1129 ± 36 Ma; the sixth spot is plotted as a dashed ellipse.

FC04-1B, Spotted Orthogneiss

Samples of gneiss were collected near the junction of Fines Creek Road and I-40, from an outcrop north of the westbound I-40 onramp. A variety of different lithologies are exposed here including augen gneiss with K-feldspar augen, as well as an intermediate spotted orthogneiss, that does not fit clearly into either the biotite gneiss or biotite augen gneiss classifications. These lithologies were mapped as part of the Spring Creek Granitoid Gneiss unit of Merschat and Cattanach (2008), and commonly assigned to the western Blue Ridge basement complex (e.g. Hatcher et al., 2005). Zircon morphology from FC04-1B separates is different relative to most of the other basement complex samples; zircons from FC04-1B are brown with rounded terminations, in contrast to the more frequent pink zircons that are common in most of the other orthogneiss samples. Also present in sample FC04-1B is a generation of spherical zircons that appear to be of metamorphic origin (Corfu et al., 2003). A slab of the sample, CL images of zircons, and a concordia diagram of the four points determined from the zircons are given in Figure 4.35. The four points appear to belong to three different age modes. Two points from xenocrystic cores of spherical zircons were averaged to yield an age of 1336 ± 51 Ma, an age represented in most detrital zircon data sets (e.g., Chakroborty et al., 2011) and in some Hbl-Bt orthogneisses (Moecher, pers. comm., 2011). The other ages from this sample are 1145 ± 41 Ma, from a single point determined from the core of an ovoid-shaped brown grain, and 1047 ± 79 Ma determined from a spherical grain that appears to lack a xenocrystic core.

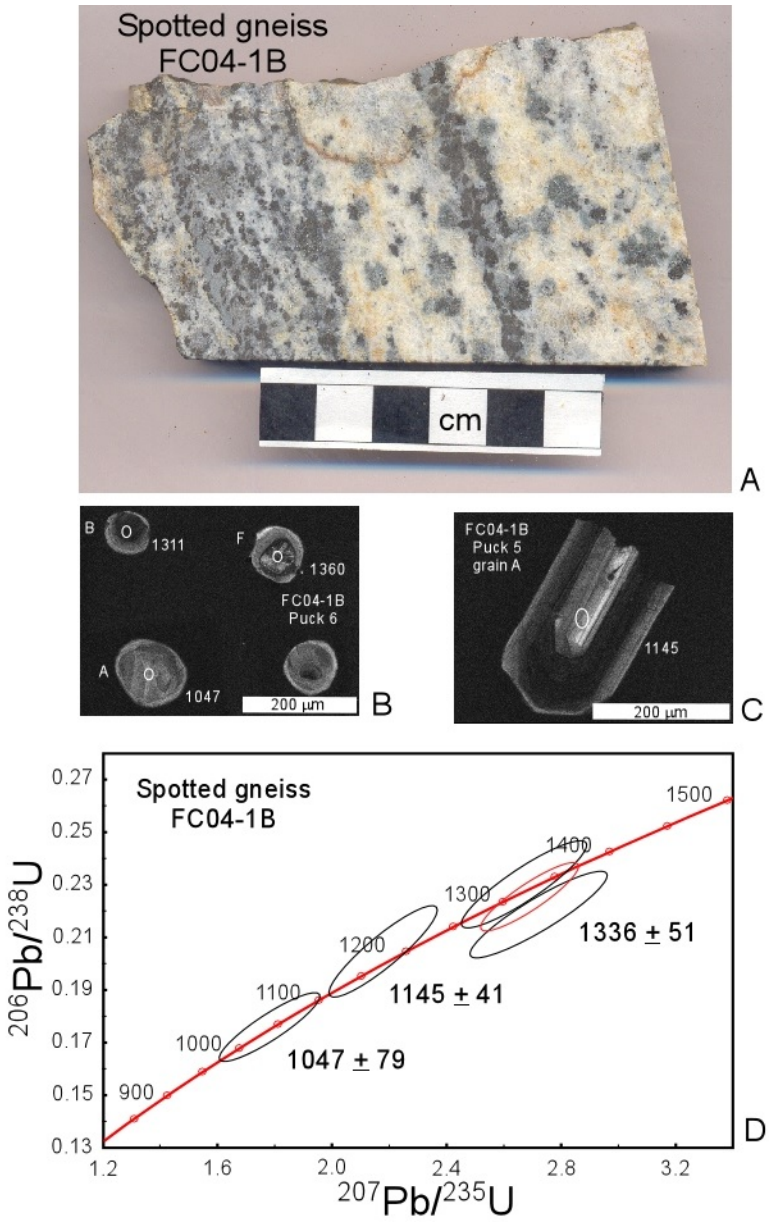

Figure 4.35. Zircon images and concordia plot from spotted gneiss, FC04-1B. A) Image of slab with dark spots composed of biotite. B) CL images of spherical zircons with spot locations and concordia ages (Ma). C) CL images of a fractured grain that appears brown under transmitted light. D) Summary plot with three distinct age modes.

Monazite Ages: Results and Interpretation

Monazite was separated from five schists and one orthogneiss sample. Th-Pb ages were determined using the CAMECA IMS-1270 at UCLA (Table 4.2, Appendix L). The "unmix ages" function of Isoplot V.3.5 (Sambridge and Compston, 1994; Ludwig, 2003) was used to delineate age modes. Previous chemical age and elemental mapping studies (EMPA) from the same formations have demonstrated the existence of distinct age domains within single monazite crystals (Moecher et al., 2003), and the relatively large ion probe spot size was expected to sample material from a mixture of monazite age domains. Although monazites were not characterized prior to analysis, it would be possible to conduct follow-up EMPA studies of the monazites examined here.

Four dates were determined from the cores of four monazite grains that were separated from the Wading Branch Formation, lower Snowbird Group (sample #CCG03-3B). The sample is a Grt-Chl phyllite with crenulation cleavage (Figure 4.11.C,D), sampled west of Cove Creek Gap. The results appear to show a bimodal age distribution with one age determined to be 463 $\pm$ 40 Ma, and three younger aged points yielding a weighted average age of 417 $\pm$ 17 Ma (Figure 4.36).

Six spots from six monazites were determined from a Great Smoky Group Grt-Ky-Ms-Bt-Pl-Kfs schist (sample MV02-1B), collected near Maggie Valley, NC, below Leatherwood Top. The weighted average Th-Pb age determined from this Great Smoky Group schist is 426 $\pm$ 12 Ma, with no auxiliary age mode apparent (Figure 4.37).

A St-Grt schist from the Mineral Bluff Formation, sample MB02-4 from the Murphy Belt (junction of NC 141 and Kinner's Cove Road, Marble quadrangle) shows a bimodal age distribution of monazite Th-Pb ages: one point was determined to have an Acadian age of 380 $\pm$ 30 Ma, while the seven other points determine a weighted average of 416 $\pm$ 11 Ma (Figure 4.38).

A Grt-St-Ky-Ms-Bt-Qtz-Pl-Rt schist from the Great Smoky Group, (GT02-2, sampled near Big Witch Gap, Blue Ridge Parkway, Bunches Bald quadrangle) records a variety of monazite U-Th ages. Four age modes were estimated using Isoplot V.3.5: 128 $\pm$ 8.5 Ma, 311 $\pm$ 16, 406 $\pm$ 23, and 450 $\pm$ 26 Ma, using the "unmix ages" function (Figure 4.38). The significance of the ~127 Ma ages is unclear (lead loss?). The 310 and 450 Ma ages appear to have resulted from the Alleghanian and Taconic orogenies, and the 406 Ma age may result from a mixture of Alleghanian, Acadian, and Taconic age domains, sampled by a relatively large ion beam. If, however, ages younger than 380 Ma are excluded from the age-unmixing routine, three age modes are resolved that more closely match the results from the other four monazite populations analyzed here: 384 $\pm$ 34, 429 $\pm$ 20, and 458 $\pm$ 32 Ma (Figure 4.40).

Results of Th-Pb monazite dating from migmatitic biotite gneiss (MM-22) were presented above (Figure 4.17). Monazite ages appear to show a bimodal distribution; the younger 434 $\pm$ 9.5 Ma is more frequent than a Taconic age of 457 $\pm$ 31 Ma.

In summary, all five samples from the Ocoee, Murphy belt, and central Blue Ridge migmatite contain monazites that fall within the age range of 434-416 Ma. This age is tentatively interpreted as the time of a distinct Middle- to Late-Silurian tectophase

that occurred in the western and central Blue Ridge (Cherokee orogeny of Hibbard et al., 2010). If these metamorphic monazite domains were produced during prograde metamorphism (e.g. the Staurolite-in isograd) related to the Taconic metamorphic event at ~460 Ma, monazite ages would be expected to be *older* than 460 Ma. The tectonic events related to the 434-416 Ma monazite ages are unclear. The dates may be related to a post-metamorphic thermal pulse indicated by a pulse of trondhjemite dikes (Hadley and Goldsmith, 1963; Merschat and Wiener, 1990). 420 Ma trondhjemitic to granodioritic plutonism is reported in the eastern Blue Ridge (Miller et al., 1997), that appear to be correlated to small trondhjemite dikes mapped in the SE portion of the Dellwood quadrangle (Hadley and Goldsmith, 1963). The 434-416 monatite ages and trondhjemite dike plutonic episode may be related to terrane accretion events that occurred east of the Great Smoky Mountains, for example at the boundary of the Carolinian Slate belt and Charlotte belt, where the Newberry eclogite formed via the subduction of Parr Shoals amphibolites prior to 415 Ma (Shervais et al., 2003). Hibbard et al. (2010) proposed that Carolinia docked with Laurentia during the late Ordovician Cherokee orogeny in the southern Appalachians. This model, which implicates closure of Iapetus by the Silurian and northwest directed continental subduction of Carolinia beneath Laurentia is supported by the monazite ages determined here.

This age mode (434-416 Ma) is dominant in the present study and strikingly absent in recent detrital monazite studies of the eastern Blue Ridge/French Broad River drainage basin, occurring to the east (Hietpas et al., 2010; Moecher et al., 2011). Unlike the disparity between EMPA and ion probe SIMS data sets, the lack of 434-416 Ma monazite ages in the French Broad River drainage basin is difficult to dismiss because both data sets (this study and Hietpas et al., 2010) were determined using the same instrument, and the same analytical protocols.

Other points that are pertinent to the discussion of monazite ion-probe results determined here are:

- The ion probe and statistical unmixing is capable of resolving distinct age modes at ~460 and 434-416 Ma. These ages probably correspond to the "weak modes" determined via EMPA chemical dating at ~480 and ~440 Ma from sample GT02-2 (Moecher et al, 2003).

- No ages ranging from 510-540 Ma were determined in the present study. Monazite age modes in this range were previously determined in EMPA studies of samples from the same outcrops (GT02-2, MM-22, Moecher et al, 2002, 2003). This may be due to the large ion-probe spot size that precludes the resolution of volumetrically-small age domains.

- Corrie and Kohn (2007) interpreted U-Pb monazite ID-TIMS ages that clustered around 450 Ma as being the products of Taconic metamorphism, with a possible Acadian overprinting event occurring later in the Paleozoic (~380 Ma). Corrie and Kohn (2007) note that the high MSWD (mean square of the weighted deviates) imply that monazites do not belong to a single population. When

concordia ages of Corrie and Kohn (2007) are evaluated using the unmixing routine of Isoplot (Sambridge and Compston, 1994; Ludwig, 3003), the resulting age distribution contains two age modes at 448 ± 1 Ma and 421 ± 2 Ma, results that are broadly similar to the monazite age distribution determined here.

In summary, three of the samples examined here have Taconic monazite modes of ~460 Ma, statistically identical to high precision U-Pb zircon ages determined from the Wayah Bald metamorphic core complex, and zircons from the Lick Ridge eclogite. Clearly the Great Smoky Group (GT02-2) and Snowbird Group (CCG03-3B) experienced Taconic metamorphism. However, monazite age modes of the present study suggest that effects of the Silurian "Cherokee" orogeny (Hibbard et al., 2010) were also important in the regional metamorphic history of the western and central Blue Ridge. The poly-metamorphic textures evident in some Great Smoky group schists, expressed as multiple phases of garnet growth evident in Figure 4.11 may have resulted from Taconic metamorphism that was overprinted by a later Cherokee tectonometamorphic event. The irregular distribution of monazite ages (e.g. Cherokee and Taconic ages in the Great Smoky Mountains, and predominantly Taconic ages in the French Broad River drainage to the east, Hietpas et al., 2010; Moecher et al., 2011) allow for the possibility that strike-slip faulting and Devonian terrane dispersal recognized in the Piedmont (Dennis, 2007) may have also caused some reconfiguration of the central and western Blue Ridge terranes. Two of the samples were determined to have Acadian monazite ages (~380 Ma), the significance of which is presently poorly understood in the eastern Great Smoky Mountains.

Table 4.2. Summary of Th-Pb Monazite Data (SIMS) from the Western and Central Blue Ridge

			Age modes (2σ, Ma)				
Sample	Formation	Affiliation	Pre-Alleghanian	Alleghanian	Acadian	Middle to Late Silurian	Taconic
CCG03-3B	Wading Branch	WBR				417 ± 17	462 ± 40
MV02-1B	Great Smoky Group	WBR				426 ± 12	
MB02-4	Mineral Bluff	WBR			380 ± 30	416 ± 11	
GT02-2	Great Smoky Group	WBR	~128	~310	384 ± 34	429 ± 20	458 ± 32
MM-22	Migmatitic biotite gneiss	CBR				434 ± 9.5	457 + 31

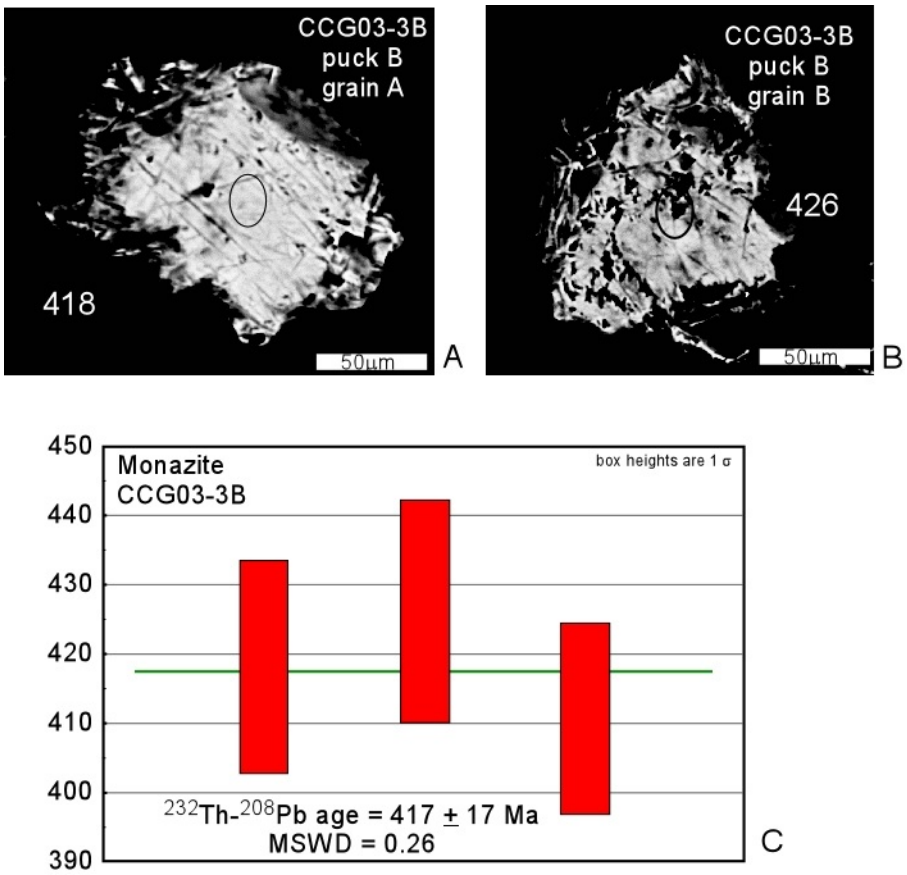

Figure 4.36. Monazite grains and weighted average Th-Pb age from Wading Branch phyllite. Sample CCG03-3B. A, and B) Representative BSE images of polished monazite grains with spot locations and Th-Pb ages. C) Weighted average plot from three monazite spots. The fourth Taconic-aged spot (463 ± 20 Ma) was excluded from this calculation as it represents a distinct age mode.

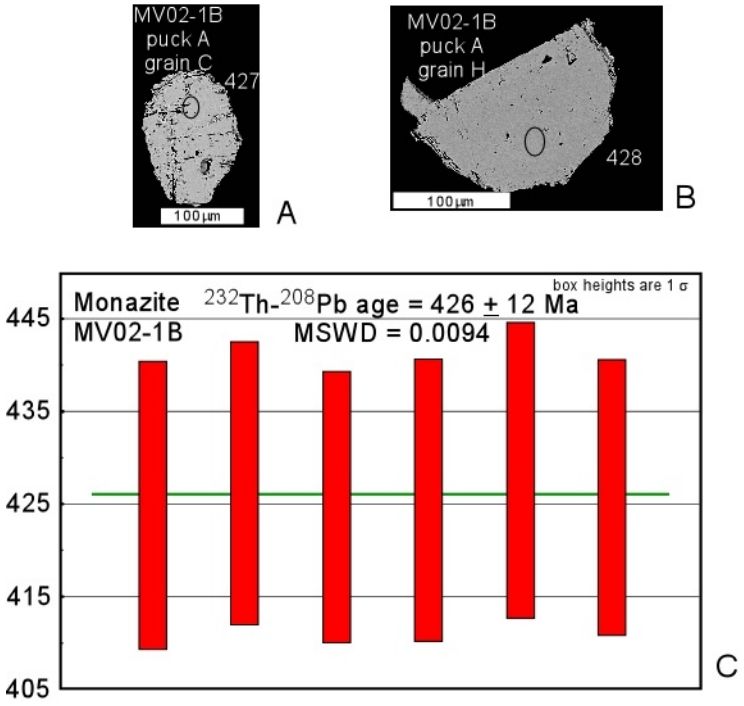

Figure 4.37. Monazite grains and weighted average Th-Pb monazite age from Great Smoky Group schist. A) and B) Representative BSE images of monazite separates from sample MV02-1B with ion probe analysis locations and Th-Pb ages. C) Weighted average age estimate determined from all points from MV02-1B.

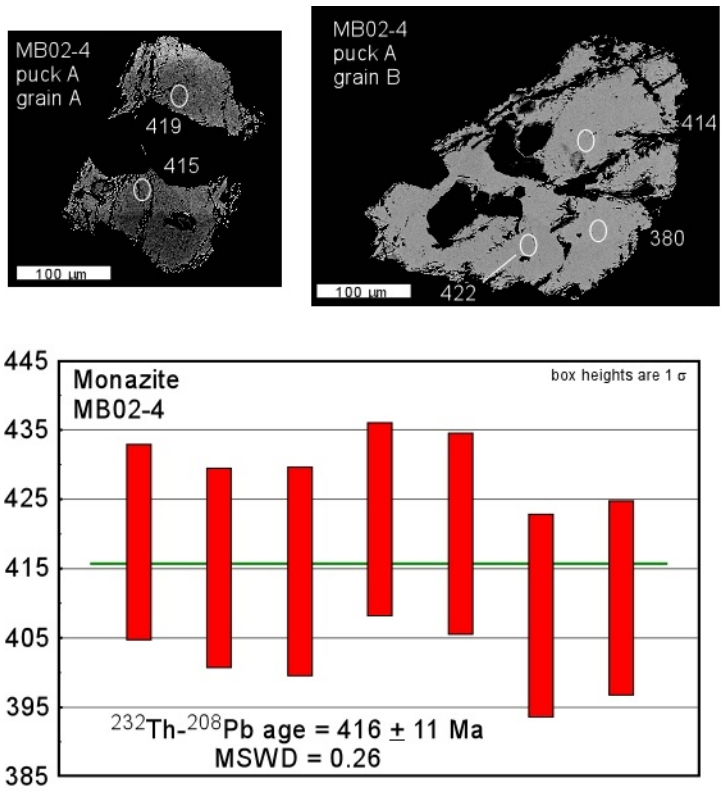

Figure 4.38. Monazite grains and weighted average Th-Pb monazite age from Mineral Bluff Formation, Murphy Belt. A) and B) Representative BSE images of monazite separates from sample MB02-4 with ion probe analysis locations and Th-Pb ages. C) Weighted average age estimate determined from seven points determined from MB02-4. The eighth point yielded a Acadian age (380 ± 15 Ma), defines a second age mode, and was excluded from the weighted average calculation.

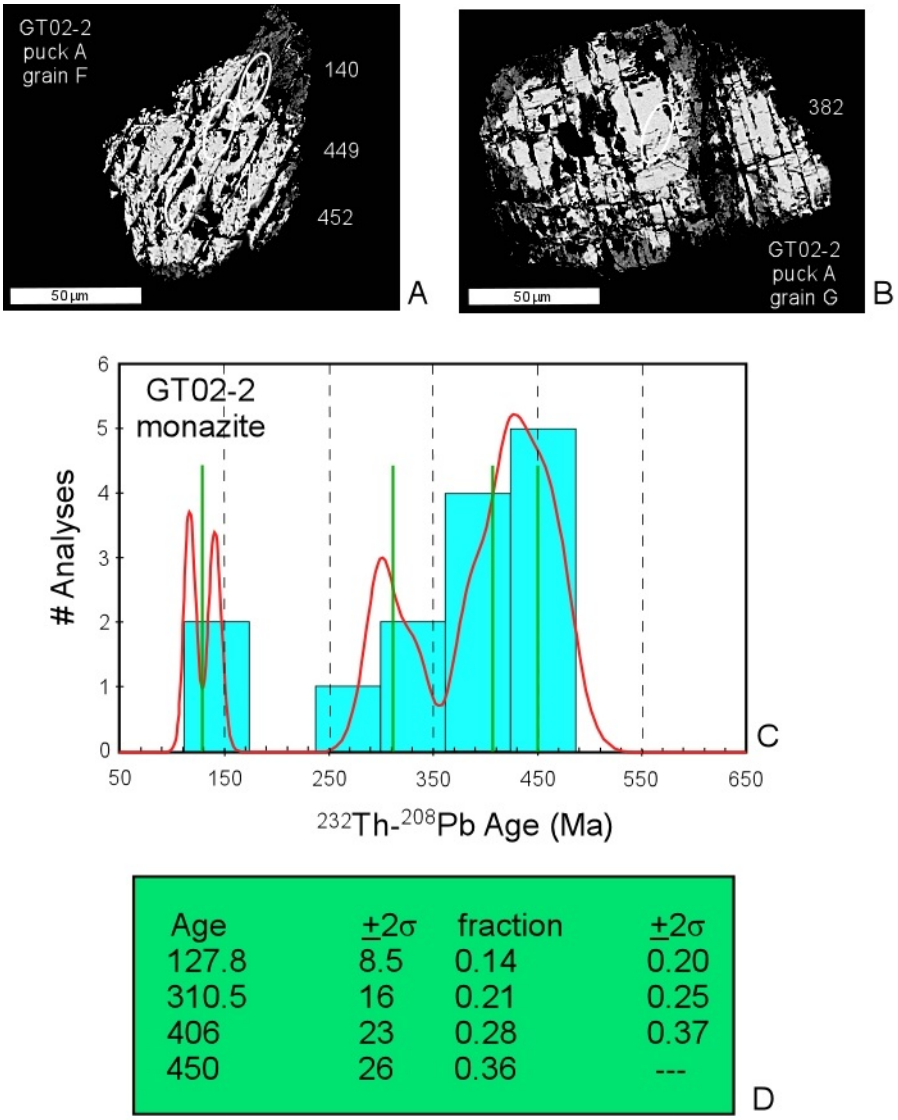

Age	±2σ	fraction	±2σ
127.8	8.5	0.14	0.20
310.5	16	0.21	0.25
406	23	0.28	0.37
450	26	0.36	---

D

Figure 4.39. Monazite grains and Th-Pb monazite unmixing ages from Great Smoky Group schist, GT02-2. A) and B) Representative BSE images of monazite separates from sample GT02-2 with ion probe analysis locations and Th-Pb ages. C and D) Age distribution and age modes determined for all points using Isoplot V 3.5.

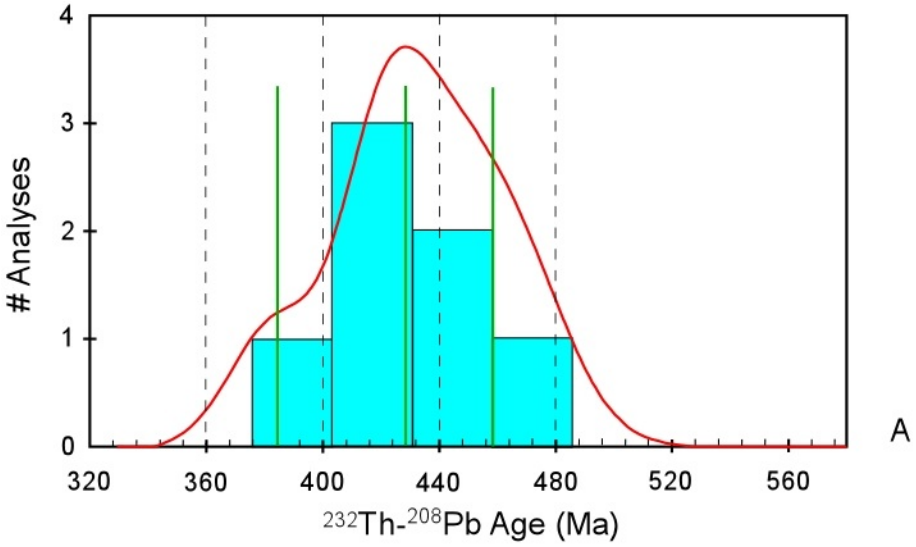

Age	±2σ	fraction	±2σ
384	34	0.14	0.30
429	20	0.56	0.67
458	32	0.30	----

B

Figure 4.40. Preferred Th-Pb monazite age modes, Great Smoky Group schist, GT02-2. A) and B) Age histogram and preferred age modes determined from monazite spots older than 380 Ma, using unmixing calculations from Isoplot v.3.5.

CHAPTER 5: MAJOR AND TRACE ELEMENT GEOCHEMISTRY OF BASEMENT ROCKS, DELLWOOD AREA, WESTERN NORTH CAROLINA

Methods

Whole rock major element compositions, and some trace-element compositions were determined using a Bruker S4 Pioneer X-Ray fluorescence spectometer at the Kentucky Geological Survey (KGS) X-Ray analytical laboratory. The mass of samples ranged from roughly 5 – 15 kg, with some lithologically distinct layers-in-gneiss samples having a lower mass (< 2 kg). Crushed rocks were reduced to powders using a shatterbox with iron-alloy pucks. To test for Fe- and potentially V-contamination of samples from the shatterbox, two blanks were prepared by pulverizing pure-quartz sand with the shatterbox. XRF analyses of the blanks, yielded 0.14 wt.% Fe_2O_3, suggesting that Fe-contamination effects from the pulverization process were minor. Fused glass beads were prepared using a dilution ratio of 9:1 (nine parts C-type Li-tetraborate flux, and one part rock sample, by mass) and an automated fluxer. A second batch of pressed pellets was prepared for trace-element analysis, with no dilution, and a binding agent. Calibration curves were constructed by analyzing reference material standards obtained from the U.S. Geological Survey, SARM (Service d'Analyse des Roches et des Min/ Centre National de la Recherche Scientifique), and CCRMP (Canadian Certified References Materials Project). The proprietary data reduction system software of Bruker was used to calculate major element compositions in the unknowns. Statigraphics and Excel software were used to construct the calibration curves for estimating trace element data determined from the undiluted pressed-pellet runs. To evaluate the accuracy of the XRF data, seven standards were analyzed as unknowns (BVN-1, OU-1, OU-2, OU-3, OU-4, OU-5, and GSP-2). The deviations between the determined value and the recommended values of standards were used to estimate 2σ values that are reported at the end of Appendix M. This procedure was used to assess the instrumental accuracy of the data for pressed pellets and fused glass beads (major and minor elements).

Whole Rock Geochemistry Results

Major element, trace element, and CIPW normative estimations are compiled in Appendix M. The purpose here is to look for igneous trends in orthogneisses of the central and western Blue Ridge, to recognize differences between the 1020-60, 1140-70, and 1244-92 Ma igneous events, and potentially to discriminate the tectonic setting of the three granitic suites. In addition to XRF data determined here, data from Loughry (2010) are also examined and plotted. These data are available online in electronic thesis format, and are not replicated here. Most of Loughry's whole-rock compositional data are determined from hornblende-biotite gneiss ("the Carolina Gneiss"), although some biotite gneiss and amphibolite analyses were also determined. Loughry subdivided the hornblende-biotite gneiss samples into "metaplutonic orthogneiss", "deformed

orthogneiss", and "hornblende migmatites". In the present study, these rock types are lumped together and plotted as "hornblende-biotite gneiss".

The first step towards distinguishing magmatic trends in the sample set is to cull the data set of analyses that appear to be non-igneous in origin. Developing a robust culling method to differentiate between orthogneiss and immature metasedimentary rocks derived from orthogneiss is difficult, if not impossible, and the methods used here are not considered ideal. Two criteria were used after Ownby et al. (2004) and Werner (1987). If normative calculations determined >1.5% corundum, they were culled from the data set. Typical intermediate to felsic plutonic igneous rocks lack normative corundum, and the presence of significant normative corundum may be an indication of chemical and mechanical weathering processes. However, some igneous rocks, specifically strongly-peralumious granitoids and S-type granites, are corundum-bearing (Barker, 1983). Consequently, not all of the samples that show normative corrundum in CIPW norm calculations were culled, and the 1.5% cutoff point is somewhat arbitrary. The second criterion is an evaluation of P_2O_5/TiO_2 versus MgO/CaO (Figure 5.1). Samples were culled that plot far within the "sedimentary" field determined by Werner (1987) in a study of igneous and sedimentary protoliths related to Saxonian granulites. Twenty six analyses were culled, including all of the muscovite-biotite gneisses and several biotite gneiss analyses. Muscovite-biotite gneiss and schist appears to have a sedimentary protolith (metagraywacke?). Biotite gneiss appears to have mixed origins; some samples appear to have sedimentary protoliths, and zircon U-Pb ion-probe age distributions from DEL03-1 also support a sedimentary-protolith heritage. Other biotite gneisses appear to be meta-igneous rocks having survived the culling criterion. Some orthogneiss and amphibolite analyses were culled as well. Field relations and textural relationships suggest that these rocks are meta-igneous, however chemical weathering is suspected of altering the ancient chemical compositions. Amphibolites from the present study are included in some of the geochemical plots for comparative purposes. Their mafic compositions imply an igneous origin, but the crystallization ages of the metabasites was not determined here, and it is entirely possible that these rocks are unrelated to the Mesoproterozoic orthogneisses of the central Blue Ridge basement complex.

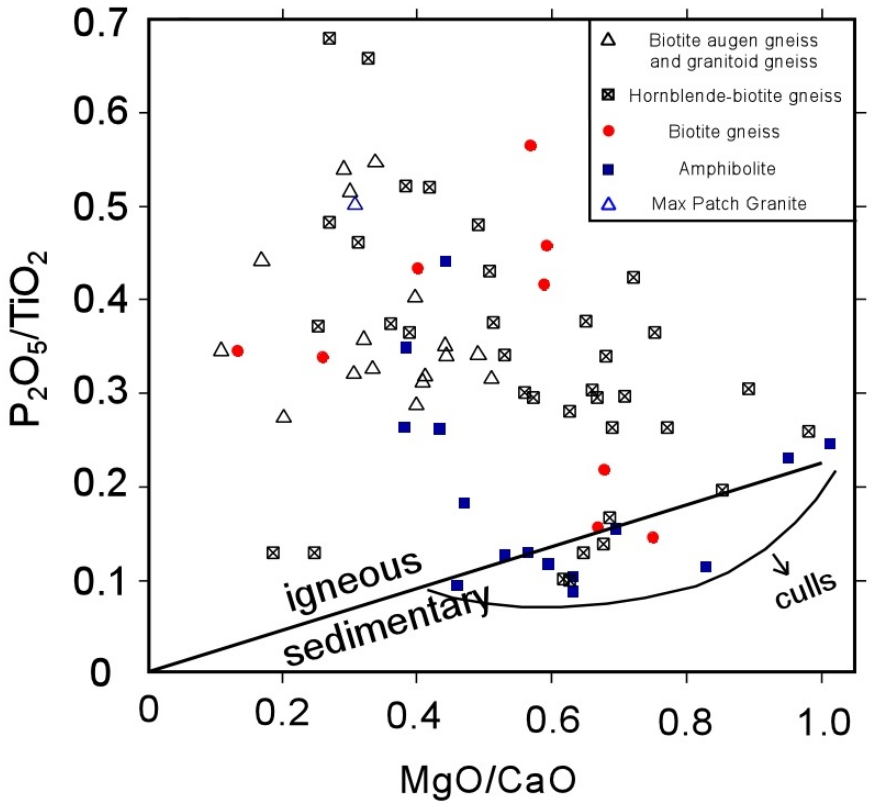

Figure 5.1. Sedimentary-igneous discrimination diagram. Plot of P_2O_5/TiO_2 versus MgO/CaO after Werner, (1987) with all samples used for geochemical plots (culls not shown).

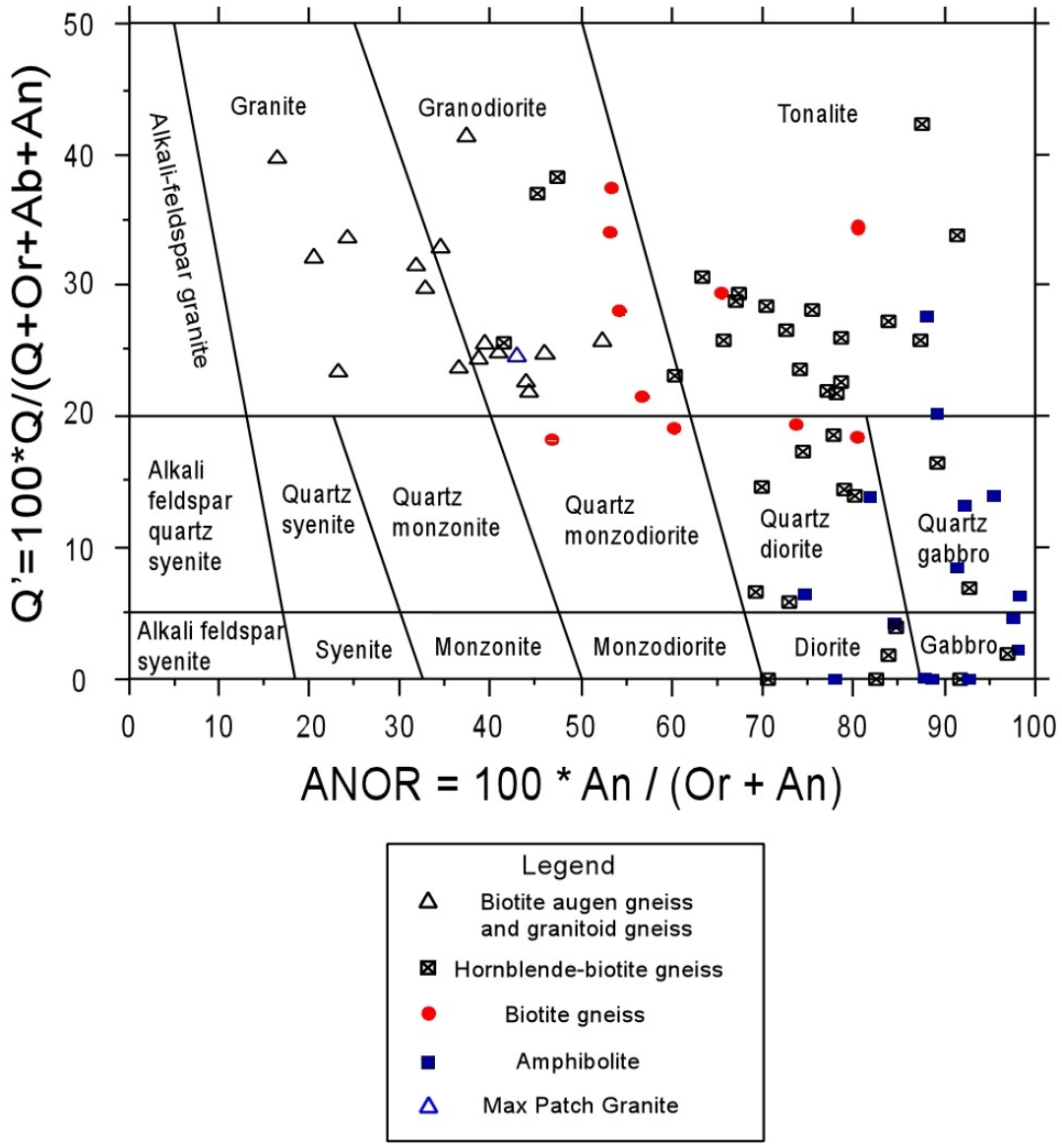

Figure 5.2. Q' versus ANOR. Normative rock classification after Streckheisen and Le Maître (1979).

Orthogneisses from the central and western Blue Ridge are classified using the normative classification scheme devised by Streckheisen and Le Maître (1979) in Figure 5.2. Biotite augen gneiss and granitoid gneiss are restricted to the granodioritic and granitic fields. These lithologies also appear to have slightly lower ANOR values relative to biotite gneiss. The hornblende-biotite orthogneisses have much higher ANOR values, and are predominantly tonalities and quartz diorites. Some of the more mafic hornblende-biotite gneiss analyzed by Loughry (2010) and amphibolites from the central Blue Ridge plot within the diorite and gabbro fields.

Variation diagrams are shown in Figures 5.3 and 5.4. Notable trends include the relatively restricted compositional range of biotite augen gneiss and granitoid gneiss. The Al_2O_3-SiO_2 field is circled in Figure 5.3 to illustrate the relatively restricted range relative to the wider compositional ranges exhibited by the hornblende-biotite gneiss and biotite gneiss suites. Extremely narrow compositional ranges are circled in Figure 5.4.G, and H, to illustrate compositional similarities between the Max Patch granite (one sample; MP04-2, blue triangle) and orthogneisses of the Cherokee-Raven Fork Belt, (CH02-1,2,4). These tightly-clustered composition fields indicate a remarkable degree of compositional similarity between a sample of Max Patch Granite (Lemon Gap quad) and biotite augen gneiss of the Cherokee-Raven Fork Belt that were sampled over 30 kilometers apart (Lemon Gap, Whittier, and Smokemont quadrangles). The restricted compositional range of "biotite augen gneiss and granitoid gneiss" is also apparent in the variation diagrams of Figure 5.4. Other notable trends can be seen in plots of FeOt vs MgO and CaO vs MgO. Specifically, there appear to be at least three chemically distinct types of amphibolite within the basement complex of the Dellwood region. Pl-Hbl amphibolites analyzed from the Hemphill Creek/Purchase Knob exposure (H03-4) have MgO content of ~3.2-4.03 wt.% with FeO concentrations ~ 13 wt.%. The "Dellwood metabasite body" (DEL03 samples) shows higher MgO concentrations (~6-7 wt.%) and higher FeO concentrations (13.5-17 wt.%) relative to the other amphibolites. Amphibolites sampled by Loughry (2010) show FeO-MgO variations that coincide with the nearly linear FeO-MgO variations of the hornblende-biotite gneiss suite, suggesting that a third group of amphibolites exists that is co-genetic with the ~1244-1292 Ma hornblende-biotite suite.

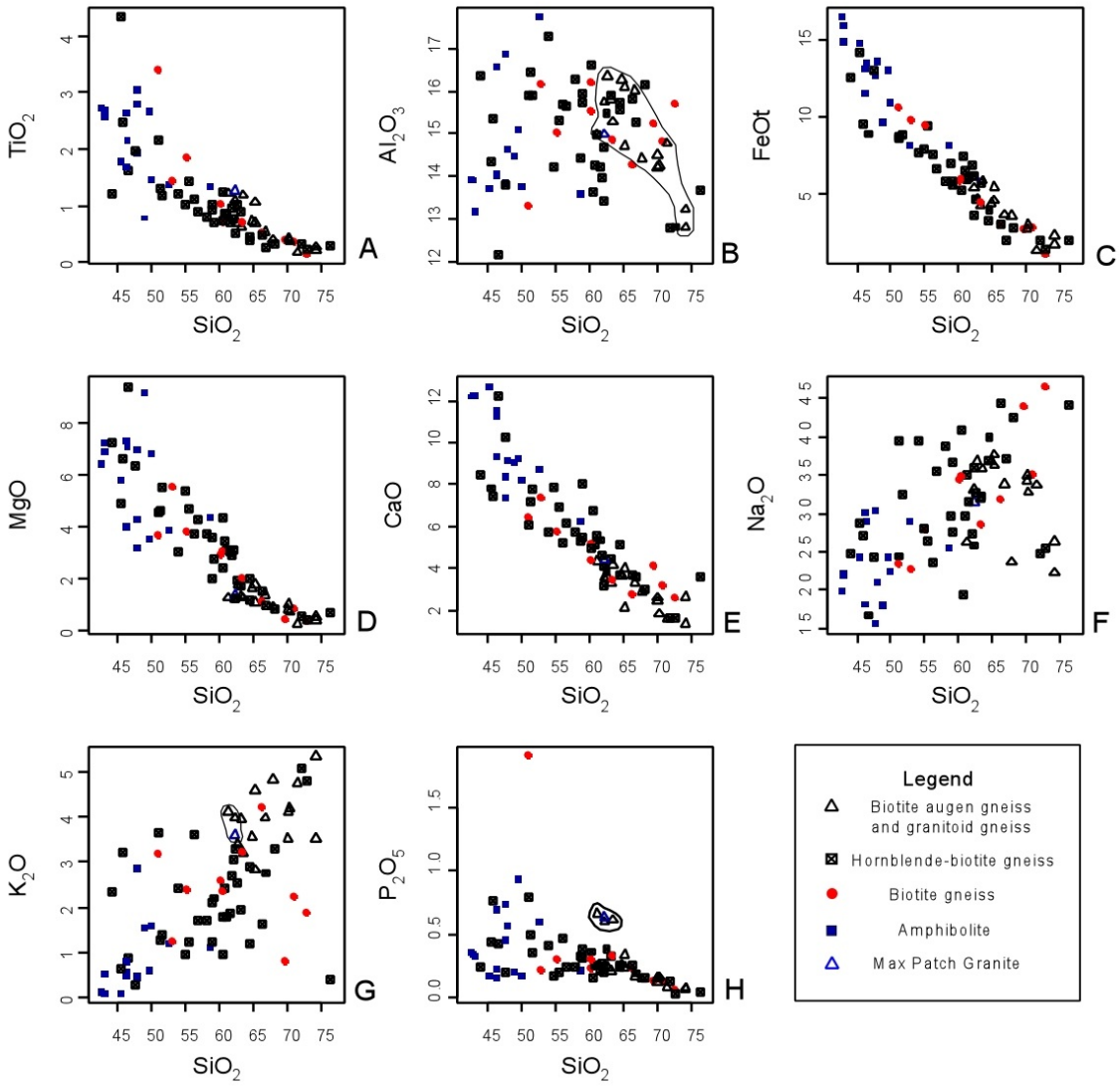

Figure 5.3. Variation diagrams; major elements versus SiO_2.

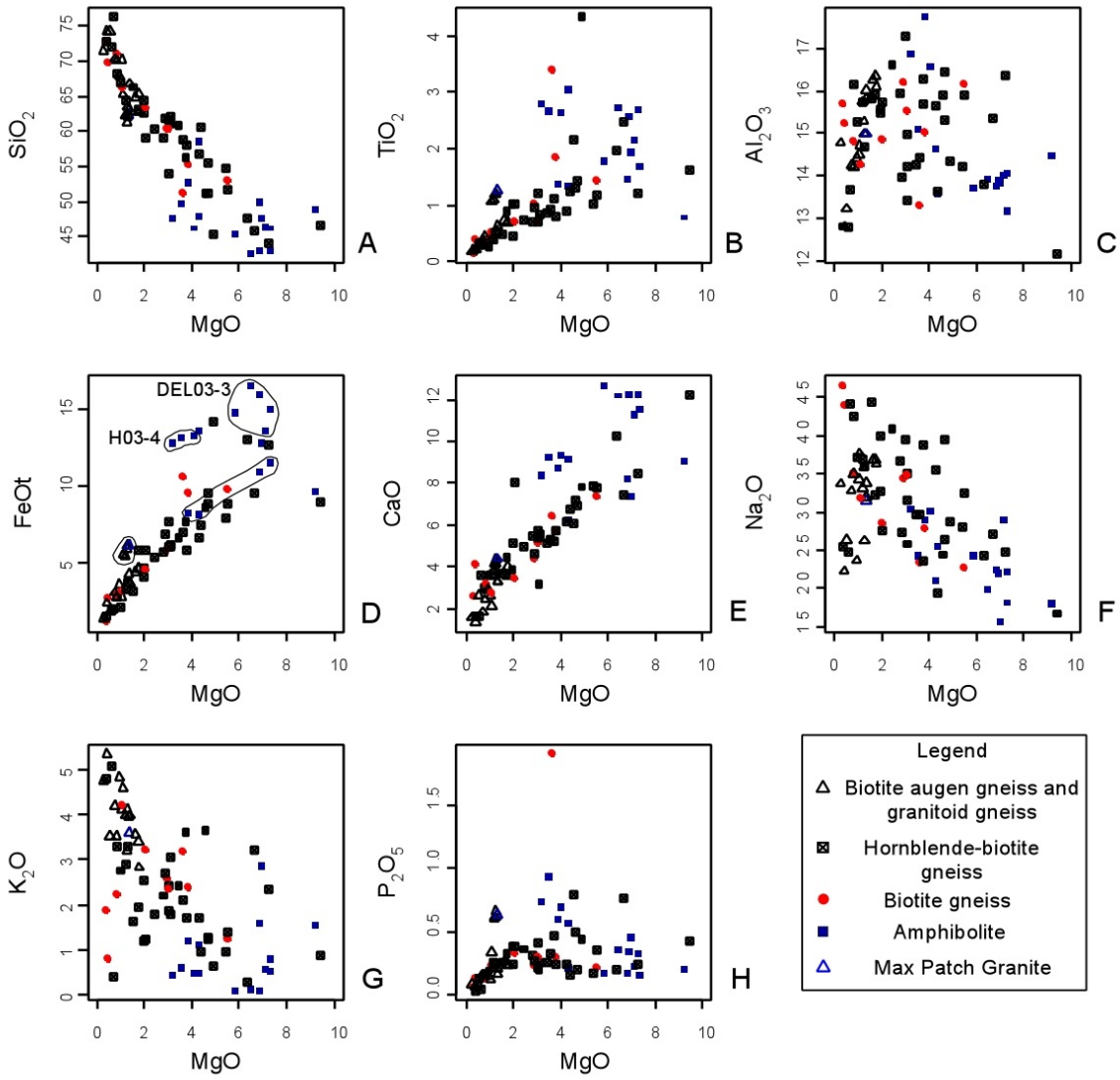

Figure 5.4. Variation diagrams; major elements versus MgO.

An AFM ternary plot after Irving and Baragar (1971) is shown in Figure 5.5. (A = alkalis: [K_2O + Na_2O]; F = [FeOt]; M = [MgO]; A+F+M=100). Most of the biotite augen gneiss and granitoid gneiss, biotite gneiss, and hornblende-biotite gneiss suites plot within the calc-alkaline series field. The sample of Max Patch granite and samples CH02-1 and CH02-2 from the Cherokee-Raven fork belt plot just within the tholeiitic series. Amphibolites from the Hemphill Creek and Dellwood metabasite outcrops plot as distinct fields within the tholeiitic series (circled).

In an effort to classify the granitoid gneisses further, the three tiers of the classification scheme of Frost et al. (2001) were applied with mixed results. Before plotting additional classification diagrams, the XRF data set was culled further to exclude samples with <52 wt. % silica; the granitoid classification scheme does not distinguish among various basalts, and the 52% cuttoff point is suggested by Frost and Frost (2008). All the amphibolite samples were culled. The first tier of Frost et al. (2001) is determined by the FeO/(FeO + MgO) of the granitoids, with a plot of Fe* versus SiO_2 given in Figure 5.6 with Fe* = FeOtot/(FeOtot + MgO).

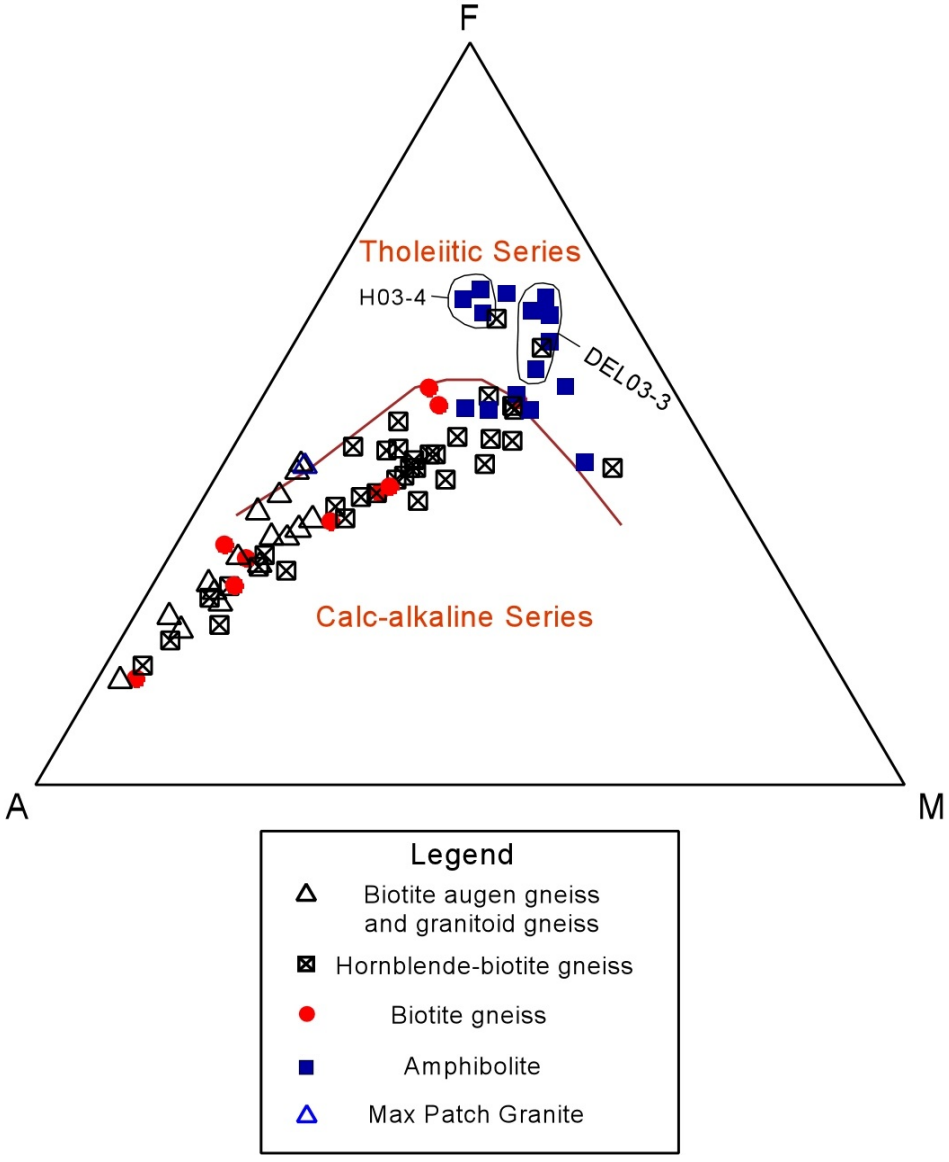

Figure 5.5. AFM ternary plot after Irving and Baragar (1971).

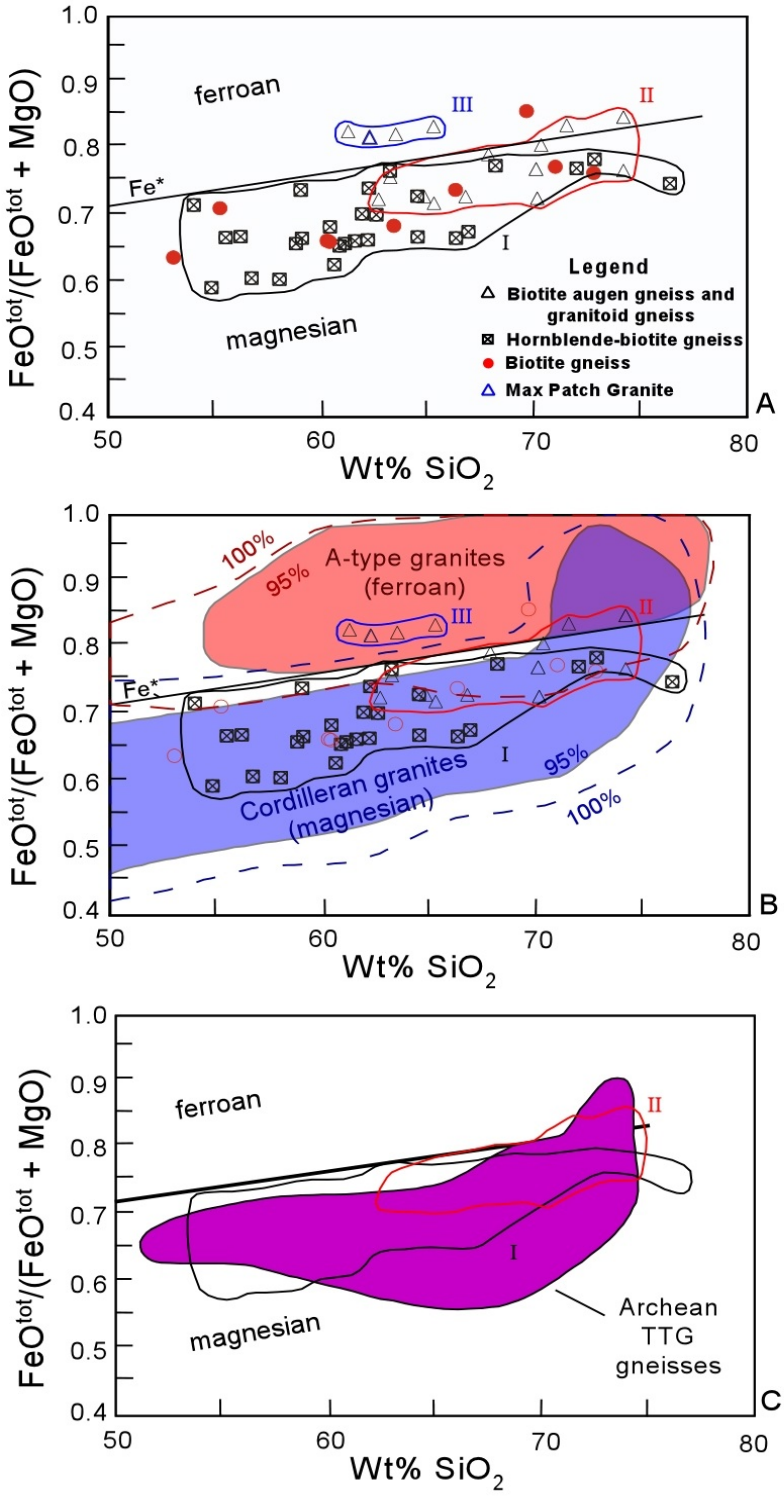

Figure 5.6. Fe* versus SiO_2 granite classification diagrams. (Legend follows)

Figure Legend 5.6: A) Granitoids from the central and western Blue Ridge with compositional outlines for Group I (hornblende-biotite gneiss; ~1244-1292 Ma), Group II (~1140-1170 Ma biotite augen gneiss and granitoid gneiss, and group III (Max Patch granite and 1030-1060 Ma biotite augen gneiss of the western Blue Ridge). Line "Fe*" is the boundary between ferroan and magnesian granitoids. B) Central and western Blue Ridge granitoids with compositional fields from A-type granites and Cordilleran granites. Solid color = 95% interval; dashed lines = 100% interval. Fields based on the analysis of 486 A-type granites and 538 Mesozoic magnesian batholiths from North America, with references in Frost et al. (2001). C) Comparative plot of group I and group II granitoids of the central and western Blue Ridge with Archean TTG (tonalitic, trondhjemitic, and granodioritic) gneisses. (n=55, references in Frost et al., 2001).

Fe* versus SiO_2 is an evolution of the "tholeiitic" versus "calc-alkaline" trends established by Miyashiro (1970) in a study of arc related granites from Northern Japan that underwent iron enrichment (tholeiites). Frost and Frost (2002) observe that if plutons are reduced [fayalite-magnetite-quartz,"FMQ" or below; Frost and Lindsley (1992)] fractional crystallization drives the pluton towards iron enrichment, with an example being the A-type granites with high FeO/(FeO + MgO) first recognized by Loiselle and Wones (1979) (Frost and Frost, 2008). If the plutons are relatively oxidized (FMQ +2 or more), the fractional crystallization of magnetite prohibits Fe-enrichment of the remaining liquid, resulting in Fe* characteristic of the most abundant granitic plutons on Earth referred to as "volcanic arc granites" (Pearce et al., 1984) or "Cordilleran batholiths" (Frost et al., 2001). Because it is oxygen fugacity that controls the Fe-number, a value unrelated to alkalinity, Frost et al. (2001) suggest that the terms "calc-alkalic" and "tholeiitic" should be abandoned in favor of "magnesian" and "ferroan".

Interpretation of the Fe* versus SiO_2 plot (Figure 5.6), and the use of compositional comparisons to previously studied granites allows for inferences to be made regarding the tectonic settings of the orthogneisses analyzed here. The hornblende-biotite gneiss suite (Group I, 1292-1244 Ma) has Fe* values that lie in the magnesian field, with a range in compositions that is broadly similar to the Mesozoic Cordilleran granites of North America, but more similar to Archean TTG gneisses. The Cordilleran granites are widely interpreted to have formed in a volcanic-arc tectonic setting. Archean TTG gneisses may have formed in volcanic arcs, but "TTG-like" rocks may form via the partial melting of hydrated basaltic material at the base of magmatically or tectonically thickened crust (Smithies, 2000). Although U-Pb zircon geochronology (Loughry, 2010; and this study) clearly demonstrate that the Group I gneisses are not Archean, similar ranges of Fe* versus SiO_2 for Group I gneiss and Archean TTGs suggests that Group I gneiss may have originated as a TTG-like suite, a hypothesis that requires further examination. Biotite gneiss compositions have values that closely mimic Group I gneiss, suggesting that they are petrogenetically related. Biotite gneiss may be the volcanic expression of the ~1292-1244 Ma magmatic event(s). Group II gneiss is also largely magnesian, but more evolved relative to the Group I gneisses, suggesting that a second episode of volcanic arc magmatism occurred *circa* 1170-1140 Ma, involving the recycling of Group I granitoids. Group III gneisses are represented by one sample of Max Patch Granite (Lemon Gap quad), three samples of granodioritic orthogneiss from the Cherokee-Raven fork belt, and one sample from a small basement sliver exposed in the Cove-Creek Gap quadrangle. Group III gneisses are distinctly ferroan, and may represent A-type (anorogenic, anhydrous, and sometimes alkaline) granitoids that are not arc-related. Group III was recognized by restricted compositional ranges in variation diagrams (Figures 5.3, 5.4). The age of group III gneiss is constrained by SHRIMP analyses of zircons from a Raven Fork orthogneiss age of 1022 $\pm$ 4 Ma (Aleinikoff et al., 2007) and a U-Pb zircon age of 1020 $\pm$ 30 Ma determined for the Max Patch Granite (Berquist et al., 2005)

The second tier of the Frost et al. (2001) geochemical classification scheme is based on the alkali-lime classification of Peacock (1931), designed to classify rock suites.

Frost et al. (2002) apply the modified alkali-lime index (MALI), plotting $Na_2O + K_2O - CaO$ versus SiO_2 to expand the range of SiO_2 through which four classes of granites can be distinguished: calcic, calc-alkalic, alkali-calcic, and alkalic. The gneisses from group I, II, and III, and biotite gneiss have compositions that belong to several of the alkali-lime classes (Figure 5.7). Group I (hornblende-biotite gneiss) is mostly calc-alkalic, with several calcic samples, and three alkali-calcic samples. Group II (1140-1170 biotite gneiss) is calc-alkalic and alkali-calcic with one calcic sample. Group III is calc-alkalic, and alkali-calcic to alkalic.

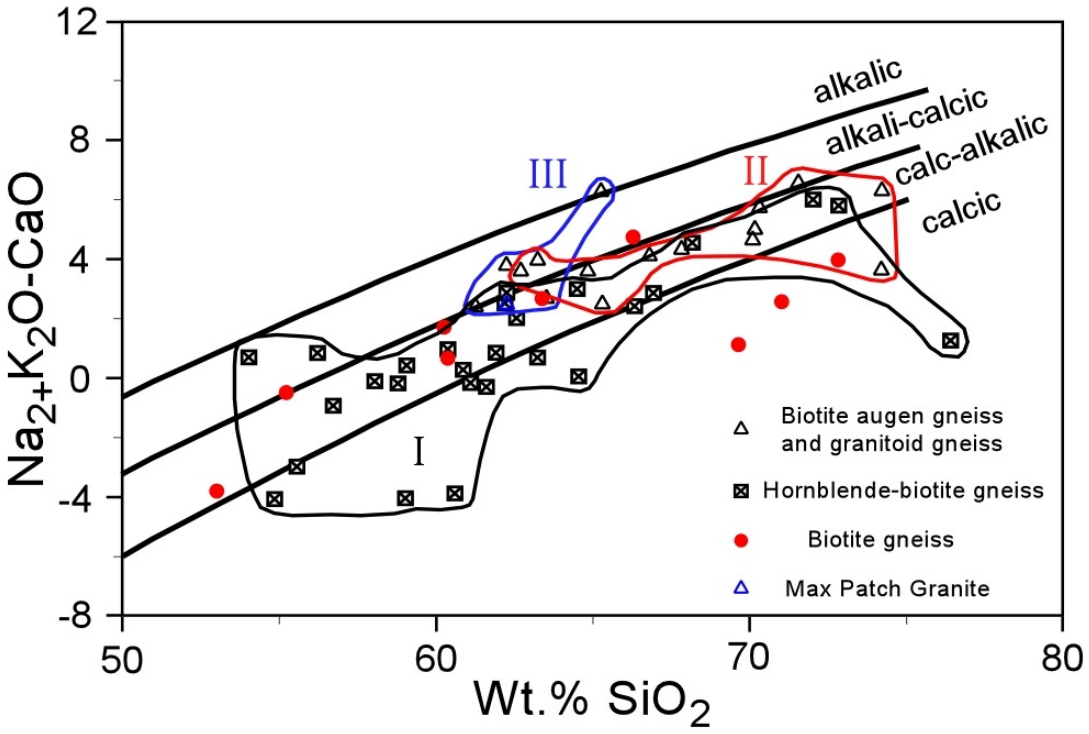

Figure 5.7. MALI versus SiO_2 after Frost et al. (2001) and Peacock (1931). Group I (1292-1244 Ma hornblende-biotite gneiss) outlined in black, Group II ~1170-1140 Ma granitoid gneiss outlined in red, and Group III (Max Patch granite and 1060-1030 Ma granitoid gneiss)outlined in blue.

An examination of the aluminum saturation index (ASI) of orthogneisses from the central and western Blue Ridge is shown in Figure 5.8. This is the third tier of the Frost et al. (2001) granitic classification scheme, and is essentially the same as the "alumina

saturation“ classification of Shand (1951) with a correction for apatite. Shand (1951) divided igneous rocks into three groups, based on Al-saturation: peraluminous, $Al_2O_3 > (CaO + Na_2O + K_2O)$; metaluminous, $Al_2O_3 < (CaO + Na_2O + K_2O)$, and peralkaline, $Al_2O_3 < (Na_2O + K_2O)$. No correction for apatite was applied in Figure 5.8, where x-axis is the molecular ratio of A/CNK or $Al_2O_3/(CaO + Na_2O + K_2O)$ and the y-axis is the molecular ratio A/NK or $Al_2O_3/ (Na_2O + K_2O)$. Group I gneisses (1292-1244 Ma hornblende-biotite gneiss) are metaluminous to peraluminous, Group II gneisses (1170-1140 Ma) are also metaluminous to peraluminous, and Group III gneisses (1060-30 Ma) are metaluminous. No peralkaline samples were identified in the study area, and the biotite gneisses have a distribution that closely mimics the hornblende-biotite gneiss ASI distribution. Examining the ASI allows for the prediction of modal phases that may have been present in the granitoid plutons of the central and western Blue Ridge prior to metamorphism. Metaluminous igneous rocks contain excess Ca that is commonly accomodated by hornblende and Ca-rich augite (Mišković et al., 2009). Other characteristic modal phases of metaluminous plutons include melilite, olivine, and biotite (Barker, 1983). Weakly peraluminous igneous rocks typically contain abundant feldspar, with biotite as the mafic phase. Strongly peraluminous granitoids commonly contain muscovite, cordierite, and garnet or Al_2SiO_5 polymorph, with pressure being a factor related to which phases form (Mišković et al., 2009). Other characteristic modal phases of peraluminous granitoids include corundum, biotite, topaz, and tourmaline (Barker, 1983).

K_2O versus SiO_2 is plotted in Figure 5.9 after Peccerillo and Taylor (1976) to draw attention to the unusually K-rich compositions of the Group II and Group III meta-granodiorites and meta-granites. About half of the Group I gneisses (primarily meta-tonalites and meta-quartz diorites) are also K-rich.

Summary

Results of geochemical classification of the orthogneisses from the central and western Blue Ridge are combined with geochronologic data of Chapter 4 and sumarized in Table 5.1. The oldest rocks examined are the Group I gneisses, with Fe* trends and whole-rock chemical compositions consistent with a tonalite-quartz diorite plutonic episode related to volcanic arc magmatism. Multiple “age modes” of the hornblende-biotite gneiss suite determined by Loughry (2010) indicate plutonism at circa 1292-1244 Ma followed by second plutonic event at circa 1170-1140 Ma. Group II gneiss also appears to be arc-related as determined from Fe* versus SiO_2 trends. Group III gneisses show Fe* trends consistent with an A-type tectonic setting that was not arc-related. The inferred tectonic setting for the Group II gneisses contrasts with the 1180-1160 Ma intrusives of the Shenandoah massif in the Virginia Blue Ridge to the north. The Shenandoah orthogneisses mostly plot above Fe*, in the ferroan field of Frost (2001), consistent with an A-type magmatism, not the volcanic arc tectonic setting inferred for the French Broad massif rocks of the Dellwood area (Tollo et al., 2004a).

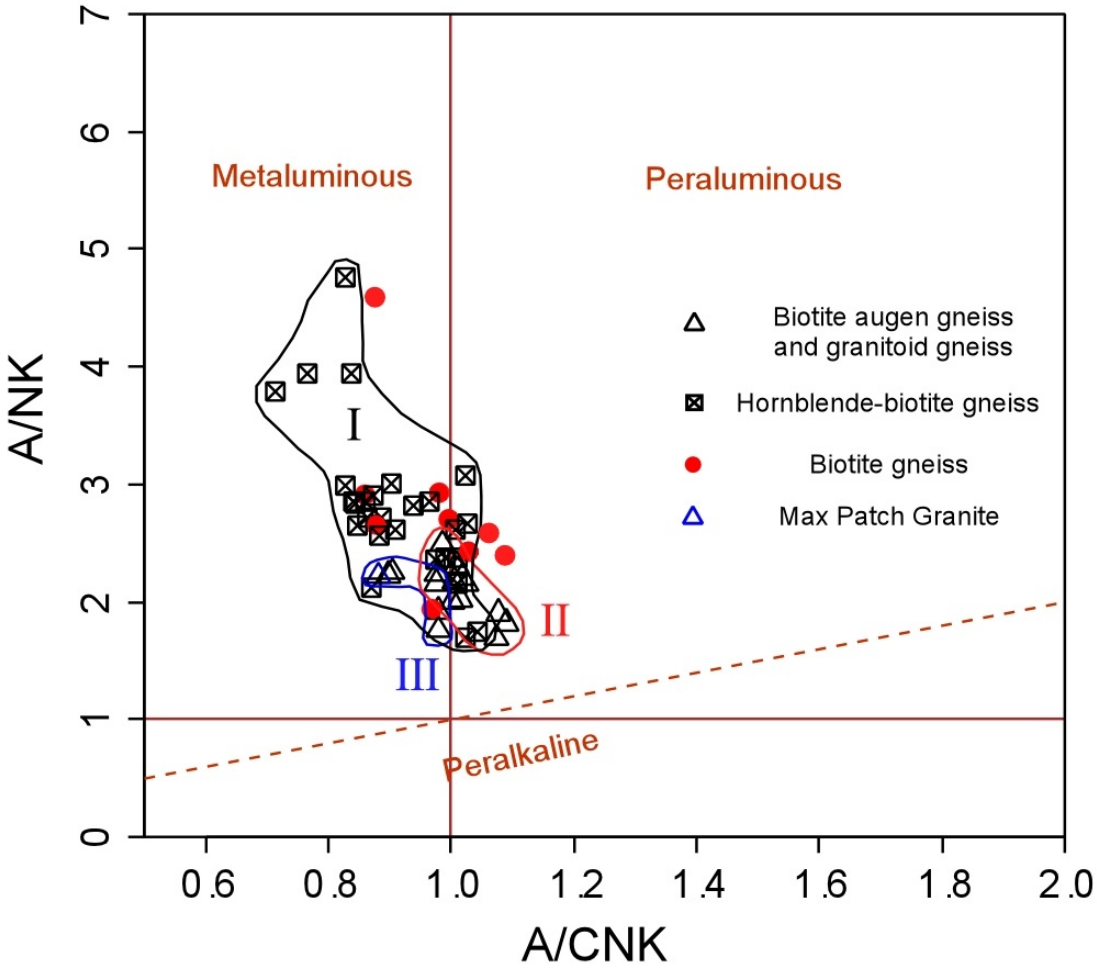

Figure 5.8. A/NK versus A/CNK (After Shand, 1951). Solid lines outline Group I (~1292-1244 Ma hornblende-biotite gneiss), Group II (~1170-1140 Ma granitoid gneiss), and Group III (Max Patch granite and 1060-1030 Ma granitoid gneiss).

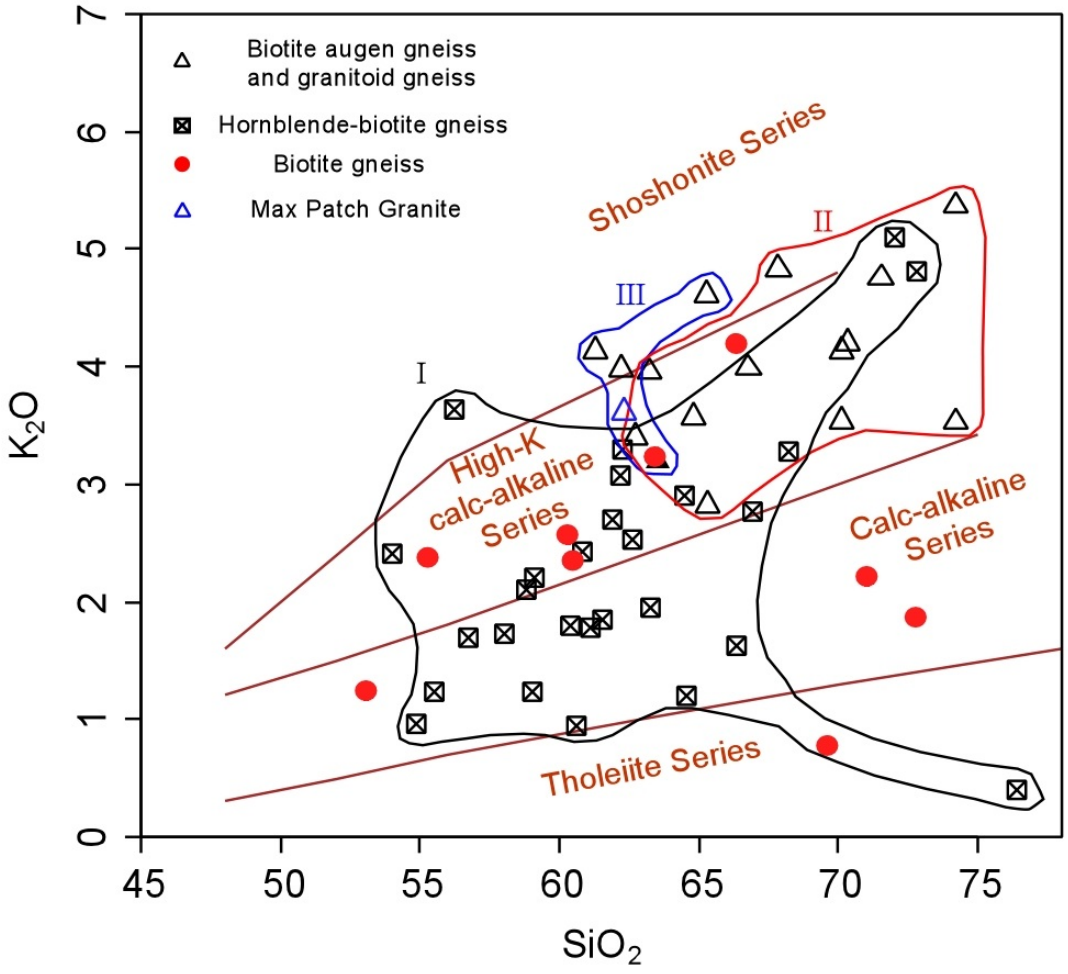

Figure 5.8. K_2O versus SiO_2 after Peccerillo and Taylor (1976).

Table 5.1. Summary of Geochemical Trends, Central and Western Blue Ridge Orthogneiss.

	Group I, hornblende-biotite gneiss	biotite gneiss	Group II biotite augen gneiss and granitoid gneiss	Group III Max Patch Granite and biotite augen gneiss equivalents
Age (Ma)	1292-1244	1292-1244??	1170-1140	1060-1020
rock types	tonalite, qtz diorite diorite, qtz gabbro some granodiorite	dacite-andesite?	granite granodiorite	granite granodiorite
Fe*	Magnesian	magnesian	magnesian	ferroan
MALI / alkali-lime index	calc-alkalic to calcic	calc-alkalic to calcic	calc-alkalic to alkali-calcic	calc-alkalic to alkali-calcic
ASI / alumina saturation	metaluminous to peraluminous	metaluminous to peraluminous	metaluminous to peraluminous	metaluminous
K, potassium	some end members high-K	variable K	high-K	high-K

CHAPTER 6: APPLICATION OF NEW GEOCHRONOLOGY AND GEOCHEMISTRY TO TECTONIC MODELS OF THE PRECAMBRIAN AND EARLY PALEOZOIC TECTONIC EVOLUTION OF THE SOUTHERN BLUE RIDGE

Introduction

After evaluating the geochronology and geochemistry of the Blue Ridge basement complex of western North Carolina, a potential lithologic correlation has been recognized that links Mesoproterozoic basement of Laurentia to the Mesoproterozoic Arequipa-Antofalla block of western South America. Although both margins (eastern Laurentia and western South America) have experienced extensive tectonic reconfiguration since the Mesoproterozoic, the lithologic correlation proposed here may help to understand the tectonic interactions between Laurentia and western South America. The lithologic correlation potentially constrains the paleogeography of Rodinia, an ancient supercontinent widely believed to have contained Laurentian and Amazonian elements (e.g. Valentine and Moores, 1970; McMennemin and McMenemin, 1990; Moores, 1991; Dalziel, 1991; Hoffman, 1991, Weil et al., 1998; Li et al., 2008). The correlation may also help to understand the early Paleozoic evolution of the southern Blue Ridge and the tectonic history of the Mars Hill terrane. To put the reconstruction in context, the geology of southwestern South America from the Mesoproterozoic through Cambrian is summarized. More details and alternate interpretations related to the geology of western South American are given in Ramos (2008, 2010a,b), Steenken et al. (2011), Mišković et al. (2009), Chew et al. (2010), and Collo et al. (2009) among others. The geologic overview is followed by a presentation of isotopic data interpreted as demonstrating a potential lithologic correlation between the Mars Hill terrane/southern Blue Ridge of Laurentia and the Arequipa-Antofalla block of South America. Finally, the tectonic evolution of the central Blue Ridge from the Precambrian through early Paleozoic is discussed.

Introduction to the Geology of South America

The Amazonian Craton of South America is composed of two Archean blocks and five Proterozoic tectonic provinces (Figure 6.1). The age distribution of geologic provinces suggests a geologic history of crustal accretion events that young away from a central Amazonian core. There are three Mesoproterozoic metamorphic belts located on the southwest margin of the Amazonian Craton: the Sunsás, Aguapei, and Nova Brasilândia belts (Figure 6.1.B). The Sunsás and Aguapei belts have geochronologic ages that overlap with the "Grenville age" lithologies of Laurentia and consequently have been central to studies that invoke a western Amazonia/eastern Laurentia connection during the Precambrian (e.g. Dalziel, 1991; Hoffman, 1991; Weil et al., 1998; Tohver et al., 2002). However, different workers connect the southwestern Amazonian Craton with different regions of Laurentia such as the Llano Uplift (Tohver et al., 2002), the Grenville

Province, eastern Canada (Sadowski and Bettencourt, 1996), and the central and southern Appalachian Blue Ridge (Loewy et al., 2003; Tohver et al., 2004; D'Agrella-Filho et al., 2008; Fisher et al., 2010).

Some workers, such as Cordani et al. (2010) extend the Sunsás belt (Figure 6.2) to a much wider geographic extent due to scattered occurrences of ~1.0-1.2 Ga rocks preserved along the Andean margin that may represent the country rock into which Andean volcanics intruded. These scattered outcrops of Grenville-Sunsás-age (~1.0-1.2 Ga) rocks imply that there was once a continuous Mesoproterozoic orogenic belt that rimmed most of the western Amazonian Craton, that is now largely dismembered or covered (Cardona et al., 2010; Chew et al., 2010). Several other Mesoproterozoic blocks occur south and southwest of the Amazon Craton. These include Arequipa, Antofalla, (Figure 6.1.C) Pampia ("Sierras Pampeanas" in Figure 6.1.A), and the Paragua Craton (Figure 6.1.B) (Teixeira et al, 1989; Bettencourt et al., 1999; Tohver et al, 2004, 2005; Boger et al., 2005; Ramos 2008; Ramos et al., 2010).

Mesoproterozic Blocks of Southwestern South America (Arequipa-Antofalla and Pampia)

There is a general consensus that Laurentia and western Gondwana were part of Rodinia (e.g. Li et al., 2008) having been linked by compressional tectonic episodes during the Grenville-Sunsás orogeny (Tohver et al., 2004, D'Agrella-Filho et al., 2008). However, the relative locations of the continents and constituent terranes that composed Rodinia remain a subject of debate. Neoproterozoic, Paleozoic, and Mesozoic tectonics have precluded accurate paleogeographic reconstructions of Rodinia. Some isotopic signatures such as whole-rock Pb isotopic compositions and Sm-Nd isotope data have been applied to correlate continents and mobile terranes. Isotope data, U-Pb zircon ages, and paleomagnetic data were used to develop the model of Laurentia and Amazonia shown in Figure 6.3. In this model (Ramos, 2008), the Arequipa and Antofalla terranes were sutured between Laurentia and the Amazonian margin in a collisional even at ~1050 Ma (Loewy et al., 2004). Two east-dipping subduction zones formed above the Arequipa and Amazonian craton margins. The location of the rift in Rodina shown in Figure 6.3 is consistent with whole rock Pb-isotopic studies of Mesoproterozoic basement of the southeastern Appalachian Blue Ridge, in which radiogenic Pb compositions from the southern Blue Ridge indicate an exotic (South American) origin for the central and southern Appalachian basement (e.g. Tohver et al., 2004; Fisher et al., 2010).

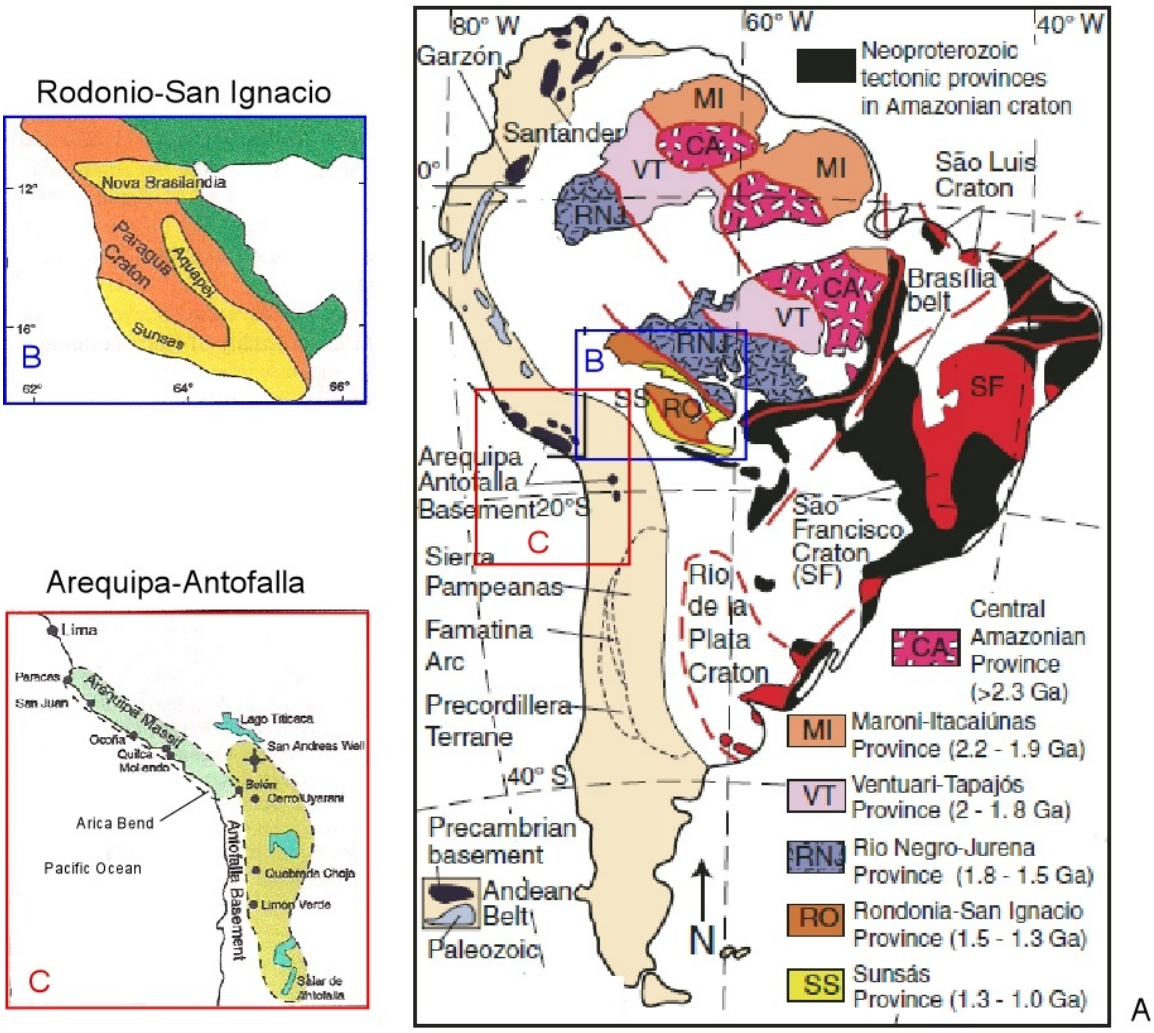

Figure 6.1. Map of South America with major tectonic provinces. A) Tectonic map from Chew et al. (2007, 2010) modified from Cordani et al. (2000). Ages are of most recent metamorphic events. B) Detail of Rodinio-San Ignacio Province; C) Detail of Arequipa-Antofalla block.

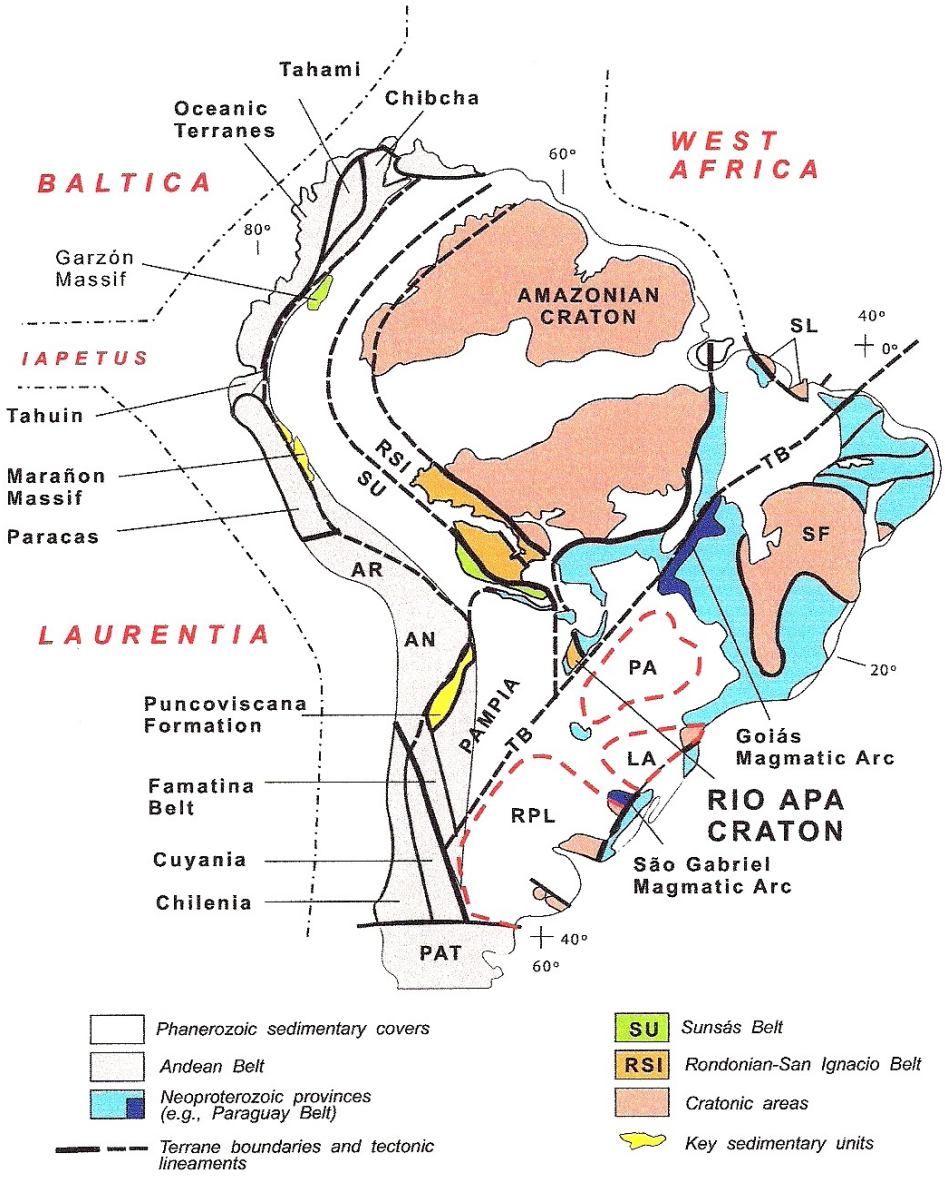

Figure 6.2. Geotectonic sketch of South America. From Cordani et al. (2010). Abbreviations: RSI=Mesoproterozoic Rodonian-San Ignacio(or Paragua Craton); SU=Sunsás; AR=Arequipa; AN=Antofalla; SL=São Luis; TB=Transbrasiliano Lineament; SF=São Francisco; PA=Paranapanema; LA=Luiz Alvez; RPL=Rio de La Plata; PAT=Patagonia.

The Arequipa and Antofalla blocks are composed of polydeformed granulite facies orthogneiss, metabasic gneiss, dioritic gneiss, and foliated migmatites with a complex history and a variety of chronologic and tectonic interpretations (e.g. Cobbing et al., 1977; Shackleton et al., 1979; Martignole and Martelat, 2003; Loewy et al. 2003, 2004; Ramos, 2008, 2010; Casquet et al, 2010). Both terranes (Arequipa, Antofalla) contain outcrops of Mesoproterozoic orthogneiss, and are considered exotic or parautochthonous to South America (Ramos, 2008). Ramos (2008) considers Arequipa and Antofalla to be distinct from each other due to contrasting early Paleozoic histories. The Arequipa block, appears to have remained attached to Amazonia through the Ordovician (Ramos, 2008). In contrast, the Antofalla block, defined by a few small outcrops of late Proterozoic gneiss in Chile (Ramos, 1988; Damm et al., 1990) may have partially separated from the Amazonian craton in the early Paleozoic and re-attached at the end of the Paleozoic (Ramos, 2008). Paleomagnetic studies of Conti et al. (1996) and Forsythe et al. (1993) produced tectonic models in which the the Famatinian terrane and Antofalla basement experienced structural rotations related to the closure of ocean-floored back-arc basins during the Cambrian-Early Ordovician. These models were based on paleomagnetically determined counterclockwise rotations of ~90^{o} for the western Puna and clockwise rotations of ~40^{o} for Eastern Puna, northwestern Pampean and Famatinia terranes with respect to the Gondwanan margin. Mobile blocks were believed to have reaccreted to the western Gondwanan margin during the early Paleozoic based on the presence of late Paleozoic oceanic rocks occurring between the Mejillones peninsula and the Sierra de Limón Verde (Ramos, 2008). More recently, a model of strike-slip displacement along the Gondwanan margin has been proposed by Spagnuolo et al. (2011) in which counter-clockwise rotation of the Western Puna (Forsythe et al., 1993; Rapalini et al., 2002) and clockwise rotations in Ordovician rocks of the Famatina Ranges, Pampean Ranges and Eastern Puna occured in response to the collision and emplacement of the Precordillera terrane against Gondwana (Spagnuolo et al., 2011). However, the strike-slip model of Spagnuolo et al. (2011) does not fully explain the extensive plutonism that occurs along the eastern margin of the Arequipa block. Three extensive plutonic belts include the Neoproterozoic-Early Cambrian Puncoviscana belt (Ramos, 1988; Pankhurst et al.,1998), and the early Paleozoic eastern and western Puna erruptive belts (Faja Eruptiva de la Puna Orientale and Occidental; Palma et al., 1986; Ramos, 1988). Consequently, the Paleozoic tectonic evolution of the Antofalla terrane of northwestern Argentina and northern Chile remains an unsolved problem (Rapalini et al., 2002).

In isotopic and U-Pb zircon-based studies of the Arequipa and Antofalla blocks, Loewy et al. (2004) interpret the Arequipa and Antofalla basement to have formed as a single block that is referred to as the "Arequipa-Antofalla block". Subsequent studies of Casquet et al. (2010) note that the U-Pb zircon ages of the Arequipa massif are similar to the Rio Apa block of the Amazonian craton (Figure 6.2) and the Maz domain in the Western Sierras Pampeanas. Casquet et al. (2010) suggest that the Arequipa, Rio Apa, and Maz blocks may have been part of a larger Paleoproterozoic craton that was reworked by the Grenville-Sunsás orogeny prior to reaccretion of the Arequipa massif to the Amazonian craton at *circa* 1050 Ma. Casquet et al. (2010) also note diachronous

Mesoproterozoic metamorphism in the Arequipa massif that is attributed to internal tectonic juxtaposition of domains.

The timing of the docking of the Pampia block (Sierras Pampeanas) is also critical to Rodinian paleogeographic reconstructions. Although most of Pampia is covered by Phanerozoic sediments of the Chaco basin (Cordani et al., 2010), there are several Mesoproterozoic basement outcrops in the western Sierras Pampeanas (e.g. the Sierra de Pie de Palo, McDonough et al., 1993; Sierras de Maz and Espinal, Casquet et al., 2004). On the basis of abundant Grenville-age peaks in detrital zircon studies, several workers have proposed that a Mesoproterozoic belt may have extended along the present western margin of Argentina as far south as Patagonia (Santos et al., 2008; Chericoff et al., 2009; Ramos, 2009). Consequently, Amazonia, Pampia, and the Arequipa-Antofalla block have been interpreted as being part of Rodinia (e.g. Brito Neves et al., 1999; Kroner and Cordani, 2003; Ramos et al., 2010). Some models of the Pampian-Amazonian suture call for the subduction of Pampia beneath the Amazon craton resulting in intra-crustal S-type magmatism in the Sunsás belt, north of the Tucavaca aulacogen that occurred at ~1000 Ma (Cordani et al., 2009, Ramos et al., 2010). The collision followed consumption of oceanic crust attached to the Pampian block beneath the Amazonian craton to produce the Sunsás magmatic arc (Ramos, 2010).

An alternate interpretation for the docking of the Pampean terrane calls for a southern extension of the Arequipa-Antofalla block that docked with the Amazonian margin during the Brasiliano orogeny (560-630 Ma; Collo et al., 2009). This interpretation is based on prominent peaks that fall within this age range in detrital zircon studies based in the Famatina belt.

Neoproterozoic Rifting, South America

The geologic record of the breakup of the Laurentian-Amazonian realm of Rodinia is poorly preserved along the western margin of South America (Chew et al., 2010). The scant record includes: 1) A-type granitic plutonism has been documented in the Eastern Cordillera of Peru (Mišković et al., 2009; dated at 775 – 690 Ma) and in the Grenville-Sunsás basement of the Precordillera (Baldo et al., 2006; dated at 774 $\pm$ 6 Ma); 2) Extensional magmatic dacite dikes dated 635 $\pm$ 4 Ma that occur in the Antofalla basement of northern Chile (Loewy et al., 2004); and 3) Late Proterozoic ultra-potassic mafic dikes and alkaline lava flows occur in the Puncoviscana Basin of northern Chile, with ages of "Pampean granitoids" interpreted as 550-530 Ma (Omarini, 1983; Omarini et al., 1999).

A major spike in the U-Pb zircon age spectrum at 550-650 Ma was determined in a detrital zircon provenance study of the Eastern Cordilleras of Peru and Equador. The spike was attributed to a Neoproterozoic magmatic arc that is speculated to lie buried beneath the modern Andean foreland (Chew et al., 2007). The presence of a Neoproterozoic arc along the western margin of Amazonia would indicate at least partial separation of Gondwana and Laurentia occurred prior to 650 Ma.

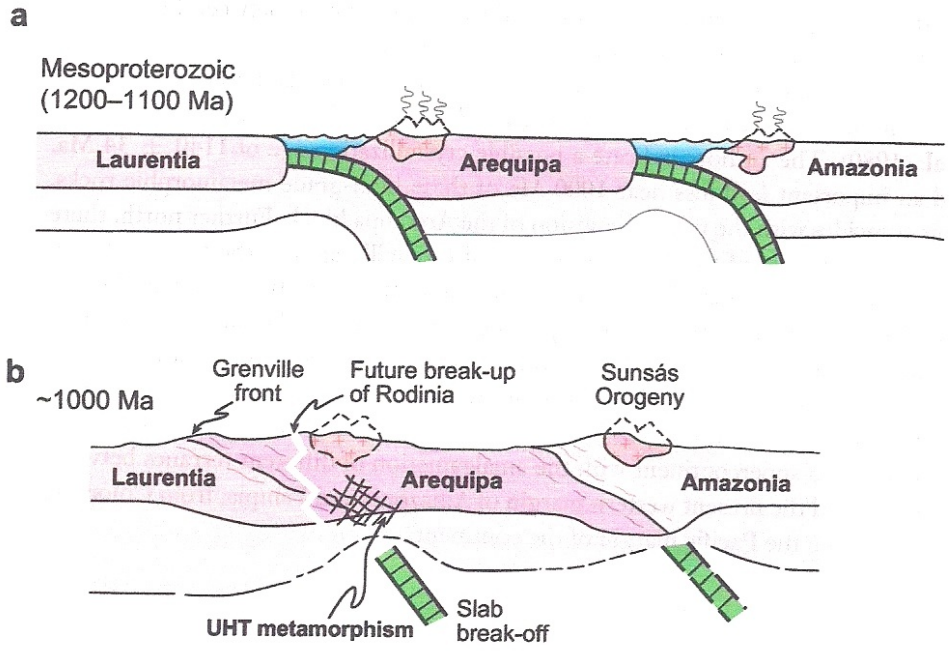

Figure 6.3. Model of the Grenville-Sunsás orogeny and collision between Laurentia, Arequipa, and Amazonia. A) Juvenile arcs in the Arequipa and Sunsás belts related to subducted oceanic crust. B) Collision and slab break-off event, with location of future rift of Rodinia. From Ramos (2008).

Neoproterozoic Rift Record in Laurentia, and Opening of the Iapetus Ocean

Laurentian rift-related events can be inferred from igneous complexes that intrude the Mesoproterozoic basement of the southern Blue Ridge. The intrusions are widely believed to have occurred in two temporal pulses (Aleinikoff et al., 1995, Brewer and Thomas, 2000, Owens and Tucker 2003). Intrusive events include volcanism from the Mount Rogers Formation, the Crossnore Complex, the Catoctin Formation, the Robertson River Igneous Suite, the Bakersville mafic dike swarm, and A-type plutonism in the Goochland terrane. Zircon U-Pb TIMS ages range from 758 $\pm$ 12 Ma for the Mount Rogers rhyolites to 564 $\pm$ 9 Ma rhyolites of the Catoctin Formation (Aleinikoff et al, 1995). Consequently, rift-related magmatism has been documented along the southeast margin of Laurentian that spans a ~200 Ma interval during the Neoproterozoic. Bimodal volcanics intruded the Mars Hill terrane at 726 $\pm$ 29 Ma (Goldberg et al., 1986). These intrusions are part of the Bakersville dike swarm that is associated with the granitic Crossnore Plutonic Complex. The suite is also referred to as Appalachian Blue Ridge A-type granites and bimodal volcanics with an age range of 765-680 Ma as determined by Tollo et al. (2004b) that defines the early rift-related magmatic pulse. Occurrences of these dominantly felsic, within-plate A-type plutons are restricted to the southern Appalachians with no associated rift-drift stratigraphic record (McCausland et al., 2007).

From an examination of data related to rifting in Newfoundland, Cawood et al. (2001) suggested that the Iapetus Ocean or Proto-Atlantic Ocean opened at circa 570 Ma, with rafting of a string of peri-Laurentian terranes occurring later at 540-535 Ma. However, subsequent paleomagnetic-based studies of McCausland et al. (2007) indicate that Amazonia and east Laurentia may have been well-separated by a substantial tract of Iapeus Ocean crust by the late Neoproterozoic (Figure 6.4). If these paleomagnetic observations are correct, the timing of the opening of Iapetus remains unresolved. Opening of Iapetus is constrained by 920-750 Ma post-Grenville extension (Dalziel and Soper, 2001) as an older age limit, and the onset of rift magmatism to form the peri-Laurentian microcontinents at ~570 Ma as a younger limit. McCausland et al. (2007) suggest that the opening of the Iapetus Ocean may have coincided with the early magmatic pulse, the timing of which is only preserved in the southern Blue Ridge (760-680 Ma; Badger and Sinha, 1988; Aleinikoff et al., 1995; Tollo et al., 2004). The craton-wide transgressive Sauk sequence (Sloss, 1963) that is Early Cambrian-aged along the Blue Ridge, but latest Cambrian-aged in the interior of North America (Thomas, 1991) may be partly related to thermal subsidence that followed the rafting of peri-Laurentian terranes from the continental margin. This would imply that the Chilhowie (siliciclastics) – Shady dolostone (carbonate) rift-drift transitional stratigraphic sequence was deposited at the margin of the "Taconic Seaway", and not at the margin of the Iapetus Ocean (McCausland et al., 2007; Hibbard et al., 2007). In summary, the Early Cambrian rift-to-drift stratigraphic interval interpreted as marking the opening of the Iapetus Ocean does not agree with paleomagnetic constraints that indicate an earlier time of separation.

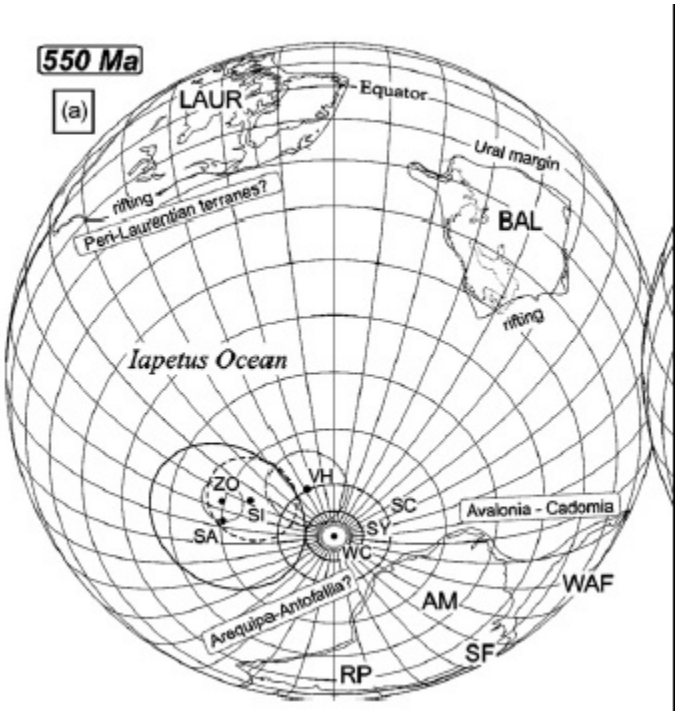

Figure 6.4. Paleomagnetically determined circum-Pacific paleogeography for the Late Ediacarian (550 Ma). From McCausland et al., (2007), based on Hoffman, (1991) and Cawood and Pisarevsky (2006). Continent abbreviations: AM, Amazonia; BAL, Baltica; LAUR, Laurentia; RP, Rio de la Plata; SF, Sao Francisco; WAF, West Africa.

Proterozoic-Early Cambrian Orogenies of South America

Tectonic events that occurred in South America during the Neoproterozoic-Cambrian interval are briefly examined here to determine which South American terranes should be included in late Neoproterozoic plate reconstructions. Recent tectonic models call for a trans-continental collision that closed the Clymene Ocean basin and completed the assembly of Gondwana in the Early to Middle Cambrian. The age of the suture, shown in Figure 6.5, was determined from a combined paleomagnetic-geochronologic study of Amazon-West Africa and São Franciso-Congo craton collisional orogens (Trindade et al., 2006; Tohver et al., 2006; Tohver et al., 2010). The model of Tohver et al., 2010 may be consistent with early models for the Pampean orogeny that call for collision between the Rio de Plata and Pampia blocks (Ramos et al.,1986, 1988; Rapela et al., 1998, 2007). Evidence for closure of the Clymene ocean basin between Pampia and Rio de Plata may include intrusion of calc-alkaline volcanics into marine turbidites of the Puncoviscana Formation at 555-525 followed by peraluminous magmatism and high-grade metamorphism at 525-515 Ma (Rapela et al., 2007; Tohver et al., 2010).

There are two basic models for the Pampean orogeny. In the collisional model an orogen formed between the Rio de Plata and Pampia blocks with a magmatic arc forming on the Pampia block prior to collision (Ramos et al., 1986; Ramos, 1988). In the non-collisional model, long-lived subduction persisted from 555-525 Ma that formed a calc-alkaline magmatic arc and an accretionary wedge prism. A short-lived pulse of high-grade metamorphism occurred due to the subduction of a mid-ocean ridge (Schwartz et al., 2008). The latest model of Tohver et al. (2010) appears to be an extension of the collisional model. In this model, the Clymene ocean closed during the Early to Middle Cambrian. Associated plutonic and metamorphic episodes occurred along a ~3000 km mega-suture zone that includes the Pampean, Paraguai, and Araguaia belts (Tohver et al., 2010). In this model, volcanic rocks from the Brasilia belt with ages that range from 570-700 Ma (Brasiliano orogeny, or Brasiliano-Pan-African orogeny) may be related to the construction of volcanic arcs on the Sao Francisco craton that occurred prior to the closure of the Clymene Ocean. In a study of detrital zircons from low-grade rocks of the Famatina belt, central Andes, Collo et al. (2009) determined distinct age spectra peaks with a Pampean age defined near 520 Ma and a Brasiliano age defined near 635 Ma.

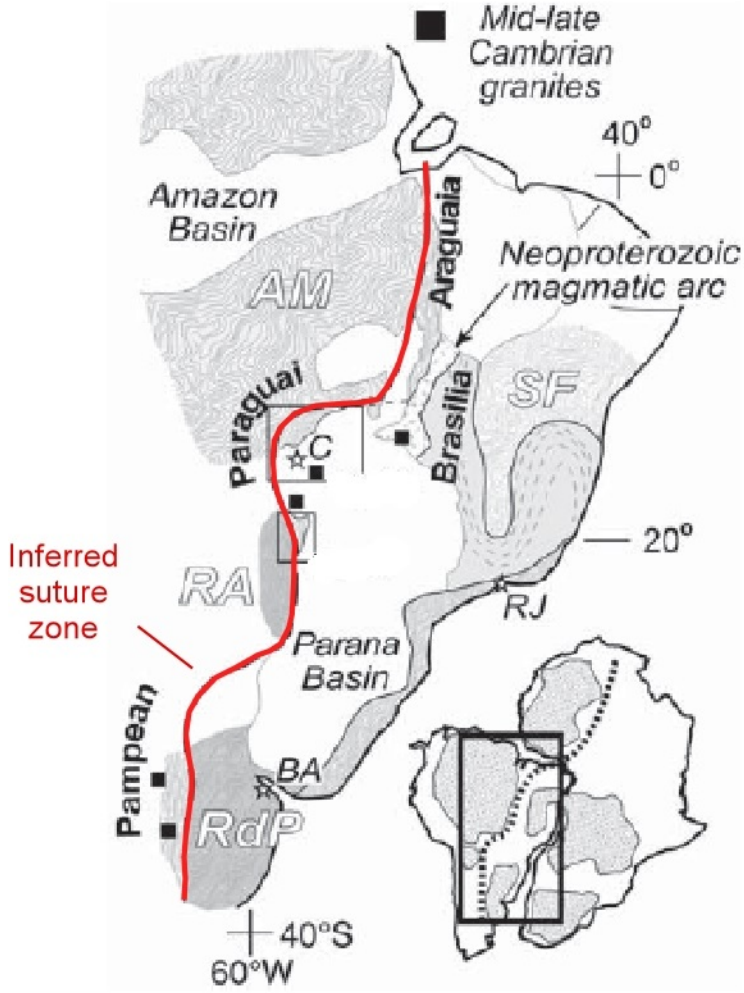

Figure 6.5. Pampean-Age suture zone. Major cratons: AM-Amazon, SF-Sao Francisco, RdP-Rio de Plata, RA-Rio Apa. RJ-Rio de Janeiro, BA-Buenos Aires, C-Culaba. A proposed Early – Middle Cambrian suture zone is shown as a red line. From Tohver et al., 2010.

Geochronological Comparison of the Arequipa-Antofalla Block with the Mars Hill /Southern Blue Ridge

Early reconnaissance excursions to the "Arequipa Massif" by Cobbing et al. (1977) recognized the complex igneous relations and poly-metamorphic nature of gneiss exposed in Peru near the Arica bend. These early isotopic studies detected disturbances in Rb-Sr and K-Ar systems, but a 6-point whole-rock Rb-Sr determined from gneiss of the Mollendo-Quilca region yielded an age of 1811 $\pm$ 39 Ma. The remarkable similarity of these results to the early whole rock Rb-Sr isochron age determination from Roan Mountain/Mars Hill terrane (Southern Appalachian Blue Ridge; 1815 $\pm$ 31 Ma; Monrad and Gulley, 1983) led to the more detailed comparison presented here. The following section is a comparison of geochronologic and whole-rock Pb isotopic data that have been determined from these South American (northern and central domains of the Arequipa Antofalla block) and Laurentian Mesoproterozoic gneiss complexes (primarily from the Mars Hill Terrane with some analyses from the central Blue Ridge of western North Carolina). Figure 6.5 shows approximate sample locations and the boundaries between the northern, central, and southern domains of the Arequipa-Antofalla block (Loewy et al., 2004).

One of the more insightful geochronologic studies of the Arequipa block is arguably a U-Pb TIMS zircon investigation of four samples of granulitic gneiss (Wasteneys et al., 1995). Analyses from the "Quilca Domain" (Figure 6.1.C, 6.5.A) determined a granulite facies metamorphic event at 1198 +6/-4 Ma that deformed ~1200 Ma and ~1900 Ma granitoids (Figure 6.6). At Mollendo (Figure 6.1.C, 6.5.A), granulite facies metamorphism occurred at 970 $\pm$ 23 Ma resulting in deformation of ~1900 Ma protoliths, ages that were determined from a 10-point concordia plot (Wasteneys et al., 1995).

As part of a metamorphic study, Martignole and Martelet (2003) determined metamorphic monazite ages via electron microprobe chemical dating from granulites in the Mollendo region, determining a Th-U monazite age of ~ 989 $\pm$ 11 Ma for a metamorphic episode that altered 1900 Ma protoliths. The event was identified as a geologically rare ultrahigh-temperature (UHT) metamorphic event expressed along a ~100 kilometer segment of the Peruvian coast in the Mollendo-Camana region. The UHT event was potentially caused by the upwelling of asthenospheric mantle into an overthickened crust.

In the present study and previous studies of the Mars Hill terrane (Carrigan et al., 2003; Ownby et al., 2004) a similar age distribution is inferred from the zircon U-Pb SHRIMP data. There is strong evidence for the existence of ~1200 Ma orthogneiss on the Laurentian side. For example, sample RM30 (Carvers Gap Gneiss from Roan Mountain) has a pooled $^{207}Pb/^{206}Pb$ age of 1190 $\pm$ 19 Ma. One of the main conclusions of Ownby et al. (2003) is that cumulatively, the SHRIMP data document a circa 1200 Ma magmatic event. In the Dellwood area the Group I orthogneisses (1244-1292 Ma) are older than the ~1200 Ma gneisses of the northern Arequipa-Antofalla block but may

correlate with 1254 +97/-94 Ma migmatite and 1213 + 28/-25 Ma orthogneiss that occurs in the central domain at Quebrada Choja (Damm et al., 1990). In the Mars Hill terrane, a felsic orthogneiss from the Cloudland Gneiss (MBCL4) also appears to belong to this age group, with an upper intercept age determined to be 1257 ± 26 Ma, and mean age from the ten most concordant points determined to be 1245 ± 18 Ma ($^{207}Pb/^{206}Pb$ age, Ownby et al., 2004).

The existence of a 1900 Ma granulitic orthogneiss counterpart in the southern Blue Ridge is more tentative. However a whole rock Rb-Sr isochron from Mollendo-Quilca (Cobbing et al., 1977) yields results that are identical (within error) to the whole rock Rb-Sr isochron from Roan Mountain (Monrad and Gulley, 1983). The Arequipa whole rock isochron yields 1811 ± 39 Ma; the Mars Hill isochron yields 1815 ± 31 Ma. There is a population of older inherited zircons in the 1200 Ma orthogneisses of the Mars Hill terrane. RM30 and RM30C, interpreted as felsic and mafic orthogneisses, contain inherited zircons that yield concordant ages at 1658, 1672, and a discordant age of 1782 ± 201 in RM30C (Ownby et al., 2004). A Paleoproterozoic age for the protoliths of the Mars Hill gneisses is inferred from Sm-Nd depleted mantle model ages (T_{DM}) of *circa* 2.3-1.7 Ga determined from two felsic orthogneisses, two mafic gneisses, and a paragneiss (DePaolo, 1980; Carrigan et al., 2003; Ownby et al, 2004). T_{DM} estimates from the northern domain of the Arequipa-Antofalla block range from 2.3-1.9 Ga, with the exception of Ordovician intrusions and one 1.8 Ga amphibolite (Loewy et al., 2004). The presence of ~1900 Ma lithologies in the Cartoogechaye terrane is more tentative; a single detrital grain from DEL03-1L yields a U-Pb SIMS age of 1911 ± 39 Ma. Additional U-Pb zircon ages of ~1900 Ma were determined from detrital zircon populations separated from Cartoogechaye terrane, Dahlonega gold belt, and Mineral Bluff Formations metasedimentary rocks (Merschat et al., 2010, SHRIMP ages). Similar laser-ablation U-Pb ages were determined from detrital zircon grains of the Ocoee (~1800 Ma, Chakraborty et al., in submission).

There is a strong case for correlation of Neoproterozoic and Mesoproterozoic metamorphic events between the Arequipa-Antofalla block and the Mars Hill terrane. Specifically, the 970 ± 23 Ma metamorphic U-Pb zircon TIMS age from the northern domain of the Arequipa-Antofalla block (Wasteneys et al., 1995) correlates with a metamorphic $^{207}Pb/^{206}Pb$ zircon SHRIMP age of 975 ± 31 Ma from a banded paragneiss from the Roan Mountain location, Mars Hill terrane (Sample #RM30B, Ownby et al., 2004). The seven zircons from RM30B are described as unzoned with bright and dark interiors and rims, and were interpreted as having a metamorphic origin. The metamorphic rim ages determined from the Dellwood area are somewhat different; the 997 ± 18 Ma age (weighted mean from 7 points, DEL03-1, DEL03-1L) is slightly older, but within error of the metamorphic age from Mollendo, but nearly identical to the monazite age (989 ± 11 Ma) determined by Martignole and Martelet (2003). The second metamorphic age of 897 ± 31 Ma determined from a weighted mean of 4 points from Cartoogechaye terrane migmatite #DEL03-1 and DEL03-1L has not been recognized in Mars Hill, but a correlative metamorphic age occurs in the Atico domain of the Arequipa-

Antofalla block where Grenville metamorphic U-Pb SHRIMP zircon ages range from ~1000-840 Ma (Casquet et al, 2010).

Correlation of the earlier 1198 +6/-4 Ma metamorphic event in the Arequipa "Quilca domain" (Wasteneys et al., 1995) is less definitive. The interpretation that high grade metamorphism at Quilca began at 1200 Ma by dehydration reactions, followed by anatectic melting as late as 1185 Ma was made in part from observations related to Th/U ratios (Wasteneys et al., 1995). A SHRIMP Pb-Pb age of ~1199 Ma was determined from a Cloudland Gneiss zircon (sample MBCL-3B, Mars Hill terrane) having extremely low Th/U relative to zircon core analyses from the same sample (Ownby et al., 2004). Thus there is evidence for a correlated 1199 Ma metamorphic event, but more data are required to confirm it on the Laurentian side.

There is a weak case for the correlation of Neoproterozic rifting events between the Arequipa and Antofalla block and the Mars Hill terrane. The older phase of Neoproterozic rift intrusives of the Laurentian margin is widespread in the The Mars Hill terrane (Bakersville dike swarm; 726 $\pm$ 29 Ma,Goldberg et al., 1986). Neoproterozic sedimentation occurred in the San Juan and Quebrada Choja domains of the Arequipa-Antofalla block, however only one dacite dike has been dated from Quebrada Choja that supports Neoproterozoic rifting. A lower intercept age of 635 $\pm$ 5 Ma was interpreted as the time of crystallization of the dacite dike (Loewy et al., 2004). Three middle Neoproterozoic A-type quartz monzonite and alkali feldspar granites have been determined to the north of the Arequipa-Antofalla block in the south-central Eastern Cordillera of Peru (Mišković et al., 2009). Ages ranging from 752-691 were interpreted as being part of a larger suite that complements the 765-680 Ma ages from the Appalachian Blue Ridge.

Lower Ordovician through Lower Silurian metamorphic ages determined from the central Blue Ridge (478 $\pm$ 22 to 434 $\pm$ 10 Ma; this study, Chapter 4) broadly overlap with the emplacement age of the arc-related San Nicolás batholith that intrudes the northern Arequipa domain. Refined age estimates of the San Nicolás batholith range from 468 to 440 Ma (Mukasa and Henry, 1990; Loewy et al., 2004). However, these events are interpreted here as occurring at the same time, but in different places, as supported by paleomagnetic studies of Mac Niocaill et al. (1996) and Precordillera "microcontinent" models of Thomas and Astini, (1996, 1999, 2003), Astini and Thomas (1999), and Thomas et al. (2002).

Selected ages of intrusive and metamorphic events from the Mars Hill, central Blue Ridge and Arequipa-Antofalla basement are compared in Table 6.1. Additional comparisons of the whole rock Pb isotopic compositions of the Mars Hill and Arequipa blocks are plotted in Figure 6.7. The whole rock Pb-isotopic compositions from the Laurentian and South American terranes overlap in $^{207/204}$Pb - $^{206/204}$Pb space, and plot in the U-enriched area, above the reference line of Stacey and Kramers (1975). The Pb isotope data (Figure 6.7) would suggest that *all* of the southern Blue Ridge basement samples plotted may be petrogenetically related to the Arequipa-Antofalla block, and not the Mars Hill terrane alone.

The ages and whole-rock Pb-isotopic compositions compared in Table 6.1 and Figure 6.8 are not unique to the Mars Hill terrane and the Arequipa-Antofalla block. Similar ages have been observed in the Maz domain of the western Sierras Pampeanas and the Rio Apa block south of the present day Amazonian craton (Casquet et al., 2010). Gneiss terranes with similar age distributions could potentially be found elsewhere internal to the Amazonian craton (e.g. Bettencourt et al., 1999). Although the geochronology and isotopic compositions of the Laurentian and South American blocks are strengthened by the somewhat weak evidence for Neoproterozoic rifting at each location (poorly preserved on the South American side, Loewy et al., 2004) the geochronologic and isotope-based correlation between the southern Blue Ridge and the Arequipa-Antofalla block presented here is by no means bullet-proof. Some of the metamorphic ages from the Dellwood region have large errors, and the Mesoproterozoic basement of the central Blue Ridge shows a large magmatic age interval. The paleogeographic correlation presented here is regarded as a hypothesis that needs to be tested by further geochronology and geochemistry.

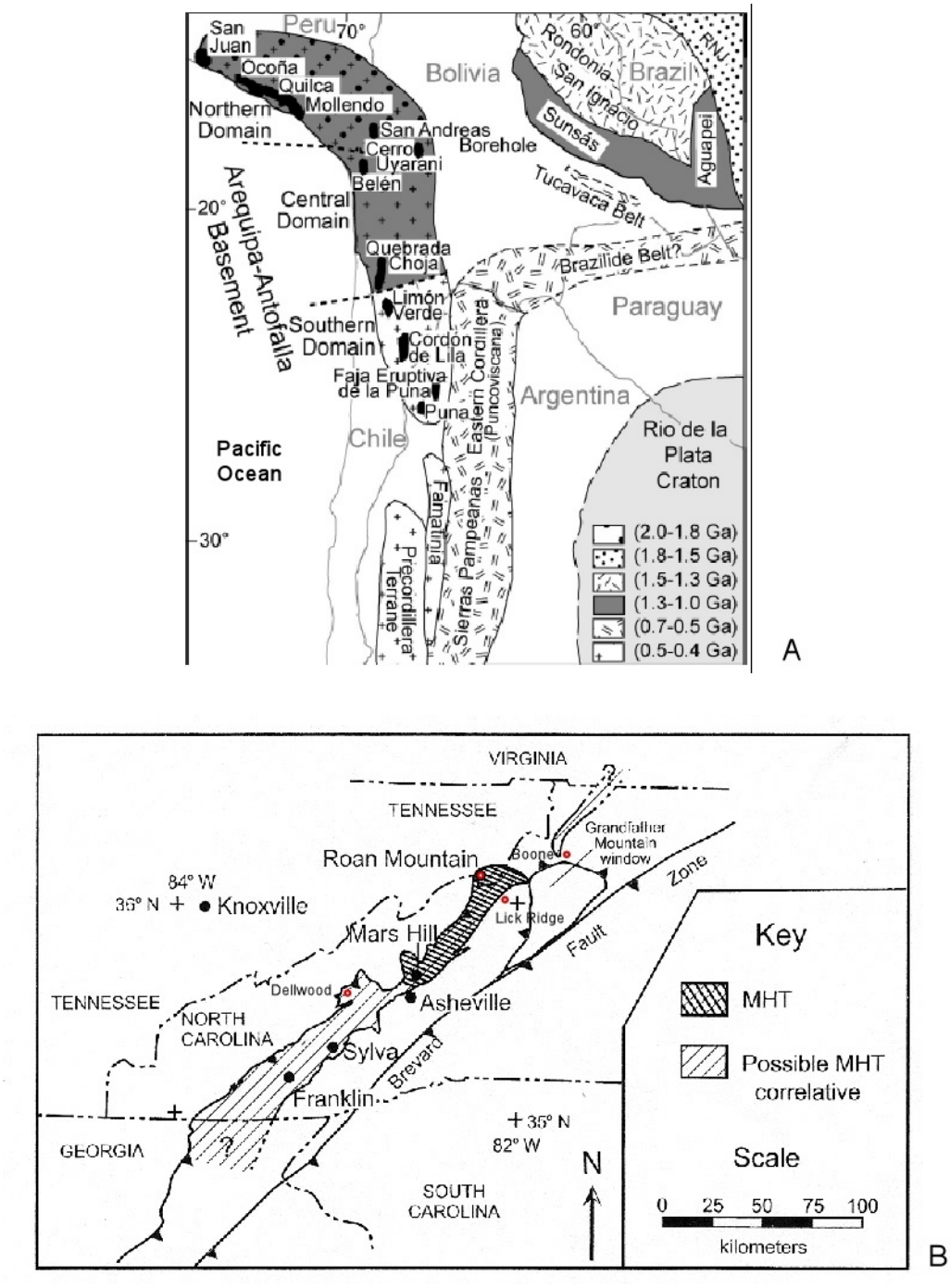

Figure 6.5. Locations in the Arequipa-Antofalla and southern Blue Ridge. A) Arequipa-Antofalla basement gneiss localities and domain subdivisions from Loewy et al. (2004). B) Mars Hill and Dellwood locations from Ownby et al. (2004).

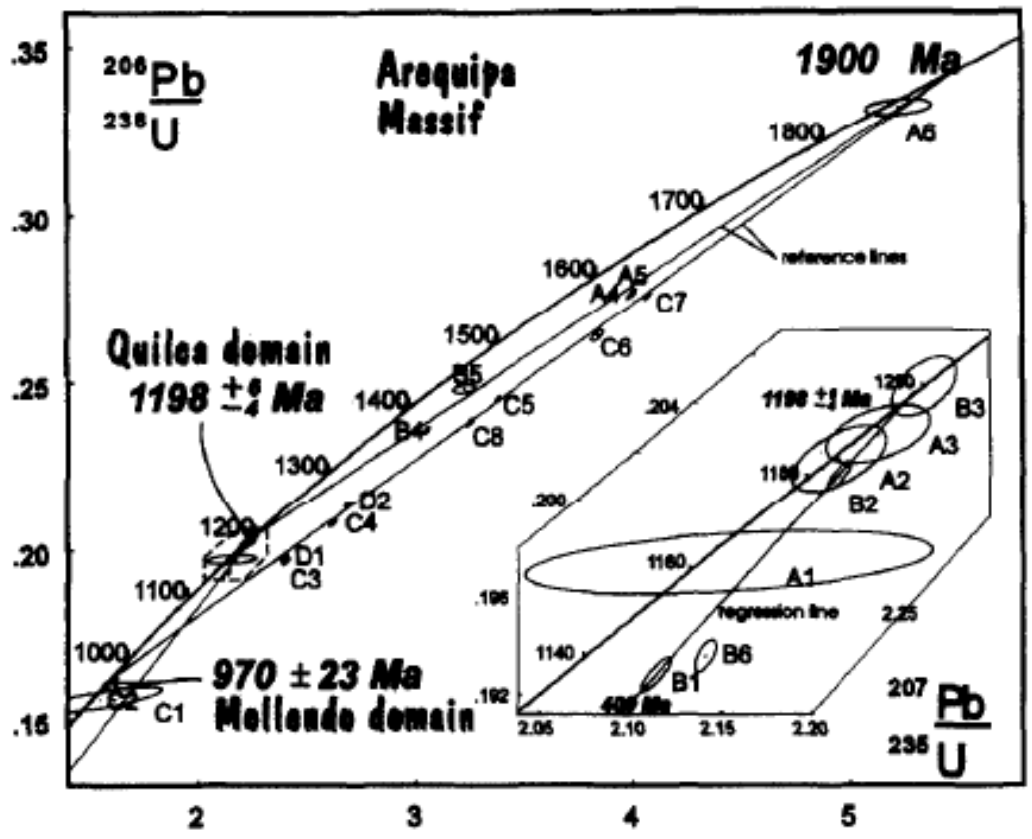

Figure 6.6. Concordia plot of TIMS U-Pb data from Quilca and Mollendo. (Arequipa Block). Distinct discordant arrays are plotted from protolith zircons. Lower intercepts correspond with concordant metamorphic zircon ages. Inset is the discordia from metamorphic zircons from the two Quilca samples. From Wasteneys et al. (1995).

Table 6.1. Comparison of Laurentian Blue Ridge and Arequipa Tectonic Events.

Mars Hill and Central Blue Ridge	Arequipa-Antofalla
765-680 Ma A-type suite, bimodal volcanics ~630 Ma, Goochland terrane	752-691 Ma A-type suite, eastern Cordillera 635 Ma dacite dikes, Quebrada Choja
997 Ma met (zircon), Dellwood 975 Ma met (zircon), Mars Hill	989 Ma met (monazite), Mollendo 970 Ma met (zircon), Mollendo
1198 Ma met (Mars Hill, tentative)	1198 Ma met (Quilca)
1200 Ma magmatism, Mars Hill	1200 Ma magmatism, Quilca
1292-1244 Ma arc magmatism (Dellwood, central Blue Ridge)	1254, 1213 Ma orthogneiss Quebrada Choja
Rb/Sr 1815 Ma Mars Hill, whole rock	Rb/Sr 1811 Ma Mollendo-Quilca, whole rock
inherited zircons 1658, 1672 Ma Mars Hill Detrital zircons: ~1800, 1911 Ma Central Blue Ridge T_{DM} 2.3-1.7 Ga (Mars Hill)	1900 Ma zircons, upper intercept T_{DM} 2.3-1.9 Ga (northern domain)

References and errors given in text.

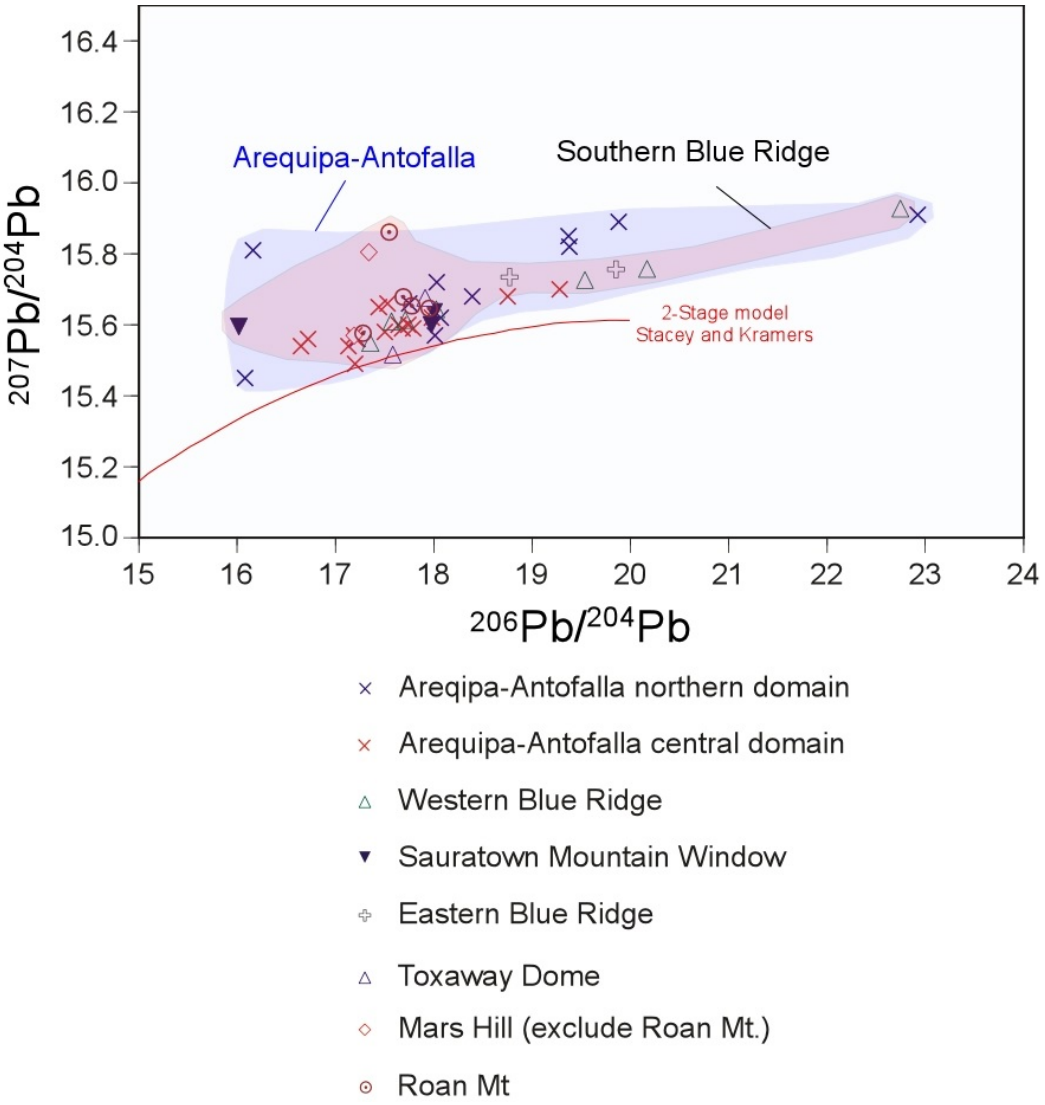

Figure 6.7. Whole-rock Pb compositions of the Arequipa-Antofalla block and southern Blue Ridge. Compositions of the Arequipa-Antofalla block northern domain include analyses of Paleoproterozoic (~1.8 Ga) crystalline basement occurrences from San Juan, and Mollendo, Peru and one Ordovician intrusive from Ocoña, Peru. Central domain compositions (Arequipa-Antofalla) were determined from ~1.4 Ga gneisses, amphibolites, and ultramafics as well as seven analyses of Ordovician granodiorites from Belén, Chile; data from Loewy et al. (2004), data repository item 2004028. Southern Blue Ridge compositions were determined from various felsic and mafic gneiss and granulites with inherited zircon ages ranging from 1019-1765 Ma. Data from Berquist,

(2005); Carrigan et al. (2003); Ownby et al. (2004); Hatcher et al. (2004); and Fischer et al. (2010), with a compilation in Fischer et al. (2010), Table 4. Average crustal Pb evolution line from the two-stage model of Stacey and Kramers (1975).

Tectonic Synthesis

Tectonic Framework of the Mesoproterozoic

Loewy et al. (2004) suggest that the Arequipa-Antofalla block was accreted to Amazonia during the Sunsás orogeny (1.2-1.0 Ga). The significance of the 1198 +6/-4 metamorphic age from Quilca (Wasteneys et al., 1995) and the widespread ~1200 Ma arc magmatism in the Mars Hill and central Blue Ridge terranes (~1200 Ma, Ownsby et al., 2004; 1292-1244 Ma, this study) is unclear. The P-T conditions related to the ~1198 Ma metamorphic event in the Blue Ridge of western North Carolina is presently poorly constrained. The interval 1170-1140 Ma was an interval of prolific arc magmatism in which ocean crust was subducted beneath the Arequipa-Antofalla block generating the abundant ~1170-1140 Ma magnesian, calc-alkalic to alkali-calcic, high-K granites and granodiorites in the central Blue Ridge (Chapters 4,5, Figure 6.8.A) that may be part of a broader Shawinigan orogenic suite (1190-1140 Ma) that is widespread in the basement gneisses that compose the Appalachian inliers (McLelland et al., 2010). It was during this interval that the central and southern Blue Ridge (SCAB) was transferred from Amazonia to Laurentia. The paleomagnetic-based study of D'Agrella-Filho estimates the transfer at 1150 Ma. An estimate based on Pb and Nd isotopes also yields an age of 1150 Ma (Tohver et al. 2004a). Tohver et al. (2004b) and D'Agrella-Filho et al. (2008) suggest that there was continued sinistral lateral motion between Laurentia and Amazon craton during the Grenville-Sunsás orogeny.

Arc magmatism terminated with the collision of Amazonia and Laurentia (Grenville Orogeny) in a protracted collision evident in the central Blue Ridge at *circa* 1060-1020 Ma (Chapters 4, 5) that would appear to be part of the Ottawan phase of the Grenville (-Sunsás) orogeny (Figure 6.8.B, Rivers, 1997; Rivers et al., 2002; Hynes and Rivers, 2010). In the central Blue Ridge orthogneiss examined here, the younger Proterozoic rocks (1060-1020) are ferroan-granitoids, not magnesian granites typical of a volcanic arc. The change from magnesian to ferroan granites in the Central Blue Ridge supports the hypothesis that a change in tectonic modes occurred during the Mesoproterozoic. The group I and group II orthogneiss (1292-1244 and 1170-1140 Ma) are magnesian; the group II orthogneiss (1060-1030 Ma) is ferroan. However, the distribution of magnesian and ferroan granites may be related to the Taconian suture or Hayesville fault as mapped by Montes (1997); the older hornblende-biotite gneiss is abundant in the Hayesville thrust sheet and the ferroan granites and granodiorites (Max Patch Granite) are abundant to the northwest of the fault. Alternatively, strike-slip motion occurred between the Peri-Laurentian margin and Laurentia during the time interval bracketed by Neoproterozoic rifting and Taconian collision.

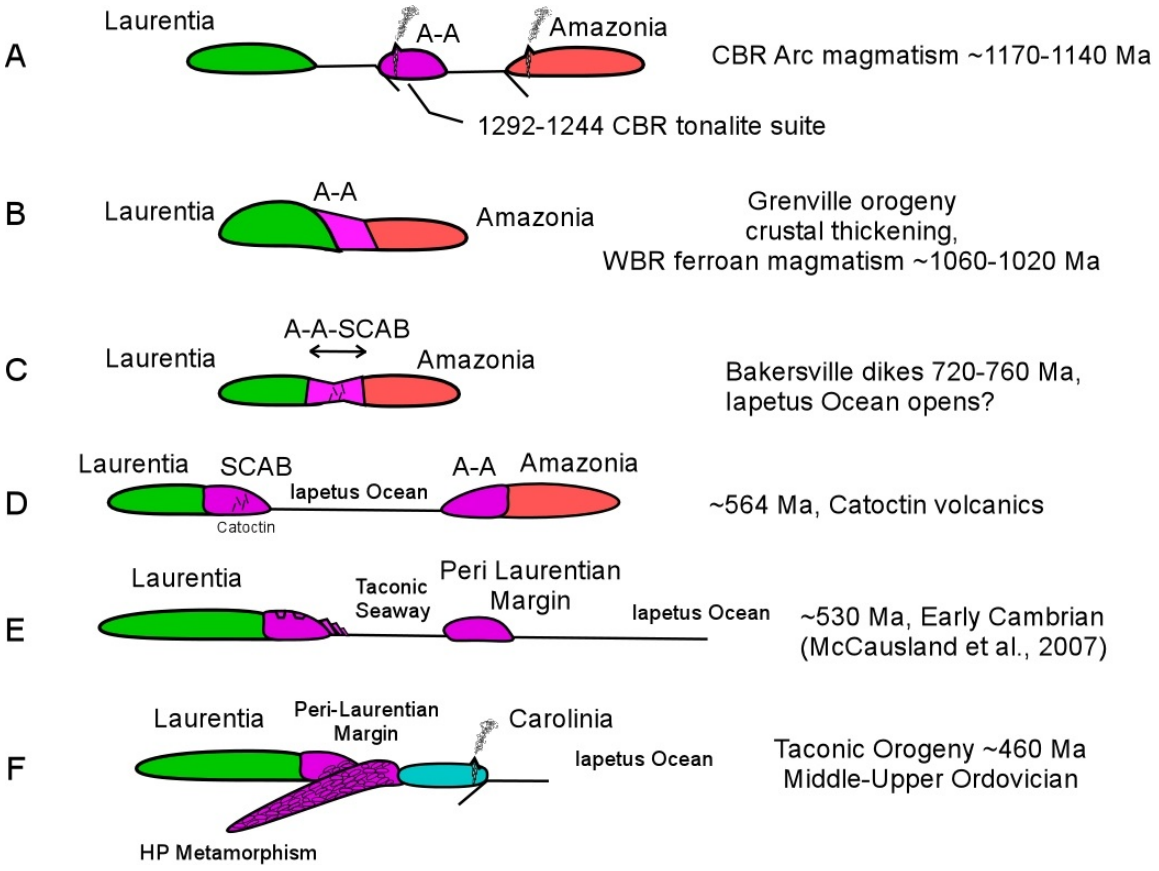

Figure 6.8. Depiction of the tectonic history of the central Blue Ridge of western North Carolina, Mesoproterozoic through Middle Ordovician. AA: Arequipa-Antofalla block; CBR: central Blue Ridge; WBR: western Blue Ridge; SCAB: southern and central Blue Ridge.

Neoproterozoic Paleogeographic Reconstruction

Using the previously described lithologic correlation, it is possible to reconstruct a crude estimate of the paleogeography of the Laurentian-Amazonian section of Rodinia (Figure 6.9). On the Laurentian side, the palinspastically restored rifted margin of Thomas (2006) is used to estimate the shape of the North American margin. No palinspastic correction was applied to the western margin of South America. It is doubtful that the ancient South American coastline resembles the modern one due to Paleozoic tectonic events, and tectonic erosion related to Andean subduction zones.

There is a large gap that occurs when the restored margin of Thomas (2006) is placed against the modern South American coastline due to the Arica bend (Figure 6.1.C). The terranes that belong in the Arica bend are unclear. It is conceivable that the shape of the Arica bend is related to Paleozoic tectonic indentation, and not Precambrian rifting. In Figure 6.9 the gap at the Arica bend is filled with "peri-Laurentian terranes".

To estimate the shape and terrane distribution in South America prior to the break up of Rodinia, the terranes southeast of the Pampean-Brasiliano suture zone (Tohver et al., 2010) were stripped away from the geotectonic sketch map of Cordani et al. (2010). The Famatina belt and Chilenia terranes were stripped from the southwest coast, and the Precordillera was left in its Precambrian position (the Ouachita embayment of Laurentia; Thomas and Astini, 1996; Astini and Thomas, 1999; Thomas et al., 2002). The locations of Paracas and Oaxaquia are from the interpretations of Ramos (2010). By restoring the Mars Hill terrane to a position adjacent to the central domain of the Arequipa-Antofalla block, the Precordillera is juxtaposed with Pampia and Oaxaquia is nestled into the Quebec embayment. This northern position for Oaxaquia appears questionable, given the amount of dextral translation required to move it to its present position in central Mexico. No geochemical comparisons of Oaxaquia to the Mesoproterozoic basement of Quebec were undertaken here

A model of the break up of the Laurentian-Amazonian realm of Rodinia is depicted in Figures 6.8.(C,D,E). A two-phase rift model is applied, following the arguments of McCausland et al. (2007) and Hibbard et al. (2007). In this model of rifting along the Laurentian margin, the Iapetus Ocean opens first, followed by a second rifting event that occurred inboard of the Laurentian margin, forming a ribbon of terranes along the southeast coast of Laurentia (Hibbard et al., 2007).

The paleogeographic reconstruction (Figure 6.9) and proposed lithologic correlation support the hypotheses proposed by Tohver et al. (2004a), Ramos (2008), and Fisher et al. (2010). These hypotheses suggest that the southern and central Blue Ridge basement rocks are exotic to Laurentia, having been tranferred from western Amazonian during the Grenville-Sunsás orogeny.

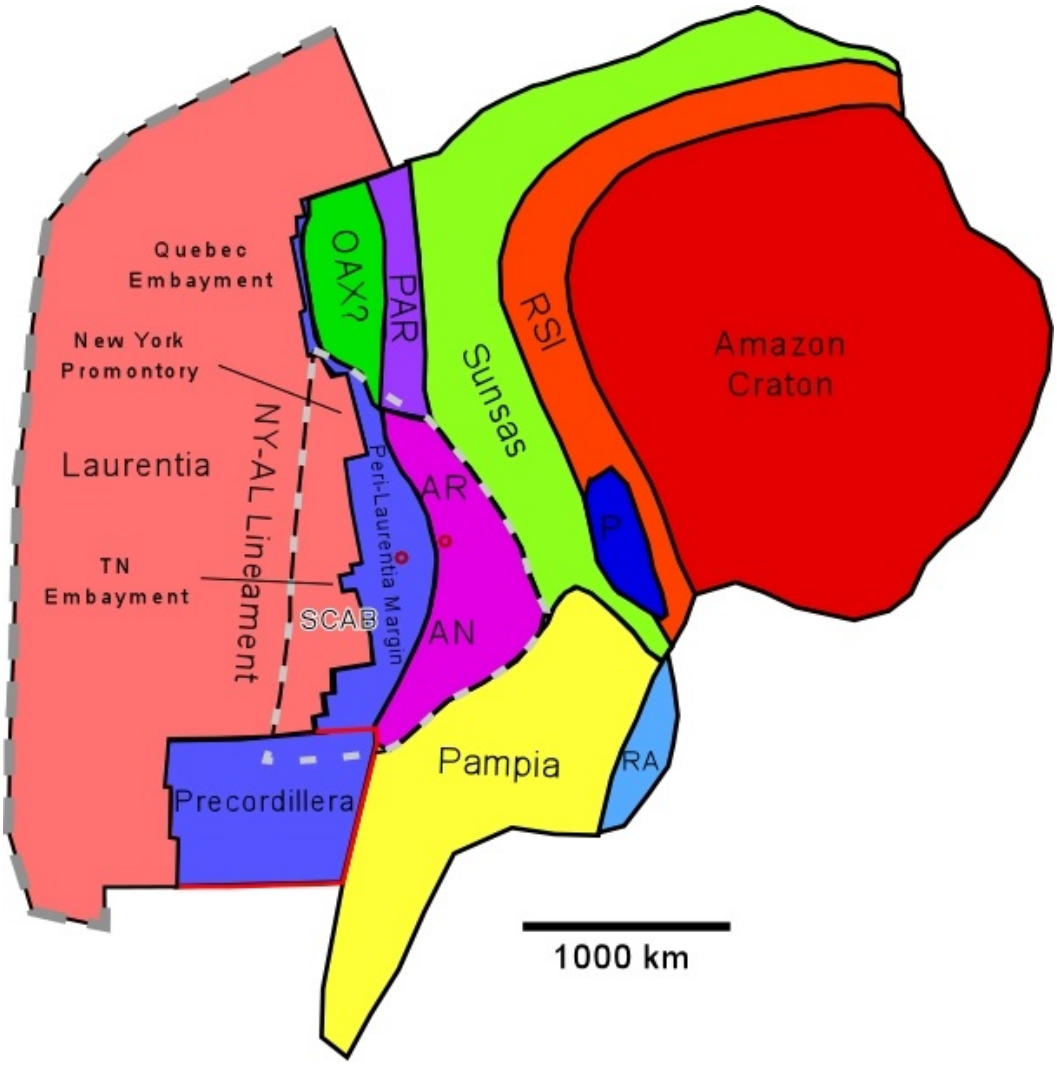

Figure 6.9. Paleogeographic reconstruction of the Laurentian-Amazonian region of Rodinia at 920 Ma. Eastern Laurentian margin after Thomas (2006). Amazonian configuration after Cordani et al. (2010), Ramos (2010), and Tohver et al. 2010. Abbreviations: RSI -Rodonia-San Ignacio; AR-Arequipa; AN-Antofalla; Paragua; PAR-Paracas; OAX-Oaxaquia; SCAB-southern and central Appalachian Basement. Potential outline of restored Arequipa-Antofalla block + SCAB shown with thick black dash. Approximate locations of correlated formations shown as red dots (Mars Hill terrane and central domain, Arequipa-Antofalla block).

CHAPTER 7: SUMMARY OF NEW FINDINGS

Summary of Chapter 2

The examination of eclogite-facies metabasites in the present study indicates that the net omphacite-breakdown reaction is essentially Omp = Di-Hd (ss) + Pl $\pm$ Hbl $\pm$ Qtz, and not a simple combination of Jd + Qtz = Ab and CaTs + Qtz = An. In Dellwood samples the reaction appears to be low-Na Ac or high-Na Di = Di-Hd (ss) + Pl + Hbl + Qtz. The temperature range for formation of the Cpx-Pl symplectites examined is ~650 to 775 ^{o}C. Boone symplectites are an exception, formed at higher temperatures (~ 760 – 825 ^{o}C). Cpx-Pl symplectites form over a pressure interval of ~ 3 – 16 kbar that appears to be correlated with X_{Jd} in omphacite, with high-X_{Jd} Cpx breaking down at higher pressures, low- X_{Jd} Cpx reacting at lower pressures during decompression.

The widespread occurrence of symplectic textures in rapidly decompressed HP and UHP rocks is the fingerprint of rapid eduction or uplift and significant over-stepping of a strongly pressure-dependent reaction along a nearly isothermal decompression path. Although decompression is rapid, the degree of cooling through the isothermal interval is obviously low, thus maintaining favorable reaction kinetics at nearly peak-T conditions. The reaction may be considered wholesale breakdown of the omphacite lattice, with product phases nucleating at the site of breakdown. In contrast, nucleation of 'exsolution' lamellae and diffusion-controlled coarsening is diagnostic of low degrees of overstepping of the omphacite-breakdown reaction along P-T paths with a greater component of cooling, and longer periods of time at high T, with a longer characteristic length scale for diffusion.

In most of the broadbeam comparisons the Cpx-Pl symplectites appear to be largely isochemical with adjacent unreacted clinopyroxene.

The paradox that quartz occurs within some Cpx-Pl symplectites after omphacite (quartz should be consumed by the reactions Jd + Qtz = Ab and CaTs + Qtz = An) can be explained by the presence of Ca-Eskola component in precursor clinopyroxene. Significant amounts of CaEs are indicated when reintegrated Cpx-Pl symplectite compositions are recalculated as pyroxenes. The reintegrated symplectites from Flatraket, Lick Ridge and Dellwood have X_{CaEs} that ranges from 4-15 mole % when endmember calculation methods of Katayama et al., (2000) and Page et al., (2005) are applied. If CaEs was a component of these pyroxenes at high pressure (>15 kbar), it is plausible that all of the following reactions occurred during the breakdown of clinopyroxene to form Cpx-Pl symplectite:

$$\text{CaEs} + \text{Jd} = 1.5\ \text{Pl}\ (\text{Ab}_{67}\text{An}_{33})\ \text{(Vogel, 1966)}$$
$$\text{Jd} + \text{Qtz} = \text{Ab}$$
$$\text{CaTs} + \text{Qtz} = \text{An}$$
$$2\ \text{CaEs} = \text{CaTs} + 3\ \text{Qtz}\ \text{(Smyth, 1980)}$$
$$\text{CaEs} = \text{An} + 2\ \text{Qtz}\ \text{(Gasparik, 1986)}$$

Summary of Chapter 3

The similarity of the P-T paths of the Blue Ridge metabasites and P-T paths of continental subduction complexes (Figure 3.11B) indicates that HP-metabasites of western North Carolina could represent another continental crustal subduction complex. Peak-pressure conditions from Blue Ridge metabasites allow for the estimate of burial/subduction of crustal material to depths of at least 65 km. The nearly-isothermal trend of decompression paths (Figure 3.8), new zircon U-Pb and hornblende ^{40}Ar-^{39}Ar age estimates from the Dellwood metabasites of the central Blue Ridge basement complex, and preservation of prograde growth zoning in garnet are consistent with rapid eduction of the central and eastern Blue Ridge to depths of 25-30 km. U-Pb zircon age determinations from the Lick Ridge eclogite (Miller et al. 2006, 2010) indicate a Taconic age for the Lick Ridge eclogite. A ^{40}Ar-^{39}Ar hornblende age of ~450 Ma from the Dellwood HP amphibolite body (Kunk et al., 2006) is interpreted as a cooling age that marks the eduction of the Taconic continental subduction complex. Boone eclogites remain undated, but are in all likelihood Taconic due to similarities in the P-T paths and tectonic settings.

Taconic continental subduction may have produced a mega- mélange that is referred to in the literature as the "Cullowhee terrane" Raymond et al. (1989) and the "eastern Blue Ridge mélange" Lacazette and Rast (1989). Determining the polarity of Taconic continental subduction in western North Carolina is nontrivial due to widespread late Paleozoic retrograde metamorphism and deformation that may have involve hundreds of kilometers of compressional and dextral transpressional translation. Seismic studies have produced data that can potentially support a model of westward subduction of continental crust below the Middle Ordovician Laurentian margin. COCORP imaging reveals west-dipping reflectors below the Charlotte belt and Carolina Slate belt of Carolinia labeled "J" in Figure 3.13, 3.14. Hibbard et al. (2010) interpret this same "reflector J" as the Silurian-aged (pre ~430 Ma) suture between Carolinia and Laurentia, having formed via continental subduction during the "Cherokee" orogeny, an alternate scenario to the one presented here.

Geophysical modeling studies support the concept of westward subduction. Specifically, Coakley and Gurnis (1995) proposed that westward subduction occurred below the Laurentian margin based on lithospheric modeling of far-field tilting of the Michigan Basin to accommodate the deposition of the Black River and Trenton stratigraphic intervals. The best-fit model of Coakley and Gurnis (2005) invokes westward subduction of a slab of negatively buoyant crust, descending at moderate dip (20-30^{o}) for 10-15 Ma.

In summary, the P-T pathways determined from the Taconian metabasites of the eastern and central Blue Ridge metabasites are strongly indicative of a continental subduction event. The polarity of subduction in the southern Blue Ridge remains speculative, and polarity may not have been consistent along strike. Late Silurian reconstructions of Dennis, (2007) suggest that the Inner Piedmont may not have been in

its present position at the time of the Taconic orogeny. The Inner Piedmont is an important component of widely-accepted models that invoke the eastward subduction of ocean crust material beneath a Piedmont arc. The absence of a Piedmont arc outboard of the central and eastern Blue Ridge during the Taconic orogeny, and the possibility of a southern extension of Carolinia are discussed.

Summary of Chapter 4

Using petrographic criterion and classifications of others (Southworth et al., 2005; Merschat and Cattanach, 2008), six subdivisions are used to classify samples from the present study: migmatitic-biotite gneiss, hornblende-biotite gneiss, muscovite-biotite gneiss, biotite augen gneiss, amphibolite, and metasedimentary cover sequences. U-Pb zircon (SIMS) ages were determined from central and western Blue Ridge rocks and combined with additional data from Loughry (2010). Plutonic ages of the central and western Blue Ridge mainly fall into three broad groups: Group I (1292-1244 Ma); Group II (1170-1140), and Group III (1060-1020). Some plutonic zircons have ages that are older than Group I, and others have ages that are younger than Group III, indicating that the complex geochronologic record of the central Blue Ridge is by no means fully understood. Three metamorphic events were determined from a central Blue Ridge migmatite (Sample DEL03-1): 997 $\pm$ 18 Ma, 897 $\pm$ 31 Ma, and 460 $\pm$ 11 Ma.

Th-Pb monazite ages (SIMS) were determined from four cover sequence schists and one central Blue Ridge migmatite. Of these samples, three record Taconic ages (~460 Ma), all five record Cherokee ages (434-416 Ma), two record Acadian ages (~380), and one records a Alleghanian age (~310 Ma). Monazite ages distributions suggest that effects of the Silurian "Cherokee" orogeny (Hibbard et al., 2010) were critical to the regional metamorphic history of the western and central Blue Ridge. The poly-metamorphic textures evident in some Great Smoky group schists, expressed as multiple phases of garnet growth (Figure 4.11.A,B) may have resulted from Taconic metamorphism that was overprinted by Cherokee metamorphism. The irregular distribution of monazite ages (e.g. Acadian ages in the Murphy Belt, and only ~460 Ma ages in the French Broad River drainage, Hietpas et al., 2010) allow for the possibility that the effects of Devonian terrane dispersal recognized in the Piedmont (Dennis, 2007) may have been active in the central and western Blue Ridge during the Devonian.

Summary of Chapter 5

After determining geochemical compositions from samples of gneiss of the central and western Blue Ridge basement complex, criteria were applied to cull the data set prior to plotting a variety of classification diagrams. The classification of Frost et al. (2001) and Frost and Frost (2008) were applied, and geochronologic data of Chapter 4 were used to distinguish three Mesoproterozoic age orthogneiss suites that compose the central and western Blue Ridge basement complex examined here. Results are summarized in Table 5.1 and are not repeated here. Migmatitic biotite gneiss samples that survived the culling

process show geochemical trends that are similar to Group I orthogneiss. Some migmatitic biotite gneiss may represent dacite-andesite, or volcanic equivalents of the Group I (tonalite-diorite-gabbro) suite. Most of the biotite gneiss and all of the muscovite-biotite gneiss samples were culled. These rocks may be metasedimentary or metavolcanic in origin, and require further investigation. Group I and Group II orthogneiss represent magnesian granitoid suites, typically produced by arc plutonism. Group III gneiss represents a ferroan granitoid suite that commonly forms via the melting of overly-thickened crust. Group III gneiss is Grenville-age, and occurs in the western Blue Ridge.

Summary of Chapter 6

A potential correlation between the Mars Hill terrane (southern Blue Ridge) and the Arequipa-Antofalla block of Peru is proposed, based on isotopic similarities between orthogneiss in these terranes. The correlation may help to clarify the early Paleozoic evolution of the southern Blue Ridge and the tectonic history of the Mars Hill terrane. To put the correlation and paleogeographic reconstruction in context, the geology of southwestern South America from the Mesoproterozoic through Cambrian is summarized. The geologic overview is followed by a presentation of isotopic data interpreted as demonstrating a potential lithologic correlation between the Laurentian and Gondwanan terranes. Finally, a paleogeographic reconstruction is presented and the tectonic evolution of the central Blue Ridge from the Precambrian through early Paleozoic is discussed.

APPENDICES

Appendix A. Representative mineral compositions from the Appalachian Blue Ridge and WGR, Norway.

Clinopyroxene

	1	2	3	4	5	6
SiO_2	52.86	51.15	51.83	49.98	50.71	51.51
TiO_2	0.22	0.36	0.26	0.27	0.3	0.18
Al_2O_3	8.97	6.64	7.31	5.62	6.55	2.23
FeO	5.58	7.06	9.72	11.33	9.64	10.84
MnO	0.05	0.03	0.06	0	0.02	0.07
MgO	10.52	12.38	9.27	9.86	9.81	11.92
CaO	17.18	20.72	18.71	21.07	20.62	22.23
Na_2O	3.98	1.76	3.19	1.5	2.31	0.96
Sum	99.36	100.1	100.34	99.64	99.96	99.94
Si	1.92	1.873	1.904	1.878	1.879	1.928
^{IV}Al	0.08	0.127	0.096	0.122	0.121	0.072
^{VI}Al	0.304	0.159	0.221	0.127	0.165	0.027
Ti	0.044	0.073	0.088	0.09	0.105	0.104
Fe^{3+}	0.006	0.01	0.007	0.008	0.008	0.005
Fe^{2+}	0.57	0.676	0.508	0.552	0.542	0.665
Mg	0.126	0.143	0.211	0.266	0.194	0.235
Mn	0.002	0.001	0.002	0	0.001	0.002
Ca	0.669	0.813	0.737	0.848	0.819	0.892
Na	0.28	0.125	0.227	0.109	0.166	0.07
Sum	4	4	4	4	4	4
Jd	0.24	0.05	0.14	0.02	0.06	0
Ac	0.04	0.07	0.09	0.09	0.1	0.07
I*	0.01	0.01	0.01	0.01	0.01	0.01
Ess	0	0	0	0	0	0.03
CaTs	0.07	0.11	0.08	0.11	0.1	0.03
Jo	0	0	0	0	0	0
CaEs	0	0	0	0	0	0
Wo	0.3	0.35	0.32	0.37	0.35	0.41
En	0.28	0.34	0.25	0.28	0.27	0.33
Fs	0.06	0.07	0.11	0.13	0.1	0.12
Sum	1	1	1	1	1	1
class (IMA)	omp	Di	omp	di	di	di

Table caption follows

Appendix A (Table caption):

Cations calculated on the basis of 6 oxygen with Fe^{3+} estimated using the method of Droop, 1987. 1) Lick Ridge eclogite, matrix Cpx core; 2) Lick Ridge eclogite, matrix Cpx rim; 3) Dellwood garnet granulite, matrix Cpx core (sample DEL05-3B2); 4) Dellwood garnet granulite, matrix Cpx rim (DEL05-3B2); 5) Dellwood garnet granulite, inclusion in Grt; 6) Dellwood HP-amphibolite, symplectic Cpx (DEL03-3B). *I = Ca-Ti Tschermak component ($CaTiAl_2O_6$); IMA: International Mineralogical Association.

Appendix A (continued). Representative clinopyroxene compositions from the Appalachian Blue Ridge and WGR, Norway.

	7	8	9	10	11	12	13
SiO_2	50.2	50.29	54.57	52.22	52.4	53.2	50.17
TiO_2	0.33	0.36	0.04	0.16	0.1	0.13	0.28
Al_2O_3	5.68	4.26	11.49	10.08	7.22	8.93	2.86
FeO	10.79	11.11	7.48	8.25	9.92	9.04	11.27
MnO	0.09	0.1	0	0.09	0.06	0.01	0.31
MgO	10.38	11.07	6.85	8.33	9.55	7.41	11.72
CaO	20.1	22.61	11.74	14.38	16.64	15.28	22.15
Na_2O	2.01	1.05	6.95	5.66	3.98	5.92	0.49
Sum	99.57	100.84	99.12	99.18	99.94	99.92	99.25
Si	1.874	1.867	1.972	1.899	1.921	1.929	1.9
^{IV}Al	0.126	0.133	0.028	0.101	0.079	0.071	0.1
^{VI}Al	0.124	0.054	0.462	0.331	0.233	0.311	0.028
Ti	0.129	0.134	0.051	0.16	0.124	0.169	0.091
Fe^{3+}	0.009	0.01	0.001	0.004	0.003	0.004	0.008
Fe^{2+}	0.578	0.613	0.369	0.452	0.522	0.401	0.662
Mg	0.208	0.211	0.176	0.091	0.18	0.106	0.266
Mn	0.003	0.003	0	0.003	0.002	0	0.01
Ca	0.804	0.9	0.455	0.56	0.654	0.594	0.899
Na	0.145	0.076	0.487	0.399	0.283	0.416	0.036
Sum	4	4	4	4	4	4	4
Jd	0.02	0	0.44	0.24	0.16	0.25	0
Ac	0.13	0.08	0.05	0.16	0.12	0.17	0.04
I*	0.01	0.01	0	0	0	0	0.01
Ess	0	0.06	0	0	0	0	0.06
CaTs	0.11	0.05	0.03	0.09	0.07	0.06	0.03
Jo	0	0	0	0	0	0	0.01
CaEs	0	0	0	0	0	0	0
Wo	0.34	0.39	0.21	0.23	0.29	0.26	0.4
En	0.29	0.31	0.18	0.23	0.26	0.2	0.33
Fs	0.1	0.11	0.09	0.05	0.09	0.05	0.13
Sum	1	1	1	1	1	1	1
class (IMA)	di	Di	omp	omp	omp	omp	di

7) Dellwood HP-amphibolite, matrix cpx core (DEL03-3B); 8) Boone eclogite, symplectic Cpx; 9) Flatraket eclogite, matrix Cpx core; 10) Flatraket eclogite, symplectic Cpx; 11) Flatraket eclogite, symplectic Cpx; 12) Gurskøy eclogite, matrix Cpx; 13) Gurskøy garnet granulite, symplectic Cpx.

Appendix A (continued). Representative garnet analyses from the Appalachian Blue Ridge and WGR, Norway.

	1	2	3	4	5	6
SiO_2	38.74	39.41	38.26	37.61	37.22	37.99
TiO_2	n.d.*	n.d.	n.d.	n.d.	0	0.12
Al_2O_3	21.75	22.13	21.84	21.59	21.24	21.01
FeO	20.67	21.17	22.72	24.84	25.34	25.67
MnO	0.39	0.43	0.43	0.45	0.45	0.86
MgO	7.92	8.5	7.11	3.08	3.79	4.19
CaO	9.2	8.31	8.46	11.46	10.86	10.11
Sum	98.67	99.95	98.83	99.03	98.89	99.97
Si	2.995	3.001	2.978	2.981	2.961	2.988
Ti	n.d.	n.d.	n.d.	n.d.	n.d.	< 0.01
Al	1.982	1.986	2.004	2.016	1.992	1.947
Fe	1.337	1.348	1.479	1.647	1.686	1.688
Mn	0.026	0.028	0.028	0.03	0.03	0.057
Mg	0.912	0.965	0.825	0.364	0.449	0.491
Ca	0.762	0.678	0.706	0.973	0.926	0.852
Alm	44	45	48	55	54	55
Grs	25	23	24	32	31	28
Prp	30	32	27	12	14	16
Sps	1	1	1	1	1	2

Cations calculated on the basis of 12 oxygen, all Fe assumed to be Fe^{2+}. 1) Lick Ridge core; 2) Lick Ridge, peak Mg/Fe; 3) Lick Ridge, rim; 4) Dellwood core (sample DEL03-3B2); 5) Dellwood peak Mg/Fe (sample DEL05-3B2); 6) Dellwood core (DEL03-3B)*n.d. not determined

Appendix A (continued). Representative garnet analyses from the Appalachian Blue Ridge and WGR, Norway.

	7	8	9	10	11	12	13
SiO_2	38.36	36.92	37.33	38.14	38.09	38.47	39.35
TiO_2	0.19	0.06	n.d.	n.d.	n.d.	n.d.	n.d.
Al_2O_3	20.88	21.02	20.76	20.96	21.44	21.1	21.81
FeO	25.83	27.39	27.01	25.12	27.58	26.54	21.37
MnO	0.83	1.11	1.27	0.47	0.56	0.48	1.1
MgO	4.17	3.18	3.47	5.21	5.93	5.24	8.37
CaO	10.15	9.8	9.38	8.79	5.72	8.16	8.2
Sum	100.41	99.48	99.22	98.7	99.33	99.98	100.2
Si	3.002	2.95	2.982	3.012	2.995	3.009	3.001
Ti	0.011	< 0.01	n.d.	n.d.	n.d.	n.d.	n.d.
Al	1.926	1.98	1.954	1.951	1.987	1.945	1.961
Fe	1.691	1.83	1.804	1.659	1.814	1.736	1.363
Mn	0.055	0.075	0.086	0.032	0.037	0.032	0.071
Mg	0.487	0.379	0.413	0.614	0.695	0.611	0.951
Ca	0.851	0.839	0.802	0.744	0.482	0.684	0.67
Alm	54	59	58	54	60	56	44
Grs	28	27	26	24	16	23	22
Prp	16	12	13	20	23	20	31
Sps	2	2	3	1	1	1	2

7) Peak Mg/Fe (DEL03-3B); 8) Dellwood rim (DEL03-3B); 9) Boone core; 10) Flatraket core; 11) Flatraket rim; 12) Gurskøy core; 13) Gurskøy rim.

Appendix A (continued). Representative plagioclase analyses from the Appalachian Blue Ridge and WGR, Norway.

	1	2	3	4	5	6	7	8	9	10	11
SiO_2	61.26	61.21	63.75	61.94	63.50	62.20	56.46	59.11	58.47	65.23	58.18
Al_2O_3	24.80	23.72	22.31	23.55	22.40	23.38	27.88	25.65	26.43	20.80	26.31
FeO	0.18	0.25	0.25	0.25	0.20	0.23	0.66	0.41	0.40	0.38	0.28
CaO	5.66	5.47	3.68	4.82	3.76	4.41	9.12	7.67	8.25	2.23	7.81
Na_2O	8.52	8.41	10.10	8.91	9.28	8.95	6.64	7.44	7.23	10.22	7.10
K_2O	0.06	0.08	0.00	0.04	0.03	0.01	0.02	n.d.*	n.d.	0.00	0.28
sum	100.47	99.14	100.09	99.51	99.17	99.18	100.77	100.28	100.77	98.87	99.95
Si	2.707	2.738	2.816	2.756	2.825	2.775	2.524	2.637	2.601	2.896	2.607
Al	1.292	1.251	1.162	1.235	1.175	1.229	1.469	1.349	1.386	1.089	1.390
Fe	0.007	0.009	0.009	0.009	0.007	0.009	0.025	0.015	0.015	0.014	0.010
Ca	0.268	0.262	0.174	0.230	0.179	0.211	0.437	0.366	0.393	0.106	0.375
Na	0.730	0.729	0.865	0.769	0.800	0.774	0.575	0.643	0.623	0.880	0.617
K	0.003	0.004	0.000	0.002	0.002	0.000	0.001	n.d.	n.d.	0.000	0.016
Z	4.006	3.998	3.987	4.001	4.007	4.013	4.017	4.001	4.002	3.999	4.007
X	1.001	0.996	1.039	1.001	0.981	0.985	1.013	1.009	1.016	0.986	1.007
Ab	73	73	83	77	82	79	57	64	61	89	61
An	27	26	17	23	18	21	43	36	39	11	37
Or	0	0	0	0	0	0	0	n.d.	n.d.	0	2

Formulae calculated on the basis of 8 oxygen. 1) Lick Ridge, rim on Grt; 2) Lick Ridge, symplectite; 3) Dellwood, matrix core (DEL03-3B); 4) Dellwood matrix rim (DEL03-3B); 5) Dellwood, symplectite core (DEL03-3B); 6) Dellwood, symplectite rim (DEL03-3B); 7) Dellwood inclusion in Grt (DEL05-3B2) 8) Boone symplectite; 9) Boone symplectite; 10) Flatraket symplectite; 11) Gurskøy, rim on Grt. *n.d. = not determined

Appendix A (continued). Representative amphibole analyses from the Appalachian Blue Ridge and WGR, Norway.

	1	2	3	4	5	6	7	8
SiO_2	46.52	45.29	41.41	43.77	34.81	41.94	42.72	41.63
TiO_2	0.64	0.68	1.82	1.54	1.07	1.47	0.43	0.77
Al_2O_3	10.45	11.88	12.59	11.96	21.13	12.24	12.55	13.61
Cr_2O_3	n.d.*	n.d.	n.d.	n.d.	n.d.	n.d.	n.d.	n.d.
Fe_2O_3	5.16	6.96	3.42	3.04	5.76	4.67	12.14	8.27
FeO	6.66	6.16	16.08	14.11	14.73	14.39	5.07	10.64
MnO	0.04	0.09	0.05	0.10	0.07	0.05	0.10	0.12
MgO	14.33	13.97	8.41	10.25	5.68	9.53	12.43	10.13
CaO	11.69	11.79	11.52	11.57	12.11	11.97	10.08	11.63
Na_2O	1.72	1.93	2.51	2.45	2.73	2.36	3.40	1.59
K_2O	0.10	0.22	0.10	0.25	0.10	0.00	0.00	1.24
F	n.d.	n.d.	n.d.	n.d.	0.00	n.d.	n.d.	n.d.
Cl	n.d.	n.d.	n.d.	n.d.	1.88	n.d.	n.d.	n.d.
H2O	n.d.	n.d.	n.d.	n.d.	n.d.	n.d.	n.d.	n.d.
Sum	97.31	98.98	97.91	99.04	100.06	98.60	98.92	99.63
Si	6.707	6.463	6.244	6.432	5.281	6.248	6.182	6.110
^{IV}Al	1.293	1.537	1.756	1.568	2.719	1.752	1.818	1.890
^{VI}Al	0.482	0.461	0.481	0.503	1.059	0.397	0.323	0.464
Ti	0.069	0.073	0.206	0.171	0.122	0.164	0.047	0.085
Cr	n.d.	n.d.	n.d.	n.d.	n.d.	n.d.	n.d.	n.d.
Fe^{3+}	0.560	0.748	0.388	0.335	0.657	0.524	1.322	0.913
Fe^{2+}	0.803	0.736	2.028	1.734	1.869	1.792	0.614	1.306
Mn	0.005	0.010	0.007	0.013	0.009	0.006	0.012	0.015
Mg	3.080	2.972	1.890	2.244	1.284	2.117	2.683	2.217
Ca	1.806	1.803	1.861	1.822	1.968	1.910	1.563	1.829
Na^M	0.194	0.197	0.139	0.178	0.032	0.090	0.437	0.171
Na^A	0.287	0.339	0.595	0.519	0.771	0.592	0.517	0.281
K	0.018	0.040	0.019	0.047	0.019	0.000	0.000	0.232

Formulae normalized to 13 cations, excluding Na, Ca, K. Fe^{2+}/Fe^{3+} estimated by stoichiometry (Droop, 1987). 1) Lick Ridge, at garnet rim; 2) Lick Ridge, hornblende with quartz caps in clinopyroxene; 3) Dellwood garnet granulite symplectite, (DEL05-3B2); 4) Dellwood HP amphibolite matrix (DEL03-3C); 5) Dellwood garnet granulite, inclusion in garnet (DEL05-3B2); 6) Boone eclogite, at garnet rim; 7) Flatraket symplectite; 8) Gurskøy, at garnet rim. *n.d. = not determined.

Appendix B. Broadbeam analyses of clinopyroxene and adjacent Cpx-Pl symplectite.

location	Lick Ridge	Lick Ridge	Dellwood	Dellwood	Dellwood	Dellwood
lithology	eclogite	eclogite	granulite[1]	granulite	HP-amph[2]	HP-amph
	Cpx	Symp.	Cpx	Symp.	Cpx	Symp.
SiO_2	54.09	53.72	49.08	49.48	50	52.47
TiO_2	0.26	0.24	0.28	0.26	0.27	0.22
Al_2O_3	8.85	10.17	6.24	7.23	6.48	8.08
FeO	5.56	5.54	10.61	9.43	10.81	8.4
MnO	0.02	0.03	0.06	0.04	0.07	0.07
MgO	10.5	9.37	10.8	10.17	10.55	9.38
CaO	17.64	16.27	19.69	18.78	19.91	17.61
Na_2O	4	3.45	2.68	2.98	2.5	2.87
K_2O	n.d.	n.d.	n.d.	n.d.	n.d.	n.d.
Total	100.93	98.8	99.45	98.37	100.59	99.1
Si	1.937	1.978	1.818	1.847	1.837	1.949
^{IV}Al	0.063	0.022	0.182	0.153	0.163	0.051
^{VI}Al	0.31	0.419	0.091	0.165	0.118	0.303
Ti	0.007	0.007	0.008	0.007	0.007	0.006
Fe^{3+}	0.017	0	0.268	0.189	0.208	0
Fe^{2+}	0.15	0.171	0.061	0.105	0.124	0.261
Mn	0.001	0.001	0.002	0.001	0.002	0.002
Mg	0.561	0.515	0.597	0.566	0.578	0.519
Ca	0.677	0.642	0.782	0.751	0.784	0.701
Na	0.278	0.246	0.192	0.216	0.178	0.207
Sum	4	4	4	4	4	4
Jd	0.26	0.23	0	0.01	0	0.2
Ac	0.02	0	0.27	0.2	0.22	0
CaTs	0.07	0.02	0.18	0.17	0.17	0.05
CaEs[3]	0	0.15	0.01	0.01	0.01	0.06
CaEs[4]	0	0.11	0	0	0	0.04
Il[5]	0.01	0.01	0.02	0.02	0.02	0.01
Aug	0.57	0.51	0.41	0.48	0.47	0.58
Opx	0.08	0.08	0.12	0.12	0.12	0.1
n	9	97	7	41	6	55

Table caption follows.

Appendix B (continued). Broadbeam analyses of pyroxene and adjacent Cpx-Pl symplectite.

Location	Flatraket	Flatraket	Gurskøy	Gurskøy	Gurskøy	Gurskøy
Lithology	eclogite	eclogite	eclogite	eclogite	eclogite	eclogite
	Cpx	Symp.	Cpx	Symp.	Cpx	Symp.
SiO_2	55.04	55.34	53.25	55.34	54.05	57.93
TiO_2	0.08	0.14	0.14	0.11	0.16	0.14
Al_2O_3	11.53	12.71	8.37	13.02	7.71	9.44
FeO	6.85	6.55	9.08	5.32	8.93	5.84
MnO	0.02	0.04	0.02	0.04	0.03	0.05
MgO	7.43	7.14	9.17	7.33	8.42	8.26
CaO	11.64	11.69	15.57	13.42	15.15	15.18
Na_2O	7.08	5.95	5.08	4.48	5.8	4.69
K_2O	n.d.	n.d.	n.d.	n.d.	n.d.	n.d.
Total	99.66	99.55	100.67	99.06	100.25	101.52
Si	1.971	2.001	1.919	2.026	1.952	2.074
^{IV}Al	0.029	0	0.081	0	0.048	0
^{VI}Al	0.458	0.542	0.274	0.562	0.28	0.398
Ti	0.002	0.004	0.004	0.003	0.004	0.004
Fe^{3+}	0.058	0	0.155	0	0.166	0
Fe^{2+}	0.147	0.198	0.119	0.163	0.103	0.175
Mn	0	0.001	0.001	0.001	0.001	0.001
Mg	0.397	0.385	0.492	0.4	0.453	0.441
Ca	0.447	0.453	0.601	0.527	0.586	0.582
Na	0.491	0.417	0.355	0.318	0.406	0.325
Sum	4	4	4	4	4	4
Jd	0.43	0.4	0.2	0.3	0.24	0.33
Ac	0.06	0	0.16	0	0.17	0
CaTs	0.03	0	0.08	0	0.05	0
CaEs[3]	0	0.12	0	0.23	0	0.07
CaEs[4]	0	0.09	0	0.2	0	0.15
Il[5]	0	0.01	0.01	0.01	0.01	0.01
Aug	0.39	0.38	0.45	0.39	0.5	0.56
Opx	0.08	0.09	0.09	0.07	0.03	0.03
N	5	34	9	28	4	16

Table caption follows.

Appendix B (Table caption). Broadbeam microprobe analyses of pyroxene and adjacent symplectite. Pyroxene formulae calculated on the basis of 6 oxygen, with Fe^{3+} estimated by stoichiometry (Droop 1987). Notes: [1]) Dellwood garnet granulite (DEL05-3B2); [2]) HP-amphibolite, sample DEL03-3B; [3]) CaEs component calculated using the method of Katayama et al. (2000); [4]) CaEs calculated using the method of Page et al. (2005); [5]) endmember II = $Na(Mg,Fe)_{0.5}Ti_{0.5}Si_2O_6$. Endmembers calculated after Katayama et al. (2000). n = number of analyses averaged.

Appendix C. Broadbeam reintegrations of hornblende-quartz inclusions and surrounding clinopyroxene.

	Lick Ridge eclogite	Dellwood granulite[1]	Dellwood HP-amph[2]	Gurskøy eclogite
SiO_2	53.67	51.64	50.55	53.53
TiO_2	0.29	0.3	0.79	0.2
Al_2O_3	6.95	7.23	6.61	8.09
FeO	7.84	12.39	12.77	9.4
MnO	0.03	0.03	0.08	0.03
MgO	11.95	10.12	10.05	8.38
CaO	17.67	15.75	16.98	15
Na_2O	1.85	1.97	1.71	4.06
K_2O	n.d.	n.d.	n.d.	n.d.
Total	100.26	99.42	99.54	98.69
Si	1.97	1.939	1.904	1.991
^{IV}Al	0.03	0.061	0.096	0.009
^{VI}Al	0.27	0.258	0.198	0.346
Ti	0.008	0.008	0.023	0.005
Fe^{3+}	0	0	0	0
Fe^{2+}	0.241	0.389	0.402	0.292
Mn	0.001	0.001	0.002	0.001
Mg	0.654	0.567	0.564	0.465
Ca	0.695	0.633	0.686	0.598
Na	0.131	0.143	0.125	0.293
Sum	4	4	4	4
Jd	0.11	0.13	0.08	0.28
Ac	0	0	0	0
CaTs	0.03	0.06	0.1	0.01
CaEs[3]	0.12	0.07	0.02	0.05
CaEs[4]	0.08	0.05	0.02	0.04
Il[5]	0.02	0.02	0.05	0.01
Aug	0.57	0.48	0.51	0.55
Opx	0.15	0.24	0.24	0.1
n	20	8	20	12

Table caption follows.

Appendix C. (Table caption):

Pyroxene formulae calculated on the basis of 6 oxygen, with Fe^{3+} estimated by stoichiometry (Droop 1987). Notes: [1]) Dellwood garnet granulite (DEL05-3B2); [2]) HP-amphibolite, sample DEL03-3B; [3]) CaEs component calculated using the method of Katayama et al. (2000); [4]) CaEs calculated using the method of Page et al. (2005); [5]) endmember II = $Na(Mg,Fe)_{0.5}Ti_{0.5}Si_2O_6$. Endmembers (with the exception of [4]) calculated after Katayama et al. (2000). n = number of analyses averaged.

Appendix D. Equilibria used for P-T estimates.

Metamorphic assemblage: omphacite + garnet		
Equilibria	Program	References:
[2] Jd + Qtz = Ab	TWQ 2.02	Holland (1980, 1983)
[3] Di + Alm = 3 Hd + Prp	TWQ 2.02	Berman (1988)
		Berman and Aranovich (1996)
		Berman et al. (1995)
Assemblage: hornblende + clinopyroxene + plagioclase (symplectites)		
[4] Ed + Ab = Ri + An	Hb-Plag	Holland and Blundy, 1994
[5] 8 Jd + Tr + Ts = 2 Prg + 6 Ab	TWQ 1.02	Berman (1988)
		Berman (1990)
		Fuhrman and Lindsley (1988)
		Mader et al. (1994)
		Holland (1980, 1983)
Assemblage: garnet (rim) + plagioclase + hornblende + quartz		
[6] 3 Tr + 22 Prp + 8 Grs + 24 An = 27 Ts	TWQ 1.02	Berman (1988)
[7] An + Grs + 2 Prp + Qtz + 2 H_2O = 3 Tr + 21 Ts	TWQ 1.02	Berman (1990)
[8] 25 Qtz + 26 Prp + 16 Grs + 24 H_2O = 3 Tr + 21 Ts	TWQ 1.02	Fuhrman and Lindsley (1988)
[9] 27 Qtz + 10 Prp + 11 Grs + 6 H_2O = 21 An + 3 Tr	TWQ 1.02	Mader et al. (1994)
[10] 3 Ts + 12 Qtz + 2 Prp + 4 Grs = 12 An + 3 Tr	TWQ 1.02	
[11] 5 Ts + 11 Qtz + 3 Grs = 13 An + 3 Tr + 2 H_2O	TWQ 1.02	
[12] 11 Ts + 8 Qtz = 16 An + 6 Prp + 3 Tr + 8 H_2O	TWQ 1.02	

Table caption follows.

Appendix D (continued). Equilibria Used for P-T Estimates.

Assemblage: garnet + plagioclase + clinopyroxene + quartz		
[13] 2 Grs + Prp + 3 Qtz = 3 Di + 3 An	TWQ 2.02	Berman (1988)
[14] Alm + 2 Grs + 3 Qtz = 3 Hd + 3 An	TWQ 2.02	Berman and Aranovich (1996)
[15] Alm + 3 Di = Prp + 3 Hd	TWQ 2.02	Berman et al. (1995)
Assemblage: garnet (rim) + plagioclase + hornblende (no quartz)		
[16] 3 Tr + 22 Prp + 8 Grs + 24 An + 24 H_2O = 27 Ts	TWQ 1.02	Berman (1988)
[17] 3 Tr + 5 FeTs = 5 Ts + 3 FeTr	TWQ 1.02	Berman (1990)
[18] 4 FeTs + 3 Prg = 3 FePa + 4 Tsc	TWQ 1.02	Fuhrman and Lindsley (1988)
[19] 3 FeTr + 22 Py + 8 Grs + 24 An + 24 H_2O = 22 Ts + 5 FeTs	TWQ 1.02	Mader et al. (1994)
[20] 81 FeTr + 110 Prp + 40 Grs + 120 An + 120 H_2O = 66 Tr + 135 FeTs	TWQ 1.02	
[21] 81 FePa + 12 Tr + 88 Prp + 32 Grs + 96 An + 96 H_2O = 108 FeTs + 81 Prg	TWQ 1.02	
[22] 5 FePa + 4 Tr = 4 FeTr + 5 Prg	TWQ 1.02	
[23] 33 FePa + 6 FeTr + 44 Prp + 16 Grs + 48 An + 48 H_2O = 54 FeTs + 33 Prg	TWQ 1.02	
[24] 96 An + 32 Grs + 88 Prp + 12 FeTr + 15 Prg + 96 H_2O = 15 FePa + 108 Ts	TWQ 1.02	

Table caption follows.

Appendix D, (Table caption).
Metamorphic assemblages, equilibria, and applications used for P-T estimates. Abbreviations: Jd jadeite, Qtz quartz, Ab albite, Di diopside, Hd hedenbergite, Alm almandine, Prp pyrope, Grs grossular, Ed edenite, Ri richterite, An anorthite, Tr tremolite, FeTr ferro-tremolite, Ts tschermakite, FeTs ferro-tschermakite, Prg pargasite, FePa ferro-pargasite, TWQ (Thermobarometry With Estimation of Equilibration State).

Appendix E. Summary of Blue Ridge tectonometamorphic events, Great Smoky Mountains region.

	Neoproterozoic.	Cambrian-Early Ord.	Middle Ordovician (Taconian)	Siluro-Devonian (Acadian)	Permo-Carboniferous (Neo-Acadian to Alleghanian) Miss.	Penn-Perm.
WBR[1]	Rifting of Grenville basement; mafic dikes	Passive margin	Collision with Piedmont; formation of subduction complex	Initial strike-slip motion?	Collision with Carolina terrane; thin-skinned deformation	Collision with Africa; foreland fold-thrust belt
	Ocoee Supergroup	Chilhowee-Shady-Rome-Knox passive margin seq,	Sevier foreland sequence	Foreland sedimentation	Pennington-Lee clastic wedge	
			Greenschist-upper amphibolite facies meta., migmatites in Ocoee + isoclinal folding	Retrograde meta.?	Retrograde greenschist facies metamorphism, tight-open refolding, crenulation cleavage	
CBR[2]	Coweeta Gp., Otto Fm. and related clastics		Isoclinal folding of migmatitic layering		Folding, crenulation cleavage	
		Mafic-ultramafic complexes	Upper amphibolite, HP granulite facies meta.; migmatites	Retrograde amhibolite facies metamorphism of eclogites		
EBR[3]	Rifting of Grenville basement to form internal massifs		Eclogite facies meta. Granitic plutonism	Granitic plutonism; Pegmatites	Granitic plutonism	
	Ashe-Tallulah Falls Fm. deposition	Mafic-ultramafic complexes			Upper amphibolite facies, Sil-grade migmatites	

(Table legend follows)

Appendix E (Table legend). Sources: Hatcher (2002); Hatcher et al. (2005); Massey and Moecher (2005); Moecher et al. (2004); Kunk et al. (2006); Miller et al. (2006); Southworth et al. (2005); Anderson and Moecher, (2007); Clemons and Moecher (2009). 1: western Blue Ridge; 2: central Blue Ridge: Cartoogechaye and Cowrock terranes; 3: eastern Blue Ridge.

Appendix F. Summary of thermobarometric methods (Chapter 3).

Metamorphic assemblage: omphacite + garnet		
Equilibria	Program	References:
[1] Jd + Qtz = Ab	TWQ 2.02	Holland (1980, 1983)
[2] 3 Di + Alm = 3 Hd + Prp	TWQ 2.02	Berman (1988)
		Berman and Aranovich (1996)
		Berman et al. (1995)
Assemblage: hornblende + clinopyroxene + plagioclase (symplectites)		
[3] Ed + Ab = Ri + An	Hb-Plag	Holland and Blundy, 1994
[4] 8 Jd + Tr + Ts = 2 Prg + 6 Ab	TWQ 1.02	Berman (1988)
		Berman (1990)
		Fuhrman and Lindsley (1988)
		Mader et al. (1994)
		Holland (1980, 1983)
Assemblage: garnet (rim) + plagioclase + hornblende + quartz + H_2O		
[6] 3 Tr + 22 Prp + 8 Grs + 24 An = 27 Ts	TWQ 1.02	Berman (1988)
[7] An + Grs + 2 Prp + Qtz + 2 H_2O = 3 Tr + 21 Ts	TWQ 1.02	Berman (1990)
[8] 25 Qtz + 26 Prp + 16 Grs + 24 H_2O = 3 Tr + 21 Ts	TWQ 1.02	Fuhrman and Lindsley (1988)
[9] 27 Qtz + 10 Prp + 11 Grs + 6 H_2O = 21 An + 3 Tr	TWQ 1.02	Mader et al. (1994)
[10] 3 Ts + 12 Qtz + 2 Prp + 4 Grs = 12 An + 3 Tr	TWQ 1.02	
[11] 5 Ts + 11 Qtz + 3 Grs = 13 An + 3 Tr + 2 H_2O	TWQ 1.02	
[12] 11 Ts + 8 Qtz = 16 An + 6 Prp + 3 Tr + 8 H_2O	TWQ 1.02	

Table caption follows

Appendix F (Continued). Summary of thermobarometric methods (Chapter 3).

Metamorphic assemblage: omphacite + garnet		
Equilibria	Program	References:
[1] Jd + Qtz = Ab	TWQ 2.02	Holland (1980, 1983)
[2] 3 Di + Alm = 3 Hd + Prp	TWQ 2.02	Berman (1988)
		Berman and Aranovich (1996)
		Berman et al. (1995)
Assemblage: hornblende + clinopyroxene + plagioclase (symplectites)		
[3] Ed + Ab = Ri + An	Hb-Plag	Holland and Blundy, 1994
[4] 8 Jd + Tr + Ts = 2 Prg + 6 Ab	TWQ 1.02	Berman (1988)
		Berman (1990)
		Fuhrman and Lindsley (1988)
		Mader et al. (1994)
		Holland (1980, 1983)
Assemblage: garnet (rim) + plagioclase + hornblende + quartz + H_2O		
[6] 3 Tr + 22 Prp + 8 Grs + 24 An = 27 Ts	TWQ 1.02	Berman (1988)
[7] An + Grs + 2 Prp + Qtz + 2 H_2O = 3 Tr + 21 Ts	TWQ 1.02	Berman (1990)
[8] 25 Qtz + 26 Prp + 16 Grs + 24 H_2O = 3 Tr + 21 Ts	TWQ 1.02	Fuhrman and Lindsley (1988)
[9] 27 Qtz + 10 Prp + 11 Grs + 6 H_2O = 21 An + 3 Tr	TWQ 1.02	Mader et al. (1994)
[10] 3 Ts + 12 Qtz + 2 Prp + 4 Grs = 12 An + 3 Tr	TWQ 1.02	
[11] 5 Ts + 11 Qtz + 3 Grs = 13 An + 3 Tr + 2 H_2O	TWQ 1.02	
[12] 11 Ts + 8 Qtz = 16 An + 6 Prp + 3 Tr + 8 H_2O	TWQ 1.02	

Table caption follows

Appendix F (Continued). Summary of thermobarometric methods (Chapter 3).

Assemblage: garnet + muscovite + biotite + plagioclase + quartz + H_2O		
[25] Ann + 2 Pg + 3 Qtz = Ms + Alm + 2 Ab + 2 H_2O	TWQ 2.02	Berman (1988)
[26] Ms + Gr + Alm = Ann + 3 An	TWQ 2.02	Berman and Aranovich (1996)
[27] Gr + 2 Pg + 3 Qtz = 3 An + 2 Ab + 2 H_2O	TWQ 2.02	Berman et al. (1995)
Assemblage: Hbl + Qtz + Grt + H_2O		
[28] 21 Ts + 3 Tr = 16 Grs + 26 Prp + 24 Qtz + 24 H_2O	TWQ 1.02	Berman (1988)
[29] 3 Tr + 5 Alm = 5 Prp + 3 FeTr	TWQ 1.02	Berman (1990)
[30] Ts + Alm = Prp + FeTs	TWQ 1.02	Fuhrman and Lindsley (1988)
[31] 24 Qtz + 21 Prp + 16 Grs + 5 Alm + 24 H_2O = 3 FeTr + 21 Ts	TWQ 1.02	Mader et al. (1994)
[32] 63 Tr + 120 Qz + 80 Grs + 130 Alm + 120 H_2O = 78 FeTr + 105 Ts	TWQ 1.02	
[33] 24 Qz + 5 Prp + 16 Grs + 21 Alm + 24 H_2O = 3 Tr + 21 FeTs	TWQ 1.02	
[34] 5 Ts + 24 Qz + 16 Grs + 26 Alm + 24 H_2O = 3 Tr + 26 FeTs	TWQ 1.02	
[35] 26 Alm + 16 Grs + 24 Qz + 24 H_2O = 21 FeTs + 3 FeTr	TWQ 1.02	
[36] 3 FeTr + 26 Ts = 5 FeTs + 24 Qz + 26 Prp + 16 Grs + 24 H_2O	TWQ 1.02	
[37] 78 Tr + 105 FeTs = 63 FeTr + 120 Qz + 130 Prp + 80 Grs + 120 H_2O	TWQ 1.02	

Appendix F. Metamorphic assemblages, equilibria, and applications used to estimate P-T conditions in the present study. Most abbreviations after Kretz (1983). Other abbreviations: Ri = richterite, FeTs = ferrotschermakite, FeTr = ferrotremolite, FePa = ferropargasite, TWQ = Thermobarometry With Estimation of Equilibration State (Berman, 1988).

Appendix G. Representative analyses, Chapter 3

	Garnet							Amphibole				
Location	Boone	Boone	Boone	Dellwood	Dellwood	Dellwood	Dellwood	Boone	Boone			
Sample	Z05-1B	Z05-1B	Z05-1B	DEL05-3B2	DEL05-3B2	DEL05-3B2	MV02-7	Z05-1B	Z05-1B	DEL05-3B2	DEL05-3B2	DEL05-3B2
lithology	R	R	R	G	G	G	S	R	R	G	G	G
Texture	core	rim	max Mg/Fe	core	rim	max Mg/Fe	core	grt rim	incl in grt	incl	incl	grt rim
SiO_2	38.04	37.69	37.90	37.93	37.24	38.36	37.29	37.72	41.70	39.35	42.18	40.87
TiO_2	n.d.	n.d.	n.d.	n.d.	n.d.	n.d.	n.d.	0.72	1.60	1.53	1.59	1.40
Al_2O_3	21.54	21.55	22.14	21.77	21.67	22.00	21.13	17.69	12.07	16.93	14.25	14.17
Fe_2O_3	0.00	0.00	0.00	0.00	0.00	0.00	0.00	7.71	2.84	2.66	1.59	4.09
FeO	25.29	25.14	24.96	25.50	26.34	25.13	33.81	11.74	14.55	15.38	14.41	14.78
MnO	1.90	1.19	1.27	0.72	0.63	0.27	2.90	0.50	0.08	0.06	0.04	0.03
MgO	2.80	3.04	3.98	2.53	2.73	4.22	2.60	7.54	9.58	7.58	9.74	8.68
CaO	10.61	10.78	10.08	11.15	9.93	9.74	2.91	12.01	12.01	11.70	11.88	11.78
Na_2O	n.d.	n.d.	n.d.	n.d.	n.d.	n.d.	n.d.	1.80	1.92	2.61	2.59	2.52
K_2O	n.d.	n.d.	n.d.	n.d.	n.d.	n.d.	n.d.	0.41	0.28	0.18	0.09	0.10
Cl-	n.d.	n.d.	n.d.	n.d.	n.d.	n.d.	n.d.	n.d.	n.d.	1.15	0.07	n.d.
Totals	100.17	99.38	100.32	99.59	98.54	99.73	100.64	97.01	97.01	97.98	98.36	98.42
Si	2.994	2.984	2.961	2.995	2.978	2.997	2.990	5.676	6.318	5.903	6.233	6.105
Ti	n.d.	n.d.	n.d.	n.d.	n.d.	n.d.	n.d.	0.081	0.183	0.172	0.177	0.157
Al	1.998	2.011	2.038	2.026	2.042	2.026	1.997	3.137	2.156	2.993	2.482	2.495
Fe^{3+}	n.d.	n.d.	n.d.	n.d.	n.d.	n.d.	n.d.	0.874	0.324	0.300	0.177	0.460
Fe^{2+}	1.665	1.664	1.631	1.684	1.762	1.642	2.267	1.477	1.843	1.929	1.781	1.846
Mn	0.127	0.080	0.084	0.048	0.043	0.018	0.197	0.064	0.011	0.007	0.004	0.004
Mg	0.328	0.359	0.463	0.297	0.325	0.492	0.311	1.691	2.165	1.695	2.146	1.933
Ca	0.895	0.914	0.844	0.943	0.851	0.816	0.250	1.936	1.950	1.880	1.881	1.886
Na	n.d.	n.d.	n.d.	n.d.	n.d.	n.d.	n.d.	0.525	0.564	0.760	0.741	0.730
K	n.d.	n.d.	n.d.	n.d.	n.d.	n.d.	n.d.	0.078	0.054	0.034	0.017	0.02

Appendix G (Table legend): Representative garnet and amphibole analyses. Garnet formulae calculated on the basis of 12 O. Amphibole formulae calulated on the basis of 13 cations. $Fe^{2+}/Fe^{3+}$of amphibole estimated after Droop (1987). Lithologies: R-retrograde eclogite; G-garnet granulite; S-schist. n.d.= not determined.

Appendix G. Representative analyses, Chapter 3 (continued).

	Clinopyroxene					Plagioclase						Muscovite	Biotite
Location	Boone	Dellwood	Dellwood	Dellwood	Dellwood	Boone	Dellwood	Dellwood	Dellwood	Dellwood	Dellwood	Dellwood	Dellwood
Sample	Z05-1B	DEL05-3B2	DEL05-3B2	DEL05-3B2	DEL05-3B2	Z05-1B	DEL05-3B2	DEL05-3B2	DEL05-3B2	DEL05-3B2	MV02-7	MV02-7	MV02-7
lithology	R	G	G	G	G	R	G	G	G	G	S	S	S
Texture	incl in grt	matrix	matrix	incl in grt	incl in grt	grt rim	incl grt	incl grt	grt rim	grt rim	incl grt	incl grt	incl grt
SiO_2	50.85	52.53	49.83	50.45	51.48	59.99	59.46	61.48	61.16	60.37	59.06	45.57	35.49
TiO_2	0.26	0.22	0.28	0.31	0.16	n.d.	n.d.	n.d.	n.d.	n.d.	n.d.	1.36	2.55
Al_2O_3	2.36	7.19	6.89	5.41	2.54	25.64	25.84	24.37	24.15	25.05	25.35	34.48	19.21
Fe_2O_3	5.76	1.75	2.44	5.18	4.44	n.d.	n.d.	n.d.	n.d.	n.d.	n.d.	n.d.	n.d.
FeO	6.70	8.26	8.09	5.05	6.10	0.31	0.88	0.71	0.44	0.41	0.21	1.88	20.99
MnO	0.14	0.05	0.11	0.03	0.05	n.d.	n.d.	n.d.	n.d.	n.d.	n.d.	0.00	0.06
MgO	11.52	8.63	8.97	11.02	11.78	n.d.	n.d.	n.d.	n.d.	n.d.	n.d.	1.26	9.06
CaO	22.92	18.68	19.54	22.05	23.50	7.29	7.00	5.39	5.46	6.13	6.05	0.00	0.02
Na_2O	0.93	3.32	2.29	1.64	0.96	7.27	7.64	8.53	8.17	7.98	7.76	0.48	0.16
K_2O	0.00	0.00	0.00	0.00	0.00	0.04	0.04	0.02	0.00	0.00	0.30	10.01	9.30
Totals	101.43	100.64	98.45	101.14	101.02	100.58	100.87	100.50	99.38	99.94	98.72	0.00	0.00
	Ions on the basis of 6 O					Ions on the basis of 8 O							
Si	1.894	1.932	1.887	1.861	1.912	2.659	2.638	2.722	2.731	2.688	2.665	6.097	5.348
Ti	0.007	0.006	0.008	0.009	0.005	n.d.	n.d.	n.d.	n.d.	n.d.	n.d.	0.137	0.289
Al	0.106	0.312	0.308	0.235	0.111	1.340	1.352	1.272	1.272	1.315	1.348	5.436	3.412
Fe^{3+}	0.162	0.049	0.070	0.144	0.124	n.d.	n.d.	n.d.	n.d.	n.d.	n.d.	n.d.	n.d.
Fe^{2+}	0.209	0.254	0.256	0.156	0.190	0.012	0.033	0.026	0.017	0.015	0.008	0.210	2.645
Mn	0.004	0.002	0.003	0.001	0.002	n.d.	n.d.	n.d.	n.d.	n.d.	n.d.	0.000	0.008
Mg	0.639	0.473	0.506	0.606	0.652	n.d.	n.d.	n.d.	n.d.	n.d.	n.d.	0.252	2.036
Ca	0.915	0.736	0.793	0.871	0.935	0.346	0.333	0.256	0.261	0.292	0.293	0.000	0.004
Na	0.067	0.237	0.168	0.118	0.069	0.625	0.657	0.732	0.707	0.689	0.679	0.125	0.046
K	0.000	0.000	0.000	0.000	0.000	0.002	0.002	0.001	0.000	0.000	0.017	1.708	1.788

Representative clinopyroxene, plagioclase, muscovite, and biotite analyses. Fe^{2+}/Fe^{3+} of pyroxene estimated after Droop (1987). Lithologies: R-retrograde eclogite; G-garnet granulite; S-schist. n.d. = not determined. Mica formulae calculated on the basis of 24 O.

Appendix H. U-Pb zircon data (SIMS) from Central Blue Ridge migmatite DEL03-1, DEL03-1L.

Puck#.Sample #.grain ID.	Ages (Ma)						Radiogenic	Corrected atomic ratios						Correlation of	
	$^{206}Pb/^{238}U$	$^{206}Pb/^{238}U$	$^{207}Pb/^{235}U$	$^{207}Pb/^{235}U$	$^{207}Pb/^{206}Pb$	$^{207}Pb/^{206}Pb$	^{206}Pb	$^{206}Pb^*/^{238}U$	$^{206}Pb^*/^{238}U$	$^{207}Pb^*/^{235}U$	$^{207}Pb^*/^{235}U$	$^{207}Pb^*/^{206}Pb^*$	$^{207}Pb^*/^{206}Pb^*$	Concordia	Common
leucocratic dike plotted:		1 s.e.		1 s.e.		1 s.e.	(%)		1 s.e.(%)		1 s.e. (%)		1 s.e. (%)	Ellipses	Pb corr.
m6 DEL03-1L gr C spot 2	435.8	20.33	437.4	34.39	445.8	171	97.78	0.06995	4.824	0.5385	9.675	0.05584	7.695	0.62	(204Pb)
m6 DEL03-1L gr e	448.6	21.27	419	37.69	258.8	209.3	98.16	0.07208	4.907	0.5108	10.98	0.0514	9.11	0.57	(204Pb)
m5 DEL03-1L gr c	471.5	23.15	466.9	49.02	444	261	97.64	0.07589	5.091	0.5838	13.1	0.05579	11.74	0.45	(204Pb)
DEL03-1L gr b spot 1	442	19.86	417.1	39.85	281.7	232.1	95.55	0.07097	4.648	0.508	11.65	0.05192	10.15	0.50	(204Pb)
DEL03-1L gr f spot 1	456.2	24.72	402.9	75.48	107.9	488.6	94.29	0.07333	5.612	0.4871	22.7	0.04818	20.68	0.47	(204Pb)
DEL03-1L gr g spot 1	485.7	26.77	478	31.18	441.2	126.2	98.2	0.07826	5.723	0.6012	8.177	0.05572	5.675	0.72	(204Pb)
DEL03-1L gr h spot 1	474.6	22.8	493.2	55.15	580.8	263.4	96.35	0.0764	4.983	0.6254	14.12	0.05937	12.13	0.55	(204Pb)
plotted points:															
DEL03-1 gr a spot 1	474.5	20.31	467	35.83	430.1	166.6	98.5	0.07639	4.44	0.584	9.572	0.05544	7.475	0.65	(204Pb)
DEL03-1 gr k spot 1	481.9	9.786	477.8	8.41	457.8	13.77	99.92	0.07763	2.107	0.6008	2.207	0.05614	0.6206	0.96	(204Pb)
DEL03-1 gr k spot 2	494.1	10.38	485.5	8.685	445.2	20.06	99.9	0.07967	2.183	0.6132	2.25	0.05582	0.9023	0.92	(204Pb)
DEL03-1 gr k spot 3	517.4	11.01	503.1	9.047	438.7	14.19	99.88	0.08358	2.215	0.6414	2.28	0.05566	0.6378	0.96	(204Pb)
DEL03-1 gr k spot 4	489.8	10.48	487.3	8.881	475.5	17.25	99.91	0.07894	2.222	0.6159	2.295	0.05659	0.7803	0.94	(204Pb)
DEL03-1 gr f spot 2	445.4	17.52	419.1	45.46	277.1	276.4	96.84	0.07153	4.07	0.511	13.24	0.05181	12.07	0.43	(204Pb)
DEL03-1 gr j spot 2	448.6	13.45	431.2	15.48	339.5	72.72	99.19	0.07206	3.104	0.5291	4.407	0.05325	3.211	0.69	(204Pb)
excluded points:															
m6 DEL03-1L gr A spot 2	394.3	16.69	397.9	47.79	418.9	285.9	97.82	0.06307	4.364	0.4797	14.52	0.05516	12.8	0.52	(204Pb)
m5 DEL03-1L gr c tip	845.4	42.92	871.8	32.91	939.3	37.46	99.64	0.1401	5.416	1.36	5.625	0.07037	1.827	0.95	(204Pb)
m5 DEL03-1L gr c spot 2	990.7	49.81	995.6	34.14	1006	20.11	99.82	0.1661	5.425	1.666	5.38	0.07273	0.9913	0.98	(204Pb)
m5 DEL03-1L gr b spot 2	306.2	18.13	332.6	72.13	521.5	504.8	93.44	0.04865	6.062	0.3876	25.43	0.05778	23.01	0.50	(204Pb)
m5 DEL03-1L gr b spot 3	975.9	43.47	987.7	30.4	1014	8.321	99.78	0.1634	4.8	1.645	4.813	0.073	0.4106	1.00	(204Pb)
m5 DEL03-1L gr a	410.4	18.79	363.5	34.01	74.45	229.2	97.49	0.06573	4.725	0.4305	11.13	0.0475	9.645	0.51	(204Pb)
m5 DEL03-1L gr b	945.5	39.87	966.7	28.59	1015	11.43	99.39	0.158	4.534	1.591	4.585	0.07304	0.5639	0.99	(204Pb)
m5 DEL03-1L gr d	872.2	37.34	901.5	27.82	973.8	16.61	99.78	0.1449	4.577	1.43	4.657	0.07157	0.8147	0.98	(204Pb)
m5 DEL03-1L gr f	899.7	37.65	921.4	27.68	973.7	21.55	99.62	0.1498	4.483	1.478	4.571	0.07157	1.057	0.97	(204Pb)

Appendix H (continued). U-Pb zircon data (SIMS) from Central Blue Ridge migmatite DEL03-1, DEL03-1L.

Puck#.Sample #.grain ID.	Ages (Ma)						Radiogenic	Corrected atomic ratios						Correlation of	
	$^{206}Pb/^{238}U$	$^{206}Pb/^{238}U$	$^{207}Pb/^{235}U$	$^{207}Pb/^{235}U$	$^{207}Pb/^{206}Pb$	$^{207}Pb/^{206}Pb$	^{206}Pb	$^{206}Pb^*/^{238}U$	$^{206}Pb^*/^{238}U$	$^{207}Pb^*/^{235}U$	$^{207}Pb^*/^{235}U$	$^{207}Pb^*/^{206}Pb^*$	$^{207}Pb^*/^{206}Pb^*$	Concordia Ellipses	Common Pb corr.
excluded points:		1 s.e.		1 s.e.		1 s.e.	(%)		1 s.e.(%)		1 s.e. (%)		1 s.e. (%)		
DEL03-1L gr a spot 1	1024	39.99	1093	31.08	1233	37.47	98.58	0.1721	4.224	1.933	4.644	0.08146	1.91	0.91	(204Pb)
DEL03-1L gr c spot 1	866.9	37.27	876.1	39.93	899.6	93.93	97.12	0.1439	4.595	1.37	6.803	0.06903	4.554	0.75	(204Pb)
DEL03-1L gr e spot 1	1005	31.69	1004	23.14	1003	19.05	99.73	0.1687	3.406	1.688	3.629	0.07259	0.9383	0.97	(204Pb)
DEL03-1L gr g spot 2	454.2	23.73	376.9	80.67	-1	0.01084	94.22	0.073	5.41	0.4495	25.62	0.04465	24.28	0.35	(204Pb)
DEL03-1L gr l spot 1	1012	53.33	994.8	51.52	957.5	108.1	97.55	0.1699	5.695	1.664	8.124	0.071	5.286	0.76	(204Pb)
DEL03-1L gr j spot 2	574.1	35.93	506.6	92.65	212.6	505.6	93.29	0.09314	6.541	0.647	23.23	0.05038	21.82	0.35	(204Pb)
DEL03-1L gr l spot 1	1272	42.08	1279	27.43	1290	15.94	99.78	0.2182	3.644	2.524	3.772	0.0839	0.819	0.98	(204Pb)
DEL03-1L gr l spot 2	1266	43.98	1241	28.44	1197	12.96	99.78	0.217	3.825	2.393	3.971	0.07998	0.6572	0.99	(204Pb)
DEL03-1 gr c spot 1	1395	49.5	1411	31.49	1436	23.03	99.38	0.2417	3.945	3.015	4.13	0.09047	1.207	0.96	(204Pb)
DEL03-1 gr f spot 1	321.2	15.29	291.9	116.5	63.78	1043	76.12	0.05109	4.879	0.3331	45.92	0.04729	43.8	0.48	(204Pb)
DEL03-1 gr j spot 1	759.2	29.55	753.8	38.89	737.8	122.1	97.03	0.125	4.125	1.101	7.309	0.06388	5.769	0.62	(204Pb)
DEL03-1 gr d spot 1	1590	49.04	1609	29.56	1635	20.19	99.32	0.2797	3.481	3.88	3.661	0.1006	1.087	0.95	(204Pb)
DEL03-1 gr d spot 2	1188	29.12	1196	21.07	1211	16.07	99.77	0.2023	2.685	2.247	2.999	0.08057	0.8165	0.96	(204Pb)
DEL03-1 gr f spot 1	1022	20.24	1030	14.34	1048	8.59	99.55	0.1718	2.141	1.759	2.216	0.07425	0.4261	0.98	(204Pb)
DEL03-1 gr h spot 1	1836	37.66	1874	22.09	1916	13.08	99.85	0.3296	2.356	5.333	2.583	0.1174	0.7289	0.96	(204Pb)
DEL03-1 gr h spot 2	1008	23.27	976.8	19.72	907.8	38.09	98.36	0.1692	2.495	1.617	3.143	0.0693	1.849	0.81	(204Pb)
DEL03-1 gr i spot 1	1263	37.81	1307	25.32	1380	22.42	99.42	0.2165	3.296	2.623	3.444	0.0879	1.167	0.94	(204Pb)
DEL03-1 gr i spot 2	825.4	16.32	892.5	15.53	1062	21.27	99.72	0.1366	2.107	1.408	2.616	0.07477	1.057	0.92	(204Pb)
DEL03-1 gr j spot 1	1001	21.08	1007	14.92	1021	8.119	99.94	0.168	2.273	1.697	2.335	0.07324	0.401	0.99	(204Pb)
m5 DEL03-1L gr b spot 1	459.7	31.32	283.5	79.6	-1	0.00955	95.11	0.07392	7.057	0.3221	32.18	0.0316	30.23	0.38	(204Pb)
DEL03-1L gr d spot 1	486.9	50.08	278.7	110.9	-1	0.01274	85.52	0.07845	10.68	0.3158	45.5	0.02919	43.64	0.29	(204Pb)
DEL03-1L gr m spot 1	433.3	18.35	321.3	75.63	-1	0.01022	91.28	0.06953	4.378	0.3722	27.46	0.03882	26.32	0.34	(204Pb)
DEL03-1 gr d spot 1	365.7	11.61	458.2	21.52	953.3	101.1	96.47	0.05837	3.267	0.5703	5.835	0.07086	4.941	0.53	(204Pb)

Appendix I, Sample locations.

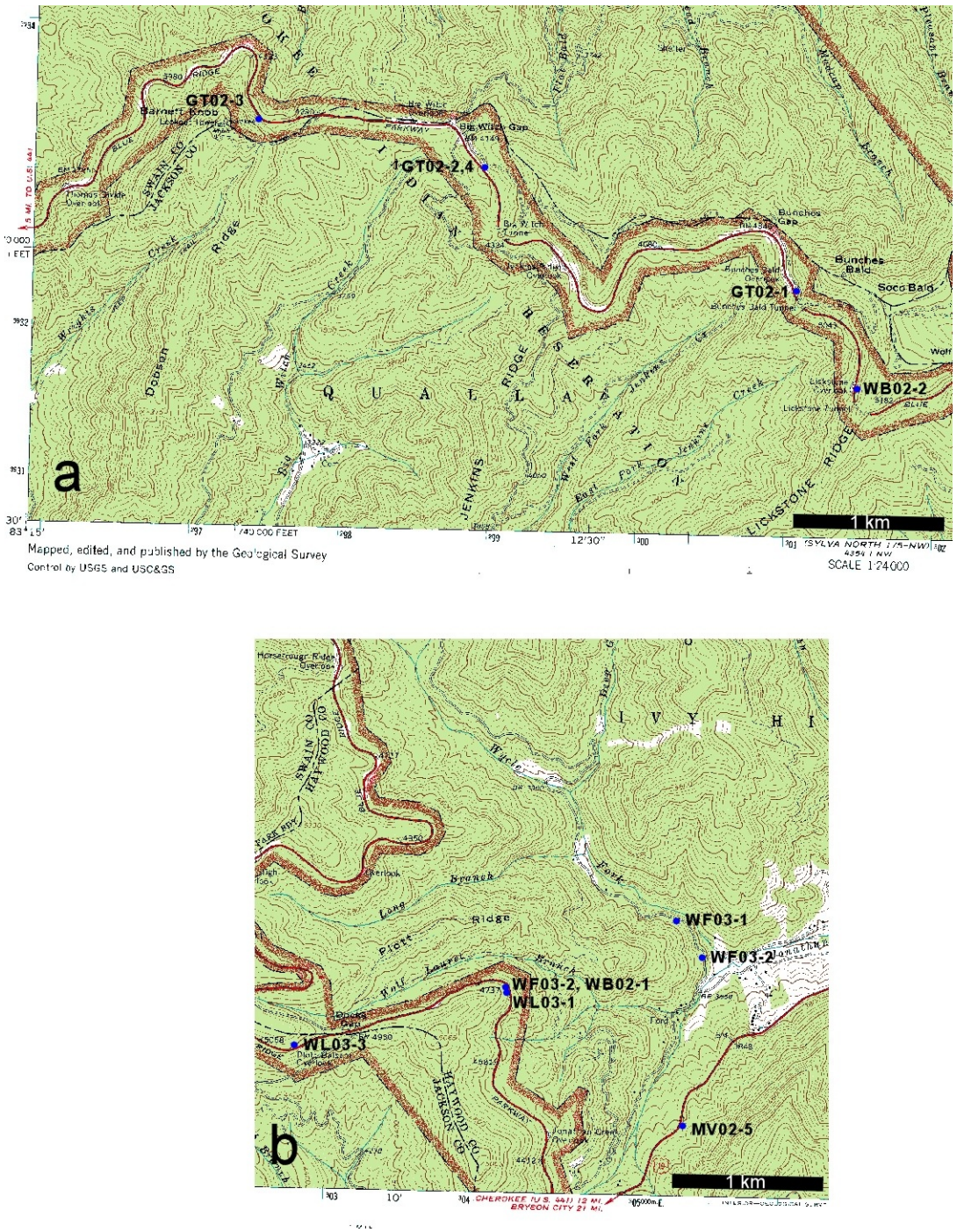

Appendix I. Sample locations from the Bunches Bald quadrangle, Great Smoky Mountains, western North Carolina.

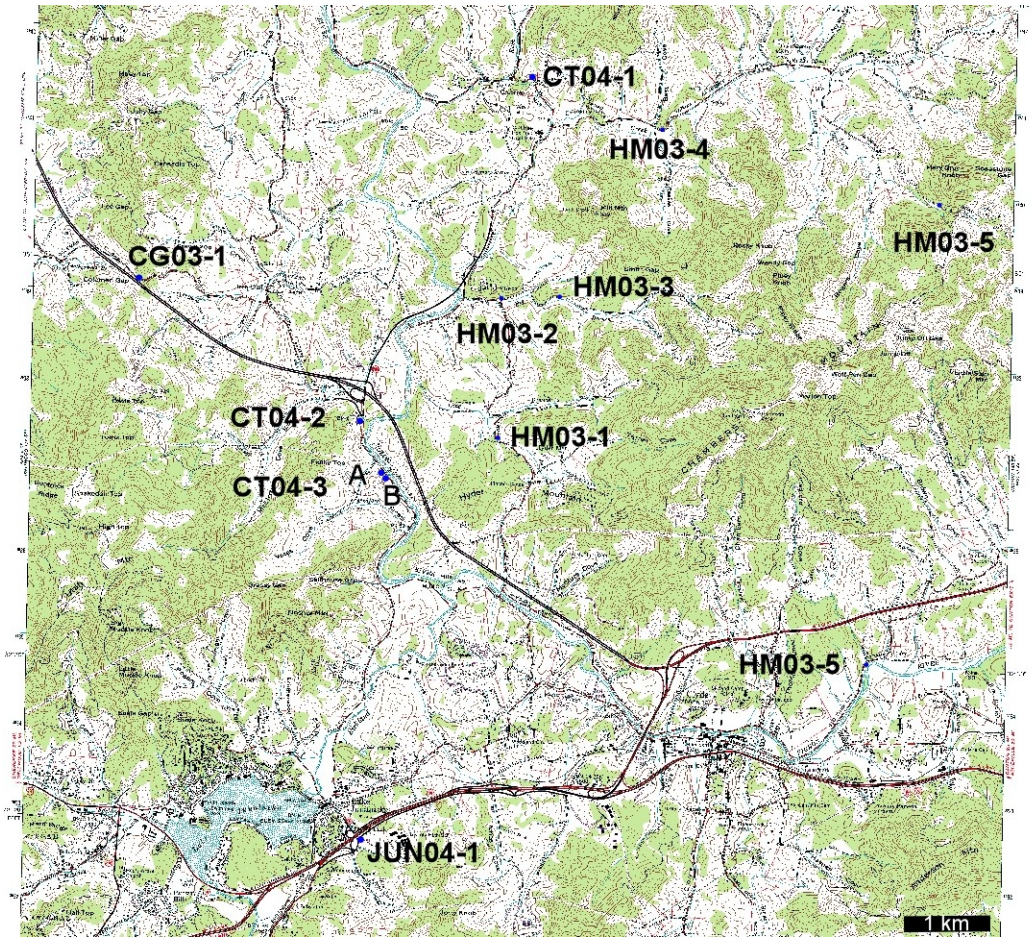

Appendix I. Sample locations from the Clyde quadrangle, eastern Great Smoky Mountains, western North Carolina.

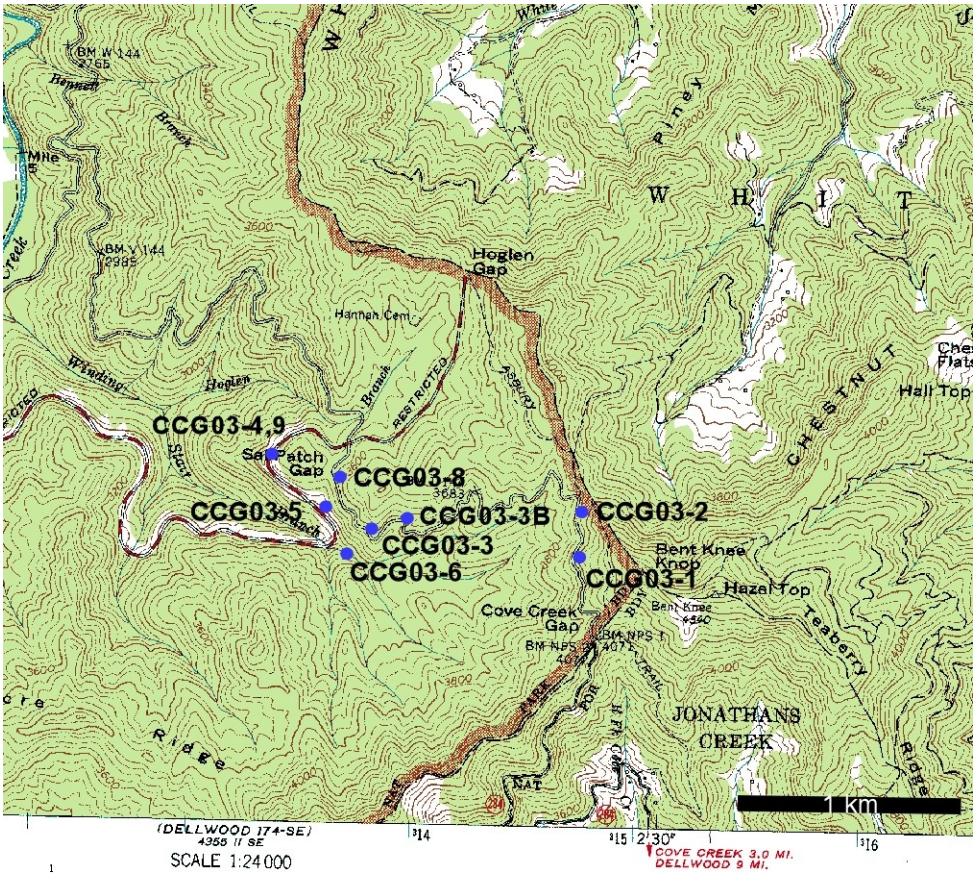

Appendix I. Sample locations from the Cove Creek quadrangle, Great Smoky National Park, western North Carolina.

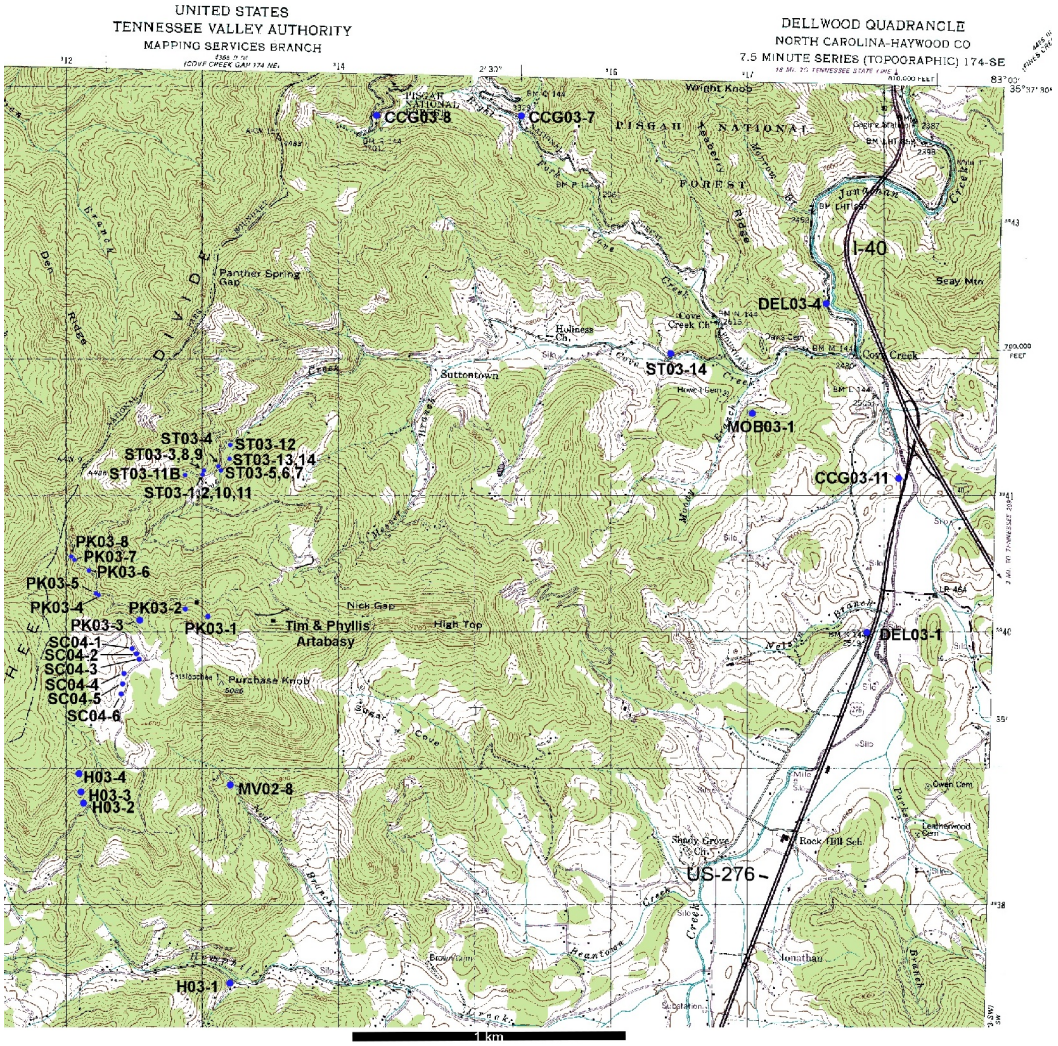

Appendix I. Sample locations of schist, orthogneiss, and amphibolite from the northern half of the Dellwood quadrangle, eastern Great Smoky Mountains, western North Carolina.

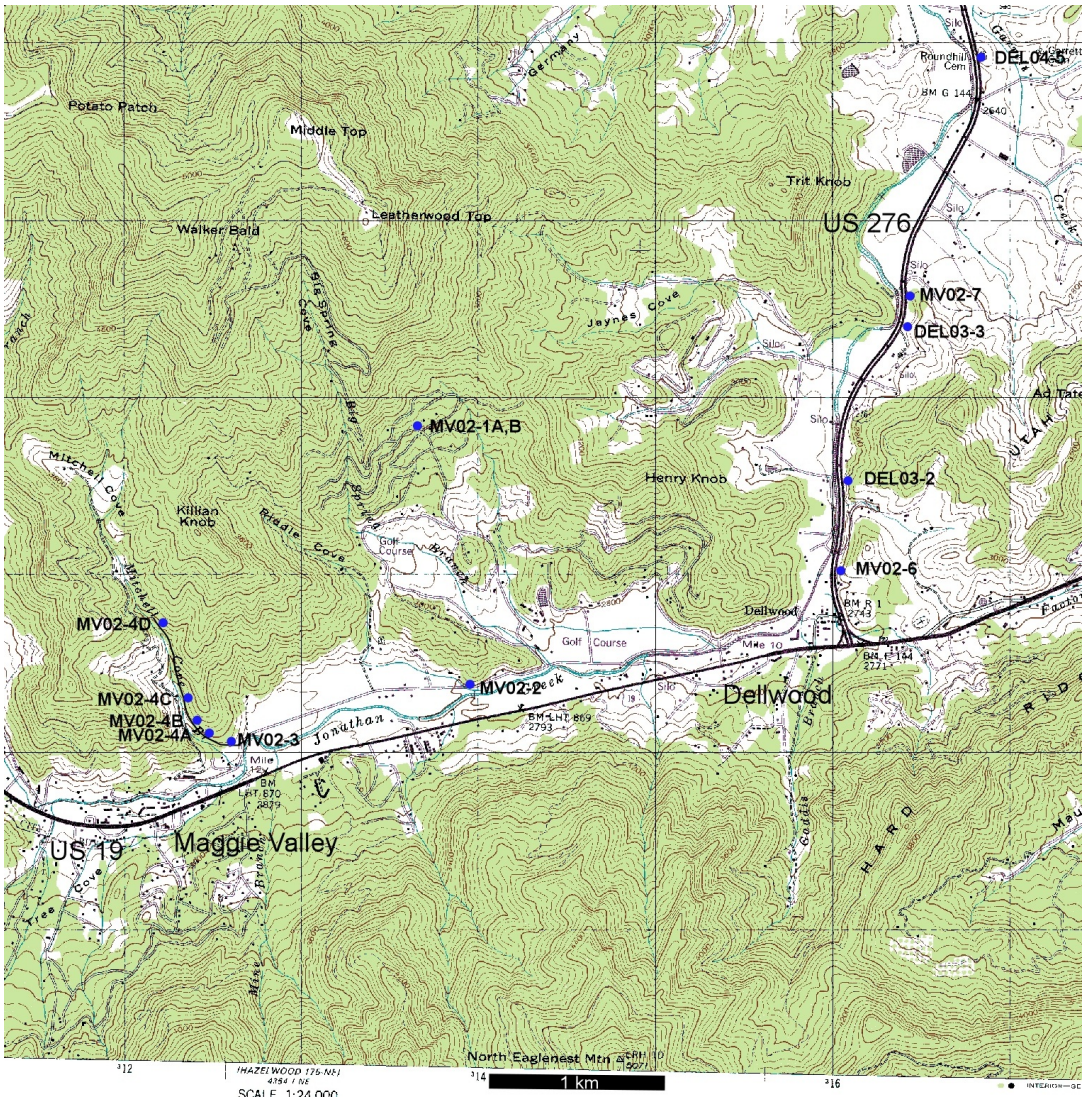

Appendix I. Sample locations from the Dellwood quadrangle, (southern portion) eastern Great Smoky Mountains, western North Carolina.

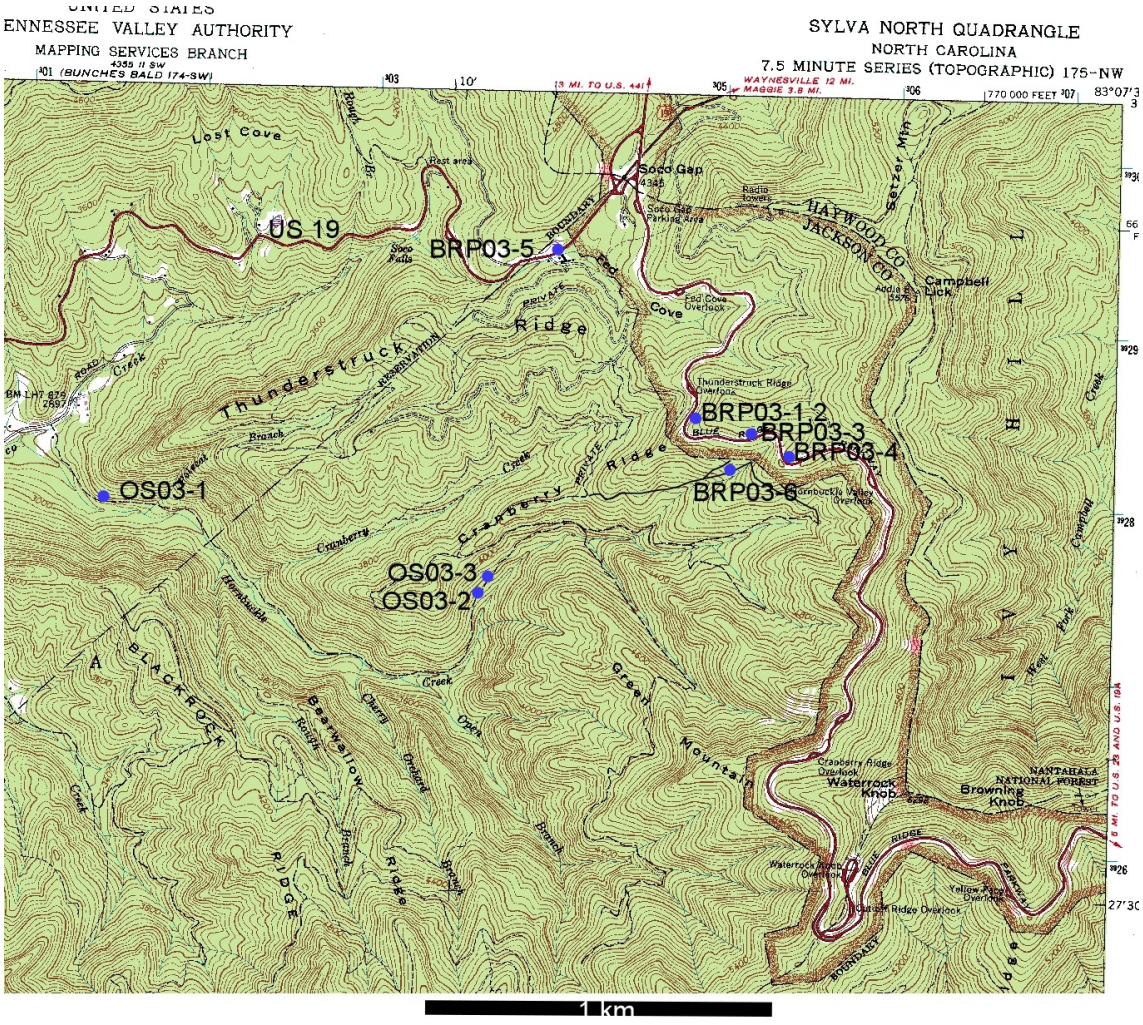

Appendix I. Sample locations, northern portion of the Sylva North quadrangle, eastern Great Smoky Mountains, western North Carolina.

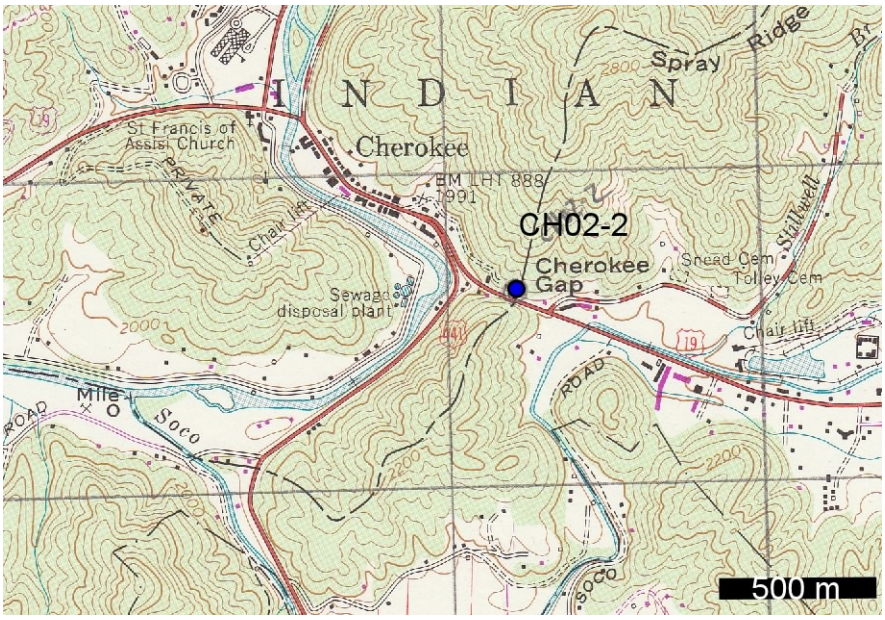

Appendix I. Sample location of biotite augen gneiss, Cherokee-Raven Fork belt, western Blue Ridge basement, Whittier Quadrangle, North Carolina.

Appendix I. Sample locations from the central and western Blue Ridge, western North Carolina.

Sample Locations and Rock names						
	UTM coordinates			USGS 7.5 minute	Location Notes	Lithology
	(1927 N.A. datum)			series topo map		
Sample #	Zone	Easting	Northing			
Cove Creek Gap						
CCG03-1	17N	314180	3945460	Cove Creek Gap	0.5 km N of Cove Creek Gap, within GSMNP	calc-silicate
CCG03-2	17N	314180	3945660	Cove Creek Gap		meta-arkose
CCG03-3A	17N	313750	3945340	Cove Creek Gap		orthogneiss
CCG03-3B	17N	314000	3945450	Cove Creek Gap		grt-chl phyllite
CCG03-4	17N	313350	3945640	Cove Creek Gap	quality roadcut, 250m NW of Sal Patch Gap	meta-arkose
CCG03-9	17N	313350	3945640	Cove Creek Gap	quality roadcut, 250m NW of Sal Patch Gap	meta-arkose
CCG03-5	17N	313640	3945330	Cove Creek Gap		mylonitic orthogneiss
CCG03-6	17N	313720	3945180	Cove Creek Gap	sampled from creek bed	cld-grt phyllite
CCG03-7	17N	315450	3943620	Dellwood		meta-graywacke
CCG03-8	17N	314280	3943810	Dellwood		meta-graywacke
CCG03-10	17N	314750	3944640	Cove Creek Gap	200m SW of Cove Creek Gap	
Maggie Valley						
MV02-1A	17N	313660	3933830	Dellwood	Near 24 Valley View Dr.	ky-grt schist
MV02-1B	17N	313660	3933830	Dellwood	Near 24 Valley View Dr.	ky-grt schist
MV02-2	17N	313960	3.9E+07	Dellwood	State Rt. 1307, N of Jonathan Creek	biotite gneiss
MV02-3	17N	312580	3932090	Dellwood	State Rt. 1307, N of Jonathan Creek	orthogneiss
MV02-4A	17N	312450	3932150	Dellwood	Mitchell Cove	orthogneiss
MV02-4B	17N	312400	3932250	Dellwood	Mitchell Cove	orthogneiss
MV02-4C	17N	312340	3932430	Dellwood	Mitchell Cove	ky-grt schist
MV02-4D	17N	312220	3932740	Dellwood	Mitchell Cove	ms-grt schist
MV02-5A	17N	305350	3930850	Bunches Bald	roadcut SE of SR 19	mylonitic orthogneiss
MV02-5B	17N	305350	3930850	Bunches Bald	roadcut SE of SR 19	mylonitic orthogneiss
MV02-5C	17N	305350	3930850	Bunches Bald	roadcut SE of SR 19	mylonitic orthogneiss

Appendix I, (continued). Sample locations from the central and western Blue Ridge, western North Carolina.

	UTM coordinates			USGS 7.5 minute	Location Notes	Lithology
	(1927 N.A. datum)			series topo map		
Sample #	Zone	Easting	Northing			
MV02-5D	17N	305350	3930850	Bunches Bald	roadcut SE of SR 19	mylonitic orthogneiss
MV02-6	17N	316050	3933050	Dellwood	Near Dellwood, Clearwood Drive west of Route 19, 0.5 km N	biotite gneiss
					of Route 276	
MV02-7	17N	316430	3934560	Dellwood	Roadcut east of SR 276	biotite gneiss
MV02-8	17N	313220	3938880	Dellwood	Large boulder in Ned Branch of Hemphill Creek	mylonitic orthogneiss
NB04-1A	17N	313220	3938880	Dellwood	Ned Branch outcrop near creek	mylonitic orthogneiss
NB04-1B	17N	313220	3938880	Dellwood	Ned Branch outcrop near creek	mylonitic orthogneiss
Hemphill Creek						
H03-1	17N	313190	3937420	Dellwood	Junction of Tumbling Fork Rd. and Hemphill Creek Rd.	biotite gneiss
H03-2	17N	312100	3938700	Dellwood	Uphill from Hemphill Creek Rd	amphibolite
H03-3	17N	312100	3938810	Dellwood	Uphill from Hemphill Creek Rd	amphibolite
H03-4	17N	312080	3938950	Dellwood	Uphill from Hemphill Creek Rd	amphibolite
Science Center						
SC04-1	17N	312480	3939900	Dellwood	Hemphill Creek Rd, below science center	orthogneiss
SC04-2	17N	312510	3939870	Dellwood	Hemphill Creek Rd, below science center	orthogneiss
SC04-3	17N	312520	3939820	Dellwood	Hemphill Creek Rd, below science center	orthogneiss
SC04-4	17N	312420	3939700	Dellwood	Hemphill Creek Rd, below science center	orthogneiss
SC04-5	17N	312430	3939630	Dellwood	Hemphill Creek Rd, below science center	orthogneiss
SC04-6	17N	312410	3939530	Dellwood	Hemphill Creek Rd, below science center	orthogneiss
Suttontown						
ST03-1	17N	313000	3941160	Dellwood	above gravel road, NW of Cove Creek	quartz vein
ST03-2	17N	313000	3941160	Dellwood	above gravel road, NW of Cove Creek	
ST03-3	17N	313010	3941220	Dellwood	above dirt road/trail, NW of Cove Creek	graphitic schist
ST03-4	17N	313120	3941280	Dellwood	near junction with Smoky Boundary Ranch Dr, NW of Cove Creek	meta-graywacke
ST03-5	17N	313170	3941200	Dellwood	below Cove Creek Road, above the falls	meta-arkose

Appendix I, (continued). Sample locations from the central and western Blue Ridge, western North Carolina.

	UTM coordinates			USGS 7.5 minute	Location Notes	Lithology
	(1927 N.A. datum)			series topo map		
Sample #	Zone	Easting	Northing			
ST03-6	17N	313170	3941200	Dellwood	below Cove Creek Road, above the falls	meta-arkose
ST03-7	17N	313170	3941200	Dellwood	below Cove Creek Road, above the falls	meta-arkose
ST03-8	17N	313010	3941220	Dellwood	above dirt road/trail, NW of Cove Creek	quartz vein + feldspar
ST03-9	17N	313010	3941220	Dellwood	above dirt road/trail, NW of Cove Creek	
ST03-10	17N	313000	3941160	Dellwood	above gravel road, NW of Cove Creek	
ST03-11A	17N	313000	3941160	Dellwood	above gravel road, NW of Cove Creek	
ST03-11B	17N	312850	3941150	Dellwood	adjacent to creek bed	grt-schist
ST03-12	17N	313200	3941380	Dellwood	Private drive near Cove Creek, below falls	meta-arkose
ST03-13A	17N	313220	3941260	Dellwood	base of waterfall	meta-arkose
ST03-13B	17N	313220	3941260	Dellwood	base of waterfall	
ST03-14	17N	316450	3942040	Dellwood	Suttontown Road, 0.5 km west of Cove Creek Rd.	
Great Smoky Group Traverse						
GT02-1A	17N	301080	3932170	Bunches Bald	Blue Ridge Parkway (BRP)	ms schist
GT02-1B	17N	301080	3932170	Bunches Bald	Blue Ridge Parkway (BRP)	mu-bt-grt schist
GT02-2	17N	299010	3932980	Bunches Bald	BRP, 0.5 km SE of Big Witch Gap	mu schist
GT02-3	17N	297460	3933360	Bunches Bald	BRP, 0.25 km ENE of Barnett Knob	mu schist
GT02-4	17N	299010	3932980	Bunches Bald	BRP, 0.5 km SE of Big Witch Gap	mu-bt-grt schist
WB02-1, WL03-2	17N	304220	3931800	Bunches Bald	BRP, NW of Soco Gap, mile marker 457	meta-arkose
WB02-2	17N	301480	3931500	Bunches Bald		mu-bt schist
Wolf Laurel						
WL03-1	17N	304225	3931790	Bunches Bald	BRP, south of quartzite outcrop near mile marker 457	mu-grt schist
WL03-2	17N	304220	3931800	Bunches Bald	BRP, NW of Soco Gap, mile marker 457	meta-arkose
WL03-3	17N	302780	3931400	Bunches Bald	On trail, near BRP, above Plott Balsam Overlook	meta-arkose
WL03-4A	17N	302360	3931700	Bunches Bald	flote from Wolf Laurel Branch, just west of BRP extension	ky-grt schist
WL03-4B	17N	302360	3931700	Bunches Bald	flote from Wolf Laurel Branch, just west of BRP extension	

Appendix I (continued). Sample locations from the central and western Blue Ridge, western North Carolina.

	UTM coordinates			USGS 7.5 minute	Location Notes	Lithology
	(1927 N.A. datum)			series topo map		
Sample #	Zone	Easting	Northing			
Wycle Fork						
WF03-1	17N	305350	3932230	Bunches Bald	Wycle Fork, NW of Jonathan Creek	meta-arkose
WF03-2A	17N	305520	3931960	Bunches Bald		
WF03-2B	17N	305520	3931960	Bunches Bald		grt-ky schist
WF03-3						orthogneiss
Blue Ridge Parkway						
BRP03-1	17N	304810	3928580	Sylva North	BRP, 0.15 km SSE of Thunderstruck Ridge Overlook	
BRP03-2	17N	304810	3928580	Sylva North	BRP, 0.15 km SSE of Thunderstruck Ridge Overlook	
BRP03-3	17N	305130	3928460	Sylva North	BRP	meta-graywacke
BRP03-4A	17N	305330	3928340	Sylva North	BRP, drive 0.7 km NW of Hornbuckle Valley Overlook	meta-arkose
BRP03-4B	17N	305330	3928340	Sylva North	BRP, drive 0.7 km NW of Hornbuckle Valley Overlook	chlorite schist
BRP03-4C	17N	305330	3928340	Sylva North	BRP, drive 0.7 km NW of Hornbuckle Valley Overlook	meta-conglomerate
BRP03-5	17N	303980	3929510	Sylva North	SR 19, 0.65 km SW of Soco Gap	meta-arkose
BRP03-6A	17N	304920	3928210	Sylva North	Dirt road SE of Cranberry Ridge	leucocratic pegmatite
BRP03-6B	17N	304920	3928210	Sylva North	Dirt road SE of Cranberry Ridge	meta-graywacke
Old Soco Road						
OS03-1	17N	301380	3928080	Sylva North	Rough gravel road up Hornbuckle Creek, SE of Old Soco Rd.	orthogneiss
OS03-2	17N	303530	3927500	Sylva North	Hornbuckle Creek, SE of Cranberry Ridge	meta-graywacke
OS03-3	17N	303590	3927585	Sylva North	Hornbuckle Creek, SE of Cranberry Ridge	meta-graywacke
Cherokee						
CH02-1	17N	290130	3930550	Whittier	Behind Bob's Big Boy, Cherokee, N.C.	orthogneiss
CH02-2	17N	290200	3927610	Whittier	Cherokee Gap, U.S. 19	orthogneiss
CH02-3	17N	296520	3937910	Bunches Bald	North of junction of Raven Fork and Straight Fork	meta-arkose
CH02-4	17N	294760	3939950	Smokemont	North end of Big Cove loop road, bridge over Raven Fork	orthogneiss
CH02-5	17N	293120	3932380	Smokemont	BRP, 1.1 km southeast of Ballhoot Scar Overlook	

Appendix I, (continued). Sample locations from the central and western Blue Ridge, western North Carolina.

	UTM coordinates			USGS 7.5 minute	Location Notes	Lithology
	(1927 N.A. datum)			series topo map		
Sample #	Zone	Easting	Northing			
Purchase Knob						
PK03-1	17N	313040	3940115	Dellwood	Private community, gravel roads, NW of Purchase Knob	Biotite augen gneiss
PK03-2	17N	312880	3940180	Dellwood	Private community, gravel roads, NW of Purchase Knob	Biotite augen gneiss
PK03-2B	17N	312880	3940180	Dellwood	Private community, gravel roads, NW of Purchase Knob	Biotite augen gneiss
PK03-4A	17N	312280	3940275	Dellwood	Private community, gravel roads, NW of Purchase Knob	Biotite augen gneiss
Purchase Knob (continued)						
PK03-4B	17N	312280	3940275	Dellwood	Private community, gravel roads, NW of Purchase Knob	Biotite augen gneiss
PK03-5	17N	312255	3940265	Dellwood	Private community, gravel roads, NW of Purchase Knob	Biotite augen gneiss
PK03-6	17N	312165	3940450	Dellwood	Private community, gravel roads, NW of Purchase Knob	meta-graywacke
PK03-7	17N	312075	3940530	Dellwood	Private community, gravel roads, NW of Purchase Knob	meta-graywacke
PK03-8	17N	312050	3940600	Dellwood	Private community, gravel roads, NW of Purchase Knob	meta-graywacke
Dellwood						
DEL03-1	17N	317880	3939990	Dellwood	US 276, below parachute park	Migmatitic biotite gneiss
DEL03-2	17N	316050	3933060	Dellwood	east side US 276, across from school	biotite gneiss
DEL03-3	17N	316450	3934400	Dellwood	east of US 276, north of Dellwood, NC	amphibolite, granulite
DEL03-4	17N	317560	3942430	Dellwood	roadcut 0.5 km NW of Cove Creek	metagraywacke
DEL03-5	17N	316840	3935860	Dellwood	east of 276, near Roundhill Cemetary	Hornblende-biotite gneiss
DEL05-3B2	17N	316250	3934500	Dellwood	ridge west of 276	garnet granulite
Hemphill Creek						
H03-1	17N	313190	3937420	Dellwood	Junction of Tumbling Fork Rd. and Hemphill Creek Rd.	2-mica schist
H03-2	17N	312100	3938700	Dellwood	Up steep hill above Hemphill Creek Rd.	amphibolite
H03-3	17N	312100	3938810	Dellwood	Up steep hill above Hemphill Creek Rd.	amphibolite
H03-4A	17N	312080	3938950	Dellwood	Up steep hill above Hemphill Creek Rd.	amphibolite
H03-4C	17N	312080	3938950	Dellwood	Up steep hill above Hemphill Creek Rd.	amphibolite
H03-4F	17N	312080	3938950	Dellwood	Up steep hill above Hemphill Creek Rd.	amphibolite

Appendix I, (continued). Sample locations from the central and western Blue Ridge, western North Carolina.

	UTM coordinates			USGS 7.5 minute	Location Notes	Lithology
	(1927 N.A. datum)			series topo map		
Sample #	Zone	Easting	Northing			
Hyder Mountain						
HM03-1	17N	324160	3937300	Clyde	Hyder Mt. Rd, 0.9 km N of Fincher Chapel	paragneiss
HM03-2	17N	324210	3938880	Clyde	"T" junction of Hyder Mt. Rd and Big Branch Rd.	migmatitic gneiss
HM03-3	17N	324890	3938900	Clyde	Big Branch Rd.	migmatitic gneiss
HM03-4	17N	326050	3940850	Clyde		migmatitic gneiss
HM03-5A	17N	329240	3939970	Clyde		migmatitic gneiss
HM03-5B	17N	329240	3939970	Clyde		Hornblende-biotite gneiss
HM03-6	17N	328400	3934590	Clyde		meta-volcanic?
Mount Lyn Lowry						
MLL04-1A	17N	309680	3923780	Hazelwood	BRP, Mt. Lyn Lowry Overlook	intermediate gneiss
MLL04-1B	17N	309680	3923780	Hazelwood	BRP, Mt. Lyn Lowry Overlook	felsic gneiss
MLL04-1C	17N	309680	3923780	Hazelwood	BRP, Mt. Lyn Lowry Overlook	mafic gneiss
Carver Mountain						
CM04-1	17N	310700	3918500	Sylva North	SR 74, 23, north side of roadway	mafic gneiss
CM04-2	17N	307030	3919780	Hazelwood	SR 74, 23, east of roadway	amphibolite
Fines Creek						
FC04-1A	17N	319430	3948820	Fines Creek	Junction of I40, Fines Creek Rd.	spotted gneiss
FC04-1B	17N	319430	3948820	Fines Creek	Junction of I40, Fines Creek Rd.	intermediate gneiss
FC03-2	17N	323360	3950120	Fines Creek	"T" intersection of Max Patch and Fines Creek Rds.	augengneiss
Coleman Gap						
CG03-2	17N	320000	3939115	Clyde	above Coleman Gap Rd (2-lane)	migmatitic gneiss

Appendix J. U-Pb zircon data (SIMS)

puck#/Sample #/grain ID	Ages (Ma)							Radiogenic ^{206}Pb (%)	Corrected atomic ratios						Correlation of Concordia Ellipses
	$^{206}Pb/^{238}U$	$^{206}Pb/^{238}U$ 1 s.e.	$^{207}Pb/^{235}U$	$^{207}Pb/^{235}U$ 1 s.e.	$^{207}Pb/^{206}Pb$	$^{207}Pb/^{206}Pb$ 1 s.e.	concordia age		$^{207}Pb^*/^{235}U$	$^{207}Pb^*/^{235}U$ 1 s.e. (%)	$^{206}Pb^*/^{238}U$	$^{206}Pb^*/^{238}U$ 1 s.e.(%)	$^{207}Pb^*/^{206}Pb^*$	$^{207}Pb^*/^{206}Pb^*$ 1 s.e. (%)	
M5 DEL03-1L gr B@2	294.4	11.28	321.3	68.86	521.5	504.8	292	93.44	0.3722	25	0.04672	3.919	0.05778	23.01	0.5671
M6 DEL03-1L gr A@2	396.2	15.23	398.5	48.12	412	289.4	396	97.46	0.4806	14.6	0.06339	3.964	0.05499	12.94	0.5294
M6 DEL03-1L gr A	412.2	17.31	363.5	34.17	62.9	233.7	411	97.08	0.4304	11.18	0.06604	4.335	0.04727	9.811	0.4908
PB DEL03-1L gr M	422.7	22.84	314.3	74.83	-1	0.01022	423	91.28	0.3628	27.69	0.06777	5.582	0.03882	26.32	0.3395
PB DEL03-1L gr B	430.6	24.63	407.9	41	281.7	232.1	429	95.55	0.4944	12.2	0.06907	5.913	0.05192	10.15	0.5611
M6 DEL03-1L gr C@2	438.2	18.69	438.3	34.22	439	173.5	438	97.42	0.5398	9.614	0.07033	4.411	0.05566	7.796	0.6026
M5 DEL03-1L gr B @1	440.1	19.92	272.5	75.85	-1	0.009554	444	95.11	0.3078	31.74	0.07065	4.683	0.0316	30.23	0.3873
PB DEL03-1L gr G@2	441.9	28.16	368	79.97	-1	0.01084	442	94.22	0.4369	25.9	0.07095	6.592	0.04465	24.28	0.3652
PB DEL03-1L gr F	444.5	28.49	394.1	74.99	107.9	488.6	446	94.29	0.4742	22.96	0.07138	6.633	0.04818	20.68	0.4706
M6 DEL03-1L gr E	451.4	19.56	420.1	37.74	251.9	212.4	453	97.86	0.5125	10.97	0.07253	4.487	0.05125	9.235	0.5606
PB DEL03-1L gr H	461.2	28.36	481.7	56.2	580.8	263.4	460	96.35	0.6071	14.65	0.07416	6.373	0.05937	12.13	0.5792
PB DEL03-1L gr G	470.1	32.95	465.2	34.83	441.2	126.2	468	98.2	0.5812	9.331	0.07565	7.268	0.05572	5.675	0.794
PB DEL03-1L gr D	473.9	50.61	271.9	108.8	-1	0.01274	446	85.52	0.3071	45.6	0.07628	11.08	0.02919	43.64	0.2945
M6 DEL03-1L gr C	474.3	21.16	467.9	49.23	436.7	264.7	474	97.25	0.5854	13.13	0.07635	4.628	0.05561	11.89	0.4316
PB DEL03-1L gr J	556.5	41.51	493.8	92.4	212.6	505.6	554	93.29	0.6263	23.63	0.09017	7.786	0.05038	21.82	0.3878
M5 DEL03-1L gr C rightTip	812	18.16	846.8	16.24	939.3	37.46	836	99.64	1.303	2.828	0.1342	2.38	0.07037	1.827	0.7669
PB DEL03-1L gr C	843.5	47.92	859.1	45.61	899.6	93.93	853	97.12	1.33	7.868	0.1398	6.061	0.06903	4.554	0.8168
M6 DEL03-1L gr D	879.9	33.5	906.9	24.97	973.5	16.64	957	99.74	1.443	4.164	0.1462	4.073	0.07156	0.816	0.9806
M6 DEL03-1L gr F	907.1	33.85	926.6	24.93	973.2	21.64	962	99.55	1.491	4.102	0.1511	4.001	0.07155	1.061	0.966
M5 DEL03-1L gr B@3	940.9	16.41	963.1	11.87	1014	8.321	976	99.78	1.582	1.909	0.1572	1.874	0.073	0.4106	0.9766
M5 DEL03-1L gr C core	951.5	20.25	968.2	13.72	1006	20.11	979	99.82	1.595	2.199	0.159	2.289	0.07273	0.9913	0.9032
M6 DEL03-1L gr B	953.1	35.77	971.8	25.62	1014	11.49	1009	99.29	1.604	4.097	0.1593	4.037	0.07302	0.5671	0.9904

Appendix J (continued). U-Pb zircon data (SIMS).

puck#/Sample #/grain ID	Ages (Ma)							Radiogenic	Corrected atomic ratios						Correlation of
	$^{206}Pb/^{238}U$	$^{206}Pb/^{238}U$ 1 s.e.	$^{207}Pb/^{235}U$	$^{207}Pb/^{235}U$ 1 s.e.	$^{207}Pb/^{206}Pb$	$^{207}Pb/^{206}Pb$ 1 s.e.	concordia age	^{206}Pb (%)	$^{207}Pb^*/^{235}U$	$^{207}Pb^*/^{235}U$ 1 s.e. (%)	$^{206}Pb^*/^{238}U$	$^{206}Pb^*/^{238}U$ 1 s.e.(%)	$^{207}Pb^*/^{206}Pb^*$	$^{207}Pb^*/^{206}Pb^*$ 1 s.e. (%)	Concordia Ellipses
PB DEL03-1L gr E	984.1	41.86	989.8	30.06	1003	19.05	1000	99.73	1.651	4.755	0.1649	4.587	0.07259	0.9383	0.9805
PB DEL03-1L gr I	985.6	62.19	977	56.02	957.5	108.1	979	97.55	1.617	8.928	0.1652	6.804	0.071	5.286	0.8071
PB DEL03-1L gr A	997.1	52.91	1074	40.04	1233	37.47	discordant	98.58	1.879	6.042	0.1673	5.727	0.08146	1.91	0.9487
PB DEL03-1L gr L@2	1240	55.85	1224	36.01	1197	12.96	1202	99.78	2.339	5.063	0.2121	4.952	0.07998	0.6572	0.9916
PB DEL03-1L gr L@1	1245	55.3	1262	35.96	1290	15.94	1285	99.78	2.465	4.978	0.2131	4.884	0.0839	0.819	0.9864
PB DEL03-1 gr F	314.5	17.45	286.5	114.9	63.78	1043	316	76.12	0.326	46.01	0.04999	5.684	0.04729	43.8	0.4418
PB DEL03-1 gr D	359.1	14.49	451.4	23.22	953.3	101.1	discordant	96.47	0.5598	6.372	0.05729	4.149	0.07086	4.941	0.6317
PA DEL03-1 gr F@2	445.4	17.52	419.1	45.46	277.1	276.4	446	96.84	0.511	13.24	0.07153	4.07	0.05181	12.07	0.4283
PA DEL03-1 gr J@2	448.6	13.45	431.2	15.48	339.5	72.72	443	99.19	0.5291	4.407	0.07206	3.104	0.05325	3.211	0.6852
PB DEL03-1 gr A	463.1	25.02	457.6	37.38	430.1	166.6	463	98.5	0.5694	10.15	0.07448	5.599	0.05544	7.475	0.6902
PA DEL03-1 gr K@1	481.9	9.786	477.8	8.41	457.8	13.77	479	99.92	0.6008	2.207	0.07763	2.107	0.05614	0.6206	0.9597
PA DEL03-1 gr K@4	489.8	10.48	487.3	8.881	475.5	17.25	488	99.91	0.6159	2.295	0.07894	2.222	0.05659	0.7803	0.9408
PA DEL03-1 gr K@2	494.1	10.38	485.5	8.685	445.2	20.06	483	99.9	0.6132	2.25	0.07967	2.183	0.05582	0.9023	0.9176
PA DEL03-1 gr K@3	517.4	11.01	503.1	9.047	438.7	14.19	discordant	99.88	0.6414	2.28	0.08358	2.215	0.05566	0.6378	0.9601
PB DEL03-1 gr J	742.2	36.8	741.1	42.07	737.8	122.1	742	97.03	1.075	7.999	0.122	5.25	0.06388	5.769	0.6937
PA DEL03-1 gr I@2	825.4	16.32	892.5	15.53	1062	21.27	discordant	99.72	1.408	2.616	0.1366	2.107	0.07477	1.057	0.922
PA DEL03-1 gr J@1	1001	21.08	1007	14.92	1021	8.119	1003	99.94	1.697	2.335	0.168	2.273	0.07324	0.401	0.9852
PA DEL03-1 gr H@2	1008	23.27	976.8	19.72	907.8	38.09	988	98.36	1.617	3.143	0.1692	2.495	0.0693	1.849	0.8087
PA DEL03-1 gr F@1	1022	20.24	1030	14.34	1048	8.59	1044	99.55	1.759	2.216	0.1718	2.141	0.07425	0.4261	0.9815
PA DEL03-1 gr D@2	1188	29.12	1196	21.07	1211	16.07	1206	99.77	2.247	2.999	0.2023	2.685	0.08057	0.8165	0.9647
PA DEL03-1 gr I@1	1263	37.81	1307	25.32	1380	22.42	1349	99.42	2.623	3.444	0.2165	3.296	0.0879	1.167	0.941
PB DEL03-1 gr C	1365	63.26	1393	40.07	1436	23.03	1426	99.38	2.942	5.288	0.2359	5.142	0.09047	1.207	0.9736
PA DEL03-1 gr D@1	1590	49.04	1609	29.56	1635	20.19	1628	99.32	3.88	3.661	0.2797	3.481	0.1006	1.087	0.9549
PA DEL03-1 gr H@1	1836	37.66	1874	22.09	1916	13.08	1911	99.85	5.333	2.583	0.3296	2.356	0.1174	0.7289	0.9606

Appendix J (continued). U-Pb zircon data (SIMS).

puck#/Sample #/grain ID	Ages (Ma)							Radiogenic	Corrected atomic ratios						Correlation of
	$^{206}Pb/^{238}U$	$^{206}Pb/^{238}U$ 1 s.e.	$^{207}Pb/^{235}U$	$^{207}Pb/^{235}U$ 1 s.e.	$^{207}Pb/^{206}Pb$	$^{207}Pb/^{206}Pb$ 1 s.e.	concordia age	^{206}Pb (%)	$^{207}Pb^*/^{235}U$	$^{207}Pb^*/^{235}U$ 1 s.e. (%)	$^{206}Pb^*/^{238}U$	$^{206}Pb^*/^{238}U$ 1 s.e.(%)	$^{207}Pb^*/^{206}Pb^*$	$^{207}Pb^*/^{206}Pb^*$ 1 s.e. (%)	Concordia Ellipses
PB MM22 gr A	462.8	22.69	447.4	28.57	368.5	122.1	461	98.14	0.5536	7.896	0.07444	5.08	0.05394	5.42	0.7327
PB MM22 gr I	467.6	22.94	458.9	27.57	415.2	115.5	466	98.56	0.5713	7.469	0.07524	5.086	0.05507	5.169	0.7231
PB MM22 gr H	475.6	26.19	473.8	38.84	465.2	169	476	97.02	0.5947	10.26	0.07657	5.712	0.05633	7.627	0.6798
PB MM22 gr C	521.7	27.15	455	26.21	130.6	99.74	discordant	97.35	0.5653	7.148	0.08429	5.418	0.04864	4.241	0.8065
PB MM22 gr D	546.6	31.03	560.5	41.84	617.2	170.1	549	97.12	0.7367	9.714	0.0885	5.921	0.06038	7.879	0.5854
PB MM22 gr F	560.4	33.86	491.5	55.34	182.3	283.2	553	95.84	0.6227	14.2	0.09082	6.309	0.04973	12.16	0.523
PB MM22 gr B	912.1	46.15	967.8	37.34	1097	56.69	982	99.09	1.594	5.985	0.152	5.426	0.07606	2.832	0.8813
PB CG03-2 gr J	410.4	21.42	381	56.99	206.1	382.1	411	94.97	0.4553	17.94	0.06573	5.387	0.05024	16.47	0.4108
PB CG03-2 gr D	521.3	38.84	525.7	160.8	545	802.9	521	84.79	0.6783	39.18	0.08423	7.755	0.0584	36.74	0.4038
PB CG03-2 gr G	699.1	45.53	798	46.62	1085	116.2	732	98.48	1.194	8.436	0.1145	6.872	0.07563	5.795	0.7314
PB CG03-2 gr H	734.8	40.85	720.3	104.4	675.2	406.7	734	94.01	1.033	20.23	0.1207	5.882	0.06203	19.02	0.3448
PB CG03-2 gr B	819.5	61.79	727.8	182.9	454.8	736.2	819	87.47	1.048	35.21	0.1356	8.029	0.05606	33.17	0.36
M6 CG03-2 gr D	963.4	40.68	939.5	36.33	883.9	78.7	946	99.29	1.523	5.928	0.1612	4.546	0.06851	3.806	0.7666
M6 CG03-2 gr A	971.3	40.21	992.5	30.88	1040	42.58	1003	99.47	1.658	4.877	0.1626	4.459	0.07393	2.109	0.9017
M6 CG03-2 gr C	1012	54.31	1084	59.8	1230	137.7	1033	98.14	1.907	8.977	0.1701	5.796	0.08134	7.015	0.6243
M6 CG03-2 gr B	1063	66.96	1062	83.49	1058	185.4	1063	98.39	1.845	12.68	0.1794	6.83	0.07461	9.21	0.7076
PB CH02-2B gr A	599	73.42	337.3	494.4	-1	0.04951	604	78.39	0.394	172.3	0.09738	12.83	0.02935	168.7	0.3098
PB CH02-2B gr B	849.6	51.84	883.2	36.81	968.5	66.25	898	98.37	1.387	6.24	0.1409	6.512	0.07138	3.247	0.8712
PB CH02-2B gr G	934.9	83.56	959.1	126.7	1015	330.3	936	96.52	1.572	20.41	0.1561	9.602	0.07304	16.3	0.62
PB CH02-2B gr E	939.7	48.53	990.2	64.08	1104	159.6	946	97.75	1.652	10.13	0.1569	5.551	0.07634	7.982	0.6201
PA CH02-2B gr B @1	989.5	28.03	1022	26.49	1092	43.23	1010	99.58	1.736	4.112	0.1659	3.056	0.0759	2.158	0.859

Appendix J (continued). U-Pb zircon data (SIMS).

puck#/Sample #/grain ID	Ages (Ma)							Radiogenic ^{206}Pb (%)	Corrected atomic ratios						Correlation of Concordia Ellipses
	$^{206}Pb/^{238}U$	$^{206}Pb/^{238}U$ 1 s.e.	$^{207}Pb/^{235}U$	$^{207}Pb/^{235}U$ 1 s.e.	$^{207}Pb/^{206}Pb$	$^{207}Pb/^{206}Pb$ 1 s.e.	concordia age		$^{207}Pb^*/^{235}U$	$^{207}Pb^*/^{235}U$ 1 s.e. (%)	$^{206}Pb^*/^{238}U$	$^{206}Pb^*/^{238}U$ 1 s.e.(%)	$^{207}Pb^*/^{206}Pb^*$	$^{207}Pb^*/^{206}Pb^*$ 1 s.e. (%)	
M6 MV02-2 gr G	1121	43.11	1125	29.54	1132	22.18	1129	99.63	2.027	4.344	0.1899	4.191	0.07741	1.114	0.9666
M5 MV02-2 gr C	927.2	21.55	946.6	17.88	991.9	28.1	949	99.75	1.54	2.904	0.1547	2.496	0.07221	1.382	0.8797
M6 MV02-2 gr D	1033	40.22	1035	37.28	1037	67.96	1034	98.79	1.77	5.745	0.1738	4.213	0.07385	3.366	0.8145
M6 MV02-2 gr F	1140	44.79	1114	30.79	1065	21.21	1079	99.77	1.997	4.55	0.1934	4.287	0.07487	1.055	0.9733
M6 HM03-5B gr B	983.3	38.7	1005	31.73	1054	50.07	1009	99.48	1.692	4.973	0.1648	4.244	0.07446	2.486	0.8662
M6 HM03-5B gr C	1060	67.58	1086	98.33	1137	254.3	1064	97.31	1.913	14.75	0.1788	6.913	0.0776	12.78	0.4996
M6 HM03-5B gr D	1153	49.97	1145	34.9	1132	36.44	1139	99.49	2.089	5.083	0.1958	4.734	0.0774	1.83	0.9329
M6 HM03-5B gr A	1181	57.04	1173	38.99	1158	30.42	1162	99.44	2.174	5.606	0.201	5.287	0.07845	1.534	0.962
M6 OS03-1B gr F	1098	45.32	1129	42.25	1190	77.96	1117	98.27	2.041	6.199	0.1857	4.488	0.07971	3.949	0.7724
M6 OS03-1B gr B	1136	57.27	1106	41.18	1048	47.3	1094	99.34	1.972	6.112	0.1927	5.498	0.07423	2.346	0.9237
M5 OS03-1 gr F	1169	45.58	1134	40.36	1069	86.55	1144	98.83	2.056	5.908	0.1988	4.265	0.07501	4.306	0.6856
M6 OS03-1B gr A	1202	55.29	1191	42.41	1170	57.75	1187	98.69	2.231	6.049	0.205	5.041	0.07893	2.917	0.8772
M6 PK03-3B gr A	1163	50.32	1177	45.62	1203	78.27	1173	98.97	2.187	6.547	0.1977	4.728	0.08023	3.972	0.7987
M6 PK03-3B gr C	1194	53.35	1159	39.1	1093	49.51	1139	99.19	2.13	5.658	0.2035	4.895	0.07592	2.472	0.9002
M6 PK03-3B gr F	1208	49.72	1198	36.96	1181	48.98	1193	99.04	2.254	5.255	0.206	4.514	0.07934	2.478	0.8822
M6 FC04-1B gr A	1053	43.66	1044	40.71	1025	75.01	1047	98.81	1.796	6.243	0.1774	4.494	0.0734	3.708	0.8095
M5 FC04-1B gr A	1153	28.06	1144	20.66	1127	47.16	1139	99.63	2.085	3.01	0.1958	2.658	0.07721	2.367	0.6577
M6 FC04-1B gr F	1284	53	1340	41.07	1430	50.01	1360	98.55	2.742	5.519	0.2204	4.552	0.0902	2.62	0.882
M6 FC04-1B gr B	1347	52.84	1327	37.08	1296	34.77	1311	99.61	2.696	5.006	0.2324	4.347	0.08414	1.788	0.9365

Appendix J (continued). U-Pb zircon data (SIMS).

puck#/Sample #/grain ID	Ages (Ma)							Radiogenic ^{206}Pb (%)	Corrected atomic ratios						Correlation of Concordia Ellipses
	$^{206}Pb/^{238}U$	$^{206}Pb/^{238}U$ 1 s.e.	$^{207}Pb/^{235}U$	$^{207}Pb/^{235}U$ 1 s.e.	$^{207}Pb/^{206}Pb$	$^{207}Pb/^{206}Pb$ 1 s.e.	concordia age		$^{207}Pb^*/^{235}U$	$^{207}Pb^*/^{235}U$ 1 s.e. (%)	$^{206}Pb^*/^{238}U$	$^{206}Pb^*/^{238}U$ 1 s.e.(%)	$^{207}Pb^*/^{206}Pb^*$	$^{207}Pb^*/^{206}Pb^*$ 1 s.e. (%)	
M6 SC04-6 gr A	1108	44.17	1122	37.04	1148	63.02	1121	98.31	2.019	5.455	0.1876	4.338	0.07805	3.173	0.8137
M6 SC04-6 gr F	1113	47.48	1125	35.91	1149	50.59	1129	98.87	2.029	5.28	0.1885	4.644	0.07808	2.547	0.8759
M6 SC04-6 gr D	1117	51.64	1085	56.46	1021	137.8	1104	97.57	1.911	8.47	0.1892	5.034	0.07326	6.805	0.5954
M6 SC04-6 gr H	1128	45.02	1141	37.19	1166	53.86	1143	98.41	2.077	5.426	0.1913	4.349	0.07874	2.719	0.868
M6 SC04-6 gr I	1169	52.39	1150	46.3	1116	91.58	1155	97.87	2.104	6.727	0.1987	4.902	0.0768	4.589	0.7312
M6 SC04-6 gr G	1228	62.37	1216	42.96	1195	50.68	1209	99.26	2.313	6.06	0.2099	5.576	0.07992	2.569	0.9058
M6 DEL04-5 gr B	1314	56.04	1296	40.19	1266	40.81	1283	99.52	2.583	5.491	0.2261	4.715	0.08286	2.09	0.9273
M5 DEL04-5 gr A core	1240	33.14	1252	22.88	1272	27.62	1259	99.66	2.431	3.179	0.2122	2.937	0.08312	1.416	0.8958
M5 DEL04-5 gr C	1262	25.86	1247	17.52	1223	25.42	1242	99.73	2.416	2.44	0.2162	2.257	0.08105	1.294	0.8511
M6 DEL04-5 gr C	1223	57.34	1215	46.4	1201	75.34	1215	98.58	2.308	6.549	0.2088	5.149	0.08016	3.822	0.8124
M6 DEL04-5 gr E	1149	49.43	1144	37.01	1135	44.92	1142	99.53	2.087	5.391	0.1952	4.695	0.07754	2.257	0.909
M5 MV02-3 gr C	1161	30.1	1167	23.3	1180	33.2	1169	99.71	2.157	3.359	0.1973	2.834	0.0793	1.679	0.8664
M5 NB04-1A gr A	1279	32.47	1230	22.61	1146	13.51	1231	99.92	2.359	3.171	0.2194	2.799	0.07797	0.6799	0.9818

Appendix K. U-Pb zircon ion-tunneling data (SIMS).

puck#/Sample #/grain ID	Ages (Ma)						Radiogenic ^{206}Pb (%)	Corrected atomic ratios						Correlation of Concordia Ellipses	number of blocks
	$^{206}Pb/^{238}U$	$^{206}Pb/^{238}U$ 1 s.e.	$^{207}Pb/^{235}U$	$^{207}Pb/^{235}U$ 1 s.e.	$^{207}Pb/^{206}Pb$	$^{207}Pb/^{206}Pb$ 1 s.e.		$^{207}Pb^*/^{235}U$	$^{207}Pb^*/^{235}U$ 1 s.e. (%)	$^{206}Pb^*/^{238}U$	$^{206}Pb^*/^{238}U$ 1 s.e.(%)	$^{207}Pb^*/^{206}Pb^*$	$^{207}Pb^*/^{206}Pb^*$ 1 s.e. (%)		
DEL03-1gr D@2	453.9	14.62	408.6	39.3	159.7	242.4	96.89	0.4954	11.68	0.07296	3.336	0.04925	10.36	0.5167	5
Block 2	460.9	13.09	482.9	27.4	588.7	135.7	98.25	0.609	7.129	0.07412	2.943	0.05959	6.256	0.4847	5
Block 3	473.2	11.6	527.8	26.33	771.6	113.8	98.84	0.6817	6.398	0.07617	2.544	0.06492	5.408	0.5579	5
Block 4	469.9	11.45	457.4	36.74	395.3	203.4	97.59	0.5691	9.976	0.07561	2.526	0.05459	9.072	0.4683	5
Block 5	446.4	13.85	472.5	35.56	600.9	189.7	97.81	0.5925	9.413	0.07171	3.212	0.05993	8.764	0.3657	5
Block 6	443.3	16.38	452.5	40.03	499.6	218.5	97.53	0.5615	10.96	0.07118	3.825	0.05721	9.922	0.4339	4
CH02-2 gr G	437.1	45.17	493.2	85.83	762.9	413.4	99.34	0.6254	21.97	0.07016	10.69	0.06465	19.61	0.4519	1
Block 2	527.9	56.16	621	120.8	976.7	467	98.39	0.8433	26.02	0.08533	11.08	0.07167	22.91	0.4763	1
Block 3	588.7	61.93	799.4	73.87	1443	195.4	100	1.197	13.35	0.09563	11.01	0.09081	10.26	0.6609	1
Block 4	576.8	57.08	714.9	66.32	1177	209.1	100	1.022	12.92	0.0936	10.35	0.07918	10.57	0.607	1
Block 5	717.6	75.69	818.3	76.11	1103	211.5	100	1.239	13.55	0.1177	11.15	0.07631	10.58	0.6486	1
Block 6	823	90.23	836.1	80.76	870.9	228.4	100	1.278	14.18	0.1362	11.68	0.06808	11.02	0.6519	1
Block 7	1004	122.4	1046	116.1	1135	271.7	99.55	1.801	17.78	0.1685	13.17	0.07754	13.65	0.6477	1
Block 8	1045	131.7	964.9	153.4	786.8	432.9	98.73	1.586	24.63	0.176	13.66	0.06539	20.62	0.5471	1
Block 9	1153	149.3	1125	109.5	1070	219.3	100	2.027	16.11	0.1958	14.15	0.07507	10.91	0.7472	1
Block 10	1063	135.6	1017	124.3	918.9	312.3	99.53	1.723	19.35	0.1794	13.83	0.06968	15.19	0.6258	1
Block 11	929.9	112.5	952	142.8	1003	397.1	98.69	1.554	23.11	0.1552	12.99	0.07262	19.56	0.5332	1
Block 12	999	127.2	1062	104.3	1193	230	100	1.846	15.84	0.1676	13.75	0.07985	11.66	0.6979	1

Appendix L. Th-Pb monazite data (SIMS).

Sample I.D./	Age (Ma)	Age (Ma)	ThO_2/	isobaric interference		Nd	Common Pb corrections		
Grain I.D.	$^{208}Pb/^{232}Th$	$^{208}Pb/^{232}Th$ 1 s.e.	Th	207.9766/ ^{208}Pb	203.4689/ ^{204}Pb	correction	$^{206}Pb/^{204}Pb$	$^{207}Pb/^{204}Pb$	$^{208}Pb/^{204}Pb$
ccg03-3b ga	418.1	15.45	0.5682	8.053	0.1053	0.2106	1.83	1.53	3.71
ccg03-3b gb	426.1	16.15	0.5573	8.135	0.0699	0.13988	1.98	1.65	4
ccg03-3b gd	410.7	13.76	0.6403	6.797	0.0888	0.17764	2.26	1.89	4.58
ccg03-3b ge	462.8	20	0.4949	7.280	0.0531	0.1061	2.3	1.92	4.65
gt02-2 gc	395	16.58	0.5054	8.017	0.0206	0.04116	2.24	1.87	4.53
gt02-2 gd	467.3	22.68	0.4673	6.147	0.0012	0.002446	3.03	2.54	6.14
gt02-2 gd@2	296	16.73	0.4572	7.271	0.0013	0.002696	2.56	2.14	5.19
gt02-2 gd@3	331.9	13.97	0.5432	7.470	0.0043	0.008586	2.48	2.07	5.02
gt02-2 ge	424.6	15.73	0.578	8.091	0.1840	0.368	1.46	1.22	2.96
gt02-2 ge@2	416.2	13.92	0.6298	8.811	0.0121	0.02426	2.04	1.73	4.19
gt02-2 gf@1	140.8	6.268	0.5061	6.985	0.0013	0.00254	2.67	2.23	5.41
gt02-2 gf@2	449.4	17.98	0.5334	8.199	0.0085	0.016932	2.24	1.87	4.54
gt02-2 gf@3	452.1	17.82	0.5377	8.941	0.0102	0.02042	2.05	1.71	4.15
gt02-2 gg@1	382.7	14.79	0.5476	6.906	0.0191	0.0381	2.6	2.18	5.27
gt02-2 gh@1	116.9	5.754	0.4553	7.303	0.0020	0.003908	2.55	2.13	5.16
gt02-2 gi@1	301	12.89	0.5024	6.548	0.0015	0.003012	2.85	2.38	5.76
gt02-2 gj@1	472.3	17.07	0.5851	6.175	0.0119	0.02378	2.96	2.47	5.99
gt02-2 gk@1	429.9	15.93	0.5777	6.554	0.0652	0.13046	2.48	2.07	5.02
mb02-4 ga@1	418.8	14.07	0.6465	8.002	0.0147	0.0294	2.27	1.9	4.59
mb02-4 ga@2	415.1	14.36	0.6255	8.202	0.0313	0.06262	2.14	1.79	4.33
mb02-4 gb@1	414.6	15.02	0.5928	7.886	0.1265	0.253	1.77	1.48	3.59
mb02-4 gb@2	380	14.99	0.5371	9.342	0.0329	0.06572	1.87	1.56	3.79
mb02-4 gb@3	422.2	14	0.6458	9.213	0.1919	0.3838	1.25	1.05	2.53
mb02-4 gc@1	420	14.51	0.6126	7.843	0.1101	0.2202	1.86	1.55	3.76
mb02-4 gd@1	408.2	14.55	0.5957	7.794	0.0603	0.12056	2.11	1.76	4.27
mb02-4 ge@1	410.8	13.99	0.6225	7.977	0.0332	0.0663	2.19	1.83	4.43
mm22a ga@1	426.8	15.44	0.5929	8.253	0.1653	0.3306	1.52	1.27	3.07
mm22a ga@2	431.4	14.93	0.6081	9.304	0.1721	0.3442	1.32	1.1	2.67
mm22a gc@1	437.2	14.83	0.6189	7.671	0.1023	0.2046	1.94	1.62	3.93
mm22a ge @3	468.4	15.39	0.6475	5.049	0.1601	0.3202	2.52	2.1	5.1
mm22a ge@1	431.6	15.1	0.6022	8.415	0.2194	0.4388	1.25	1.04	2.52
mm22a ge@2	464.6	18.29	0.5523	4.891	0.1490	0.298	2.68	2.24	5.43
mm22a gf @1	433.9	15.26	0.5992	8.094	0.1383	0.2766	1.67	1.4	3.38
mm22a gi @1	427.2	15.78	0.5937	7.911	0.1253	0.2506	1.77	1.48	3.59
mm22a gi @2	447.5	12.76	0.7328	6.600	0.2434	0.4868	1.45	1.22	2.94
mm22a gi @3	450.4	14.48	0.6595	7.904	0.2058	0.4116	1.39	1.16	2.82
mm22a gl@1	427.2	15.15	0.5972	7.582	0.2440	0.488	1.26	1.06	2.56
mm22a gm @1	425.3	15.51	0.5811	7.988	0.3071	0.6142	0.9	0.75	1.83
mv02-1b ga@1	424.9	15.53	0.5912	8.629	0.1157	0.2314	1.67	1.39	3.37
mv02-1b gc@1	427.2	15.27	0.588	8.853	0.1136	0.2272	1.63	1.36	3.3
mv02-1b gd@1	424.7	14.69	0.6104	8.197	0.0395	0.07898	2.1	1.76	4.25
mv02-1b ge@1	425.5	15.17	0.5997	8.703	0.1438	0.2876	1.53	1.28	3.1
mv02-1b gh@1	428.6	16.01	0.6022	8.422	0.0853	0.17058	1.84	1.54	3.73
mv02-1b gi@1	425.7	14.9	0.6052	8.420	0.1320	0.264	1.63	1.37	3.31

Appendix L (continued). Th-Pb monazite data (SIMS).

Calibration	Age (Ma)	Age (Ma)	Th O_2/	isobaric interference		Nd	Common Pb corrections		
	$^{208}Pb/^{232}Th$	$^{208}Pb/^{232}Th$ 1 s.e.	Th	207.9766/ ^{208}Pb	203.4689/ ^{204}Pb	correction	$^{206}Pb/^{204}Pb$	$^{207}Pb/^{204}Pb$	$^{208}Pb/^{204}Pb$
554_g1@1	47.56	1.638	0.6795	8.105	0.0891	0.17826	1.9	1.58	3.84
554_g1@2	49.17	2.09	0.5211	5.936	0.2329	0.4658	1.68	1.41	3.41
554_g2@1	46.87	1.91	0.6333	7.741	0.4572	0.9144	0.21	0.17	0.42
554_g2@2	45.63	1.97	0.6329	7.873	0.1426	0.2852	1.7	1.42	3.44
554_g3@1	45.9	1.75	0.6181	7.615	0.3637	0.7274	0.67	0.56	1.36
554_ga@1	45.57	1.732	0.5892	7.934	0.2123	0.4246	1.36	1.13	2.75
554_ga@2	44	1.831	0.5514	8.395	0.2334	0.4668	1.19	0.99	2.4
554_ga@4	45.93	1.786	0.5752	6.141	0.1479	0.2958	2.14	1.79	4.34
554_ga@5	44.12	1.595	0.6403	8.015	0.1318	0.2636	1.72	1.44	3.48
554_ga@a4	44.76	1.727	0.6006	6.693	0.1742	0.3484	1.82	1.52	3.69
554_ga@a5	43.57	1.645	0.5973	9.752	0.1569	0.3138	1.32	1.1	2.66
554_gb puck b@1	43.8	1.901	0.5907	7.691	0.0770	0.15404	2.06	1.72	4.16
554_gb@1	44.74	1.927	0.5672	7.390	0.0957	0.19134	2.05	1.71	4.14
554_gb@3a	44.8	1.72	0.5737	8.660	0.2992	0.5984	0.87	0.72	1.76
554_gb@4	44.58	1.475	0.6541	9.022	0.3549	0.7098	0.6	0.5	1.22
554_gb@a5	45.98	1.679	0.6039	6.546	0.1683	0.3366	1.9	1.58	3.84
554_gc@1	44.57	1.635	0.618	8.817	0.0932	0.18646	1.73	1.44	3.49
554_gc@4	45.49	1.64	0.6282	7.290	0.2277	0.4554	1.4	1.17	2.83
554_gd@a1	44.1	1.836	0.5544	7.584	0.1229	0.6164	0.95	0.79	1.91
554_gd2@a1	43.9	1.829	0.5544	7.584	0.1229	0.2458	1.86	1.55	3.77
554_gf@1	44.75	2.066	0.546	7.957	0.2509	0.5018	1.17	0.98	2.37
554_gf@2	44.28	1.971	0.521	7.816	0.2014	0.4028	1.43	1.19	2.89

Standard: 554: 45.3 $\pm$ 1.4 Ma
Calibration curve: Slope = 0.285
X-intercept: 0.02 + 0.02 (1 stdev)
X=Pb/Th; Y=ThO_2/Th
Th/U relative sensitivity factor = 1.36

Appendix M. Whole rock chemical compositions (XRF).

Sample	CCG03-3	CCG03-5	CG03-1	CG03-2	CH02-1	CH02-2	CH02-4	CT04-3B
quad[1]	CCG	CCG	C	C	W	W	S	C
lithology[2]	1	1	2	3	1	1	1	4
SiO_2 (%)	65.27	75.47	59.98	55.50	61.26	63.50	62.24	52.71
TiO_2 (%)	1.06	0.14	1.07	1.44	1.22	1.19	1.09	1.36
Al_2O_3 (%)	14.72	13.48	16.19	15.30	15.00	15.28	15.74	17.74
$Fe_2O_3^T$ (%)	6.10	1.95	8.46	10.53	6.78	6.51	6.03	9.10
MnO (%)	0.10	0.05	0.14	0.18	0.14	0.10	0.09	0.12
MgO (%)	1.08	0.33	3.38	4.69	1.27	1.25	1.19	3.86
CaO (%)	2.12	0.92	3.73	6.93	4.36	4.17	3.53	8.74
Na_2O (%)	3.76	2.66	2.66	2.65	2.62	3.58	3.30	2.89
K_2O (%)	4.61	3.72	2.62	1.23	4.13	3.20	3.98	1.19
P_2O_5 (%)	0.34	0.02	0.21	0.20	0.66	0.61	0.60	0.60
Ba (ppm)	1672	984	841	325	2179	1395	2070	1485
V (ppm)	60	19	159	206	74	69	65	172
Cr (ppm)	303	439	495	442	332	418	260	304
Ni (ppm)	5	14	52	54	8	19	6	52
Ga (ppm)	21	24	21	18	20	21	22	21
Rb (ppm)	99	86	69	27	86	80	93	23
Y (ppm)	65	30	42	36	52	56	60	28
Zr (ppm)	652	237	219	195	462	467	579	296
Sr (ppm)	337	116	196	166	557	507	549	650
LOI	1.35	0.95	0.35	0.97	1.04	0.52	0.54	0.30
SUM	100.83	99.87	98.97	99.78	98.84	100.21	98.71	98.89
CIPW norm calculated on the basis of $Fe^{2+}/Fe_{(total)}$=.75								
Qtz	18.39	42.52	18.78	11.55	18.53	19.22	18.05	6.84
Cor	0.49	3.46	2.70	0.00	0.00	0.00	1.02	0.00
Or	27.26	22.00	15.48	7.30	24.41	18.90	23.52	7.03
Ab	31.83	22.47	22.48	22.42	22.15	30.27	27.96	24.42
An	8.30	4.43	17.15	26.20	16.97	16.20	13.59	31.93
Ne	0.00	0.00	0.00	0.00	0.00	0.00	0.00	0.00
Di	0.00	0.00	0.00	5.62	0.32	0.42	0.00	6.17
Hy	7.43	2.69	15.63	17.75	8.24	7.86	7.56	13.95
Ol	0.00	0.00	0.00	0.00	0.00	0.00	0.00	0.00
Mt	2.21	0.71	3.07	3.82	2.46	2.36	2.19	3.30
Ilm	2.02	0.27	2.02	2.74	2.32	2.25	2.08	2.58
Ap	0.79	0.04	0.49	0.48	1.56	1.45	1.41	1.42
LOI	1.35	0.95	0.35	0.97	1.04	0.52	0.54	0.30
Sum	100.07	99.53	98.13	98.85	97.99	99.45	97.92	97.93

[1]quadrangle:
CCG=Cove Creek Gap
C=Clyde
W=Whittier
S=Smokemont

[2]lithology:
1=biotite augen gneiss and granitic gneiss
2=muscovite biotite gneiss
3=hornblende biotite gneiss
4=amphibolite

Appendix M (continued). Whole rock chemical compositions (XRF).

Sample	DEL03-1	DEL03-1L	DEL03-2	DEL03-3	DEL03-3B	DEL03-3C	DEL03-3D	DEL04-5
quad[1]	D	D	D	D	D	D	D	D
lithology[2]	5	5	5	4	4	4	4	3
SiO_2 (%)	70.66	74.77	65.58	46.38	43.04	42.67	43.10	68.18
TiO_2 (%)	0.56	0.08	0.85	2.15	2.58	2.72	2.70	0.33
Al_2O_3 (%)	14.07	14.03	14.01	14.03	13.92	13.94	13.16	16.16
$Fe_2O_3^T$ (%)	4.72	1.01	5.89	15.02	17.70	18.34	16.58	3.13
MnO (%)	0.06	0.02	0.09	0.24	0.29	0.30	0.31	0.04
MgO (%)	1.22	0.20	1.64	7.12	6.89	6.47	7.30	0.81
CaO (%)	2.26	1.41	1.44	11.27	12.21	12.19	12.27	3.00
Na_2O (%)	2.93	2.56	1.86	2.89	2.20	2.00	2.21	4.24
K_2O (%)	3.35	5.45	5.41	0.54	0.08	0.11	0.52	3.29
P_2O_5 (%)	0.15	0.09	0.18	0.23	0.34	0.35	0.32	0.16
Ba (ppm)	675	1830	1304	243	174	221	217	1580
V (ppm)	65	16	90	365	355	340	407	48
Cr (ppm)	469	268	126	453	455	417	313	196
Ni (ppm)	31	9	21	47	64	53	55	11
Ga (ppm)	22	19	21	17	16	16	18	22
Rb (ppm)	121	111	153	12	6	8	8	73
Y (ppm)	53	32	59	30	40	43	38	31
Zr (ppm)	225	72	293	134	184	212	169	185
Sr (ppm)	280	502	215	127	70	68	81	918
LOI	0.36	0.40	0.54	0.53	0.21	0.26	0.38	0.17
SUM	100.53	100.29	97.73	100.55	99.59	99.48	98.98	99.81
CIPW norm calculated on the basis of $Fe^{2+}/Fe_{(total)}$=.75								
Qtz	32.72	35.56	26.80	0.00	0.00	0.00	0.00	22.49
Cor	1.87	1.59	2.90	0.00	0.00	0.00	0.00	0.55
Or	19.78	32.18	31.99	3.21	0.48	0.67	3.07	19.41
Ab	24.78	21.64	15.76	22.66	17.67	16.88	14.61	35.87
An	10.26	6.39	5.97	23.73	27.86	28.74	24.45	13.86
Ne	0.00	0.00	0.00	0.96	0.51	0.00	2.24	0.00
Di	0.00	0.00	0.00	25.12	25.11	24.30	28.10	0.00
Hy	7.09	1.45	8.92	0.00	0.00	1.68	0.00	4.79
Ol	0.00	0.00	0.00	13.01	14.18	12.80	12.87	0.00
Mt	1.71	0.37	2.14	5.44	6.42	6.65	6.01	1.14
Ilm	1.07	0.15	1.62	4.09	4.91	5.17	5.13	0.63
Ap	0.35	0.21	0.42	0.53	0.80	0.83	0.76	0.38
LOI	0.36	0.40	0.54	0.53	0.21	0.26	0.38	0.17
Sum	99.98	99.93	97.07	99.29	98.14	97.97	97.62	99.28

[1]quadrangle:
D=Dellwood

[2]lithology:
3=hornblende-biotite gneiss
4=amphibolite
5=mylonitic biotite gneiss

Appendix M (continued). Whole rock chemical compositions (XRF).

Sample	DEL05-3B2	FC04-1A	FC04-1B	FC03-2	H03-1	H03-2	H03-4B	H03-4D
quad[1]	D	FC	FC	FC	D	D	D	D
lithology[2]	4	5	5	1	2	5	4	4
SiO_2 (%)	45.39	51.09	69.70	66.77	73.68	69.64	49.63	46.24
TiO_2 (%)	1.78	3.38	0.66	0.54	0.65	0.39	2.68	2.63
Al_2O_3 (%)	13.73	13.31	15.48	16.01	11.90	15.21	15.09	16.55
$Fe_2O_3^T$ (%)	16.40	11.74	4.46	4.08	3.95	3.01	14.52	14.66
MnO (wt.%)	0.19	0.13	0.08	0.07	0.06	0.05	0.23	0.21
MgO (%)	5.84	3.64	1.03	1.36	1.30	0.45	3.53	4.05
CaO (%)	12.69	6.42	1.67	3.32	1.06	4.11	9.23	9.33
Na_2O (%)	2.44	2.33	2.49	3.38	1.36	4.40	2.43	3.00
K_2O (%)	0.07	3.16	4.43	3.99	2.97	0.78	0.57	0.47
P_2O_5 (%)	0.17	1.91	0.07	0.17	0.16	0.13	0.93	0.69
Ba (ppm)	170	3276	1169	1880	725	278	257	234
V (ppm)	291	227	51	62	64	56	203	209
Cr (ppm)	405	126	420	166	351	299	281	80
Ni (ppm)	48	14	17	9	31	6	21	18
Ga (ppm)	16	19	20	21	20	25	20	20
Rb (ppm)	6	49	95	86	111	40	10	10
Y (ppm)	34	40	47	36	53	26	34	28
Zr (ppm)	108	492	206	187	273	198	297	229
Sr (ppm)	141	755	342	600	143	651	389	486
LOI (%)	0.29	0.40	0.53	0.52	1.06	0.60	0.49	0.41
Sum	99.12	98.00	100.84	100.50	98.32	98.93	99.49	98.36
CIPW norm calculated on the basis of $Fe^{2+}/Fe_{(total)}$=.75								
Qtz	0.00	9.18	31.69	21.59	49.19	30.81	8.30	0.28
Cor	0.00	0.00	3.72	0.48	4.88	0.00	0.00	0.00
Or	0.42	18.70	26.15	23.59	17.55	4.63	3.39	2.78
Ab	20.63	19.71	21.10	28.62	11.54	37.19	20.55	25.41
An	26.31	16.51	7.83	15.39	4.26	19.46	28.57	30.29
Ne	0.00	0.00	0.00	0.00	0.00	0.00	0.00	0.00
Di	29.40	2.34	0.00	0.00	0.00	0.07	9.26	9.55
Hy	1.65	14.68	6.23	6.82	6.34	3.64	15.17	16.52
Ol	9.33	0.00	0.00	0.00	0.00	0.00	0.00	0.00
Mt	5.95	4.25	1.62	1.48	1.43	1.09	5.26	5.31
Ilm	3.38	6.42	1.25	1.02	1.24	0.73	5.09	4.99
Ap	0.41	4.52	0.17	0.40	0.37	0.32	2.21	1.63
LOI	0.29	0.40	0.53	0.52	1.06	0.60	0.49	0.41
Sum	97.77	96.71	100.27	99.90	97.85	98.55	98.29	97.16

[1]quadrangle:
D=Dellwood
F=Fines Creek

[2]lithology:
1=biotite augen gneiss and granitic gneiss
2=muscovite-biotite gneiss
4=amphibolite
5= migmatitic biotite gneiss

Appendix M (continued). Whole rock chemical compositions (XRF).

Sample	H03-4E	HM03-2	HM03-3	HM03-4	HM03-5A	HM03-5B	JUN04-1A	MLL04-1A
quad[1]	D	C	C	C	C	C	C	H
lithology[2]	4	5	3	5	4	3	5	5
SiO_2 (%)	47.72	70.99	63.23	72.79	48.86	76.37	53.05	60.27
TiO_2 (%)	2.80	0.37	0.90	0.15	0.79	0.29	1.44	1.01
Al_2O_3 (%)	16.85	14.83	15.88	15.67	14.49	13.68	16.15	16.18
$Fe_2O_3^T$ (%)	14.13	3.19	6.39	1.27	10.71	2.22	10.87	6.44
MnO (wt.%)	0.26	0.06	0.07	0.02	0.22	0.04	0.21	0.08
MgO (%)	3.20	0.83	1.73	0.35	9.22	0.67	5.52	2.93
CaO (%)	8.40	3.20	4.46	2.61	9.10	3.57	7.36	4.33
Na_2O (%)	3.04	3.50	3.21	4.66	1.79	4.41	2.27	3.42
K_2O (%)	0.43	2.22	1.95	1.87	1.55	0.39	1.24	2.57
P_2O_5 (%)	0.74	0.13	0.33	0.05	0.19	0.04	0.21	0.22
Ba (ppm)	310	1709	1120	404	513	202	278	501
V (ppm)	198	49	99	16	156	38	223	111
Cr (ppm)	106	250	297	145	620	304	295	289
Ni (ppm)	11	17	16	10	177	5	54	47
Ga (ppm)	20	21	20	24	18	20	20	21
Rb (ppm)	6	53	85	43	27	12	30	89
Y (ppm)	31	27	35	18	26	14	40	37
Zr (ppm)	245	236	330	147	115	103	169	201
Sr (ppm)	460	675	440	738	298	687	129	353
LOI (%)	0.59	0.22	0.36	0.24	0.67	0.18	0.36	0.48
Sum	98.29	99.84	98.75	99.84	97.79	102.00	98.80	98.09
CIPW norm calculated on the basis of $Fe^{2+}/Fe_{(total)}$=.75								
Qtz	4.21	33.15	23.50	32.07	0.00	40.08	8.56	15.20
Cor	0.00	1.16	1.17	1.36	0.00	0.00	0.00	0.44
Or	2.57	13.10	11.51	11.06	9.14	2.32	7.30	15.16
Ab	25.69	29.60	27.19	39.41	15.14	37.27	19.21	28.96
An	31.08	15.05	19.95	12.62	26.94	16.39	30.22	20.02
Ne	0.00	0.00	0.00	0.00	0.00	0.00	0.00	0.00
Di	4.81	0.00	0.00	0.00	13.68	0.90	4.01	0.00
Hy	16.00	4.85	9.54	1.97	22.43	3.10	21.03	12.41
Ol	0.00	0.00	0.00	0.00	2.95	0.00	0.00	0.00
Mt	5.12	1.16	2.32	0.46	3.88	0.81	3.94	2.34
Ilm	5.32	0.71	1.72	0.29	1.50	0.56	2.73	1.93
Ap	1.75	0.30	0.78	0.13	0.46	0.09	0.50	0.53
LOI	0.59	0.22	0.36	0.24	0.67	0.18	0.36	0.48
Sum	97.13	99.30	98.04	99.60	96.80	101.70	97.87	97.45

[1]quadrangle:
D=Dellwood
C=Clyde
H=Hazelwood

[2]lithology:
3=hornblende-biotite gneiss
4=amphibolite
5= migmatitic biotite gneiss

Appendix M (continued). Whole rock chemical compositions (XRF).

Sample	MLL04-1B	MLL04-1C	MP04-2	MV02-2	MV02-3	MV02-4A	MV02-6B	MV02-6HB
quad[1]	H	H	LG	D	D	D	D	D
lithology[2]	5	5	1	1	1	1	1	3
SiO_2 (%)	57.97	55.23	62.27	65.42	62.69	63.24	74.19	51.35
TiO_2 (%)	0.91	1.86	1.27	0.94	0.70	0.64	0.27	0.38
Al_2O_3 (%)	19.65	15.04	14.99	15.45	16.35	15.79	13.24	17.10
$Fe_2O_3^T$ (%)	6.87	10.53	6.79	6.66	5.15	4.72	1.96	8.43
MnO (wt.%)	0.09	0.13	0.12	0.08	0.09	0.08	0.04	0.16
MgO (%)	2.72	3.82	1.35	2.67	1.75	1.35	0.53	9.25
CaO (%)	4.60	5.71	4.38	3.25	3.55	3.27	2.62	6.90
Na_2O (%)	4.38	2.78	3.14	3.03	3.68	3.20	2.64	2.14
K_2O (%)	2.68	2.39	3.61	2.68	3.40	3.96	3.53	3.03
P_2O_5 (%)	0.23	0.29	0.63	0.12	0.24	0.20	0.07	0.08
Ba (ppm)	569	538	1467	957	1384	1765	1666	443
V (ppm)	103	158	65	123	72	65	27	84
Cr (ppm)	217	240	199	403	184	187	238	654
Ni (ppm)	35	32	3	89	8	9	10	279
Ga (ppm)	23	19	22	20	20	20	19	18
Rb (ppm)	85	61	92	82	101	113	55	74
Y (ppm)	46	33	59	37	37	38	24	28
Zr (ppm)	269	149	472	223	267	226	176	91
Sr (ppm)	507	298	559	432	562	608	577	426
LOI (%)	0.45	0.44	0.23	0.36	0.26	0.41	0.11	0.43
Sum	100.73	98.36	99.09	100.88	98.12	97.16	99.48	99.45
CIPW norm calculated on the basis of $Fe^{2+}/Fe_{(total)}$=.75								
Qtz	6.37	10.25	18.53	24.48	16.78	19.24	38.41	0.00
Cor	1.74	0.00	0.00	1.95	0.74	0.79	0.51	0.00
Or	15.83	14.11	21.35	15.83	20.11	23.39	20.86	17.90
Ab	37.03	23.49	26.60	25.61	31.11	27.08	22.31	18.11
An	21.33	21.52	16.14	15.35	16.06	14.88	12.49	28.10
Ne	0.00	0.00	0.00	0.00	0.00	0.00	0.00	0.00
Di	0.00	4.02	1.20	0.00	0.00	0.00	0.00	4.50
Hy	12.53	15.57	7.90	12.11	8.66	7.32	2.97	16.26
Ol	0.00	0.00	0.00	0.00	0.00	0.00	0.00	9.35
Mt	2.49	3.82	2.46	2.41	1.87	1.71	0.71	3.05
Ilm	1.73	3.53	2.41	1.78	1.34	1.22	0.51	0.71
Ap	0.54	0.69	1.50	0.28	0.57	0.48	0.18	0.19
LOI	0.45	0.44	0.23	0.36	0.26	0.41	0.11	0.43
Sum	100.04	97.43	98.31	100.15	97.48	96.51	99.05	98.60

[1]quadrangle:
H=Hazelwood
LG=Lemon Gap
D=Dellwood

[2]lithology:
1=biotite augen gneiss and granitic gneiss
3=hornblende-biotite gneiss
5= migmatitic biotite gneiss

Appendix M (continued). Whole rock chemical compositions (XRF).

Sample	MV02-7	MV02-8	NB04-1B	OS03-1B	OS03-1GN	PK03-1	PK03-2	PK03-5
quad[1]	D	D	D	SN	SN	D	D	D
lithology[2]	2	1	1	1	1	1	1	1
SiO_2 (%)	64.91	64.83	65.29	71.52	70.32	62.55	67.85	67.05
TiO_2 (%)	0.85	0.73	0.69	0.18	0.39	0.54	0.40	0.65
Al_2O_3 (%)	14.86	16.27	16.09	14.78	14.26	17.56	14.42	15.09
$Fe_2O_3^T$ (%)	6.17	4.91	5.09	1.53	3.38	4.69	3.98	4.32
MnO (wt.%)	0.10	0.09	0.10	0.02	0.05	0.06	0.06	0.09
MgO (%)	1.75	1.63	1.78	0.27	0.73	0.88	0.93	1.34
CaO (%)	1.63	3.69	4.02	1.58	1.82	3.39	2.90	2.30
Na_2O (%)	1.83	3.68	3.63	3.37	3.28	2.93	2.36	3.58
K_2O (%)	3.37	3.58	2.82	4.76	4.20	4.58	4.84	3.62
P_2O_5 (%)	0.20	0.26	0.24	0.08	0.16	0.25	0.14	0.20
Ba (ppm)	879	1570	827	1512	1326	3589	2208	1114
V (ppm)	91	71	80	18	38	52	47	68
Cr (ppm)	334	178	104	238	500	379	246	149
Ni (ppm)	27	12	9	6	13	9	11	6
Ga (ppm)	22	20	22	21	21	21	19	22
Rb (ppm)	111	97	89	87	93	92	93	121
Y (ppm)	55	38	44	27	35	40	53	46
Zr (ppm)	302	252	189	133	238	320	188	223
Sr (ppm)	203	595	478	554	446	545	557	445
LOI (%)	1.09	0.27	0.57	0.46	0.88	1.42	0.43	0.89
Sum	96.97	100.20	100.49	98.79	99.74	99.35	98.65	99.33
CIPW norm calculated on the basis of $Fe^{2+}/Fe_{(total)}$=.75								
Qtz	33.46	18.28	20.82	29.57	29.29	18.29	26.80	24.39
Cor	5.72	0.24	0.32	1.41	1.38	2.23	0.38	1.57
Or	19.93	21.13	16.68	28.11	24.84	27.07	28.59	21.38
Ab	15.51	31.17	30.71	28.49	27.73	24.79	19.99	30.31
An	6.77	16.62	18.39	7.31	8.01	15.14	13.42	10.11
Ne	0.00	0.00	0.00	0.00	0.00	0.00	0.00	0.00
Di	0.00	0.00	0.00	0.00	0.00	0.00	0.00	0.00
Hy	9.51	8.07	8.72	1.99	4.74	6.23	5.86	6.88
Ol	0.00	0.00	0.00	0.00	0.00	0.00	0.00	0.00
Mt	2.24	1.78	1.85	0.55	1.23	1.70	1.44	1.56
Ilm	1.61	1.39	1.31	0.34	0.74	1.03	0.77	1.23
Ap	0.47	0.61	0.56	0.19	0.37	0.60	0.34	0.48
LOI	1.09	0.27	0.57	0.46	0.88	1.42	0.43	0.89
Sum	96.31	99.56	99.93	98.42	99.22	98.51	98.01	98.80

[1]quadrangle:
D=Dellwood
SN=Sylva North

[2]lithology:
1=biotite augen gneiss and granitic gneiss
2=muscovite-biotite gneiss

Appendix M (continued). Whole rock chemical compositions (XRF).

Sample	SC04-1	SC04-2	SC04-3	SC04-4	SC04-5	SC04-6	error	
quad[1]	D	D	D	D	D	D	2σ	
lithology[2]	1	1	1	1	1	1		
SiO_2 (%)	74.19	70.13	70.08	67.28	71.94	66.56	1.49	(wt%)
TiO_2 (%)	0.21	0.43	0.45	0.48	0.38	0.57	0.06	(wt%)
Al_2O_3 (%)	12.82	14.51	14.22	15.44	14.69	15.17	0.43	(wt%)
$Fe_2O_3^T$ (%)	2.62	3.07	3.06	3.88	3.72	3.64	0.37	(wt%)
MnO (wt.%)	0.04	0.06	0.06	0.05	0.05	0.06	0.01	(wt%)
MgO (%)	0.42	1.03	0.81	1.20	1.21	1.22	0.18	(wt%)
CaO (%)	1.36	2.59	2.44	2.53	4.13	2.14	0.14	(wt%)
Na_2O (%)	2.23	3.43	3.50	2.72	3.15	2.99	0.62	(wt%)
K_2O (%)	5.37	4.13	3.54	3.66	0.44	4.65	0.07	(wt%)
P_2O_5 (%)	0.07	0.12	0.15	0.19	0.14	0.19	0.03	(wt%)
Ba (ppm)	1233	692	880	1010	405	1990	153	(ppm)
V (ppm)	31	42	42	61	48	51	30	(ppm)
Cr (ppm)	953	237	164	225	235	170	24	(ppm)
Ni (ppm)	28	9	6	24	18	10	16	(ppm)
Ga (ppm)	19	21	21	22	21	21	8	(ppm)
Rb (ppm)	126	112	85	107	23	86	22	(ppm)
Y (ppm)	32	42	38	36	20	37	24	(ppm)
Zr (ppm)	156	160	204	190	200	225	64	(ppm)
Sr (ppm)	354	401	415	428	698	609	52	(ppm)
LOI (%)	0.76	0.39	0.56	1.34	0.89	0.86		
Sum	100.37	100.08	99.04	98.97	100.90	98.36		
CIPW norm calculated on the basis of $Fe^{2+}/Fe_{(total)}$=.75								
Qtz	36.24	26.48	29.01	29.26	40.20	24.15		
Cor	1.03	0.00	0.55	2.86	1.86	1.77		
Or	31.72	24.43	20.91	21.65	2.59	27.47		
Ab	18.84	28.99	29.63	23.01	26.64	25.33		
An	6.31	12.00	11.11	11.32	19.57	9.39		
Ne	0.00	0.00	0.00	0.00	0.00	0.00		
Di	0.00	0.03	0.00	0.00	0.00	0.00		
Hy	3.47	5.13	4.54	6.29	6.31	5.96		
Ol	0.00	0.00	0.00	0.00	0.00	0.00		
Mt	0.95	1.11	1.11	1.41	1.35	1.32		
Ilm	0.40	0.82	0.86	0.90	0.72	1.09		
Ap	0.16	0.29	0.35	0.45	0.34	0.45		
LOI	0.76	0.39	0.56	1.34	0.89	0.86		
Sum	99.88	99.68	98.64	98.48	100.46	97.77		

[1]quadrangle: D=Dellwood

[2]lithology: 1=biotite augen gneiss and granitoid gneiss

REFERENCES

Abbott R.N. and Raymond (1997), Petrology of pelitic and mafic rocks in the Ashe and Alligator Back Metamorphic Suites, northeast of the Grandfather Mountain window. In: K.G. Stewart, M.G. Adams, and C.H. Trupe (eds.), 1997 Field Trip Guidebook, Carolina Geological Society: Durham, 87-100.

Abbott R.N. and Greenwood J.P. (2001), Retrograde metamorphism of eclogite in the southern Appalachian Mountains, U.S.A.-A case involving seamount subduction? Journal of Metamorphic Geology, 19: 433-443.

Aceñolaza, F.G., and Toselli, A. (1976) Consideraciones estratigráficas y tectónicas sobre el Paleozoico inferior del noroeste argentino. 2 º. Congreso Latinoamericano de Geología*,* Actas, 2:755-763.

Aceñolaza, F.G, Miller, H., Toselli, A.J. (2002), Proterozoic-Early Paleozoic evolution in western South America – a discussion. Tectonophysics, 354: 121-137.

Adams M.G., Stewart K.G., Trupe C.H., and Willard R.A. (1995), Tectonic significance of high-pressure metamorphic rocks and dextral strike-slip faulting along the Taconic suture. In: Hibbard J.P., van Staal C.R., and Cawood P.A. (eds.) Current Perspectives in the Appalachian-Caledonian Orogen. Geological Association of Canada, Special Paper, 41: 21-42.

Adams, M.G., and Trupe, C.H., (1997), Conditions and timing of metamorphism in the Blue Ridge thrust complex, northwestern North Carolina and eastern Tennessee. In: Stewart, K.G., Adams, M.G., and Trupe, C.H., (eds.), 1997 Field Trip Guidebook, Carolina Geological Society: Durham, 33-48.

Aleinikoff, J.N., Zartman, R.E., Walter, M., Rankin, D.W., Lyttle, P.T., and Burton, W.C. (1995), U–Pb ages of metarhyolites of the Catoctin and Mount Rogers Formations, central and southern Appalachians: Evidence for two pulses of Iapetan rifting. American Journal of Science 295: 428-454.

Aleinikoff, J.N., Horton, J.W., Jr., Drake, A.A., Jr., and Fanning, C.M. (2002), SHRIMP and Conventional U-Pb ages of Ordovician granites and tonalites in the central Appalachian Piedmont: Implications for Paleozoic tectonic events. American Journal of Science, 302: 50-75; doi:10.2475/ajs.302.1.50

Aleinikoff, J.N., Wintsch, R.P., Horton, J.W., Jr., Drake, A.A., Jr., and Fanning, C.M. (2004), Deciphering Mesoproterozoic and Paleozoic events preserved in the isotopic compositions of zircon and titanite; SEM imaging, SHRIMP U-Pb geochronology, and EMP analysis. Geological Society of America Abstracts with Programs, 36, 2, 80.

Aleinikoff, J.N., Southworth, S., and Kunk, M.J. (2007), SHRIMP U-Pb geochronology of zircon and titanite and 40Ar/39Ar of hornblende and muscovite from Mesoproterozoic rocks of the western Blue Ridge, Great Smoky Mountains National Park Area, TN and NC. Geological Society of America, Abstracts with Programs, 27-6.

Amato J.M., Johnson C.M., Baumgartner L.P., and Beard B.L. (1999), Rapid exhumation of the Zermatt-Saas ophiolite deduced from high-precision Sm-Nd and Rb-Sr geochronology. Earth and Planetary Science Letters, 171:425-438.

Andersen T.B., Jamveit B., Dewey J.F., and Swensson, E. (1991), Subduction and eduction of continent crust: major mechanisms during continent-continent collision and orogenic extensional collapse, a model based on the south Norwegian Caledonides. Terra Nova, 3:303-310.

Anderson, E.D., and Moecher, D.M. (2007), Omphacite breakdown reactions and relation to eclogite exhumation rates, Contributions to Mineralogy and Petrology, 154: 253-277, doi: 10.1007/s00410-007-0192-x.

Anderson, E. D., and D. P. Moecher (2009), Formation of high-pressure metabasites in the southern Appalachian Blue Ridge via Taconic continental subduction beneath the Laurentian margin, Tectonics, 28, TC5012, doi:10.1029/2008TC002319.

Astini, R.A., Thomas, W.A., (1999), Origin and evolution of the Precordillera of western Argentina: a drifted Laurentian orphan. In: Ramos, V.A., Keppie, J.D. (eds.), Laurentia–Gondwana Connections Before Pangea. Geological Society of America Special Paper 336: 1- 20.

Badger, R.L., and Sinha, K.A. (1988), Age and Sr-isotopic signature of the Catoctin volcanic province: Implications for sub-crustal mantle evolution. Geology, 16: 692-695.

Baldo, E.G., Casquet, C., Pankhurst, R.J., et al. (2006), Neoproterozoic A-type magmatism in the Western Sierras Pampeanas (Argentina): evidence for Rodinia break-up along a proto-Iapetus rift? Terra Nova, 18: 388-394.

Baldwin S.L., Monteleone B.D., Webb L.E., Fitzgerald P.G., Grove M., and Hill E.J. (2004), Pliocene eclogite exhumation at plate tectonic rates in eastern Papua New Guinea. Nature, 431:263-267.

Banno, S. (1970), Classification of eclogites in terms of physical conditions of their origin, Physics of the Earth and Planetary Interiors, 3: 405-421.

Barineau, C.I., Holm-Denoma, C.S., and Tull, J.F. (2008), An Ordovician accretionary orogen in the southern Appalachians: Part 2. Tectonic model: Geological Society of America Abstracts with Programs, 40, 6, p. 450.

Barker, D.S. (1983), Igneous Rocks. Prentice-Hall, Incorporated: Englewood Cliffs, New Jersey.

Bartholomew, M.J., and Lewis, S.E. (1988), Peregrination of middle Proterozoic massifs and terranes within the Appalachian orogen, eastern USA. Trabajosde Geología, 17: 155–165.

Bartholomew, M.J., and Lewis, S.E. (1992), Appalachian Grenville massifs: Pre-Appalachian translational tectonics. In: R.Mason (ed.), Basement tectonics 7: Dordrecht, The Netherlands, Kluwer Academic Publishers, 363–374.

Berman, R.G. (1988), Internally-consistent thermodynamic data for minerals in the system Na_2O-K_2O-CaO-MgO-FeO-Fe_2O_3-Al_2O_3-SiO_2-TiO_2-H_2O-CO_2. Journal of Petrology, 29:445-522.

Berman, R.G. (1990), Mixing properties of Ca-Mg-Fe-Mn garnets. American Mineralogist, 75:328-344.

Berman, R.G., Aranovich, L.Y, and Pattison, D.R.M. (1995), Reassessment of the garnet-clinopyroxene Fe−Mg exchange thermometer: II. Thermodynamic analysis. Contributions to Mineralogy and Petrology, 119:30-42.

Berman, R.G. and Aranovich, L.Y. (1996), Optimized standard state and solution properties of minerals. I. Model calibration for olivine, orthopyroxene, cordierite, garnet, and ilmenite in the system Feo-MgO-CaO-Al_2O_3-TiO_2-SiO_2. Contributions to Mineralogy and Petrology, 126: 1-24.

Bernard-Griffiths, J., and Jahn, B.M. (1981), REE geochemistry of eclogites and associated rocks from Sauviat-sur-Vige, Massif Central, France, Lithos, 14(4): 263-274.

Berquist, P.J., Miller, C., Wooden, J., Fullagar, P., Ownby, S., and Carrigan, C. (2003), The Mars Hill terrane: extent, age, and origin of the oldest rocks in the southeastern USA. Geological Society of America Abstracts with Programs, 35 (1) 19.

Berquist, P. J., Fisher, C. M., Miller, C. F., Wooden, J. L., Fullagar, P. D., and Loewy, S. L., 2005, Geochemistry and U-Pb zircon geochronology of Blue Ridge basement, western North Carolina and eastern Tennessee: Implications for tectonic assembly. In: R.D. Hatcher Jr., and A.J. Merschat (eds.), 2005 Field Trip Guidebook, Carolina Geological Society: Durham, 33-44.

Bettencourt, J.S., Tosdal, R.M., Leite, W.B., Jr., and Payola, B.L. (1999), Mesoproterozoic rapakivi granites of the Rondônia Tin Province, southwestern border of the Amazonian craton, Brazil- I.Reconnaissance U–Pb geochronology and regional implications. Precambrian Research 95: 41-67.

Bird, J.M., and Dewey, J.F. (1970), Lithosphere plate-continental margin tectonics and the evolution of the Appalachian orogen, Geolical Society of America Bulletin, 81: 1031-1060, doi: 10.1130/0016-7606(1970)81[1031:LPMTAT]2.0.CO;2

Blümel, P. (1983), The western margin of the Bohemian Massif in Bavaria, Fortschritte der Mineralogie, 61: 171-195.

Blümel, P. (1986), Metamorphic processes in the Variscan crust of the central segment, In: R. Freeman et al. (eds.), Proceedings of the 3rd workshop on the European Geotraverse (EGT) Project: The Central segment, 149-155, European Science Foundation: Strassbourg.

Boger, S.D., Raetz, A., Giles, D., Etchart, E., and Fanning, C.M. (2005), U-Pb age data from the Sunsás region of Eastern Bolivia, evidence for the allochthonous origin of the Paragua Block: Precambrian Research, 139(3–4): 121–146.

Boland, J.N., and van Roermund, H.L.M. (1983), Mechanisms of exsolution in omphacites from high temperature, type B, eclogites. Physics and Chemistry of Minerals, 9: 30-37.

Bream, B.R., Hatcher, R.D., Jr., Miller, C.F., and Fullagar, P.D. (2004), Detrital zircon ages and Nd isotopic data from the southern Appalachian crystalline core, Georgia, South Carolina, North Carolina, and Tennessee: New provenance

constraints for part of the Laurentian margin. In: R.P.Tollo et al.(eds.), Proterozoic tectonic evolution of the Grenville orogen in North America: Geological Society of America Memoir 197: 459–475, doi: 10.1130/0-8137-1197-5.459.

Brewer, M.C., and Thomas, W.A., (2000), Stratigraphic evidence for Neoproterozoic-Cambrian two-phase rifting of southern Laurentia. Southeastern Geology, 39, no 2: 91-106.

Brewer, R.C., and Woodward, N.B. (1988), The amphibolitic basement complex in the Blue Ridge Province of western North Carolina, Proto-Iapetus? American Journal of Science, 288: 953–967.

Briand, B., Piboule, M., and Bouchardon, J-L. (1988), Diversité géochemique des métabasites des groupes leptyno-amphiboliques du Rougergue et de marvejois (Massif central). Origine et implications, Bulletin de la Societe géologique France, 8(IV), 489-498.

Brito Neves, B.B., Campos Neto, M.C., Fuck, R.A., (1999), From Rodinia to Western Gondwana: An approach to the Brasiliano-Pan African cycle and orogenic collage. Episodes 22, 155–166.

Brown, W.R. (1970), Investigations of the sedimentary record in the Piedmont and Blue Ridge of Virginia, In: G.W. Fisher et al., (eds.) Studies of Appalachian Geology – Central and Southern*,* 335-349, Wiley-Interscience: New York.

Brueckner, H.K., and Medaris, L.G. (2000), A general model for the intrusion of 'mantle' garnet peridotites in high-pressure and ultra-high-pressure metamorphic terranes, Journal of Metamorphic Geology, 18: 123-133, doi: 10.1046/j.1525-1314.2000.00250.x

Bucher, K., Fazis, Y., De Capitani, C., and Grapes, R. (2005), Blueschists, eclogites and decompression assemblages of the Zermatt-Saas ophiolite: High-pressure metamorphism of subducted Tethys lithosphere. American Mineralogist, 90: 821-835.

Carrigan, C.W., Miller, C.F., Fullagar, P.D., Hatcher, R.D., Jr., Bream, B.R., and Coath, C.D. (2003), Ion microprobe age and geochemistry of southern Appalachian basement, with implications for Proterozoic and Paleozoic reconstructions. Precambrian Research, 120:1–36, doi: 10.1016/S0301-9268(02)00113-4.

Carswell, D.A. (1990), Eclogites and the eclogite facies: definitions and classification, In: D.A Carswell (ed.) Eclogite facies rocks, Chapman and Hall: New York, 1-13

Carswell, D.A., and Jamtveit, B. (1990), Variscan Sm-Nd ages for the high-pressure granulites: examples from the Moldanubian Zone of the Bohemian Massif in Lower Austria. Neues Jahrbuch für Mineralogie, 162: 69-78.

Casquet, C., Rapela, C.W., Pankhurst, R.J., Galindo, C., Dahlquist, J., Baldo, E.G., Saavedra, J., González Casado, J.M., Fanning, C.M., (2004). Grenvillian massif-type anorthosites in the Sierras Pampeanas. Journal of the Geological Society, London 162: 9-12.

Casquet, C., Fanning, C.M., Galindo, C., Pankhurst, R.J., Rapela, C.W., and Torres, P. (2010), The Arequipa Massif of Peru: New SHRIMP and isotope constraints on a

Paleoproterozoic inlier in the Grenville orogen. Journal of South American Earth Sciences, 29: 128-142. doi: 10.1016/j.sames.2009.08.009
Cawood, P.A., McCausland, P.J.A., and Dunning, G.R., (2001), Opening Iapetus: constraints from the Laurentian margin of Newfoundland. Geological Society of America Bulletin, 113(4): 443-453.
Cawood, P.A., Pisarevsky, S.A., 2006. Was Baltica right-way-up or upside-down in the Neoproterozoic? Journal of the Geological Society, London, 163: 1-7.
Chakraborty, S., Moecher, D.P., Samson, S.D., and Loughry, D. (2010), Provenance analysis of the Neoproterozoic Ocoee Supergroup eastern Great Smoky Mountains, NC/TN. Geological Society of America Abstracts with Programs, 42, 1, 58.
Chakraborty, S., Moecher, D.P., and Samson, S.D. (2011), Provenance of the Ocoee Supergroup, Journal of Geology, in submission.
Chernicoff, C.J., Zappettini, E.O., Villar, L.M., Hernández, F.C., Jr. (2009), The belt of metagabros of La Pampa: Lower Paleozoic back-arc magmatism in southcentral Argentina. Journal of South American Earth Sciences, 28(4): 383–397.
Chew, D.M., Schaltegger, U., Kosler, J., Whitehouse, M., Gutjahr, M., Spikings, R.A., and Mišković, A. (2007), U-Pb geochronologic evidence for the evolution of the Gondwanan margin of the north-central Andes. Geological Society of America Bulletin, 119(5/6): 697-711, doi: 10.1130/B26080.1
Chew, D.M., Cardoni, A., and Mišković, A. (2010), Tectonic evolution of western Avalonia from the assembly of Rodinia to its break-up. International Geology Review, iFirst article, 1-12.
Church W.R. (1969), Metamorphic rocks of the Burlington Penninsula and adjoining areas of Newfoundland and their bearing on continental drift in the North Atlantic. In: M. Kay (ed.), North Atlantic Geology and Continental Drift. American Association of Petroleum Geologists Memoir 12: 212-233.
Clemons, K.M., and Moecher, D.P. (2009), Reinterpretation of the Greenbrier fault, Great Smoky Mountains: New petrofabric constraints and implications for southern Appalachian tectonics. Geological Society of America Bulletin, 121(7-8): 1108-1122. doi: 10.1130/B26480.1
Coakley, B., and Gurnis, M. (1995), Far-field tilting of Laurentia during the Ordovician and constraints on the evolution of a slab under an ancient continent. Journal of Geophysical Research, 100(B4): 6313-6327.
Cobbing, E.J., Ozard, J.M., and Snelling, N.J. (1977), Reconaissance geochronology of the crystalline basement rocks of the Coastal Cordillera of southern Peru. Geological Society of America Bulletin, 88: 241-246.
Coira, B., Davidson, J., Mpodozis, C., and Ramos, V. (1982), Tectonic and magmatic evolution of the Andes Northern Argentina and Chile. Earth Science Reviews, 18: 303-332.
Coleman, R.G., Lee, D.E., Beatty, L.B., and Brannock, W.W. (1965), Eclogites and eclogites: their differences and similarities. Geological Society of America Bulletin, 76: 483-508, doi: 10.1130/0016-7606(1965)76[483:EAETDA]2.0.CO;2

Coler, D. G., Samson, S. D., and Hibbard, J. P., (1998), New constraints on the age and Nd isotopic composition of the Chopawamsic terrane, VA. Geological Society of America Abstracts with Programs, v. 30, no. 7, A-125.

Collo G., Astini R.A., Cawood P., Buchan C., Pimentel M. (2009), U-Pb detrital zircon ages and Sm-Nd isotopic features in low-grade metasedimentary rocks of the Famatina belt: implications for late Neoproterozoic-Early Paleozoic evolution of the proto-Andean margin of Gondwana. Journal of the Geological Society of London 166:303–319.

Connelly, J.B., and Dallmeyer, R.D. (1993), Polymetamorphic evolution of the western Blue Ridge: evidence from $^{40}Ar/^{39}Ar$ whole-rock slate/phyllite and muscovite ages. American Journal of Science, 293: 322-359.

Conti C.M., Rapalini A.E., Coira, B., Koukharsky, M. (1996), Paleomagnetic evidence of an early Paleozoic rotated terrane in Northwestern Argentina, a clue for Gondwana–Laurentia interaction? Geology 24: 953-956.

Cook, F.A., Albaugh, D.S, Brown, L.D., Kaufman, S., Oliver, J.E., and Hatcher, R.D., Jr. (1979), Thin-skinned tectonics in the crystalline southern Appalachians; COCORP seismic-reflection profiling of the Blue Ridge and Piedmont. Geology, 7: 563-567, doi: 10.1130/0091-7613(1979)7<563:TTITCS>2.0.CO;2

Cook, F.A., Brown, L.D., Kaufman, S, Oliver, J.E., and Petersen, T.A. (1981), COCORP seismic profiling of the Appalachian orogen beneath the Coastal Plain of Georgia. Geological Society of America Bulletin, 92: 738-748.

Cook, F.A., and Vausdevan, K. (2006), Reprocessing and enhanced interpretation of the initial COCORP Southern Appalachian traverse. Tectonophysics, 420: 161-174, doi:10.1016/j.tecto.2006.01.022

Copeland, P., Parrish, R.R., and Harrison, T.M. (1988), Identification of inherited radiogenic Pb in monazite and its implication for U-Pb systematics. Nature, 333: 760-763.

Cordani, U.G., and Sato, K, (2000), Crustal evolution of the South American Platform, based on Nd isotopic systematics on granitoid rocks. Episodes, v. 22, no. 3: p.167-173.

Cordani, U.G., Teixeira, W., Tassinari, C.G.C., Coutinho, J.M.V., and Ruiz, A.S. (2010), The Rio Apa Craton in Mato Grosso do Sul (Brazil) and northern Paraguay; geochronological evolution, correlations and tectonic implications for Rodinia and Gondwana (*in* Alfred Kroener special issue; Part I) American Journal of Science, 310(9): 981-1023.

Corfu, F., Hanchar, J.M., Hoskin, P.W.O., and Kinny, P. (2003), Atlas of zircon textures. In: Hanchar J.M, Hoskin P.W.O. (eds.), Zircon. Reviews in Mineralogy and Geochemistry, v. 53, Mineralogical Society of America, 469-500; DOI: 10.2113/0530469

Corfu, F., Krogh Ravna, E., and Kullerud, K. (2002), A Late Ordovician U-Pb age for HP metamorphism of the Tromsdalstind eclogite in the uppermost allochthon of the Scandinavian Caledonides. Goldschmidt Conference Abstracts, A153

Costa, S., Maluski, H., and Lardeaux, J., -M. (1993), $^{40}Ar/^{39}Ar$ chronology of Variscan tectono-metamorphic events in an exhumed crustal neppe: the Monts du Lyonnais complex (Massif Central, France). Chemical Geology, 105: 339-359.

Cotkin S.J., Valley J.W., and Essene, E.J. (1988), Petrology of a margarite-bearing meta-anorthosite from Seljeneset, Nordfjord, western Norway: Implications for the P-T history of the Western Gneiss Region during Caledonian uplift. Lithos, 21:117-128.

Cuthbert, S.J., Harvey, M.A., and Carswell, D.A. (1983), A tectonic model for the metamorphic evolution of the basal gneiss complex, western south Norway. Journal of Metamorphic Geology, 1: 63-90.

Cuthbert S.J., Carswell D.A., Krogh-Ravna E.J., and Wain A. (2000), Eclogites and eclogites in the Western Gneiss Region, Norwegian Caledonides. Lithos, 52:165-195. doi:10.1016/S0024-4937(99)00090-0.

D'Agrella-Filho, M.S., Tohver, E., Santos, J.O.S., Elming, S.-Å., Trindade, R.I.F., Pacca, I.I.G., and Geraldes, M.C. (2008), Direct dating of paleomagnetic results from Precambrian sediments in the Amazon Craton: Evidence for Grenvillian emplacement of exotic crust in SE Appalachians of North America. Earth and Planetary Science Letters, 267 (1–2): 188–199.

Dalla Salda, L.H., Cingolani, C., and Varela, R. (1992a), Early Paleozoic orogenic belt of the Andes in southwestern South America: Results of Laurentia-Gondwana collision? Geology, 20: 617-620.

Dalla Salda, L.H., Dalziel, I.W.D., Cingolani, C.A., and Varela, R. (1992b), Did the Taconic Appalachians continue into southern South America? Geology 20: 1059-1062.

Dallmeyer, R.D. (1974), Eclogite inclusions in an alpine peridotite sill, Georgia-North Carolina: their chemistry and petrogenetic evolution, American Journal of Science, 274: 356-377.

Dallmeyer, R.D. (1975), Incremental $^{40}Ar/^{39}Ar$ ages of biotite and hornblende from rretrograde basement gneisses of the southern Blue Ridge: Their bearing on the age of Paleozoic metamorphism. American Journal of Science, 275: 444-460.

Dallmeyer, R.D., Wright, J.E., Secor, D.T., Jr., and Snoke, A.W. (1986), Character of the Alleghanian orogeny in the southern Appalachians: Part II. Geochronological constraints on the tectonothermal evolution of the east Piedmont in South Carolina. Geological Society of America Bulletin, 97: 1329-1344.

Dallmeyer, R.D. (1988), Late Paleozoic tectonothermal evolution of the western Piedmont and eastern Blue Ridge, Georgia: controls on the chronology of terrane accretion and transport in the Southern Appalachian Orogen. Geological Society of America Bulletin, 100: 702-713.

Dallmeyer, R.D., Neubauer, F., and Höch, V. (1992), Chronology of late Paleozoic tectonothermal activity in the southeastern Bohemian Massif, Austria (Moldanubian and Moravo-Silesian zones) $^{40}Ar/^{39}Ar$ mineral age controls. Tectonophysics, 210: 135-153.

Dalziel, I.W.D. (1991), Pacific margins of Laurentia and East Antarctica–Australia as a conjugate rift pair: evidence and implications for an Eocambrian supercontinent. Geology 19: 598-601.

Dalziel, I.W.D. (1997), Neoproterozoic-Paleozoic geography and tectonics: review, hypotheses, environmental speculation. Geological Society of America Bulletin 109: 16-42.

Dalziel, I.W.D., and Soper, N.J. (2001), Neoproterozoic extension on the Scottish Promontory of Laurentia; paleogeographic and tectonic implications. Journal of Geology 109: 299-317.

Damm, K.W., Pichowiak, S., Harmon, R.S., Todt, W., Kelley, S., Omarini, R., and Niemeyer, H. (1990), Pre-Mesozoic evolution of the central Andes; The basement revisited. In: S.M. Kay and C.W. Rapela (eds.), Plutonism from Antarctica to Alaska, Geological Society of America Special Paper 241:101–125.

Davies, J.H., and von Blanckenburg, F. (1995), Slab break off: a model of lithospheric detachment and its test in the magmatism and deformation of collisional orogens. Earth and Planetary Science Letters, 129: 85-102.

Day, H.W. and Mulcahy S.R. (2007), Excess silica in omphacite and the formation of free silica in eclogite. Journal of Metamorphic Geology, 25: 37-50.

Dennis, A.J. (1991), Is the central Piedmont suture a low-angle normal fault? Geology,19: 1081–1084, doi: 10.1130/0091-7613(1991)019 <1081:ITCPSA>2.3.CO;2.

Dennis, A.J., (2007), Cat Square basin, Catskill clastic wedge: Silurian-Devonian orogenic events in the central Appalachians and the crystalline southern Appalachians, In: Sears, J.W., Harms, T.A., and Evenchick, C.A., (eds.), Whence the Mountains? Inquiries into the Evolution of Orogenic Systems: A Volume in Honor of Raymond A. Price: Geological Society of America Special Paper 433, 313–329, doi: 10.1130/2007.2433(15).

Dennis, A.J., and Wright, J.E. (1997a), Middle and late Paleozoic monazite U-Pb ages, Inner Piedmont, South Carolina. Geological Society of America Abstracts with Programs, 29, 3, 12.

Dennis, A.J., and Wright, J.E. (1997b), The Carolina terrane in northwestern South Carolina, U.S.A.: Late Precambrian–Cambrian deformation and metamorphism in a peri-Gondwanan oceanic arc. Tectonics, 16: 460–473, doi: 10.1029/97TC00449.

DePaolo, D.J. (1980), Crustal growth and mantle evolution: inferences from models of element transport and Nd and Sr isotopes. Geochimica et Cosmochimica Acta, 44: 1185-96.

DeWindt, J.T. (1975), Geology of the Great Smoky Mountains, Tennessee and North Carolina, with road log for field excursion, Knoxville - Clingmans dome – Maryville. Compass, 52: 73-129.

Dobrzhinetskaya, L.F., Eide, E.A., Larsen, R.B., Sturt, B.A., Tronnes, R.G., Smith, D.C., Taylor, W.R., and Poskhovar, T.V. (1995), Microdiamond in high-grade metamorphic rocks of the Western Gneiss Region, Norway. Geology, 23: 597-600, doi: 10.1130/0091-7613(1995)023<0597:MIHGMR>2.3.CO;2

Droop G.T.R. (1987) A general equation for estimating Fe^{3+} concentrations in ferromagnesian silicates and oxides from microprobe analyses, using stoichiometric criteria. Mineralogical Magazine, 51:431-435.

Droop G.T.R., Lombardo, B., and Pognante, U. (1990), Formation and distribution of eclogite facies rocks in the Alps. In: D.A. Carswell (ed.) Eclogite Facies Rocks. Chapman and Hall: New York. 225-259.

Drummond, M.S., Allison, D.T., and Wesolowski, D.J. (1994), Igneous petrogenesis and tectonic setting of the Elkahatchee Quartz Diorite, Albama Appalachians: Implications for Penobscotian magmatism in the eastern Blue Ridge. American Journal of Science, 294: 173-236.

Dufour, E. (1985), Granulite facies metamorphism and retrogressive evolution of the Monts du Lyonnais metabasites (Massif Central, France). Lithos, 18: 97-113.

Dunn S.R. and Medaris L.G. Jr. (1989), Retrograded eclogites in the Western Gneiss Region, Norway, and thermal evolution of a portion of the Scandinavian Caledonides. Lithos, 22:229-245.

Eckert, J.O., Jr. (1984), Stratigraphy, structure, and metamorphism of the eastern half of the Wayah bald quadrangle, North Carolina: Evidence for granulite facies metamorphism in the southern Appalachians. M.S. thesis, University of South Carolina, Columbia, 411 p.

Eckert, J.O., Jr. (2002), Monazite EMPA dates from the amphibolite-granulite metamorphic progression to the Wayah granulite core, western North Carolina: confirmation of Taconian peak metamorphism. Geological Society of America Abstracts with Programs, 37-0.

Eckert, J.O. Jr., Hatcher, R.D., Jr., and Mohr, D.W. (1989), The Wayah granulite-facies metamorphic core, southwestern North Carolina: High-grade culmination of Taconic metamorphism in the southern Blue Ridge. Geological Society of America Bulletin, 101: 1434-1447, doi: 10.1130/0016-7606(1989)101<1434:TWGFMC>2.3.CO;2.

Emilio, M.C. (1998), Metamorphic evolution of the Buck Creek mafic-ultramafic complex, Clay County, North Carolina, USA. MS thesis, University of South Florida, Tampa.

Engvik, A.K., Austrheim, H., and Andersen, T.B. (2000), Structural mineralogical and petrophysical effects on deep crustal rocks of fluid-limited polymetamorphism, Western Gneiss Region, Norway. Journal of the Geological Society of London, 157: 121-134.

Ernst, W.G. (1988), Tectonic history of subduction zones inferred from retrograde blueschist P-T paths. Geology, 16: 1081-1084, doi: 10.1130/0091-7613(1988)016<1081:THOSZI>2.3.CO;2

Ernst, W.G. (2006), Preservation/exhumation of ultrahigh-pressure subduction complexes. Lithos, 92: 321-335, doi: 10.1016/j.lithos.2006.03.049

Eskola P. (1921) On the eclogites of Norway. Videnskapsselskapets Skrifter, I Mat-Naturv Klasse, 8:1-118.

Faure, G. (1986), Principles of isotope geology. Wiley and Sons: New York.

Fisher, C.M., Loewy, S.L., Miller, C.F., Berquist, P., Van Schmus, W.R., Hatcher, R.D., Jr., Wooden, J.L., and Fullagar P.D. (2010), Whole-rock Pb and Sm-Nd isotopic constraints on the growth of southeastern Laurentia during Grenvillian orogenesis. Geological Society of America Bulletin, 122(9-10):1646-1659.

Forsythe, R.D., Davidson, I., Mpodozis, C., Jesinskey, C. (1993), Paleozoic relative motion of the Arequipa block and Gondwana: paleomagnetic evidence from Sierra de Almeida of northern Chile. Tectonics 12: 219-236.

Franz, G., Thomas, S., and Smith, D.C. (1986), High pressure phengite decomposition in the Weissenstein eclogite, Münchberg Gneiss Massif, Germany. Contributions to Mineralogy and Petrology, 92: 71-85, doi: 10.1007/BF00373964

Frost, B.R., Barnes, C.G., Collins, W.J., Arculus, R.J., Ellis, D.J., and Frost, C.D. (2001), A geochemical classification of granitic rocks. Journal of Petrology, 42: 2033–2048, doi: 10.1093/petrology/42.11.2033

Frost, R.B., and Frost, C.D. (2008), A geochemical classification for feldspathic igneous rocks. Journal of Petrology, 49: 1955-1969, doi:10.1093/petrology/egn054

Frost, B. R., and Lindsley, D. H. (1992). Equilibria among Fe-Ti oxides, pyroxenes, olive, and quartz: Part II. Application. American Mineralogist, 77: 1004-1020.

Fuhrman, M.L. and Lindsley D.H. (1988), Ternary-feldspar modeling and thermometry. American Mineralogist, 73: 201-215.

Fullagar, P.D., and Odom, A.L. (1973), Geochronology of Precambrian gneisses in the Blue Ridge Province of northwestern North Carolina and adjacent parts of Virginia and Tennessee. Geological Society of America Bulletin, 84: 3065-3080.

Fullagar, P.D., Hatcher, R.D., Jr., and Merschat, C.E. (1979), 1200 m.y.-old gneisses in the Blue Ridge province of North and South Carolina. Southeastern Geology, 20: 69-77.

Gasparik, T. (1986) Experimental study of subsolidus phase relations and mixing properties of clinopyroxene in the silica-saturated system CaO-MgO-Al_2O_3-SiO_2. American Mineralogist, 71:686-693.

Gaugh, S.J. (2002), Subduction-related metamorphism, structure and tectonic evolution of the Kohistan-arc and Main Mantle thrust zone, Pakistan Himalaya. Ph.D. thesis, Oxford University, 250 p.

Gibbons, W., Waters, C., and Warburton, J. (1986), The blueschist facies schistes lustres of Alpine Corsica: a review. Geological Society of America Memoirs, 164: 301-12.

Gilotti, J.A., and McClelland, W.C. (2007), Characteristics of, and a tectonic model for, ultrahigh-pressure metamorphism in the overriding plate of the Caledonian orogen. International Geology Review, 49: 777-797, doi: 10.2747/0020-6814.49.9.777

Goldberg, S.A., Butler, J.R., and Fullagar, P.D. (1986), The Bakersville dike swarm: Geochronology and petrogenesis of Late Proterozoic basaltic magmatism in the Southern Appalachian Blue Ridge. American Journal of Science, 286: 403-430.

Griffin, W.L. and Råheim, A. (1973), Convergent metamorphism of eclogites and dolerites, Kristiansund area, Norway. Lithos, 6:21-40.

Griffin, W.L., Austrheim, H., Brastad, K., Bryhni, I., Krill, A.G., Krogh, E.J., Mork, M.B.E., Qvale, H., and Torudbakken, B. (1985), High-pressure metamorphism in the Scandanavian Caledonides. In: D.G.Gee and B.A. Sturt (eds.), the Caledonide Orogen-Scandinavian and Related Areas, vol. 2, John Wiley and Sons: Chichester, UK. 783-801.

Grove, M., and Harrison, T.M. (1999) Monazite Th-Pb age depth profiling. Geology, 27: 487-490.

Guthrie, G.M., Steltenpohl, M.G., and Gastaldo, R.A. (1995), Alleghanian timing constraints on Laurentian margin orogenesis: new fossils and radiometric data from the Alabama Blue Ridge. In: Guthrie, G.M. (ed.), The timing and tectonic mechanisms of the Alleghanian orogeny, Alabama Piedmont. Alabama Geological Society 32nd annual field trip guidebook. Tuscaloosa, AL, p. 1-15.

Hacker B.R., Calvert, A., Zhang, R.Y., Ernst, G.W., and Liou J.G. (2003), Ultrarapid exhumation of ultrahigh-pressure diamond-bearing metasedimentary rocks of the Kokchetav Massif, Kazakhstan? Lithos, 70: 61-75.

Hadley, J.B., and Goldsmith, R. (1963), Geology of the eastern Great Smoky Mountains, North Carolina and Tennessee. U.S. Geological Survey Professional Paper 349-B, 118p.

Hanan, B.B. and Sinha, A.K. (1989), Petrology and tectonic affinity of the Baltimore mafic complex, Maryland. Geological Society of America Special Paper 231, 1-18.

Harrison, T.M., McKeegan, K., and LeFort, P. (1995), Detection of inherited monazite in the Manaslu leucogranite by 232Th-208Pb ion microprobe dating: Crystallization age and tectonic implications. Earth and Planetary Science Letters, 133: 271–282, doi: 10.1016/0012-821X(95)00091-P.

Harrison, T. M., Grove, M., McKeegan, K. D., Coath, C. D., Lovera, O. M., and LeFort, P. (1999), Origin and episodic emplacement of the Manaslu intrusive complex: Journal of Petrology, 40: 3–19.

Hatcher, R.D., Jr. (1978), Tectonics of the western Piedmont and Blue Ridge, southern Appalachians: Review and speculation. American Journal of Science, 278: 276-304.

Hatcher, R.D., Jr. (1989), Tectonic synthesis of the U.S. Appalachians. In: R.D. Hatcher Jr. et al. (eds.), The Appalachian-Ouachita Orogen in the United States, The Geology of North America (v. F-2), Geological Society of America, Boulder, 511-535

Hatcher, R.D., Jr. (2002), An Inner Piedmont primer. In: Hatcher, R.D., Jr., and Bream, B.R. (eds.), Field Trip Guidebook, Carolina Geological Society: Durham, 1-18.

Hatcher, R.D., Jr., and Butler, J.R., (1979), Guidebook for Southern Appalachian Field Trip in the Carolinas, Tennessee and Northeastern Georgia: Blacksburg, Virginia, International Geological Correlation Program, Caledonide Orogen Program Symposium, 117 p.

Hatcher, R.D. Jr., Bream, B.R., Miller, C.L, Eckert, J.O. Jr., Fullagar, P.D., and Carrigan,C. (2004), Paleozoic structure of Southern Appalachian Blue Ridge

Grenvillian internal basement massifs. In: R.P. Tollo et al. (eds.), Proterozoic evolution of the Grenville orogen in North America, Geological Society of America Memoir 197: 525-547.
Hatcher, R.D., Jr., Merschat, A.J., and Thigpen, J.R. (2005), Blue Ridge Primer. In: R.D. Hatcher Jr. and A.J. Merschat (eds.), 2005 Field Trip Guidebook, Carolina Geological Society: Durham, 1-24.
Hatcher, R.D., Jr. (2010), The Appalachian orogen: A brief summary. In: Tollo, R.P., et al. (eds.), From Rodinia to Pangea: the Lithotectonic Record of the Appalachian Region: Geological Society of America Memoir 206: 1-19. doi: 10.1130/2010.1206(01)
Heinrich, C.A. (1982), Kyanite-eclogite to amphibolite facies evolution of hydrous mafic and pelitic rocks, Adula Nappe, Central Alps. Contributions to Mineralogy and Petrology, 81:30-38.
Hibbard, J.P. (2000), Docking Carolina. Geology 28: 127-130.
Hibbard, J.P., Stoddard, E.F., Secor, D.T., and Dennis, A.J. (2002), The Carolina Zone: Overview of Neoproterozoic to early Paleozoic peri-Gondwanan terranes along the eastern flank of the southern Appalachians. Earth Science Reviews, 57: 299-339.
Hibbard, J.P., van Staal, C.R., and Rankin, D.W. (2007), A comparative analysis of pre-Silurian crustal building blocks of the northern and the southern Appalachian orogen. American Journal of Science, 307: 23-45.
Hibbard, J.P., van Staal, C.R., and Rankin, D.W. (2010), Comparative analysis of the geological evolution of the northern and southern Appalachian orogen: Late Ordovician-Permian. In: R.P.Tollo, M.J. Bartholomew, J.P. Hibbard, and P.M. Karabinos, (eds.), From Rodinia to Pangea: The Lithotectonic Record of the Appalachian Region: Geological Society of America Memoir 206, Boulder, 51-69, doi: 10.1130/2010.1206(26).
Hietpas, J., Samson, S., Moecher, D.P., and Schmitt, A. (2010), Recovering tectonic events from the sedimentary record: Detrital monazite plays in high fidelity. Geology, 38 (2): 167-170, doi: 10.1130/G30265.1
Higgins, M. W., Sinha, A. K., Zartman, R. E., and Kirk, W. S. (1977), U-Pb zircon dates from the central Appalachian Piedmont: A possible case of inherited radiogenic lead: Geological Society of America Bulletin, 88: 125–132.
Hill, E.J. and Baldwin, S.L. (1993), Exhumation of high-pressure metamorphic rocks during crustal extension in the D'Entrecasteaux region, Paupua New Guinea. Journal of Metamorphic Geology, 11:261-277.
Hoffman, P.F. (1991), Did the breakout of Laurentia turn Gondwanaland insideout? Science 252: 1409-1412.
Holland, T.J.B. (1980) The reaction albite = jadeite + quartz determined experimentally in the range 600-1200 °C. American Mineralogist, 65:129-134.
Holland, T.J.B. (1983), The experimental determination of activities in disordered and short-range ordered jadeitic pyroxenes. Contributions to Mineralogy and Petrology, 82:214-220.

Holland, T.J.B. and Blundy, J.D. (1994), Non-ideal interactions in calcic amphiboles and their bearing on amphibole plagioclase thermometry. Contributions to Mineralogy and Petrology, 116:433-447.
Holland, T.J.B. and Powell, R. (1998), An internally consistent thermodynamic data set for phases of petrologic interest. Journal of Metamorphic Geology, 16: 309-343.
Holm-Denoma, C.S., and Das, R. (2010), Bimodal volcanism as evidence for Paleozoic extensional accretionary tectonism in the southern Appalachians. Geological Society of America Bulletin, 122, no 7/8: 1220-1234, doi: 10.1130/B30051.1.
Horton, J.W., Jr., Blake, D.E., Wylie, A.S., Jr., and Stoddard, E.F., (1986), Metamorphosed mélange terranes in the eastern Piedmont of North Carolina. Geology, 14(7): 551-553.
Horton, J.W., Jr., Drake, A.A., Jr., and Rankin, D.W. (1989), Tectonostratigraphic terranes and their Paleozoic boundaries in the central and southern Appalachians. Geological Society of America Special Paper 230: 213-244.
Horton, J. W., Jr., Aleinikoff, J. N., Drake, A. A., Jr., and Fanning, C. M., (1998), Significance of middle to late Ordovician volcanic-arc rocks in the central Appalachian Piedmont, Maryland and Virginia Geological Society of America Abstracts with Programs, 30, 7, A-125.
Horton, J.W., Aleinikoff, J.N., Drake, A.A., Jr., and Fanning, M.C., (2010), Ordovician volcanic-arc terrane in the Central Appalachian Piedmont of Maryland and Virginia: SHRIMP U-Pb geochronology, field relations, and tectonic significance. In: Tollo, R.P., et al. (eds): From Rodinia to Pangea: the Lithotectonic Record of the Appalachian Region: Geological Society of America Memoir 206: 621-660. doi: 10.1130/2010.1206(25).
Hurford, A.J., Flisch, M., and Jäger, E. (1989), Unravelling the thermotectonic evolution of the Alps: a contribution from fission track analysis and mica dating. In: M.D. Coward, D. Dietrich, and R.G. Park (eds.), Alpine Tectonics, Geological Society of London Special Publication 45: 369-398.
Hurford, A.J., Hunziker, J.C., and Stöckhert, B. (1991), Constraints on the Late Thermotectonic evolution of the Western Alps: evidence for episodic rapid uplift. Tectonics, 10:758-769.
Hynes, A., and Rivers, T. (2010), Protracted continental collision – evidence from the Grenville Orogen. Canadian Journal of Earth Sciences, 47: 591-620, doi: 10:1139/E10-003
Irving, E. (1975), Structural evolution of the northeast Andes, Columbia. U.S. Geological Survey Professional Paper 846, 47 p.
Irving, T.N, and Baragar, W.R.A. (1971), A guide to the chemical classification of the coman volcanic rocks. Canadian Journal of Earth Sciences, 8: 523-548.
Jamtveit, B. (1987) Metamorphic evolution of the Eiksunddal eclogite complex, Western Norway, and some tectonic implications. Contributions to Mineralogy and Petrology, 95:82-99.
Johnston, S., Hacker, B.R., and Ducea, M.N. (2007), Exhumation of ultrahigh-pressure rocks beneath the Hornelen segment of the Nordfjord-Sogn Detachment Zone,

western Norway, Geological Society of America Bullletin, 119(9/10): 1232-1248, doi: 10.1130/B26172.1; 8
Katayama, I., Parkinson, C.D., Okamoto, K., Nakajima, Y., and Maruyama, S. (2000), Supersilicic clinopyroxene and silica exsolution in UHPM eclogite and pelitic gneiss from the Kokchetav massif, Kazakhstan. American Mineralogist, 85:1368-1374.
Keith, A. (1904), Description of the Asheville Quadrangle, North Carolina. U.S. Geological Survey Geological Atlas, Folio 116.
Kerr, W.C. (1875), Report of the Geological Survey of North Carolina, Volume I: Physical geography, resume, economical geology, North Carolina Geological Survey, 325 p.
King, P.B., Hadley, J.B., Neuman, R.B., and Hamilton, W. (1958), Stratigraphy of the Ocoee Series, Great Smoky Mountains, Tennessee and North Carolina, Geological Society of America Bullletin, 69: 947-966, doi: 10.1130/0016-7606(1958)69[947:SOOSGS]2.0.CO;2
Klein, H., and Wimmenauer, W. (1984), Eclogites and their retrograde transformation in the Schwartzwald (Fed. Rep. Germany). Neues Jahrbuch für Mineralogie Monatshefte, 1:25-38.
Kohn, M.J. (2001), Timing of arc accretion in the southern Appalachians: Perspectives from the Laurentian margin. Geological Society of America Abstracts with Programs, 110-0.
Kohn, M.J. and Malloy, M.A. (2004), Formation of monazite via prograde metamorphic reactions among common silicates: Implications for age determinations. Geochimica et Cosmochimica Acta, 68(1): 101-113.
Krabbendam, M., Wain, A., and Andersen, T.B. (2000), Pre-Caledonian granulite and gabbro enclaves in the Western Gneiss Region, Norway: indications of incomplete transition at high pressure. Geological Magazine, 137:235-255.
Kraemer, P.E., Escayola, M.P., Martino, R.D., 1995. Hipótesis sobre la evolución tectónica neoproterozoica de las Sierras Pampeanas de Córdoba (30º40'-32º40'). Revista Asociación Geológica Argentina, 50: 47–59.
Kretz, R. (1983), Symbols for rock-forming minerals. American Mineralogist, 68: 277-279.
Krogh, E.J. (1980), Geochemistry and petrology of glaucophane-bearing eclogites and associated rocks from Sunnfjord, Western Norway. Lithos, 13(4): 355-380.
Krogh, E.J., Oh, C.W., and Liou, J.G. (1994), Polyphase and anticlockwise P-T evolution for Franciscan eclogites and blueschists from Jenner, California, USA. Journal of. Metamorphic Geology, 12: 121-134, doi: 10.1111/j.1525-1314.1994.tb00008.x
Kröner, A., Jaeckel, P., Reischmann, T., and Kroner, U. (1998), Further evidence for an early Carboniferous (~340 Ma) age of high-grade metamorphism in the Saxonian granulite complex. Geologische Rundschau, 86: 751-766.
Kröner, A., Cordani, U., (2003), African, southern Indian and South American cratons were not part of the Rodinia supercontinent: evidence from field relationships and geochronology. Tectonophysics 375: 325–352.

Kuijper, R.P., Vogel, D.E., and Den Tex, E. (1985), Eclogite-plagiopyrigarnite relations in the catazonal complexes of Northwest Spain, Chemical Geology, 50: 163-171.

Kunk, M.J., Southworth, S., Aleinikoff, J.N, Naeser, N.D., Naeser, C.W., Merschat, C.E., and Cattanach, B.L. (2006). Preliminary U-Pb, 40Ar/39Ar and fission-track ages support a long and complex tectonic history in the western Blue Ridge in North Carolina and Tennessee. Geological Society of America Abstracts with Programs, 38 (3) 66.

Kunuziga, K., Takasu, A., and Banno, S. (1986), The origin and metamorphic history of the ultramafic and metagabbro bodies in the Sanbagawa metamorphic belt. In: B.W. Evans and E.H. Brown (eds.), Blueschists and eclogites, Geological Society of America Memoir 164, 375-385. Geological Society of America: Boulder.

Labrousse, L. (2001), L'exhumation des roches métamorphiques de très haute pression: le cas des Calédonides de Norvège. Ph.D thesis, Univerité Pierre & Marie Curie, 423 p.

Labrousse, L., Jolivet, L., Andersen, T.B., Agard, P., Hébert, R., Maluski, H., and Schärer, U. (2004), Pressure-temperature-time deformation history of the exhumation of ultra-high pressure rocks in the Western Gneiss Region, Norway. In: D.L.Whitney, C. Teyssier, and C.S. Siddoway (eds.), Gneiss domes in Orogeny. Geological Society of America Special Paper 380, Geological Society of America: Boulder, 155-183.

Lacazette, A.J., Jr., and Rast, N. (1989), Tectonic mélange at Chunky Gal Mountain, North Carolina, In: J.W. Horton Jr. and N. Rast (eds.), Mélanges and olistostromes of the U.S. Appalachians, Geological Society of America Special Paper 228, Geological Society of America: Boulder, 217-227.

Laird, J., and Albee, A.L. (1981), High-pressure metamorphism in mafic schist from northern Vermont. American Journal of Science, 281:97-126.

Leake, B.E., Woolley, A.R., Arps, C.E.S., Birch, W.D., Gilbert, M.C., Grice, J.D., Hawthorne, F.C., Kato, A., Mandarino, J.A., Maresch, W.V., Nikel, E.H., Rock, N.M.S., Schumacher, J.C., Smith, D.C., Stephenson, N.C.N., Ungaretti, L, Whittaker, E.J.W., and Youzhi, G. (1997), Nomenclature of amphiboles: Report of the Subcommittee on Amphiboles of the International Mineralogical Association, Commission on New Minerals and Mineral Names. American Mineralogist, 82:1019-1037.

Li, Z.X., Bogdanova, S.V., Collins, A.S., Davidson, A., De Waele, B., Ernst, R.E., Fitzsimons, I.C.W., Fuck, R.A., Gladkochub, D.P., Jacobs, J., Karlstrom, K.E., Lu, S., Natapov, L.M., Pease, V., Pisarevsky, S.A., Thrane, K., Vernikovsky, V., (2008), Assembly, configuration, and break-up history of Rodinia: A synthesis. Precambrian Research,160 (1-2): 179-210, doi: 10.1016/j.precamres.2007.04.021.

Liou, J.G., Tsujimori, T., Zhang, R.Y., Katayama, I., and Maruyama, S. (2004), Global UHP Metamorphism and Continent Subduction/Collision: The Himalayan Model. International Geology Review, 46: 1-27, doi: 10.2747/0020-6814.46.1.1

Lister, G.S., and Snoke, A.W. (1984), S-C mylonites. Journal of Structural Geology, 6 (6): 617-638.
Loewy, S.L., Connelly, J.N., Dalziel, I.W.D., and Gower, C.F. (2003), Eastern Laurentia in Rodinia: constraints from a whole-rock Pb and U/Pb geochronology. Tectonophysics, 375: 169-197.
Loewy, S.L., Connelly, J.N., and Dalziel, I.W.D. (2004), An orphaned basement block: the Arequipa-Antofalla Basement of the central Andean margin of South America. Geological Society of America Bulletin, 116(1/2): 171-187, doi: 10.1130/B25226.1
Loiselle, M. C., and Wones, D. (1979). Characteristics and origin of anorogenic granites. Geological Society of America, Abstracts with Programs, 11, 468.
Loughry, D.F. (2010), Origin of Blue Ridge basement rocks, Dellwood quad, western NC: Evidence from U-Pb zircon geochronology and whole rock geochemistry. M.S. thesis, University of Kentucky, Lexington, 136 p.
Ludwig, K.R., 2003. User's manual for Isoplot 3.0: a geochronological toolkit for Microsoft Excel. Berkeley Geochronology Center Special Publication, No. 4., 70p.
Mac Niocaill, C., van der Pluijm, B.A., and Van der Voo, R. (1996). Ordovician paleogeography and the evolution of the Iapetus ocean. Geology 25: 159-162.
Mader, U. K., Percival, J.A., and Berman, R. G. (1994), Thermobarometry of garnet-clinopyroxene-hornblende granulites from the Kapuskasing structural zone. In: Percival, J.A. (ed.) The Kapuskasing transect of Lithoprobe. Canadian Journal of Earth Science, 31:1134-1145.
Maggs, W.W., Cheney, J.T. and Spear, F.S. (1986), Probable retrograded eclogites in the Berkshire Massif. Geological Society of America Abstracts with Programs, 18:32.
Markl, G., and Bucher, K. (1997), Proterozoic eclogites from the Lofoten islands, northern Norway. Lithos, 42:15-35.
Martignole, J., and Martelat, J.E. (2003), Regional-scale Grenvillian-age UHT metamorphism in the Mollendo-Camana block (basement of the Peruvian Andes). Journal of Metamorphic Geology, 21: 99-120.
Martino, R.D., Law, R.D., Simpson, C. (1993), Evidence for orthogonal contractional orogeny in the Pampean Ranges of Córdoba, Central Argentina. EOS 74(16), 302. American Geophysical Union, Spring Meeting, Baltimore.
Massey, M. A., and Moecher, D.P. (2005), Deformation and metamorphic history of the Western Blue Ridge–Eastern Blue Ridge terrane boundary, southern Appalachian Orogen, Tectonics, 24, TC5010, doi:10.1029/2004TC001643.
McCausland, P.J.A., Van der Voo, R.A., and Hall, C.M. (2007), Circum-Iapetus paleogeography of the Precambrian–Cambrian transition with a new paleomagnetic constraint from Laurentia. Precambrian Research 156: 125-152.
McClellan, E.A., Steltenpohl, M.G., Thomas, C., and Miller, C.F. (2007), Isotopic age constraints and metamorphic history of the Talladega Belt: New evidence for timing of arc magmatism and terrane emplacement along the southern Laurentian margin. Journal of Geology, 115: 541-561. doi: 10.1086/519777.

McClelland, J.M., Selleck, B.W., and Bickford, M.E. (2010), Review of the Proterozoic evolution of the Grenville Province, its Adirondack outlier, and the Mesoproterozoic inliers of the Appalachians. In: Tollo, R.E., et al. (eds.), From Rodinia to Pangea: the Lithotectonic Record of the Appalachian Region: Geological Society of America Memoir 206: 621-660. doi: 10.1130/2010.1206(02)

McConnell, K.I., (1988), Geology of the Sauratown Mountains anticlinorium: Vienna and Pinnacle 7.5 minute quadrangles. In: R.D.Hatcher, Jr., (ed.), 1988 Field Trip Guidebook, Carolina Geological Society: Durham, 51–66.

McConnell, K.I., and Abrams, C.E. (1984), Geology of the greater Atlanta region. Georgia Geological Survey Bulletin 96, 127 p.

McDonough, M.R., Ramos, V.A., Isachsen, C.E., Bowring, S.A., Vujovich, G.I. (1993), Edades preliminares de circones del basamento de la Sierra de Pie de Palo, Sierras Pampeanas occidentales de San Juán: sus implicancias para el supercontinente proterozoico de Rodinia. In: XII Congreso Geológico Argentino y II Congreso de Exploración de Hidrocarburos, Mendoza, Actas, vol. 3, pp. 340–342.

McMenamin, M.A.S., McMenamin, D.L.S. (1990), The Emergence of Animals: The Cambrian Breakthrough. Columbia University Press: New York, 217 p.

McSween, H.Y., Jr., Abbott, R.N., and Raymond, L.A. (1989), Metamorphic conditions in the Ashe Metamorphic Suite, North Carolina Blue Ridge. Geology, 17:1140-1143.

McSween, H.Y., Jr., and Harvey, R.P., (1997), Concord plutonic suite; pre-Acadian gabbro-syenite intrusions in the southern Appalachians. In: A.K. Sinha, J.B. Whalen, and J.P. Hogan (eds.), The Nature of Magmatism in the Appalachian Orogen, Geological Society of America Memoir 191: 221–234.

Medaris, G., Jr., Jelínek, E., and Mísař, Z. (1995), Czech eclogites: Terrane settings and implications for Variscan tectonic evolution of the Bohemian Massif. European Journal of Mineralogy, 7:7-28.

Medaris, L.G., Jr., Ghent, E.D., Wang, H.F., Fournelle, J.H., and Jelínek, E. (2006), The Spačice eclogite: constraints on the P-T-t history of the Gföhl granulite terrane, Moldanubian Zone, Bohemian Massif. Mineralogy and Petrology, 86:203-220.

Meen, J.K. (1988), Mineral chemical variations in the Lake Chatuge mafic-ultramafic complex, North Carolina-Georgia; the P-T history of rocks in the Blue Ridge. Southeast Geology, 29: 1-27.

Merschat, A.J., and Kalbas, J.L. (2002), Geology of the southwestern Brushy Mountains, North Carolina Inner Piedmont: A summary and synthesis of recent studies. In: Hatcher, R.D., Jr. and Bream, B.R. (eds.), 2002 Field trip guidebook, Carolina Geological Society: Durham, p. 101-126.

Merschat, A.J., Hatcher, R.D., Jr., Bream, B.R., Miller, C.F., Byars, H.E., Gatewood, M.P., and Wooden, J.L. (2010), Detrital zircon geochronology and provenance of southern Appalachian Blue Ridge and Inner Piedmont crystalline terranes, In: R.P.Tollo, M.J. Bartholomew, J.P. Hibbard, and P.M. Karabinos, (eds.), From

Rodinia to Pangea: The Lithotectonic Record of the Appalachian Region: Geological Society of America Memoir 206, Boulder, 661–699, doi: 10.1130/2010.1206(26).
Merschat, C.E., and Wiener, L.S. (1988), Geology of the Sandymush and Canton quadrangles, North Carolina. North Carolina Geological Survey, Bulletin 90, 66 p.
Merschat, C.E., and Wiener, L.S. (1990), Geology of Grenville-Age basement and younger cover rocks in the west central Blue Ridge, North Carolina. 1990 Field Trip Guidebook, Carolina Geological Society: Durham.
Merschat, C.E., and Cattanach, B.L. (2008), Bedrock geologic map of the western half of the Asheville 1:100,000 scale quadrangle, North Carolina and Tennessee. North Carolina Geological Survey Geologic Map Series – 13.
Mesigga, B., and Bettini E. (1990), Reactions behaviour during kelyphyte and symplectite deformation: a case study of mafic granulites and eclogites from the Bohemian Massif. European Journal of Mineralogy, 2**:**125-144.
Miller, B.V., Stewart, K.G., Miller, C.F., and Thomas, C.W. (2000), U-Pb ages from the Bakersville, North Carolina eclogite: Taconian eclogite metamorphism followed by Acadian and Alleghanian cooling. Geological Society of America Abstracts with Programs, 32:62.
Miller, B.V., Fetter, A.H., and Stewart, K.G. (2006), Plutonism in three orogenic pulses, Eastern Blue Ridge Province, southern Appalachians. Geological Society of America Bulletin, 118:171-184.
Miller, B.V., Stewart, K.G., and Whitney, D.L. (2010), Three tectonothermal pulses recorded in eclogite and amphibolite of the Eastern Blue Ridge, Southern Appalachians. In: Tollo, R.P., et al. (eds): From Rodinia to Pangea: the Lithotectonic Record of the Appalachian Region: Geological Society of America Memoir 206: 701-724. doi: 10.1130/2010.1206(27)
Miller, C.F., Fullagar, P.D., Sando, T.W., Kish, S.A., Solomon, G.C., Russell, G.S., and Wood, L.F. (1997), Lowpotassium, trondhjemitic to granodioritic plutonism in the eastern Blue Ridge, southwestern North Carolina–northeastern Georgia. In: A.K. Sinha, and J.B. Whalen (eds.) The nature of magmatism in the Appalachian orogen, Geological Society of America Memoir 191, p. 235–254.
Mišković, A., Spikings, R.A., Chew, D.M., Košler, J., Ulianov, A., and Schaltegger, U. (2009), Tectonomagmatic evolution of Western Amazonia: Geochemical characterization and zircon U-Pb geochronologic constraints from the Peruvian Eastern Cordilleran granitoids. Geological Society of America Bulletin, 121(9/10): 1298-1324.
Misra, K.C., and McSween, H.Y., Jr. (1984), Mafic rocks of the southern Appalachians: A review. American Journal of Science, 284: 294-318.
Miyashiro, A. (1970), Volcanic rock series in island arcs and active continental margins. American Journal of Science, 19: 321-355.
Moecher, D.M., and Wintsch, R.P. (1994), Deformation-induced reconstitution and local resetting of mineral equilibria in polymetamorphic gneisses: tectonic and

metamorphic implications, Journal of Metamorphic Geology, 12(4): 523-538, doi: 10.1111/j.1525-1314.1994.tb00040.x
Moecher, D.P., Tracy, R.J., and Massey, M.A. (2002), Monazite chemical ages reveal more than one "Great Smoky Group" in southern Blue Ridge, Appalachian orogen. Geological Society of America Abstracts with Programs, 25-15.
Moecher, D.P., Tracy, R.J., and Anderson, E.D. (2003), Taconian metamorphism in eastern Great Smoky Mountains inferred fro U-Th-Pb monazite chemical ages. . Geological Society of America Abstracts with Programs, 10-4.
Moecher, D.P., Massey, M.A., and Tracy, R.J. (2005), Timing and pattern of metamorphism in the western and central Blue Ridge, TN and NC: Status and outstanding problems. In: R.D Hatcher Jr. and A.J. Merschat (eds.), 2005 Field Trip Guidebook, Carolina Geological Society: Durham. 57-66.
Moecher, D.P., Samson, S.D., and Miller, C.F. (2004), Precise time and conditions of peak Taconian granulite facies metamorphism in the southern Appalachian orogen, U.S.A., with implications for zircon behavior during crustal melting events, Journal of Geology, 112: 289-304, doi: 10.1086/382760.
Möller C. (1998), Decompressed eclogites in the Svenconorwegian (-Grenvillian) orogen of SW Sweden: petrology and tectonic implications. Journal of Metamorphic Geology, 16:641-656.
Monrad, J.R., and Gulley, G.L., Jr. (1983), Age and P-T conditions during metamorphism of granulite-facies gneisses, Roan Mountain, NC-TN, In: S. Lewis (ed.), 1983 Field Trip Guidebook, 41-51, Carolina Geological Society: Durham.
Monrad, J.R., and Gulley, G.L., Jr. 1983, Age and P-T conditions during metamorphism of granulite-facies gneisses, Roan Mountain, NC-TN. In: S.E. Lewis (ed.), 1983 Field Trip Guidebook, Carolina Geological Society: Durham, 1-18.
Montes, C. (1997) The Greenbrier and Hayesville faults in central-western North Carolina. M.S. thesis, University of Tennessee, Knoxville 145p.
Montes, C., and Hatcher R.D., Jr. (1999), Documenting Late Proterozoic rifting in the Ocoee basin, western Blue Ridge, North Carolina. Southeastern Geology, 39 (1): 37-50.
Moores, E.M. (1991), Southwest U.S.–East Antarctic (SWEAT) connection: a hypothesis. Geology 19: 425-428.
Morimoto, N., Fabries, J., Ferguson, A.K., Ginzburg, I.V., Ross, M., Siefert, F.A., Zussman, J., Aoki, K., and Gottardi, G. (1988), Nomenclature of pyroxenes, American Mineralogist, 73:1123-1133.
Mottana, A. (1986), Crystal-chemical evaluation of garnet and omphacite microprobe analyses: Its bearing on the classification of eclogites, Lithos, 19:171-186.
Mukasa, S.B., and Henry, D.J. (1990), The San Nicolás batholith of coastal Peru: early Palaeozoic continental arc or continental rift magmatism? The Journal of the Geological Society, London, 147: 27-39.
Munhá, J., and Marques, F. (1987), A model for the Lower Continental Crust (Morais and Bragança Massifs, NE Portugal) II. Petrology, Terra Cognita 7, 161.

Mysen, B. and Griffin, W.L. (1973), Pyroxene stoichiometry and the breakdown of omphacite. American Mineralogist, 58:60-63.
O'Brien, P.J. (1989a), The petrology of retrograded eclogites of the Oberpfalz Forest, NE Bavaria, West Germany. In: R. Meissner and D. Gebauer (eds.), The Evolution of the European Continental Crust: Deep Drilling, Geophysics, Geology, and geochemistry, Tectonophysics, 157: 195-212.
O'Brien, P.J. (1989b), A study of retrogression in eclogites of the Oberpfalz Forest, north-east Bavaria, West Germany, and their significance in the tectonic evolution of the Bohemian Massif. In: J.S.Daly et al. (eds.), Evolution of Metamorphic Belts, Geological Society of London Special Publication 43: 507-512.
O'Brien, P.J. (2000), The fundamental Variscan problem: high-temperature metamorphism at different depths and high-pressure metamorphism at different temperatures. In: W. Franke et al. (eds.), Orogenic processes: quantification and modeling in the Variscan belt, Geological Society of London Special Publication 179: 369-386.
O'Brien, P.J., Carswell, D.A., and Gebauer, D. (1990), Eclogite formation and distribution in the European Variscides. In: D.A. Carswell (ed.), Eclogite Facies Rocks, 204-224, Chapman and Hall: New York.
O'Brien, P. J., and Rötzler, J. (2003), High-pressure granulites: Formation, recovery of peak conditions and implications for tectonics. Journal of Metamorphic Geology, 21: 3-20, doi:10.1046/j.1525-1314.2003.00420.x.
Officer, N.D., Berquist, P.J., Miller, C.F., Fullagar, P., Wooden, J., and Carrigan, C.W. (2003), Western Blue Ridge basement of northeast TN and northwestern NC: Age, geochemistry, and possible relationships to Proterozoic rocks of the southeastern USA. Geological Society of America Abstracts with Programs, 10, 2.
Okamoto, K., Liou, J.G., and Ogasawara, Y. (2000), Petrology of the diamond-grade eclogite in the Kokchetav Massif, northern Kazakhstan. Island Arc, 9:379-399.
Omarini, R.H. (1983), Caracterizacion litologica diferenciacion y genesis de la Formacion Puncoviscana entre el Valle de Lerma y la Faja Eruptiva de la Puna. PhD thesis.University Nacional, Salta. 202 pp.
Omarini, R.H., Sureda, R.J., Götze, H.J., Seilacher, A., Plüger, F. (1999), Puncovicana fold belt in Northwestern Argentina: testimony of Late Proterozoic Rodinia fragmentation and pre-Gondwana collisional episodes. International Journal of Earth Sciences 88: 76-97.
Ortega-Obregon, C., Keppie, J.D., Murphy, J.B., Lee, J.K.W., and Ortega-Rivera, A. (2009), Geology and geochronology of Paleozoic rocks in western Acatlan Complex, southern Mexico: Evidence for contiguity across an extruded high-pressure belt and constraints on Paleozoic reconstructions. Geological Society of America Bulletin, 121(11/12): 1678-1694, doi: 10.1130/B26597.1
Osmundsen, P.T., Braathen, A., Nordgulen, Ø., Roberts, D., Meyer, G.B. and Eide, E., (2003), The Devonian Nesna shear zone and adjacent gneiss-cored culminations,

North-Central Norwegian Caledonides. Journal of the Geological Society of London, 160: 137–150.
Owens, B.E., and Tucker, R.D. (2003), Geochronology of the State Farm Gneiss and associated Neoproterozoic granitoids, Goochland Terrane, Virginia. Geological Society of America Bulletin, 115: 972-982.
Ownby, S.E., Miller, C.F., Berquist, P.J., Carrigan, C.W., Wooden, P.D., and Fullagar, P.D. (2004), U-Pb geochronology and geochemistry of a portion of the Mars Hill terrane, North Carolina-Tennessee: Constraints on origin, history, and tectonic assembly. In: Tollo et al. (eds.), Proterozoic tectonic evolution of the Grenville orogen in North America, Geological Society of America Memoir 197, Boulder, Colorado, 609-632.
Paces, J. B., and Miller, J.D., Jr. (1993), Precise U-Pb ages of Duluth Complex and related mafic intrusions, northeastern Minnesota: Geochronological insights to physical, petrogenetic, and paleomagnetic, and tectonomagmatic processes associated with the 1.1 Ga Midcontinent Rift system, Journal of Geophysical Research, 98:13,997-14,013, doi:10.1029/93JB01159.
Page, F.Z., Essene, E.J., and Mukasa, S.B. (2003), Prograde and retrograde history of eclogites from the Eastern Blue Ridge, North Carolina, USA. Journal of Metamorphic Geology, 21:685-698.
Page, F.Z., Essene, E.J., and Mukasa, S.B. (2005), Quartz exsolution in clinopyroxene is not proof of ultrahigh pressures: Evidence from eclogites from the Eastern Blue Ridge, Southern Appalachians, U.S.A. American Mineralogist, 90:1092-1099.
Palma, M.A., Parica, P.D., and Ramos, V.A. (1986), El Granito Archibarca, su edat y significado tectónico, Revista Asciación Geológica Agentina, 41, no 3-4, p. 414-419, Buenos Aires.
Pankhurst, R.J., Rapela, C.W., Saavedra, J., Baldo, E., Dahlquist, J., Pascua, I., Fanning, C.M. (1998), The Famatinian magmatic arc in the Central Sierras Pampeanas: an early to mid-Ordovician continental arc on the Gondwana margin. In: R.J. Pankhurst and C.W.Rapela, (eds.), The Proto-Andean Margin of Gondwana. Geological Society: London, Special Publication 142, 343–367.
Parrish, R.R., Gough, S.J., Searle, M.P., and Waters, D.J. (2006), Plate velocity exhumation of ultrahigh-pressure eclogites in the Pakistan Himalaya. Geology, 34: 989-992.
Peacock, M.A. (1931), Classification of igneous rock series. Journal of Geology, 39: 54-67.
Peacock, S.M. and Goodge, J.W. (1995), Eclogite-facies metamorphism preserved in tectonic blocks from a lower crustal shear zone, central Transarctic Mountains, Antarctica. Lithos, 36:1-13.
Pearce, J.A., Harris, N.B.W, and Tindle, A.G. (1984), Trace element discrimination diagrams for the tectonic interpretation of granitic rocks. Journal of Petrology, 25: 956-983.

Peccerillo, A., and Taylor, S.R. (1976), Geochemistry of Eocene calc-alkaline volcanic rocks from the Kastamonu area, Northern Turkey. Contributions to Mineralogy and Petrology, 58: 63-81.

Peterson, V., Ryan, J.G., and research experiences for undergraduates site program participants (2009), Petrogenesis and structure of the Buck Creek mafic-ultramafic suite, southern Appalachians: constraints on ophiolite evolution and emplacement in collisional orogens. Geological Society of America Bulletin, 121 (3/4): 615-629, doi: 10.1130/B26302.1

Powell, R. (1985) Regression diagnostics and robust regression in geothermometer/geobarometer calibration. The garnet-clinopyroxene thermometer revisited. Journal of Metamorphic Geology, 3:231-243.

Ramos, V.A., Jordan, T.E., Allmendinger, R.W., Mpodozis, C., Kay, S.M., Cortes, J.M., and Palma, M. (1986), Paleozoic terranes of the central Argentine-Chilean Andes. Tectonics, 5: 855-880.

Ramos, V.A. (1988), Late Proterozoic-Early Paleozoic of South America – a collisional history. Episodes, 11: 168-174.

Ramos, V.A. (2008), The basement of the central Andes: the Arequipa and related terranes, Annual Review of Earth and Planetary Sciences, 36: 289-324. doi: 10.1146/annurev.earth.36.031207.124304.

Ramos, V.A., (2009), The Grenville-Age Basement of the Andes. Journal of South American Earth Sciences.doi: 10.1016/j.jsames.2009.09.004.

Ramos, V.A. (2010), The Grenville-age basement of the Andes, Journal of South American Earth Sciences, 29: 77-91, doi: 10.1016/j.sames.2009.09.004.

Ramos, V.A., Vujovich, G., Martino, R., and Otamendi, J. (2010), Pampia: a large cratonic block missing in the Rodinia supercontinent. Journal of Geodynamics, 50: 243-255, doi: 10.1016/j.jog.2010.01.019

Rankin, D.W. (1970), Stratigraphy and structure of Precambrian rocks in northwestern North Carolina. In: G.W. Fisher et al. (eds.), Studies of Appalachian geology: Central and southern, 227-245, Interscience: New York.

Rankin, D.W., Espenshade, G.H., and Shaw, K.W. (1973), Stratigraphy and structure of the metamorphic belt in northwestern North Carolina and southwestern Virginia; A study from the Blue Ridge across the Brevard fault zone to the Sauratown Mountains anticlinorium. American Journal of Science (Cooper volume), 273-A: 1-40.

Rankin, D.W. (1975), The continental margin of eastern North America in the southern Appalachians: the opening and closing of the Proto-Atlantic Ocean. American Journal of Science, 275-A: 298-336.

Rankin, D.W., Drake, A.A., Jr., Glover, L., III, Goldsmith, R., Hall, L.M., Murray, D.P., Ratcliffe, N.M., Read, J.F., Secor, D.T., Jr., and Stanley, R.S. (1989), Pre-orogenic terranes. In: R.D. Hatcher, Jr. et al. (eds.), The Appalachian-Ouachita Orogen in the United States, The Geology of North America v. F-2, Geological Society of America: Boulder, 7-100.

Rankin, D.W., Drake, A.A., Jr., and Ratcliffe, N.M. (1990), Geologic map of the U.S. Appalachians showing the Laurentian margin and the Taconic orogen. In: R.D. Hatcher Jr. et al. (eds.), The Appalachian-Ouachita Orogen in the United States, The Geology of North America, v. F-2, (plates), Geological Society of America: Boulder.

Rapalini, A.E., Velasco, M.S., Koukharsky, M. (2002), New paleomagnetic data from the western Puna of Argentina: some tectonic speculations on its early Paleozoic evolution. 5th International Symposium on Andean Geodynamics, Extended Abstracts, pp 505–508.

Rapela, C.W., Pankhurst, R.J., Casquet, C., Baldo, E., Saavedera, J., Galindo, C., and Fanning, C.M. (1998), The Pampean Orogeny of the southern proto-Andes: Cambrian continental collision in the Sierras de Córdoba. In: R.J. Pankhurst and C.W.Rapela, (eds.), The Proto-Andean Margin of Gondwana. Geological Society: London, Special Publication 142: 181-217.

Rapela, C.W., Pankhurst, R.J., Casquet C., Fanning, C.M., Baldo, E.G., Gonzáles-Casado, J.M., Galindo, C., Dahlquist, J. (2007), The Río de la Plata craton and the assembly of Gondwana. Earth Science Reviews, 83:49–82.

Rast, N., and Kohles, K.M. (1986), The origin of the Ocoee Supergroup. American Journal of Science, 286: 593-616.

Raymond, L.A. (1987), Terrane amalgamation in the Blue Ridge belt, southern Appalachian orogen, U.S.A., Geological Society of America, Abstracts with Programs 19, 2, 125.

Raymond, L.A. (1995), Petrology: the study of igneous, sedimentary, and metamorphic rocks, Wm. C. Brown: Dubuque, 667-674.

Raymond, L.A., Yurkovich, S.P., and McKinney, M. (1989), Block-in-matrix structures in the North Carolina Blue Ridge belt and their significance for the tectonic history of the southern Appalachian orogen. In: J.W. Horton Jr., and N. Rast (eds.) Mélanges and Olistostromes of the U.S. Appalachians, Geological Society of America Special Paper 228, 195-215.

Rivers, T. (1997), Lithotectonic elements of the Grenville Province: review and tectonic implications. Precambrian Research, 86: 117-154.

Rivers, T., Ketchum, J., Indares, A., and Hynes, A. 2002. The High-Pressure belt in the Grenville Province: architecture, timing and exhumation. Canadian Journal of Earth Sciences, 39(5): 867-893. doi:10.1139/e02-025.

Roberts, D., Nordgulen, Ø., and Melezhik, V. (2007), The Uppermost Allochthon in the Scandinavian Caledonides: From a Laurentian ancestry through Taconian orogeny to Scandian crustal growth on Baltica. In: R.D.Hatcher Jr., M.P. Carlson, J.H. McBride, and J.R. Martínez Catalán (eds.), 4-D Framework of Continental Crust: Geological Society of America Memoir 200: 357–377, doi: 10.1130/2007.1200(18).

Rubie, D.C. (1990), Role of kinetics in the formation and preservation of eclogites. In: Carswell D.A. (ed.), Eclogite Facies Rocks, Chapman and Hall: New York, 111-140.

Russell, G.S., Odom, A.L., and Russell, C.W. (1987), Uranium-lead and rubidium-strontium isotopic evidence for the age and origin of granitic rocks in the Northern Alabama Piedmont. In: M.S. Drummond and N.L. Green (eds.), Granites of Alabama, Geological Survey of Alabama, Special Publication, Tuscaloosa, 239-249.

Ryan, J.G., Yurkovich, S., Peterson, V., Burr, J., and Kruse, S. (2005), Geology and petrogenesis of mafic and ultramafic rocks of the Willets-Addie area, central Blue Ridge, NC. In: R.D. Hatcher, Jr., and A.J. Merschat (eds.), 2005 Field Trip Guidebook, Carolina Geological Society: Durham, 91-98.

Sadowski, G.R., and Bettencourt, J.S., (1996), Mesoproterozoic correlations between eastern Laurentia and the western border of the Amazon craton. Precambrian Research, 76: 213-227.

Sambridge, M.S., and Compston, W. (1994), Mixture modeling of multi-component data sets with application to ion-probe zircon ages. Earth and Planetary Science Letters, 128: 373-390.

Santos, J.O.S., Rizzotto, G.J., Potter, P.E., McNaughton, N.J., Matos, R.S., Hartmann, L.A., Chemale, F., and Quadros, M.E.S. (2008), Age and autochthonous evolution of the Sunsás Orogen in West Amazon Craton based on mapping and U-Pb geochronology. Precambrian Research,165 (3–4): 120–152.

Schliestedt, M. (1990), Occurrences and stability conditions of low-temperature eclogites. In: D.A. Carswell (ed.), Eclogite Facies Rocks, Chapman and Hall: New York, 160-179.

Schwartz, J.J., Gromet, L.P., Miro, R. (2008), Timing and duration of thecalc-alkaline arc of the Pampean orogeny: implications for the late Neoproterozoic to Cambrian Evolution of Western Gondwana. Journal of Geology, 116:39–61.

Shackleton, R.M., Ries, A.C., Coward, M.P., and Cobbold, P.R. (1979), Structure, metamorphism and geochronology of the Arequipa Massif of coastal Peru. Geological Society [London] Journal, 136: 195–214.

Shand, S.J. (1951), The study of rocks. Thomas Murby and Company: London. 236 p.

Shärer, U., and Labrousse, L. (2003), Dating the exhumation of UHP rocks and associated crustal melting: the Norwegian Caledonides. Contributions to Mineralogy and Petrology, 144:758-770.

Shatsky, V.S., Jagoutz, E., Kozmenko, O.A., and Sobolev, N. (1999), The age of the UHP metamorphism and protoliths. In: Dobretsov NL, Sobolev NV, and Shatsky VS (eds.), Fourth International Eclogite Symposium Field Guide Book. United Institute of Geology, Geophysics, and Mineralogy, Siberian Branch of Russian Academy of Sciences: Novosibirsk, 50-52.

Shervais, J.W., Dennis, A.J., McGee, J.J. and Secor, D. (2003), Deep in the Heart of Dixie: Pre-Alleghanian eclogite and HP granulite metamorphism in the Carolina terrane, South Carolina, USA. Journal of Metamorphic Geology, 21:65-80.

Sinha, A.K., Hund, E.A., and Hogan, J.P. (1989), Paleozoic accretionary history of the North American Plate margin (central and southern Appalachians): Constraints from the age, origin, and distribution of granitic rocks. In: J.W Hillhouse (ed.), Deep structure and past kinematics of accreted terranes, Geophysical Monograph 50, AGU: Washington, D.C., 219-238.

Sinha, A. K., Hanan, B. B., and Wayne, D. M., 1997, Igneous and metamorphic U-Pb zircon ages from the Baltimore mafic complex, Maryland Piedmont. In: Sinha, A. K., Whalen, J. B., and Hogan, J. P., (eds.), The Nature of Magmatism in the Appalachian Orogen: Boulder, Colorado, Geological Society of America Memoir 191: 275–286.

Sloss, L.L. (1963), Sequences in the cratonic interior of North America. Geological Society of America Bulletin, 74: 93-114.

Smith, D.C. (1984), Coesite in clinopyroxene in the Caledonides and its implications for geodynamics. Nature, 310:641-644.

Smith, D.C. (1988), A review of the peculiar mineralogy of the "Norwegian Coesite Eclogite Province", with crystal-chemical, petrological, geochemical and geodynamical notes and an extensive bibliography. In: D.C. Smith (ed), Eclogites and Eclogite-facies Rocks. Elsevier: Amsterdam, 1-206.

Smith, D.C. (2006), The SHAND quaternary system for evaluating the supersilicic or subsilicic crystal-chemistry of eclogite minerals, and potential new UHPM pyroxene and garnet end-members. Mineralogy and Petrology, 88: 87-122.

Smithies, R.H., 2000, The Archaean tonalite-trondhjemite-granodiorite (TTG) series is not an analogue of Cenozoic adakite. Earth and Planetary Science Letters, 182: 115-125.

Smyth, J.R. (1980), Cation vacancies and the crystal chemistry of breakdown reactions in kimberlitic omphacites. American Mineralogist, 63: 1185-1191.

Southworth, S., Schultz, A., and Denenny, D., (2005a), Geologic Map of the Great Smoky Mountains National Park Region, Tennessee and North Carolina, US Geological Survey open file report 2005-1225.

Southworth, S., Aleinikoff, J. N., Kunk, M. J., Naeser, C. W., and Naeser, N. D., (2005b), Geochronology of the Great Smoky Mountains Nation Park region, TN/NC, with correlation to the rocks and orogenic events of the Appalachian Blue Ridge. In: R.D. Hatcher, Jr., and A.J. Merschat, (eds.), 2005 Field Trip Guidebook, Carolina Geological Society: Durham, 45-56.

Spagnuolo, C.M., Rapalini, A.E., and Astini R.A., (2011), Reinterpretation of the Ordovician rotations in NW Argentina and Northern Chile: a consequence of the Precordillera collision? International Journal of Earth Sciences, 100:603-618. doi: 10.1007/s00531-010-0578-2.

Spear, F.S. (1995), Metamorphic phase equilibria and pressure-temperature-time paths. Mineralogical Society of America Monograph. Mineralogical Society of America: Washington, DC., 437-439.

Steltenpohl, M., Hames, W., Andresen, A., and Markl, G. (2003), New Caledonian eclogite province in Norway and potential Laurentian (Taconic) and Baltic links. Geology, 31: 985-988, doi: 10.1130/G19744.1

Stacy, J.S., and Kramers, J.D. (1975), Approximation of terrestrial lead isotope evolution by a two-stage model. Earth and Planetary Science Letters, 26: 207-221.

Steenken, A., Lopez de Luchi, M.G., Martinez Dopico, C., Drobe, M., Wemmer, K., and Siegesmund, S. (2011), The Neoproterozoic-early Paleozoic metamorphic and magmatic evolution of the Eastern Sierras Pampeanas: an overview. International Journal of Earth Sciences, 100: 465-488.

Stewart, K.G., Adams, M.G., and Trupe, C.H. (1997), Paleozoic structural evolution of the Blue Ridge thrust complex, western North Carolina. In: K.G. Stewart et al. (eds.), 1997 Field Trip Guidebook, Carolina Geological Society: Durham, 21-31.

Štípská, P., and Powell, R. (2005), Constraining the P-T path of a MORB-type eclogite using pseudosections, garnet zoning and garnet-clinopyroxene thermometry: an example from the Bohemian Massif. Journal of Metamorphic Geology, 23:725-743.

Storey, C.D., Brewer, T.S., and Parrish, R.R. (2004), Late Proterozoic tectonics in northwest Scotland: one contractional orogeny or several? Precambrian Research 134: 227-247. doi:10.1016/j.precamres.2004.06.004

Streckheisen, A.L., and Le Maître, R.W. (1979), A chemical approximation to the modal QAPF classification of the igneous rocks. Neues Jahrbuch für Mineralogie Abhandlungen, 136: 169-206.

Swanson, S.E., Raymond, L.A, Warner, R.D., Ryan, J.G., Yurkovich, S.P., and Peterson, V.L. (2005), Petrotectonics of mafic and ultramafic rocks in Blue Ridge terranes of western North Carolina and northern Georgia, In: R.D. Hatcher, Jr., and A.J. Merschat, (eds.), 2005 Field Trip Guidebook, Carolina Geological Society: Durham, 73-90.

Terry, M.P., Robinson, P., Hamilton, M.A., and Jercinovic, M.J. (2000), Monazite geochronology of UHP and HP metamorphism, deformation, and exhumation, Nordøyane, Western Gneiss Region, Norway. American Mineralogist, 85:1651-1664.

Teixeira, W., Tassinari, C.C.G., Cordani, U.G., Kawashita, K., (1989), A review of the geochronology of the Amazonian craton: tectonic implications. Precambrian Research 42: 213–227.

Thomas, W.A. (1977), Evolution of Appalachian-Ouachita salients and recesses from reentrants and promontories in the continental margins.American Journal of Science, 277: 1233-1278.

Thomas, W.A. (1991), The Appalachian-Ouachita rifted margin of southeastern North America. Geological Society of America Bulletin, 103: 415-431, doi: 10.1130/0016-7606(1991)103<0415:TAORMO>2.3.CO;2.

Thomas, W.A. (2006), Tectonic inheritance at a continental margin, GSA today, v. 16, no. 2, doi: 10.1130/1052-5173(2006)016<4:TIAACM>2.0.CO;2.

Thomas, W.A., and Astini, R.A. (1996), The Argentine Precordillera: a traveler from the Oauchita embayment of North American Laurentia. Science, 273: 752-757.
Thomas, W.A. and Astini, R.A., (1999), Simple-shear conjugate rift margins of the Argentine Precordillera and the Ouachita embayment of Laurentia. Geological Society of America Bulletin 111, 1069– 1079.
Thomas, W.A., and Astini, R.A. (2003), Ordovician accretion of the Argentine Precordillera terrane to Gondwana: a review. Journal of South American Earth Sciences, 16: 67-79.
Thomas, W.A., Astini, R.A., and Bayona, G. (2002), Ordovician collision of the Argentine Precordillera with Gonddwana, independent of the Laurentian Taconic orogeny. Tectonophysics, 345: 131-152.
Tilton, G. R., Doe, B. R., and Hopson, C. A. (1970), Zircon age measurements in the Maryland Piedmont with special reference to Baltimore Gneiss problems, In: G.W. Fisher et al. (eds), Studies of Appalachian geology-Central and southern, Interscience Publishers: New York, 429–434.
Tohver, E., van der Pluijm, B.A., Van der Voo, R., Rizzotto, G., Scandolara, J.E. (2002), Paleogeography of the Amazon craton at 1.2 Ga: early Grenvillian collision with the Llano segment of Laurentia. Earth and Planetary Science Letters 199: 185-200.
Tohver, E., Bettencourt, J.S., Tosdal, R., Mezger, K., Leite, W.B., and Payolla, B.L. (2004a), Terrane transfer during the Grenville orogeny: tracing the Amazonian ancestry of southern Appalachian basement through Pb and Nd isotopes. Earth and Planetary Science Letters, 228: 161-176. doi: 10.1016/j.epsl.2004
Tohver, E., van der Pluijm, B.A., Mezger, K., Scandolara, J.E., and Essene, E.J., (2004b), Significance of the Nova Brasilaˆndia Metasedimentary Belt in western Brazil: Redefining the Mesoproterozoic boundary of the Amazon craton: Tectonics, v. 23, ~20 pp. TC6004, doi: 10.1029/2003TC001563.
Tohver, E., van der Pluijm, B.A., Scandolara, J.E., Essene, E.J., (2005), Late Mesoproterozoic deformation of SW Amazonia (Rondônia, Brazil): geochronological and structural evidence for collision with southern Laurentia. Journal of Geology, 113: 309-323.
Tohver, E., Teixiera, W., van der Pluijm, B., Geraldes, M.C., Bettencourt, J.S., and Rizotto, G. (2006), Restored transect across the exhumed Grenville orogen of Laurentia and Amazonia, with implications for crustal architecture. Geology, 34. no. 8: 669–672; doi: 10.1130/G22534.1
Tohver, E., Trindade, R.I.F., Solum, J.G., Hall, C.M., Riccomini C., and Nogueira, A.C., (2010), Closing the Clymene ocean and bending a Brasiliano belt: Evidence for the Cambrian formation of Gondwana, southeast Amazon craton. Geology, 38, no.3: p. 267–270; doi: 10.1130/G30510.1
Tollo, R.P., Bailey, C.M., Borduas, E.A., and Aleinikoff, J.N. (2004a), Mesoproterozoic geology of the Blue Ridge province in north-central Virginia: Petrologic and structural perspectives on Grenvillian orogenesis and Paleozoic tectonic processes. In: S. Southworth and W. Burton (eds.), Geology of the National

Capital Region-Field Trip Guidebook, US Geological Survey Circular 1264, 17-75.
Tollo, R.P., Aleinikoff, J.N., Bartholomew, M.J., and Rankin, D.W. (2004b), Neoproterozoic A-type granitoids of the central and southern Appalachians; intraplate magmatism associated with episodic rifting of the Rodinian supercontinent. Precambrian Research, 128: 3-38.
Tollo, R.P., Bartholomew, M.J., Hibbard, J.P., and Karabinos, P.M. (2010) Preface. In: R.P. Tollo, M.J. Bartholomew, J.P. Hibbard and P.M. Karabinos (eds.), From Rodinia to Pangea: The Lithotectonic Record of the Appalachian Region: Geological Society of America Memoir 206, Boulder, 51-69, doi: 10.1130/2010.1206(26).
Treloar, P.J., O'Brien, P.J., Parrish, R.R., and Kahn, M.A. (2003), Exhumation of early Tertiary, coesite-bearing eclogites from the Pakistan Himalaya. Journal of the Geological Society, 160:367-376.
Trindade, R.I.F., D'Agrella Filho, M.S., Epof, I., and Neves, B.B.B. (2006), Paleomagnetism of Early Cambrian Itabaiana mafic dikes (NE Brazil) and the final assembly of Gondwana: Earth and Planetary Science Letters, 244: 361-377, doi: 10.1016/j.epsl.2005.12.039.
Tsujimori, T., Matsumoto, K., Wakabayashi, J., and Liou, J.G. (2006), Franciscan eclogite revisited: Reevaluation of the P-T evolution of tectonic blocks from Tiburon Peninsula, California, U.S.A., Mineralogy and Petrology, 88: 243-267.
Tull, J.F. (1978), Structural development of the Alabama Piedmont northwest of the Brevard zone. American Journal of Science. 278: 442-460.
Tull, J.F. (1998), Analysis of a regional middle Paleozoic unconformity along the distal southeastern Laurentian margin, southernmost Appalachians: Implications for tectonic evolution, Geological Society of America Bulletin, 110(9), 1149-1162, doi: 10.1130/0016-7606(1998)110<1149:AOARMP>2.3.CO;2.
Tull, J.F., Barineau, C.I., Mueller, P.A., and Wooden, J.L. (2007), Volcanic arc emplacement onto the southernmost Appalachian Laurentian shelf: Characteristics and constraints. Geological Society of America Bulletin, 119, 261-274, doi: 10.1130/B25998.1.
Valentine, J.W., Moores, E.M. (1970), Plate-tectonic regulation of animal diversity and sea level: a model. Nature, 228: 657-659.
van Breeman, O., Aftalion, M., Bowes, D.R., Dudek, A., Mísař, Z., Povondra, P., and Vrána, S. (1982), Geochronological studies of the Bohemian Massif, Czechoslovakia, and their significance in the evolution of Central Europe. Transactions of the Royal Society of Edinburgh: Earth Sciences, 73: 89-108.
van Staal, C.R., Ravenhurst, C.E., Winchester, J.A., Roddick, J.C., and Langdon, J.P. (1990), Post-Taconic blueschist suture in the northern Appalachians of northern New Brunswick, Canada, Geology, 18: 1073-1077, doi: 10.1130/0091-7613(1990)018<1073:PTBSIT>2.3.CO;2

Vogel, D.E. (1966) Nature and chemistry of the formation of clinopyroxene-plagioclase symplectite from omphacite. Neues Jahrbuch für Mineralogie-Monatshefte, 6: 185-189.

Wain, A.L. (1997) New evidence for coesite in eclogite and gneisses: defining an ultrahigh pressure province in the Western Gneiss Region of Norway. Geology, 25: 927-930.

Wain, A.L., Waters, D.J., and Austrheim, H. (2001) Metastability of granulites and processes of eclogitisation in the UHP region of western Norway. Journal of Metamorphic Geology, 19: 607-623.

Wakabayashi, J. (1999), Subduction and the rock record: Concepts developed in the Franciscan Complex, California, Geological Society of America Special Paper 338: 123-133.

Walsh, E.O., Hacker, B.R., Gans, P.B., Grove, M., and Gehrels, G. (2007), Protolith ages and exhumation histories of (ultra)high-pressure rocks across the Western Gneiss Region, Norway, Geological Society of America Bulletin, 119(3-4): 289-301, doi: 10.1130/B25817.1

Warner, R.D., and Hepler, C.W. (2005), Petrology of the Dark Ridge metaultramafic body, North Carolina. In: R.D. Hatcher and A.J. Merschat (eds.), 2005 Field Trip Guidebook, Carolina Geological Society: Durham, 99-112.

Wasteneys, H.A., Clark, A.H., Farrar, E., and Langridge, R.J. (1995), Grenvillian granulite-facies metamorphism in the Arequipa Massif, Peru: a Laurentia-Gondwana link. Earth and Planetary Science Letters, 132: 63-73.

Waters, C.L., Hewitt, K., Stewart K.G., and Miller, B.V. (2000), Tectonothermal evolution of the Ashe metamorphic suite south of the Grandfather Mountain Window, NC; implications for Paleozoic orogenic events in the eastern Blue Ridge. Geological Society of America Abstracts with Programs, 32:81.

Waters D.J. (2002), Clinopyroxene-amphibole-plagioclase symplectites in Norwegian eclogites: microstructures, chemistry and the exhumation P-T path. Mineralogical Society, Winter Conference, Derby, January 2002.

Waters, D.J., and Martin, H.N. (1993), Geobarometry in phengite-bearing eclogites. Terra Abstracts, 5:410-411.

Weil, A.B.,Van der Voo, R., Mac Niocaill, C., Meert, J.G. (1998), The Proterozoic supercontinent Rodinia: paleomagnetically derived reconstructions for 1100 to 800 Ma. Earth Planetary Science Letters 154: 13–24.

Werner, C.D. (1987), Saxonian granulites—igneous or lithogeneous? A contribution to the geochemical diagnosis of the original rocks in highmetamorphic complexes. In: H. Gerstenberger (ed.), Contributions to the geology of the Saxonian granulite massif: Sächsisches Granulitegebirge, Zfl-Mitteilungen Nr., 133: 221–250.

Wiedenbeck, M. (1995), An example of reverse discordance during ion microprobe zircon dating: An artifact of enhanced ion yields from a radiogenic labile Pb. Chemical Geology, 125: 197-218.

Will, T.M., and Schmädicke, E. (2001), A first find of retrogressed eclogites in the Odenwald Crystalline Complex, Mid-German Crystalline Rise, German: evidence for a so far unrecognized high-pressure metamorphism in the Central Variscides. Lithos, 59: 109-125, doi: 10.1016/S0024-4937(01)00059-7

Willard, R.A. and Adams, M.G. (1994), Newly discovered eclogite in the southern Appalachian orogen, northwestern North Carolina. Earth and Planetary Science Letters, 123:61-70.

Woodward, N.B., Connelly, J.B., Walters, R.R., and Lewis, J.C. (1991), Tectonic evolution of the Great Smoky Mountains: Studies of Precambrian and Paleozoic stratigraphy in the western Blue Ridge, In: S.A. Kish (ed), 1991 Field Trip Guidebook, Carolina Geological Society: Durham, 57-68.

Yang, T.N. (2004), Retrograded textures and associated mass transfer: evidence for aqueous fluid action during exhumation of the Qinglongshan eclogite, Southern Sulu ultrahigh pressure metamorphic terrane, eastern China. Journal of Metamorphic Geology, 22: 653-669.

Zhang, J.X., Yang, J.S., Mattinson, C.G., Xu, Z.Q., Meng, F.C., and Shi, R.D. (2005), Two contrasting eclogite cooling histories, North Qaidam HP/UHP terrane, western China: Petrological and isotopic constraints. Lithos, 84:51-76.

Zhao, G., Cawood, P.A., Wilde, S.A. and Lu, L. (2001), High-pressure granulites (retrograded eclogites) from the Hengshan Complex, North China craton: petrology and tectonic implications. Journal of Petrology, 42: 1141-1170.

VITA

Eric D. Anderson
Born: August 31, 1962, San Francisco, California

Education
M.S. 1995 (Geology), University of Kentucky
B.S. 1985 (Geology) Virginia Polytechnic Institute and State University

Publications, and Thesis:

Anderson, E.D., and Moecher, D.P. (2009), Formation of high-pressure metabasites in the southern Appalachian Blue Ridge via Taconic continental subduction beneath the Laurentian margin. Tectonics, 28, TC5012, doi:10.1029/2008TC002319.

Anderson, E.D., and Moecher, D.P. (2007), Omphacite breakdown reactions and relation to eclogite exhumation rates. Contributions to Mineralogy and Petrology, 154(3): 253-277, doi: 10.1007/s00410-007-0192-x.

Moecher, D.P., Anderson, E.D., Cook, C.A., and Mezger, K. (1997), The petrogenesis of metamorphosed carbonatites in the Grenville Province, Ontario. Canadian Journal of Earth Science, 34: 1185-1201.

Anderson, E.D. 1995. The stable isotope and chemical composition of calcite from calcite-apatite-biotite rocks, marble and skarn, Southwestern Grenville Province, Ontario; constraints on the origin of potential meta-carbonatites. University of Kentucky, thesis. 62 p.